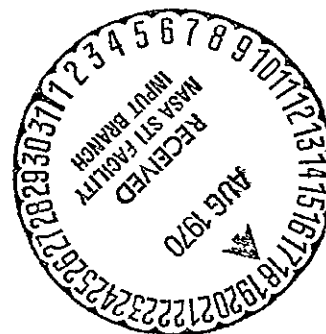


EARTH RESOURCES TECHNOLOGY SATELLITE FINAL REPORT

4. OBSERVATORY SUBSYSTEMS STUDY

PREPARED FOR
GODDARD SPACE FLIGHT CENTER
NATIONAL AERONAUTICS
AND SPACE ADMINISTRATION
UNDER CONTRACT NAS5-11260



FACILITY FORM 602

N70-34412
(ACCESSION NUMBER) (THRU)

529
(PAGES)

CR-10911
(NASA CR OR TMX OR AD NUMBER)

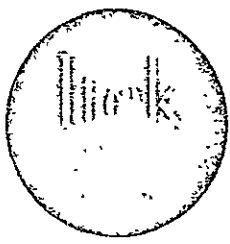
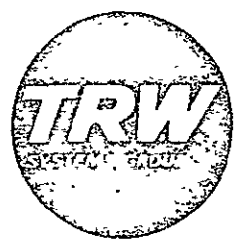
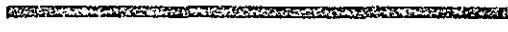
31
(CODE) (CATEGORY)

Reproduced by
**NATIONAL TECHNICAL
INFORMATION SERVICE**
Springfield, Va. 22151

EARTH RESOURCES TECHNOLOGY SATELLITE FINAL REPORT

4. OBSERVATORY SUBSYSTEMS STUDY

PREPARED FOR
GODDARD SPACE FLIGHT CENTER
NATIONAL AERONAUTICS
AND SPACE ADMINISTRATION
UNDER CONTRACT NAS5-11260



N70-34412

(ACCESSION NUMBER)

(THRU)

529

(PAGES)

(CODE)

CR-109117

(NASA CR OR TMX OR AD NUMBER)

31

(CATEGORY)

Reproduced by
**NATIONAL TECHNICAL
INFORMATION SERVICE**
Springfield, Va. 22151

EARTH RESOURCES TECHNOLOGY SATELLITE

FINAL REPORT

Volume 4. Observatory Subsystems Study

February 11, 1970

prepared for

National Aeronautics and Space Administration
Goddard Space Flight Center

Contract NAS5-11260

item 3a

TRW Systems Group
One Space Park · Redondo Beach
Los Angeles County
California 90278

PREFACE

The final report for the ERTS Phase B/C study consists of the 12 volumes that are submitted now and additional volumes to be delivered in April covering the results of the study of the Ground Data Handling System for ERTS. The contents of the first volumes of the report are as follows:

Volume

1. (to be completed in April). Summarizes all significant conclusions of the study and indicates where the supporting analyses are presented. The system specification is included as an appendix.
2. (to be completed in April). Contains all system interface studies.
3. Describes the design of ERTS resulting from the study, to a block diagram level of detail.
4. Presents the detailed results of the study supporting the design in Volume 3, including backup tradeoffs and analyses.
5. Presents both the design of the data collection system and the supporting analyses.
- 6-12. Present the plans prepared for the ERTS Phase D program on the Phase B/C program.

CONTENTS

	Page
1. OVERALL STUDY RESULTS	1-1
1.1 Introduction	1-1
1.2 Body Orientation	1-3
1.3 Wideband Tape Recorder Installation	1-8
1.4 Uncompensated Momentum	1-11
1.5 Flexibility for Scanning Mirrors and Antennas	1-12
2. SPACECRAFT PAYLOAD COMPATIBILITY	2-1
2.1 Introduction	2-1
2.2 Electrical Power	2-5
2.3 Commands	2-8
2.4 Telemetry	2-10
2.5 Timing Signals	2-12
2.6 Video Tape Recorder Search Channel	2-13
2.7 Fault Protection	2-14
2.8 Mechanical Interface	2-14
2.9 Thermal Interface	2-19
2.10 Uncompensated Momentum	2-20
2.11 Recommended Payload Changes	2-22
2.12 Krypton Effect on Radiative Cooler	2-22
3. SYSTEM LIFETIME	3-1
4. STRUCTURE	4-1
4.1 Equipment Layout	4-1
4.2 Boost Vibration and Acceleration Environment	4-2
4.3 Vibration and Acceleration Testing of Assemblies	4-8
4.4 Observatory Qualification Testing	4-9
4.5 Boost Separation	4-13
4.6 Spacecraft Vibrations in Orbit	4-14
4.7 Payload Thermal Alignment Shift	4-15
4.8 Effect of Array Rotation on Mass Properties	4-17
4.9 Structural Strength Analysis	4-19

CONTENTS (Continued)

	Page
5. ATTITUDE CONTROL SYSTEM	5-1
5.1 Normal Mode Performance Analysis	5-1
5.2 Attitude Control Configuration Study	5-6
5.3 Yaw Attitude Control Subsystem Preliminary Analysis and Design	5-8
5.4 Control Gas Requirements	5-16
5.5 Acquisition Studies	5-17
5.6 Attitude Control System Accuracy During Velocity Corrections	5-17
5.7 Moon Avoidance	5-19
5.8 Albedo Errors in Sun Sensor	5-20
5.9 Solar Array Deployment and Slew	5-23
5.10 Horizon Tracker Operation in South Pole Winter	5-24
5.11 Non-Nominal Orbital Performance	5-27
6. ATTITUDE DETERMINATION	6-1
6.1 The Selected System	6-5
6.2 Earth Sensor Assembly/Gyro	6-8
6.3 Systems Using Star Sensors	6-21
6.4 Conclusion Concerning Orbital Attitude Determination	6-25
6.5 Relative Attitude Determination	6-26
6.6 Systems Using Reaction Wheel Data	6-28
6.7 Systems Using Gyro Reference Assemblies	6-34
6.8 Conclusion Concerning Relative Attitude Determination	6-35
6.9 Celestial Attitude Reference from the RBV Camera	6-35
7. VELOCITY CORRECTION	7-1
7.1 System Interactions	7-1
7.2 Thruster Design	7-2
7.3 Thruster Placement	7-6
7.4 Choice of Propellant	7-9

CONTENTS (Continued)

	Page
8. DATA HANDLING	8-1
8.1 Stored Command Programmer	8-1
8.2 Narrowband Tape Recorder	8-13
8.3 Spacecraft Clock	8-18
8.4 Telemetry List	8-20
8.5 Command List	8-31
8.6 Command Reliability	8-36
9. COMMUNICATIONS	9-1
9.1 Power Amplification of Wideband Video Signals	9-1
9.2 Traveling Wave Tube Selection	9-5
9.3 Carrier Intermodulation By Limiting of Two FM Signals, Wideband Link	9-8
9.4 MSS and RBV Downlink Intermodulation Interference	9-11
9.5 Effect of RF Link on RBV Signal-to-Noise Ratio	9-14
9.6 Unified S-Band Downlink Intermodulation Interference	9-16
9.7 VHF Transmitter Design Alternatives	9-20
9.8 Communication Link Power Budgets	9-21
10. ANTENNAS	10-1
10.1 VHF Antenna Pattern Test	10-1
10.2 Unified S-Band Omnidirectional Antenna Pattern Test	10-21
11. ELECTRICAL POWER	11-1
11.1 Power System Sizing	11-1
11.2 Solar Array Design Factors	11-4
11.3 Alternate Array Designs	11-4
11.4 Depth of Battery Discharge	11-10
11.5 Negative Bus Peak Current Source	11-10
12. ELECTRICAL INTEGRATION	12-1
12.1 Junction Box Requirements	12-1
12.2 Grounding and Bonding	12-1

CONTENTS (Continued)

	Page
12.3 Command Distribution Unit	12-2
12.4 Harnesses	12-7
12.5 Electromagnetic Interference	12-10
13. THERMAL	13-1
14. SPACECRAFT HARDWARE	14-1
15. PERFORMANCE ASSURANCE	15-1
15.1 The Spacecraft Reliability Model	15-2
15.2 Review of Existing Assemblies, Extent of Compliance with ERTS Requirements	15-16
15.3 Configuration Management	15-16
15.4 Consolidated Parts, Materials, and Process List	15-20
15.5 Reliability Program Plan	15-20
15.6 Quality Program Plan	15-20
15.7 Test Monitoring and Control Plan	15-21
15.8 Program Plan for Soldered Electrical Connections	15-22
15.9 Review of TRW Failure Reporting Procedures	15-22
16. INTEGRATION, TEST, AND LAUNCH	16-1
16.1 Observatory Qualification	16-1
16.2 Pneumatic Leak Test Study	16-3
16.3 Observatory Shock Test Study	16-5
16.4 Thermal Deformation Checks	16-6
16.5 ERTS Payload Study	16-8
16.6 Functions Not Tested in All-Up Spacecraft Testing	16-10
17. GROUND SUPPORT EQUIPMENT	17-1
17.1 Thermal-Vacuum Fixture	17-1
17.2 Observatory Handling Fixture	17-2
17.3 Center of Gravity Fixture	17-3
17.4 Alignment Table Adapter	17-4
17.5 Sensor Installation Equipment	17-4
17.6 ERTS RF Station	17-5

CONTENTS (Continued)

	Page
17.7 Test Control Center	17-6
17.8 Peripheral EGSE	17-6
17.9 Launch Site Signal Monitoring	17-7
APPENDIX A. PAYLOAD INTERFACE SPECIFICATION	A-1
APPENDIX B. DESIGN ANALYSIS REPORT	B-1
APPENDIX C. ERTS-A AND -B PARTS, MATERIALS, AND PROCESSES LISTS	C-1

CONTENTS

	Page
1. OVERALL STUDY RESULTS	1-1
1.1 Introduction	1-1
1.2 Body Orientation	1-3
1.3 Wideband Tape Recorder Installation	1-8
1.4 Uncompensated Momentum	1-11
1.5 Flexibility for Scanning Mirrors and Antennas	1-12

1. OVERALL STUDY RESULTS

1.1 INTRODUCTION

The spacecraft portion of the ERTS study has been aimed at the application of OGO technology to the creation of an ERTS vehicle. In many instances this consisted merely of verifying the applicability of an existing item or technique. In other instances, modifications were required and the study was concerned with finding the form of the modification which was simplest, most reliable, cost effective, and capable of completion on the ERTS schedule. Finally, certain ERTS function had no counterparts on OGO and entirely new equipment was required. The new functions required for ERTS but not for OGO which lead to new or modified equipments are:

- Orbit velocity adjustment; a precisely controlled orbit is required
- Body alignment to orbit velocity vector
- Reduced body rotational rates
- Command execution beyond the line of sight of a ground station
- Accuracy in knowledge of body pointing consistent with an accuracy of 2 nautical miles in locating picture elements
- Payload sensors needing high power and wideband data transmission
- A data collection and relay capability for on-ground measurements
- A redundant unified S-band command, data and tracking system for use with the Manned Space Flight Network

The results of our studies have been most satisfactory. The needs of the ERTS mission can be met largely with existing OGO designs modified for the new functions as follows:

- An addition to the OGO pneumatic system of three heated gas thrusters provides the needed orbit adjustment. Residual krypton gas weighing up to 48 pounds is available to extend the life of the attitude control system after orbit adjustment is complete.

- The existing OGO OPEP gyro system connected as a gyro-compass provides body yaw alignment to the orbit plane. Alterations to the gyro are minor.
- Lower body rates are provided by reducing the on-off hysteresis of the existing OGO reaction wheel control loops. Solid state modules replace the magnetic amplifier bi-stables of OGO.
- A new programmer connected to the existing OGO decoder provides command storage and clocked execution.
- Accuracy in earth pointing is obtained from the existing OGO horizon tracker design incorporating the advanced OGO tracker for its improved CO₂ optics and low instrument errors. Yaw pointing accuracy requirements are met with error read-out of the yaw gyrocompass.
- The physical requirements of the payload are accommodated in the OGO body. Video tape recorders are installed at the +Y outside end of the spacecraft. Power for 20-minute sensor operation is assured by a slightly enlarged OGO solar array on the existing OGO frame. A new video transmission system is required.
- The relatively small airborne weight and power for the new data collection system are readily accommodated.
- S-band duplication of STADAN command, tracking and data functions is provided using equipment already designed and space qualified.

A second study requirement has been the determination of the modifications required to accept detailed characteristics of the payload already being designed to the Nimbus interface. The study has defined six requirements in this objective:

- Negative 24-volt power bus
- Negative analog telemetry voltages
- Command matrix driver, -24 volt pulse
- Coded time clock, 36 bit
- Physical shape
- Location of connectors

All but one of these requirements can be met with relatively simple adaptation of the OGO designs:

- A new -24 volt solid state converter-regulator will supply most loads; a small battery will serve the high current pulse of the RBV.
- A minor change in the analog data handling system, a phase inverter, will allow accepting negative inputs into the positive input OGO system.
- Matrix-drive -24 volt pulses can be obtained with isolating relays
- Physical shape and connector location will be accommodated by installation design.

The 36-bit standard clock format cannot be provided without significant redesign of the OGO data system. On the other hand, a binary clock format is already available in OGO to 1.152-second granularity; and we believe this is adequate for the ERTS mission. Finer granularity than 1.152 seconds is required for picture location determination, and this can readily be generated from existing timing signals. The aspect of the Nimbus standard clock format which is incompatible with the OGO format is the decimal telemetry frame which it implies. Section 2 discusses the problem in detail.

Most of the design choices made during this study have been shown to have no effects beyond the affected subsystem. Three areas, however, have had significant effects throughout the spacecraft, body orientation, the installation of the wideband tape recorder, and uncompensated body momenta.

1.2 BODY ORIENTATION

Thermal control, power supply, and attitude control are affected by the choice of body orientation. In our June 1969 proposal we selected a configuration with the solar array shaft perpendicular to the orbit plane to maximize power. The addition on ERTS-B of a radiative cooler for the multispectral line scanner, however, has caused re-examination of that choice.

The effect of the radiative cooler on the preferred orientation in our Phase B/C proposal was found to be severe. The 4-foot length of the MSS resulted in interference with solar array panels in the folded configuration, since the MSS orientation must be with its long axis

normal to the orbit plane. A configuration which would eliminate the interference was found (Figure 1-1) but it required lowering the array drive to the +Y outboard end of the spacecraft, removing the outer rows of solar modules from the array, and locating the sensor outside the body.

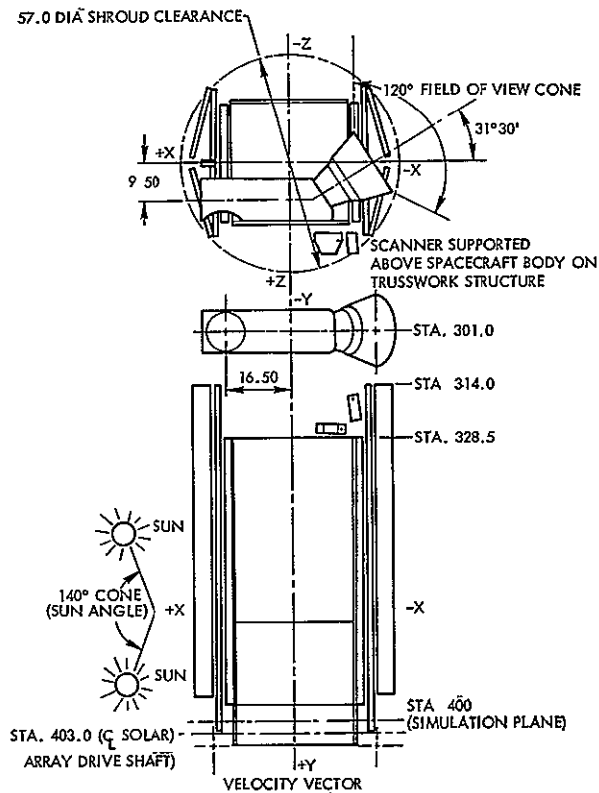


Figure 1-1
ALTERNATE CONFIGURATION
for MSS

The most significant effect of body orientation is in power developed by the solar array. To a first approximation (neglecting body shading) the efficiency of the configuration having its array shaft normal to orbit plane is

$$E = \frac{\cos \Psi}{2\pi \rho} \Delta V_e$$

That for the array shaft in the orbit plane is expressible as an elliptic integral,

$$E = \frac{1}{\pi} \int_0^{\Delta V_e} \sqrt{1 - \sin^2 \psi \sin^2 x} \, dx$$

where Ψ is the angle between sun line and orbit plane normal and V_e is half the fraction of the orbit in sunlight (expressed in radians).

For the two orientations the ranges of sun angle and eclipse duration for one year are shown on Figure 1-2 and the computed values of total array efficiency are shown on Figure 1-3. It is clear that a slip in launch time is detrimental when the array shaft is in the orbit plane; for a 9:30 a. m. node crossing the two cases are nearly equal.

Several other advantages of the configuration with the array shaft in the orbit plane emerged upon closer examination:

- 1) The array drive can be fully deactivated during picture taking with negligible effect on power (less than 1 percent for 20-minute exposure).
- 2) Wrap-ups for array wiring can be retained as on OGO and the need for a new slip ring design (as in the Phase B/C proposal) is avoided.
- 3) Even in drifting orbit (booster failure) the worst case sun condition produces sufficient power for 15 minutes of payload sensor operation (see Figure 1-4). This is not true of the alternate approach where a morning orbit produces low power.
- 4) There is no post-eclipse array turn. Thus, about one minute of array power is gained.

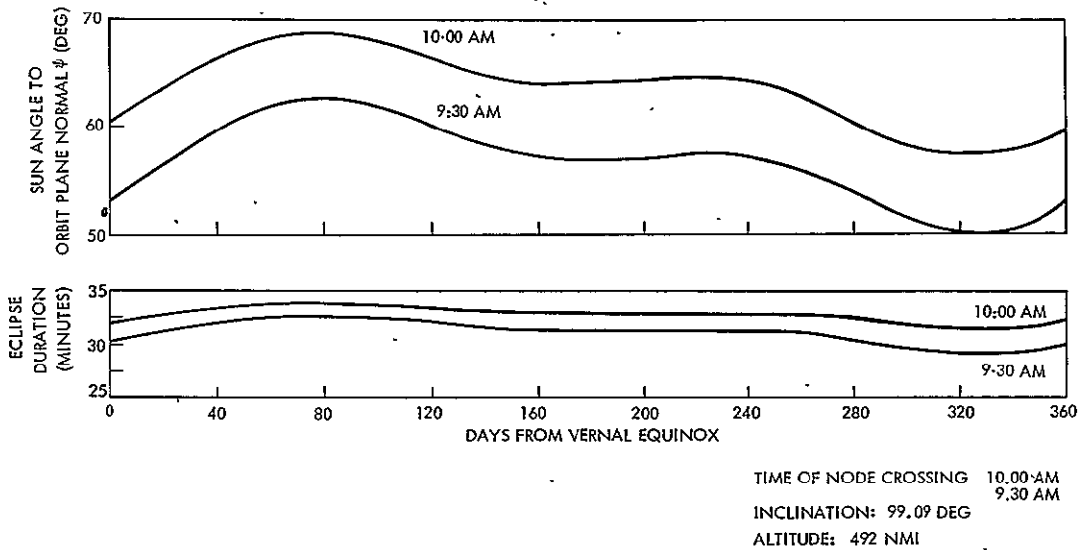


Figure 1-2
ECLIPSE AND SUN ANGLE CONDITIONS vary throughout the year

To summarize: the difficulty of accommodating the line scanner in the structure has led to our decision to rotate the spacecraft by 90 degrees from our configuration in the Phase B/C proposal. The effects of this decision on power are summarized in Figure 1-5. The design point for the array sizing reflected in Figure 1-5 is 20 minutes of payload operation (half real time, half playback in eclipse) under the following conditions:

- 1) Launch in spring of 1972 and 1973
- 2) One-year radiation degradation of array
- 3) Worst day of year eclipse and sun angle conditions
- 4) Sun-earth distance for the same day as (2) above
- 5) One-half hour launch slip
- 6) Body shading based on model tests

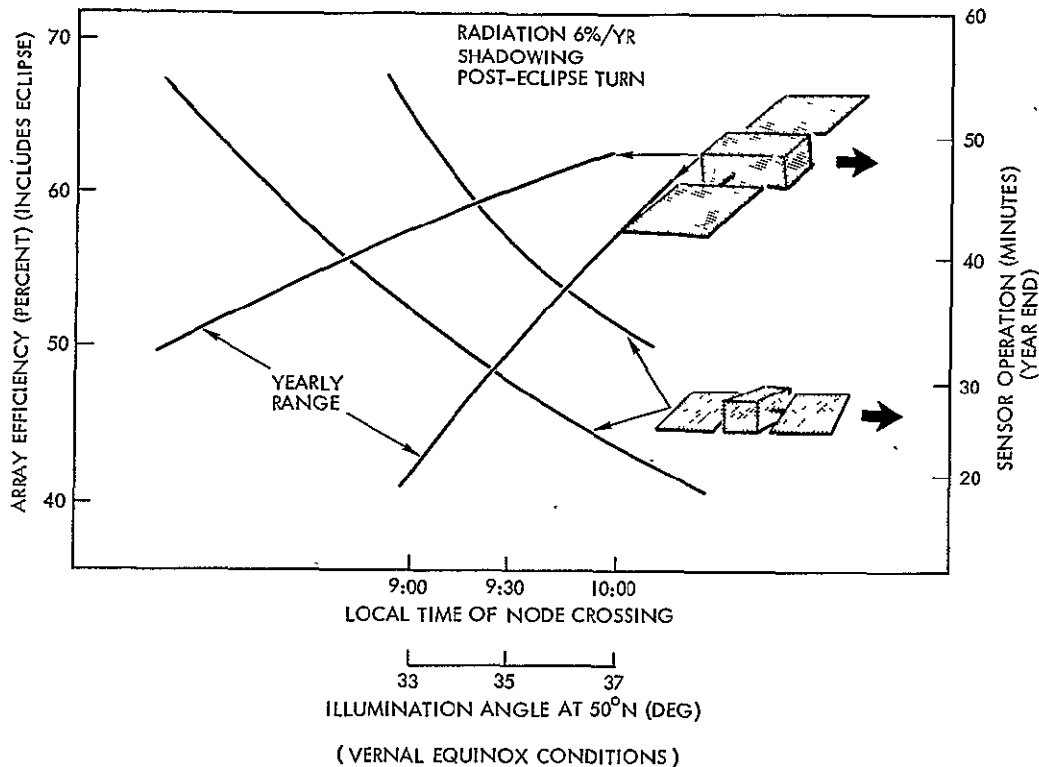


Figure 1-3
POWER SYSTEM PERFORMANCE (worst case)

Design of the solar array is conservative in that power is provided to operate sensors every revolution whereas they may not be operated very often over clouds and oceans. It is further conservative in that a half-hour launch slip is unlikely; Thor-Delta launches have repeatedly demonstrated an ability to stay within a five-minute launch window.

Implementing the revised body attitude has the following effects on other subsystems.

- 1) The yaw gyro must, of course, be rotated 90 degrees.
- 2) Thermal design is somewhat eased since each X panel is exposed to sunlight for a brief time whereas one panel endured a continuous exposure in the previous attitude.

The resultant spacecraft configuration is shown in Figure 1-6.

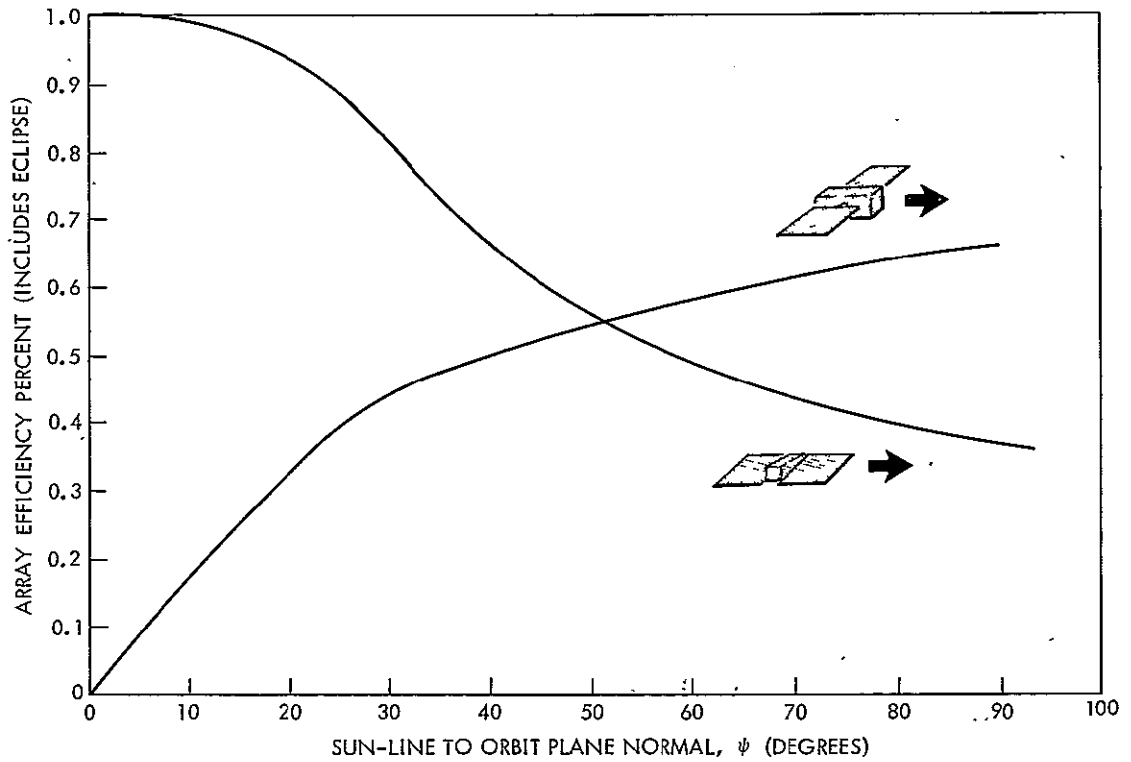


Figure 1-4
ERTS ARRAY OUTPUT as a function of sun line

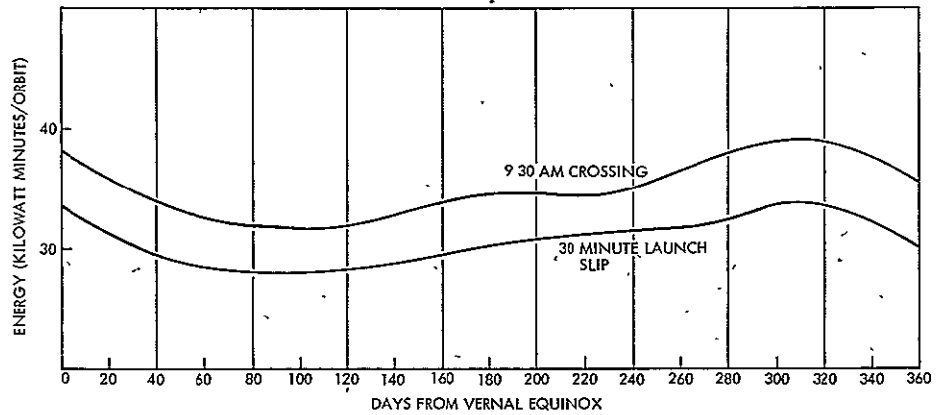


Figure 1-5
ARRAY OUTPUT ENERGY

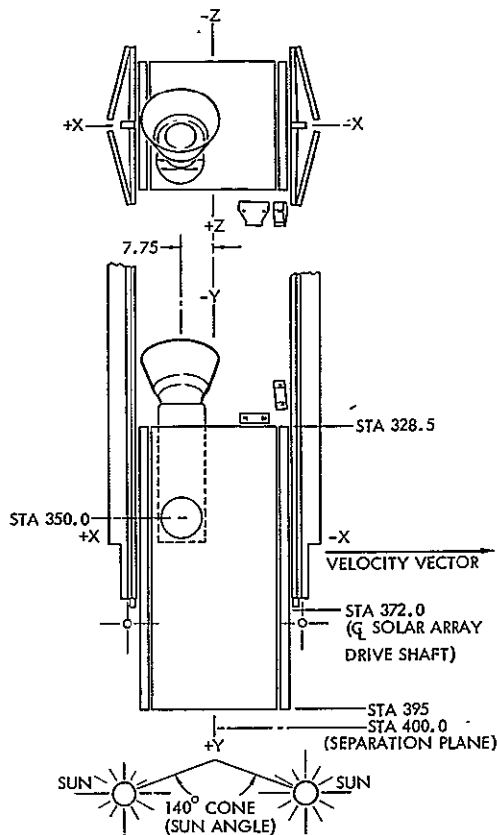


Figure 1-6
SPACECRAFT CONFIGURATION places
sun away from line scanner cooler

1.3 WIDEBAND TAPE RECORDER INSTALLATION

A second study which cuts across several subsystems is the effect of including the wideband tape recorder. The study specification, Paragraph 7.1.4, asks us to study two spacecraft configurations (a) ERTS-A and -B having no provisions for wideband tape recorder installation and (b) ERTS-A and -B both carrying a pair of wideband tape recorders.

The two wideband tape recorders have the following general characteristics:

Weight:	136 pounds
Volume:	4 cubic feet
Power:	166 watts record 152 watts play-back

which clearly place significant requirements on a spacecraft in terms of all three factors. Our approach to the two alternates has been (1) to devise a spacecraft design which will accept the two recorders, but (2) to maximize the simplifications which result if they are not required.

The possibility that wideband video tape recorders may not be a part of ERTS-A and -B has been recognized in the baseline design. These units are housed together in an area at the +Y end of the spacecraft which can be entirely eliminated if desired. Thus, the greatest potential saving in weight and spacecraft complexity is presented. The major savings, if a decision is made at the initial phase of the program, are as follows:

Weight reduction:	160 pounds
Body volume reduction:	10 cubic feet

Array area reduction: 14 percent

However, none of these savings are possible if the decision to eliminate the tape recorders is made late in the program. Ballasted assemblies would be needed for flight to replace tape recorders to avoid the c. g. shift that would degrade the performance of the attitude control thrusters.

Everywhere in this study report, except this section, the discussion presumes a design which includes two tape recorders. In this section, the simplifications allowed by their removal are described.

Structure Impact. The baseline spacecraft carries the two tape recorder assemblies at its outer +Y end. Hence their elimination has relatively minor effects:

- Support structure weight reduces: 23 pounds
- Spacecraft center of gravity moves about 5.1 inch in the -Y direction
- Spacecraft inertia (deployed) is reduced as follows:

I_{xx}	32 percent
I_{yy}	3 percent
I_{zz}	17 percent

As a result of the c. g. shift the X panel orbit adjust thrusters would move correspondingly.

Power System. The two wideband tape recorders require about 3200 watt minutes per orbit from a 28-volt bus for 10 minutes of record and 10 minutes of playback. This is about 12 percent of the solar array capability at its design end point. One row of modules on the two solar paddles theoretically provides 14 percent of the array power. Because of body shading the in-board modules are not fully effective and elimination of the in-board row of modules on each paddle would about balance the reduction of 12 percent in required energy. Array weight would hence be reduced about 13 pounds if the recorders were eliminated.

A secondary effect results from the fact that playback of video data in eclipse would not be required. Depth of battery discharge would

be lessened by about 1 ampere-hour per two batteries. Depth of discharge would then be about 13 percent rather than 2 percent. Depth of discharge is a factor in the seriousness of the effects of battery.

Elimination of the tape recorders could argue for a reduction in the ERTS battery size. There is no inducement for this move, however, since weight is not a problem on ERTS.

Communication. The elimination of the requirement to transmit 1 kbit/sec PCM housekeeping telemetry for the tape recorders via two subcarriers would simplify design of the baseband part of the unified S-band system. Two subcarriers would be eliminated. Modulation power used for the subcarriers could be applied to increasing margins in the 32 kbit/sec playback and 1 kbit/sec real time channels. These two subcarrier links have slightly over 6-db excess margin in the baseline design.

Thermal Control. Were the recorders to be eliminated at the outset, a design and fabrication effort in connection with thermal control elements to accommodate the heat rejected by the tape recorders would be avoided.

Attitude Control. There is no apparent effect on the attitude control system design if wideband tape recorders are deleted. Inertia and center of gravity shifts will be felt but such effects can be accommodated without changing the attitude control design. Control gas consumption will not change appreciably.

Electrical Integration System. The obvious effects here if the tape recorders are eliminated are reduced cabling requirements as the following functions are deleted:

- 18 Commands
- 20 Analog telemetry words
- 28 Bilevel telemetry words
- 4 Power wires

Testing. Depending on the time of decision a considerable amount of test planning and checkout time would be saved by elimination of the tape recorders. The savings can be easily identified in Volume 12.

1.4 UNCOMPENSATED MOMENTUM

The effects of uncompensated momentum on the performance of the spacecraft and on image distortion have been studied, assuming the following observatory inertias:

<u>Axis</u>	<u>Inertia (slug-ft²)</u>
I_{xx}	150
I_{yy}	250
I_{zz}	350

The analysis proceeded on the basis that body motion occurs within the deadband of the control system threshold, and this is found to be justified. Figure 1-7 shows the allowable torque which may be uncompensated as a function of oscillating frequency of application. Ground error of 2000 feet corresponds to 0.04 degree body pointing error, which is well within the gas threshold of the attitude control system. Hence control system operation is unaffected by any condition reflected on Figure 1-7.

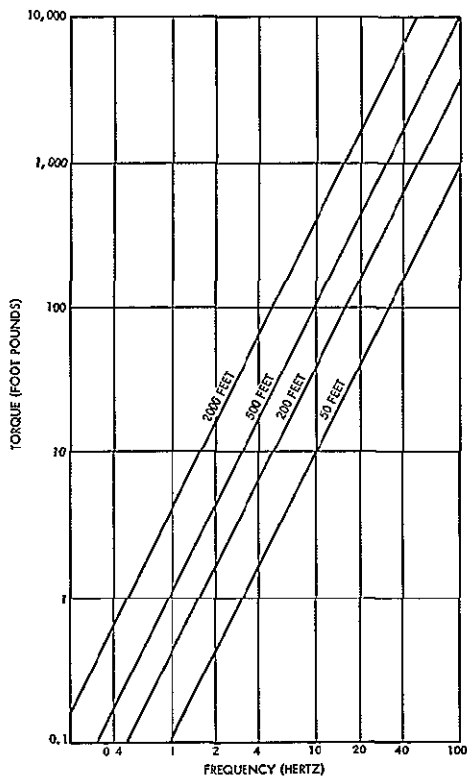


Figure 1-7
PICTURE ERROR caused by pulsating torque on most sensitive axis of ERTS observatory

The effect of steady but unknown momentum is more serious in terms of picture error. For the 27-second duration of an MSS picture the error in relative image element location is as shown on Figure 1-8. If this momentum is known it can be removed in ground processing. For example, the error from a tape recorder may be reduced by noting time of turn-on and turn-off. These errors will be affected by spacecraft inertias and are slightly conservative today.

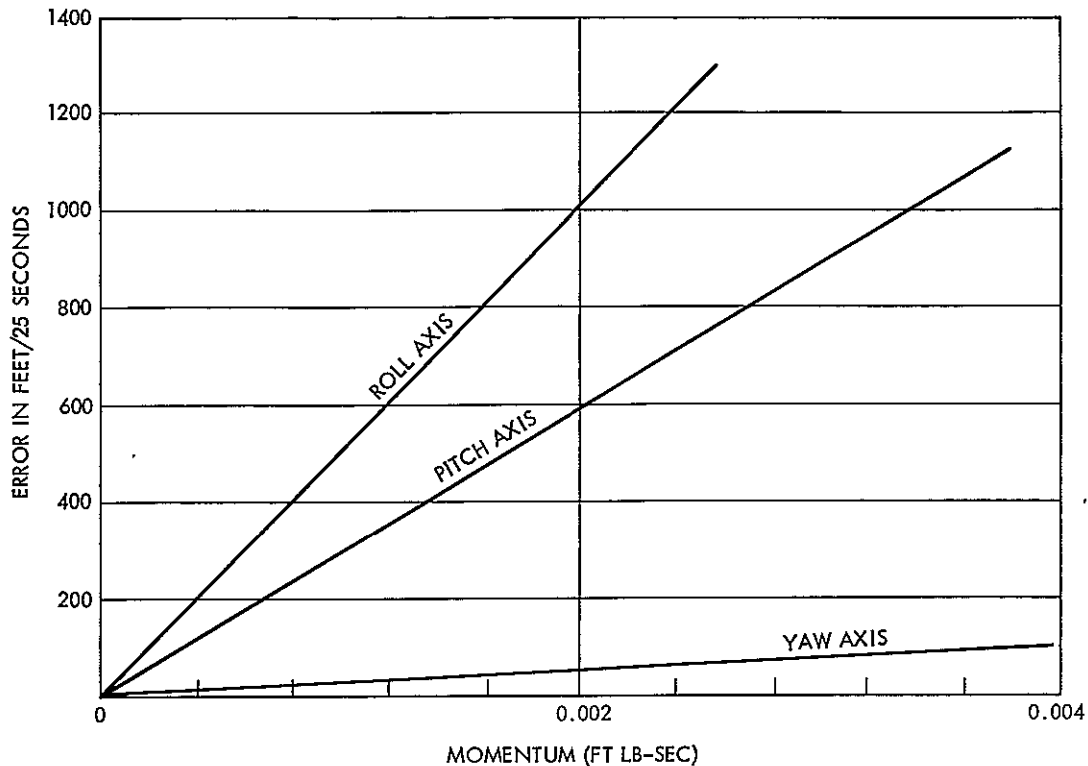


Figure 1-8

RELATIVE MSS PICTURE ELEMENT ERROR as caused by steady uncompensated momentum for 25 seconds

1.5 FLEXIBILITY FOR SCANNING MIRRORS AND ANTENNAS

The Study Specification, Paragraph 7.3 specifies a task aimed at demonstrating "spacecraft flexibility for mounting and deploying large scanning mirrors, foldable antennas, radiative coolers and equipment for communicating with ATS-F and -G." This has been studied and the effect on structure, attitude control, and power system determined. There appears to be no significant effect on communication or thermal system designs. The approach used, lacking numerical definition of the objectives, was to determine the limit of each subsystem in accommodating such structures.

The general problem presented by this task was: To what extent can large structures be stowed for launch, deployed in orbit and then operated without seriously compromising performance of the mission of ERTS? What array shadowing will result, what effect will the deployed structure have on the attitude control system? This study has not

attempted to answer questions of design of the structure to be supported such as: How will a data relay antenna be slewed and fixed on the relay satellite?

The general conclusion of this study is that significantly large and complex structures can be deployed, little effect on electric power is likely but that detailed study of attitude control interactions are required to determine effect on control system performance.

The OGO design on which ERTS is based has a long history demonstrating deployment and successful use of long booms. This history conclusively proves that interaction between oscillating structure and attitude control loops must be understood and accommodated in control loop design. Three separate cases of boom oscillations were first detected in orbit then corrected by redesign.

- OGO 3: first bending mode of 20-foot experiment booms
- OGO 4: thermally generated 60-foot DeHavilland antenna oscillations at 35-second period
- OGO 4, 5: array bending in pitch (Mode 2 condition)

This experience convinces us that detailed design of resilient structure which can couple to the attitude control loops must be well understood and accounted for in the attitude control design. This has been accomplished on OGO with the aid of orbital experience. Figure 1-9 shows a deployed OGO 5 including two 20-foot booms, Yagi antenna and various other deployed appendages. Clearly the OGO design can accommodate complex deployed structures.

It is presumed in this study that the ERTS objective must also be met with the additional deployed appendages, antennas, etc. The most apparent conflict then becomes one of body pointing stability versus picture smear, geometric error, etc. The ERTS picture quality objective—one resolution element—translates into body motion of about 0.004-degree arc in pitch or roll. OGO experience has shown that deployed booms have very low damping—about 0.25 percent. Hence body control forces may be followed for minutes by decaying boom-body transient motion. Note that a torque pulse on the solar array produces

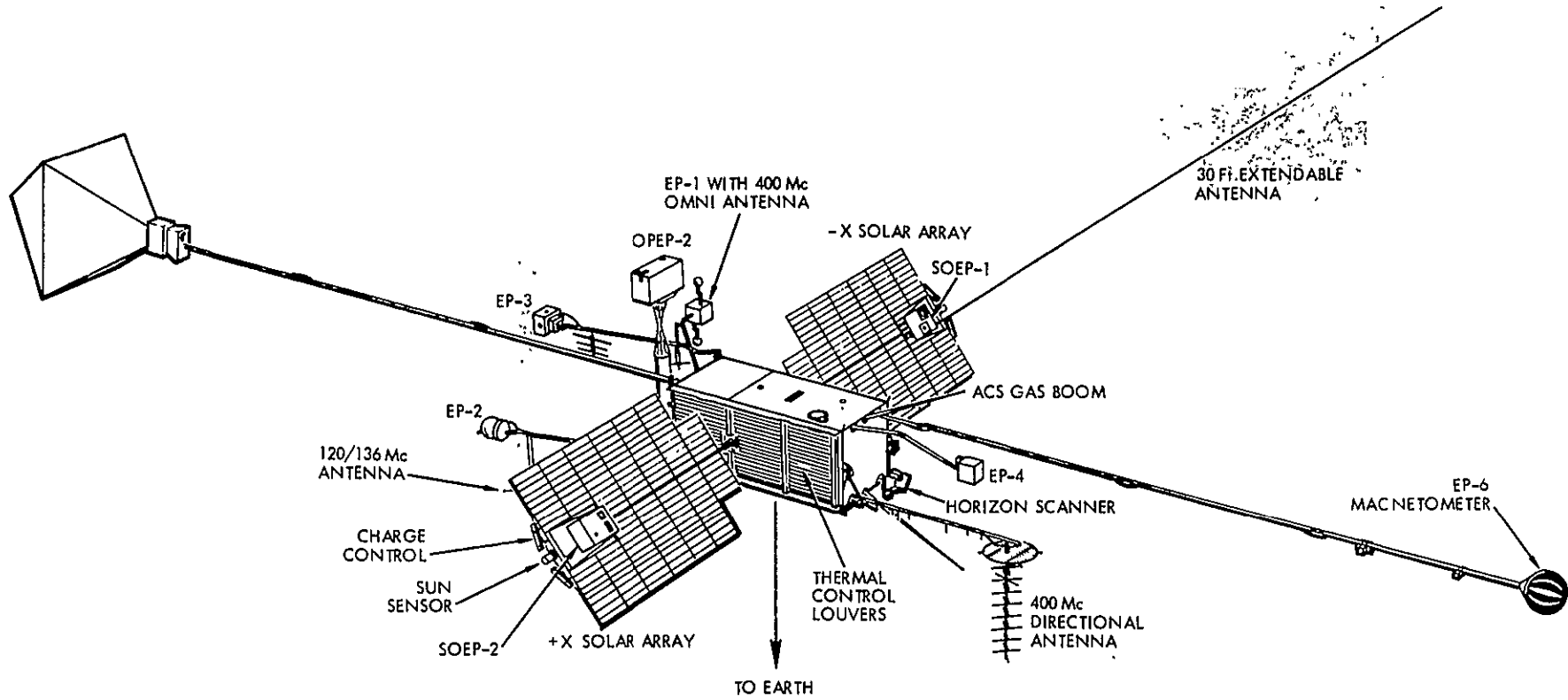


Figure 1-9
DEPLOYED OGO 5

body deflection equivalent to 50 feet on the ground, 50 seconds after the pulse occurs (Section 4).

Our first conclusion is that long, under damped (low frequency) structures are incompatible with the ERTS mission objectives.

Figure 1-10 shows a possible installation of an antenna which would be useful for data relay. Such an antenna would be stowed for launch above the -Y end of the spacecraft and released for deployment just as OGO booms are handled. An example of an unfolding reflector for such an installation is given on Figure 1-11. Array shading produced by the parabolic reflector was estimated with the aid of a model and light source (Figure 1-12). This test showed only 2.5 percent reduction in energy over the full orbit. This result is accounted for by the geometry. With the array shaft in the orbit plane, maximum power is obtained at noon yet the deployed antenna shadow does not fall on the array panels.

A structure such as shown on Figure 1-10 would affect attitude control performance in several respects:

- Center of gravity would shift about 2 inches increasing cross coupling and gas consumption slightly
- Center of pressure for aerodynamic and solar pressures would be offset several feet resulting in significantly higher control gas consumption
- The increased inertias in pitch and roll would be significant but probably would not bar normal control and reacquisition
- Principal axes would be maintained reasonably orthogonal in folded and deployed configuration
- Reaction from antenna tracking motion on the attitude control and determination functions would require special precaution

There appears to be no fundamental reason why the attitude control concept would not function in event a deployed antenna were added. Increased gas consumption due to solar pressures is estimated as 10 pounds of krypton per year for the configuration of Figure 1-10. This is within the excess capability of the storage system shown for ERTS in Volume 3, Section 3.

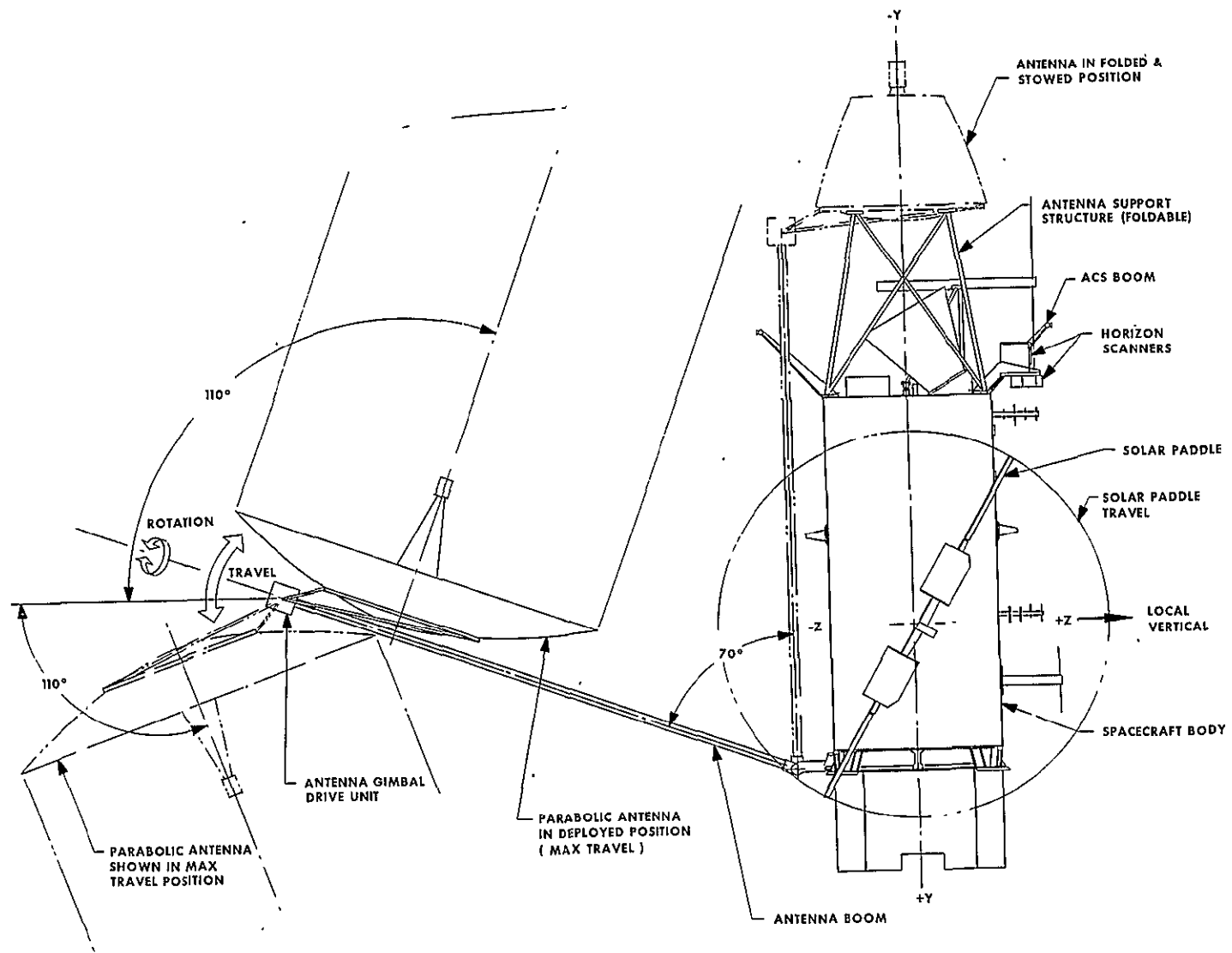


Figure 1-10

THE ABILITY OF THE ERTS DESIGN TO MOUNT ADDITIONAL EQUIPMENT is illustrated by a possible configuration for an antenna to relay data to ATS-F and -G.

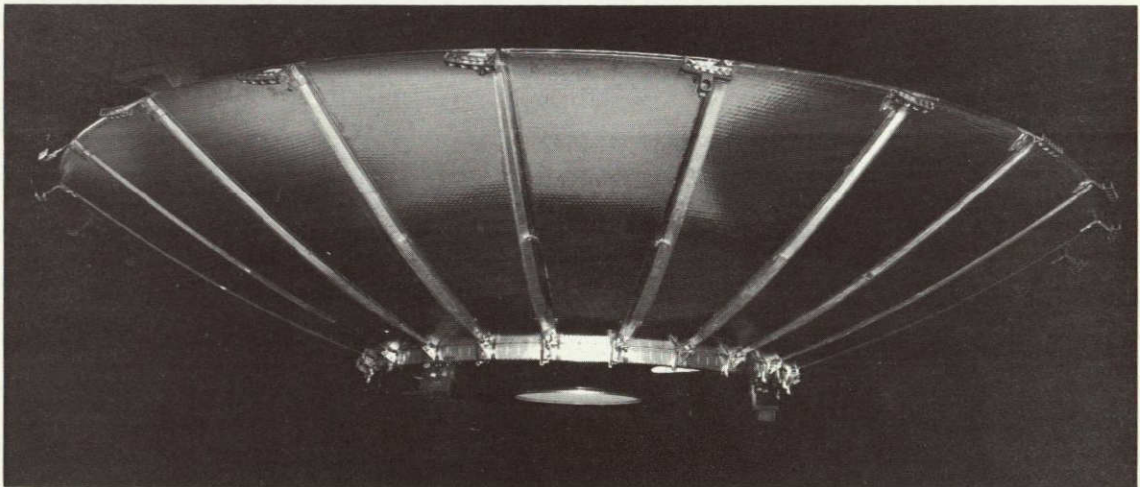
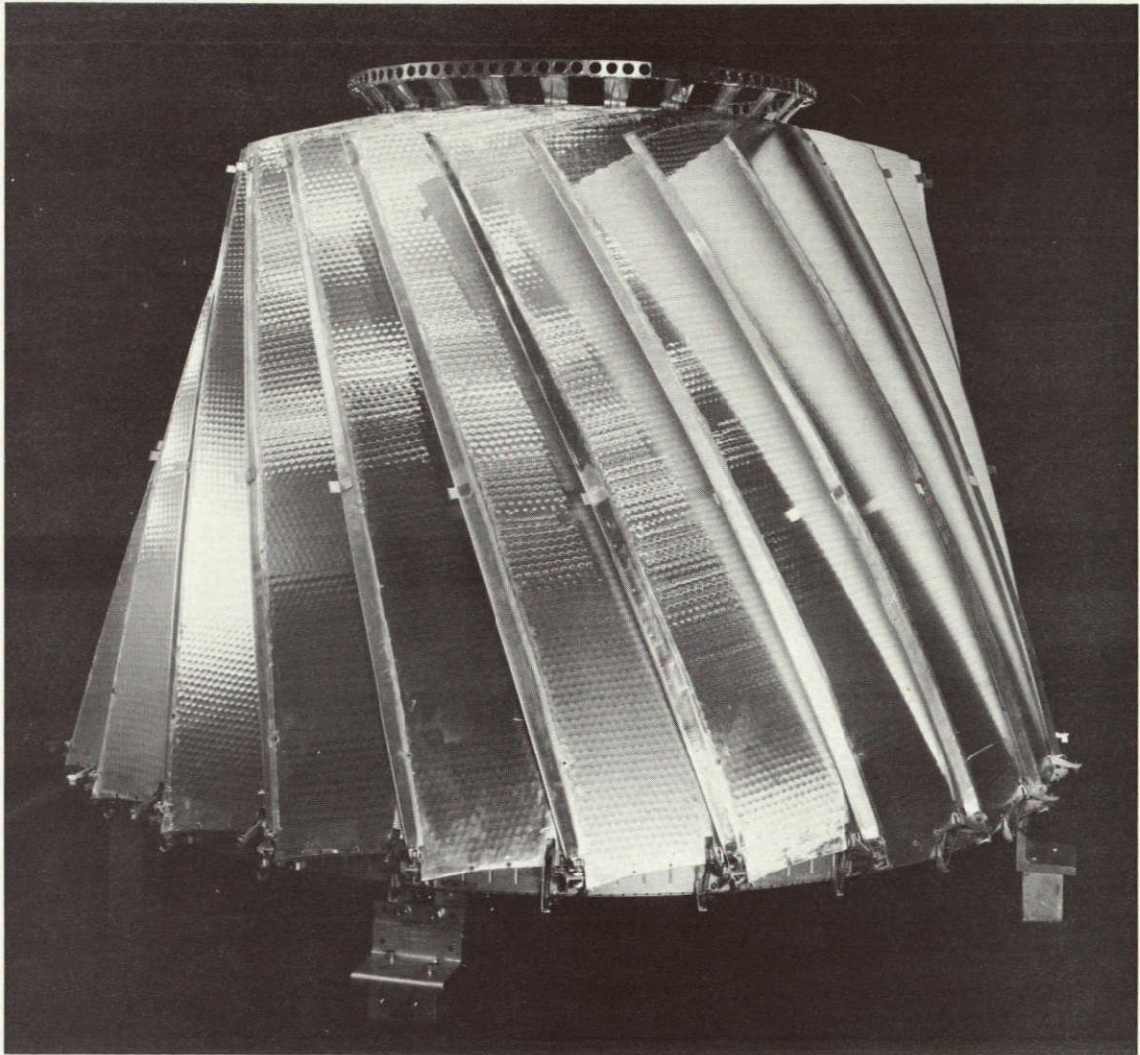


Figure 1-11
UNFOLDING PARABOLIC ANTENNA visualized for data relay application

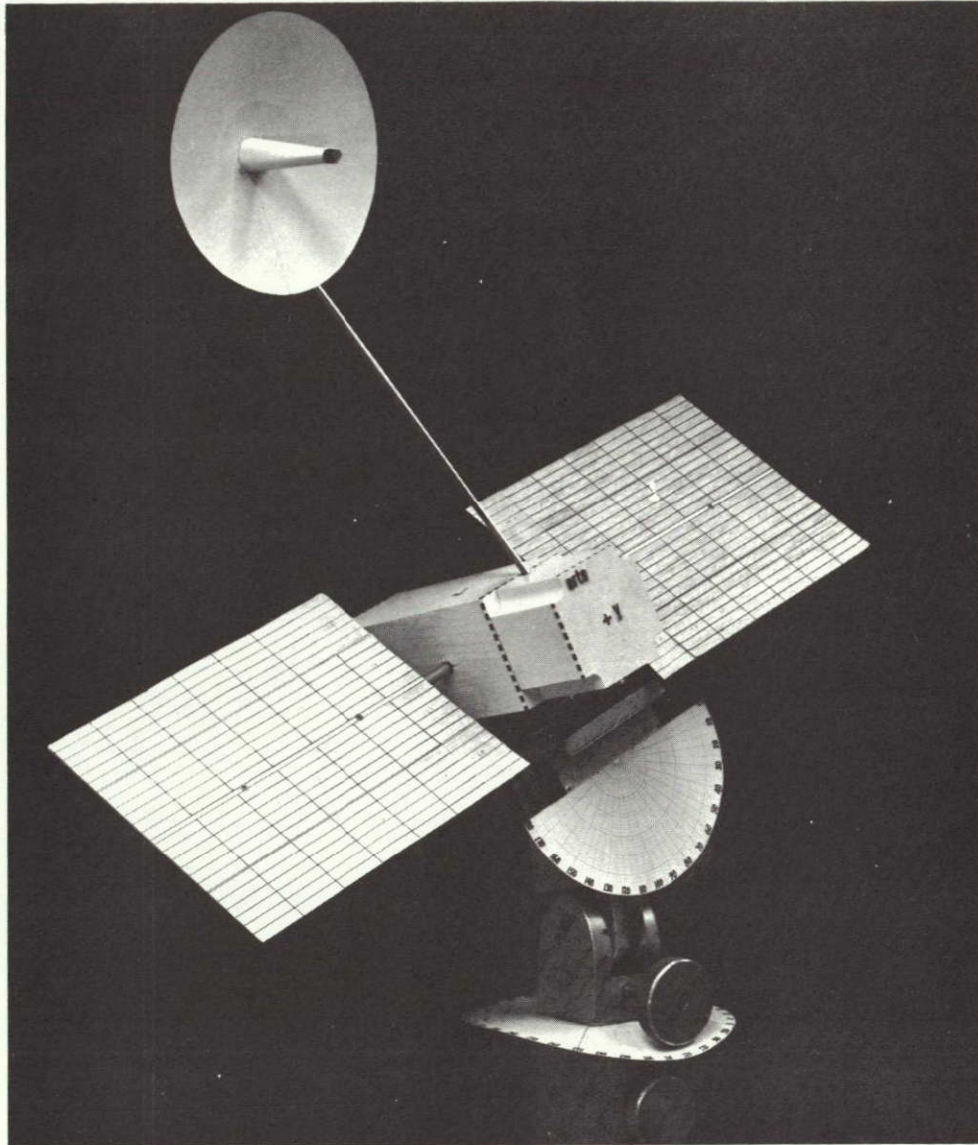


Figure 1-12

SHADOW TEST SETUP shows data relay antenna deployed off ERTS
-Z panel

A detailed analysis of a specific mission proposal would be required to confirm suitability of the spacecraft subsystem designs for the added structure. The most critical item to be examined in this analysis would be the vibration characteristics of the deployed structure and its effect on image geometric accuracy. If the added structure exerts torques on the structure these should be less than figures shown in Section 1. 4.

CONTENTS

	Page
2. SPACECRAFT PAYLOAD COMPATIBILITY	2-1
2.1 Introduction	2-1
2.2 Electrical Power	2-5
2.3 Commands	2-8
2.4 Telemetry	2-10
2.5 Timing Signals	2-12
2.6 Video Tape Recorder Search Channel	2-13
2.7 Fault Protection	2-14
2.8 Mechanical Interface	2-14
2.8.1 Volume and Weight	2-14
2.8.2 Look Angles	2-15
2.8.3 Mounting Provisions	2-17
2.9 Thermal Interfaces	2-19
2.10 Uncompensated Momentum	2-20
2.10.1 Video Tape Recorder	2-20
2.10.2 Return Beam Vidicon	2-21
2.10.3 Multispectral Scanner System	2-21
2.11 Recommended Payload Changes	2-22
2.12 Krypton Effect on Radiative Cooler	2-22

2. SPACECRAFT PAYLOAD COMPATIBILITY

2.1 INTRODUCTION

During the Phase B/C study of the compatibility of the ERTS payload with the spacecraft, three types of activity have been pursued:

- 1) Monitor evolving payload characteristics regarding such factors as weight, volume, view area, power requirements, commands, telemetry words, data bandwidth, unbalanced momentum, deployment. Maintain current specifications for requirements placed on the spacecraft to satisfy the payload.
- 2) Work with GSFC and sensor manufacturers regarding the ease with which payload specifications can be altered from Nimbus-D to OGO. Trade off the effect on the overall program including cost and schedule of setting payload interface specifications to meet OGO or some suitable compromise rather than Nimbus-D.

In keeping with GSFC's desire that the data collection system study be considered in, but separate and distinct from, the spacecraft and ground data handling system reports and proposals, the DCS is considered here only as it pertains to the overall payload characteristics, requirements, and interface specifications. The detailed DCS system description and studies are contained in Volume 5.

A series of formal and informal meetings with GSFC and sensor personnel has been held to discuss payload characteristics and requirements, and all payload documentation received (specifications, reports, studies) has been reviewed. This activity has indicated that payload development is sufficiently simple that in all but four instances Nimbus interface specifications are appropriate. The four exceptions are: serial digital telemetry words, coded-clock signal to indicate RBV shuttering time, polarity of RBV shuttering pulse, and DCS equipment polarity. Rather than literally meeting the Nimbus specification in each of the above areas, TRW has sought the minimum deviation from OGO without requiring payload modifications. Using this approach, a baseline spacecraft/payload interface has been established which not only fulfills all known requirements, but provides growth potential and flexibility as well, since it is recognized that in this state of development changes in the payload interface requirements are to be expected.

In several instances, however, TRW feels that a better overall system results from establishing the specification more nearly like OGO than Nimbus. These and the baseline approach are discussed in the following pages of this section.

In addition to interface requirements, other areas of special consideration relative to the payload have been investigated and described in other sections of this report. Of particular significance are the following:

- MSS Radiative Cooler Protection. In the standard earth acquisition mode, the -Y end of the observatory was oriented toward and normal to the sunline vector until the earth was acquired. Since sunlight impinging on the IR detector can cause permanent damage in a short time, the body axis has been rotated 180 degrees for this maneuver. Thus, if earth reacquisitions are ever performed after the protective cover on the cooler has been deployed, the cooler will face opposite to the sunline and be shaded by the observatory body.
- MSS Handling Fixtures. Due to the weight of the MSS scanner (approximately 100 pounds), special handling fixtures are being designed to facilitate its integration into the spacecraft.
- Krypton Effect on MSS Cooler. A rough analysis indicates no problem will be encountered with krypton condensation.
- Array Torque In Orbit. To preclude possibility of MSS picture distortion, array motion will be inhibited when that sensor is turned on.

The OGO-6 and Nimbus-D interface characteristics are detailed in Table 2-1. Although many of the differences are not relevant to the studies reported here they have been included for completeness and future reference. Primary and significant differences are apparent, especially in the areas of power, command techniques, telemetry, timing signals, and the mechanical installation. These variances have been evaluated in detail, and the proposed means to establish total system compatibility are presented. Other differences, such as the large number and variety of connectors required by Nimbus D as opposed to OGO 6 are not considered significant since the ERTS design has sufficient versatility to easily accommodate such requirements.

Although the payload is being designed basically to the Nimbus-D interface specification, the proposed interface more than satisfies the

Table 2-1. OGO 6 and Nimbus D Payload Interfaces

	OGO 6	Nimbus D
Payload weight, lb	150 in main body (maximum)	300 allotted to experiments
Mounting provisions	24 modules 8 × 8 × 8 in. Maximum experiment size ~26 × 16.5 × 30.5 in. as measured along X, Y, and Z, respectively Mounting surface on outward-looking surface (+Z) of experiment assembly	18 full bays in sensory ring, 6 × 8 × 13 in. Nonmodular size sensors, mounted to cross-beam inside sensory ring and outside (+Z) below sensory ring Mounting surfaces parallel to equator plane of sensory ring. Removable tabs on top and bottom of bay modules at center of each module.
Thermal control	Mounting surfaces are heat sinks. Conductive material (RTV) applied to spacecraft experiment interface (except assemblies requiring precise alignment) Main body temperature 20 ± 15°C Mounting surface coatings: aluminum: Iridite 14, Alodine 1200 magnesium: Dow 23 Other surface coatings: flat black with $\epsilon > 0.72$	Experiments preloaded against outer surface of sensory ring, ring is heat sink. Experiments preloaded to 144 ± 7 ± lb. Interface coated with silicon grease. Sensory ring temperature 25 ± 10°C Surface coatings, magnesium Dow 23, aluminum Alodine 600, steel, electroless nickel 5°C maximum day-night variation, 10°C maximum instantaneous difference
Attitude control system restraints	Not applicable Maximum payload angular momentum: 0.05 ft-lb-sec	Rotating parts aligned to pitch axis (Y - S/A) Maximum payload angular momentum 0.005 ft-lb-sec per experiment
Electrical I/F connectors	Cannon D type, brass case	Standard. Bendix JTN, Cannon D High clock frequency: twin-axial (one/signal) Analog or digital B telemetry. Bendix FTJ
Connector locations	Access required when ±Z doors are open Separate connectors for ordnance	Connectors located on top of module or mounting tab faces (-Z surface) Separate connectors for power, low frequency, each high frequency, commands, analog telemetry, digital B telemetry, timing, HDRSS output and each HV
Power	50 watts average, 80 watts peak plus 10 watts, average heater power Unregulated power: +28 ^{+5.5} _{-4.5} vdc Sync power converters to 2461 5 or 7384.5 Hz Transient tolerance: +50 volt (peak) for 10 msec or less Voltage variation. 0 to 42 volt, over 33.5 volt for 10 minutes Payload noise tolerance: 450 mv p-p 5 to 50 kHz Feedback. 20 mv at all frequencies > 0.01 Hz Supply Z: < 1.5 ohms (0 to 50 kHz); 4.0 ohms thereafter	Nominal 100 watts for payload Regulated power -24.5 ± 0.5 vdc Unregulated power: -26.5 to -37.5 vdc No requirement for sync Transient -18 or -39 volts for 40 msec during regulated switching Voltage variation -20 and -34.5 volt continuous at 35°C 250 mv p-p at all frequencies 25 mv maximum p-p or 10% of steady-state current, whichever is smaller
Timing	Available frequency. 3555.6, 222.22, 13.889, 0.86806, 0.05425, 0.00339 pps Accuracy: 1 part/10 ⁵ /year 1 part/10 ⁶ /hour True: 7 ± 3 volts False: 0 ± 1.5 volts	1, 10, 500 Hz; 2.4, 5, 10, 50 kHz, 0.2, 0.4, 1.6 MHz; 400 Hz (Phase B), 100 Hz (Phase B) Accuracy: (not stated) True. 5.25 ± 0.75 volts (no load) 1.3 ^{+0.3} _{-0.2} volts (600-ohm load) False: 0 2 ^{+0.1} _{-0.15} volts (no load) 1.3 ^{+0.3} _{-0.2} volts (600-ohm load)
Stored commands	None	30 command storage (two memory modules) timing in 2-second increments, 18 hour maximum time to first execution; 9-hour maximum recycle period. Has readout capability.

Table 2-1. OGO 6 and Nimbus D Payload Interfaces (Continued)

OGO 6		Nimbus D								
Nonstored commands	236 commands for experiment use 100 power commands 136 impulse commands Impulse commands: ground command line for 50 to 65 msec through nonlatching relay	512 commands total including spacecraft and stored Duration: 45 msec Matrix A (open circuit) <u>Energized</u> -23.5 ±1 volt Z = 30 ±5 ohms Matrix B (open circuit) -0.5 ±0.0 volt Z = 30 ±5 ohms Maximum load (either) 200 ma								
	Relays: +28 volt, 2 amp resistive 28 volt, 2 amp resistive, 1 amp inductive Four 10-amp rated relays available for high current experiments									
Telemetry										
	<u>Main Commutator</u>	<u>Sub-commutator</u>	<u>Range</u>	<u>Bits/Word</u>	<u>Fault Voltage</u>	<u>Quantity</u>	<u>Range</u>	<u>Bits/Word</u>	<u>Input Z</u>	<u>Output</u>
Analog	68	88	0 to +5.1 V	8	±33.5 V	Analog	576	0 to -6.375 V	8	≤10 megohm -10 kohm
(Serial) Digital	20	16	0 ≤ V ₀ ≤ 1.3 V 5.2 ≤ V ₁ ≤ 9.0 V	9	0 to +33.5 V without Series R or ±33.5 V with 14,000 ohm in series	(Serial) Digital (Bilevel) Digital B	16	0 ±0.8 V = 0 5 ±0.8 V = 1	10	-
							320	0 to -1.0 V = 0 -5 to -10 V = 1	1	-
						Analog and Digital B		Fault voltage: -25 vdc to +0.8 vdc range		≤1 megohm on ≤50 kohm off
Spacecraft clock	25-bit binary coded, 1.152 sec/pulse increments (0.86806 pps)									Standard NASA 36-bit time code (PWM-BCD) (IRIG Document 104-59)

payload requirements. The study has also revealed areas where the payload items have deviated from the Nimbus-D requirements, but which can be readily adapted in the initial system design.

It is suggested that two major differences between the proposed design and the Nimbus-D specifications be allowed to remain: Nimbus 10-bit compressed sampling of serial digital data and inclusion of the NASA standard 36-bit time-coded clock. These are not required or used by the payload and extensive hardware changes are involved in providing them. The standard OGO 9-bit noncompressed serial digital data can be used if ever needed, and the 25-bit binary coded OGO clock provides all required spacecraft time correlation.

A proposed preliminary specification, ERTS-A, and -B payload interfaces, is contained in Appendix A.

2.2 ELECTRICAL POWER

The OGO spacecraft system bus voltage has always been an unregulated +28 volt (+23.5 to +33.5 volts) system. The payload design, except possibly for the data collection system, is based on the Nimbus D regulated -24.5 ± 0.5 volt power supply system.

As presently known, the power requirements of the payload are as follows:

		<u>Watts (at -24.5 volt)</u>	
RBV	Peak	163	163
	Average	155	
	Warm-up	75	
MSS	ERTS-A	65	
	ERTS-B	70	70
VTR	Record (2 x 83) =	166	166
	Playback (2 x 76) =	152	
DCS		<u>1</u>	<u>1</u>
Total maximum			400

All except the MSS are per Reference (1) attachments. The latest MSS data were obtained during the interface meeting at Hughes Aircraft Company on 17 December 1969. Also, per a meeting held at GSFC on 14 January 1970, it is recognized that the RBV power profile may be outdated. It is an RCA action item to provide an updated profile, particularly including the thermoelectric cooler characteristics.

To supply the regulated negative power required by the payload, three payload converters will be provided with two active and the third redundant and switchable as required. Output voltage will have the same characteristics and tolerances as Nimbus D, -24.5 ± 0.5 volt. The design will provide an excess capacity to allow for growth with self-protection incorporated. Pertinent design features of each converter are:

¹ "Design Study Specifications for the Earth Resources Technology Satellite, ERTS-A and ERTS-B, S-701-P-3," April 1969, revised November 1969.

- 300 watts nominal output (at -24.5 volts)
- 450 watts maximum load; above this the converter will automatically turn off until the abnormal load is removed
- Direct short circuit of output will not damage the converter
- Recover normal operation after exposure to abnormal input levels or transients

Since a contractor for the DCS has not yet been selected, no power requirements have been established except that the airborne receiver will require approximately 1 watt. At this stage of development and design, it should be immaterial whether this power is supplied from a negative or positive bus. (The TRW design will specify either polarity, but will be positive if the system is selected for use on TRW ERTS.)

The RBV double-blade focal plane shutters require two high current pulses which activate solenoids in the shutter drive circuitry. Since exposure is simultaneous for all three cameras, each pulse is 18 amperes. The shutter solenoid power can be supplied from a negative unregulated bus, which in the case of Nimbus D is -26.5 to -37.5 volts. As indicated in Section 11.5, the most feasible method of supplying the pulse energy is by a small battery. Battery trickle charging is performed by an AC output from an added winding on the power control unit transformer, with rectification circuitry at the battery.

Discussions with GSFC and reviewing the RCA shutter drive schematic indicate it would not be difficult to change the RBV shutter circuitry to operate from the normal OGO +28 volt unregulated bus. Changing a transistor and several drivers on one board in each camera would be required. By making this change, the following spacecraft advantages and cost savings can be obtained:

- Elimination of -24 volt battery and rectifier
- Overall weight saving of approximately 5 pounds
- Simplification of power control unit and cabling by eliminating extra transformer winding and PCU-battery interconnection
- Reduction of spacecraft internal volume requirements by approximately 90 in.³

In addition to the shutter transient, the Study Specification indicates a 12-ampere supply from the regulated bus is required during initial turn-on. The transient is specified with a rise time of 90 ma/microsec. This 0.133-millisecond spike would be well within the ripple limits of the converter and will not drive it out of regulation or turn-off.

Per discussions with GSFC on 16 January 1970, this turn-on transient has the following characteristics for each of the three cameras:

- 18 amperes at 20 microsec
- 0 ampere at 40 microsec
- 17 amperes at 500 microsec
- 8 amperes at 1.5 millisec
- 4 amperes at 4.5 millisec

Thus, a maximum transient spike of 54 amperes is experienced for the simultaneous turn-on of all three cameras. By first analysis, it appears that the converter output capacitance will easily tolerate such transients, being much higher than the apparent capacitive load.

The video tape recorder headwheel motor starts on a low impedance winding, then automatically switches to high impedance "run" windings when the rotary speed of 18,750 rpm is reached. This requires approximately four seconds, during which a peak initial transient load of approximately 250 watts per recorder decreases to average power (83 watts in record mode). TRW obtained the transient response curve (current vs time) on 9 January 1970, and it is apparent that the video tape recorders should operate from separate converters; likewise for the RBV and MSS. Thus, the high initial turn on transient will at worst drive the converter out of regulation (above 300 watts output) for a few seconds and not trip the overload circuit set at 450 watts. (This assumes an RBV or MSS is on simultaneously. If not, then the converter will not even reach the out-of-regulation limit.)

Alternatives to this problem have been examined:

- Extend Wheel Startup Time. Per discussions with GSFC, this is possible but would result in a sacrifice of torque capability.

- Convert Headwheel and Momentum Compensation Motors to Positive Bus. Although not considered difficult for the video tape recorders to implement, positive bus regulation would be required (+24.5 ± 0.5 volt) during normal running, with out-of-limits voltage allowable during the transitory startup. Thus, either a series regulator, which would create a power loss, or a separate converter would be required.

No MSS transients were known to exist until 21 January 1970. Preliminary data indicates that the inclusion of mirror scanning compensation has induced an approximately 1 ampere spike of 0.015-second duration at twice the scan frequency (30 Hz). This transient is well within the specified loads and should present no problems.

Although not specified as a requirement, separate power for both the MSS uncaging and uncapping pyrotechnics and the radiation cooler outgassing heater can be supplied from existing circuitry identical to that used on OGO. In each case, power is from the unregulated +28 volt bus and commandable through latching relays in the command distribution unit. This provides an additional degree of safety since two commands (one to turn the appropriate bus on in the spacecraft and the other executed by commands now assigned to the MSS) would be required. Thus, a single command could not initiate the nonreversible squib action or turn the heaters on.

For protection from high current loads caused by short-circuited bridge wires after squib firing, current limiting resistors will be included in the power lines. Similarly, solid-state slow-blow fuses will be used in the heater lines. Both of these protective devices have been standard practice on OGO.

2.3 COMMANDS

The ERTS command system provides two types of commands to the payload:

- Power commands supply power through magnetic latching relays in the command distribution unit. In the ON condition, payload buses (-24.5 volt) is provided; OFF provides an open circuit.
- The Nimbus command system uses a matrix driver arrangement whereby two complementary signal lines provide momentary (45 millisecond) pulses to activate relays inside the payload.

When non-energized, the signal levels are reversed from the energized state on the two lines. Steering and suppression diodes are included in the payload to provide the desired command routing. To comply with the Nimbus specification, the OGO impulse command concept will be expanded and modified to provide the required energized (-23.5 + 1 volt) and non-energized (essentially ground) voltage levels for 50 to 65 milliseconds. Also redundant command storage capability is provided.

The total payload command requirements as now understood are as follows:

	<u>Commands</u>
RBV	34
MSS (ERTS-B)	48
VTR 2 x 9 =	18
DCS (TRW design)	<u>4</u>
Total	104

This does not include commands used to perform video switching for maximum redundancy at the interface between the VTR input and RBV and MSS outputs. At this stage of development it has not been possible to define which of the above require execution from storage.

With the exception of the RBV, all payload commands are of the matrix type at the payload interface. For the RBV, four commands are used as power commands implemented with high-current latching relays in the spacecraft payload converters. This applies power to any or all of the three cameras, depending on the previously selected state of the three camera relays, as shown in Figure 2-1.

To provide an adequate growth margin, a total of 160 commands is available for exclusive use by the payload. Of these assigned, 32 may be executed either in real time or by the stored command programmer. An additional 32 commands have been reserved for optional storage or real time use for the spacecraft or payload as required. Stored commands may be executed in increments as short as 0.5 second. The stored load can be verified via the narrowband telemetry system.

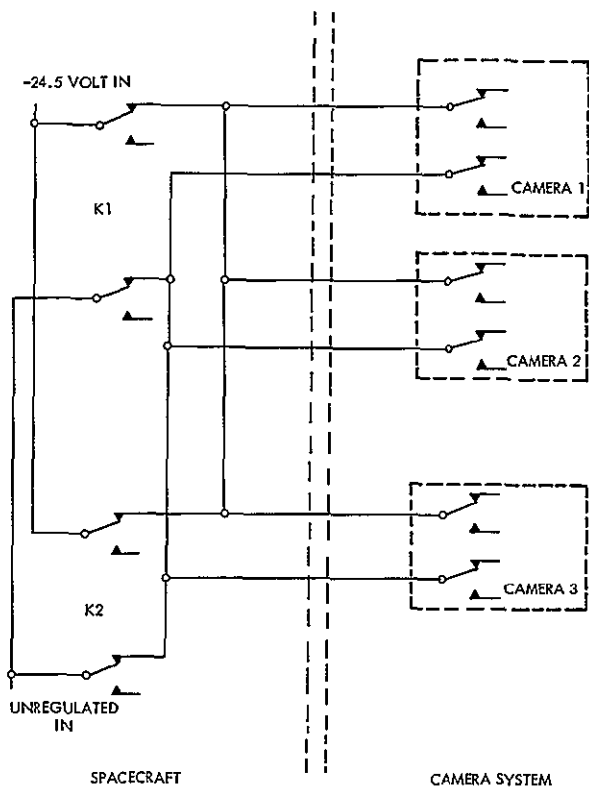


Figure 2-1
RBV POWER WIRING configuration
(simplified)

All available information specifies that command status monitoring is telemetered by each payload item. Therefore, no requirement is assumed to exist for redundant monitoring by the spacecraft.

To preclude the possibility of undervoltage resulting from excessive current drain should a command shut-off fail, individual high-current payload items will be turned off automatically by a timer approximately 24 minutes after turn-on. A commandable override feature is incorporated for use in the event of a timer failure.

2.4 TELEMETRY

On OGO, analog output signals from the payload were positive and vary between 0 and +5.12 volts. On Nimbus D, the outputs lie between 0 and -6.375 volts. Both systems use 8-bit quantization. An inherent difference between the systems is that the maximum output impedance on Nimbus is 10 kohms for 1 percent accuracy, while the OGO is 8 kohms.

To convert the OGO equipment to accommodate the negative outputs, inversion circuitry is added in the analog-to-digital conversion processing described in Section 5, Volume 3. It is our understanding, however, that the analog outputs from the RBV, MSS, and VTR's vary between 0 and -5.0 volts rather than -6.375 volts and to utilize the full quantization range, the inversion circuitry is being designed for these limits instead.

Except for their range, the bilevel (Nimbus Digital B) signals are treated as equivalent to negative analog. These signals are used to

indicate status, such as relay on-off, with an output of -7.5 ± 2.5 volts for the on condition and -0.5 ± 0.5 volt for the off condition.

To conserve telemetry slots, several of these signals are combined into a single analog word. The voltage range of each individual signal is stabilized and four such signals are summed in the payload integration assembly and treated thereafter as a negative analog signal.

Narrowband serial digital data (Nimbus Digital A) is not generated by the payload, but the ability to handle such data in a slightly different format exists in the present system. In OGO equipment, 9-bit serial digital words are shifted out at the bit rate in current use. On Nimbus, 10-bit compressed sampling is used. To convert the OGO equipment to Nimbus specifications would necessitate extensive hardware modifications. Although such changes are quite possible, a better overall system would result from altering the payload to deliver its data at the bit rate rather than by compressed sampling should the need ever arise.

Payload requirements for narrowband telemetry as presently defined are:

	<u>Analog</u>	<u>Bilevel</u>
RBV	17	17
MSS	26	24
VTR (X2)	20	28
DCS (TRW design)	2	-
	<hr/>	<hr/>
Totals	65	69 (69/4 = 18)

Thus, $65 + 18 = 83$ analog word slots are required. These words are assigned to the main commutator, where the sampling rate of 1.152 seconds/sample is sufficient to meet the payload requirements. To permit payload growth 96 main-commutator analog word slots are provided for both payload and spacecraft use.

For wideband telemetry, six video outputs (RBV and MSS real time and RBV and MSS playback data from each VTR), including 15-MHz clock with each MSS output, are routed through a channel switching assembly to the video transmission system. The channel switching assembly

provides cross-strapping to achieve maximum redundancy between the payload video outputs and the S-band transmission system.

The data collection system receiver and the auxiliary channel (1 kbit/sec spacecraft housekeeping telemetry) output of each VTR are applied to redundant unified S-band subcarrier oscillator baseband assemblies for transmission as part of the composite unified S-band signal. No incompatibilities are anticipated.

2.5 TIMING SIGNALS

All necessary timing signals are supplied by adding redundant timers, oscillators, and countdown networks to the existing OGO timing system. Since all spacecraft timing is derived from a basic flight-proven oscillator, accuracy is insured by using countdown logic clocked by a single high frequency source. To minimize interaction and interference, separate buffered outputs are used. Short and long-term stability is 1 part in 10^6 .

The timing signals (coherent square waves) required by the payload are 1 Hz, 50 kHz, and 1.6 MHz for the RBV and 50 kHz for the video tape recorders. Hardware changes are necessitated by these requirements.

The OGO clock consists of 25-bit binary coded time, read out as three consecutive words within the narrowband telemetry format. Clock update, synchronous with the PCM telemetry data, occurs once every 1.152 seconds. The update is known to an accuracy better than one bit period of the PCM data rate. Since the narrowband telemetry output is provided to both video tape recorders simultaneously for recording on the auxiliary channels, coded time is available, along with all spacecraft housekeeping data, with the recorded sensor imagery.

Although not now required by the payload, the following signals are available for optional use on ERTS-A or future missions:

- 2461.5-Hz power converter synchronization signal
- Narrowband telemetry operational signals

Switch. Indicates which of the redundant equipment groups is operating in real time during real time transmissions. At all other times, it indicates which equipment group is handling recorded data.

Mode. Indicates whether the equipment groups are operating in their normal real-time mode or alternate storage mode.

Bit Rate. Indicates the bit rate of the real time telemetry system

- Index pulses. Indicates that a particular serial digital word or words in one equipment group is being read out

2.6 VIDEO TAPE RECORDER SEARCH CHANNEL

A 12-bit recorded binary code is available on longitudinal tracks. The digital readout is intended to allow spacecraft control of the location of data for the selective recording and reproduction of data. The signals are present whenever the tape is moving, forward or rewind at normal or fast speed.

No requirements have been specified for utilization of this channel. Equipment ranging from a simple digital readout via the narrowband telemetry system to a small on-board computer for complete automatic control can be visualized. A more reasonable compromise is a semi-automatic device to run the tape to a commanded position, then stop and perhaps remain in standby, turnoff, or start recording.

To utilize this feature, ground bookkeeping will be necessary to maintain a log of recorded data and available locations for additional recording. However, since tape speeds are known, commanded recordings and playback times are known and logged, spacecraft clock data is available from the auxiliary channel during playbacks, tape speed can be periodically calibrated in orbit, and end-of-tape and beginning-of-tape times are known via narrowband telemetry bilevel monitors, it is believed that tape locations can be adequately controlled and monitored by computer operations in the Operations Control Center. Further details will be provided in that report.

Therefore, no interface with the video tape recorder search channel is planned.

2.7 FAULT PROTECTION

Adequate protection from fault voltages will be provided at all observatory/payload interfaces. New circuitry will incorporate protection in the initial design, while some existing circuits may require minor modifications. Fault protection limits are ± 30 volts. All power lines to the payload are fused with solid-state slow-blow fuses to prevent a single payload failure from shortening the overall mission lifetime. For protection from high-current loads caused by short-circuited bridge wires after squib firings, current limiting resistors are included in series with the ordnance lines. Both of these protective devices have been reliably used as standard practice on OGO.

2.8 MECHANICAL INTERFACE

2.8.1 Volume and Weight

The displacement volume of all the payload components within the spacecraft structure is 11 cubic feet. To this must be added about 20 percent for installation clearances and payload interassembly harnesses. With the addition of the video tape recorder compartment at the +Y end of the structure, the volume available in the spacecraft exceeds the 13 cubic feet demand. Because of the irregular shapes and large sizes of the RBV cameras and MSS, payload assemblies are not confined to the -Y end of the spacecraft structure as were experiments on OGO, but are distributed throughout the main body. All components of one payload assembly, however, are grouped to minimize the distance between sensors or recorders and their associated logic and control electronics.

The following payload assembly weights are based on the latest available information from GSFC and payload subcontractors:

	<u>Weight (lb)</u>	<u>Payload Assembly Total</u>
MSS-A	105.0	114.8 (ERTS-A)
MSS-B	120.0	129.8 (ERTS-B)
MSS multiplexer	9.8	
RBV camera housing (3 ea)	31.2 ea	160.6

	<u>Weight (lb)</u>	<u>Payload Assembly Total</u>
RBV camera electronics (3 ea)	12.0 ea	
Camera controller	7.0	
Video combiner	9.0	
Baseplate	15.0	
VTR 1 transport	-	68.0
VTR 1 electronics	-	
VTR 2 transport	-	68.0
VTR 2 electronics	-	
DCS receiver (2 each)	2.50	5.80
DCS antenna	0.80	
Payload harnesses (estimate)	-	18.0
Payload total: ERTS-A		<u>435.20</u>
ERTS-B		<u>450.20</u>

The payload weight of 450 pounds is easily accommodated by OGO without additional structural support. Upwards of 50 pounds of excess weight capacity is available for potential payload growth.

2.8.2 Look Angles

Fields of view relative to the payload are listed below with their required look angles. The accommodations for each on ERTS are summarized in the following paragraphs.

	<u>Field of View Requirements</u>	<u>Source of Data</u>
RBV cameras (3 ea)	16.25 deg unobstructed FOV representing the diagonal of a 100 x 100 n mi ground scene	GSFC Spec S-731-P-79
MSS mirror	9 in. column \pm 15 deg perpendicular to, and \pm 10 deg parallel to orbit track	GSFC Spec S-701-P-3, Attachment III

	<u>Field of View Requirements</u>	<u>Source of Data</u>
MSS calibration mirror	Included view angle 55 deg in X-Y plane with centerline 52.5 deg from Y-H axis; with lower extremity of FOV 5 deg above X-Y plane, and upper extremity 35 deg below X-Y plane	SBRC drawing 24469, 16 Dec 1969
MSS radiative cooler	118 deg cone with centerline 31 deg off X-Y plane in -Z direction	SBRC drawing 24469

The three RBV cameras projecting through the +Z (earth-looking) panel of the spacecraft have an unobstructed field of view greatly in excess of a 16.25-degree cone. In the baseline configuration, no reflections from light impinging on any part of the satellite during normal orbital operations can be seen by the cameras.

The required field of view for the MSS rocking mirror is easily obtained with the scanner installed at the -Y end of the main body with the aperture in the +Z panel. The entire field of view is unobstructed by any protrusions from the satellite and is free from any reflected light impinging directly on the scan mirror during normal operation, except from the calibration mirror.

The small mirror provided with the MSS as the primary calibration device is supposed to look in a direction where it will see the sun at various times during the year when the satellite is in view of the Ulaska station. The mirror location on the scanner as shown on SBRC drawing 24353, 10 November 1969 and SBRC drawing 24469, 16 December 1969, does not extend through the cutout in the +Z panel of the spacecraft. TRW has arbitrarily extended the mirror support in the +Z (earth-looking) direction several inches so the stated field of view will be unobstructed by the main body of the spacecraft. However, even in the extended configuration, the outboard half of one of the wideband telemetry antennas is within the field of view and the -X solar array sweeps several degrees in and out. Further coordination with GSFC and Hughes will be required to assure a suitable location for the calibration mirror.

The original MSS radiative cooler design for ERTS-B has been incorporated into the baseline configuration. This design incorporates

the cooler radiation cone centerline tilted 31 degrees from the XY plane in the -Z or outer space direction. According to Hughes, this cooler is more efficient than the "universal" concept which utilizes a cooler of smaller proportions with the centerline parallel to the Y-Y or long axis of the MSS. The universal concept is undesirable to TRW since it precludes the mounting of the VHF omni antenna to the -Y panel of the spacecraft and the cooler would be uncomfortably close to a gas-jet boom. In the tilted configuration, the 118-degree conical field of view to cold space is unobstructed by satellite components.

2.8.3 Mounting Provisions

The RBV and MSS with their associated electronics and control units are installed close to one another in the -Y end of the spacecraft main body. Reasons for locating these precision instruments at this end of the structure include nearness to the horizon scanners, which minimizes alignment shifts caused by thermal bending of the spacecraft structure. Also, the -Y end of the spacecraft will never be in sunlight during normal orbital operation. The MSS cooler extends through this panel and radiates toward cold space.

The baseline approach for integration of the RBV cameras into the spacecraft is to shock-mount the cameras to a common baseplate which will be hard mounted at three points to rigid structural longerons at each side of the -X panel within the spacecraft. The baseplate is essential to provide a rigid mounting surface to provide better maintenance of camera-to-camera alignment.

TRW reviewed a mounting technique from RCA which proposed hard mounting the cameras to another baseplate, which in turn would be shock mounted to the rigid baseplate. This was expected to afford better maintenance of camera-to-camera alignment. An analysis of the proposed configuration revealed the system was not as dynamically stable as the baseline configuration and there is not enough room to add in the second baseplate and the associated installation hardware. Camera-to-camera alignment in the baseline configuration is not expected to be a problem if the vibration isolators are carefully designed by RCA.

Installation requirements are met by mounting the cameras in the same orientation on the baseplate with the lens axis pointing earthward. The mounting feet of the cameras are coplanar and at right angles to the orbit plane. Following integration onto the spacecraft, the camera-to-camera alignments will be rechecked and camera-to-spacecraft alignments will be made to within the 0.1-degree tolerance specified.

Center-to-center camera spacing in the baseline configuration is 9.0 inches, which is somewhat lower than the 13.0-inch constraint initially required by the payload contractor to accommodate the single camera collimators used during assembly level testing. The smaller dimension is necessary to keep the cameras within the available payload envelope. RCA has indicated that a smaller, less complex collimator may be specified for spacecraft testing which will still suffice to monitor camera resolution and to detect performance changes.

RBV interassembly cable lengths have been kept short by mounting the camera electronics, controller and video combiner units as close together as practical. Mechanical interface requirements are straightforward and require no special provisions other than the mounting adapter bracket designed to convert from the Nimbus module mounting arrangement to OGO.

Several compromises have been attempted to define an envelope for the MSS which provide adequate volume and remain mechanically compatible with OGO and Nimbus.

Adequate volume within the spacecraft body exists for accommodating the MSS, but incompatibilities exist in the most recent envelope drawing received from Hughes. The latest interface drawing, SBRC drawing 24469, 16 December 1969, indicates significant growth in size of the scanner from the previous MSS interface control drawing, SBRC drawing 24353, 10 November 1969. The changes between the two drawings which affect the spacecraft interface are listed below:

<u>Change</u>	<u>Effect on Spacecraft</u>
Increase in height from 13 to 16 inches	14-inch maximum clearance is available between intercostal extension and +Z panel

<u>Change</u>	<u>Effect on Spacecraft</u>
Move mounting feet from -Z surface to along sides of scanner	No spacecraft attachment points
Increase in width from 11 to 15 inches over entire length of scanner	12.5-inch maximum width at the -Y end of spacecraft body structure. Portions of support longerons would need to be cut away.
Remove the 31-degree tilt of the cooler; cooler centerline along long axis of scanner	Cannot mount VHF omni antenna on -Y end of spacecraft and cooler close to gas jet boom

One of the action items resulting from the 17 December 1969 interface meeting with GSFC and Hughes was for TRW to prepare a space envelope drawing indicating the available space within the spacecraft in which the MSS scanner would fit considering the larger volume requirements. TRW Layout Drawing L121193, which has been transmitted to GSFC and Hughes for review, shows the preferred volume restraint, recommended envelope, preferred mounting surface, and connector location areas. TRW will continue to coordinate this interface in order to accommodate the final MSS configuration within the spacecraft design.

A new compartment was added to the +Y end of the spacecraft structure to accommodate the two video tape recorders and their associated electronics. Within this addition, the transports are mounted on opposing X panels to minimize torques and momentum effects on the spacecraft, and the electronics are attached to the adjacent surfaces. Since the design of the new compartment took into consideration the non-standard Nimbus and OGO mechanical installation interface, no special mounting adaptors are required.

2.9 THERMAL INTERFACES

The thermal control system within the main body structure of the spacecraft is designed to maintain the temperature at $20 \pm 10^{\circ}\text{C}$ during normal operation. The primary method of heat elimination is by means of radiating panels under bimetallic spring-operated louvers located on the \pm X sides of the spacecraft body. The only time the temperature could normally exceed these limits is during initial sun acquisition when

the temperature could drop as low as 5°C. During this period, the payload is not operated.

Based on currently available information relating to payload thermal characteristics, operating temperature limits of the payload assemblies encompass the spacecraft temperature range and no special provisions for heating or cooling are required (see Section 9, Volume 3).

Operating temperature ranges of the flight model payload items based on the latest available information are as follows:

	<u>Operating Temperature Range (°C)</u>	<u>Source of Information</u>
MSS	+10 to +35	S 701-P-3
RBV	0 to +40 Prefer 25	S 701-P-3
VTR	+10 to +40	Nimbus D handbook
DCS (TRW design)	+ 5 to +35	OGO acceptance limits

2.10 UNCOMPENSATED MOMENTUM

Uncompensated momentum in the payload produces internal disturbance torques in the spacecraft which in turn can create errors in the location of RBV and MSS picture components and distortions in the imagery by contributing to the body turning rates.

2.10.1 Video Tape Recorder

To compensate for the average angular momentum in the plane of the tape reels a flywheel with a momentum of 0.1008 ft-lb-sec at the rewind speed (four times record speed) has been incorporated and a second compensator for the video headwheel is being included.* However, per GSFC Specification S-731-P-79, total uncompensated angular momentum "shall not exceed 0.005 ft-lb-sec" per recorder. No indication of

*RCA, Defense Communication System Division, "Second Quarterly Report for Design, Fabrication, Development, and Test of a 0 to 4 MHz Recorder/Reproducer," 1 April 1969 to 1 July 1969, EBC-R043, Contract NAS5-11643.

the present uncompensated momentum is made in Attachment II of GSFC Specification S-701-P-3. As we have learned in discussions with GSFC, some residual momentum will remain after compensation and the original value of 0.005 ft-lb-sec should be included. This number is therefore assumed as applicable for each video tape recorder.

Deletion of the headwheel compensation motor assembly would result in uncompensated momentum of approximately 0.05 ft-lb-sec, a power saving of about 6 watts running and 55 watts startup, and a weight saving of 4 to 5 pounds per recorder.

As may be seen from Section 1.4, the error in picture element location produced by 0.05 ft-lb-sec uncompensated momentum is dependent on the axis in which it occurs.

<u>Axis</u>	<u>MSS Error Per 25 seconds (ft)</u>
Pitch	15,000
Roll	25,000
Yaw	1,250

As installed in the spacecraft this momentum is in yaw—hence the value 0.05 ft-lb-sec is allowable only if accounted for in ground data processing.

2.10.2 Return Beam Vidicon

The shutter blade momentum of 0.025 ft-lb is specified as compensated.

2.10.3 Multispectral Scanner System

Per specification, the uncompensated moment of inertia is less than 1×10^{-3} slug-ft² at 15.2 Hz, the mirror scan rate. Mirror impulses of 0.7 in.-lb-sec occur twice each mirror scan cycle, each opposite in direction. Effects on the spacecraft from either the mirror rotation or the impulses are insignificant. Further, mirror compensation may be incorporated to eliminate jitter at the beginning of scan cycles.*

* Hughes Aircraft Co., Monthly Progress Report No. 2, Multispectral Scanner System for ERTS, November 1969, NASA Contract NAS5-11255.

2.11 RECOMMENDED PAYLOAD CHANGES

The designs of all payload items except the data collection system are in advanced stage, and it is realized that their specifications must be established as early as possible to avoid delays in development. Obviously, from our standpoint, the ultimate in payload changes would be a complete conversion to the OGO interface specification. It is recognized that this is neither possible nor practical for many reasons. For example, changing to a positive bus from the regulated negative bus would cause serious delays in payload deliveries and probably significant additional costs since designs and parts procurements have been based on the negative supply.

Changes which we feel are practical from both a cost and schedule standpoint are as follows:

- 1) Convert RBV shutter pulse to a positive bus. The implications and advantages are described in Section 2.2.
- 2) Require DCS receiver to operate from a positive bus. These advantages and tradeoffs are detailed in Section 2.2.
- 3) Maintain MSS radiative cooler at 31 degrees canting angle as depicted on SBRC Drawing 24353, 10 November 1969. (A reduction to 27 degrees is the minimum that can be tolerated for the present baseline spacecraft configuration.) Also restrict scanner growth to the envelope shown in TRW Drawing L121193, 19 December 1969. See Section 2.8.3.
- 4) If serial digital data is ever required, the OGO interface should be used since it would be a new design item for the payload regardless of which interface specification is used. See Section 2.4.

2.12 KRYPTON EFFECT ON RADIATIVE COOLER

The MSS radiative cooler is designed to maintain a detector element at a temperature of about 90°K. Since krypton is used in attitude control jets near the cooler opening the effect of such gas emissions on the cooler thermal properties must be evaluated. A rough estimate of the significance of this problem indicates that it is not serious in normal operation of the spacecraft.

The mass flow rate of control gas for attitude control is estimated based on two 0.5-second pulses of gas per day:

$$\begin{aligned} \text{Mass flow per pulse} &= \frac{\text{thrust} \times \text{time}}{I_{sp}} \\ &= \frac{0.05}{37} \times 1/2 = 0.00087 \text{ lb/pulse} \end{aligned}$$

These gas pulses are constrained by design to occur when the MSS is not being used but this is disregarded in the analysis. Analysis indicates that the mass of gas which arrives at the cooler opening is believed to be far less than 1 percent of the total expended since jets are directed away from the cooler. Jets used (Figure 2-2) cannot be predicted in advance but all may be used in normal control. Jet number 4 would be most likely to contaminate the cooler. Jet 4 is used in normal control only in conjunction with 1 to correct a pitch error. The mass arriving at the cooler opening is less than 0.01×0.00087 pound or 0.0192 gram $\approx 10^{20}$ krypton atoms.

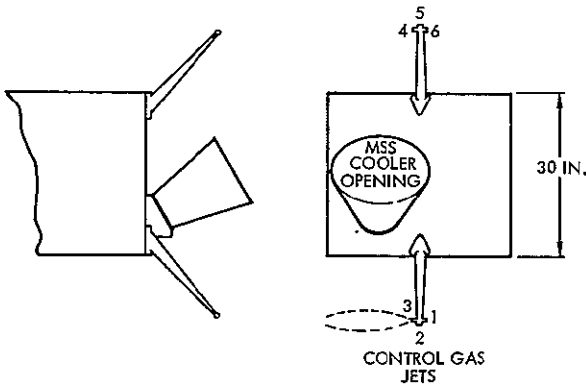


Figure 2-2

GEOMETRICAL RELATION between control gas jets and MSS cooler opening

Given an initial coverage of a few monolayers thickness, a surface will condense an impinging gas vapor at the following rate*

$$\frac{dx}{dt} = \frac{1}{n} \left[\Gamma_{ar} - \frac{P(T)}{\sqrt{2\pi mkT}} \right]$$

where $\frac{dx}{dt}$ is the rate of condensate thickness buildup

n is the density of the condensate

Γ_{ar} is the atom arrival rate incident on the surface

*Hall, D. H., "Evaluation of Electric Propulsion Beam Divergence and Effects on Spacecraft," Final Report, TRW 08965-6013-R000, September 2, 1969.

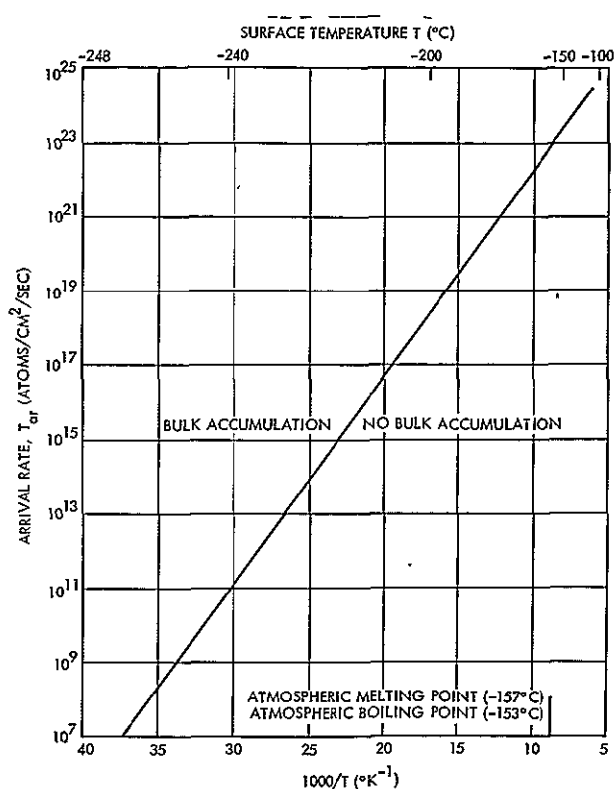
T is the absolute temperature of the surface

m is the molecular weight of the gas

k is the Boltzmann gas constant

P(T) is the vapor pressure* of the incident gas temperature T

Figure 2-3 shows the solution of this equation for krypton with dx/dt set equal to zero. Any combination of surface temperature and arrival rate falling below the $dx/dt = 0$ line on Figure 2-3 will not sustain condensation of more than a few monolayers.



KRYPTON CONDENSATION at a cold surface as a function of temperature and arrival rate

Entering Figure 2-3 with 10^{20} atoms/cm² one sees that mass accumulation occurs at a cold surface if that surface is about -180°C and if all the mass arrives at a square centimeter of surface. After the pulse period of mass flow the gas begins to sublime and leave the cold surface. Since gas pulsing is predicted to be at about 12-hour intervals the time when the cooler could be affected is severely limited.

The conservatism in the above approach is believed substantial. A more exact analysis requires detailed knowledge of the cooler design and is in process at Hughes Aircraft.

* Hanig, R. E., "Vapor Pressure Data for the More Common Elements," RCA Review, Vol 18, pp-194-204, June 1957.

3. SYSTEM LIFETIME

Lifetime studies have been undertaken to identify the limiting factors for life of an ERTS spacecraft and where appropriate recommend changes to reinforce their ability to survive. Broadly, these factors can be grouped as follows:

- Launch survivability
- Orbit maintenance
- Expendable usage
- Mechanical wearout
- Material degradation
- Overheating
- Random electronic failure

The principal cause of failure during boost is the vibration environment. Good design and adequate testing are the means of ensuring boost survivability. Sections 4 and 16 deal with this aspect in detail and together with past orbital experience with OGO, ensure a high likelihood of launch survivability.

Section 3 of Volume 2 deals with attaining and maintaining the desired orbit. Calculations show that an ample supply of krypton gas exists to correct launch insertion errors having far less than a 3σ probability of occurring. That section also indicates that by proper initial biasing, the orbit will remain satisfactory throughout the first year without additional thrusting. To operate beyond one year, however, requires correction of approximately 8 ft/sec (5.1 pounds) per year. Assuming any but the most unlikely launch errors, enough gas will remain after initial orbit adjustment for several years of orbit maintenance. The simplicity of the thrust system discussed in Section 7 ensures that periodically renewed operations over many years can be expected, i. e., there are no elements which degrade with time.

The only expendable aboard ERTS is the supply of krypton gas. Its application to orbit maintenance was discussed in the previous paragraph. It is also used for attitude control. Predicted consumption for the first year for this purpose is as follows:

	<u>Impulse/Year</u> <u>(lb-sec)</u>
Aerodynamic	0
Magnetic	102
Solar	6
Gravity gradient	30
ΔV firing	30
Acquisition (5)	<u>180</u>
Total	348 (9.4 lb krypton)

In subsequent years the weight used per year is only 3.0 lb because no more compensation for velocity correction is required and the need for reacquisitions is quite unlikely. Assuming a 1 σ orbit is attained by the launch vehicle, 8.4 pounds (13 ft/sec) of krypton would be used for initial orbit adjustment. With 3.0 pounds per year required for attitude control after the first year and with 57 pounds of gas carried, it can be seen that approximately 5.5 years of controlled operation can be expected. Even if a 3 σ launch prevails approximately 3.3 years of operation are possible. Table 3-1 shows the predicted life for those elements subjected to wear and/or degradation. Material degradation is primarily associated with the solar modules. Orbital experience of solar cells indicates that a 6 percent per year degradation is appropriate. Thus, the ERTS solar array will provide adequate power capability for three years' operation.

Other surface materials such as thermal reflective and insulation materials have been chosen to provide specification performance for at least three years in orbit.

Table 3-1. Predicted Life for ERTS Elements
Subjected to Wear and/or Degradation

	Predicted Life (years)
Aluminized teflon	>3
Solar array	3
Solar array drive	2
Yaw gyro (2)	4
Pitch gyro	5
Battery	5
Reaction wheels	7
Wrap-ups	3
Narrowband tape recorder (2)	2
Relays, valves, switches	>3
Traveling wave tube	3

The nickel cadmium batteries to be used on ERTS are identical in design to those proven on five orbiting OGO spacecraft. Over five years of experience and 100,000 hours on five spacecraft have demonstrated their failure-free performance. The batteries used on the first OGO launched in 1964 currently display a virtually unchanged capacity from that available on launch.

All mechanical moving parts on ERTS are based on proven design from TRW Systems orbiting spacecraft or are based on conservative design proven by qualification and experimental testing on parameters in excess of those predicted for ERTS application.

In-orbit experience on gyros used on ERTS has demonstrated a life capability in excess of 2.5 gyro years without failure. For the yaw control, redundant gyros are included in the design, thus assuring a high probability of mission success. The pitch rate gyro is required for a few hours during the acquisition phase. Based on experimental test wear data and orbital experience, the pitch rate gyro success probability approaches unity.

The ERTS array drive design is identical to that used on six orbiting OGO spacecraft. Performance over the five-year span has been troublefree, thus proving the design concept and mechanical arrangement.

TRW Systems orbital experience on reaction wheels has demonstrated the ERTS reaction wheel design capability for long-term operation. This experience is further substantiated by seven years of failure-free bench life testing. With 14 years of accumulated orbital experience and seven years of bench testing without failure the ERTS reaction wheel design is assured of mission success.

The wrap-up design used on ERTS is proven by TRW Systems life tests in excess of 20,000 actuations in ground testing and verified by successful in-orbit operation of 12 wrap-up configurations on six TRW Systems spacecraft. These accumulated operating data prove the design will perform the wrap-up operation for ERTS for the one year in orbit without failure.

Performance of the narrowband tape recorders used on ERTS is backed by orbital operation on six spacecraft. Limited life items within the recorders are currently being redesigned to extend the tape recorder life considerably beyond the one year in orbit requirements. Particular emphasis is centered on lubrication improvements. The improvements are based on known accepted design principles. Ground life tests will be conducted to verify the operational life improvement.

TRW Systems orbital and ground experience on limit switches, relays, pneumatic switches and other related items shows that the concept of conservative design backed by detailed specifications, vendor requirements, testing and operational records assures that these items are trouble free. Orbital operation on the Vela, Pioneer, Intelsat, and OGO spacecraft has proven the ERTS use of these items.

Overheating has proved a problem on two previous OGO spacecraft; the first, roll motor drive mag-amps, from failure mode operation outside design limits and the second caused by solar energy trapping through the -Z panel of OGO 5. The combination of spacecraft attitude

and orbit for ERTS make the latter occurrence unlikely. The shakedown given all OGO components during five launches makes the former difficulty improbable.

Electronic parts used on ERTS are not subject to wear-out but are dependent upon the exponential failure law, i. e., the failure rates are constant with time. ERTS electronic parts are controlled by specifications equal to or exceeding those prescribed by the GSFC/NASA Preferred Parts List PPL-10. Similarly, materials used on ERTS are controlled by detailed specifications. Detailed specifications describe the operational requirements to be met and each electronic part is qualified to those requirements. This coupled with operational burn-in and component (assembly) acceptance testing eliminates infant mortality. Conservative circuit design with proven derating for electrical stress and temperature assures the lowest possible exponential failure rate. TRW Systems orbit experience and that of other space vehicle contractors shows that the failure rates for the benign conditions in orbit are considerably less than those predicted prior to launch. For example, the predicted orbital reliability for the OGO, Pioneer, Vela, and other systems has been far exceeded by the demonstrated orbital reliability.

Orbital experience and ground life testing by TRW Systems, other spacecraft contractors, and the manufacturer has proven the conservative design of the ERTS traveling wave tubes. The life of the ERTS design is conservatively estimated at greater than 30,000 hours. This life coupled with the use of redundant traveling wave tubes shows that the predicted life is much greater than the one year in orbit requirement. In addition, the ERTS traveling wave tubes are qualified for Mariner '69 requirements.

Reliability model calculations from Section 15 indicate a 0.85 probability of survival for one year at 65 percent confidence. The previous paragraphs backed up by the flight history of OGO give positive evidence that a much longer time can be anticipated.

CONTENTS

	Page
4. STRUCTURE	4-1
4.1 Equipment Layout	4-1
4.2 Boost Vibration and Acceleration Environment	4-2
4.2.1 Unmodified Components	4-2
4.2.2 Interstage	4-5
4.2.3 Honeycomb Panels	4-7
4.2.4 Intercostal	4-7
4.2.5 Solar Arrays	4-8
4.3 Vibration and Acceleration Testing of Assemblies	4-8
4.4 Observatory Qualification Testing	4-9
4.5 Boost Separation	4-13
4.6 Spacecraft Vibrations in Orbit	4-14
4.7 Payload Thermal Alignment Shift	4-15
4.8 Effect of Array Rotation on Mass Properties	4-17
4.9 Structural Strength Analysis	4-19
4.9.1 Interstage and Separation System	4-19
4.9.2 Main Body Structure	4-20
4.9.3 Solar Paddles	4-22
4.9.4 Antennas, Supports, and Other Appendages	4-22
4.9.5 Thermal Distortion and Mechanical Alignment	4-22

4. STRUCTURE

The OGO structure has been reviewed for any features requiring modifications for application to ERTS. Particular attention has been directed toward equipment layout such that the payload operates in the proper environment and is rigidly interconnected with attitude determination and control sensors. Stress and dynamics analyses have been performed to assure survival in the launch environment and maintenance of alignment tolerances. The impact of inclusion or deletion of the video tape recorders on system design has been reviewed. Finally, the ability to incorporate large scanning mirrors and deployable antennas has been studied. No inherent limitations on the application of the OGO structure to the ERTS mission have been found though several minor modifications will be required.

4.1 EQUIPMENT LAYOUT

Equipment layout has proceeded through several stages, as equipment requirements and specifications evolved. A preliminary mass properties analysis indicated that weight would not be a serious problem and that sufficient layout flexibility existed to minimize potential mass distribution problems. Payload placement became the first pressing problem. The need for an earth viewing area for the MSS and a cool-space looking area for its radiative cooler dictated placement of the MSS at the -Y end of the spacecraft. This was doubly convenient because it provided close structural proximity to the horizon sensors and the yaw reference gyro. Growth in MSS size has presented an access problem but this is solvable by providing a removable end brace in the main structure. The RBV attached to a common base also are mounted in the -Y end of the body.

Placement of wideband video tape recorders off the +Y end of the spacecraft was studied and found feasible. This arrangement facilitates deletion of these units if that occurs. A key requirement to be able to remove and replace units while on-stand was met by use of two hinged panels.

With the major payload items fixed in position the remainder of the black boxes were located with these ground rules:

- S-band assemblies near antennas for low loss in coaxial loads
- Antennas generally separated for minimum pattern distortion
- VHF antenna as clear of body shadow as feasible but not on deployed boom
- Thermal balance, i. e. , equal dissipations on opposing panels
- Principal axes to be along body axes
- Accessibility for connectors and box replacement
- Place boxes used on OGO in same location as on OGO 6 to minimize harness redesign

The layout which resulted is shown in Volume 3, Section 2.

4.2 BOOST VIBRATION AND ACCELERATION ENVIRONMENT

The stated vibration and thrust data for the ERTS spacecraft has been analyzed in its relation to required test levels for black box components based upon designs chosen for interstage, panels, intercostal and solar arrays. A test approach for existing unchanged designs and for new designs has been worked out from this.

In summary it appeared that vibratory responses experienced by OGO components installed in ERTS will be equal to or less than those experienced in OGO. Requalification testing will not be required on existing designs.

4.2.1 Unmodified Components

Unmodified OGO components previously qualified for OGO applications will not have to undergo requalification testing for ERTS. Basically, OGO components are rugged since they have been designed and fabricated in a program which featured:

- Rugged, conservative design criteria (see Figure 4-1)
- Thorough qualification testing at the component level, covering acceleration, shock, sine vibration, and random vibration tests

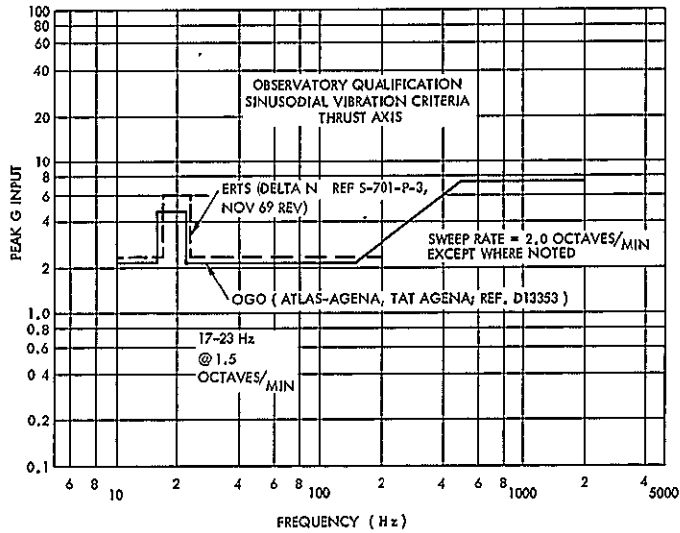
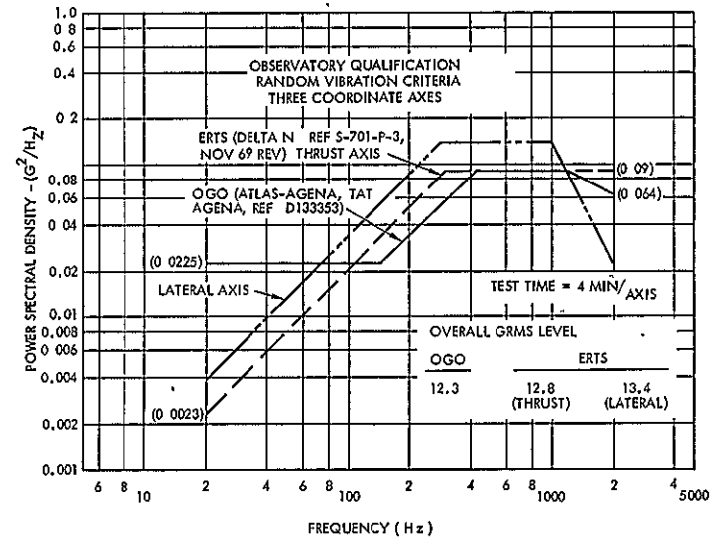
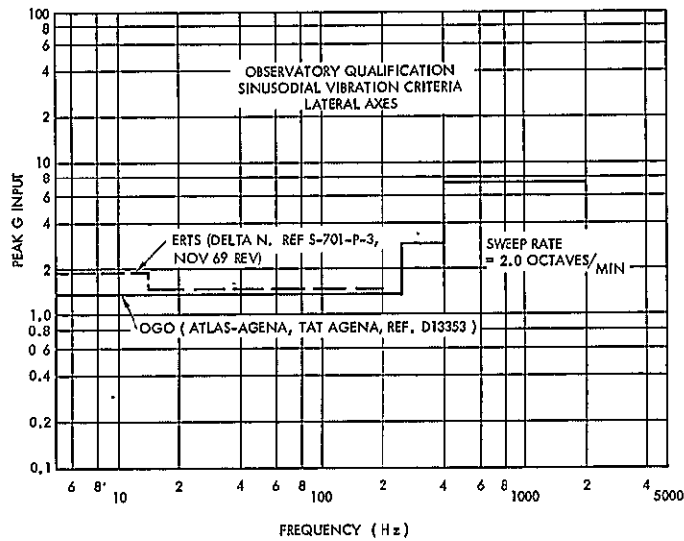


Figure 4-2

OBSERVATORY VIBRATION TEST LEVELS.
Similarity between Thor-Agena and Thor-Delta is marked.



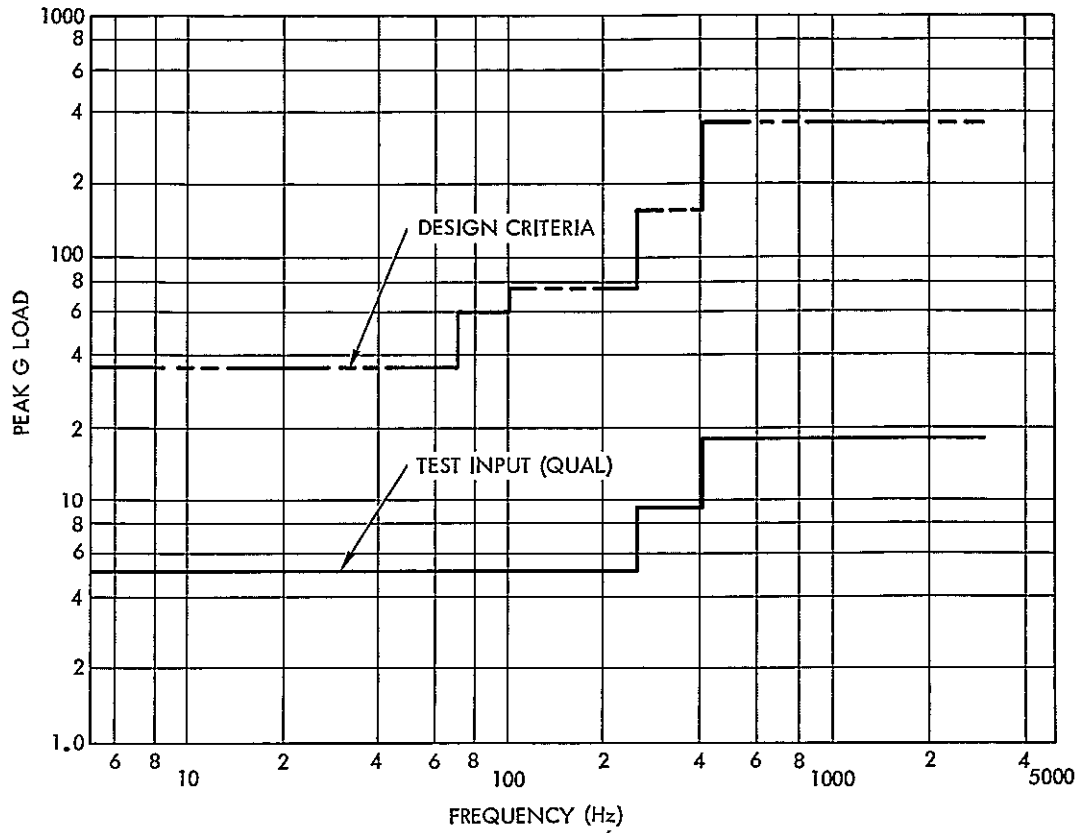


Figure 4-1

DESIGN CRITERIA FOR ELECTRONIC ASSEMBLIES. Allowable stress levels in the design aim at 7 to 20 times the stress of the qualification vibration test.

- Vibration qualification testing at the spacecraft level
- Pyrotechnic shock qualification testing at the spacecraft level

The OGO and ERTS dynamic environments are similar; therefore, it is not proposed to revise OGO component qualification vibration test levels and retest OGO components. As shown in Figure 4-2, the predicted spacecraft vibration spectra are the same for both the Delta N and the OGO boosters; Atlas-Agena and TAT Agena. The OGO hardware has operated satisfactorily throughout six flight exposures and has satisfactorily passed OGO qualification tests.

While the OGO and ERTS environments are the same in magnitude, they are applied at different locations in tests. ERTS vibration is applied

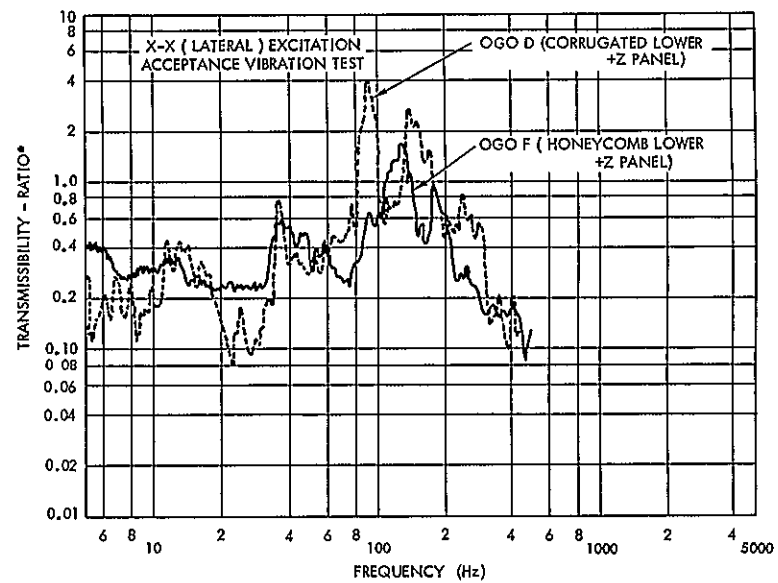
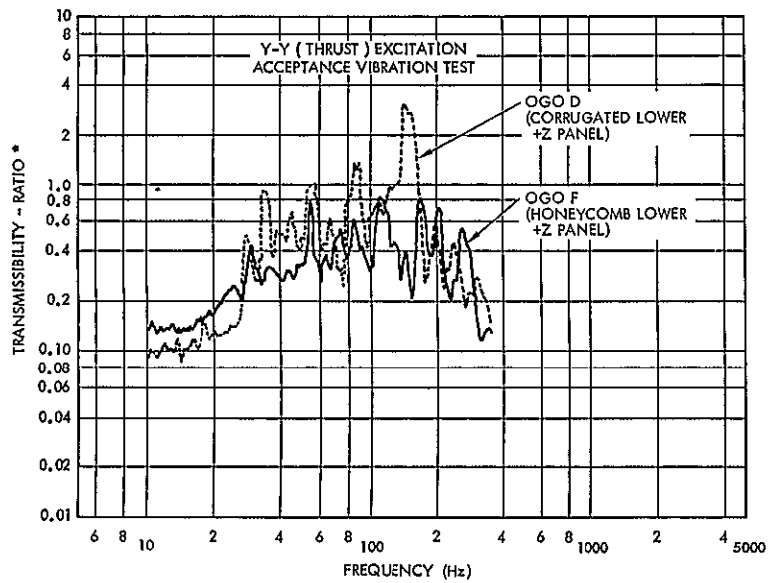
at the lower surface of the interstage, OGO at the upper interface or separation plane. The interstage on ERTS will thus have a tendency to act as a spring, producing resonance amplification at certain frequencies and isolation at the higher frequencies. This could result in higher response levels for some components during spacecraft testing, which could exceed the levels to which the parts have been OGO-qualified. To offset this possibility, the following measures are planned:

- 1) The interstage will be stiffened to avoid amplification in the critical high energy, low frequency spacecraft, and system modes.
- 2) Honeycomb panels similar to those utilized on OGO 6 will be used in place of corrugated core sandwich panels throughout the box structure. Honeycomb panels show a marked increase in damping over corrugated core panels (see Figure 4-3).
- 3) A stiffer intercostal will be used to aid in supporting the relatively heavy interior components in the top of the box and also to provide better stiffening for the -X and +X side panels.
- 4) The vibration energy exhibited by the solar arrays on OGO will be significantly reduced by the removal of the sun-oriented experiment package for ERTS.

By incorporating these design changes into ERTS, it is believed that the component dynamic responses measured throughout ERTS will be similar to those measured in OGO tests. This conclusion will be checked in the dynamic analyses described in the following sections. Further verification will be obtained in the proto-flight qualification program. The similarity in environment makes it unnecessary to re-qualify OGO components due to the change in location of the spacecraft test input.

4.2.2 Interstage

The responses of OGO structure in the lower sectors of the box were strongly influenced in the 25 to 55 Hz band by a coupled mode consisting primarily of pressure bottle and OPEP modes, augmented somewhat by lateral and torsion modes of the spacecraft. OPEP will not be carried by ERTS. By stiffening the interstage, the second lateral spacecraft mode can be raised into the 50 to 60 Hz band; a simple



* BASED ON RESPONSE NORMAL TO PANEL (Z) + BY INPUT RESPONSE
(AVG EXCITATION AT SEPARATION PLANE)

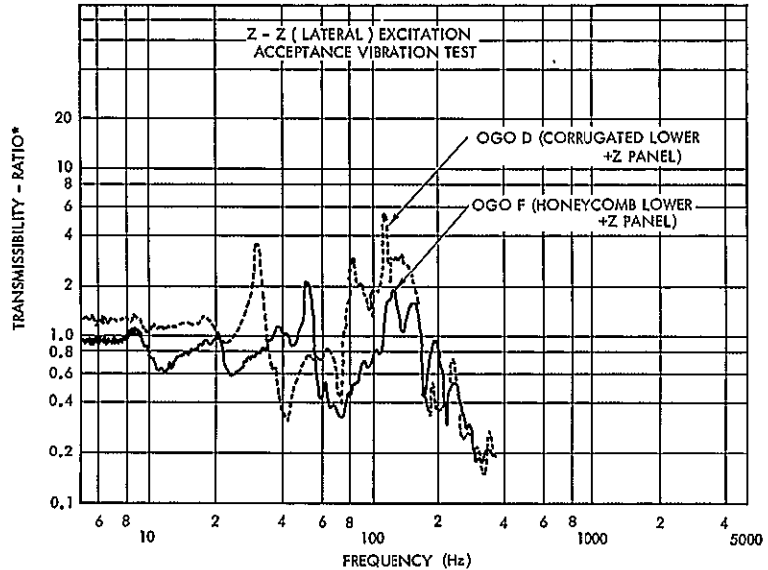


Figure 4-3

VIBRATION TEST TRANSMISSIBILITIES
at lower Z panel. OGO 6 with honey-
comb panels showed lower amplitude.

addition of diagonal stiffeners between bipods raises the second lateral frequency to 52 Hz (see Appendix B). These two changes should reduce the responses in the 25 to 55 Hz band. A detailed dynamic analysis to verify this assumption, considering the addition of new components unique to ERTS, will be performed early in Phase D. The assumption will also be verified in the proto-flight vibration test. From the analyses to date (Appendix B), it does not appear that the higher modes associated with the interstage will be affected by the simple stiffening considered. It is expected that the isolating characteristics of the interstage will be similar to OGO (see Figure 4-4). The onset of interstage isolation occurred in OGO at about 80 Hz. If this occurs in ERTS, the response in the 70 to 150 Hz band will be significantly reduced. This effect will also be checked by the analysis and test of Phase D.

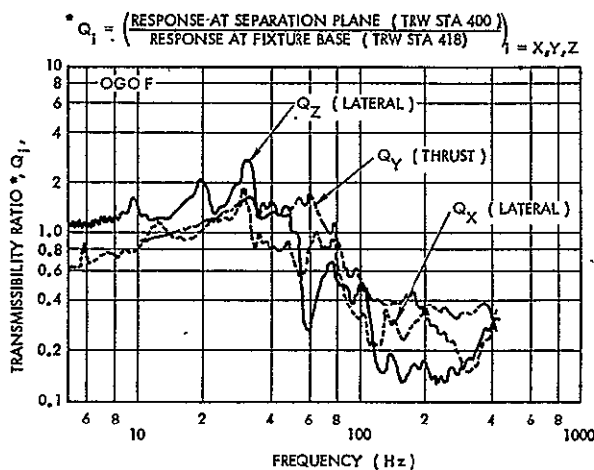


Figure 4-4
VIBRATION TRANSMISSION of the OGO interstage. ERTS interstage will be cross-braced to raise lateral response frequency.

box. All panels are well loaded and panel damping should increase over previous panels used, an especially helpful effect in the 70 to 150 Hz band where component-panel local modes occur.

4.2.4 Intercostal

It is planned to carry the MSS and RBV camera loads via the longerons and intercostal into the box structure. Ideally the intercostal

4.2.3 Honeycomb Panels

The +Z lower panel in OGO 6 differed from those of other OGO's by the fact that it was fabricated from aluminum honeycomb sandwich material. In all OGO's, the +Z lower panel carries two tape recorders (with attendant electronics) only. The reduction in response, across all frequency bands, due to the structural damping inherent in the honeycomb used was significant (see Figure 4-3). ERTS will utilize honeycomb panels throughout the spacecraft

would consist of a stiffened shear beam or panel inserted amidships into the ERTS box, connecting the -X and +X panels. Undoubtedly, cut-outs will be installed in which equipment chasses will be fitted. In each case, the chassis will be capable of carrying intercostal web shear loads. The heavily loaded X panels will thus be stiffened significantly and panel natural frequencies and, to some extent, component-panel local modes will be raised accordingly. Any raising of local mode natural frequencies, together with the increase in damping, should be helpful since modal energy is inversely proportional to the square of the modal frequency, assuming a constant generalized modal mass, a condition approached in many component-panel local mode situations.

4. 2. 5 Solar Arrays

In the frequency band from 6 to 16 Hz, responses induced by the solar array modes are seen at significant levels throughout the OGO. The sun oriented experiment packages, located out of plane, at the extreme cantilevered ends of the folded solar arrays, had a strong effect on solar array response. Current analysis (Appendix B) indicates that the removal of these packages will affect the solar array natural frequencies as follows:

<u>Mode</u>	<u>OGO 5 Modal Frequency (Hz)</u>	<u>ERTS Modal Frequency (Hz)</u>
1	6	8
2	11	21

4. 3 VIBRATION AND ACCELERATION TESTING OF ASSEMBLIES

Based on the above described analysis of spacecraft vibration a test requirement was formulated for components mounted in ERTS. This test includes centrifuge acceleration, shock, random vibration, and sine wave vibration. Table 4-1 shows the tests to be performed in qualifying new black boxes. These tests are identical to levels used in qualifying OGO equipment.

Table 4-1. OGO Component Qualification Dynamic Environments are to be applied to ERTS components (new or modified OGO components) requiring qualification

Environment	Test Axis	Description (OGO Specification D 13351)
Acceleration	Thrust (Y-Y)	Centrifuged acceleration of 13 g (+10%) applied for 3 minutes (-0, +10%) in each direction
	Lateral (X-X and Z-Z)	Centrifuged acceleration of 3 g (+10%) applied for 3 minutes (-0, +10%) in each direction per axis
Shock	Thrust (Y-Y)	A single 45 g, 2.2 millisecc terminal peak sawtooth shock pulse applied in one direction
	Lateral (X-X and Z-Z)	A single 22 g, 4.4 millisecc terminal peak sawtooth shock pulse applied in one direction per axis
Vibration		
a) Sinusoidal	Each of three coordinate axes	One sweep per axis from 5 to 3000 Hz at 1/2 octave/minute. Input from 5 to 15.6 Hz limited to 0.4-inch double amplitude, from 15.6 to 250 Hz at 5.0 g peak, from 250 to 400 Hz at 9.2 g peak and from 400 to 3000 Hz at 18.4 g peak
b) Random	Each of three coordinate axes	Input spectrum from 20 to 1000 Hz at 0.10 g ² /Hz and 12 db/octave roll off from 1000 to 2000 Hz. Time = 12 minutes per axis. Overall g rms level ≥ 11.3 g rms.

4.4 OBSERVATORY QUALIFICATION TESTING

The technical need for proof or qualification tests of a fully assembled spacecraft was studied since a substantial cost is associated with qualification testing. An entire spacecraft must usually be built for the purpose. For this reason the validity of previous OGO qualification level tests was examined in light of ERTS requirements. The most severe environment is vibration associated with longitudinal acceleration. The conclusion reached in the analysis next described is that a test should

be performed on the first flight spacecraft consisting of (1) normal flight acceptance, (2) brief duration qualification level tests.

The study specification defines the Thor Agena vibration environment as shown on Figure 4-2 where sine and random inputs are plotted in comparison with TAT-Agena-OGO test levels. The close similarity in levels is natural in view of the fact that the source of highest levels is the first booster stage and this is Thor for OGO and ERTS. To a close approximation it may be said that the ERTS spacecraft environment will be the same as seen by the most recent OGO launched. It may therefore be inferred that OGO would survive a Thor-Delta launch with a high degree of confidence of success.

The next logical question is how different from OGO is ERTS in ways which would affect its performance in the environment. The answer to this question may be summarized from data presented elsewhere in this report:

- Weight of ERTS is 1430 pounds vs OGO 6 weight of 1394 pounds
- Weight distribution is comparable to OGO (Volume 3, Section 2)
- Added weight is concentrated closest to the booster. Video tape recorders at the +Y end weigh 136 pounds.
- Array weight is reduced by elimination of 20-pound experiment packages and thus array modes are increased in frequency. Interaction with the body will be reduced (Section 4. 2).
- Deployed booms are eliminated
- Cross bracing added to ERTS interstage should reduce lateral responses of the spacecraft in the 25 to 50 Hz band (Section 4. 2)
- Honeycomb panels provide increased damping as evident from Figure 4-3 and Section 4. 2

It was concluded that the proposed observatory structure would have little risk of failure in an ERTS qualification test. In Section 4. 2 this same conclusion was reached with regard to existing electronic assemblies.

For those new parts of the ERTS spacecraft, there is little risk that a properly pretested unit will fail in a spacecraft qualification test. Past experience has shown few instances of electronic assembly failure in spacecraft qualification test. There are two reasons for this:

- Criteria for design of electronic packaging are quite conservative ranging from 7:1 to 20:1 greater than qualification test levels (Figure 4-1).
- Testing at box qualification levels is generally more punishing than spacecraft qualification. The lower level of Figure 4-1 may be compared to spacecraft input levels of Figure 4-2. Generally, the electronic assembly vibration problem is at the higher frequencies and these are attenuated by structural transmission (see Figure 4-4).

The ERTS design proof test concept was evolved from the above stated background and relies upon a brief exposure to qualification levels of vibration for the first flight spacecraft. There would seem to be little risk of failure yet this test would provide assurance of flight success. The approach proposed for the dynamic qualification of ERTS covers the following five points:

- 1) Early in Phase D, a detailed dynamic model of the spacecraft will be generated. This mathematical model will be used to predict gross dynamic responses at various structural locations throughout the spacecraft, and in spacecraft flight loads analyses.
- 2) Also early in the program, a static loads test will be performed on a structural model spacecraft to ERTS design load levels. Pyrotechnic devices used for spacecraft separation and solar array deployment will be fired.
- 3) All modified OGO components and new components unique to ERTS will be subjected to OGO component-level qualification acceleration, shock, sine vibration, and random vibration tests. These tests will be performed as the components become available and as early in the program as possible.
- 4) All OGO components previously qualified for OGO, and used on ERTS in unmodified form, will not be subjected to re-qualification tests as components.
- 5) ERTS-A will be designated a proto-flight spacecraft. All components installed on it will be subjected to OGO/ERTS component acceptance vibration tests prior to installation. The proto-flight spacecraft will then be subjected to ERTS

spacecraft qualification test levels but at flight acceptance durations. Sinusoidal vibration and acoustic tests will be applied separately. Pyrotechnic devices used for spacecraft separation and solar array deployment will be fired.

Both the OGO and ERTS dynamic qualifications emphasize component testing. In the OGO program, this concept was extremely successful. Components so tested passed the all-up spacecraft tests without problems. Though the proto-flight model qualification tests will occur rather late in the program, the OGO successes, the ERTS structural model static tests, and successful qualification vibration testing of components result in a high degree of confidence that any problems encountered with the proto-flight model will be minor. However, prior to applying qualification test levels to the proto-flight spacecraft, at least one sinusoidal vibration evaluation test at low input levels will be run. Responses will be compared with those predicted by analysis as a workmanship check prior to the qualification test runs.

OGO qualification vibration tests consisted of a sine vibration test followed by a random vibration test. As specified in S-320-G-1, the ERTS proto-flight qualification tests will consist of a sine vibration test followed by an acoustic test. The component responses induced by acoustic testing of the spacecraft should be less than those already experienced in random vibration tests of the OGO spacecraft. Flight responses measured during the OGO flight program have never equaled or exceeded those induced in shaker-excited ground tests. Furthermore, all OGO components have been subjected to random vibration qualification tests at the component level. It appears clear, therefore that unmodified OGO components used in ERTS will pass the ERTS proto-flight acoustic test without failure, malfunction, or out-of-tolerance performance, and that requalification at the component level due to the addition of an acoustic test in the spacecraft qualification program is not necessary.

The use of sine and acoustic vibration environments (applied separately) to simulate boost loadings is a much more realistic approach to the simulation of the boost environment than the sine and random vibration environments applied to OGO.

During boost, the spacecraft will experience oscillatory loadings which are transmitted across the booster-spacecraft interface. In addition, oscillatory loadings will result from the direct impingement of acoustic noise upon spacecraft components and supporting structure.

The sine test provides a good simulation of the interface loadings. These result from the excitation of booster modes by engine operation, acoustic noise, guidance maneuvers, or Pogo effects, all of which appear as narrowband random or sinusoidal responses at the booster-spacecraft interface.

The acoustic test realistically excites spacecraft component and structural modes via nearly the same load paths as in flight.

4.5 BOOST SEPARATION

Separation velocity and tipoff characteristics are within acceptable limits. Analysis of the current ERTS observatory configuration with the OGO spring separation system clearly indicates acceptable performance. A minimum relative separation velocity of 4.2 ft/sec is calculated as compared to the previous OGO specification value of 4.5 ± 0.5 ft/sec.

For the folded ERTS configuration, worst-case separation tipoff rates are calculated as

0.68 deg/sec roll	(about ERTS X-X axis)
0.99 deg/sec yaw	(about ERTS Z-Z axis)
0.32 deg/sec pitch	(about ERTS Y-Y axis)

Transcribed to the deployed ERTS configuration, these residual tipoff rates are

0.96 deg/sec roll	(about ERTS X-X axis)
0.77 deg/sec yaw	(about ERTS Z-Z axis)
0.08 deg/sec pitch	(about ERTS Y-Y axis)

These values are within the previous OGO specification value of 1 deg/sec about each control axis.

ERTS is different from OGO in that the moment of inertia ratio (folded configuration value to deployed configuration value) for the X-X

axis becomes greater than 1.0 (approximately 1.4). Applying conservation of angular momentum, this infers a 40 percent (approximately) increase in roll tipoff rate for the deployed configuration over that existing for the folded configuration. Primarily because of its boom-mounted experiments, the OGO moment of inertia ratios (again, folded configuration to deployed configuration) were significantly less than one for all control axes. Typically, they ranged from 0.2 to 0.4. Even so, the ERTS tipoff rates (deployed configuration) can readily be maintained, if required, to within the ± 1 deg/sec limits by making use of procedures and techniques developed for OGO. These involve:

- Use of two left-hand wound separation springs diametrically opposite each other and two right-hand wound springs for the other two locations
- Precise matching, as a set, four separation springs and marking the direction of spring force inclination, per spring
- Precise alignment of the separation springs and spring cups in the separation subsystem installation and shimming of springs or cups where necessary. Direction of force inclination mark on each spring orientated as a set either all radially in towards the center or all radially out from the center

4.6 SPACECRAFT VIBRATIONS IN ORBIT

Because of the sensitivity of ERTS optical sensors to small body pointing errors an investigation was conducted into in-orbit vibration sources and resultant pointing errors. Excitation of the solar array by reaction wheel unbalance, reaction wheel control torques, tape recorder switching and its own drive motor was investigated in a simplified manner.

The numerical results are summarized in Table 4-2. The magnitude of jitter and jitter rate resulting from reaction wheel unbalance, control torques and tape recorder switching do not appear to be large enough to blur the camera image. This is based on the worst case angle of 0.57 arc second which will produce an image movement of 7.2 feet on the earth's surface, assuming the spacecraft altitude to be 500 miles. The allowable image movement is about 50 feet.

The time required for decay of torsional vibration initiated by solar panel positioning was briefly checked. If a typical array step motion is 0.2 degree and the resultant body reaction 0.01 degree

Table 4-2. Predicted Jitter Amplitude and Rate Responses indicates that the values are sufficiently low

Jitter Source	Solar Panel Response Mode			
	Flexure		Torsion	
	Amplitude (arc sec)	Rate Response (arc sec/sec)	Amplitude (arc sec)	Rate Response (arc sec/sec)
Reaction wheels				
Static imbalance	0.25	4.28	0.02	0.32
Dynamic imbalance	0.10	1.71	0.008	0.13
Control torques	0.288	4.60	0.02	0.36
Tape recorder switching	0.57	9.80	0.04	0.72

(from inertia ratios) the initial picture error in the roll axis will be 500 feet. This will reduce to 10 percent or 50 feet in 55 seconds (see Figure 4-5).

4.7 PAYLOAD THERMAL ALIGNMENT SHIFT

The objectives for imaging payload installation include alignment stability consistent with the picture element position accuracy objectives. These objectives are of two orders (1) long term drift should be small compared to the two-mile absolute requirements, and (2) short term drift should be small compared to the resolution element accuracy objective over about 25 seconds. With time constants of many minutes the latter requirement is assured if the first is met. Reduced to numbers these objectives are

- 1) Alignment drift in pitch and roll less than 0.05 degree over all orbits
- 2) Alignment drift in pitch and roll less than 0.004 degree over any 25 seconds

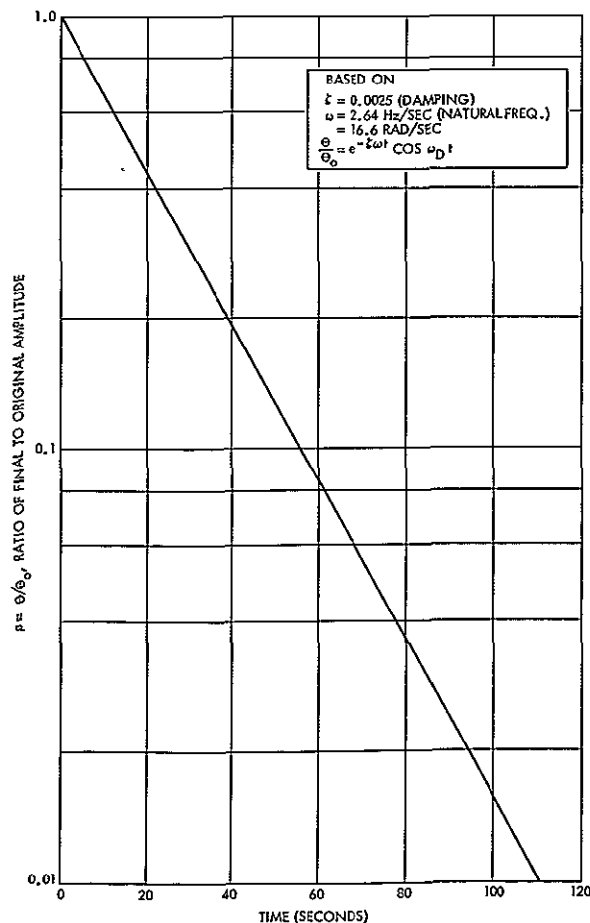
These requirements apply to the mounting of RBV and MSS with respect to the body coordinates measured at the horizon tracker bracket.

Several designs were analyzed for thermal deformation. First was direct mounting of RBV cameras on the side honeycomb panel.

A 2°F temperature differential across the two faces of this panel produced 0.02 degree sensor misalignment. The 2°F temperature differential was believed realistic for hot to cold sensor operation and type of honeycomb to be used. A second design utilized a second 0.5-inch thick honeycomb mounted inside and apart from the X radiating panel (Figure 4-6). This design is baseline and is described in Volume 3, Section 2. The temperature differential estimated for such a design was 0.5°F and total alignment shift, hot to cold was 0.0028 degree arc.

The thermal distortion in the body due to a 10°F temperature differential between opposing Z panels was found to be 0.0074 degree arc. This is negligibly small and represents the largest in-orbit thermal distortion in the spacecraft structure which can affect the alignment of sensors to spacecraft.

These analyses are included as part of Appendix B.



4.8 EFFECT OF ARRAY ROTATION ON MASS PROPERTIES

In the ERTS orbit the solar array will rock back and forth around the 0-degree (+Y looking) position by about 60 degrees (Figure 4-7). This action has negligible effect on center of gravity, a minor effect on inertias and products of inertia. Yaw principal axes shift by about 2.7 degrees maximum. Table 4-3 shows the data produced by the mass properties computer program.

Figure 4-5
DECAY OF BODY OSCILLATION after solar array motion

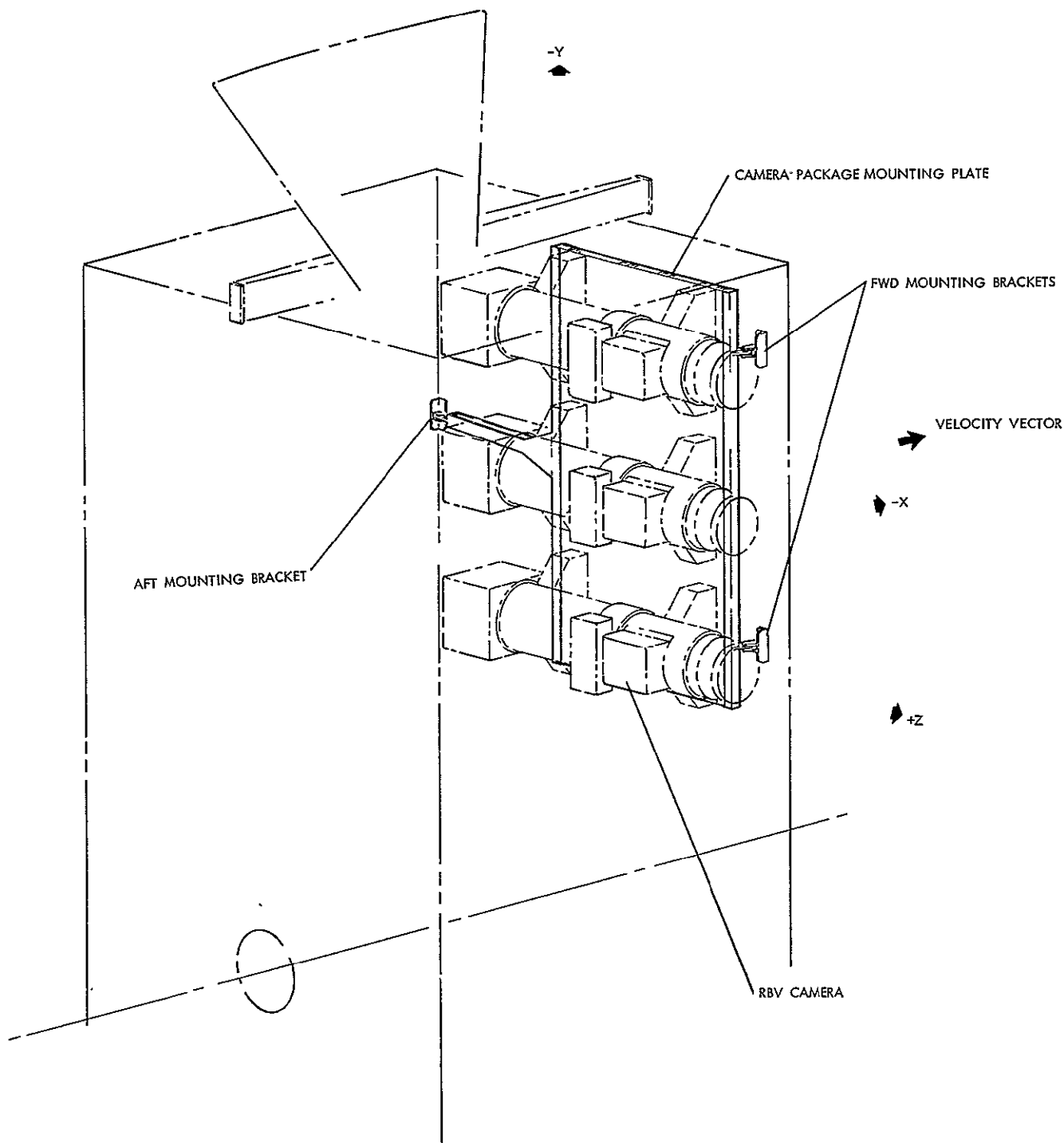


Figure 4-6
 RBV INSTALLATION on honeycomb panel minimizes thermal deformation.

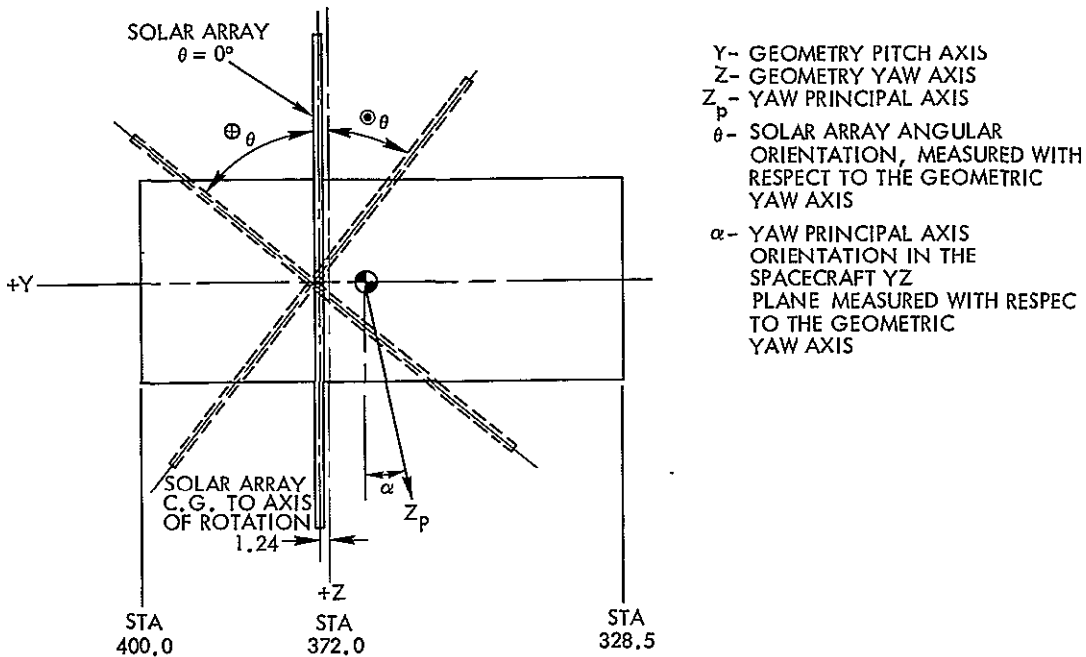


Figure 4-7
 SOLAR ARRAY ROTATION affects spacecraft mass properties

Table 4-3. Mass Properties Shifts Induced by Solar Array Rotation

Solar Array Angular Position (deg)	Moment of Inertia (slug-ft ²)			Product of Inertia (slug-ft ²)			Yaw Principal Axis Angle (in YZ plane degree)
	I_X	I_Y	I_Z	I_{XY}	I_{XZ}	I_{YZ}	α
0	210	251	393	1.2	-0.8	-2.4	0.97
15	210	250	394	1.2	-0.9	-4.8	1.92
30	210	248	395	1.2	-0.9	-6.6	2.66
45	210	246	398	1.2	-1.0	-7.1	2.68
60	210	244	400	1.2	-0.9	-6.5	2.38
-15	210	250	394	1.2	-0.9	-0.1	-0.05
-30	210	248	395	1.2	-0.8	1.6	-0.63
-45	210	246	398	1.2	-0.8	2.2	-0.85
-60	210	244	400	1.2	-0.8	1.6	-0.58

4.9 STRUCTURAL STRENGTH ANALYSIS

The design of the structure was reviewed in light of ERTS load requirements and changes in dynamics as reported above. In some areas strength increase is required and this will generally be accomplished by section wall thickness increases.

4.9.1 Interstage and Separation System

The strength requirements of the band and clamp will be satisfied by thickness increases. The band and clamp assembly, consisting of four V-groove aluminum clamps and interconnecting band, restrains the spacecraft at its four corners during launch. In a loading condition that places a corner of the box in tension, the separation flanges of the corner fittings are forced apart, inducing clamp cross-sectional bending and band tension. These components are critical under the liftoff condition of 3.0 g forward combined with 2.0 g lateral. Since these load factors represent an increase from OGO (2.5 g forward and 1.0 g lateral), a minor redesign will permit higher clamp tension loads and resultant higher band tension preload. The most efficient way to increase structural capability is to simply increase the local thickness of the clamp and band in areas of high tensile and bending stress.

The structural integrity of the bipod legs at ultimate load will be insured by thickening the flange walls in order to prevent flange crippling. Each of the four interstage lower bipod fittings consist of a bipod truss with the apex of the legs at the spacecraft corner fittings. Each leg is critical in flange compressive crippling under overall column loading. Under the burnout condition (10.1 g aft and 2.0 g lateral), with a spacecraft weight of 1500 pounds, the column loads in the bipod legs are estimated to reach 3790 pounds compression, a somewhat higher level than the OGO design loads. Consequently, flange thicknesses will be increased from the present 0.060 inch to 0.080 inch in order to maintain structural integrity. The webs transferring load from the bipod legs to the separation flange will also require a corresponding increase in thickness to carry higher bipod compression.

The interstage assembly will require cross-bracing between adjacent bipods in order to raise the second spacecraft lateral dynamic modal

frequency from the present 35 to 52 Hz. In order to reduce dynamic coupling between interstage modal responses and secondary structure modal responses, in the 25 to 50 Hz frequency range, the interstage assembly will require stiffening. Specifically, the second lateral modal frequency, estimated to occur at 35 Hz, may induce excessive input vibration levels to the pressure vessel and other heavy equipment mounted on secondary structure. This modal frequency can be increased appreciably by including cross-braced tubular members between adjacent bipod pairs to prevent diagonal warping of the interstage truss. The weight incurred by this structural change is estimated to be less than 5 pounds, and will not require a major change in the bipod configuration.

4.9.2 Main Body Structure

The box structure has been reviewed and structurally analyzed, utilizing 0.600-inch thick honeycomb on all four sides, and has been shown structurally acceptable for all loading conditions. The primary box structure load-path consists of four rectangular honeycomb side panels which carry equipment loads in out-of-plane bending and in-plane shear to the tapered thickness corner longeron angles attached to corner fittings at the bottom of the box. Diagonal I-beams attached to the corner fittings close out the bottom of the box and carry diagonal compression from box shear or separation band preload. These beams also support the pressure vessel. Cross-beams extend across the center, at the top and middle sections of the box to carry concentrated loads from the solar array and MSS instrument. A secondary standoff structure has also been included near the top of the box to support the RBV cameras away from the side panels. This method of support will minimize thermal distortions. The box structure, with the exception of the bottom diagonal I-beam assembly, is in general designed for stiffness (local modal frequencies higher than 25 Hz) and is not structurally critical under design static load conditions. A truss model computer run has been completed to determine primary member loads, and resulted in loads far below structural allowables. The diagonal I-beams supporting the pressure vessels, however, are designed for minimum weight, and are structurally critical in cap compressive crippling under the vibration loads induced during pressure vessel sinusoidal response at 33 Hz.

Primary modal frequencies of the interstage will be shifted away from the box secondary modal frequency range of 25 to 50 Hz in order to minimize transmissibility coupling which could lead to excessive structural loads. Some strengthening of the diagonal I-beams may be required.

The tape recorder assembly will be structurally mounted to side panel extensions below the separation plane. The lower bipod fittings will be modified to include attach lugs for an auxiliary panel mounting frame below the separation plane. Side panels can then be extended down for tape recorder mounting.

The pressure vessel mounting cradle will require structural improvements to withstand high vibration levels. A certain amount of increase in vibration level will be experienced by the ERTS pressure vessel, over that for the OGO bottle, due to interstage transmissibility in the 25 to 50 Hz frequency range. The cradle and preloaded band assembly will require a corresponding redesign to carry higher loads, but this redesign will be minor if interstage modal coupling is minimized.

Secondary structure for the camera and MSS is designed to mount the instruments away from the side panels, in order to minimize thermal distortion, and maintain modal frequencies above 25 Hz. The side panels have been estimated to bow outward, under a 2°F temperature gradient through the thickness, about 0.025 inch, at their midsection near the top of the spacecraft, where the cameras are mounted. This deflection corresponds to about 5.7 minutes of arc rotation of the camera assembly and is too large to allow direct camera mounting to the side panels. A secondary honeycomb panel with minimum core thickness (0.50 inch) and maximum facesheet thickness (0.030 inch) and core density (8.0 pcf) will be used to mount the cameras off the box side panels. The secondary panel, roughly 26 inches wide and 15 inches long, will be provided with two corner attachments for -X/+Z longeron mounting, and a beam-fitting along its opposite edge to attach at a single point on the opposite -X/-Z longeron. The three-point longeron mount of the camera assembly will allow for precise alignment during ground checkout. Maximum temperature gradients across the secondary mounting panel have been estimated to be about 0.5°F , and thermal distortions will be correspondingly reduced to less than 1.0 minute of arc rotation of the camera assembly.

4.9.3 Solar Paddles

The paddles, structurally designed similar to the OGO paddles, have been analyzed for ERTS launch environment and are structurally acceptable. The solar paddles have been structurally modeled utilizing a three-dimensional frame computer program. Modal frequencies are estimated to be 8, 21, and 26 Hz for the panel lateral bending modes in the tied-down launch configuration. Modal deflections for these frequencies are 2.82 inches (18.45 g's), 0.40 inch (18.07 g's), and 0.30 inch (20.82 g's), respectively. Member loads induced in each of these sine modal response conditions are within structural limits.

Deployment dynamic analysis verifies acceptable latch and hinge loads. Because of a reduction in stored spring energy with the removal of an OGO outboard-mounted experiment on the paddle tips, and member loads are lower for the ERTS paddles under deployment latch-up than for OGO. More detailed analysis and deployment tests will be performed during Phase D to verify this conclusion.

4.9.4 Antennas, Supports, and Other Appendages

The attitude control pneumatic boom is designed as a fixed, tied-down structure similar to OGO and is expected to cause no significant mechanical problems.

The 137/154 and 400 MHz dipole antennas are now mounted rigidly to the ERTS box structure and will experience comparable dynamic environments as the corresponding OGO mount.

The horizon scanner is mounted similar to its counterparts in OGO and is expected to cause no major mechanical problems.

4.9.5 Thermal Distortion and Mechanical Alignment

Observatory alignment tolerances are ensured by mounting the horizon scanner, yaw gyro, RBV cameras and MSS sensor near the top of the structure away from the thermally distorting side panels. All distortion critical equipment has been mounted on structure that attaches to the corner longerons. This structure has been modeled as a three-dimensional truss and analyzed for longeron thermal distortion. The resulting deflections are within specifications.

CONTENTS

	Page
5. ATTITUDE CONTROL SYSTEM	5-1
5.1 Normal Mode Performance Analysis	5-1
5.2 Attitude Control Configuration Study	5-6
5.3 Yaw Attitude Control Subsystem Preliminary Analysis and Design	5-8
5.3.1 Nondisturbed Performance	5-11
5.3.2 Roll Disturbed Yaw Performance	5-11
5.3.3 Pitch Disturbed Yaw Performance	5-12
5.3.4 Yaw Attitude Biases	5-13
5.3.5 Acquisition from Sun Sensor Control	5-13
5.3.6 Yaw Bias Reduction	5-14
5.4 Control Gas Requirements	5-16
5.5 Acquisition Studies	5-17
5.6 Attitude Control System Accuracy During Velocity Corrections	5-17
5.7 Moon Avoidance	5-19
5.8 Albedo Errors in Sun Sensor	5-20
5.9 Solar Array Deployment and Slew	5-23
5.10 Horizon Tracker Operation in South Pole Winter	5-24
5.11 Non-Nominal Orbital Performance	5-27

5. ATTITUDE CONTROL SYSTEM

In the application of the OGO attitude control system to the ERTS mission, several items require special attention:

- Change in yaw attitude reference from the sun to the orbit plane
- Substantial reduction in body moment of inertias due to removal of booms
- Requirement for improved pointing accuracy and lower rates
- Operation in the presence of orbital velocity correction
- Substitution of a very particular orbit for a more general class of orbit

TRW has studied the impact of each of these and devised techniques for dealing with them which are generally simple, reliable, and make maximum use of OGO experience, designs, and equipment.

The basic implementation decisions satisfying the above items were reported in our June 1969 proposal. To summarize: The rate-gyro assembly used in OGO's orbit plane experiment package is attached to the body and used as a gyrocompass for yaw reference during normal operations. Wheel sizes are reduced and pneumatic booms shortened to compensate for the decreased body inertias. These plus tightening the hysteresis of the control channels and the use of an improved version of the horizon scanner provide the required improvements in pointing and body rates. A normal OGO acquisition followed by transfer to gyrocompass yaw reference is employed. A detailed discussion of these implementations are presented in Volume 3, Section 3. Backup analyses justifying this design approach follow.

5.1 NORMAL MODE PERFORMANCE ANALYSIS

The ERTS attitude control subsystem design has been evolved from the OGO ACS with a philosophy of minimum hardware modification consistent with the mission requirements and good design practice. Accordingly, OGO system parameters have been used as a starting point in designing the ERTS control system. Table 5-1 summarizes the current ERTS attitude control parameters with OGO values for comparison.

Table 5-1. ERTS Attitude Control Subsystem Parameters

Group	Parameter	OGO 6			ERTS		
		Roll	Pitch	Yaw	Roll	Pitch	Yaw
Control law	Vehicle inertia (slug ft ²)	779	435	1088	210	250	390
	Filter time constant						
	Lead (sec)	12.5	12.5	50	12.5	12.5	5
	Lag (sec)	1.25	1.25	5	1.25	1.25	100
	Dither double lag time constant (sec)	0.2	0.2	--	0.2	0.2	
Reaction wheel	Deadzone (deg)	0.4	0.4	1.17	0.4	0.4	0.4
	Hysteresis (deg)	0.08	0.08	0.24	0.04	0.04	0.04
	Torque (ft-lb)	0.052	0.052	0.104	0.021	0.021	0.052
	Saturation momentum (ft-lb)	1.66	1.66	8.84	0.40	0.40	1.66
	Saturation speed (rpm)	1250	1250	1250	1250	1250	1250
	Windage constant (sec ⁻¹)	0.0036	0.0036	0.0036	0.0027	0.0027	0.0036
	Inhibit time (sec)	5	5	5	5	5	5
Pneumatics	Deadzone (deg)	1	1	5.7*	1	1	1*
	Hysteresis (deg)	0.08	0.08	0.5	0.1	0.1	0.1
	Torque (ft-lb)	0.384	0.308	0.71	0.20	0.15	0.40
	Lever arm (ft)	7.68	3.08	7.10	4	2.25	4
	Inhibit logic time (sec)	15	15	--	15	15	--

*Yaw pneumatics disabled for normal control

Table 5-2 summarizes the estimated steady-state subsystem Mode 4 performance including all effects (sensor noise, system dead-bands, misalignments, etc.). Major transient phenomena causing a departure from the performance stated in the table are array drive cogging and momentum unloading. Array drive cogging produces attitude rates in the order of 0.07 deg/sec which persist for 0.5 second while momentum unloading produce attitude rates of 0.02 deg/sec which persist for approximately 20 seconds following momentum unloading. Both of these transient phenomena are suppressed during payload activity by suitable attitude control logic.

A detailed breakdown of the pointing accuracy inputs to Table 5-2 are given in Table 5-3. Analysis and analog simulation verify that the proposed system can achieve the required pointing accuracy. Body rates of 0.011 deg/sec in roll and yaw and 0.008 deg/sec in pitch are obtained using the proposed control system. A typical phase plane response of the roll control system is shown in Figure 5-1. A limit cycle in the presence of a 0.001 ft-lb disturbance torque is indicated excluding the effects of noise. The response of the system is shown for wheel unloading via a pneumatic pulse, and capture of the wheel after the pneumatics pulse.

Table 5-2. Mode 4 ACS Performance

	Performance
Pointing accuracy (deg)	
● Roll	0.44
● Pitch	0.39
● Yaw	0.65
Attitude rates (deg/sec)	
● Roll	0.011
● Pitch	0.008
● Yaw	0.011

Table 5-3. Summary of Attitude Control System Accuracy

Error Source		Magnitude (deg)
<u>Roll</u>		
1	Horizon scanner position error near null	0.102 (3σ)
2	Horizon scanner misalignment	0.070 (3σ)
3	Earth oblateness and horizon profile variations	0.13 (w.c.)
4	Horizon profile uncertainty	0.084 (3σ)
5	Limit cycle amplitude (including effects of horizon scanner noise, 0.096, 3σ)	0.163 (w.c.)
	Total*	0.44
<u>Pitch</u>		
1	Earth oblateness and horizon profile	0.11 (3σ)
2	Horizon scanner position near null	0.06 (3σ)
3	Horizon profile uncertainty	0.069 (3σ)
4	Horizon scanner misalignment	0.050 (3σ)
5	Limit cycle amplitude (including effects of horizon scanner noise, 0.078, 3σ)	0.175 (3.c.)
	Total*	0.39
<u>Yaw</u>		
1	Gyro drift, ε ₁	0.5 deg/hr
2	Gyro misalignment, ε ₂	0.05 deg
3	Roll error, ε ₃	0.44 deg
	Total**	0.65

* The total error is obtained by taking the rss value of errors 1, 2, and 4, and adding this to the remaining errors.

** The total error is obtained as follows:

$$\epsilon_{\text{total}} = \sqrt{\frac{\epsilon_1^2}{0.707 \omega_0} + \frac{\epsilon_2^2}{0.707} + \epsilon_3^2}$$

where ω_0 is the orbital rate.

Studies have also shown that the existing OGO reaction wheels could be used in the system. However, this can only be done at the cost of increased body rates during limit cycling and added subsystem weight and will not be considered further.

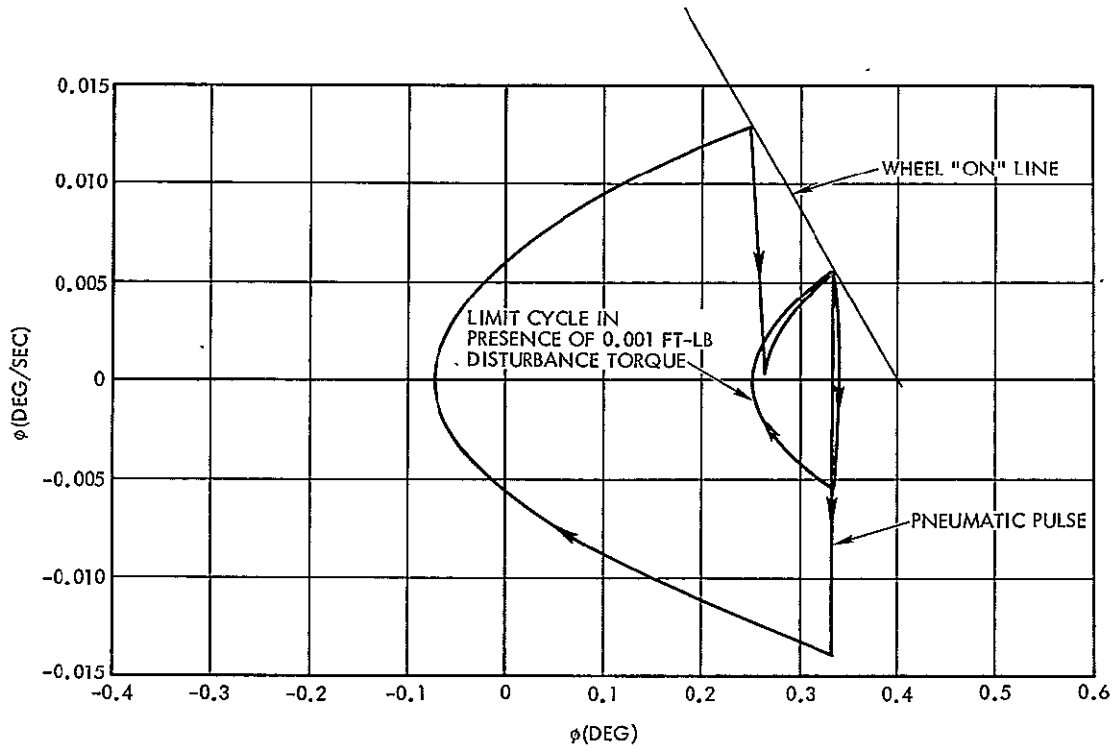


Figure 5-1

PERFORMANCE OF ROLL AXIS in presence of disturbance torque but neglecting noise, showing wheel unloading and capture.

Figure 5-2 shows the limit cycle behavior for both roll and yaw for an initial roll wheel momentum of -0.2 ft-lb-sec and zero initial yaw wheel momentum. These results, obtained from an analog simulation, show a similarity in the limit cycle behavior of roll and yaw. The roll reaction wheel windage torque causes wheel rundown, transferring wheel momentum to the body. When the roll deadband is exceeded the roll wheel speed is decreased to near its initial value. Thus, the roll wheel is activated only once during each limit cycle.

This is not the case for yaw, however. The yaw system attempts to track the roll motion sensed by the rate gyro. Assuming, for the moment, that the yaw system maintains the sensed rate near zero, the following relationship holds (for symbols see Figure 5-4).

$$\dot{\psi} \sin \beta - \omega_o \psi \cos \beta = \dot{\phi} \cos \beta + \omega_o \phi \sin \beta$$

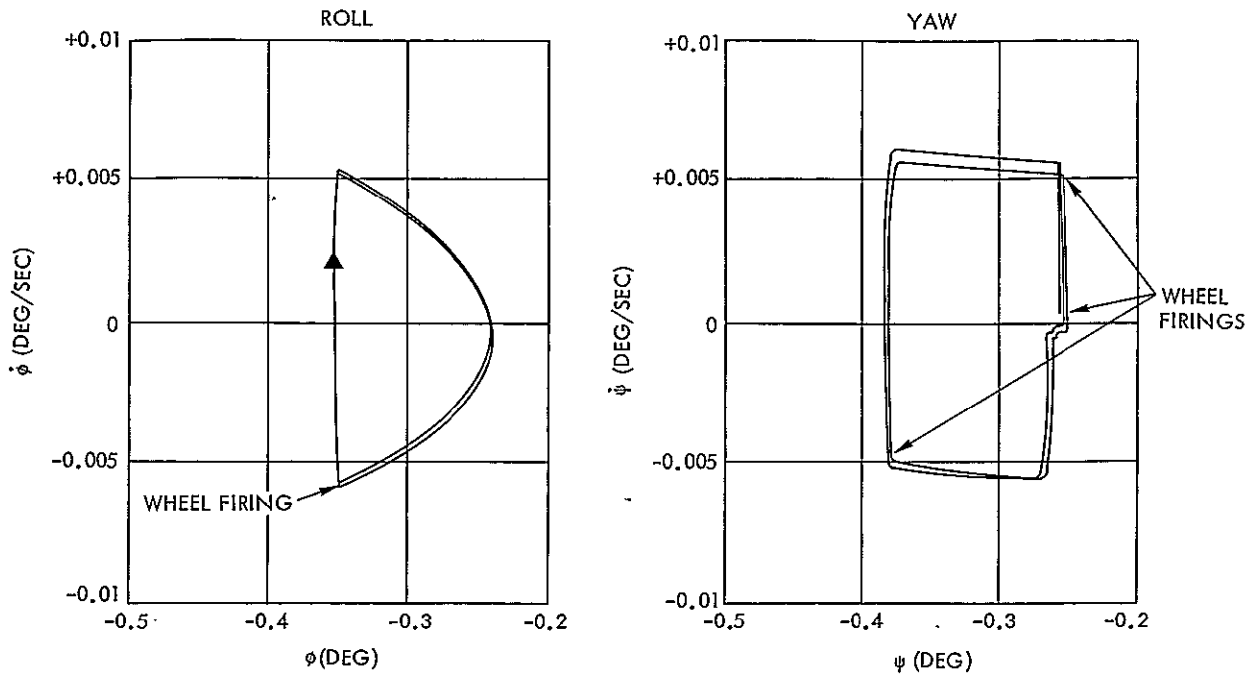


Figure 5-2

ROLL AND YAW AXIS LIMIT CYCLES ($H_{wx}(o) = -0.2$ ft-lb-sec,
 $H_{wz}(o) = 0$)

As a result of the sizable compensation lag and switch deadband, the yaw system tracks the roll limit cycle with some error and with multiple wheel firings during each limit cycle period.

5.2 ATTITUDE CONTROL CONFIGURATION STUDY

This section provides the general background for attitude control conceptual design. The baseline configuration for pitch and roll differs from OGO in four ways: reaction wheel sizes, bistable deadband and hysteresis, pneumatic lever arms, and wheel unloading technique. The pneumatic system was sized primarily from acquisition performance consideration but was also constrained by wheel desaturation requirements and by mechanical interference requirements. Wheel size and wheel bistable characteristics were selected to achieve low limit cycle rates and acceptable pointing accuracy. The new wheel unloading technique was selected to guarantee pointing accuracy during periods of payload operation during which the pneumatic system is inhibited.

Changes in wheel size and pneumatic lever arm are made possible because of the reduced inertias of ERTS over OGO. The shorter control jet booms which are now 4 feet in roll and yaw and 2.25 feet in pitch do not interfere with the payload field of view and remove the requirement for hinged deployable boom mounting since the shorter booms can be fixed mounted and still remain within the shroud envelope. The smaller wheels used for roll and pitch have a 0.4 ft-lb-sec capacity and afford an 8-pound weight reduction and adequate limit cycle rates. The wheels are the Nimbus D design modified to operate on the ERTS 115-volt, 400-Hz, two-phase square-wave power supply.

Reduction in the bistable hysteresis is made possible by the replacement of the OGO magnetic amplifiers with solid state devices which can be designed with much smaller hysteresis.

A modified wheel unloading technique is provided for better performance in roll and pitch during periods of payload operation. The proposed system is shown in functional block diagram form in Figure 5-3. In order to maintain the proven acquisition performance of the system the new wheel unloading technique is used only during Mode 4 operation.

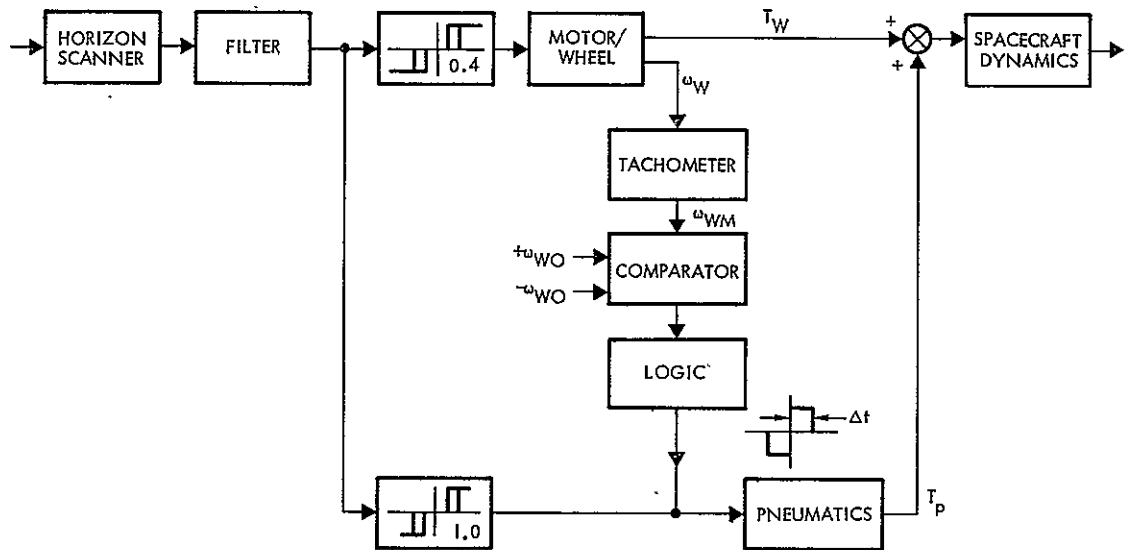


Figure 5-3
PITCH AND ROLL wheel unloading technique

During this mode the speed of the wheel is constantly monitored and compared with a reference value. (Analysis indicates that a value of one-half the maximum wheel speed is appropriate.) When the heavily smoothed measured value equals or exceeds the reference a pulse of fixed duration is applied to the pneumatic system. The selection of the pulsewidth which is 0.25 second in roll and 0.33 second in pitch is such that the wheel angular momentum is reduced 12.5 percent of maximum momentum by the pneumatic pulse. Analysis indicates that this choice of parameter values makes gas firings necessary approximately every 6.5 hours.

During picture exposure the tachometer wheel unloading technique is disabled. Wheel unloading still occurs, however, if the pointing error exceeds 1 degree. This is possible only if a wheel reaches full speed and thereby can control no more. Because at least one-half the momentum storage capacity remains when picture taking begins and an imaging sequence lasts no longer than 20 minutes, it is extremely unlikely that this will ever occur.

5.3 YAW ATTITUDE CONTROL SUBSYSTEM PRELIMINARY ANALYSIS AND DESIGN

The baseline yaw attitude control subsystem employs a caged rate integrating gyro. The gyro senses a component of orbit rate whenever there is a yaw attitude error. The input axis of the gyro is purposely tilted from the roll body axis in the roll-yaw body plane. Thus a component of yaw attitude rate is measured in addition to a component of orbit rate. Figure 5-4 shows the body axes, orbital reference frame, and the gyro input axis position. For ideal control in pitch and roll and for small attitude excursions in ψ , the sensed rate along the gyro input axis, with orbital rate ω_0 , is

$$\omega_{I.A.} = \dot{\psi} \sin \beta - \omega_0 \psi \cos \beta \quad (1)$$

Since the polarity of both the rate and position terms must agree for $\omega_{I.A.}$ to be usable as a control system error signal, the angle β must be negative. This signal, after conditioning, is input into the yaw attitude control system bistables which control the reaction wheel and pneumatics.

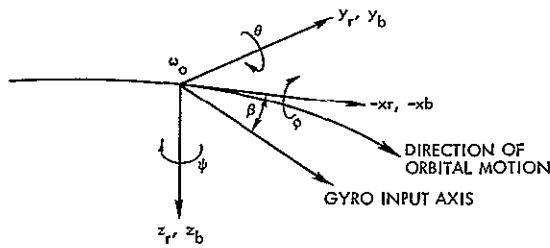


Figure 5-4
COORDINATE SYSTEM showing gyro
input axis location

The action of the torquers is to drive the error to zero, i.e., drive the yaw angle to zero.

The block diagram of the baseline yaw attitude control system and single axis yaw dynamics is shown in Figure 5-5.

The essential features of the control system are the gyro, the error signal compensation, the bistable switches and the torquers. The gyro model includes both limited gimbal travel and amplifier saturation. When the gimbal stops are reached, the gyro ceases to integrate until the sensed rate changes polarity. The compensation provides noise attenuation.

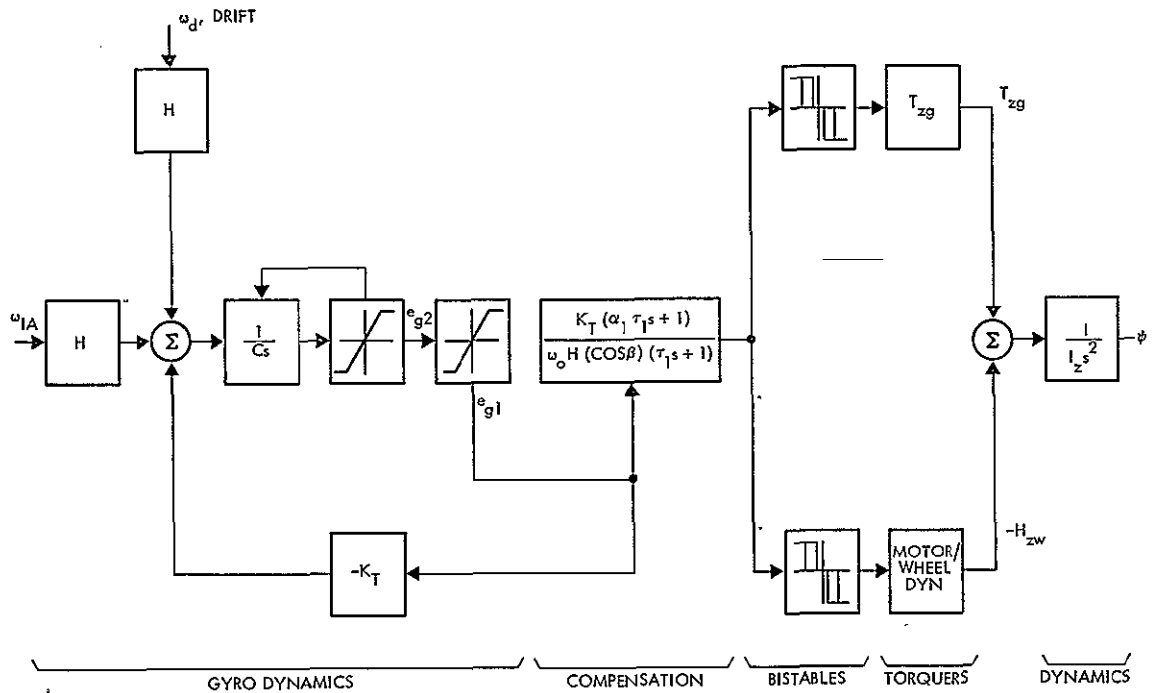


Figure 5-5
YAW CONTROL LOOP block diagram

The general expression for the rate sensed by the gyro whose input axis is tilted through the angle β from the negative roll axis in the roll-yaw plane and misaligned out of the roll-yaw plane by the small angle γ is

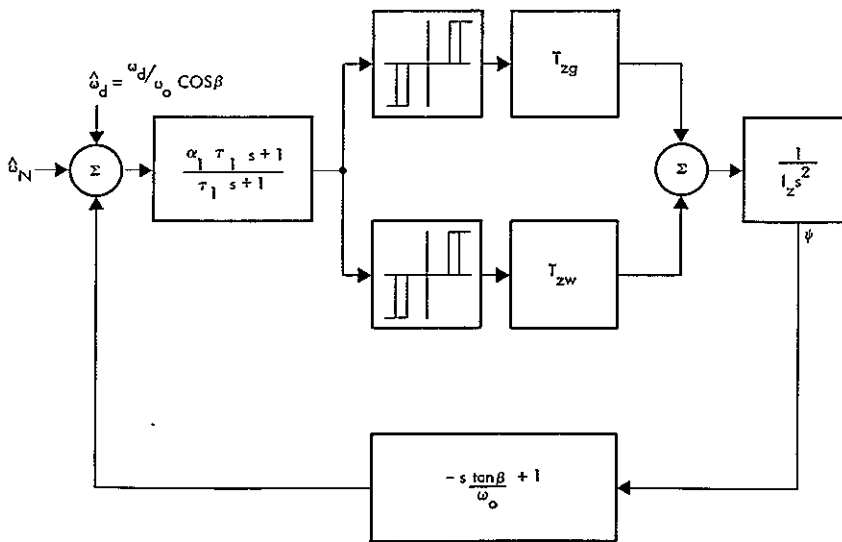
$$\omega_{I.A.} = -\omega_x \cos \beta - \omega_y (\gamma + e_{g2}) + \omega_z \sin \beta \quad (2)$$

For small angle θ and ϕ and arbitrary ψ , the body rate expressions are:

$$\begin{aligned} \omega_x &= \dot{\phi} + \omega_o \sin \psi \\ \omega_y &= \dot{\theta} + \omega_o \cos \psi \\ \omega_z &= \dot{\psi} + \omega_o \theta \sin \psi - \omega_o \phi \cos \psi \end{aligned} \quad (3)$$

Note that in Equation (2), the gimbal angle e_{g2} also appears, a result of the rotation of the gyro gimbal and, hence, input axis from its zero position. This term, however, is negligible and its effect may be ignored.

The gyro operates in the caged configuration. Since the feedback gain K_T (see Figure 5-5) of the gyro loop is generally large, the gyro gimbal angle is maintained near null and the gyro dynamics are negligible in comparison to the compensation dynamics. Also, for most analyses, the motor and wheel dynamics are represented by a torque gain equal to the stall torque of the reaction wheel motor. The resultant block diagram for small angle ψ is shown in Figure 5-6.



$$\hat{\delta}_N = [-\dot{\phi} \cos \beta - (\dot{\theta} + \omega_o) \gamma - \dot{\psi} \sin \beta] / \omega_o \cos \beta$$

Figure 5-6
SIMPLIFIED BLOCK DIAGRAM of the yaw axis control loop

5.3.1 Nondisturbed Performance

In the absence of disturbances (i. e., $\hat{\omega}_d = 0$ and $\hat{\omega}_N = 0$) the system performance is determined primarily by the gyro tilt β and compensation lag τ_1 . The lead-lag parameter α_1 is ordinarily less than 0.1 and, thus, the filter lead $\alpha_1 \tau_1$ does not affect undisturbed performance as a first-order effect.

The action of the reaction wheel for small errors is such that the input to the bistable switch is maintained within or near the switch deadband. Thus, the attitude under tight control satisfies approximately the equation

$$\psi(t) = (\psi_o - \psi_d) e^{-t/\tau} + \psi_d \quad (4)$$

where the "time constant", τ , is given by

$$\tau = -\frac{\tan \beta}{\omega_0} + (1 - \alpha_1)\tau_1 \quad (5)$$

Figure 5-7 is a graph of τ as a function of the gyro tilt angle $-\beta$, for $\alpha_1 = 0.05$ and $\tau_1 = 100$ seconds. Note the slowness of response of this system, particularly at the design value of $-\beta = +45$ deg, where the time constant is 1080 seconds. Decreasing the tilt (in a negative sense) clearly reduces the time constant of the attitude control system, a desirable feature, but at the expense of degraded pointing accuracy, as discussed below.

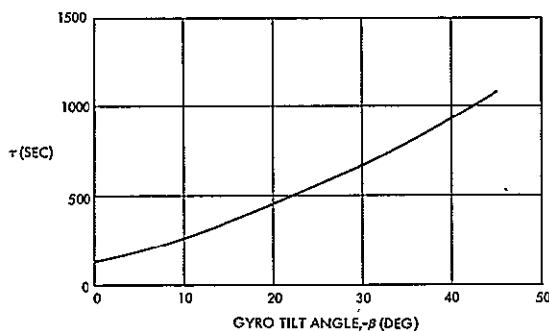


Figure 5-7
YAW AXIS TIME CONSTANT as a function of gyro tilt angle, $-\beta$

5.3.2 Roll Disturbed Yaw Performance

During fine pointing, the principal yaw disturbance arises from roll attitude error and rate being sensed by the yaw gyro. The yaw attitude control system attempts to maintain the sensed rate within the deadband of the bistable by torquing the vehicle

about the yaw axis until the yaw attitude contributions cancel the roll errors. As a first approximation, assume

- The yaw bistable is replaced by a signum function.
- The action of the yaw torquer maintains the switch input at zero, i. e., the yaw attitude follows the commanded attitude with zero error.

Under these approximations, the following relationship, obtained from Equation (2) (for small ψ and zero misalignment angle γ), holds,

$$\dot{\psi} \sin \beta - \omega_0 \psi \cos \beta = \dot{\phi} \cos \beta + \omega_0 \phi \sin \beta \quad (6)$$

If now it is assumed that the roll attitude has an average value, ϕ_0 , with a time variation, $\phi_1(t)$, it may be shown that the corresponding yaw motion is given by

$$\psi(t) = \phi_0 \tan \beta - \phi_1(t) \cot \beta \quad (7)$$

and

$$\dot{\psi}(t) = -\dot{\phi}_1(t) \cot \beta \quad (8)$$

Note that

- A large value of β reduces both the limit cycle rate and attitude variation but increases the attitude offset.
- A small value of β reduces the attitude offset but increases limit cycle rate and attitude variation.

Therefore, if consistency in peak body rates is a requirement, then the gyro tilt angle should be near -45 degrees.

5.3.3 Pitch Disturbed Yaw Performance

Pitch axis motion can be sensed by the yaw gyro if the gyro input axis is misaligned out of the roll-yaw plane. Pitch axis motion consists primarily of limit cycle motion which will not be significant since with $|\gamma| \leq 0.5$ deg and the limit cycle rate $|\dot{\theta}| \leq 0.01$ deg/sec (a reasonable upper bound) the equivalent perturbation in apparent yaw error is

$$\left| \dot{\psi} \right| \leq \left| \frac{1}{\omega_o \cos \beta} (\dot{\theta} \gamma) \right| \leq \frac{0.0087}{\cos \beta} \quad (9)$$

For $\beta = -45$ degree, this is 0.012 degree which is considerably less than the yaw reaction wheel bistable hysteresis.

5.3.4 Yaw Attitude Biases

Gyro drift and out-of-plane misalignment of the gyro input axis bias the yaw null. The former bias is given by $\omega_d / \omega_o \cos \beta$, while the latter is $-\gamma / \cos \beta$. Thus, for a gyro drift ω_d of 0.5 deg/hr and $\beta = -45$ degree, the yaw null bias is 0.2 degree. Similarly for a misalignment γ of 0.05 degree, the yaw null bias is 0.07 degree.

5.3.5 Acquisition from Sun Sensor Control

For the design orbit, the yaw error measured by the gyrocompass system prior to transfer of control authority from Mode 3 to Mode 4 will lie between -62.3 and +62.3 degrees. The gyrocompass system must successfully acquire from such initial errors.

The sensed yaw rate and yaw attitude error (for arbitrary yaw angle ψ) is

$$\omega_{I.A.} = \dot{\psi} \sin \beta - \omega_o \sin \psi \cos \beta \quad (10)$$

Assuming that the reaction wheel maintains this rate at zero, the yaw transient is the solution of

$$\dot{\psi} \sin \beta - \omega_o \sin \psi \cos \beta = 0 \quad (11)$$

or equivalently,

$$\log \tan \frac{\psi}{2} - \log \tan \frac{\psi_o}{2} = (\omega_o \cos \beta)t \quad (12)$$

Therefore the time required to perform a yaw maneuver from an initial attitude ψ_o to a final attitude ψ is

$$t = \frac{-\tan \beta}{\omega_0} \left[\log \tan \frac{\psi_0}{2} - \log \tan \frac{\psi}{2} \right] \quad (13)$$

This expression is plotted in Figure 5-8 for a final yaw attitude of 1 degree. The curves, plotted for various gyro tilt angles, show that for the maximum expected initial error of 63 degrees and the gyro tilt angle of -45 degrees, acquisition to gyrocompass can be accomplished in approximately 70 minutes. This should be acceptable. Note that this time could be reduced by changing the tilt angle at the expense of degraded limit cycle performance as described in the section above but such a change seems undesirable. Transients can be eliminated entirely by transferring from Mode 3 to Mode 4 near the equator.

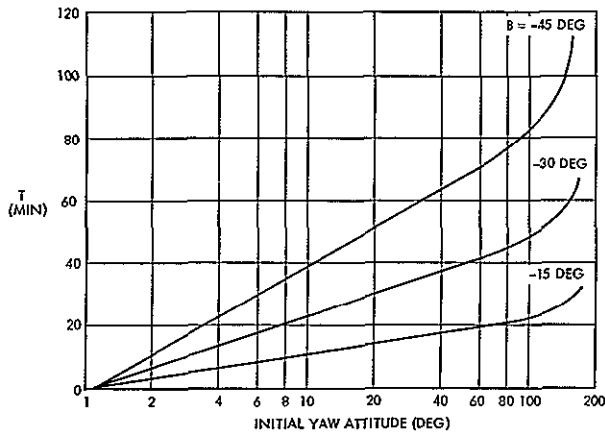


Figure 5-8
TIME REQUIRED to reduce an initial yaw attitude angle to 1 degree as a function of the gyro input axis tilt angle β

The Mode 3 OGO yaw attitude control system configuration can be used as a backup system, if desired. Transfer of control from gyrocompass, Mode 4, to Mode 3 and re-acquisition to sun sensor control can be easily accomplished with the yaw pneumatics disabled.

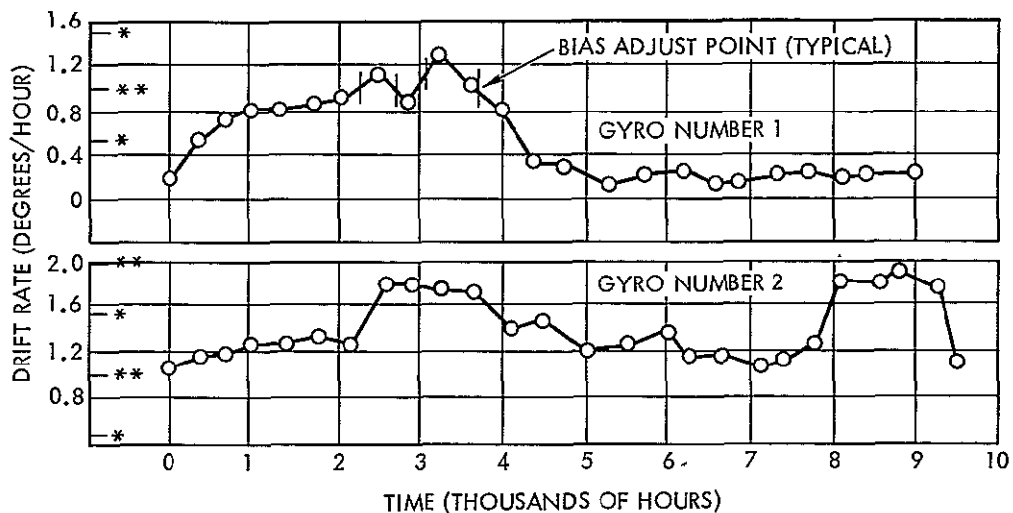
5.3.6 Yaw Bias Reduction

The fixed drift or bias associated with the OGO OPEP gyro assembly is presently specified at ± 3.6 deg/hr which is in excess of the 0.87 deg/hr required to meet 0.7-degree pointing accuracy. This value, based on the vendor's and our own experience, is conservative. However, on the other hand, requiring that the drift change never exceed 0.87 deg/hr over the life of the mission seems optimistic. Therefore, the system design includes a ground commandable bias circuit which adjusts the bias of the summed signals to within ± 0.5 deg/hr, over a range of ± 4 deg/hr. The bias will be established as a natural byproduct of image processing. Since the rate of change of gyro drift is very low, adjustments will be infrequent, in the order of two months apart.

The ERTS (and OGO OPEP) gyro is a Honeywell Model GG49E16, and long term bias data for two similar units is shown in Figure 5-9. This data was taken with each unit running continuously for a year in a manner which very closely approximates the ERTS environment. If gyro No. 1 were used in ERTS a total of four corrections would have been required, the closest two being 300 hours apart and the average separation being 1800 hours or 2.5 months. Note that this gyro was quite stable over the second half of the year, and during that period no correction changes would have been required. The second gyro exhibited slightly more stable performance and hence if used on ERTS would not require any bias correction changes from an initial value of -1.5 deg/hr over the entire period. Honeywell personnel indicate that the above data was taken in 1961 and that their present experience with these units tends to be somewhat better.

The use of higher performance gyros was considered for this application; however, none seemed to justify the additional expense and technical risks associated with its inclusion. Furthermore the use of a different

- 1) GYROS ORIENTED OUTPUT AXIS VERTICAL, INPUT AXIS APPROXIMATELY CAST
- 2) ALL EXCITATIONS CONTINUOUSLY APPLIED THROUGHOUT ENTIRE TEST
- 3) DRIFT RATE MEASURED APPROXIMATELY TWICE A MONTH



- * YAW GYRO ASSEMBLY BIAS VALUE
- ** BIAS ADJUST LEVEL, i.e., WHEN THE GYRO DRIFT CURVE PASSES THROUGH THIS LEVEL, A BIAS ADJUSTMENT WOULD BE REQUIRED

Figure 5-9

YAW GYRO BIAS versus time for two units

gyro would require extensive redesign and requalification of the yaw gyro assembly both of which tend to be incompatible with the present schedule. Had a new gyro been adopted the drift errors present in the analog circuitry, that is, slowly varying electrical biases which are independent of gyro drift and are estimated to be as large as an equivalent of 1 deg/hr would still require reduction. Based on the above reasoning, we have concluded that the existing OGO gyro is preferred based on relative performance risk and cost.

5.4 CONTROL GAS REQUIREMENTS

Fuel expenditure is required for acquisition, to remove secular disturbance torques, and to maintain control during velocity correction maneuvers. A typical acquisition requires approximately 36 lb-sec of krypton. On the basis of five acquisitions (initial plus four reacquisitions) 180 lb-sec are allotted.

To remove secular disturbance torques 138 lb-sec per year are required. The major sources of secular disturbance torques are magnetic, gravity gradient, and solar pressure. The magnetic torque is computed assuming a spacecraft magnetic moment of 9 amp-ft² which is equivalent to a magnetic field of 0.7 gamma measured 20 feet away from the spacecraft center of mass with a resulting impulse requirement of 102 lb-sec per year. The solar pressure torque is computed assuming that the center of mass lies 9 inches aft of the solar array shaft with a resulting impulse requirement of 6 lb-sec per year. The gravity gradient torque is computed assuming a principal axis offset of 1 degree with a resulting impulse requirement of 30 lb-sec per year.

The expected disturbance torque from the krypton hot gas thrusters is approximately 0.007 ft-lb. Although the reaction wheels can handle this, momentum build-up will eventually "saturate" the wheels resulting in pneumatic activation. The necessary impulse requirement is 30 lb-sec per year.

Total attitude control gas requirements are thus

Acquisition	180 lb-sec
Magnetic torques	102
Solar pressure	6
Gravity gradient	30
Orbit adjust torque	30
Total	<u>348 lb-sec</u>

5.5 ACQUISITION STUDIES

Computer simulation results indicate that an all-attitude acquisition capability is provided using an OGO configuration with minor changes.

The changes summarized in Table 5-1 are shorter moment arms for the pneumatics, smaller reaction wheels, less hysteresis in the bistables and a different yaw filter time constant. The results also indicate that the proposed ERTS system provides adequate stability margins and is relatively insensitive to torque imbalance and inertia changes.

Figure 5-10 shows performance during sun acquisition for the worst case initial rates and worst case initial attitude. About 34 lb-sec of fuel is consumed in this case. The simulation demonstrated that sun acquisition was readily achieved from initial rates of ± 2 deg/sec; nominal fuel consumption is approximately 24 lb-sec, and the vehicle acquires the sun within 200 seconds. Earth acquisition requires less than 12 lb-sec.

5.6 ACS ACCURACY DURING VELOCITY CORRECTIONS

During orbit correction, heated krypton thrusters are used for removal of velocity errors. Misalignment of thrusters and/or thrust offset from the vehicle c. g. results in disturbance torques which require enablement of the yaw pneumatics during velocity correction activity. Using 0.004 ft-lb as a maximum nominal disturbance torque, with variations down to 0.001 ft-lb, yaw ACS behavior was evaluated via the analog simulation. Figure 5-11 shows the phase plane for yaw, starting with an initial yaw wheel momenta of 1.2 ft-lb-sec and the nominal disturbance. This figure shows the saturation of the yaw wheel, followed by the pneumatics turn-on. Partial wheel desaturation is evident leading to a quasi-steady-state gas limit cycle. Runs at disturbance levels of 0.001 ft-lb

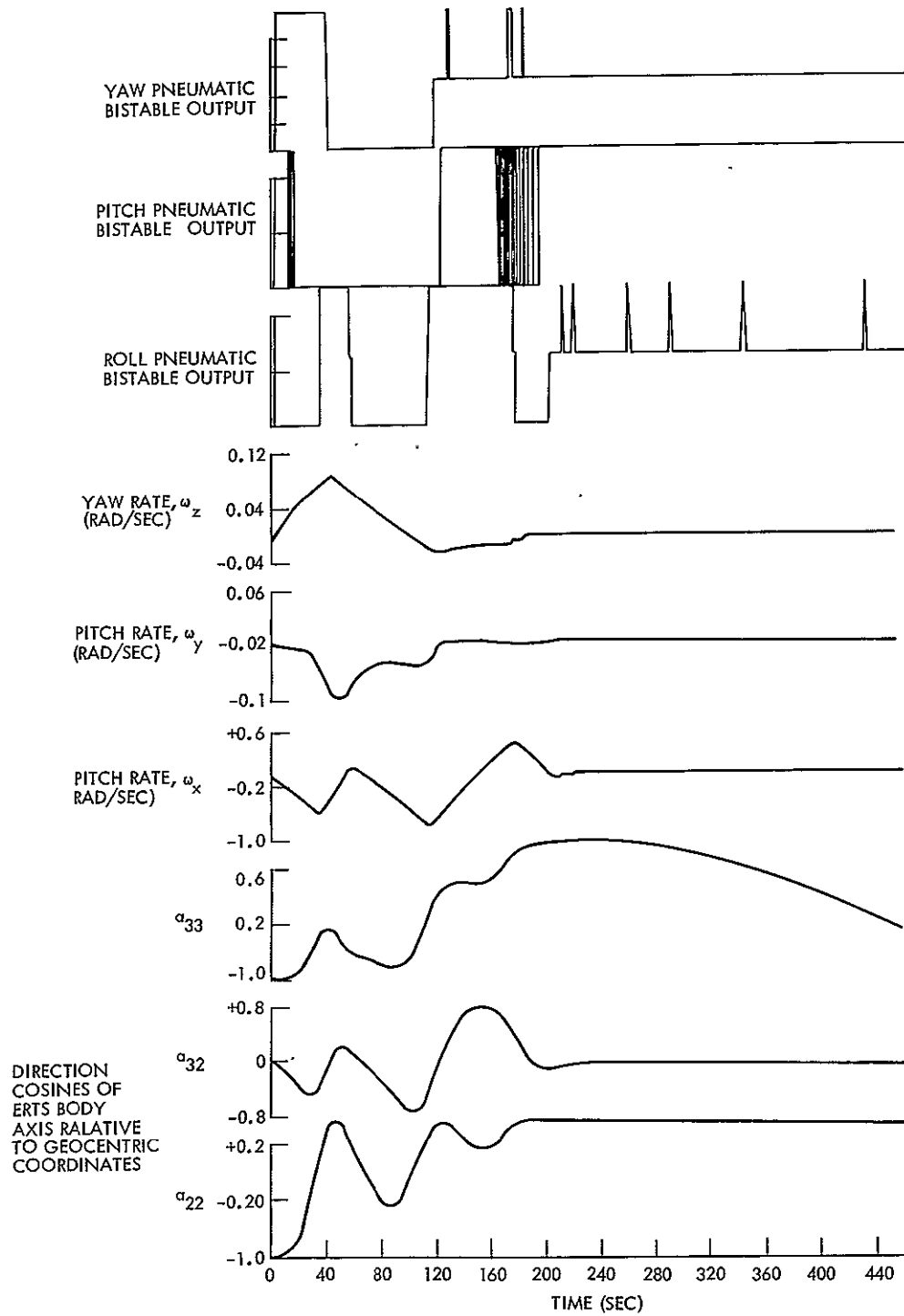


Figure 5-10

SUN ACQUISITION TIME RESPONSE for worst case initial attitude ($a_{22} = -1$) and for worst case initial body rate $\omega_x = -0.5$ deg/sec, $\omega_y = -0.5$ deg/sec, $\omega_z = +0.5$ deg/sec

showed recapture of wheel control followed by wheel saturation, gas firing and wheel recapture. In all the lower thrust disturbance cases, the peak yaw rate was in agreement with those shown in the figure. The slow drift in attitude evident in this figure is characteristic of gyrocompass systems which have comparatively large gyro tilt angles. Such motion continues until equilibrium is reached in the vicinity of the pneumatic deadband.

This analysis was completed prior to final spacecraft design definition and therefore does not reflect the anticipated 0.007 ft-lb disturbance torque level but is representative of the system operation.

5.7 MOON AVOIDANCE

Moon interference in the horizon scanners can cause significant spacecraft angular pointing error. To avoid this scanner head selection is proposed. Three scanner selections are likely to be required every lunar month.

The occurrence of moon interference is dependent on: the geometry of the horizon scanner field of view, the inclination of the moon orbit plane to the vehicle orbit plane, and the relative position of the moon orbit path ascending node (Figure 5-12).

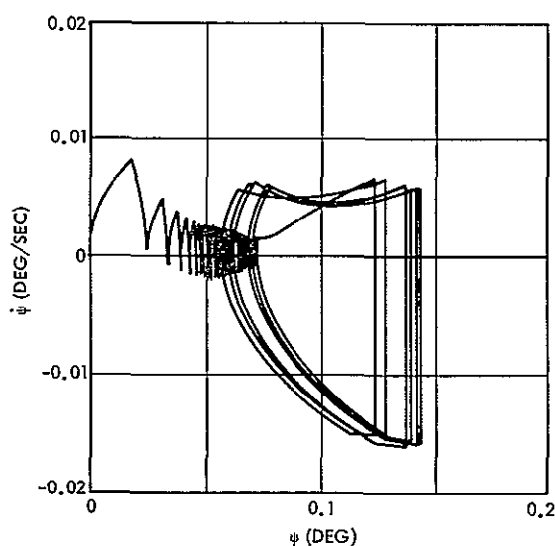


Figure 5-11
YAW AXIS PHASE PLANE for the nominal disturbance torque of 0.004 ft-lb ($H_{wz}(0) = 1.2$ ft-lb-sec)

The B-D scanner heads will be rotated about the Z_b axis by -5.8 degrees out of the $X_b - Z_b$ plane. For the ERTS orbit the earth will have a half angle of 61 degrees. The centerline of the ± 2 degree horizon scanner field of view will therefore be -5.06 degrees out of the $X_b - Z_b$ when the scanner is locked on the horizon. As the spacecraft orbits the earth, it in effect rotates about its own Y_b axis relative to the moon orbit plane. The "B" horizon scan line, therefore, describes a cone about

the Y_b axis which has an apex half angle which is the complement of the 5.06 degree scanner angle or 84.94 degrees. Similarly, the "D" head scan line describes an identical cone about the $-Y_b$ axis. Since the Y_b axis is aligned with the orbit plane normal Y_r , the cones will intersect the moon orbit path at the four locations in its orbit. The period of the moon relative to the orbit plane of the spacecraft is 29.43 days and the moon will move 0.873 degree per orbit of the spacecraft. With the ± 2 degree field of view, a rising moon will be observed on two to three successive orbits of the spacecraft at each of these four locations per lunar period.

For the A-C scan cones, the intersection with the moon orbit path is complicated by the inclination of the lunar orbit plane to the equatorial plane. The lunar orbit plane is inclined to the ecliptic by 5.145 degrees. Relative to the equatorial plane, the moon orbit inclination will be in the range of $\pm 23.44 \pm 5.145$ degrees depending on the location of the sun and moon ascending nodes. The geometry of the moon path intersection with the lunar orbit is shown in Figure 5-12. Note that the axis of the "C" head scan cone is 9.1 degrees below the equatorial plane. The moon orbit plane can be a maximum of 28.6 degrees above the equatorial plane. If the moon is more than 22 degrees above this plane, no interference will occur. The worst case will occur when the moon orbit is 9 degrees below the equatorial plane. Moon tracking will not be caused by new moons that appear in the B-D scanner field of view, because of insufficient moon radiance.

The same operational techniques will be used to operate ERTS as are now employed for OGO except that choice of tracking heads is afforded by the ERTS design. Timing for head selection is noncritical. Selection within a few days prior to the predicted interference data will be sufficient.

5.8 ALBEDO ERRORS IN SUN SENSOR

Loss of solar array power due to sun sensor bias resulting from earth albedo can be minimized by offsetting the null of the array sun sensor slightly in the direction of the bias.

The orientation of the observatory solar array is controlled by the array sun sensor, described in Volume 3, Section 3. Control action

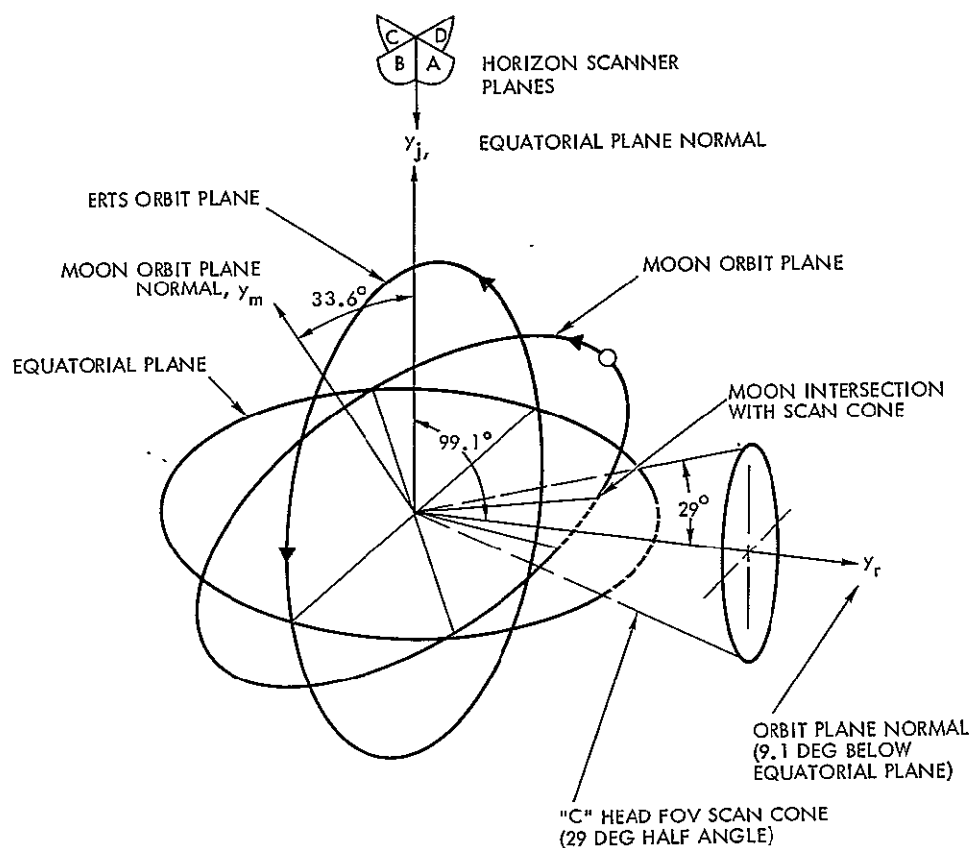


Figure 5-12
 INTERSECTION OF MOON ORBITAL PLANE with the "C" head
 horizon scanner field of view

maintains the plane containing the array axis and the array normal coincident with the plane containing the array axis and the solar vector. The array sun sensor is vulnerable to bias errors caused by stray light, since its field of view approaches 4π steradians. The only significant source of stray light is the earth, which is a relatively bright planet with an albedo of 0.36.

A conservative estimate of the earth albedo caused bias errors, and the resulting loss of available solar power has been derived for the ERTS mission. The earth was assumed to be a uniform Lambertian sphere with emissivity of 0.36. The computed array pointing error is shown in Figure 5-13 as a function of orbital position for the two extreme orbit-sun orientations. The maximum error is slightly more than 8 degrees. The available solar power for the two extreme orbits and the power available when the albedo caused bias are present are shown in Figure 5-14.

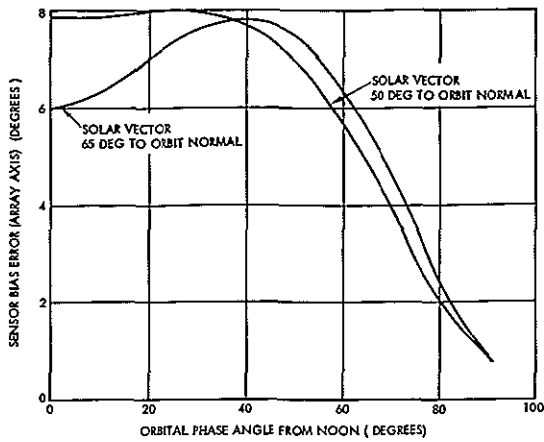


Figure 5-13

THE EARTH ALBEDO caused array sun sensor bias error varies with orbital phase

orbit due to the introduced bias is negligible. Although other solutions are possible for the albedo problem a mechanical offset is the simplest to implement and this will be done in the sensor-mounting bracket.

The loss of available solar power can be reduced by introducing a mechanical offset between the array sun sensor null, and the normal to the solar array in the direction of the albedo caused bias. The calculations indicate that a 5-degree offset will essentially eliminate the loss. With this offset, the loss for the worst orbit is less than 0.07 percent over that part of the orbit where albedo is present. The loss of power over the remainder of the orbit

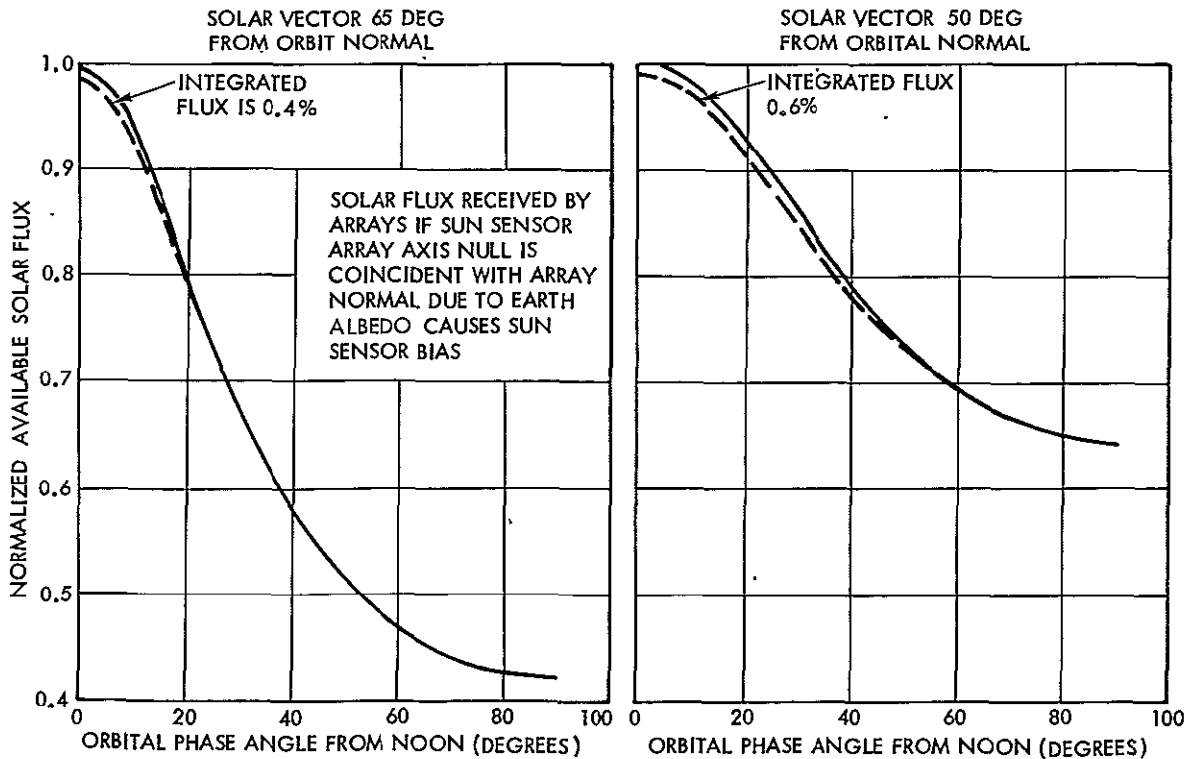


Figure 5-14

THE AVAILABLE SOLAR POWER varies with orbital phase angle

5.9 SOLAR ARRAY DEPLOYMENT AND SLEW

After the ERTS observatory separates from the booster, the solar panels are deployed or unfolded from the body such that they are aligned along the observatory roll axis with the solar cell sensitive direction parallel to the -Y or negative pitch axis. For the ERTS mission after deployment, it is desirable to have the array slew such that the solar cells are looking in the +Y direction at which time Mode 2B or sun acquisition begins.

When the observatory is in the normal cruise mode, the motion required of the solar array is approximately ± 65 degrees about the roll axis. Therefore, the largest angular motion required of the array is the initial 180 degree slew +65 or a total of 245 degrees. The flex wrap assemblies utilized on OGO have an angular capability slightly in excess of 360 degrees and since this is greater than the motion required for the new application, this space-proven hardware will be utilized for the ERTS mission. However, the array must move in the correct direction from its initial deployed position toward the shaft position transducer stable null in order not to exceed the angular capability of the flex wrap assembly, i. e., the servo must be constrained from moving in either direction from the unstable null at deployment to the stable null. To assure that the array always drives in a known direction the resolver axis of nulls is offset 5 degrees from the observatory pitch axis. Thus when the solar panels are deployed, an error corresponding to 5 degrees is present at the input to the drive electronic assembly and the servo slews in the direction associated with that error toward the stable null, 175 degrees away. Upon reaching the stable null, the array shaft stops because the error signal goes to zero. With this condition and upon completion of sun acquisition, the solar panels are thus 5 degrees away from being truly perpendicular to the sun a negligible loss of about 1/2 percent of maximum available solar power. As discussed in Section 5.8 the sun sensors are displaced 5 degrees in a compensating direction in order to minimize the earth albedo errors. This assures that the body axes are truly aligned with the sun as earth search begins. Thus the solar array drives the correct direction from its deployed position to a position 5 degrees away from

the sun line and the sun sensor is then aligned relative to the spacecraft axes.

In order to prevent the array drive servo from torquing when the panels are in a stowed position, one switch in each panel hinge will be utilized to inhibit the array servo when the arrays are folded. The circuitry is such that either switch closure at deployment actuates a 15-second delay which when completed initiates the array slew. The only other system change required as the result of this orientation of the array relative to the sun is to reverse the phasing of the Z axis control, and this can be done by a phase reversal of that portion of the sun sensor which controls the Z spacecraft axis. It appears that a simple change in the spacecraft harness will accomplish this.

5.10 HORIZON TRACKER OPERATION IN SOUTH POLE WINTER

The effective earth radiance input to the earth horizon tracker can be computed by integrating the product of the earth's spectral radiance and the total spectral-responsivity of the horizon tracker over the optical band of the horizon tracker. The total spectral responsivity of the horizon tracker shown in Figure 5-15 is the product of the spectral responsibility

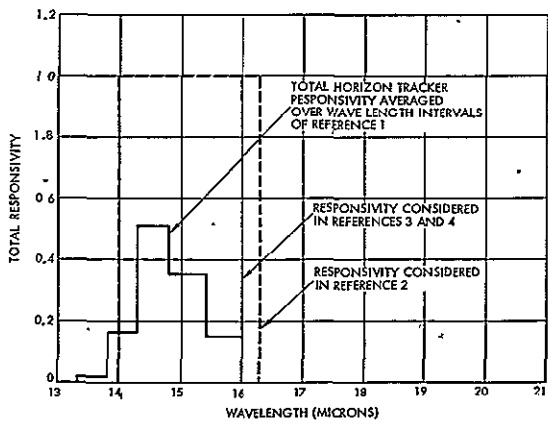


Figure 5-15
COMPARISON OF SPECTRAL RESPONSES

of the bolometer, and the transmission of the bolometer telescope optics. Although direct measurements of the earth's spectral radiance have been made, there is not sufficient data to determine the effective radiance for all anticipated conditions. It is possible, however, to calculate the earth's spectral radiance from theoretical considerations of the atmospheric radiation processes; and the variation with altitude of meteorological

parameters such as temperature, pressure, and carbon dioxide concentration. Reference 1, Wark et al, presents the results of such a calculation for eight different meteorological conditions, or atmospheres.

The mean radiance in small wave number intervals is tabulated as a function of tangent height from the earth's surface for each atmosphere. Of the eight atmospheres considered, the one designated "B" produces the largest effective radiance, 200 microwatt/cm²-steradian; and the one designated "D" produces the least, 124 microwatt/cm²-steradian.

Several authors have calculated the available earth radiance in spectral bands centered near 15 microns using bodies of meteorological data which represent valid statistical samples. Reference 2 presents calculated radiance-tangent height profiles generated from over 900 sample atmospheres of the Northern hemisphere for the spectral band between 14 and 16.2 microns as shown in Figure 5-15. The meteorological data was assembled during 1964. At a tangent altitude of 20 km, the mean radiance of a set of 900 atmospheres is 520 ± 6 microwatt/cm²-steradian, while the extreme radiance values of all atmospheres compiled are 640 ± 2 microwatt/cm²-steradian, and 370 ± 22 microwatt/cm²-steradian. The extreme values were computed from meteorological data taken over 90°N separated roughly six months in time. That is, the largest radiance variation occurs at 90°N. The winter radiance is the lowest, and the summer radiance the highest. Smaller variations can be expected at lower latitudes. The effective radiance in the horizon tracker spectral band can be extrapolated from the above data by multiplying the effective radiance in the Wark atmosphere by the ratio of the available radiance in the 14 to 16.3 micron band to that available in the appropriate Wark atmosphere. This calculation is summarized in Table 5-3.

Some authorities have suggested that the year 1964 may have been meteorologically mild. It is generally felt, however, that 1957 was meteorologically rather variable. Among the factors which may have contributed to this variability was the occurrence of peak sun spot activity. The radiance-tangent height profiles compiled in References 3 and 4 were determined largely by a body of meteorological data assembled between 1957 and 1960. References 3 and 4 present calculated available radiance-tangent height profiles for the Northern and Southern hemispheres, respectively, in the 14 to 16 micron spectral band shown on Figure 5-15. The reported values are summarized in Table 5-3.

Table 5-3. Summary of Reported Earth Radiance Extremes at 20 km Tangent Height, and Computed Effective Radiance in the ERTS Horizon Tracker Spectral Band

Reference	Description	Spectral Band	Available Radiance (microwatt/cm ² -ster)	Effective Radiance (microwatt/cm ² -ster)	Comments	
1	B	14 to 16	585	200	Maximum	
		14 to 16.2	603			
	D	14 to 16	353	124		Minimum
		14 to 16.2	362			
2	Maximum	14 to 16.2	642	213	Arctic summer	
	Minimum	14 to 16.2	348	119	Arctic winter	
3	Maximum	14 to 16	695	238	Arctic summer	
	Minimum	14 to 16	320	112	Arctic winter	
4	Maximum	14 to 16	705	241	Antarctic summer	
	Minimum	14 to 16	260	91	Antarctic winter	

The larger radiance variation in the Southern hemisphere, which occurs near 90°S is confirmed by experience. Earth sensor failures have been reported over the Antarctic during winter, which could only be attributed to low earth radiance. The radiance value reported in Reference 4 is the lowest value reported, and may be considered a worst case extreme.

Tests have been conducted to determine the least radiance that the ERTS horizon tracker can reliably track in order to establish that the

tracker would function under all anticipated conditions. During the horizon tracker development program, a breadboard electronics unit was constructed. This was connected to an OGO positor, and bolometer telescope. The earth's horizon was simulated by a heated collimated target, and the effective radiance in the OGO band calculated as a function of target temperature. The horizon tracker consistently tracked an effective radiance input of 27 microwatt/cm²-steradian. The indicated tracking angle began to increase in uncertainty at this point. However, the loss of the track check signal, as discussed in Volume 3, Section 3.1, did not occur until a somewhat lower input. If a 40 percent allowance is made for experimental uncertainty, end of life bolometer degradation, and unit temperature, the least effective radiance that would be tracked is 38 microwatt/cm²-steradian. This is a factor of 2.4 times lower than the lowest reported Antarctic winter radiance. Thus it is concluded that the horizon tracker will operate satisfactorily under all anticipated conditions.

5.11 NON-NOMINAL ORBITAL PERFORMANCE

The ERTS attitude control system will perform within the specified accuracy requirements in orbits with eccentricities as high as 0.3.

Evaluation of the attitude control system performance in non-nominal orbits was made by a study of the effects of orbital eccentricity on pointing accuracy. The orbital semimajor axis was assumed constant at 3938 nautical miles and the eccentricity was varied from 0 to 0.3. At an eccentricity of zero, this corresponds to a circular orbit with an altitude of 496 nautical miles. Over this range of eccentricities the pitch and roll control system accuracy degraded a maximum of 0.1 degree to 0.49 and 0.54 degree, respectively. The reason for this accuracy degradation is that the horizon scanner scale factor changes as a function of the earth's subtended angle, which in the case of non-zero eccentric orbits varies as a function of orbital position. The scanners are designed such that their mechanical null axes correspond to an earth's half angle of 61 degrees (496-nautical-mile circular orbit). For an eccentricity of 0.3 the earth's half angle varies from 57 to 65 degrees as the vehicle advances in its orbit. The scanners scale factor changes 2.3 percent for every degree away from the "optimum" 61 degrees

and, therefore, the above variations produce a maximum error of approximately 0.1 degree.

The yaw system accuracy is affected in two ways. The increase in roll error is reflected directly into an increase in yaw error and because of the change in orbital frequency, the contribution from gyro misalignment increases from the nominal 0.07 degree to a maximum of 0.112 degree (0.3 eccentricity) resulting in an overall yaw accuracy of 0.70 degree.

The other effect on the yaw system performance caused by increasing eccentricity is that the system time constant varies as a function of eccentricity. Figure 5-16 shows this variation.

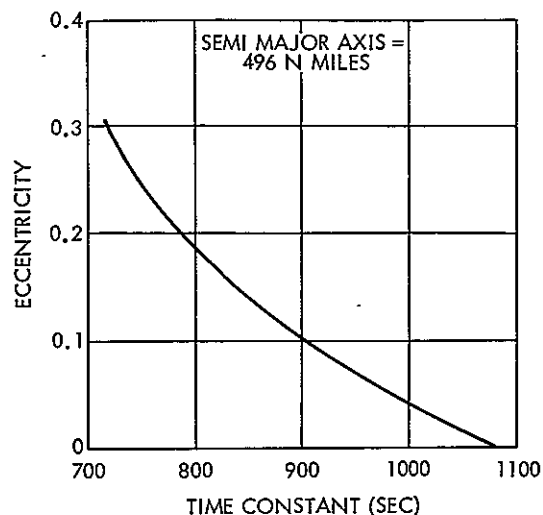


Figure 5-16
YAW SYSTEM TIME CONSTANT for
eccentric orbits

REFERENCES

1. Wark, D. Q., J. Alishouse, and G. Yamamoto, "Meteorological Satellite Laboratory Report No. 21, Calculations of the Earth's Spectral Radiance for Large Zenith Angles," October 1963.
2. Thomas, John R., Ennis E. Jones, Robert O'B. Carpenter, and George Ohring, "The Analysis of 15 μ Infrared Horizon Radiance Profile Variations over a Range of Meteorological, Geographical, and Seasonal Conditions," NASA CR-725, April 1967.
3. Burn, J. W., and P. P. Morris, "Annual High, Low, and Mean Limb Radiance Profiles for the 15-Micron Carbon Dioxide Absorption Bands," LMSC-680197, 30 October 1967.
4. Thomas, Norman L., "Earth's Radiance for CO₂ Absorption Band Horizon Sensor," LMSC-687266, 9 April 1969.

CONTENTS

	Page
6. ATTITUDE DETERMINATION	6-1
6.1 The Selected System	6-5
6.2 Earth Sensor Assembly/Gyro	6-8
6.2.1 Horizon Tracker Instrument Errors	6-10
6.2.2 Horizon Model and Atmospheric Variability	6-12
6.2.3 Horizon Tracker Accuracy Analyses	6-18
6.3 Systems Using Star Sensors	6-21
6.4 Conclusion Concerning Orbital Attitude Determination	6-25
6.5 Relative Attitude Determination	6-26
6.6 Systems Using Reaction Wheel Data	6-28
6.7 Systems Using Gyro Reference Assemblies	6-34
6.8 Conclusion Concerning Relative Attitude Determination	6-35
6.9 Celestial Attitude Reference from the RBV Camera	6-35

6. ATTITUDE DETERMINATION

Knowledge of sensor attitude as a function of time is required for use in RBV and MSS geometric image correction. The objective of the attitude determination study has been to select a candidate attitude determination system — hardware and software — which most effectively satisfies this requirement. Factors that were considered in selecting the system are impact on the spacecraft in terms of power, space, etc., increased risk in cost overrun and schedule slippage for new hardware development, reliability, and accuracy performance.

There are two distinct and different mapping objectives:

- Absolute location of all picture elements within 2 nautical miles without the aid of ground truth
- Absolute location of all picture elements approaching one resolution element (200 feet) with the aid of ground truth

For RBV images, spacecraft attitude for the 200-foot goal is only of secondary importance.* For the 2 nautical mile requirement it is important only at the instant of shutter opening. The MSS poses an entirely different problem since data is continuously collected, six lines at a time. Changes in attitude as the spacecraft moves not only interact with the indirect 2 nautical mile requirement but also distort the geometry within an image so as to make extrapolation inaccurate even if several ground truth points are identified. This then places a rate accuracy requirement on the attitude determination system. A pictorial representation of these effects on the RBV and MSS can be found in Figures 6-1 and 6-2.

The problem of attitude determination is thus one of establishing sensor attitude history to moderate accuracies for the 2 nautical mile case, and one of determining absolute attitude and attitude rate histories to a fairly high precision for the 200-foot case.

*It may also be used to remove small keystone effects.

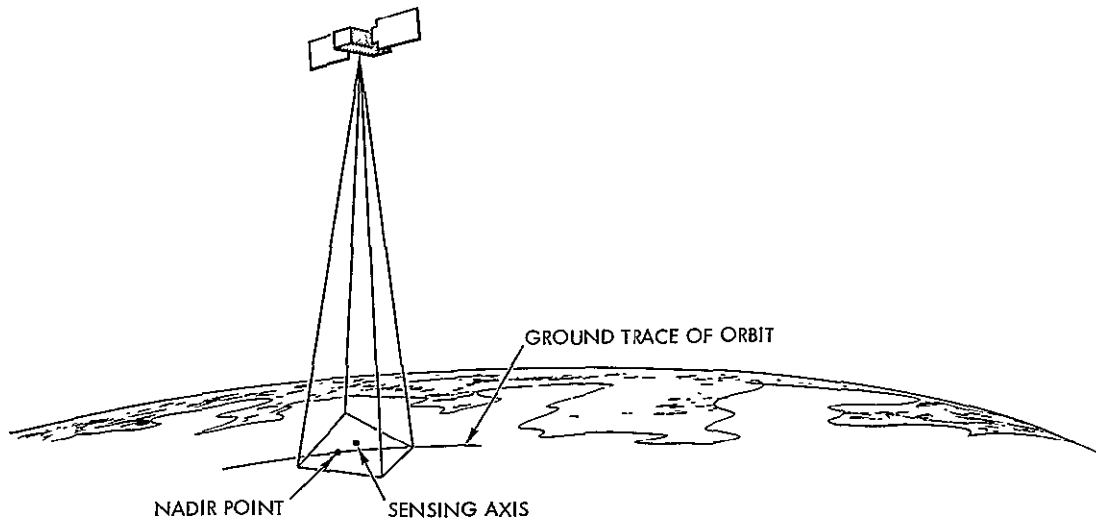


Figure 6-1

THE PRIMARY EFFECT of attitude errors on RBV images is a translation. For large errors a small keystone effect is also introduced.

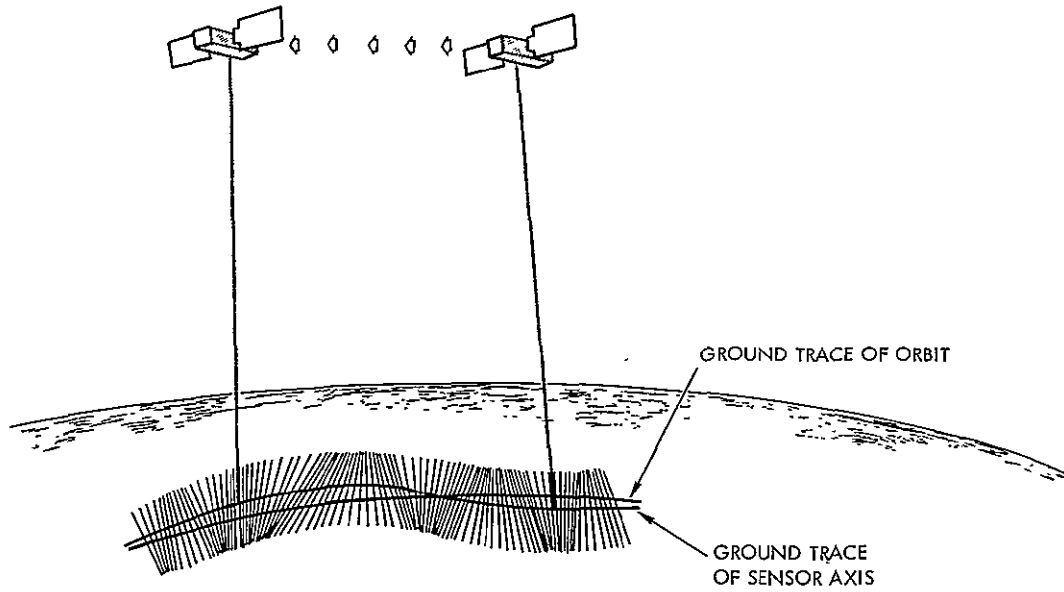


Figure 6-2

ATTITUDE RATES and absolute yaw errors produce geometric distortions in MSS images

From a practical viewpoint the 2 nautical miles required and the 200-foot desired objectives are different not only from an attitude determination viewpoint but more importantly from the overall ERTS system viewpoint. In designing an attitude determination system for 2 nautical mile accuracy the allocation of errors in the error budget need not be overly stringent. Several approaches exist which will meet this goal. The selection is between candidates providing accuracies from about 2000 to 12,000 feet, in various states of development and costing up to \$1,000,000. To achieve the 200-foot accuracy goal, however, requires not only a much more comprehensive knowledge of the error sources but the ability to smooth over and interpolate between absolute attitude fixes whether they be from the spacecraft or from ground truth. This logically suggests the addition of inertial measuring means to supplement the 2 nautical mile absolute attitude measuring equipment:

The attitude determination system selected easily fulfills the 2 nautical mile design goal and provides relative picture geometry accurate to within 750 feet without ground truth. The salient aspect of our proposed system is that from a hardware viewpoint no additional on-board equipment is required. Elements of the existing attitude control system perform the additional attitude determination functions needed for data gathering.

The selected system uses horizon sensor information for sensor pitch and roll determination, and the yaw gyro error for yaw information. Horizon sensor information is converted to pitch and roll attitude based on a calibrated horizon profile. Modeling of spacecraft inertial motions from spacecraft telemetry is used for the desired 200-foot goal. Pitch and roll attitude together with the yaw gyro input and reaction wheel data from each of the three axes are processed by filtering equations of the weighted least-square type to yield attitude rates.

The mapping accuracy of the proposed attitude determination system for the 2 nautical mile case is presented in Table 6-1. Allocation has been based on several premises. First, that relative geometric errors will be removed to the best extent possible without ground truth. Thus, knowledge of attitude rates becomes important for MSS images. Second, such factors as terrain height and film warpage which are not

Table 6-1. Allocation (in feet) of Mapping Inaccuracies
(2 nautical mile case)

	RBV	MSS
Ephemeris	1,000	1,000
Pitch and roll (0.15 deg)	11,000	11,000
Yaw (0.3 deg)	3,000	2,000
Pitch and roll rates (0.004 deg/sec)	-	4,000
Alignment	500	500
Sensor	4,000	600
Ground processing	400	400
Film warpage	600	400
Terrain	700	700
Total rms	12,150	11,950

controllable within the ERTS system will be ignored in establishing synthesis goals but included in performance evaluation. Finally, that knowledge of certain factors such as sensor alignment, constants of the spacecraft dynamic model and even geophysical parameters will be repeatedly updated as ground truth inputs permit their refinement.

In the attitude determination study various alternatives were considered. The alternatives consist of (1) an attitude reference package and, (2) a means of obtaining attitude rate information. In detail, these are:

- a) Obtain absolute attitude from either:
 - Horizon observations and gyro compass
 - Star trackers
 - Star scanner

- b) Obtain attitude rates from:
 - Inertial reference unit (i. e., rate gyro)
 - Ground modeling of spacecraft inertial motion using inputs from spacecraft telemetry

It should be noted that ground truth is also a measurement which gives absolute attitude and rate information but is not included since it is a common factor for the various alternatives.

A technical summary of the alternatives is shown in Table 6-2. The selected attitude determination system is based on the second column with standard supporting software, i. e., horizon observations and gyrocompass with ground modeling of body inertial motion. This system is discussed from an overall point of view in the next section and details of this and other systems studied follow in succeeding sections.

6.1 THE SELECTED SYSTEM

The TRW approach to the attitude determination problem is to achieve the 2 nautical mile accuracy requirement and to make a reasonable compromise on the 200-foot desired goal (for MSS image, TRW achieves 750 feet), with a system which entails minimum risk. As indicated previously, the system is:

- 1) Obtain absolute attitude data using horizon sensors and gyrocompass
- 2) Obtain rate information by the ground modeling of spacecraft inertial motion

The conversion of the horizon sensor and gyrocompass data into attitude information is well known. One point here however needs to be emphasized. That is, to achieve the 2 nautical mile accuracy using horizon scanners, TRW proposes to develop a software program to periodically update the radiance model. As will be shown, the radiance model is rather slowly varying and hence calibration is entirely feasible.

The inertial modeling is based on the integration of the laws of mechanics applied to rotating bodies. A one-dimensional example is given to convey the basic concept without introducing the maze of technical details which accompany the analysis in three dimensions. Basically we can write:

Table 6-2. Attitude Determination Technical Summary

Parameter	Earth Sensor Assemblies			Star Sensors			
	ESA (TRW)	ESA (TRW) RWD (TRW)	ESA (TRW) Gyro (TRW)	SM (ODC) RWD (TRW)	SM (ODC) Gyro (TRW)	ST (TRW) RWD (TRW)	ST (TRW) Gyro (TRW)
2 n mi performance (n mi)	1.9	1.9	1.9	0.6	0.6	0.6	0.6
200 ft performance (ft)		750	200	400	200	400	200
Model status			Breadboard	Experimental*	SM: experimental Gyro: breadboard	Development	ST: development Gyro: breadboard
Size (in.)			6 x 6 x 9	23 x 5 x 5	SM: 23 x 5 x 5 Gyro: 6 x 6 x 9	12 x 8 x 8	ST: 12 x 8 x 8 Gyro: 6 x 6 x 9
Weight (lb)			15	14	SM: 14 Gyro: 15	23	ST: 23 Gyro: 15
Power			45 w 28 vdc	8 w	SM: 8 w Gyro: 45 w 28 vdc	15 w 28 vdc	ST: 15w 28 vdc Gyro: 45 w 28 vdc
Thermal conditioning			Conduction cooling	Conduction cooling	SM: conduction Gyro: conduction	Conduction cooling	ST: conduction Gyro: conduction
Qualified environment			None	None*	SM: none* Gyro: none	None	ST: none Gyro: none
Reliability			0.965 (1 yr) (4 gyro configuration)		SM: Gyro: 0.965 (1 yr)	0.994 (1 yr)	ST: 0.994 (1 yr) Gyro: 0.965 (1 yr)
Code:	ESA	Earth Sensor Assembly		ST	Star Tracker		
	RW	Reaction Wheel Data		*Similar units space qualified			
	SM	Star Mapper					

9-9

$$T_E = (I_B + I_W) \ddot{\Theta}_B - I_W \ddot{\Theta}_W$$

where: T_E = external torques

I_B = body inertia (without the wheel)

I_W = wheel inertia

Θ_B = body angle relative to nadir

Θ_W = wheel position relative to an arbitrary reference

This equation can be integrated twice and rearranged to obtain:

$$\Theta_B = \frac{I_W}{I_B + I_W} \Theta_W + At + B + \iint_{\infty}^{tt} T_E dt$$

where A and B are constant of integration. T_E is a slowly varying function of time and therefore it is meaningful to rewrite the equation as follows:

$$\Theta_B = \frac{I_W}{I_B + I_W} \Theta_W + A(t) t + B(t)$$

where A(t) and B(t) are slowly varying functions of time and incorporate effect of the torque term. Analysis shows that over any single 100 x 100 mile picture the error introduced by holding A and B constant is negligible.

Errors in Θ_B and consequently the apparent location of points on the ground will depend on errors in the remaining terms in the foregoing equation. For relative geometric accuracies, knowledge of the B term for the pitch and roll channels need not be precise because its primary effect is a translational error which later may be removed through ground truth. The value of Θ_W is telemetered to the ground with sufficient accuracy to yield an uncertainty on the ground much less than a resolution element and therefore this error can be ignored. Uncertainty in A therefore is the only important source of error.

A physical interpretation of the importance of A is as follows: If the total angular momentum of the system is M the wheel must be biased with a speed $\omega_w = \frac{M}{I_w}$. Thus the wheel position, Θ_w , will be accumulating at a steady rate. The A term merely offsets this accumulation so that Θ_B does not change with time over the 28-second interval. While this example has assumed a steady body pointing, motion within the limit cycle is still accounted for in the deviation of the wheel position from its mean increasing value.

The value of A to use is easily determined if two ground truth points straddling an image are obtained. In this case system performance will approach 200 feet. In the absence of ground truth, horizon sensor data which is fairly noisy must be used. This limits the accuracy to about 600 feet.

6.2 EARTH SENSOR ASSEMBLY/GYRO

The first attitude determination system studied used the same hardware components and electronic mechanizations being used for the ERTS attitude control system. The parameters of the TRW advanced OGO horizon sensor and the OGO gyro assembly were used in the analysis. It was also assumed that the vehicle was stabilized in the normal attitude control mode during attitude determination. The analysis was performed assuming that all four horizon sensor heads are tracking the earth's edge.

The principle by which the earth sensor assembly determines attitude in the pitch and roll axes is illustrated in Figure 6-3. Each tracking head establishes a line-of-sight to a specific point in the horizon's radiance profile. For each sensor head the angle from the line-of-sight to the earth sensor assembly centerline is converted to an electrical voltage whose value is telemetered to earth. The attitude determination system uses the resulting values minus known error components, for estimating pitch and roll attitude errors.

The method by which yaw attitude error is determined is illustrated in Figure 6-4. The input axis of the yaw gyro nominally lies in the orbital plane tilted 45 degrees between -yaw and -roll axes. Since the gyro is electronically mechanized in a rate mode, a voltage is produced which is proportional to yaw angle times orbital rate plus some unwanted

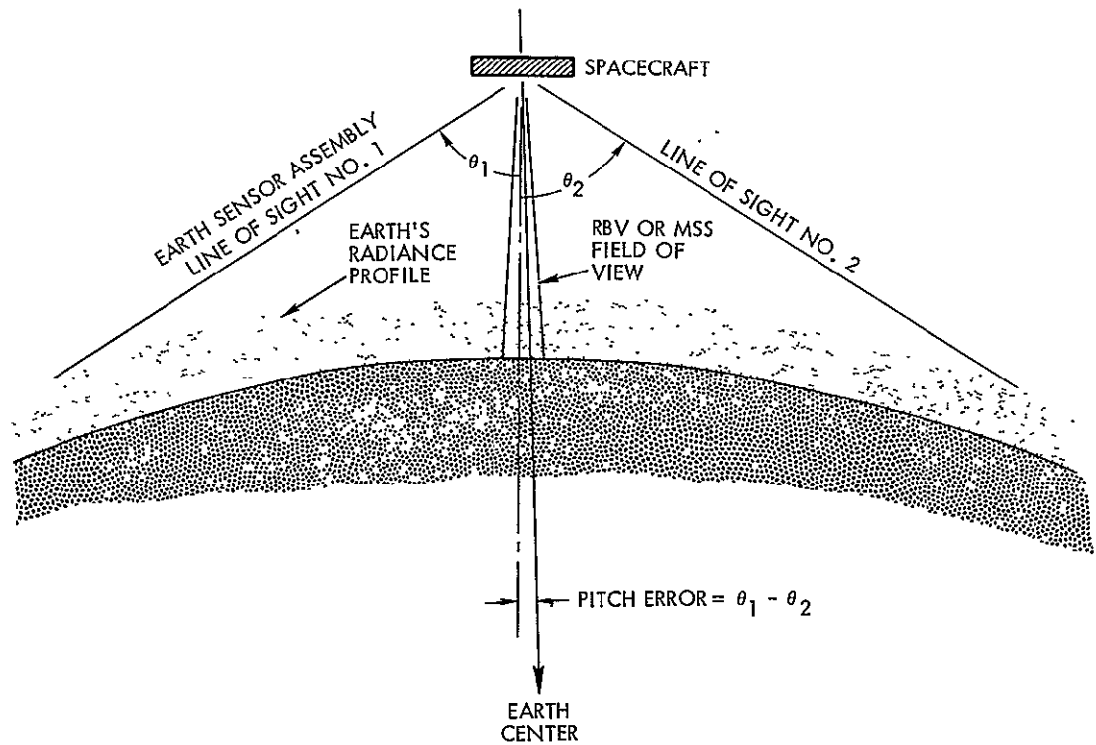
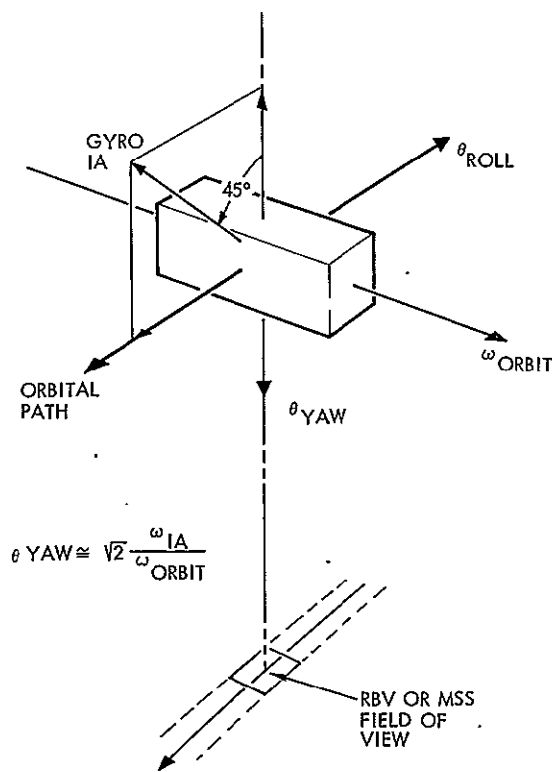


Figure 6-3
PITCH AND ROLL orbital attitude determination



$$\theta_{YAW} \cong \sqrt{2} \frac{\omega_{IA}}{\omega_{ORBIT}}$$

terms. This voltage is telemetered to earth. The attitude determination system uses this voltage signal, minus known error components, for its estimate of yaw attitude.

The evaluation of this type of attitude determination system proceeded in two parts. First, the major contributing error sources were isolated and investigated. For pitch and roll these turned out to be horizon model errors and earth sensor assembly instrument

Figure 6-4
YAW ORBITAL attitude determination

errors. For yaw the gyro drift rate and roll cross-coupling errors predominated. Next, an attitude determination mechanization was postulated and an error analysis was performed. The principal ingredients to the error analysis are listed in Table 6-3, along with their rms values derivable in the following sections.

Table 6-3. Total Horizon Tracker, Earth Horizon Model Error Components

Horizon tracker instrument errors (deg)	
Long term biases	0.028 (1 σ)
Short term, noise in 0.1 to 1.0 Hz bandwidth	0.040 (1 σ)
Horizon model accuracy (deg)	
1 km (1 σ)	0.016 (1 σ)
Atmospheric variability (deg)	
Deviation from mean in 10 to 15 deg latitude band, 1 km (1 σ)	0.016 (1 σ)
Total (long term)	0.04 (1 σ)

6.2.1 Horizon Tracker Instrument Errors

The long-term instrument error in the output of the horizon tracker contains terms which result from the failure to track a constant point on the earth's horizon radiance profile, and from nonlinearity, and gain changes in the angle readout. The total long term error is 0.028 degree (1 σ). An additional source, electronic noise, introduces a short term error of 0.04 degree (1 σ) in a 0.1 to 1.0 Hz bandwidth. The basis for these values is given in Table 6-4 and explained as follows:

- Noise. The noise expected in the 0.1 to 1.0 Hz bandwidth of the horizon tracker output is 0.040 degree (1 σ). The addition of a filter with a 1-second time constant before telemetry, could be expected to reduce this noise to 0.016 degree (1 σ), and to reduce any residual dither component to an insignificant amount. Operationally, this approach is more advantageous than ground filtering and is planned in the design.

Table 6-4. Summary of Horizon Tracker Performance Affecting Attitude Determination Accuracy

Long Term Errors (deg)	
Tracking position error	0.022*
Position error caused by earth radiance variation	0.005*
Null axis uncertainty	0.005**
Scale factor uncertainty	0.006*
Total	0.028 (1 σ)
Short Term Errors (deg)	
Noise in 0.1 to 1.0 Hz bandwidth	0.040 (1 σ)*

*Quoted error determined by actual measurement or comprehensive analog simulation.

**Estimated accuracy for each tracker.

- Total Long Term Error. The total long term error is the root sum square of the tracking position error, null axis uncertainty, and the scale factor uncertainty added to the radiance-caused position error.
- Tracking Position Error. A tracking position error occurs as gain drifts within the tracking loop cause the point tracked on the earth's horizon to shift. The gain drifts are caused primarily by environment, and aging of critical components within the loop.
- Radiance-Caused Tracking Position Shift. A simulation of the tracking process, which maintained a constant normalized horizon radiance profile showed the tracked point to be at 38 percent of the peak radiance for the minimum earth radiance, and at 33 percent of the peak radiance for the maximum earth radiance, thus shifting the tracked point.
- Null Axis Uncertainty. The alignment between the horizon tracker null axis and the payload axes will be measured on orbit using recognizable landmarks. This procedure verifies the alignment prior to launch, and corrects for alignment shifts that could result during launch.

- Scale Factor Uncertainty. The linearity of the positor and readout circuitry is within 1.7 percent near null. This number is the rss of several terms. The positor pickoff linearity over the operating temperature range is 1.1 percent. The position amplifier gain variations can be maintained to within 0.5 percent. A stability of 0.8 percent has been assumed for the signal demodulation and telemetry conditioning. The error expected over the ± 1 degree excursion of the tracker from null during normal operation introduces a possible 0.006-degree (1σ) error due to scale factor variation.

6.2.2 Horizon Model and Atmospheric Variability

The earth horizon model expresses the altitude of the mean point tracked by the earth horizon tracker in a geocentric coordinate system, so that the necessary transformation can be made from horizon tracker angle data to geocentric observatory pointing. Thus the horizon model combines the earth's physical oblateness, and the atmospheric variability which causes the tracked point to vary with respect to mean sea level. The deviation of the earth's surface from that of a sphere is well known. A detailed investigation of this deviation was not made. Rather, a simple oblate spheroid was assumed, and the study effort directed towards establishing the variation of the tracked point due to atmospheric effects.

A horizon model will be constructed during the normal operation of the observatory vehicle from the angles measured by the four horizon trackers and the known orbital position of the vehicle. The four trackers are mounted in pairs such that one pair provides attitude information about the pitch axis, while the other provides information about the roll axis. The trackers in each pair track points widely separated on the earth. The sum of the two tracker angles in a pair is the angle between tangents to the tracked points from the vehicle. This angle determines the length of the chord between the two points, and the angle between the horizon normals at the points. Motion of the vehicle within the limit cycle of the control system introduces only an insignificant error. The horizon model is constructed by filtering the telemetered tracker voltages (angles) and the approximate latitude of the tracked points which are determined from the orbital position. Although geocentric longitude is not explicitly included as a variable, any effects correlated with longitude may be accommodated by periodic updating of the model.

The important features of the horizon tracker operation are depicted in Figure 6-5. The tracker responds to radiation in the spectral band centered near 15 microns where carbon dioxide causes strong atmospheric radiation. As the instantaneous field of view is dithered across the horizon, the horizon radiance profile is optically integrated to produce the earth radiance signal. The tracking loop tracks the horizon by driving the center of the diether to the point where the duty cycle of the earth radiance signal is equal. Variations of the tracked peak-radiance point, obtained while maintaining a constant normalized horizon radiance profile is considered an instrument error and is included in Table 6-4. If the shape of the normalized radiance profile

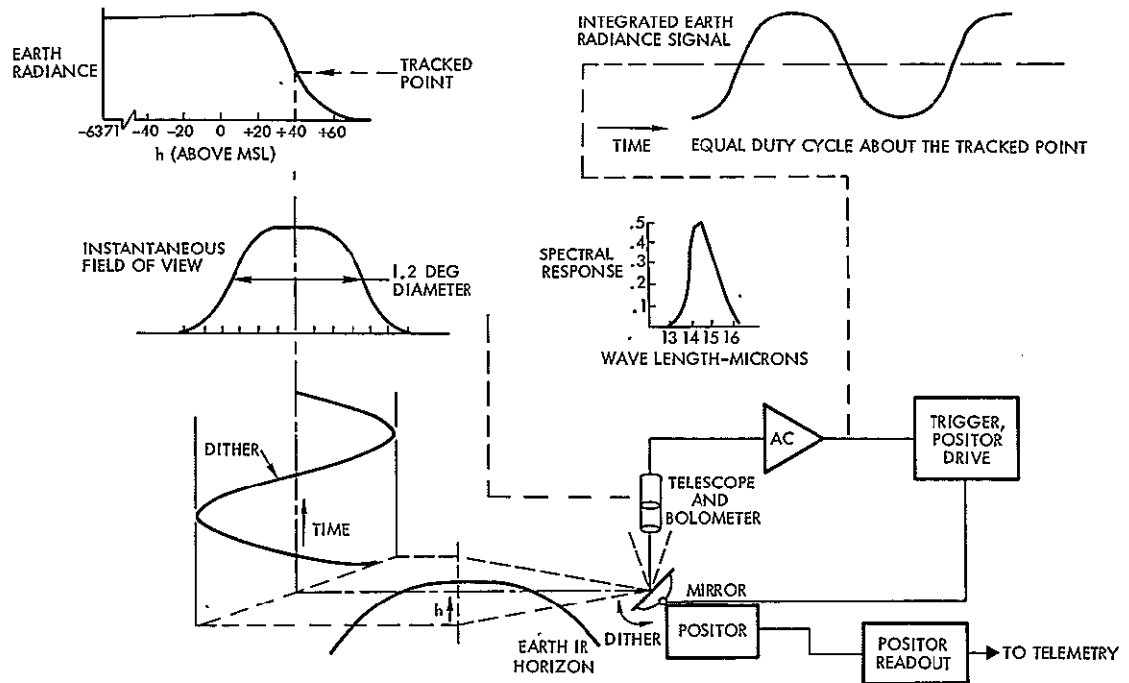


Figure 6-5
HORIZON TRACKER block diagram showing the optical integration of the earth's radiance profile

were to change with, or independently of, the value of the peak radiance, an additional tracking loop error would occur. However, no significant variation in profile shapes was observed in a volume of many normalized horizon radiance profiles covering all expected atmospheric conditions

in the 14 to 16.3 micron spectral interval.¹ Thus the system can be considered linear about the tracked point, and the principle of superposition can be used. That is, the variations in the altitude of the tracked point due to atmospheric effects can be investigated independently of the detailed interaction of the horizon radiance profile, field of view, and tracking loop.

No body of empirically measured horizon radiance profiles exists that could be used to determine the atmospheric-caused variation of the tracked point. It is possible, however, to calculate the horizon radiance profile from theoretical considerations of the atmospheric radiation processes, and measured meteorological data, such as pressure, temperature, and carbon dioxide concentration, as a function of altitude. Horizon radiance profiles calculated in this manner have shown very good agreement with actual profiles measured by high resolution radiometers.² A comprehensive body of meteorological data has been assembled for the purpose of performing these calculations.³ The meteorological data has been grouped in sets, and subsets which describe various aspects of atmospheric variability. Finally, horizon profiles of the available radiance have been computed for each subset in the 14 to 16.3 micron spectral band.¹ The effective radiance in the spectral band of the horizon tracker is directly proportional (to a high degree of accuracy) to the available radiance. Thus the variation of points on the normalized horizon profiles in the two bands will be identical.

¹ Thomas, R., Jones, E. E., Carpenter, R., and Ohring, G., "The Analysis of 15.3 Infrared Horizon Radiance Profile Variations Over a Range of Meteorological, Geographical, and Seasonal Conditions," NASA CR-725, April 1967.

² Mckee, T. B., Whitman, R. I., and Davis, R. E., "Infrared Horizon Profiles for Summer Conditions from Project Scanner," NASA TN D 4741, August 1968.

³ Peterson, R. E., Scheutz, J., Shank, W. E., and Tang, W., "Deviation of a Meteorological Body of Data Covering the Northern Hemisphere in the Longitude Region Between 60°W and 160°W from March 1964 through February 1965," NASA CR-723, April 1967.

A further study has grouped the data reported in NASA CR-723 into four sets.⁴ Each set consists of data taken during a single month over the range of latitudes available, so as to provide a seasonal comparison. Then various mathematical representations of idealized horizon sensors were generated. Each representation, or "locator," was used to determine the altitude variation of a specific point on the horizon profile over the selected set of atmospheric conditions.

Of the locators reported in NASA CR-726, the one designated "L4(5), Integral of Normalized Radiance," best describes the point tracked by the horizon tracker. The horizon tracker integrates the radiance profile optically, while the tracking loop effects a normalization of the integrated radiance. Locator L4(5) tracks a point on the radiance profile near 30 percent of the peak radiance. Of the four months studied, August 1964 and January 1965 are the extreme cases. This data is shown in Figure 6-6. The mean and standard deviation is shown for the 15-degree latitude band centered about each point. In addition, the difference between the radii of a sphere with the volume of the earth, and a simple oblate spheroid model of the earth is shown for comparison.

The standard deviation within each narrow latitude band shown in Figure 6-6 is indicative of the longitudinal and temporal variation within the band. Each latitude band contains data separated by as much as 100 degrees of longitude. Thus at any given time, the standard deviation should be interpreted as largely the variation in located horizon altitude as a function of longitude within the narrow latitude band, and longitude range of 60 to 100 degrees. At any given location within this region, temporal variations of the order of the standard deviation can also occur.

The meteorological data compiled in NASA CR-723 supports this interpretation. In the 14 to 16.3 micron spectral band, only atmospheric phenomenon above the troposphere affect the located horizon.

⁴ Thomas, J. R., "Deviation and Statistical Comparison of Various Analytical Techniques Which Define the Location of Reference Horizons in the Earth's Horizon Radiance Profile," NASA CR-726, April 1967.

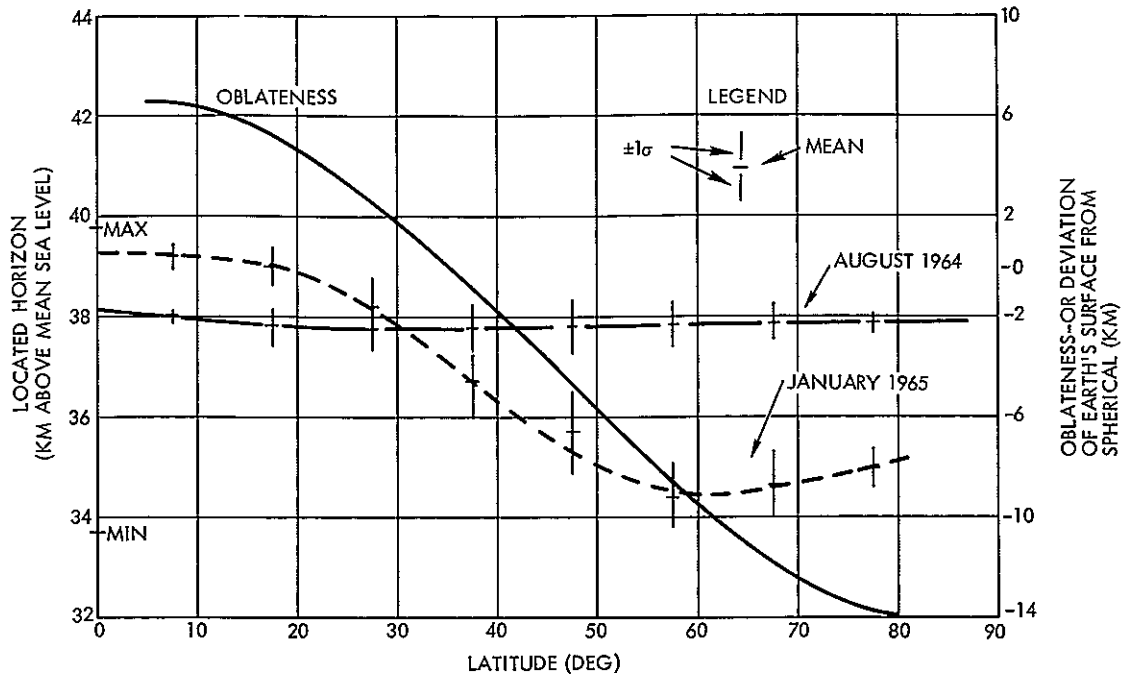


Figure 6-6

LATITUDE VARIATION of located horizon with sensor and yearly extremes

The two most important meteorological parameters are temperature and pressure. Both temperature and pressure variations with altitude are shown to be smoothly varying over both latitude and longitude at any given time. The long term variation in these parameters at a given latitude are seasonal in nature. Short term variations in the long term trend are both latitude and seasonally dependent. For example, quasi-cyclic variations in the low latitude during summer may be of the order of one month in duration. Cyclic variations in the high latitudes during winter, however, may be of three to ten days in duration. The most dramatic change occurs in the spring at high latitudes when a rapid warming occurs over a period of a few days to one week. Thus, unlike the gradual transition from summer to winter, the transition from winter to summer-like conditions is rapid. The cyclic nature of the atmospheric conditions establishes the frequency of horizon model updates. That is, during the summer, updates as seldom as once a month would seem reasonable over low altitudes, while updates may be required every orbit over the high latitudes during winter. Similar

conditions exist in the Southern hemisphere. However, slightly larger variability may be expected.

The conclusions drawn from NASA CR-726 are supported by the results of other studies, which were based on meteorological data covering more than one year. One study that provides qualitative support reports the existence of a seasonally-dependent trend in the mean located altitude with latitude.⁵ These conclusions were based on three years of meteorological data from the Northern hemisphere averaged as if they had been recorded during a single year. For the integral of normalized radiance locator, the worst case trend of 6 km occurred during November with the worst standard deviation of 3 km occurring at 80-degree latitude. The failure to separate the data from each year results in a large standard deviation since mean values can be expected to vary from year to year. Another study which was undertaken to establish the validity of the previous studies associated with NASA CR-726, and to determine the existence of any cycles longer than the one year cycles seen previously, considered each of the three years starting from 1964 independently.⁶ A body of meteorological data was assembled, horizon radiance profiles generated, and the altitude variation of points studied using a number of locators. Unfortunately, L4(5) was not one of those used. However, another integral of normalized radiance locator L4(2.5), was used. This locator tracks a point near 20 percent of the peak radiance. Even though the altitude tracked is somewhat higher than that tracked by L4(5), the standard deviation as reported in NASA CR-726 is expected to be only slightly smaller than that of L4(5). An additional complication arises, since the results of the study were only reported in wide latitude bands. This, however, tends to increase the value of the calculated standard deviation.

⁵ Dodgen, J. A., and Curfman, H. J., Jr., "Accuracy of IR Horizon Sensors as Affected by Atmospheric Considerations," NASA Langley Research Center, Hampton, Virginia, L-6951.

⁶ Bradfield, L. G., and Nelson, G. D., "Located Horizon Variation Study, Final Report," NASA CR-66748, January 1969.

Table 6-5 summarizes the computed standard deviations for L4(2.5) in summer and winter. These standard deviations closely agree with the standard deviations shown in Figure 6-6, and confirm the choice of 1 km as a conservative 1σ value. The reported quasi-biennial cycle is of only academic interest, since the horizon model is generated without a priori assuming a frequency for the variations of the deterministic latitude trend.

Table 6-5. Summary of Standard Deviations Reported in NASA CR 66748 for Locator LR(2.5)

Latitude Band (deg)	Standard Deviation (km)				
	Summer			Winter	
	August			January	(December)
	1964	1965	1966	1965	1966
0 to 20		0.5	0.4	0.5	0.7
20 to 35		0.7	0.6	0.7	0.7
35 to 55		1.1	0.75	0.75	0.75
55 to 80	0.6	0.3	0.3	0.85	1.6

6.2.3 Horizon Tracker Accuracy Analyses

The preceding paragraphs have shown that, in the case of pitch and roll, the predominant error sources are the earth's radiance profile and the earth sensor assembly. The error from the radiance profile is essentially an unobservable bias while the earth sensor assembly error consists of a small bias plus relatively large zero-mean noise. So the problem for pitch and roll attitude determination is essentially that of smoothing a noisy earth sensor assembly signal, not expecting to do any better than the rss of the radiance profile and assembly bias errors. The problem becomes a little more complicated, however, when the effect of the attitude control loop limit cycle is considered. The reaction wheel motor torques are moving the vehicle in a limit cycle, and the earth sensor assembly signal is measuring the vehicle oscillations within the limit cycle in addition to the noise and bias errors.

In view of the nature of the problem, a Kalman filter* mechanization for pitch and roll attitude determination was selected. The implication should not be made here that the final mechanization chosen for attitude determination necessarily will be a Kalman filter. Often it is more practical to use some sort of suboptimal filter or a classical controls mechanization. The advantage of using the Kalman filter for the analysis of this type of problem, however, is that it automatically produces a statistical error analysis. It also gives the best result that can be obtained for the least squares criteria.

A Kalman filter digital computer program was coded in Fortran II language in order to analyze the ERTS attitude determination problem. The single axis error model shown in Figure 6-7 was used in the filter. The model assumes that the times at which the reaction wheel motor torques occur are known. Instead of actually simulating the attitude control loop and using the simulated motor torque occurrence times, the approximation was made that they occurred periodically every 10 seconds and lasted for 0.6 second. The 10-second average period was based on actual OGO flight data. The uncertainty in torque magnitude was modeled as an exponentially correlated random variable with magnitude of 0.002 ft lb. This is one-tenth the nominal torque value. A correlation time constant of 10 seconds was selected. With a 1-second sampling time, this value was low enough to prevent the filter from estimating the torque uncertainty. It was felt that this was closer to what could really be done with an actual system. The effect of reaction wheel motor windage was also included in the error model. The windage time constant is specified to be 300 seconds.

The results of the Kalman filter analysis show that with high frequency (bandwidth greater than 1 Hz) noise of 0.06 degree (1σ) in the earth sensor assembly signal, the Kalman filter can smooth out the noise to approximately 0.01 degree. When this is added to the radiance model error and the earth sensor assembly bias, the total accuracy in

*Sorenson, H. W., "Kalman Filtering Techniques," Advances in Control Systems, Vol. 3, Academic Press Inc., New York, 1966.

either the pitch or roll axis is about 0.05 degree (1σ). A graphical representation of these results is also presented in Figure 6-7.

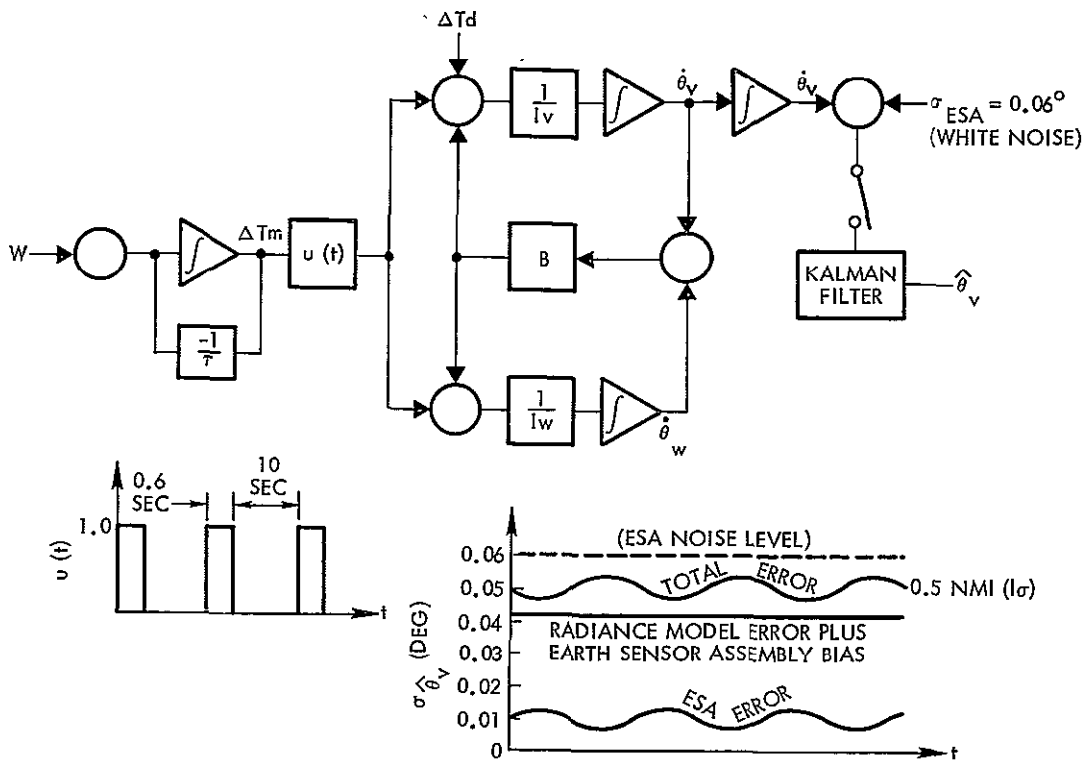


Figure 6-7
ANALYSIS OF EARTH SENSOR assembly/yaw gyro system pitch and roll errors

The error analysis of the yaw attitude determination is straightforward. Referring to Figure 6-4, the yaw error is

$$\sigma_{yaw}^2 = \frac{2\sigma_{gyro}^2}{\omega_{orbit}^2} + \sigma_{roll}^2$$

where σ_{yaw} = yaw attitude error

σ_{roll} = roll attitude error

σ_{gyro} = gyro drift rate

ω_{orbit} = orbital rate

Using a gyro drift rate of 0.17 deg/hr and a roll attitude uncertainty of 0.05 degree, the yaw attitude error is 0.08 degree (1σ).

Figure 6-8 shows the relationships between orbital attitude error and ground error to a first-order approximation. Converting the above mentioned attitude errors into mapping errors and calculating the rss, the total ground error is 1.87 nautical mile (3σ). This is primarily made up of pitch and roll errors since yaw angular errors operate on one-seventh the distance that applies for pitch or roll.

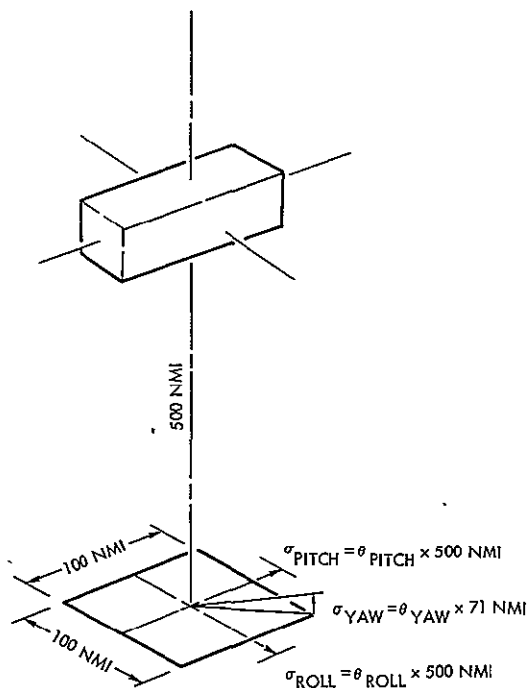


Figure 6-8
RELATIONSHIP between orbital attitude errors and mapping errors

the transit of a star across a slit. The transit times of multiple star crossings are then telemetered to a ground computer which correlates stars in a stored star catalog to transit crossings and determines spacecraft attitude. The specific star mapper considered was a unit developed by Control Data Corporation, and whose characteristics are summarized in Table 6-2.

In order to achieve 2 nautical mile mapping accuracy, both pitch orbital attitude or roll orbital attitude must be known to within 0.05 degree (1σ). If the rule-of-thumb is used, that the measuring instrument

6.3 SYSTEMS USING STAR SENSORS

The second attitude determination system studied uses star sensors to determine three-axis orbital attitude. A pictorial representation of a star mapper is presented in Figure 6-9. The star mapper is rigidly attached to the spacecraft and has no mechanical gimbals. As the spacecraft moves along the orbital path, its inertial attitude changes since it is being maintained earth-oriented by the attitude control system. As the spacecraft rotates, the star images move across the slit pattern on the reticle of the star mapper. The detector produces a pulse indicating

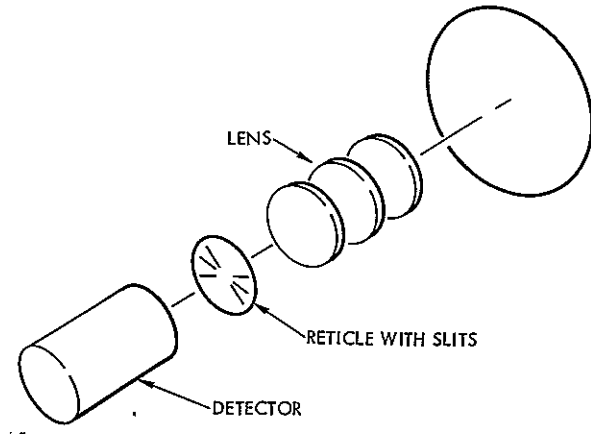


Figure 6-9
STAR MAPPER ASSEMBLY

must be 10 times better than the accuracy desired, then the star mapper should have an accuracy of 0.005 degree (1σ) or approximately 20 arc-seconds. Since this accuracy is well within the state of the art, it was used in the analysis.

Two criteria were used in the selection of the field of view of the star mapper. First, in order to optimize the use of the

stars in the star catalog, the field of view was made 10 times larger than the peak-to-peak excursions of the attitude control system. Since the yaw attitude limit cycle boundaries are ± 0.7 degree, the field of view was selected to be 15 degrees. The second criterion involved insuring that the field of view was large enough to give a sufficiently small average time between star transits. Another star mapper parameter directly connected with this criteria is the magnitude of the star which the star mapper can detect. To obtain a rationally based method for selecting these two parameters, a star frequency investigation was undertaken.

Taking into account the orbital rate of the ERTS spacecraft, and assuming the two-star-mapper configuration shown in Figure 6-10, calculations were made determining the average time between star transits for a number of values of minimum detectable star magnitude. The results of the calculations agreed with those obtained by others in the industry and are presented also in Figure 6-10.

Spacecraft rate can be estimated to an accuracy of approximately 0.0003 deg/sec. Employing the relationship

$$\Delta t = \frac{\sigma_{\text{attitude}}}{\sigma_{\text{rate}}}$$

it is seen that the maximum allowed error of 0.05 degree is reached within 170 seconds if a perfect star sighting is made.

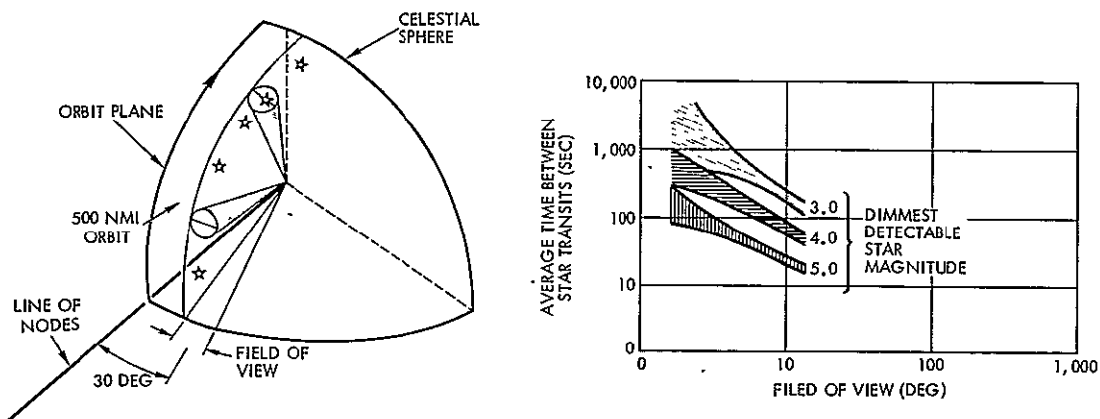


Figure 6-10
AVERAGE STAR transit interval

Combining the results of the star frequency investigation and the above calculation, it was decided to use the 15-degree field of view with a star mapper which could detect stars as dim as 4.0 M_v . This would allow a star transit approximately every 70 seconds (average) which is less than half the maximum time allowed.

Using the above performance parameter of a star mapper, a request for a proposal on such a sensor was sent to Edina Space and Defense Systems, Control Data Corporation. In response, CDC submitted a proposal for the star mapper shown in cross section in Figure 6-11. The proposal indicated compliance with all the performance parameters.

Each sensor head is 4.25 inches in diameter by 15 inches long. The size of the sensor processing electronics unit is 4 x 4 x 3 inches. The weight of the entire star mapper assembly (two heads and electronics) is 7 pounds. The power consumption of the assembly is less than 3.5 watts. The instrument exceeds the sensitivity requirement of 4.0 M_v discussed above.

Having chosen a star mapper, and having gone through the mechanics of computing the average time between star transits for a particular star mapper configuration, the next question which arose was: how good is the star mapper really going to be?

First, it was assumed that the star mapper error is an unobservable bias. In other words, it is not white noise which can be averaged

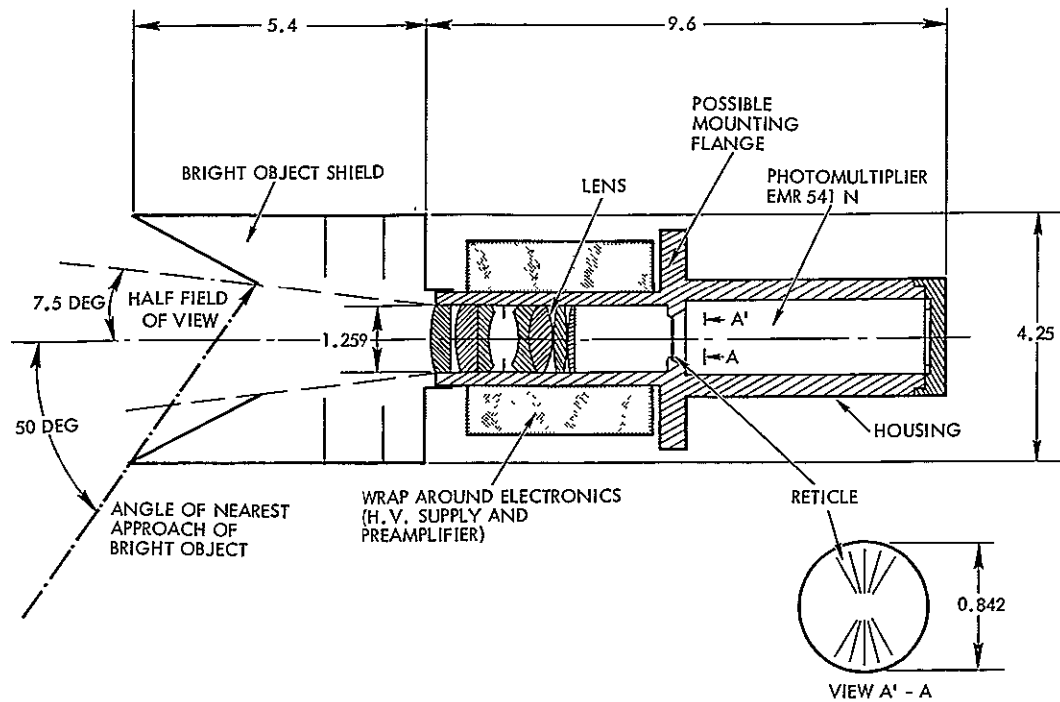
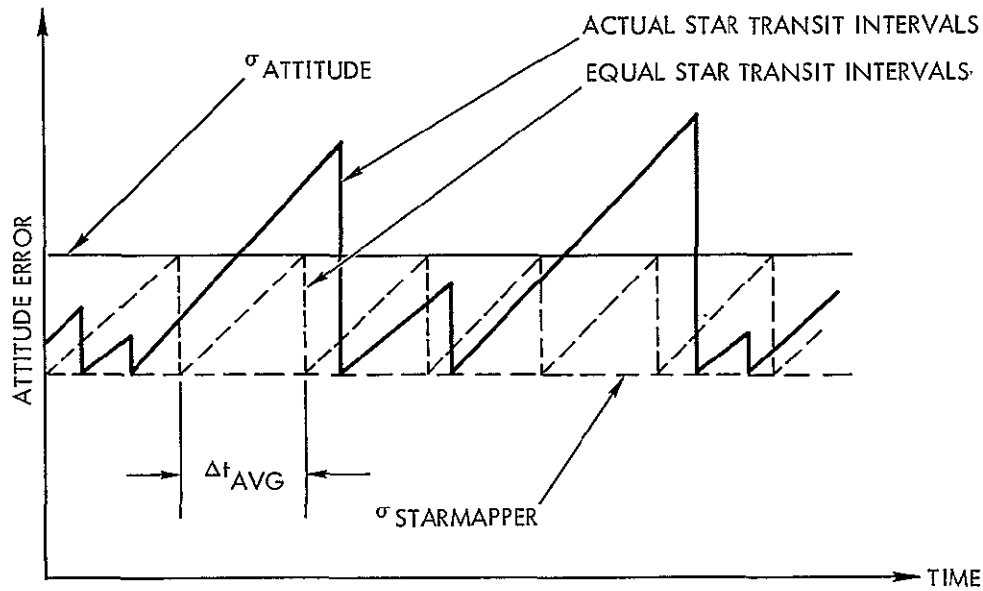


Figure 6-11
CONTROL DATA CORPORATION star mapper schematic

out with multiple transits; nor a correlated random variable which can be estimated with a Kalman filter. The accuracy at the time of a star transit will never be better than that of one star mapper sighting. The second assumption was that optimal estimation techniques using star information are not employed to improve the knowledge of vehicle rate. The final assumption was that the degraded accuracy at the end of an average star transit interval, before the new transit, is representative of the rms accuracy which would be obtained by integrating over an actual, non-equal interval, distribution of stars. The graphical and mathematical implications of these assumptions are shown in Figure 6-12.

Using the accuracy criteria specified above, the star mapper parameters, and the spacecraft rate uncertainty from Section 6.8, it was found that the single axis orbital attitude uncertainty was 0.022 degree (1σ). Converting this attitude error to mapping accuracy (refer to Figure 6-8), a total mapping error of 0.80 nautical mile (3σ) was computed. This figure is well within the ERTS requirement of 2 nautical miles.



$$\sigma_{\text{ATTITUDE}}^2 = \sigma_{\text{STARMAPPER}}^2 + (\Delta t_{\text{AVG}} \sigma_{\text{RATE}})^2$$

Figure 6-12
ATTITUDE ACCURACY using star mapper (single axis)

6.4 CONCLUSION CONCERNING ORBITAL ATTITUDE DETERMINATION

Using earth sensor assemblies and a yaw gyro mechanization results in an attitude determination system which just meets its accuracy goals—1.87 nautical miles with no additional hardware cost since the assemblies used are already on the spacecraft for the attitude control system. There is no added cost or schedule risk for developing, integrating, and testing additional hardware components. There is a minimal software cost, but such a cost will be present in any attitude determination scheme used for ERTS.

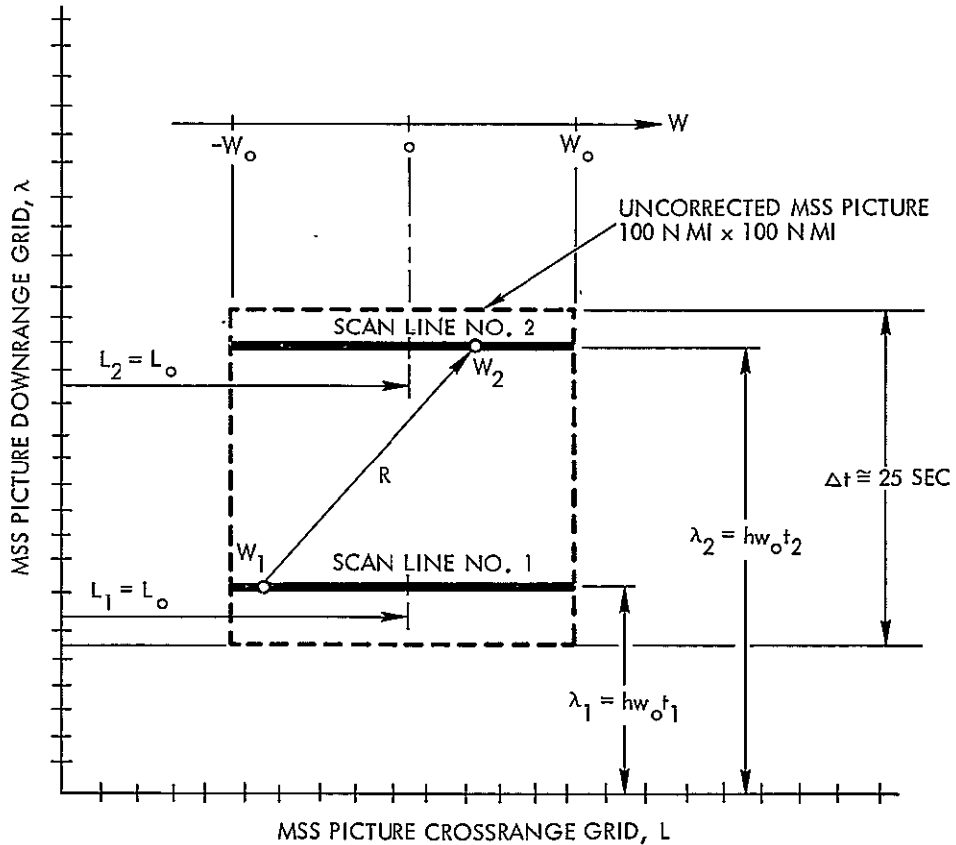
An attitude determination system using a star mapper can easily meet the accuracy requirement. The system analyzed in this study had an accuracy of 0.80 nautical mile. Such a system is well within the technical state of the art. Should a revised allocation of errors result in need for more precise attitude determination, the star-mapper instrument can be added to the spacecraft with little complication. The star mapper analyzed in this study is not a flight-proven unit, although similar units have been put in orbit.

Taking all factors into account, it is felt that the earth sensor assembly/yaw-gyro attitude determination system presents the most logical system from the standpoints of cost and accuracy. The analytical results show that it will meet the 2 nautical mile accuracy. It is definitely the lowest cost system. With analysis and application of radiance profile data, the 2 nautical mile accuracy requirement can be met and improved.

6.5 RELATIVE ATTITUDE DETERMINATION

The analysis reported here was aimed at achieving 200-foot accuracy with the aid of recognizable ground features. In order to bound the study, the design goal was set to establish 200-foot accuracy only within each 100 by 100 nautical mile picture. For example, if a crossroads was identified in the bottom left-hand corner of a picture in terms of latitude and longitude, it is desired to know the latitude and longitude of a feature in the upper right-hand corner to within 200 feet. The study concerned itself only with MSS pictures. A solution for the MSS picture automatically provides a solution for the RBV picture.

Figure 6-13 illustrates the 200-foot design goal for the case of an MSS picture. Fundamentally, the problem reduces to determining the relative distance, R , between two points, W_1 and W_2 . This distance is found in terms of downrange and crossrange distances. As shown in the figure, the nominal downrange coordinate of point W_2 is a function of the earth radius, R_e , the orbital rate, ω_o , and the absolute time, t_2 , at which the scan containing W_2 was taken. The nominal crossrange coordinate is a function of the orbital plane inclination. The length of a scan is determined by the MSS for any given orbit altitude. These nominal coordinates are for the case of zero spacecraft attitude control, i. e., the camera is kept pointing towards nadir and the scan is maintained normal to the flight path. Figure 6-10 also shows the downrange and crossrange picture first-order errors which occur when the spacecraft attitude errors are not zero. Crossrange error between points W_1 and W_2 is directly proportional to the change in roll attitude between the times scan lines 1 and 2 were taken. Downrange error between the two points is a function of three factors. First, it is



MSS PARAMETER : w_0
 ORBITAL PARAMETERS: L_0, h, w_0, t_0
 ATTITUDE ERRORS : ψ_P, ψ_R, ψ_Y

PICTURE ERRORS:

$$\begin{aligned} \delta L_1 &= h \psi_{R1} & \delta \lambda_1 &= h \psi_{P1} + w_1 \psi_{Y1} \\ \delta L_2 &= h \psi_{R2} & \delta \lambda_2 &= h \psi_{P2} + w_2 \psi_{Y2} \\ \delta (L_2 - L_1) &= h (\psi_{R2} - \psi_{R1}) & \delta (\lambda_2 - \lambda_1) &= h (\psi_{P2} - \psi_{P1}) + w_2 (\psi_{Y2} - \psi_{Y1}) \\ & & & + (w_2 - w_1) \psi_{Y1} \end{aligned}$$

Figure 6-13

MSS PICTURE ERROR due to spacecraft attitude error

directly proportional to the change in pitch attitude between the times scan lines 1 and 2 were taken. Next, depending on how close to the end of the scan line point W_2 is, it is directly proportional to the change in yaw attitude between scan lines. Finally, depending on the cross-range distance between the two points, it is a function of absolute yaw attitude. From these relationships it is easily seen that the worst total

error occurs between two points in diagonal corners. It is this case which the study analyzed in detail.

Two types of precision relative attitude determination systems were postulated and investigated. The first uses reaction wheel revolution data. This system adds no additional hardware to the spacecraft over and above that required by the attitude control system except wheel position instrumentation. It thereby avoids added cost, developmental, and schedule problems. The second uses a gyro inertial reference assembly.

6.6 SYSTEMS USING REACTION WHEEL DATA

Reaction wheel revolution data may be used to determine relative attitude change during a short time period. The study used parameters of the control reaction wheels with the vehicle stabilized in normal control and with solar array drive and gas inhibited. It was assumed that no significant momentum changes would occur from the tape recorders during the period; a verifiable assumption.

The principle from which relative body attitude may be determined from reaction wheel revolution data is basically simple. During the normal attitude control mode spacecraft motion is a direct reaction to wheel motion. The torque driving the spacecraft back and forth comes from the reaction wheel motor. The motor turns on for a fraction of a second approximately every 10 seconds under normal conditions. During this fraction of a second, a constant torque is applied to the spacecraft, and an equal and opposite torque is applied to the reaction wheel. This torque pulse produces an angular rate to both the spacecraft and the reaction wheel. Furthermore, the ratio of the spacecraft rate to the wheel rate is equal to the ratio of the wheel inertia to the spacecraft inertia. Knowing this relationship, it is a straightforward matter to compute the spacecraft attitude change due to the torque pulse if the relative rotation of the reaction wheel with respect to the spacecraft is known.

The evaluation of this type of relative attitude determination system proceeded in two parts. First, the major contributing error

sources were isolated and investigated. These turned out to be external spacecraft disturbance torques and the initial angular rates of the system. Next, a system mechanization was postulated and an error analysis was performed.

The equation expressing the relationship between the spacecraft attitude and the angle between the reaction wheel and the spacecraft is

$$\theta_v = -\frac{I_w}{I_v + I_w} \phi - \left[\theta_v(0) + \frac{I_w}{I_v} \theta_w(0) \right] - \left[\dot{\theta}_v(0) + \frac{I_w}{I_v} \dot{\theta}_w(0) \right] t$$

$$+ \frac{1}{I_v} \int_0^t \int_0^t (\Delta T_x - \dot{H}_{\text{Tape}} - \omega_y H_z + \omega_z H_y) dt dt$$

where θ_v = spacecraft inertial attitude

θ_w = reaction wheel inertial attitude

$\phi = \theta_w - \theta_v$

I_v = spacecraft inertia

I_w = reaction wheel inertia

ΔT_x = external spacecraft disturbance torques

\dot{H}_{tape} = change in tape recorder momentum

ω = cross-axis angular rate

H = cross-axis inertia

The first term on the right-hand side of the above equation is the desired relationship and would be exact except that wheel position is not known exactly. The other terms represent errors. Quantization noise arises from the fact that a digital readout of reaction wheel position is used. For every 1/8 revolution of the wheel, a pulse is sent to a summing register. Since an asynchronous, periodic sampling of the register is ordinarily used, this quantization will appear as a zero-mean, uniformly distributed, random variable with a standard deviation

of 13 degrees. In terms of spacecraft angle, this represents approximately 1 arc second (1σ), a value negligible in terms of its direct effect but very important in determining the initial angular rate.

Considering the two initial condition error terms, that representing the initial attitude is essentially unimportant, cancelling out in the analysis of relative errors, and completely determined with ground truth. The term representing initial angular rate (the coefficient of t) on the other hand is very important. In essence this term represents (through the body/wheel inertia ratio) the steady-state component (or bias) of the wheel speed that would be necessary to totally stabilize the spacecraft in the absence of limit cycle motion and external torques. When this term is not known correctly errors accumulate linearly with time in proportion to the incorrectness.

Determination of this initial angular-velocity term requires observation of the spacecraft attitude and the wheel velocity over an extended period of time in order to reduce noise components due to wheel position quantization and noise in determination of the body precise attitude. Unfortunately, the ability to smooth is limited by the presence of external torques which, when unknown, irretrievably alter the dynamic model. The predominant external spacecraft disturbance torque is expected to be magnetic. It will be largely periodic from orbit to orbit, and will be capable of calibration and compensation. The term, ΔT_x represents the uncorrected portion of the disturbance torques. Its magnitude was conservatively estimated to be 1×10^{-5} ft lb (1σ). The tape recorder momentum change and the cross-axis gyroscopic torques can be shown to be negligible relative to the other errors.

Given the reaction wheel revolution data, and the attendant errors in the data, the question is: what is the best mechanization for estimating spacecraft relative attitude? The reaction wheel data represents a noisy observation of the motion of the vehicle inside the attitude control system boundaries. Therefore, the Kalman filter appeared as a reasonable tool for the problem.

Figure 6-14 illustrates the system mechanization which was chosen for determining relative spacecraft angle. Two pieces of information per axis are sent by telemetry from the spacecraft to the ground data handling system. The reaction wheel revolution data, η_{measured} , and the earth sensor assembly signal, Ψ_{esa} . The spacecraft disturbance torque model is used to drive the spacecraft attitude model. The attitude model predicts the spacecraft attitude, Ψ_{vp} , and the wheel revolution data, η_{p} . These two predicted quantities are then differenced with the noisy observations from the telemetry and sent to the Kalman filter. The filter computes a correction to the spacecraft angle, $\hat{\theta}_{\text{p}}$, and this correction is added to the predicted value.

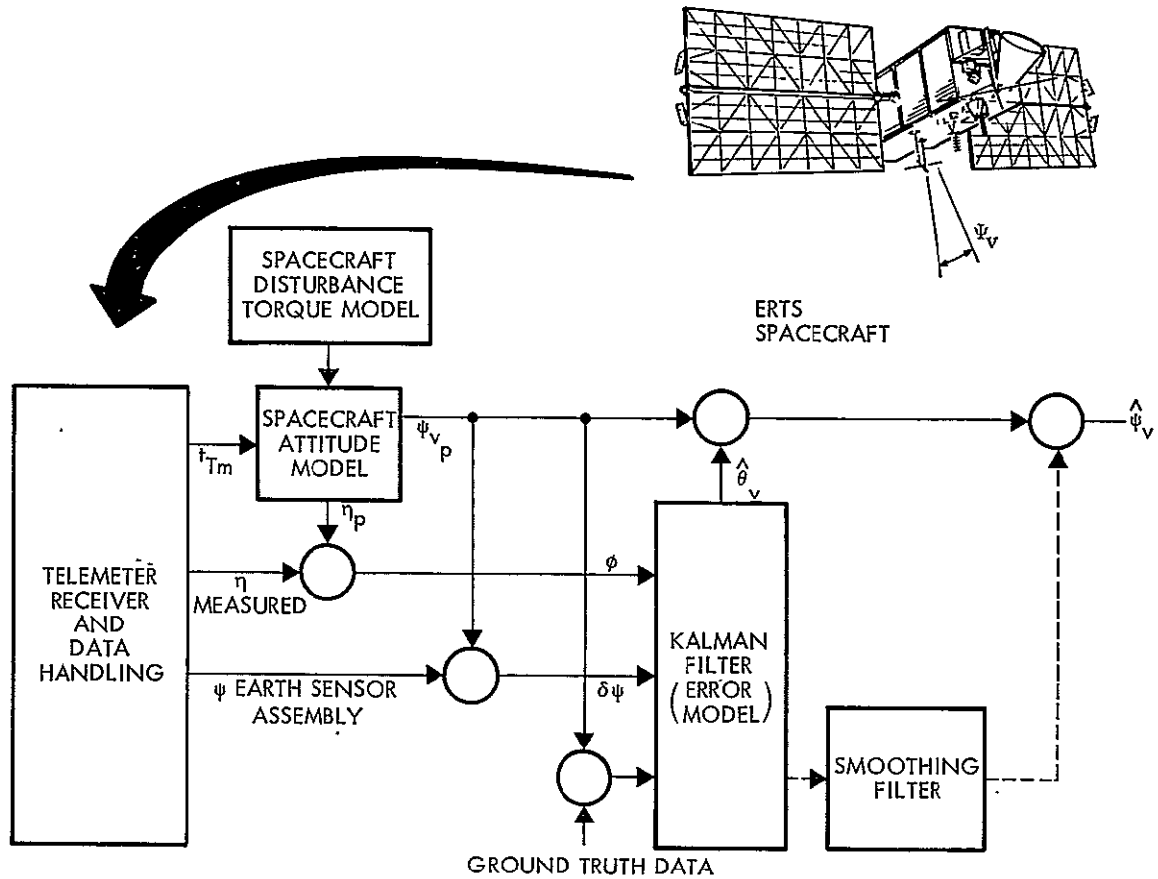
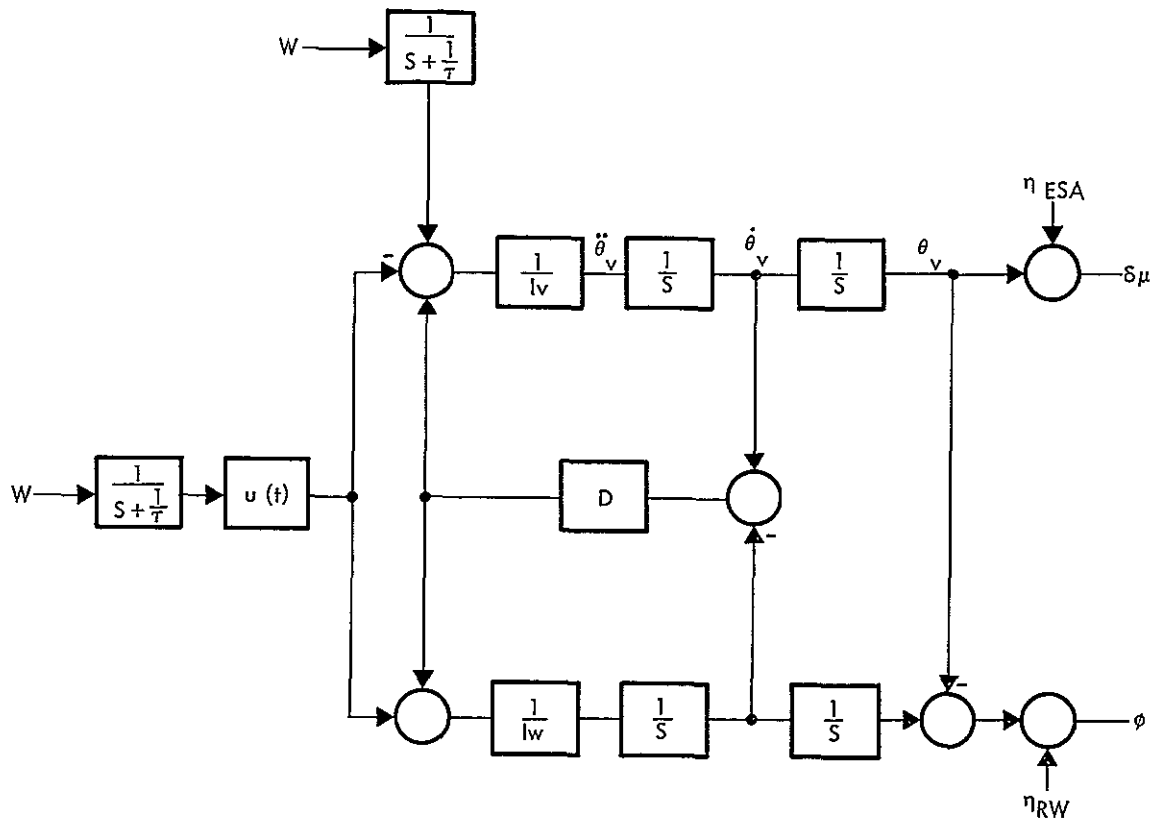


Figure 6-14
SYSTEM BLOCK DIAGRAM for relative attitude determination

The error model used in the Kalman filter is shown in Figure 6-15. As explained in Section 6.4, the reaction wheel motor torque is modeled as an exponentially correlated random variable. The uncorrected



WHERE $u(t)$ = CONTROL LAW FUNCTION
 w = WHITE NOISE

Figure 6-15
 KALMAN FILTER error block diagram

portion of the external spacecraft disturbance torques was also modeled as an exponentially correlated random variable. A 20-second time constant was used. The magnitudes of all other error sources are stated in the previous paragraphs.

The results of a digital computer analysis of the above described Kalman filter mechanization show that the relative attitude change after a 28-second time period can be detected within an uncertainty of 0.0075 degree (1σ). This represents the uncertainty in determining the change in spacecraft pitch and roll attitude angles from the time that the first MSS scan line is taken to the time that the last is taken. As before, a 100 by 100 nautical mile picture is assumed. The determination of absolute yaw is 0.08 degree using the mechanization described in Section 6.1

The impact of these uncertainties in relative attitude determination on MSS picture mapping accuracy has been shown in Figure 6-13. Assume that it is desired to know the location of a point in the top right-hand corner of the picture, given a ground truth point in the bottom left-hand corner. This is the worst case for relative positions between the two points. Using the relationships shown in the figure, the above stated attitude errors produce a crossrange error of 392 feet (1σ) and a downrange error of 928 feet (1σ).

The question now arises as to how the crossrange and downrange errors should be combined to produce a radial error. In the case of absolute attitude determination, the two predominant errors, those due to pitch and roll uncertainties, were rss combined. Statistically, this is equivalent to saying that they have a unity correlation coefficient. (They are rss combined for geometrical, not statistical reasons.) Since the errors are due to the earth's radiance model, this is a good conservative approach in view of the lack of knowledge concerning the spacial correlation of the radiance profile. However, analysis has shown that the relative attitude determination errors are due primarily to uncorrected spacecraft external disturbance torques. These errors produce the crossrange error and a small part of the downrange error. Absolute yaw attitude error produces the rest of the downrange error. Since absolute yaw error is not correlated with relative pitch or roll errors, there is only a small correlation between crossrange and downrange errors. In view of this fact, it was decided to use the formal and more commonly accepted definition of radial error; namely, circular error probability or CEP. In doing so, the downrange and crossrange errors combined to give 762 feet (CEP).

The accuracies quoted above apply to the case of one or no ground truth point. A single point allows a calibration of attitude. Two ground truth points allow a calibration of both attitude and rate. Referring to the relationships shown in Figure 6-13, roll rate can be calibrated with any two ground truth points separated in downrange distance. Pitch rate can be calibrated by two points separated downrange but in the middle of the picture. To a good approximation, pitch rate can also be calibrated by any two points separated downrange but not crossrange. This implies

neglecting the effect of yaw rate. Yaw attitude can be calibrated by any two points separated crossrange but not downrange. In view of the myriad of placements of two ground truth points, no specific results involving the use of more than one ground truth point were generated in the study. However, it was shown that for the case of two points positioned to calibrate either pitch or roll rate, the resulting mapping error from either pitch or roll was theoretically negligible compared to the 200-foot design goal.

6.7 SYSTEMS USING GYRO REFERENCE ASSEMBLIES

The second system studied for the 200-foot design goal uses a gyro reference assembly to determine relative attitude change during the time period necessary to take a 100 by 100 nautical mile MSS picture. To be specific, the study used the parameters of a gyro reference assembly currently being developed at TRW for another space program, the Precision Pointing Control Study (PPCS), a NASA/GSFC sponsored activity.

In summary, using the same ground rules that were applied in the case of the reaction wheel mechanization (one ground truth point), an error of 30 feet (1σ) is obtained with a gyro reference assembly. The gyro reference assembly will measure inertial vehicle angular rates to an accuracy of 0.01 deg/hr (1σ). This is more than sufficient to eliminate the effect of pitch or roll attitude changes during an MSS picture. In addition, the assembly can be used to determine yaw absolute attitude to an accuracy much greater than that obtainable using only one OGO gyro. Not only is the gyro drift rate less in the PPCS gyro, but the assembly measures three-axis rate information and can determine yaw attitude independent of absolute roll angle.

The major error source involved in using PPCS gyro reference assembly for the 200-foot design goal is the gyro drift rate of 0.01 deg/hr (1σ). This error limits the determination of absolute yaw attitude to approximately 10 arc-seconds. This produces a mapping error of 30 feet at the edge of an MSS picture.

It should be noted that a gyro reference assembly can also be used to determine absolute roll attitude. This capability can be used to

improve the 2 nautical mile requirement. However, the improvement is not very large since the pitch attitude error from the horizon scanners will still be present.

6.8 CONCLUSION CONCERNING RELATIVE ATTITUDE DETERMINATION

As in the case of absolute attitude determination, the tradeoff here is between a system which adds little hardware to the spacecraft and one which adds a new subsystem. Again, in this case there is a large impact on accuracy between the two systems. The gyros provide a large improvement in relative attitude determination for pitch and roll over the reaction wheels. They also greatly improve the determination of absolute yaw attitude.

On the other hand, the PPCS gyro reference assembly is still in the development stage and does not represent proven flight hardware. While more fully developed reference assemblies are available in the industry, the basic fact remains that a new hardware component is involved, with an added program cost and an increased risk in cost and schedule overrun.

The reaction wheel mechanization will provide an attitude determination error of 760 feet to an MSS picture. It was decided that the accuracy, together with the low cost of the reaction wheel mechanization, was adequate for the first ERTS missions. The added expense and risk associated with adding a gyro reference assembly to the spacecraft does not justify the increase in MSS mapping accuracy. In the future, when the PPCS gyro reference assembly is fully developed, if greater mapping accuracy is required, and other mapping error sources are appropriately small, then the assembly may well be justified.

6.9 CELESTIAL ATTITUDE REFERENCE FROM THE RBV CAMERA

A study was conducted to determine if establishing spacecraft attitude with sufficient accuracy of locate any point within the 100 x 100 nautical mile scene with an accuracy of 2 nautical miles could be accomplished using the existing return beam vidicon cameras by taking

a "double exposure" of a star field and video image. Subsequent scanning of the charge developed upon the vidicon target would result in video signal consisting of both scene and star field information, from which spacecraft attitude could be determined. Analysis determined that this idea is not feasible, due primarily to the orbit angular rate of the spacecraft which permits insufficient integration time of the optical star image on the picture element of the vidicon target.

The concept proposed is illustrated by Figure 6-16. The approach utilized a moveable mirror, which would be precisely indexed in front of the RBV camera lenses, permitting observation of stars on the dark side of the spacecraft. Two cameras would be so modified, permitting the sighting of two (or more) stars simultaneously. Using a relatively long exposure of the camera shutters the optical star image would be recorded in the form of stored electronic charge on the vidicon target.

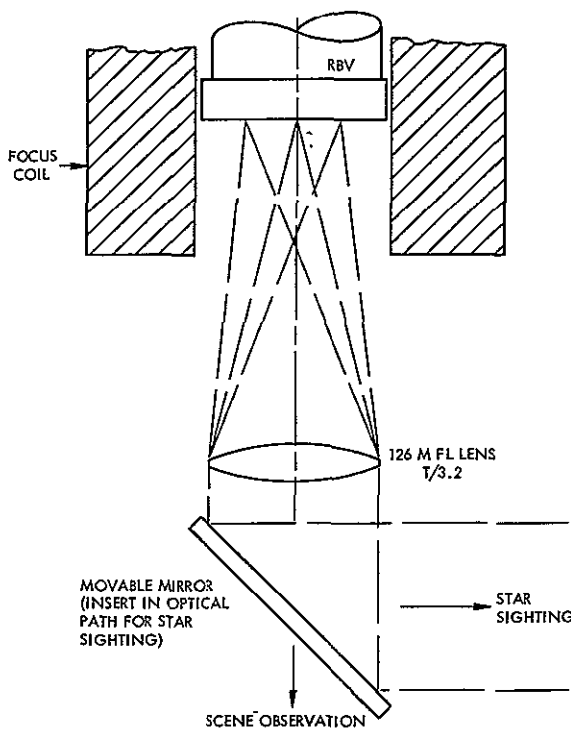


Figure 6-16
RBV CAMERA geometry

The mirrors would then be removed from in front of the RBV camera lenses, and a second exposure of the camera shutters would permit recording of the image of the scene in the form of electronic charge on the vidicon target. Subsequent scanning by the electron beam would result in obtaining a video signal containing both scene and star image data, thus permitting determination of spacecraft attitude at a known time prior to the time the imagery was obtained.

The primary constraint imposed upon the study was that any optical modification of the RBV cameras be external to the existing lens assembly. Increasing the optical field of view proved to be impractical

and therefore the only modification consisted of the addition of an external mirror, preserving the existing field of view of 11.5×11.5 degrees. With this optical field of view it is necessary to obtain sightings on stars brighter than 3.8 visual magnitude in order to be certain that at least one star is within the field of view at all times (Figure 6-17).

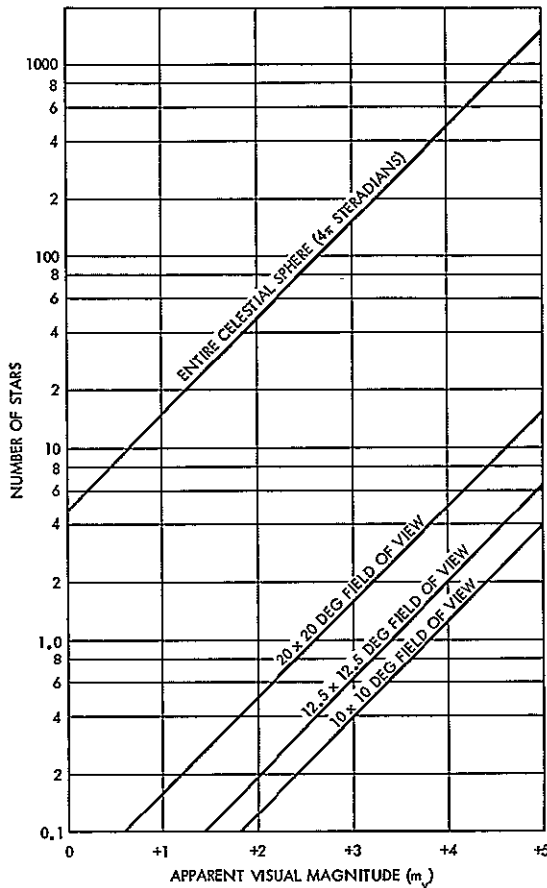


Figure 6-17
STAR POPULATION (number of stars brighter than magnitude M_v)

(Item 3.6), the allowable exposure time when observing stars would be 32 msec (Item 3.7). This would result in an integrated exposure of the optical image of 0.01 footcandle-second (Item 4.1). Referring to Figure 6-18 it is seen that an exposure of 1.0 footcandle-second is required to develop a signal of maximum amplitude from the RBV target.

The results of the computation are defined in Table 6-6. With a star of 3.8 visual magnitude, 0.98×10^{-10} lumen of light are collected by the RBV camera lens (Item 2.3), and it is assumed that this would be focused on one picture element with an area of 3.08×10^{-12} ft² (Item 2.5), resulting in an image intensity of 0.318 footcandle (Item 2.6). With the field of view of 11.5×11.5 degrees and a 4200-line raster, each line of the raster would have an angular subtend of 9.6 arc-seconds (Item 3.2). The composite angular rate of motion of the satellite (orbital rate plus limit cycle rate) is 149.5 arc-sec/sec (Item 3.5). Assuming a permissible smear, or movement of the optical image on the vidicon raster of one-half of one TV line, or 4.8 arc-seconds

Table 6-6. Calculation of Integrated Exposure of RBV Target on a +3.8 Magnitude Star
(Optical Field of View = 11.5 x 11.5 deg, 126 mm f/3.2 Lens, Line of Sight
Oriented 45 degrees from Orbit Plane)

1.0	<u>Star Availability</u>	
1.1	Total number of stars brighter than +3.8 magnitude	400
1.2	Number of stars within 11.5 x 11.5 deg field of view (average)	1.2
2.0	<u>Star Flux Intensity on RBV Target</u>	
2.1	Star flux intensity incident on RBV camera lens (0 magnitude star)	2.65×10^{-6} lumen/m ²
	(+3.8 magnitude star)	0.0802×10^{-6} lumen/m ²
2.2	Area of RBV camera lens (f1 = 126 mm, t _{no} = 3.2, transmission = 0.80, f _{no} = 2.86, dia = 44 mm)	15.3×10^{-4} m ²
2.3	Star flux on vidicon picture element (2.1 x 2.2)	0.98×10^{-10} lumens
2.4	Width of one TV line on RBV target (1/4000 in.)	0.25×10^{-3} in.
2.5	Area of one picture element (0.25×10^{-3} in. dia)	3.08×10^{-10} ft ²
2.6	Intensity of star image on picture element (2.3/2.5)	0.318 footcandle
3.0	<u>Shutter Exposure Time</u>	
3.1	Optical field of view	11.5 x 11.5 deg
3.2	Width of one TV line (11.5 deg/4200 TVL)	9.6 arc-sec/TVL
3.3	Body motion rate	0.008 deg/sec-axis = 28.8 arc sec/ sec axis
3.4	Orbital rate of line of sight	210 arc-sec/sec at zenith 149 arc-sec/sec at 45 deg to orbit plane
3.5	Composite rate of line of sight (rss of 3.3 to 3.4)	149.5 arc-sec/sec
3.6	Allowable image motion blurring exposure time (1/2 TVL)	4.8 arc-sec
3.7	Allowable shutter exposure time (3.6/3.5)	0.032 sec
4.0	<u>Integrated Exposure on Picture Element</u>	
4.1	Integrated exposure of star image (2.6 x 3.7)	0.0102 footcandle/sec
4.2	Required exposure for maximum signal from RBV target (from Picture 4)	1.0 footcandle/sec

Thus it is seen that the proposed concept is not practical as the angular rate of motion of the satellite (primarily due to orbital rate) prevents the use of an exposure time sufficiently long to result in a signal from the star which will be clearly discernible within the video signal.

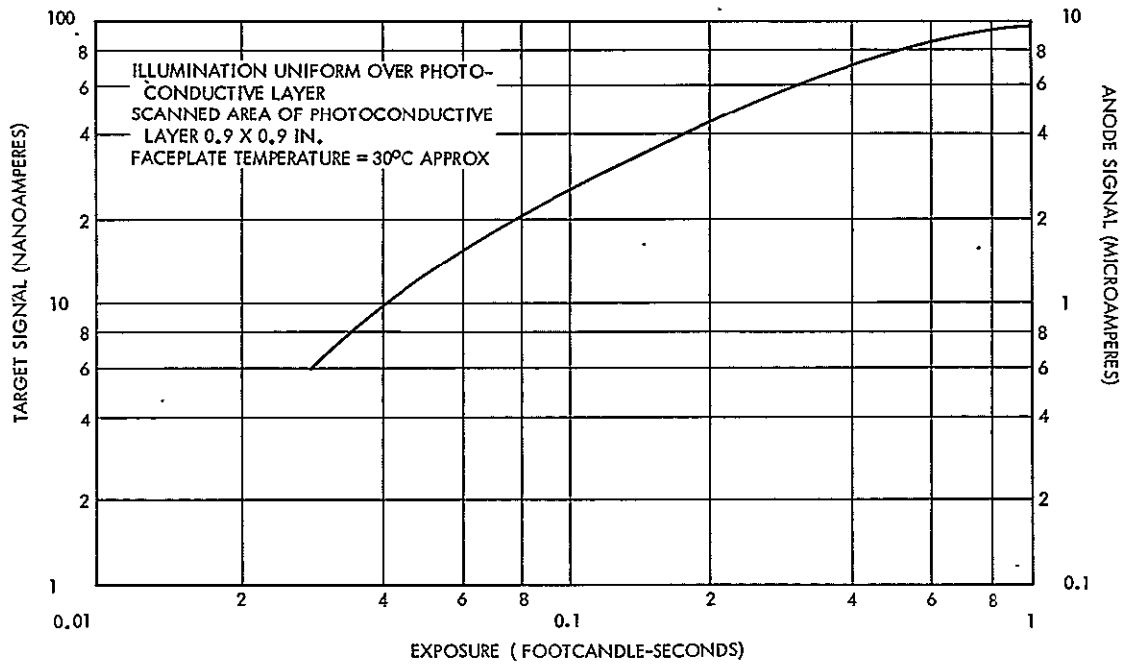


Figure 6-18
 RBV EXPOSURE, current transfer characteristics

CONTENTS

	Page
7. VELOCITY CORRECTION	7-1
7.1 System Interactions	7-2
7.2 Thruster Design	7-4
7.3 Thruster Placement	7-6
7.4 Choice of Propellant	7-9

7. VELOCITY CORRECTION

The requirement for orbit adjustment as set by the Thor-Delta injection error was shown in Volume 2 to be about 48 ft/sec. This thrust must be applied at specific positions in orbit, both in-plane and cross-plane. As a study item the choice of a suitable system for achieving this change in velocity was again reviewed. The key factors are listed here.

Two systems which will readily and reliably provide orbit adjustment are the heated gas system described in Volume 3, Section 10, and a monopropellant hydrazine system like TRW's application to Intelsat III and to Model 35 spacecraft. The characteristics of a suitable hydrazine system are described in our June 1969 proposal for ERTS Phase B/C studies, Appendix I. A brief summary of the characteristics of that system follows:

- Component Parts:

- Propellant tank assembly, bladder type (1)
- Fill and drain valve (1)
- Pressurization valve (1)
- Vent valve (1)
- Filter (1)
- Thruster, with heater and catalyst (2)
- Pressure transducer (1)
- Interconnect plumbing

- Performance Specifications:

Impulse:	5710 lb-sec
Minimum impulse:	0.3 ft/sec
Propellant weight:	26.7 lb*
Tank pressure:	600 to 200 psia
Thrust	1.7 to 3.7 lb
Specific impulse	214 sec

*A slight reduction in weight would be allowed by the 48 ft/sec objective of ERTS today.

Total installed weight with propellant:	42.4 lb
Reliability	0.99
Maneuver required	90 deg for in-plane thrust

In order of importance the tradeoff between heated krypton and hydrazine approaches is as follows:

- Volumetric efficiency. Heated krypton uses the same tankage as the attitude control pneumatics minimizing added volume. ERTS volume is more critical than weight.
- Cost. Hydrazine being a more complex system was estimated to cost about \$750,000 more than the heated krypton type.
- Operational advantage. Hydrazine thrust being high, the reliability of shutoff (using a programmer) must be high. A small timing error becomes 60 times as important with hydrazine as with heated krypton.
- Life. All krypton unused for orbit adjustment is available for extended control gas life.
- Complexity. The attitude control maneuver needed for hydrazine requires an attitude gyro. This maneuver is needed; because of high thrust torques, thrusters cannot be positioned on the X panels of the spacecraft where they would impinge on the array.
- Reliability. The heated krypton system is ideally simple having a one-year reliability of 0.999 whereas the hydrazine system bladder tank and catalyst thruster contribute to a system reliability of 0.990.
- Weight. The hydrazine system designed for 70 ft/sec would have a weight advantage of at least 20 pounds. Weight is not presently crucial to ERTS. The weight advantage of hydrazine becomes overpowering as the orbit adjust requirement grows.

7.1 SYSTEM INTERACTIONS

Since the orbit adjust system shares its propellant supply with the attitude control system, the adequacy of each OGO pneumatic component has been evaluated. The propellant tank and support structure are fully adequate for the 57 pounds of krypton. These components have a growth capability from the baseline 4000-psia storage pressure to 5175 psia.

Should this capability be utilized, the regulator and high pressure transducer would require requalification.

The flow rate for the electrothermal thrusters is approximately half that of the attitude control thrusters because of the increased specific impulse. The solenoid valve flow capability is more than adequate. The inlet pressure is identical in both cases. The cycle life requirements are significantly lower for the orbit adjust thrusters. The valve heat rejection capability is adequate for the lower flow rates and longer operating periods.

The maximum regulator flow demand time for orbit correction is 500 seconds, or about twice that of OGO. The flow rate, however, is reduced by half. The gas temperature drop across the regulator seat due to throttling (Joule-Thompson effect) will be less than that of the duty cycle tested for OGO. Based on OGO experience, no problem results from low regulator temperatures. The cycle life capability of the regulator is adequate to accommodate the additional on-off cycles imposed by orbit adjust maneuvers.

For ERTS, the system volume downstream of the pressure regulator is greater by approximately 3 cubic inches. Increased volume is usually considered a factor which reduces potential regulator-feedline coupling instabilities. However, if regulator instability is encountered during test, the system can easily be stabilized by adding more volume at the regulator outlet or by increasing the line resistance to uncouple the system from the regulator.

A flow field analysis was conducted to determine the magnitude of the disturbance torques caused by impingement of thruster exhaust on the solar panels. The net torque is less than 0.007 ft-lb. The attitude control system is capable of compensating this torque without loss of pointing accuracy. Disturbance torques caused by thrust vector misalignment and center of gravity shifts caused by propellant depletion are even smaller.

The thermal control system is unaffected by the addition of the thrusters. Since the thruster valves are within the spacecraft envelope,

additional thermal control is unnecessary. Conductive heat transfer to the spacecraft structure amounts to less than 5 watts during 500-second pulsing. Heating of the solar panels from plume impingement is negligible.

No structural changes are required except for mounting provisions for the valves and thrusters. The thruster mounting will allow a position adjustment parallel to the Y-Y axis for thrust vector alignment with the spacecraft center of gravity. The thrusters do not protrude from the spacecraft body sufficiently to interfere with the folded solar panels.

The commands and telemetry channels required for operation of the thrusters are minimized by using an existing design pressure switch to verify thruster operation and by electrically connecting the thruster valve and thruster heater in parallel.

The power and voltage requirements of the vortex thrusters are within the capabilities of the power system. Conditioned power is not required for thruster operation.

7.2 THRUSTER DESIGN

The vortex thruster, which is ideally suited to the ERTS mission, consists of a cylindrical cavity with a coaxial, spirally-wound tungsten heater element. The propellant gas is injected tangentially at high velocity. The gas spirals radially inward with high tangential, but low radial, velocity. In passing around and through the heater element, the gas is heated prior to expulsion through a propulsive nozzle. The vortex thruster, which is shown in Figure 7-1, has been under development at TRW for nearly two years. The design modifications to adapt the thruster to meet the requirements of the ERTS mission are minimal.

For ERTS, the thruster offers significant advantages over more conventional electrothermal thruster designs. The vortex heat exchange concept is more efficient than conventional single-pass designs. In the ERTS vortex thruster, the propellant temperature closely approaches the temperature of the heater element. Specific impulse is limited only by the available power and the maximum operating temperature of the element. Delivered specific impulse as a function of temperature is

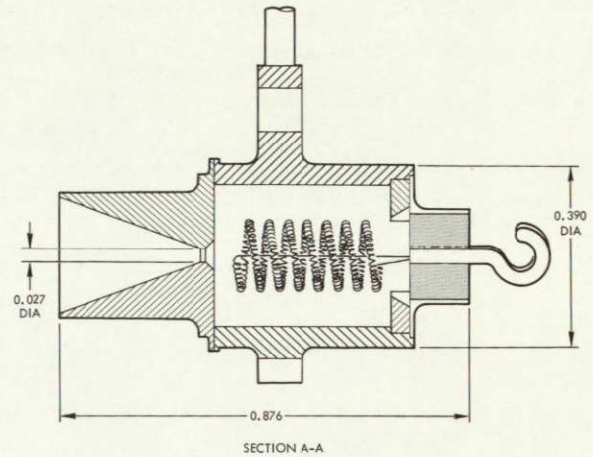
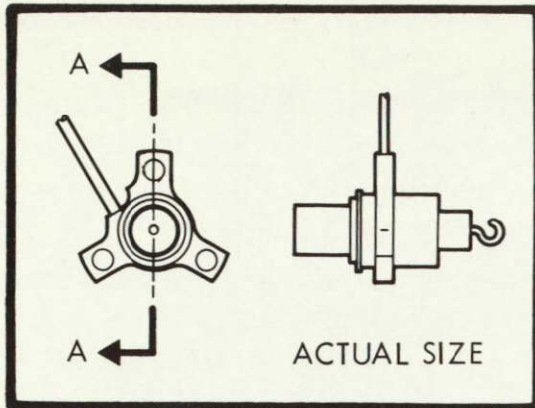


Figure 7-1
ERTS ORBIT ADJUST THRUSTERS weigh less than 0.1 pound yet deliver high performance

shown in Figure 7-2 for the three gaseous propellants considered for ERTS. The very low thermal mass of the heater element allows steady state operating temperatures to be reached quickly. Power and propellant flow are initiated simultaneously. Computer simulation of the ERTS thruster indicates that the heat-up transient degrades the average specific impulse by only 2 seconds for the 500-second ERTS thrust deviation.

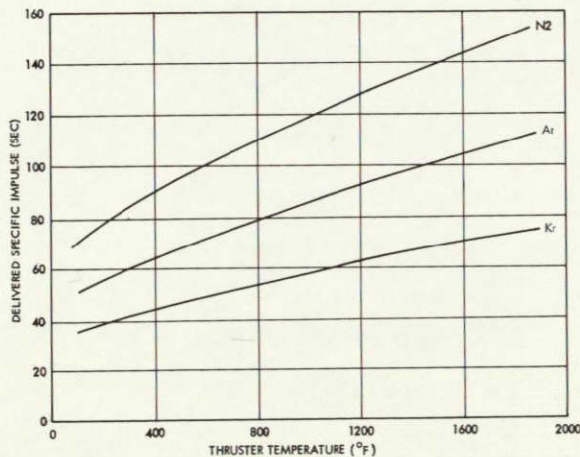


Figure 7-2
DELIVERED SPECIFIC IMPULSE of gaseous propellants is approximately doubled by heating to 1600°F. Although its specific impulse is low, krypton is optimum for ERTS due to storage density

Tangential propellant injection provides a cool layer of gas adjacent to the cavity walls. In effect, the thruster is regeneratively cooled. Thermal losses will amount to less than 5 watts (out of a total of 75 watts). No thermal insulation is required. The thruster power requirements are well within the capabilities of the spacecraft power system. Payload operation need not be interrupted. The electrical resistance of the heater can be

sized for compatibility with the spacecraft bus voltage. No power conditioning is necessary.

As shown in Figure 7-3, the body of the thruster consists of the cylindrical cavity, the nozzle, and the injection tube. The heater element is attached to an electrical insulator. The only portion of the thruster that operates at high temperature is the heater element. The predominant failure mode is thus a damaged heater, which will not impair the ability of the thruster to operate in an unheated mode. In this event, the delivered specific impulse will be equivalent to that of the attitude control thrusters, 37 seconds. In the unlikely event that all three of the thrusters must operate unheated, the baseline orbit control system would still be capable of removing 2σ launch injection errors.

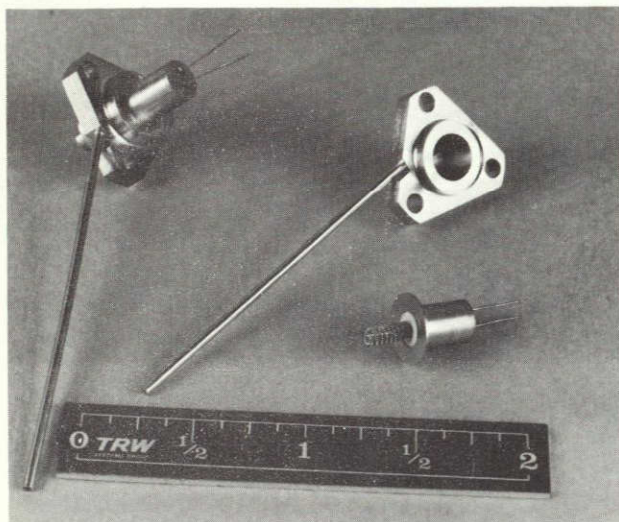


Figure 7-3

THE ORBIT ADJUST THRUSTERS have just two main components

impingement on the large solar array surface.

The design which is planned would position the X panel velocity correction nozzles at about 8 inches from the centerline of the array shaft. This is physically convenient to clear existing array support structure and is estimated to about balance torques due to plume impingement against center of gravity offset. Any torque not so balanced will be counteracted by yaw or roll control torques.

7.3 THRUSTER PLACEMENT

Ideal placement of velocity correction thruster would result in thrust through the center of gravity. This is simply arranged in the ERTS spacecraft Y direction since center of gravity is accurately measurable and does not shift with depletion of propellant. Thruster placement on the X panels requires consideration of c.g. shift and torques developed as a result (see Figure 7-4). It also requires compensation for torques produced by plume

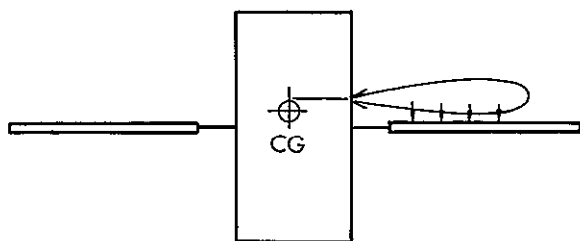


Figure 7-4
THRUSTER PLACEMENT on the X panel
balances opposing torques

The krypton gas assigned to orbit adjustment weighs 47 pounds. If this is fully depleted in its tank at Station 386 the center of gravity will shift 0.7 inch in the -Y direction. The net effect is a change in torque of 0.003 ft-lb.

Torques generated by impingement on the solar array panel have been computed for two conditions: (1) array plane parallel to the Z axis of the spacecraft, (2) array rotated 30 degrees away from condition (1) (see Figure 7-5).

The pressures on the panel were calculated by applying the Newtonian thin shock layer approximation, i. e.,

$$p_s = p + \frac{\rho v^2}{g_c} \cos^2 \beta$$

where p_s = surface pressure, lbf/ft²

p = free-stream pressure, lbf/ft²

ρ = free-stream gas density, lbf/ft³

v = free-stream velocity, ft/sec

g_c = conversion factor, 32.174 (lbf/lbm) · (ft/sec²)

β = angle between velocity vector and normal to surface

The gas density, ρ , was computed using Roberts' plume approximation.*

$$\frac{\rho}{\rho_e} = \frac{k}{2} \left(\frac{h}{r_e}\right)^{-2} (\cos \theta)^k$$

*Roberts, L., "The Action of a Hypersonic Jet on a Dust Layer," IAS Paper No. 63-50, January 1963.

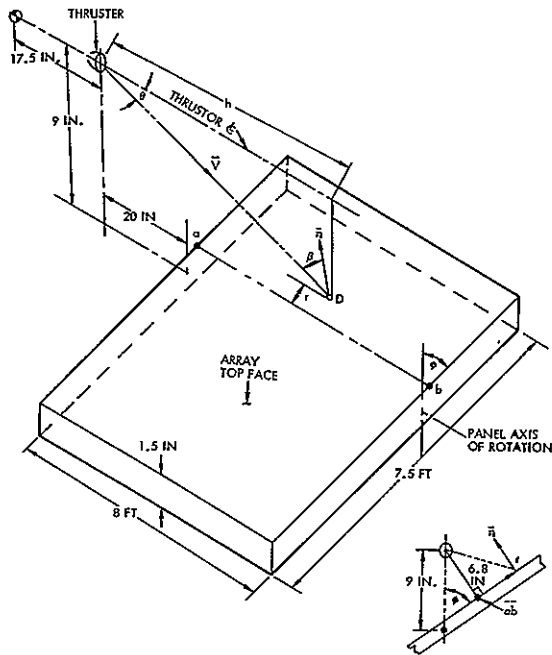


Figure 7-5
 ΔV THRUSTER, solar array geometry
 (no scale)

where $k = \gamma(\gamma - 1) M_e^2$

ρ_e = gas density at thruster exit, lbm/ft³

h = axial distance parallel to thruster axis, in.

r_e = nozzle exit radius, in.

θ = gas flow angle (assuming radial source flow), deg

γ = ratio of specific heats

The additional thruster quantities required were

$P_c = 25$ psia

$T_c = 1960^\circ R$

$\gamma = 1.667$

$F = 0.050$ lbf

$\epsilon = 100$

The surface pressure was calculated as a function of h and r for each panel orientation and then integrated to find the induced forces and torques. For $\phi = 90$ degrees it was found that the force on the top face was 0.0012.lbf and the torque about the c.g. was 0.0074 ft-lbf. For $\phi = 60$ degrees the force and torque were 0.0014 lbf and 0.0073 ft-lbf, respectively. The lower torque value for $\phi = 60$ degrees is due to the shorter moment arm of the force acting on the panel.

To a first approximation the torque developed from plume impingement can be compensated by positioning the thruster toward the -Y end of the spacecraft and away from the Y axis center of gravity.

Viewing Figure 7-4 it may be seen that plume impingement torque is clockwise whereas that due to center of gravity offset is counterclockwise. Both of these torques are small compared to the torque available from the attitude control system to correct torque unbalance.

Pitch attitude control:	0.1 lb x 28 in. = 0.23 ft-lb
Roll attitude control:	0.05 lb x 48 in. = 0.2 ft-lb
Yaw attitude control:	0.05 lb x 48 in. = 0.2 ft-lb
One-inch c.g. ΔV offset:	0.05 lb x 1.0 in. = 0.004 ft-lb
Plume impingement (6.8 in. separation):	= 0.007 ft-lb

If the set of conditions above are combined with the spacecraft center of gravity, the impulse required from the attitude control jets may be computed. The positions of key elements are:

	<u>Station</u>
Center of gravity (gas depletion)	367.1
Thruster location	364
Array plane, about	371
Torque due to c.g. offset	0.013 ft-lb
Torque due to array impingement	<u>0.007 ft-lb</u>
Difference	0.006 ft-lb

During a 500-second in-plane thrusting period the attitude control jet would be required to compensate this 0.006 ft-lb and this would require that it operate for about 15 seconds total made up of many brief pulsations.

7.4 CHOICE OF PROPELLANT

The use of krypton as a heated gas is based on its volumetric efficiency and not on weight efficiency. There is no weight problem in the ERTS design - the booster is capable of lifting substantially more than the current weight of the spacecraft. Volume on the other hand is a limiting factor - 18 cubic feet of the ERTS spacecraft are assigned to housing the payload. The problem of gas choice thus becomes one of obtaining the most impulse in a chosen tank.

Figure 7-6 shows the total impulse which is available from three gases at various pressures in the existing OGO pressure sphere.

Krypton is twice as efficient from a volumetric standpoint as its nearest competitor, argon.

The choice of krypton is based on a desire to provide as wide a margin as possible over the minimum requirements set by the Thor Delta vehicle. As time passes, this choice can be altered by procuring an alternate types of gas.

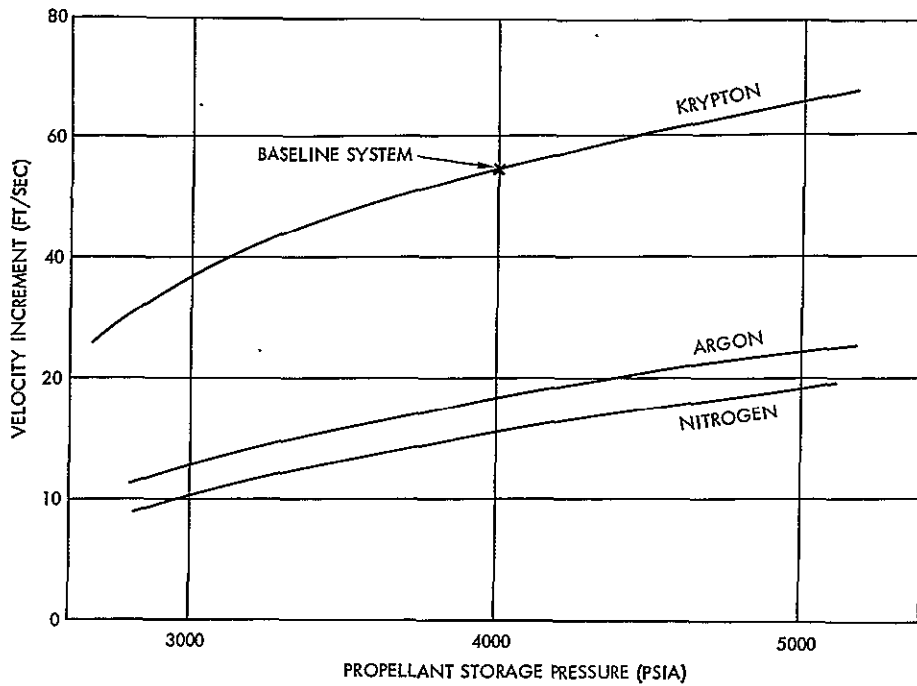


Figure 7-6

ORBIT ADJUST SYSTEM capabilities can be varied over a wide range with no component changes.

CONTENTS

	Page
8. DATA HANDLING	8-1
8.1 Stored Command Programmer	8-1
8.1.1 Breadboard Test	8-4
8.1.2 Design Approach	8-6
8.1.3 Functional Description	8-8
8.2 Narrowband Tape Recorder	8-13
8.2.1 Life Improvements	8-13
8.2.2 Playback-to-Record Ratio	8-15
8.2.3 Other Design Changes	8-17
8.3 Spacecraft Clock	8-18
8.4 Telemetry List	8-20
8.5 Command List	8-31
8.6 Command Reliability	8-36

8. DATA HANDLING

The basic data handling function described in our June 1969 proposal have been reviewed and found still applicable. Breadboard work on the stored command programmer has been completed, tests confirming the design approach. Additional functions have been assigned to the stored command programmer assembly to handle the 7-bit command address and the unified S-band interface identified at the beginning of the study. Engineering aspects of the narrowband tape recorder improvement program have been completed, and telemetry and command lists have been prepared.

8.1 STORED COMMAND PROGRAMMER

The command system for OGO is relatively simple compared with that required for ERTS since only real-time commands transmitted in one format from STADAN stations are required. The ERTS mission is based upon executing both real-time and stored commands under control of either STADAN or MSFN stations. The OGO command system has been proven on all OGO flights and consequently its retention for as much of the command function as possible is desired.

By using the OGO command decoder all command output interface problems are solved since the interface is identical to OGO. This decoder provides the following functions which are required by ERTS:

- VHF command data input interface
- Digital command decoding
- Matrix command output interfacing

Several other functions are required for ERTS which the OGO command decoder does not provide:

- Command storage
- 7-bit VHF command addresses
- Unified S-band compatible input interface

The stored command programmer design goal was to produce a unit which would interface simply with the existing command decoder, preserve all

the existing interfaces, and provide the additional ERTS functions required. This goal was successfully met.

The ERTS requirement for a 7-bit command address was found to have a very significant effect on the command decoder design. Adding this capability to the existing decoder unit would have invalidated the design qualification and would probably have made an entirely new decoder the most economical approach.

The unified S-band compatibility requirement makes it necessary for the command system to detect a 70-kHz FM subcarrier, perform bit synchronization of a 1 kbit data stream, and detect 200-bit command data by 5:1 subbit detection. New equipment was obviously needed to meet all of these requirements.

The command storage requirement also indicated the addition of a new digital memory and the logic required to control the input and output interfacing and timing.

Earlier studies considered interfacing the unified S-band, VHF, and stored commands at the command output matrix. Such an interface required a complete Apollo type decoder for the unified S-band commands and complex interface logic to convert the unified S-band commands to form a compatible command format for storage and distribution. The technique selected makes use of another interface point existing at the input to the digital portion of the command decoder. This simplified equipment requirements in two respects:

- Apollo-type command detector is not required.
- Command interface unit is not required at the command outputs.

The command detection equipment configuration chosen utilized a digital data interface at the input to the digital portion of the OGO command detector. The data at this common interface point may consist of:

- VHF command data
- Unified S-band command data

- Stored command data for execution from the command memory
- Stored command data for storage from either the VHF or unified S-band command uplinks.

Each data source also provides a synchronized clock signal to the digital interface.

Since the OGO command decoder is used, the digital command data format is that of OGO with the ERTS 7-bit address replacing the OGO 3-bit address. The unified S-band command equipment accepts an Apollo address prior to the ERTS address to prevent any possible interference with Apollo missions using the same uplink modulation. The unified S-band equipment also decodes the Apollo-type 5:1 subbit encoded signal to provide the 200-bit data from the 1-kbit uplink.

The stored command word format and size is based on the number of command types which must be stored and the number of time slots which must be checked to determine time of execution. This results in:

Commands	6 bits	64 stored command types
Time	18 bits	20.97 hr with 0.576 sec resolution
Parity	<u>1 bit</u>	
Total	25 bits per stored command word	

The single parity bit provides adequate protection from incorrect commands due to random equipment bit errors. The bit error rate for memory and logic will be quite low, less than 10^{-8} . With no parity check the unit would experience less than 263 bit errors per year at the 50-kbit internal cycle rate. Since less than 10 percent of the stored command capacity will be utilized on the average, we can determine the effect as follows:

Of each 40 errors:

- 4 fall in active stored commands and either change the command or the execution time.
- 36 fall in null commands. Of these:
 - 27 cause null commands to be executed at wrong times, thus having no effect
 - 9 change null commands to significant commands.

Thus, only 13 of each 40, or 32.5 percent, of random errors will cause spurious commands. Without parity bits this results in less than 85 spurious commands per year.

With a single parity bit in each 25-bit command word, only double errors are significant and there will be a probability of less than 0.000021 per year of such a double error causing a spurious command, assuming a random error rate. Thus, with equipment random bit error rates in the order of 10^{-8} , the single parity bit per word is seen to reduce a very significant number of spurious commands per year to an insignificant probability of any spurious command being issued over the entire mission life.

To insure that the parity check bit must deal with random bit errors only, logic is provided which switches the stored command programmer to the standby mode in case any power interruptions occur. This prevents any spurious commands being executed due to this source of error. Uplink bit errors experienced while loading stored commands will not cause spurious commands since the normal operating procedure calls for verification of loaded commands by telemetry in the standby mode before the programmer is commanded to the process mode.

8.1.1 Breadboard Test

During the summer and fall of 1969 a breadboard model of the stored command programmer proposed for ERTS was built and bench tested (Figure 8-1). The objectives for this programmer have changed little in subsequent months even with the addition of the unified S-band. The objective of this breadboard was to be able to perform the command storage and execution function in ERTS using the existing OGO digital decoder without fundamental change (see Table 8-1). This goal was achieved. With only a few wiring changes in the OGO unit, the programmer can handle all of the ERTS requirements satisfactorily.

Modifications to the digital command decoder so that it operates with the stored command programmer have not required removing any existing welded connections. In essence the modifications are OR gates, and the normal operations of the decoder are not affected.

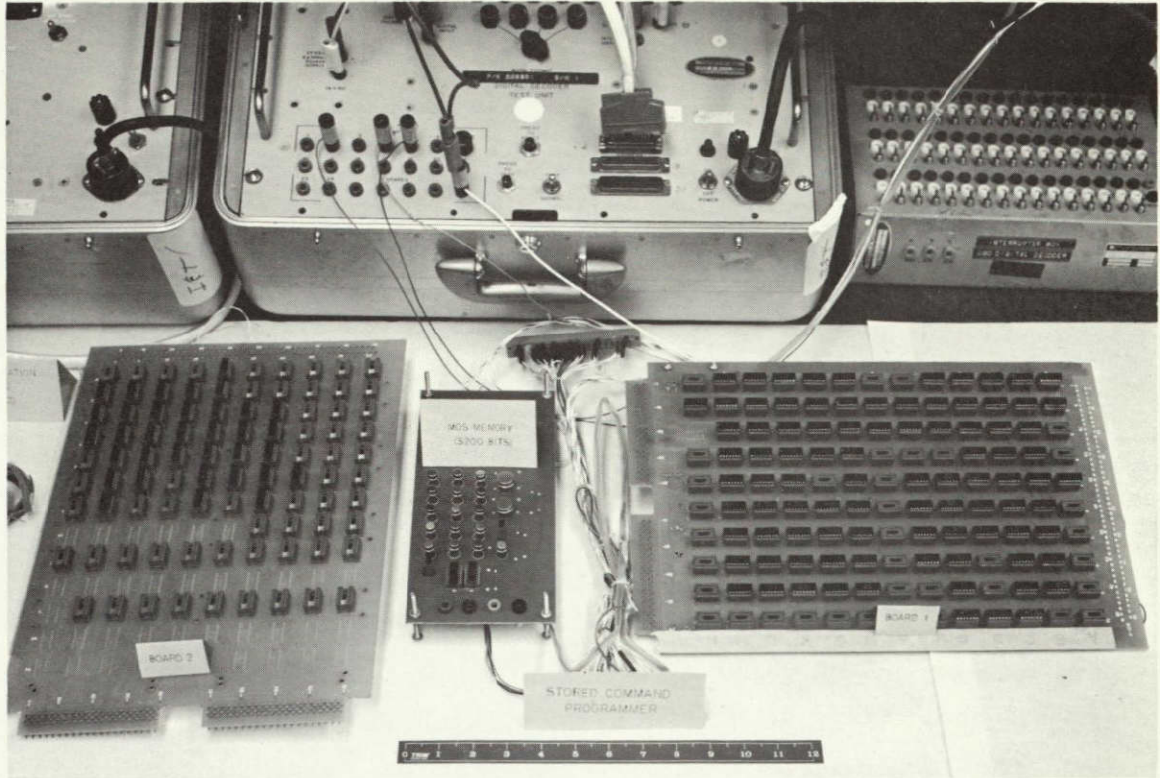


Figure 8-1

STORED COMMAND PROGRAMMER built for bench tests is an OGO command decoder modified to meet ERTS requirements.

Table 8-1. ERTS Requirements Versus Performance of Stored Command Programmer

	Requirements	Performance	Comments
Stored commands	100	128	Easily increased
Command types	32	64	Easily increased
Command centers	None specified	0.576 sec	Can be reduced by reducing the cycle time
Elapsed time clock cycle time	None specified	20.97 hr	
Total memory programming time	None specified	56.9 sec (max.)	
Total telemetry verification time	None specified	73.7 sec	1 kbit/sec telemetry rate (6 words/main frame)
Parity check on uplink command	None specified	Yes	Will flag telemetry
Parity check on command prior to execution	None specified	Yes	Command is not executed

The programmer is self-contained; it decodes modes, addresses internally and does not depend on commands from the command distribution unit. A parity bit in the stored command prevents the execution of an incorrect command. One word or all words can be filled into memory. Also one word or all words can be verified by command. The MOS memory is particularly efficient for ERTS because of its

- Minimum package count
- Low power, weight, and size
- Low design cost
- Serial operation, well suited to the operational requirement of scanning the 128 stored commands each 0.5 second for time coincidence

Operational tests indicate excellent noise immunity of the memory. Temperature test, voltage variation (± 10 percent) and clock frequency variation (10 to 270 kHz) did not affect data stored in memory. The limiting factor for the 270-kHz upper limit is the decoder, which cannot accept data at this increased rate.

8.1.2 Design Approach

The stored command programmer is designed to operate in conjunction with the OGO digital command decoder to provide the spacecraft with both real-time and stored command capability.

Commands to be stored are transmitted to the spacecraft via the command link and detected and conditioned by the command decoder. These data, which consist of mode and command information and time identification, are transferred to the programmer, and the command and time information stored in its memory for later execution. The stored commands are continuously scanned and executed back through the command decoder when the command time identification matches the content of an elapsed time counter.

The programmer operates in one of the following four modes:

- Fill mode. The memory is filled via the command link. The fill sequence can consist of one word or up to 128 words. The decoder operates in the 40 bit command word format and each stored command requires a 40 bit command. The programmer

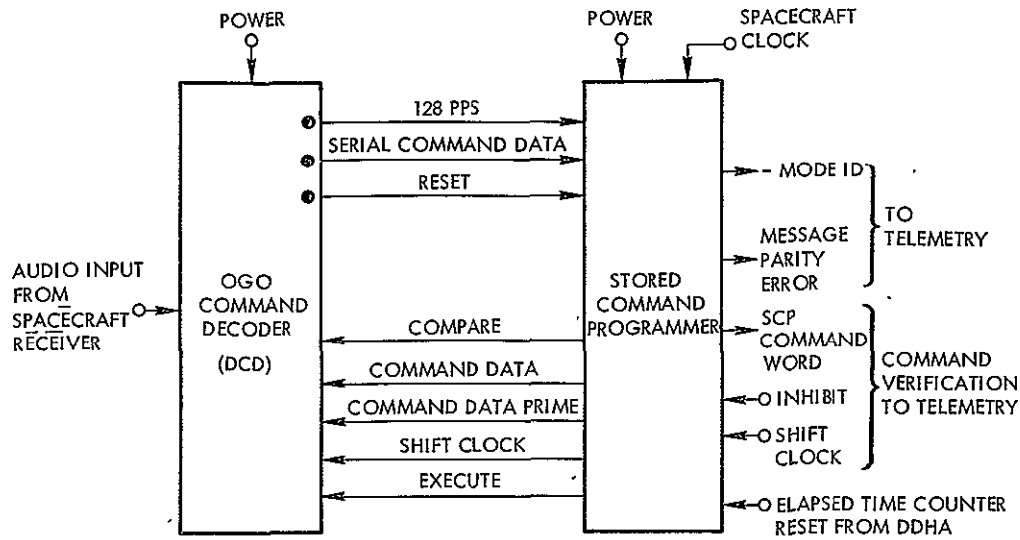
checks these 40 bits for parity before it acts on the command. The programmer can be programmed in less than 60 seconds (128 commands).

- Process mode. The time identification of each stored word is continuously compared with the contents of the elapsed time counter (18 bits) and each command is executed in accordance to its programmed time. The stored command (25 bits) is checked for parity before its execution. While in this mode the stored command has priority over the real-time command.
- Clear mode. The total memory is cleared to zero.
- Standby mode. The programmer operates normally except the commands are not executed; its output is inhibited. The entire content of the memory is telemetered to ground sequentially for memory fill verification.

In the breadboard model of the programmer another mode was also incorporated, the single telemetry mode, in which one of the stored command words is addressed by ground command and telemetered to ground for single word verification. This feature is not needed in the final version in view of the standby-mode readout of the entire memory.

The programmer will operate in only one mode at a time. The operating mode and the programming message parity is telemetered. Each mode must be entered by command except the standby mode. The programmer will automatically enter and remain in the standby mode upon detection of an abnormal power transient. A parity error detected within the uplink programming message will cause the message to be ignored and a parity indication will be transmitted to ground via telemetry.

As shown in Figure 8-2, the programmer interfaces with the digital data handling assembly as well as the command decoder. Three lines from the decoder are required to program and control the programmer. The 128-pps line provides clock signals; the serial command data line contains the 40-bit programming word; and the reset line initializes the programmer to specific states to accept programming data. As long as the reset line is inactive, the programming logic is locked up and will not accept noise.



NOTES:
 ● AVAILABLE ON
 DCD TEST CONNECTOR

Figure 8-2
 INTERFACE DIAGRAM showing data flow between programmer and decoder

Data transfer to the decoder requires five lines. The 6-bit command message is transferred via the command data and command data complement lines. A compare signal followed by shift pulses and an execute pulse is provided by the three remaining lines.

The interface with the digital data handling assembly requires six lines, one for mode ID, one for parity error, one for command word for program verification. The inhibit and shift clock require two lines, and

The interface with the digital data handling assembly requires six lines, one for mode ID, one for parity error, one for command word for program verification. The inhibit and shift clock require two lines, and the elapsed time counter requires the remaining lines. One signal is required from the spacecraft to provide spacecraft clock.

8.1.3 Functional Description

The word format of the stored command programmer (Figure 8-3) includes bits assigned as follows:

- T0 - sync bit used to synchronize operation of the decoder and the programmer
- T1 through T3 - decoder address bits (in the breadboard; a 7-bit address is employed in the final design)
- T4 and T5 - internal address
 - 00 decoder matrix command
 - 01 not used
 - 10 not used
 - 11 programmer command
- T6 through T8 - mode ID

T6	T7	T8	Mode
0	0	0	standby mode
0	0	1	telemetry mode
0	1	0	process mode
0	1	1	clear mode
1	0	0	fill mode
1	0	1	single telemetry mode
1	1	0	clear mode
1	1	1	spare
- T9 through T15 - word address to address each of 128 words
- T16 through T33 - 18 bit time ID
- T34 through T39 - 6 bit command word
- T40 - command parity bit to check 25-bit word
- T41 - message parity to check 44-bit message

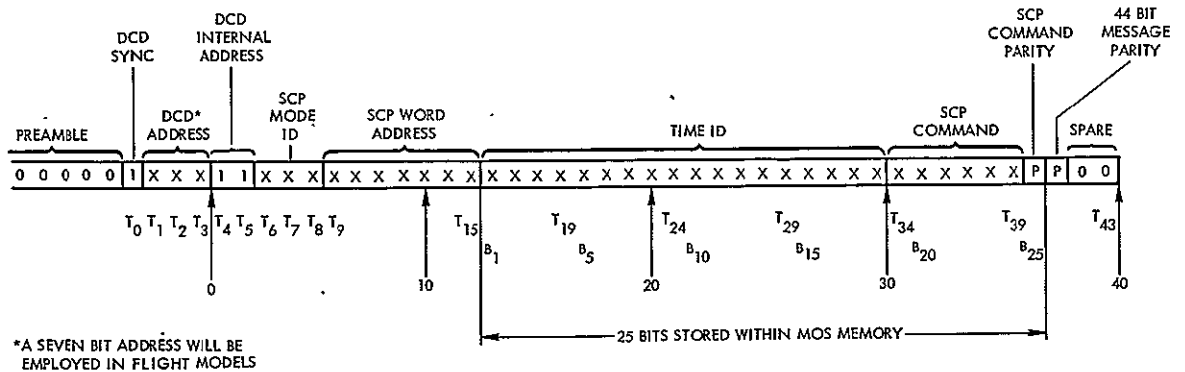


Figure 8-3
 STORED COMMAND PROGRAMMER word format used in breadboard test

as shown in Figure 8-4, the serial data enters the address and mode detector. If the command is a real-time matrix command, it is ignored. If it is a stored command, the timing generator is initiated which separates the various parts of the message. The 7-bit word address enters the address register and the remaining 25 bits (6 command, 18 time ID and one parity) are shifted into the command message register. The 40-bit command is checked for parity; if parity is correct, the command message is entered into the memory when the word counter matches the 7-bit address stored within the command address register. The memory is cleared to zero prior to filling the memory.

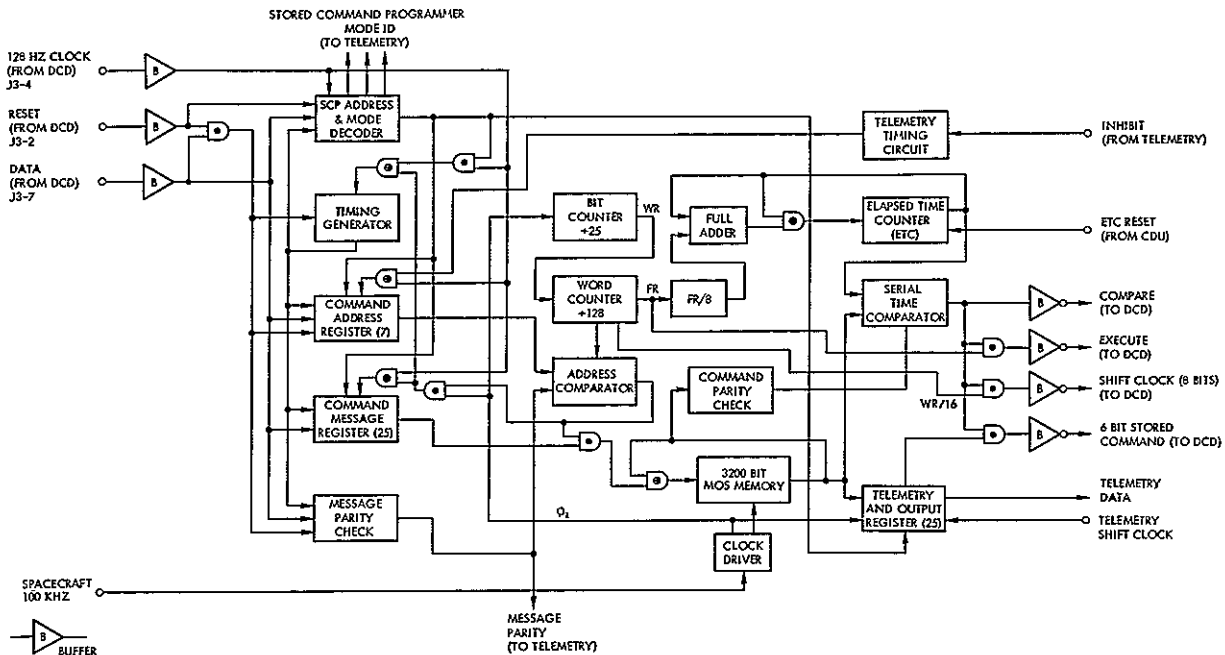


Figure 8-4
BREADBOARD STORED COMMAND PROGRAMMER block diagram

The contents of the memory are recirculated every 64 msec and a serial comparison is made between the elapsed time counter and the time ID within each of the 128 words stored within the memory. When the 18-bit count matches the stored time ID, the stored command is checked for parity and transferred serially to the command decoder. When the data transfer is complete, an execute signal is generated and the 6-bit command is decoded into one of 64 possible matrix commands. The parity is continuously checked on all 25 bits of each stored word, thus

providing continuous monitoring of the 3200-bit recirculating memory. If a single bit should be dropped within the register the programmer prevents the serial transfer of the erroneous data to the decoder.

A telemetry timing circuit synchronizes the telemetry of the digital data handling assembly rate to the operation of the programmer, to provide a means to verify the stored command information in either the single telemetry mode or the telemetry mode.

As shown in Figure 8-5, 343.2 msec are required to store a command through the decoder. A maximum of 64.25 msec is required to

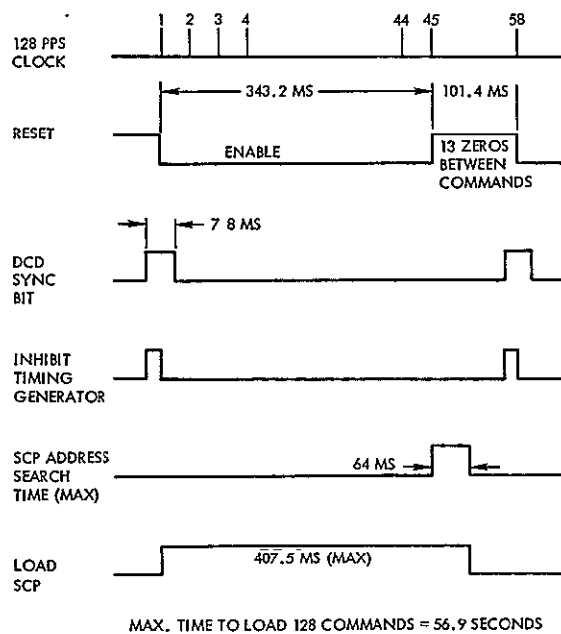


Figure 8-5
COMMAND STORAGE timing diagram
used in breadboard test

and will not require modification. The five lines from the programmer to the decoder require diodes and resistors. These parts are added to the decoder on a small terminal board. No wires are affected in this modification.

Power consumed by the breadboard is 9.69 watts. This power can be reduced to 2 watts by using low power integrated circuits. The memory portion of the breadboard consumed 507 mw at 50 kHz data rate.

store a command within the programmer. Therefore, approximately 407.5 msec are required to load each of 128 commands into the programmer. Thus, approximately 52 seconds are required to fill the total memory.

Figure 8-6 illustrates the circuit and the timing used to synchronize the 50-kHz clock to the 128-pps input data clock from the decoder.

Figure 8-7 shows the basic modification required to interface with the programmer. The three signals required from the decoder are available on the test connector

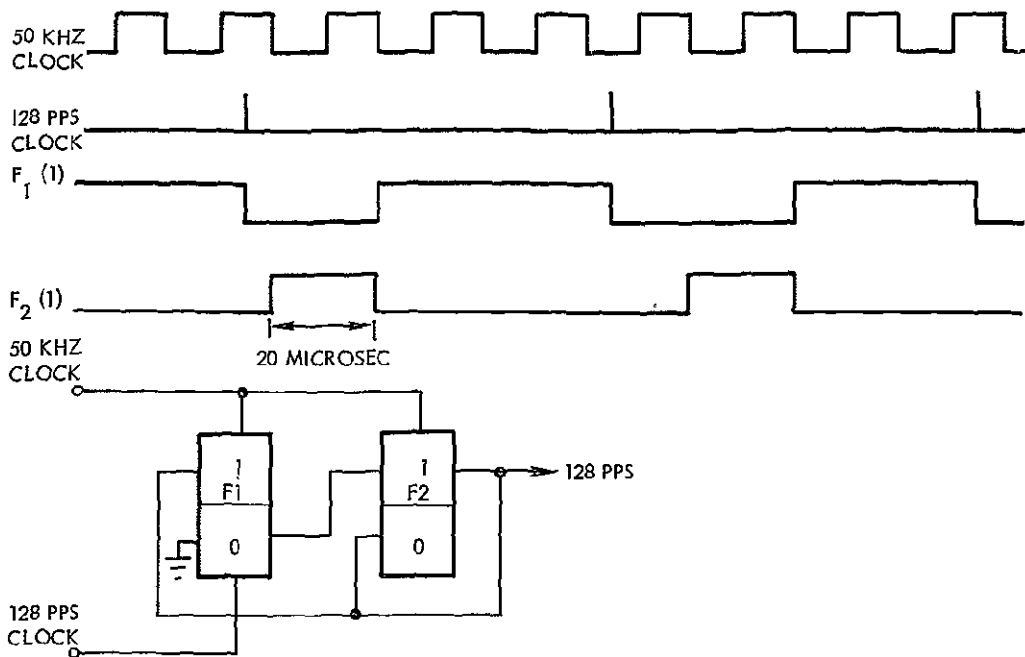


Figure 8-6

DIGITAL DECODER CLOCK (128 pps) and stored command programmer clock (50 kHz) sync timing

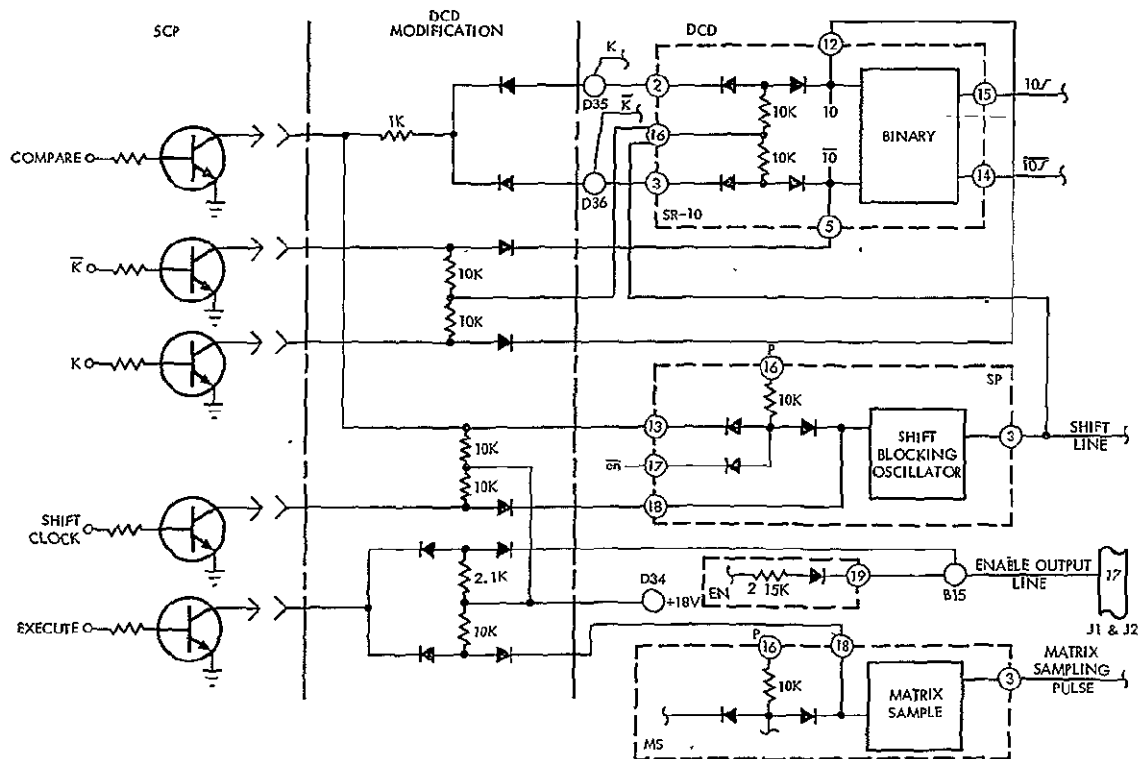


Figure 8-7

DIGITAL DECODER modifications proven out in breadboard test

Temperature test at -5 and +45°C did not affect the data stored in the memory. The power supplies (+10 and -6 volts) were varied ±10 per cent during this test.

8.2 NARROWBAND TAPE RECORDER

Studies to improve the operating life and to fulfill orbital operation requirements of the narrowband tape recorders have resulted in recommendations for incorporation of proven design changes. All of the changes considered for incorporation into the OGO tape recorders have previously been implemented on the Nimbus high data-rate storage system (HDRSS) tape recorder systems produced by RCA for GSFC. These changes are confined to the transport assembly. This system has flown on the Nimbus spacecraft and no major problems have been detected in the areas where design changes have been considered. All test history has been excellent and no difficulty is expected. The design changes require that requalification tests be conducted on the tape recorder. These tests will be conducted on the refurbished OGO prototype tape recorders.

8.2.1 Life Improvements

Four design changes have been evaluated to extend the operational life of the OGO tape recorders, lubrication changes, brake changes, optical end-of-tape sensors, and magnetic head cleaning.

Changes in the bearings of the record motor, motor gear train and the playback motor to use type G-6 grease instead of type 0-11 and 0-16 oils will eliminate the need to refurbish the tape recorder motors after two years. Because of the direct replacement capability and the positive test results, it is planned to utilize HDRSS record and playback motors for the ERTS tape recorders. The use of these motors also permits the elimination of the record gear head, improving jitter characteristics and torque margins.

All tests by RCA on the type G-6 grease have provided excellent results, and no difficulty has been encountered on the recorder or other systems which employ this lubrication. In excess of 10,000 operating hours have been accumulated in life test of the motors in a tape transport.

A change associated with the motors that resulted from the lubrication change in the HDRSS units is the utilization of diodes across the start-to-run relay contracts. These diodes enable power to be applied to the motor during switching from the start-to-run windings, preventing changes in the magnetization of the motor rotor, and thereby sustaining the motor torque characteristics. This change is considered advisable to prevent stall-out at low temperatures. Two diodes are connected back-to-back across each relay start-to-run contact as shown in Figure 8-8. A Jan type part is used, likely a 1N4962 to MIL-S-19500/356A.

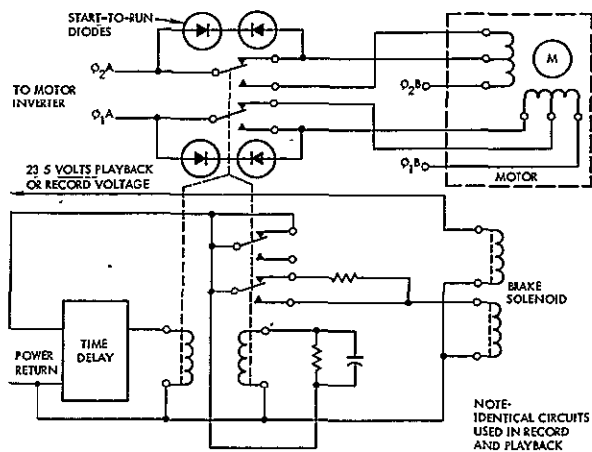


Figure 8-8
TAPE RECORDER start-to-run motor circuit

The design has also provided improved fabrication and brake adjustments. Over 9600 hours of brake system life test time on a tape transport have been accumulated without a failure.

Optical end-of-tape sensors are planned to eliminate switch damage to the magnetic tape, the OGO type microswitches are retained as a back-up.

The sensor (see Figure 8-9) uses gallium arsenide diode light sources and 2N986 photo transistor sensors with triggering circuits which have time delays to prevent false triggering. They are installed to detect end-of-tape in each direction. The backup microswitches are activated by buildup of the tape stacking diameter and are adjusted well beyond the window zone of the optical detectors. Mounting of the detectors, backup microswitches, relays, and amplifier circuits is on shear plates attached to the side of the tape transport castings.

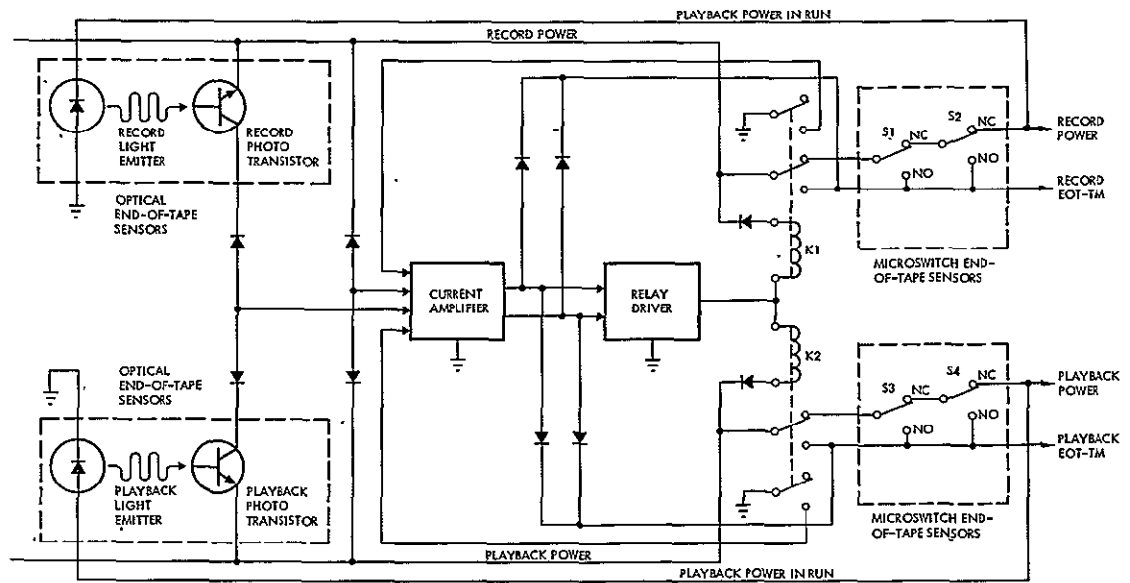


Figure 8-9
TAPE RECORDER end-of-tape sensor block diagram

Magnetic head cleaning in orbit by means of an abrasive tape at the end of playback has been studied as an optional life improvement. This technique has been implemented into HDRSS recorders scheduled for the next Nimbus flight as well as into classified tape recorders manufactured by RCA. The method, known as "green tape" places Cr_2O_3 on the end of tape in patterns which on command passes over the magnetic head and removes oxide debris that has accumulated.

Sections of green tape are placed after the optical end-of-tape window and before the microswitch end-of-tape detection. After a recorder has been played back, an "off" followed on another "playback" command will drive the recorder into the backup end-of-tape switches, permitting the green tape to pass over the heads. When the recorder is returned to the record mode the initial record time will be lost until the green tape has rewound. Prototype tape recorder life tests on the HDRSS unit have demonstrated that this head cleaning technique is effective in restoring performance.

8.2.2 Playback-to-Record Ratio

A 32:1 ratio with a bit rate of 1 kbit in record and 32 kbits in playback is required to meet orbital requirements. The record-to-

Playback ratio is changed by modifications in the transport planetary subassembly while the bit rate is changed in the electronics assembly.

Planetary subassembly from HDRSS tape recorders will be utilized as a direct replacement for the OGO subassembly. This type of planetary has a 32:1 ratio, contains the motors with the new lubrication, and includes the disc brake design. The exact record and playback speeds are set by adjustments in the diameters of two planetary pulleys. The planetary drive system is shown in Figure 8-10.

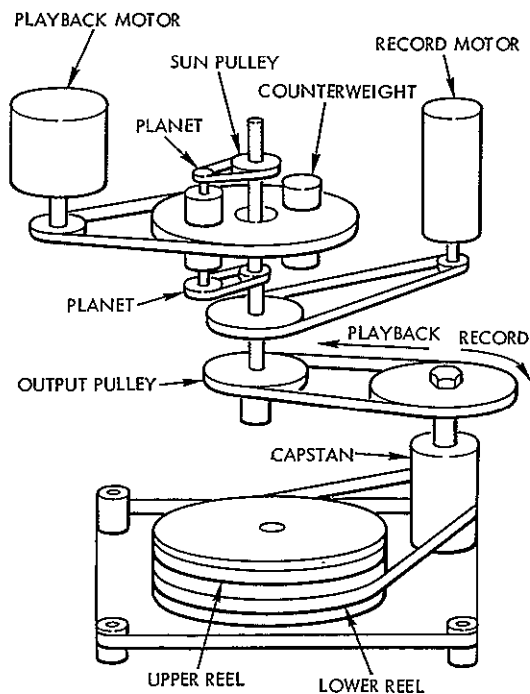


Figure 8-10
SCHEMATIC DIAGRAM of drive system
of OGO/ERTS tape recorders

The nominal operating characteristics of the ERTS tape recorders are shown along with those of OGO and HDRSS in Table 8-2. All parameters are within values previously used, and no problems are expected in operation of the tape recorders. The tape bit rate packing density has decreased because of the need to maintain the velocity of the magnetic tape across the playback head to preserve signal strength.

Several distinct advantages are gained by the use of this subassembly:

The planetary system is a direct belt drive, eliminating the gear box on the motor. This provides greatly improved characteristics of jitter and flutter.

- Torque margins are improved because of the elimination of the gear box.
- Heavier support brackets are utilized which eliminate the failures encountered during requalification of the OGO 8 kbit/sec design.
- The subassembly incorporates improved bearing mounting and mass distribution in the planetary.

Table 8-2. Tape Recorder Parameters

	ERTS-A-B	OGO 1, 3, 5	OGO 2, 4	OGO 6	HDRSS (digital)
Playback-to-record ratio	32 1	64 1	32.1	16 1	32.1
Record speed (ips)	0.592	0.296	1.18	2.36	1.34
Playback speed (ips)	18.96	18.96	37.9	37.9	42.88
Record time (hr)	6.1	12.2	3.05	1.5	2
Playback time (min)	11.4	11.4	5.7	5.7	3.75
Record bit rate (kbit/sec)	1	1	4	8	4
Playback bit rate (kbit/sec)	32	64	128	128	128
Tape packing density (bpi)	188	375	375	375	2982

The digital logic of the tape recorder is independent of the frequency. However, since the OGO system was designed for 64 and 128 kHz playback frequency with a 256-kHz oscillator frequency, a countdown circuit must be provided to obtain 32 kHz. Two techniques are feasible; the first is to change the frequency of the oscillator to 128 kHz, the second is to provide another flip-flop in the countdown circuit. The simplest and recommended approach is to change the oscillator frequency. The final determination of the method will take place after engineering tests during the initial phases of a subcontract when one of the prototype electronic assemblies will be used for modification and evaluation testing of the frequency changes.

Bandwidth of the phase-lock loop has been evaluated in view of the change in frequency. RCA does not anticipate a problem in this area because of the implementation of the belt drive system which reduces the jitter and the need for a wide bandwidth.

Pulsewidths and rise times of the phase-lock oscillator with the new frequency and operation of the recognition circuit are satisfactory.

8.2.3 Other Design Changes

Magnetic head mounting improvements have been incorporated into the transport which permits the three-axis record head mount adjustment and a swivel mount for the erase head. These changes are acceptable for inclusion into the ERTS tape recorders. Their incorporation was agreed upon for OGO, but implementation problems prevented their use.

Memorex is no longer manufacturing instrumentation tape of the type used on OGO. Therefore, a new magnetic tape must be selected for the ERTS tape recorders. In addition, the RCA/Camden Division may not produce magnetic heads of the type used for OGO. Because of these two problems it appears that a new tape and head combination must be selected. The HDRSS tape and head combination is believed to be the limiting factor in life of these tape recorders. At the time of a subcontract for ERTS tape recorders, it appears that NASA tests and data on magnetic tape will permit the selection of a tape-head combination to be tested for ERTS. The RCA proposal includes a task for the use of one of the OGO prototype tape transports for a tape cycling test at the ERTS speeds. This test will be initiated immediately after the award of a subcontract to verify the suitability of tape for the flight tape recorders.

8.3 SPACECRAFT CLOCK

The primary objective of the spacecraft clock study was to satisfy the mission requirements without imposing any change requirements on the payload and with maximum use of and minimum modifications to existing OGO equipment. The objectives to be met by a common spacecraft clock subsystem as outlined in the study specification are:

- Provide timing signals at a variety of intervals and coded relative time for the purpose of (a) sequencing of payload sensors and providing timing to the attitude determination and other spacecraft subsystems; (b) identification of the relative time at which pictures were taken, attitude measurements were made, and other engineering and scientific data samples were taken; (c) execution of stored commands through coincidence of command execute time and spacecraft clock time and; (d) as a source for synchronization pulses for wideband and narrowband formats.
- Ensure that the time of spacecraft clock update is known within 1-bit time of the PCM telemetry data rate.

The specification also states that preliminary design for the payload has considered the Nimbus clock as an interface with the spacecraft. The Nimbus clock is coded into even seconds, minutes, hours, and days; whereas the clock built into the OGO data system is binary coded with a least count of 1.152 seconds. Two approaches were examined that will meet all of the above stated requirements.

The first approach makes modifications to the existing OGO data handling equipment such that a PCM data frame rate of exactly 1 second will result. This can be done by providing a 10-bit word at a bit rate of 1280 bits/sec (10 bits/word x 128 word/frame x 1 sec/1280 bits). The format can then be used synchronously with a 36-bit NASA time code generator (1 second cycle) so that the time of clock update is known within 1-bit time of the PCM data rate. Advantages and disadvantages of this approach are:

1) Advantages

- A PCM format is obtained that can be synchronously operated with a 36-bit NASA coded-time generator (Nimbus interface).
- A 36-bit NASA coded timer in the spacecraft eliminates the need of converting and correlating to universal time at the ground station.
- The time code generator is compatible with the payload preliminary design interface.

2) Disadvantages

- Extensive design and hardware modification must be made to the digital data handling assembly and associated checkout equipment to provide a 10 bits/word format.
- Design and hardware modifications must be made to the low frequency timing assembly and associated checkout equipment to provide a bit rate of 1280 bits/sec.
- Modification of the PCM tape recorder and associated checkout equipment is required to operate at the new bit rate and word length.
- The addition of the 10th bit to the telemetry would reduce telemetry efficiency.
- Design modifications would have to be made to the existing flight proven 36-bit NASA time code generator (as used in the Nimbus system).

The second approach considered makes full use of existing flight-proven OGO hardware and was selected as the baseline timing subsystem described in Volume 3, Section 6.

1) Advantages

- No modifications are required to existing OGO hardware. Substantial expense is avoided.
- The efficient 9-bit word format is retained for PCM telemetry.
- The existing binary-coded accumulated time generator is synchronous with the PCM telemetry format and time update is known to an accuracy of better than 1-bit period of the PCM data rate.

2) Disadvantages

- Spacecraft coded time must be correlated to universal time on the ground.

All of the required timing signals are available from the chosen baseline design. The difference then between the two approaches is in the time code and least count. A conversion from binary code to UMT must be accomplished much as is now the practice with OGO operations. The binary clock is incorporated in the data frame and can be supplied for payload use as requirements are defined.

8.4 TELEMETRY LIST

The proposed telemetry list for ERB (Table 8-3) has been assembled from the following sources: (1) basic OGO design, (2) new ERTS functional needs, (3) payload needs stated by sensor manufacturers. This list in sum has demonstrated a need to retain subcommutator No. 3 of the OGO data system.

All analog words are handled as 8-bit words (accuracy ± 0.4 percent of full scale). Actual accuracy of measurement will depend also on the precision of the sensing element. Most bilevel data are handled also as analog words being summed by resistive networks to form one word of 16 states, e. g., G18A, B, C, D. This is the same technique used in OGO for status data.

Data rates available by command in ERTS are 1 and 32 kbits/sec. This choice provides the following sample rates:

Table 8-3. ERTS Observatory Instrumentation List

Item	Name	Commutator Sampling Rate
<u>Return Beam</u>		
<u>Vidicon</u>		
G1	G1 voltage	MC
G2	Target voltage	MC
G3	Vidicon cathode current	MC
G4	Video output	MC
G5	Focus current	MC
G6	Combined alignment currents	MC
G7	Horizontal deflection output	MC
G8	Vertical deflection output	MC
G9	Deflection-power supply	MC
G10	Low voltage power supply	MC
G11	Minus 28-volt shutter current	MC
G12	Temperature, faceplate	MC
G13	Temperature, yoke/focus coil	MC
G14	Temperature, electronics	MC
G15	Temperature, low voltage power supply	MC
G16	Thermoelectric cooler current	MC
G17	Temperature, camera controller	MC
G18A	Vidicon filament current	} MC
G18B	Anode voltage supply	
G18C	G2 voltage supply	
G18D	Minus 24.5-volt input voltage	
G19A	Anode/target mode (command status)	MC
G19B	Power on/off (command status)	MC
G19C	One cycle/sec rephasing	MC
G19D	50-kHz clock input	MC
G20A	Horizontal sync	} MC
G20B	Vertical sync	
G20C	Clock A-B (command status)	
G20D	Cycle, continuous/single (command status)	
G21A	P3 auto/P2-P1 (command status)	} MC
G21B	P2 auto/P3-P1 (command status)	
G21C	Mode-record/direct-record (command status)	
G21D	Mode-direct/direct-record (command status)	
G22A	Dynamic beam regulator in/out (command status)	MC
G22B	Spare	
<u>Multispectral</u>		
<u>Point Scanner</u>		
H1A	Spectral band 1 on/off	} MC
H1B	Spectral band 2 on/off	
H1C	Spectral band 3 on/off	
H1D	Spectral band 4 on/off	
H2A	Spectral band 5 on/off	} MC
H2B	Band 1 gain low/high	
H2C	Band 2 gain low/high	
H2D	Band 3 gain low/high	

Table 8-3. ERTS Observatory Instrumentation List (Continued)

Item	Name	Commutator Sampling Rate
<u>Multispectral Point Scanner</u> (Cont.)		
H3A	Band 4 gain low/high	} MC
H3B	Main inverter A on/off	
H3C	Main inverter B on/off	
H3D	Mirror pick-off on/off	
H4A	Band 1 high voltage A on/off	} MC
H4B	Band 1 high voltage B on/off	
H4C	Band 2 high voltage A on/off	
H4D	Band 2 high voltage B on/off	
H5A	Band 3 high voltage A on/off	} MC
H5B	Band 3 high voltage B on/off	
H5C	Scan mirror drive on/off	
H5D	Band 5 focus on/off	
H6	Band 5 preamplifier output voltage	MC
H7A	Calibration lamp No. 1 on/off	} MC
H7B	Calibration lamp No. 2 on/off	
H7C	Rotating shutter drive on/off	
H7D	Spare	
H8	Silicon photodiode preamplifier output	MC
H9	Silicon photodiode preamplifier output	MC
H10	Silicon photodiode preamplifier output	MC
H11	Silicon photodiode preamplifier output	MC
H12	Silicon photodiode preamplifier output	MC
H13	Silicon photodiode preamplifier output	MC
H14	Low voltage supply output	MC
H15	Low voltage supply output	MC
H16	Low voltage supply output	MC
H17	Low voltage supply output	MC
H18	Low voltage supply output	MC
H19	To be defined	MC
H20	To be defined	MC
H21A	To be defined	MC
H21B	To be defined	
H21C	To be defined	
H22	Temperature	MC
H23	Temperature	MC
H24	Temperature	MC
H25	Temperature	MC
H26	Rotating shutter housing temperature	MC
H27	Calibration lamp base temperature	MC
H28	Temperature	MC
H29	Temperature	MC
H30	Temperature	MC
H31	Temperature	MC

Table 8-3. ERTS Observatory Instrumentation List (Continued)

Item	Name	Commutator Sampling Rate
<u>Wideband Video</u>		
<u>Tape Recorders</u>		
I1	VTR 1 tape footage	MC
I2	VTR 1 pressure	MC
I3	VTR 1 temperature, electronics unit	MC
I4	VTR 1 temperature, transport unit	MC
I5	VTR 1 average record current	MC
I6	VTR 1 average playback voltage	MC
I7	VTR 1 servo voltage	MC
I8	VTR 1 capstan motor speed	MC
I9	VTR 1 DC motor current, headwheel	MC
I10	VTR 1 DC motor current, capstan	MC
I11A	VTR 1 standby power on/off	}
I11B	VTR 1 record on/off	
I11C	VTR 1 playback on/off	
I11D	VTR 1 rewind on/off	
I12A	VTR 1 fast forward on/off	}
I12B	VTR 1 primary end of tape (EOT)	
I12C	VTR 1 secondary end of tape	
I12D	VTR 1 primary beginning of tape (BOT)	
I13A	VTR 1 secondary beginning of tape	}
I13B	VTR 1 recorder current adjust levels (8)	
I13C	VTR 1 recorder current adjust levels (8)	
I13D	VTR 1 recorder current adjust levels (8)	
I14A	VTR 1 picture/wideband mode (RBV/MSS)	}
I14B	VTR 1 lap at BOT	
I14C	VTR 1 spare	
I14D	VTR 1 spare	
I15	VTR 2 tape footage	MC
I16	VTR 2 pressure	MC
I17	VTR 2 temperature, electronics unit	MC
I18	VTR 2 temperature, transport unit	MC
I19	VTR 2 average record current	MC
I20	VTR 2 average playback voltage	MC
I21	VTR 2 servo voltage	MC
I22	VTR 2 capstan motor speed	MC
I23	VTR 2 DC motor current, headwheel	MC
I24	VTR 2 DC motor current, capstan	MC
I25A	VTR 2 standby power on/off	}
I25B	VTR 2 record on/off	
I25C	VTR 2 playback on/off	
I25D	VTR 2 rewind on/off	
I26A	VTR 2 fast forward on/off	}
I26B	VTR 2 primary end of tape (EOT)	
I26C	VTR 2 secondary end of tape	
I26D	VTR 2 primary beginning of tape (BOT)	

Table 8-3. ERTS Observatory Instrumentation List (Continued)

Item	Name	Commutator Sampling Rate
<u>Wideband Video Tape Recorders</u> (Cont.)		
I27A	VTR 2 secondary beginning of tape	} MC
I27B	VTR 2 recorder current adjust levels (8)	
I27C	VTR 2 recorder current adjust levels (8)	
I27D	VTR 2 recorder current adjust levels (8)	
I28A	VTR 2 picture/wideband mode (RBV/Mss)	} MC
I28B	VTR 2 lap at BOT	
I28C	VTR 2 spare	
I28D	VTR 2 spare	
<u>Structures</u>		
B3A	Array No. 1, hinge No. 1	} SC2
B3B	Array No. 1, hinge No. 2	
B3C	Array No. 1, hinge No. 3	
B4A	Delta ERTS separation	} SC2
B4B	Array No. 2, hinge No. 1	
B4C	Array No. 2, hinge No. 2	
B4D	Array No. 2, hinge No. 3	
B7A	Predeployment array 1 (-X)	} SC2
B8B	Predeployment array 2 (+X)	
B11	Deploy bottle pressure 1	SC2
B12	Deploy bottle pressure 2	SC2
<u>Data Collection System</u>		
J1	To be defined	MC
J2	Negative analog	MC
<u>Attitude Control</u>		
A1	Gas, high pressure	SC2
A2	Gas, low pressure	SC2 X2
A3	Gas, bottle temperature	SC1
A4	Pitch error signal	MC+SC2 X2
A5	Roll error signal	MC+SC2 X2
A6A	Sun alarm signal head A	} SC2 X2
A6B	Sun alarm signal head B	
A6C	Sun alarm signal head C	
A6D	Sun alarm signal head D	
A7A	Track check signal head A	} SC2 X2
A7B	Track check signal head B	
A7C	Track check signal head C	
A7D	Track check signal head D	
A9	Horizon scanner head A temperature	SC2
A10	Yaw error signal	MC+SC2 X2

Table 8-3. ERTS Observatory Instrumentation List (Continued)

Item	Name	Commutator Sampling Rate
<u>Attitude Control</u> (Cont.)		
A11	Array error signal	SC2
A12	Array shaft angle (sine)	SC2
A13	Array shaft angle (cosine)	SC2
A16	Solar array drive	SC2 X2
A17	Reaction wheel count	MC
A18	Reaction wheel pitch count	MC
A19	Reaction wheel yaw count	MC
A21A	Gas control valve No. 1	} SC2 X8
A21B	Gas control valve No. 2	
A21C	Gas control valve No. 5	
A22A	Gas control valve No. 3	} SC2 X8
A22B	Gas control valve No. 4	
A22C	Gas control valve No. 6	
A23A	ACS modes logic	SC2 X2
A24	Pitch rate gyro demodulator signal (error)	SC2 X2
A25	Sun sensor No. 1 temperature	SC2
A26	Sun sensor No. 2 temperature	SC2
A27	Yaw gyro status	SC2
A28	Yaw gyro motor tachometer	SC2 X2
A29	Orbital switching status	SC2 X2
A30	Yaw gyro blanket temperature	SC2
A31A	Reaction wheel drive-roll	} SC2 X4
A31B	Reaction wheel drive-pitch	
A31C	Reaction wheel drive-yaw	
A32	ACS inverter temperature	SC2
A33	Yaw reaction wheel temperature	SC2
A34	Pitch reaction wheel temperature	SC2
A35	Pitch rate gyro tach	SC2 X2
A40	Head "A" angle	SC2 X4
A41	Head "B" angle	SC2 X4
A42	Head "C" angle	SC2 X4
A43	Head "D" angle	SC2 X4
A44A	CSA status, bus safe	} SC2
A44B	CSA status, bus armed	
A44C	Pitch, jets enabled	
A44D	Pitch, jets disabled	
A47A	Roll jets enable/disable	} SC2
A47B	Yaw jets enable/disable	
<u>Communication</u>		
C50	TWTA No. 1, anode voltage	SC3
C51	TWTA No. 1, helix plus anode current	SC3

Table 8-3. ERTS Observatory Instrumentation List (Continued)

Item	Name	Commutator Sampling Rate
<u>Communication</u> (Cont.)		
C52	TWTA No. 1, temperature transducer	SC3
C53A	TWTA No. 1, power mode indicator	}
C53B	TWTA No. 2, power mode indicator	
C54	TWTA No. 2, anode voltage	SC3
C55	TWTA No. 2, helix plus anode current	SC3
C56	TWTA No. 2, temperature transducer	SC3
C57	VHF transmitter No. 1, forward power	SC3
C58	VHF transmitter No. 1, reverse power	SC3
C59	VHF transmitter No. 2, forward power	SC3
C60	VHF transmitter No. 2, reverse power	SC3
C61	VHF receiver No. 1, AGC-1	SC3
C62	VHF receiver No. 1, AGC-2	SC3
C63	VHF receiver No. 2, AGC-1	SC3
C64	VHF receiver No. 2, AGC-2	SC3
C65	USB receiver "A", signal present	SC3
C66	USB receiver "A", loop stress	SC3
C67	USB receiver "B", signal present	SC3
C68	USB receiver "B", loop stress	SC3
C69	USB transmitter "A", power monitor	SC3
C70	USB transmitter "A", temperature monitor	SC3
C71	USB transmitter "B", power monitor	SC3
C72	USB transmitter "B", temperature monitor	SC3
C73	USB converter "A" +15 Vdc	SC3
C74	USB converter "A" -15 Vdc	SC3
C75	USB converter "A" +28 Vdc	SC3
C76	USB converter "B" +15 Vdc	SC3
C77	USB converter "B" -15Vdc	SC3
C78	USB converter "B" +28 Vdc	SC3
C79	Wideband driver A, Afc loop stress	SC3
C80	Wideband driver B, Afc loop stress	SC3
C81	Wideband driver C, Afc loop stress	SC3
C82	Wideband driver D, Afc loop stress	SC3
<u>Power Supply</u>		
D1	Battery 1 current amplifier	SC2 X2
D2	Battery 2 current amplifier	SC2 X2
D3A	No. 1 solar array norm/reg 2	}
D3B	No. 1 charge bus norm/parallel 2	
D3C	No. 2 solar array norm/reg 1	
D3D	No. 2 charge bus norm/parallel 1	
D4	Array 1 (-X) current amplifier	SC2
D5	Array 2 (+X) current amplifier	SC2
D6	Array 1 (-X) sec C unreg	SC1
D8	Battery 1 voltage	SC2
D9	Battery 2 voltage	SC2
D10	Load bus voltage	SC2

Table 8-3. ERTS Observatory Instrumentation List (Continued)

Item	Name	Commutator Sampling Rate
<u>Power Supply</u> (Cont.)		
D11D	No. 1 and No. 2 95°F switch norma/override	} SC1
D11E	Charge bus parallel command	
D11F	Discharge path normal/open	
D13	Array 1 (-X) Sec A thermal fin temperature	SC1
D14	Array 2 (+X) Sec A thermal fin temperature	SC1
D15	Sync signal amplifier 400 Hz	SC2
D16	Sync signal amplifier 2461 Hz 0 and 90 degrees	SC2
D17	Array 1 (-X) sec C unreg I amplifier	SC2
D20	Converter 2A + 16 volt	SC1
D21	Converter 2A + 9 volt	SC1
D22	Converter 2A + 5 volt	SC1
D23	Converter 2A - 6 volt	SC1
D28	Converter 5 + 16 (DDHA and ADHA)	SC1
D29	Converter 5 + 9 (DDHA and ADHA)	SC1
D30	Converter 5 - 6 (DDHA and ADHA)	SC1
D31	Converter 5 - 16 (DDHA and ADHA)	SC1
D32	Converter 6 + 16 volt	SC1
D33	Converter 6 + 9 volt	SC1
D34	Converter 6 - 6 volt	SC1
D35	Converter 6 - 16 volt	SC1
D36	Converter 7 + 16 volt	SC1
D37	Converter 7 + 9 volt	SC1
D38	Converter 7 - 6 volt	SC1
D39	Converter 8 + 16 volt	SC1
D40	Converter 8 + 9 volt	SC1
D41	Converter 8 - 6 volt	SC1
D42	Converter 9 + 20 volt	SC1
D43	Converter 9 + 10 volt	SC2
D44	Converter 9 - 20 volt	SC2
D45	Converter 9 + 28 volt	SC2
D46	ACS inverter 400 Hz	SC1
D50	Battery 2 (-X rad. panel)	SC1
D51	Battery 1 (+X rad. panel)	SC1
D57	No. 1 thermal fin drive volts (-X)	SC1
D58	No. 2 thermal fin drive volts (+X)	SC1
D59	Load bus	SC2
D61A	Regulator charge rate No. 1 reg/No. 2 reg trickle/1A	} SC1
D61B	No. 1 reg. normal/full array	
D61C	No. 2 reg. normal/full array	
D62A	No. 1 battery normal/recondition	} SC1
D62B	No. 2 battery normal/recondition	
D62C	No. 1 reg. No. 2 reg. charge mode. Constant volt/trackle at V_B limit	
D63A	No. 1 battery normal/disconnect	} SC2
D63B	No. 2 battery normal/didconnect	

Table 8-3. ERTS Observatory Instrumentation List (Continued)

Item	Name	Commutator Sampling Rate
<u>Power Supply</u> (Cont.)		
D64	No. 1 battery current direction	SC2
D65	No. 2 battery current direction	SC1
D75	Converter 2B + 16 volt	SC2
D76	Converter 2B + 9 volt	SC2
D77	Converter 2B + 5 volt	SC2
D78	Converter 2B - 6 volt	SC2
D79	RBV battery current	SC1
D80	RBV battery voltage	SC1
D81	Payload converter input current	SC1
D82	Payload converter output voltage	SC1
D83	Payload converter status (No. 1 or 2)	SC1
D84	Payload converter temperature	SC1
<u>Thermal Control</u>		
E1	Array 1 (inboard) -X temperature	SC3
E4	Array 2 (outboard) +X temperature	SC3
E5	Panel mid third (+X) temperature	SC3
E6	Panel aft third (+X) temperature	SC3
E7	Panel mid third (-Z) temperature	SC3
E8	Panel aft third (-X) temperature	SC3
E21	Panel top third (-Z) temperature	SC3
E22	Panel mid third (+Z) temperature	SC3
E23	Panel top third (+X) temperature	SC3
E24	Panel aft third (-X) temperature	SC3
E30	Panel (-Y) middle temperature	SC3
E50	+X panel temperature	SC3
E51	+X panel temperature	SC3
E52	-X panel temperature	SC3
E53	-X panel temperature	SC3
E54	Payload temperature sensor No. 1	SC3
E55	Payload temperature sensor No. 2	SC3
E56	Payload temperature sensor No. 3	SC3
E57	Payload temperature sensor No. 4	SC3
E58	+Y panel temperature	SC3
E59	+Z panel temperature	SC3
E60	+Z panel temperature	SC3
E61	-Z panel temperature	SC3
E62	-Z panel temperature	SC3
<u>Data Handling</u>		
F1	Tape record 1 + 9.5	SC1
F2	Tape record 1 - 9.5	SC1
F5	Tape record 1 encl. pressure	SC1
F8	Tape record 1 base temperature	SC1
F9	Tape recorder No. 2 + 9.5V	SC1

Table 8-3. ERTS Observatory Instrumentation List (Continued)

Item	Name	Commutator Sampling Rate
<u>Data Handling</u> (Cont.)		
F10	Tape recorder No. 2 - 9.5V	SC1
F13	Tape recorder pressure	SC1
F14	Clock No. 1 oscillator temperature	SC1
F15	Clock No. 2 oscillator temperature	SC1
F16	Tape recorder No 2 temperature	SC1
F17	No 1 LFTA Bd 3 temperature	SC1
F20	DDHA 1 Bd 3 temperature	SC1
F22	DDHA 2 Bd 3 temperature	SC1
F24/32	ADHA in service temperature	SC1
F25/33	Calibration No. 1	SC1
F26/34	Calibration No. 2	SC2
F27/35	Calibration No. 3	SC1
F28/36	Calibration No 4	SC2
F29/37	Calibration No 5	SC1
F30/38	Calibration No. 6	SC2
F31/39	Calibration No 7	SC1
F40A	Arm bus On	}
F40B	Payload ordnance armed	
F40C	Boom deploy	
F40E	Sequence relay switches	
F41A	SIU, Rx 1 sig present	
F41B	SIU, Rx 2 sign present	}
F41C	SIU, deployment safe	
F42	TR No. 1 status	SC2
F43	TR No. 2 status	SC2
F44	LFTA status	SC2
F45/47	DDHA status	SC2
F46/48	DDHA status	SC2
F49	Command status word No. 1	MC
F50	Command status word No. 2	MC
F51	Command status word No. 3	MC
F52	Command status word No 4	MC
F53	Command status word No 5	MC
F54	Stored command programmer No 1 verification	MC
F55	Stored command programmer No 1 verification	MC
F56	Stored command programmer No 1 verification	MC
F57	Stored command programmer No. 1 verification	MC
F58	Stored command programmer No. 1 verification	MC
F59	Stored command programmer No 1 verification	MC
F60	Stored command programmer No. 2 verification	MC
F61	Stored command programmer No. 2 verification	MC
F62	Stored command programmer No. 2 verification	MC
F63	Stored command programmer No 2 verification	MC
F64	Stored command programmer No 2 verification	MC

Table 8-3. ERTS Observatory Instrumentation List (Continued)

Item	Name	Commutator Sampling Rate
<u>Data Handling</u> (Cont.)		
F65	Stored command programmer No. 2 verification	MC
F66	Stored command programmer No. 1 temperature	SC3
F67	Stored command programmer No. 2 temperature	SC3
F68	Stored command programmer No. 1 parity	MC
F69	Stored command programmer No. 2 parity	MC
F70	Stored command programmer No. 1 +16 volt	SC3
F71	Stored command programmer No. 1 +9 volt	SC3
F72	Stored command programmer No. 1 +5 volt	SC3
F73	Stored command programmer No. 1 -5 volt	SC3
F74	Stored command programmer No. 2 +16 volt	SC3
F75	Stored command programmer No. 2 +9 volt	SC3
F76	Stored command programmer No. 2 +5 volt	SC3
F77	Stored command programmer No. 2 -5 volt	SC3
F78	Spacecraft identification	MC
F79	No. 2 LFTA Bd 3 temperature	SC1

<u>Commutator</u>	<u>Time between Samples (sec)</u>	
	<u>1 kbit/sec</u>	<u>32 kbits/sec</u>
Main Commutator	1.152	0.036
Subcommutator 1	147.45	4.61
Subcommutator 2	142.45 (1.152*)	4.61 (0.036*)
Subcommutator 3	147.45	4.61

In the sampling rate column in Table 8-3 X2 means that two samples are included in each frame, thus doubling the sampling rate.

The total requirement of Table 8-3 for each subcommutator is compared to available inputs below (Table 8-4).

* Available by command to accelerate subcommutator 2.

Table 8-4. ERTS Instrumentation List Summary

	Input Type	Capacity	Usage
Main multiplexer	Analog	68	68
	Digital	20	20
	A- -D	28	26
Submultiplexer No. 1	Analog	88	65
	Digital	16	0
	A- -D	24	0
Submultiplexer No. 2	Analog	88	74
Submultiplexer No. 3	Analog	<u>88</u>	<u>68</u>
Total inputs		420	321

8.5 COMMAND LIST

All of the commands that are judged necessary to assure reliable control of the ERTS payload and spacecraft have been identified. The total number of commands is given below where one command is one impulse. For a power on-off function two impulse commands are required.

<u>Subsystem</u>	<u>Number of Impulse Commands</u>
Return beam vidicon	34
Multispectral spot scanner	48
Data collection system	4
Video tape recorders	18
Attitude control	46
Power	31
Communication	38
Data handling	21
Command	<u>18</u>
Total	257

These totals are detailed in the following double-column list:

ERTS Command List

<u>Return Beam Vidicon</u>	<u>Multispectral Spot Scanner</u>
Clock A (spacecraft)	Spectral band 1, on
Clock B (spare)	Spectral band 2, on
Single cycle	Spectral band 3 on
Continuous cycle	Spectral band 4, on
Camera 1 on	Spectral band 5, on
Camera 1 off	Spectral band 1, off
Camera 2 on	Spectral band 2, off
Camera 2 off	Spectral band 3, off
Camera 3 on	Spectral band 4 off
Camera 3 off	Spectral band 5 off
Exposure automatic	Step gain band 1, up
Preset 1 (8 msec)	Step gain band 2 up
Preset 2 (12 msec) nominal	Step gain band 3, up
Preset 3 (16 msec)	Step gain band 4, up
Anode mode	Step gain band 1, down
Target mode	Step gain band 2, down
Dynamic beam regulator in	Step gain band 3, down
Dynamic bean regulator out	Step gain band 4, down
Record mode	Scan mirror drive, on
Direct mode	Scan mirror drive, off
Direct/record mode	Step band 5, focus, on
Start prepare	Step band 5, focus, off
Power on 1	Step band 5, focus, forward
Power off 1	Step band 5, focus, reverse
Power on 2	Mirror pick-off, on
Power off 2	Mirror pick-off, off
Aperture compensation in	Rotating shutter drive, on
Aperture compensation out	Rotating shutter drive, off
Calibrate (6 commands)	Calibration lamp 1 on
Calibration lamp 2 on	Off 1
Select calibration sequence 1	Off 2
Select calibration sequence 2	Record current adj. 1
Squib experiment ordnance	Record current adj. 2

ERTS Command List (Continued)

Squib experiment ordnance	RBV or MSS 1
Squib experiment ordnance	RBV or MSS 2
Squib experiment ordnance	Lap at BOT 1
Band 1 HV supply A	Lap at BOT 2
Band 1 HV supply B	
Band 2 HV supply A	<u>Attitude Control</u>
Band 2 HV supply B	Wheel delay
Band 3 HV supply A	Pitch rate gyro off
Band 3 HV supply B	Pitch rate gyro on
Main inverter A, on	Gas delay
Main inverter A, off	CSA arm
Main inverter B, on	CSA safe
Main inverter B, off	ACS on/jets enabled
	ACS off/jets disabled
<u>Data Collection System</u>	ACS mode 1
(1) DCS 1 power on	ACS mode 2A
(1) DCS 1 power off	ACS mode 2C
(1) DCS 2 power on	ACS mode 3
(1) DCS 2 power off	ACS mode 4
	ACS normal
<u>Video Tape Recorder</u>	ACS enable
Standby 1	ACS execute
Standby 2	Array slew CW
Record 1	Array slew CCW
Record 2	Array slew normal
Rewind 1	Array delay enable
Rewind 2	Array delay disable
Playback 1	Jet pulse execute
Playback 2	X jet disable
Fast forward 1	Y jet disable
Fast forward 2	+Y select
- Y select	Battery 2 conditioned
Yaw jet disable	Battery 2 re-conditioned
Yaw - X select	Charge rate trickle

ERTS Command List (Continued)

- Yaw select	Charge rate 3.7 amps
Y + X select	Batt. 1 charge rate normal
- X select	Batt. 1 charge rate 8.7 amps
	Batt. 2 charge rate normal
+X select	Batt. 2 charge rate 8.7 amps
Gyro auto	Charge mode control, limit
Gyro power off	Charge mode cycle
Gyro 1 select	Charge bus parallel normal
Gyro 2 select	Charge bus parallel inhibit
Gyro off, heater on	Thermal switches normal (95°)
Tracking head A disable	Thermal switches override
Tracking head B disable	U/V bus 1 reset
Tracking head D disable	U/V bus 1 override
Tracking head normal	U/V bus 2 reset
Orbit adjust arm	U/V bus 2 override
	(1) payload converter 1 enable
Orbit adjust +X thrust	(1) payload converter 2 enable
Orbit adjust -X thrust	
Orbit adjust +Y thrust	
Orbit adjust disarm	

Communications

	(1) USB transponder converter A on/B off
	(1) USB transponder converter A off/B on
<u>Power</u>	
Battery 1 normal	Baseband 1 on/2 off
Battery 1 disconnect	Baseband 2 on/1 off
Battery 2 normal	Baseband SCO's on
Battery 2 disconnect	Baseband SCO's off
Battery execute	Baseband real time SCO's only
Regulator 1 normal	Wideband Tx driver A on/B off
Regulator 1 disconnect	Wideband Tx driver B on/A off
Regulator 2 disconnect	Wideband Tx driver A & B off
Battery 1 conditioned	Wideband Tx driver C on/D off
Battery 1 re-conditioned	Wideband Tx driver D on/C off
Wideband Tx driver C & D off	Tape recorder 2 off
TWTA 1 on	Real time main commutator

ERTS Command List (Continued)

TWTA 1 off	Real time ASC
TWTA 2 on	Data storage main commutator
TWTA 2 off	Data storage ASC
TWTA 1 10W	EG 1 on
TWTA 1 10W	EG 1 off
TWTA 1 20 W	EG 1 real time
TWTA 2 10W	Clock select A on/B off
TWTA 2 20W	EG 1 HFTU
Summed Tx driver sign. on TWTA 1	EG 2 on
Summed Tx driver sign. on TWTA 2	EG 2 off
Tx driver A/B sign. normal	EG 2 real time
Tx driver C/C sign. normal	Clock select B/on A/off
VTR 1 Mss data P/B on	EG 2 HFTU
VTR 1 RBV data P/B on	Low bit rate
VTR 2 MSS data P/B on	High bit rate
VTR 2 RBV data P/B on	
MSS R/T data - ch. 1 & MSS R/T data - ch. 2	<u>Command System</u>
VTR 1 data - ch. 1 & MSS R/T data - ch. 2	SCP 1 on
RBV R/T data - ch. 1 & VTR 2 data - ch. 2	SCP 1 off
VTR 2 data - ch. 1 & RBV R/T data - ch. 2	SCP 2 on
W/B tlm. ch. 1 - pos. 1	SCP 2 off
W/B tlm. ch. 1 - pos. 2	SCP mode select 1
W/B tlm. ch. 2 - pos. 1	SCP mode select 2
W/B tlm. ch. 2 - pos. 2	SCP mode select 3
	SCP mode select 4
	SCP mode select 5
	SCP mode select 6
	Ordnance armed
	Ordnance safe
	Array deploy
	Payload ordnance on
	Payload ordnance off
	Payload heater on
	Payload heater off
	Redundant enable on

Data Handling

Tape playback

Tape recorder 1 on

Tape recorder 1 off

Tape recorder 2 on

8.6 COMMAND RELIABILITY

The ERTS study specification asks that the spacecraft be designed so that a single inadvertent command cannot cause a catastrophic or irreversible action. This has been studied with the benefit of OGO operating experience and the design found such that no single command can result in serious difficulty.

The command list given above has been analyzed for functions which might cause difficulty but are generally not catastrophic. The spacecraft commands which are critical are listed in Table 8-4 together with the arming or enabling command which must be also sent to effect them. It is clear that no catastrophic effect on the spacecraft can occur and none are apparent in the payload. One eventuality which might deplete the battery is that the payload fail to be turned off. To counter this we plan shut-off timers which automatically remove any load greater than 1 ampere 24 minutes after it is turned on (see Section 12).

The only command which appears to be a potential catastrophe is the pyrotechnic deployment of the solar array while within the shroud. As shown this requires prior spacecraft separation from the Delta which of course follows shroud ejection.

All of the command functions of Table 8-5 were also in the OGO design except "tracking head disable." OGO experience shows these functions to be adequately safed by the arming functions provided. "Tracking head disable" is only critical if one head failure has occurred since attitude control automatically continues on three heads of four.

Table 8-5. Critical Commands and Protective Measures

Function	Required Pre- or Post-requisite
ACS gas delay	CSA arm
ACS off	CSA arm
ACS mode change	ACS execute and ACS enable
Array slew	ACS arm
Control gas on 1 second	ACS arm
Tracking head disable	ACS arm + one head failure
Orbit adjust thrust	Orbit adjust arm
Battery disconnect	Battery execute
Wideband transmitter on	Timer shutoff 24 min
Pyrotechnic firing (all)	Ordnance bus arm
Array deploy	Separation switch closed

CONTENTS

	Page
9. COMMUNICATIONS	9-1
9.1 Power Amplification of Wideband Video Signals	9-1
9.2 Traveling Wave Tube Selection	9-5
9.3 Carrier Intermodulation By Limiting of Two FM Signals, Wideband Link	9-8
9.4 MSS and RBV Downlink Intermodulation Interference	9-11
9.5 Effect of RF Link on RBV Signal-to-Noise Ratio	9-14
9.6 Unified S-Band Downlink Intermodulation Interference	9-16
9.6.1 Nonranging Mode	9-16
9.6.2 Ranging Mode	9-18
9.7 VHF Transmitter Design Alternatives	9-20
9.8 Communication Link Power Budgets	9-21

9. COMMUNICATIONS

Studies of the communication system have largely been concerned with accommodating the unified S-band system, with substituting a VHF telemetry system for the 400-MHz system normally carried on OGO, and in ensuring compatibility within the wideband video transmitters for both RBV and MSS data. Verification that the remaining elements proposed in June 1969 were suitable was also accomplished.

9.1 POWER AMPLIFICATION OF WIDEBAND VIDEO SIGNALS

An analysis of the RF power requirements for the wideband video data indicates that 10 watts for each video channel is adequate for all but borderline conditions (see Section 9.8). Several choices are available for power amplifiers yielding 10 watts at 2300 MHz including solid state devices and traveling wave tube amplifiers. Considering all ERTS' needs such as dual channels, six input choices, redundancy, cross strapability and efficiency, four candidate approaches were selected.

- 1) Three 10-watt TWTA's with three-for-two redundancy, one carrier per TWTA
- 2) Two 20-watt TWTA's with two-for-one redundancy, two carriers per TWTA
- 3) Two 10/20 watt TWTA's, one carrier per TWTA normally with two-for-one redundancy, two carriers per TWTA, as a failure mode
- 4) Four solid-state 10-watt amplifiers with two-for-one redundancy.

A tradeoff matrix for these candidates is presented in Table 9-1.

An assembly of four 10-watt solid-state amplifiers (one active and one standby for each channel) complete with input and output switching is illustrated in Figure 9-1. Baseband switching allows any of the six inputs to modulate either carrier. Two SPDT coaxial switches connect selected pairs of amplifiers to the antennas.

Several potential sources of 10-watt S-band solid-state amplifiers exist. Figure 9-2 illustrates a 12-watt laboratory version being designed by TRW Systems. A complete solid-state transmitter, as illustrated in

Table 9-1. Wideband Video Data Power Amplifier Tradeoff Matrix

	3 Each, 10-Watt TWTA	2 Each, 20-Watt TWTA	2 Each, 10/20-Watt TWTA	4 Each, 10-Watt Solid-State Amplifiers
Efficiency (%)	28	22 (1)	27/22 (2)	21
Reliability	TWTA reliability high, output switching questionable	High	High	Conceptually high, low design confidence, no flight experience
Relative cost	1	0.7	0.8	1.5
Weight (lb)	27.0 (3)	19.0	21.0	22.0 (3)
Output switching	Complex	None	None	Two SPST coaxial

NOTES:

- (1) Includes 1.5 db power loss for intermodulation and carrier unbalance.
- (2) 27 percent in 10-watt mode; 22 percent in 20-watt mode including losses as in Note 1.
- (3) Does not include weight of output switches. An advanced technology TWTA to be developed and qualified for the Pioneer project may reduce the TWTA weight to 12 pounds.

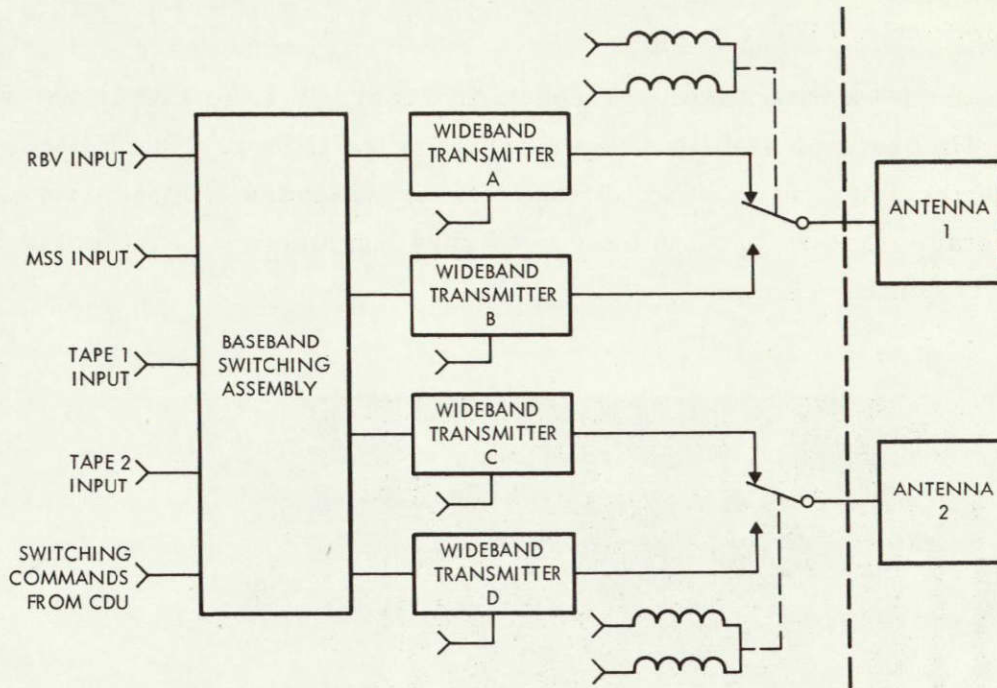


Figure 9-1
WIDEBAND TELEMETRY LINK using four 10-watt solid-state transmitters

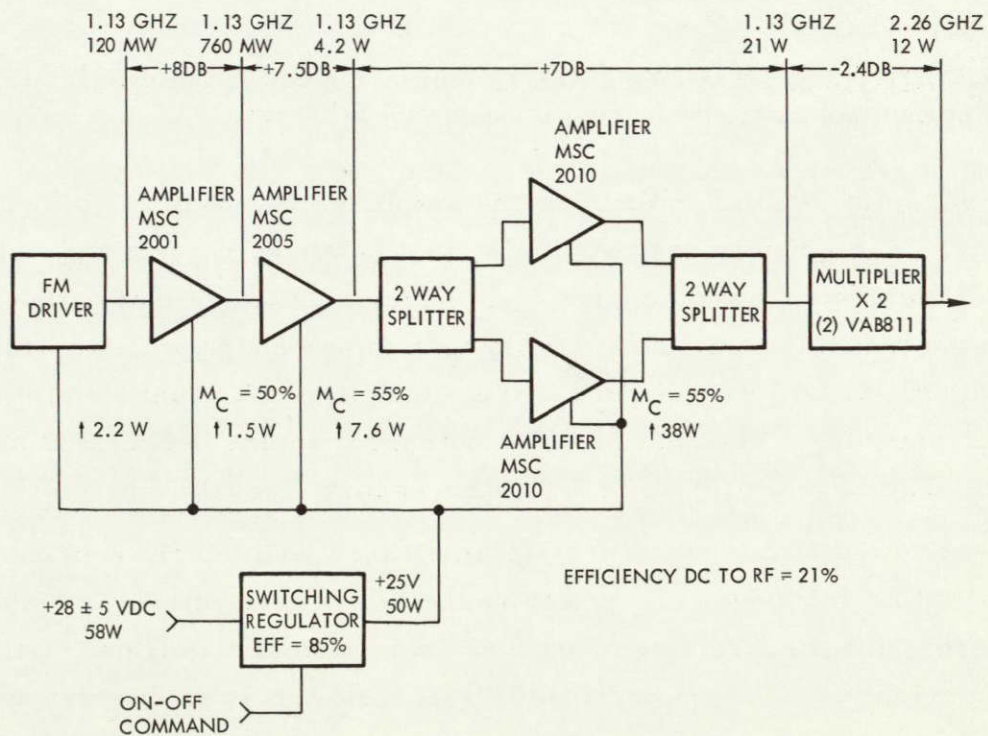


Figure 9-2
10-WATT SOLID-STATE WIDEBAND telemetry transmitter

Figure 9-1, promises size and reliability advantages over a transmitter assembled from TWTA's.

In the 10-watt transmitter shown in Figure 9-3 the FM driver uses a 1.13-gHz deviator stabilized by a sampling AFC loop. The 120 mw output of the FM driver is amplified in three cascaded transistor stages. All the stages use a common base configuration and are constructed using micro-stripline techniques.

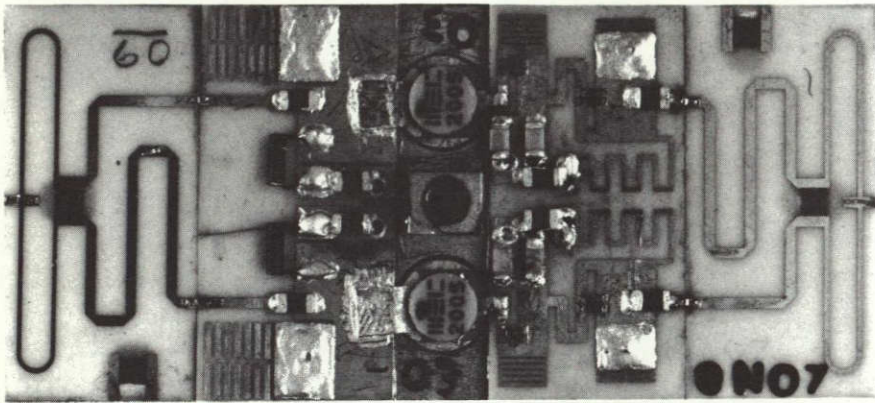


Figure 9-3

SOLID-STATE 1.4 GHz AMPLIFIER HAS 12 watts of output, 7.5 db gain, and 48 percent collector efficiency. It measures 1 x 2 inches.

A varactor doubler multiplies the amplifier output to the output frequency. The circuit uses two diodes in a balanced circuit to meet thermal requirements and suppress odd harmonics. The estimated 2.4 db loss for the multiplier includes 0.2-db loss for a bandpass filter which would be built as an integral part of the multiplier. A shunt switching regulator provides a constant 25 volts output for inputs between 23 and 32 volts. The regulator also provides necessary line filtering.

Despite the fact that solid-state amplifiers will surely replace TWTA's in this frequency and power range in the near future, the short ERTS development schedule causes their rejection at this time. Lack of flight experience with them and insufficient time for a thorough ground testing and qualification program offset the potentially more reliable design.

In selection of a traveling wave tube amplifier assembly, redundancy becomes a key question. With TWTA's redundancy is possible either through the number of amplifiers employed or, because of the dual-channel requirements, through providing for the amplification of both channels in a single TWTA should the other fail.

The use of two 20-watt TWTA's is an example of the latter. This is rejected because intermodulation products resulting from the amplification of two signals in a single saturated TWTA cause a power loss of about 1.0 to 1.5 db, a factor too large to tolerate in the normal mode of operation. The use of one 20-watt TWTA for each channel produces more RF power than is required under most circumstances and consumes more spacecraft power than is warranted.

The use of the combination of three 10-watt TWTA's falls in the former class. It is rejected despite the qualification status of both tube and power supply because of the weight penalty, the complex output switching and because the selected approach is inherently more flexible.

The dual mode 10/20 watt TWTA system suffers least from the system compromises required in the wideband video data system. It combines high efficiency, high reliability, low weight, and simple output. Efficiency drops when the 20-watt mode is required to amplify both signals should one tube fail, but it is highly probable that this mode will never be used. If required, flexibility exists in the design phase to take the resulting degradation as a signal-to-noise reduction in the downlink, or an increased DC power consumption in the spacecraft by tuning the TWTA for a higher power output (27 to 28 watts) in the high power mode.

This approach offers an additional advantage in that in those rare cases (spacecraft near the horizon) when improved communication is sought, each channel can be transmitted at the full 20 watts.

9.2 TRAVELING WAVE TUBE SELECTION

The life, efficiency and environmental tolerance of the traveling wave tube chosen is a vital link in mission success. Since a choice has been made on the basis of these factors a portrayal of the features of the chosen tube is believed pertinent. The tube chosen is a Watkins-Johnson WJ-274-9.

The encapsulated WJ-274-9 is essentially identical to the WJ-274-1, shown in Figure 9-4, except for overall length. The length of the WJ-274-9 is approximately 1 inch longer than the WJ-274-1. The WJ-274-9 is designed for long life, high reliability operation. The selection of materials is very carefully controlled so as to assure that no degradation in life can be caused by incorrect selection of material.

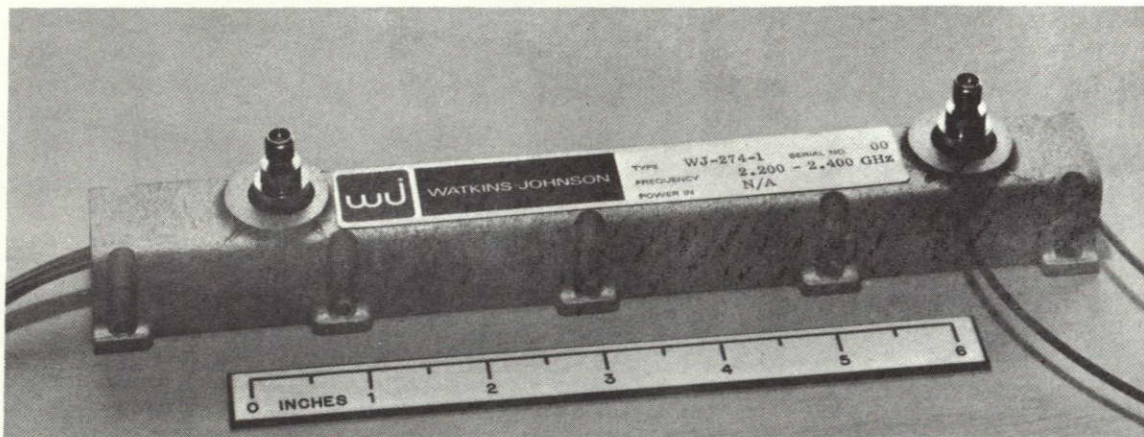


Figure 9-4

PHOTOGRAPH OF THE ENCAPSULATED WJ-274-1 which is physically identical to the proposed WJ-274-9 except for a difference in length of 1 inch.

The electron gun utilizes a high-purity doped-nickel cathode material with a barium oxide cathode coating. Life in excess of 30,000 hours can be demonstrated with this type of cathode. The electron gun is designed so as to operate the anode positive with respect to the helix in order to provide ion blockage and eliminate ion bombardment of the cathode. The collector is operated at a potential below the helix both to increase overall efficiency and to provide ion drainage into the collector. In order to reduce the internal gas pressure to an absolute minimum and maintain this low gas pressure throughout tube life, the tube is vacuum processed at 550°C for an extended length of time. The tube itself comprising the vacuum envelope is hardpotted into the enclosing cast aluminum capsule.

Figure 9-5 shows a photograph of the unencapsulated WJ-274-9 showing a completed tube with magnets and also a body with base insulator cathode and collector subassemblies ready for final assembly. The subassemblies are joined to the ends of the body by simple and rapid RF

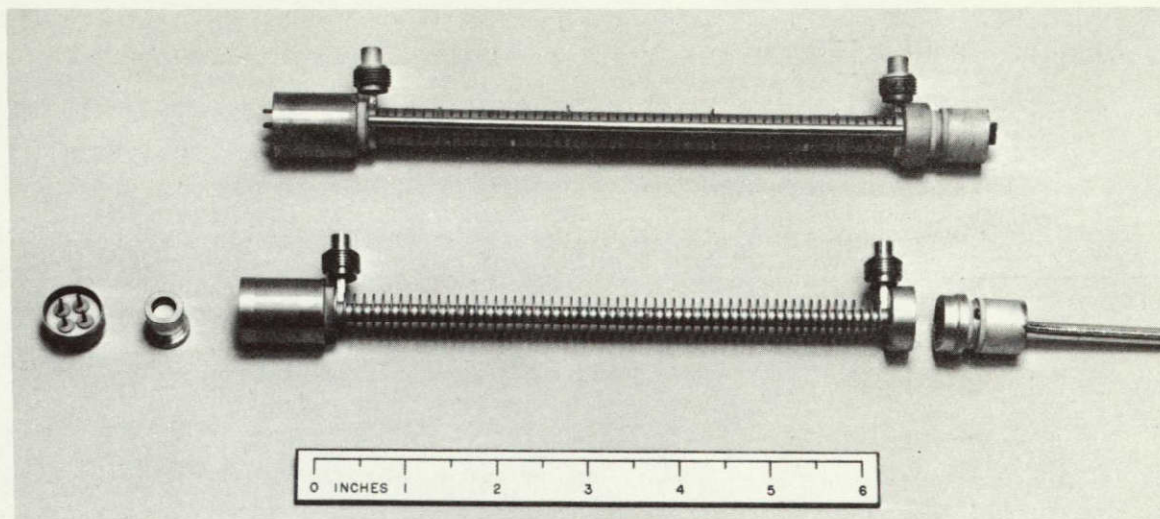


Figure 9-5

PHOTOGRAPH OF THE WJ-274-9 showing a completed tube with magnetic in place (above) and a completed body with cathode and base insulator subassemblies to the left and collector subassembly to the right (below)

induction brazes. This method of joining also allows these parts to be simply removed if they need repair or replacement. Pumping of the tube is accomplished through the collector end which allows the insulating header at the gun end to be a simple part with vacuum seals having large metalized areas for reliability.

The tube is mounted in a rectangular capsule shown in Figure 9-4. Heat is conducted from the collector, gun and body by thermal conduction through the capsule where it is transferred to the heat sink through the bottom surface. Insulation of the high voltage flying leads is accomplished by potting materials which properly insulate and support the high voltage elements and terminals from the capsule which is at ground potential. This encapsulation and mounting method performs its function of support and cooling and has been tested over a wide range of environmental conditions which include random vibration (20 g rms random, 5 to 2000 Hz), temperature (soak, turn-on, and operation in the range of -50 to $+100^{\circ}\text{C}$), mechanical shock (60 g, 11 ms and 110 g, 8 ms), static acceleration (100 g), vacuum (sea level to space vacuum through critical pressure) and thermal shock (-50 to $+100^{\circ}\text{C}$ in 5 minutes). The total weight of the unit shown in Figure 9-4 is less than 1.3 pounds.

The WJ-274-1 tube has been tested and found to successfully perform after exposure to spacecraft physical environment of the Mariner '69 mission. Jet Propulsion Laboratory Specification TS 500437 used for this testing specified the following qualification levels:

Shock	200 g
Acoustic energy	141 db (2×10^{-4} dynes/cm ²) at 300 Hz falling off at lower and higher frequencies
Vibration energy	
Random:	2.25 g ² /Hz density 50 to 150 Hz, less elsewhere
Sine wave:	7.5 to 15 g rms middle frequency range

Watkins Johnson life test programs include:

WJ-251 (4 watt X band):	12 amplifiers in orbit as of June 1969 have accumulated 160,000 hours life, two units in orbit for three years operation.
	17 amplifiers bench tested in excess of one year in vacuum.
WJ-231 (35 watt X band):	9 packages bench tested one year

Predicted life for the ERTS WJ-274-9 can be reliably estimated from past experience with other tubes of similar materials and design. Cathode material and processing are important factors. A life of 30,000 hours per tube is estimated.

9.3 CARRIER INTERMODULATION BY LIMITING OF TWO FM SIGNALS, WIDEBAND LINK

When two or more angle-modulated signals are passed through a saturated TWT power amplifier, intermodulation products of the two signals are created due to the nonlinear amplitude characteristic of the TWT. In the normal operating mode, separate TWTA's are used for the two signals and intermodulation cannot occur. If one tube fails, however,

both signals will be amplified in the remaining TWT. Hence the possibility of intermodulation interference on the wideband video downlinks requires analysis.

The nonlinear transfer function shown in Figure 9-6 is odd so only odd harmonics of each of the signals and harmonics of each of the odd-beat frequencies will be developed.

The output of the TWT can be described by:

$$V_o(t) = a_1 v_i(t) + a_3 v_i(t)^3 + a_5 v_i(t)^5 + \dots$$

where

$v_i(t)$ = input signal, in this case two FM signals

$v_i(t)^3, v_i(t)^5$ = the third and fifth order intermodulation products

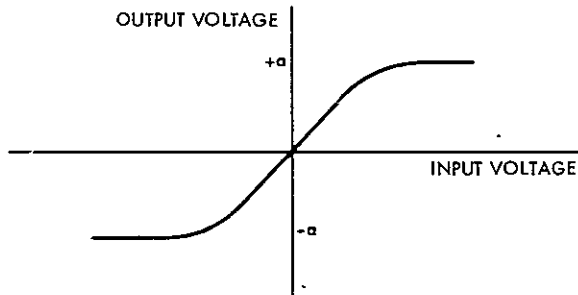


Figure 9-6

TRANSFER FUNCTION of a saturated traveling wave tube

Depending on the spacing of the signals, the resulting intermodulation spectrum may interfere with the desired signal spectrum. The primary intermodulation interference will be from the third order products. Its severity will depend on the spectral location of the products and on their amplitudes. It can be seen by cubing the sum of

two signals separated in frequency that the only potentially serious intermodulation products arise in the terms corresponding to the product of one signal with the square of the other and that the resulting spectrum is essentially the triple convolution of the one spectrum with the other twice. Section 9.4 shows that the RBV spectrum can be conservatively approximated by a gaussian shape whose 1σ value is 10 MHz. If we also approximate the MSS spectrum with a gaussian shape whose 1σ value is 9 MHz, the triple convolution is easily seen to be another gaussian function whose 1σ value is the rss combination of the 1σ values of the component parts.

The worst condition exists for the triple order products consisting of two RBV terms, and one MSS term interfering with the RBV signal. The resulting third order intermodulation band will thus be a gaussian-shaped spectrum whose 1σ width is 16.8 MHz and whose center is 36 MHz away from the center of the RBV band.

Having found the spectral shape of the intermodulation product, the portion of the total product power falling in the signal band is found by integrating one side of the gaussian spectrum from 26 to 46 MHz, which corresponds to the RBV signal detection band.

The relative intermodulation power level is given by:

$$P\left(\frac{46}{16}\right) - P\left(\frac{26}{16}\right)$$

where

$$P(X) = \frac{1}{\sqrt{2\pi}} \int_{-\infty}^X e^{-\frac{x^2}{2}} dx$$

is the distribution function of the gaussian random variable, a readily available tabulated function.

$$P\left(\frac{46}{16}\right) = 0.99801$$

$$P\left(\frac{26}{16}\right) = 0.94800$$

and

$$P\left(\frac{46}{16}\right) - P\left(\frac{26}{16}\right) = 0.05001 \text{ or } -13 \text{ db.}$$

The total intermodulation product power is -11 to -12 db referenced to the signal level in a saturated TWT.* Thus the intermodulation power -24 to -25 db referenced to the RBV signal. In the output this corresponds to a signal-to-interference level of to between 45.3 and 46.3 db since the 12.3-db FM improvement and 9.0-db peak-to-rms-ratio factors still apply.

Further study of the detailed RBV data and RF spectra is desirable to determine definitely if an interference problem exists. Since the minimum signal-to-interference ratio predicted is 45.3 db at the RBV output, and since the RBV bandwidths used are felt to be conservatively large, it seems highly probable that no interference problem exists.

*W. Kuntz, "Study of Distortion in Klystrons and Traveling Wave Tubes, Final Report," AD 632133.

If the intermodulation products should be shown to cause a significant problem at some later date, it would be possible to reduce their effect by operating the TWT in a "back-off" or quasilinear mode. As the drive to a saturated TWT is reduced, the intermodulation product power level drops rapidly. Reducing the drive would also reduce the output signal power somewhat and is thus not desirable unless required by intermodulation considerations.

Finally, there remains the possibility that the state of the art in 10-watt TWTA's will improve efficiently to make the dual-mode TWA unnecessary. Should intermodulation be shown to a problem, it would be a factor in the continuing S-band power amplifier tradeoff as discussed in Section 9.1.

9.4 MSS AND RBV DOWNLINK INTERMODULATION INTERFERENCE

The downlink intermodulation interference between the RBV and MSS video data signals was determined by finding the spectral shape of each signal and integrating that portion of each signal which fell within the bandwidth of the other data channel. The results were:

MSS interference with RBV data: +64.2 db S/I

RBV interference with MSS data: +23.3 db S/I

The actual RBV interference with MSS data should be significantly lower because of the conservative approximations used in deriving the above number. At a +23.3 db signal-to-interference ratio, however, the interference is already 10 db below thermal noise at data threshold (10^{-6} probability of bit error) and should not cause significant degradation.

The spectral model used to analyze the effect of RBV signal interference on the MSS data was a gaussian spectral shape shown in Figure 9-7 and given by:

$$G(f) = \frac{1}{\sqrt{2\pi(\Delta f)^2}} e^{-\frac{(f - f_o)^2}{2(\Delta f)^2}}$$

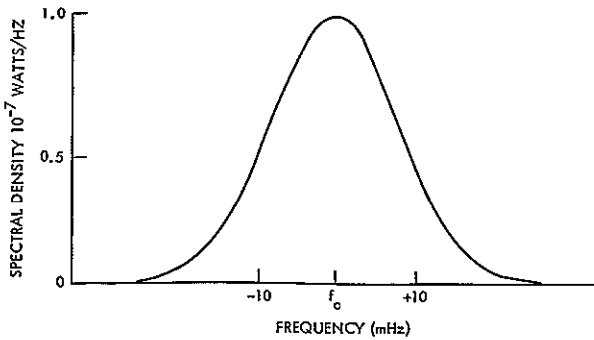


Figure 9-7
SIGNAL SPECTRUM OF RBV

shape above consists of the wideband spectral model of Schwartz, Bennett, and Stain, "Communication Systems and Techniques," with the bandwidth increased from 2β FM since β is not now much greater than one. While this approximation will not give exact spectral shapes close to the center frequency, the approximation on the tails of the gaussian frequency distribution should be excellent. This is the region of interest for this analysis since we are interested in determining that portion of the RBV TV spectrum that falls into the MSS data band.

$$\Delta f = (1.5 + 1) 4 \text{ MHz} = 10 \text{ MHz}$$

This figure for Δf is conservatively high since the peak baseband frequency is used rather than the rms baseband frequency. The rms baseband frequency is always smaller than the peak frequency, especially in the case of TV signals which normally roll-off rapidly.

The portion of this signal which interferes with the MSS data is that which falls in the frequency of 26 to 46 MHz on one side of the center. The relative power in this region is given by:

$$P \left[\frac{46}{10} \right] - P \left[\frac{26}{10} \right]$$

where $P(x)$ is the normal distribution function:

$$P(x) = \frac{1}{\sqrt{2\pi}} \int_{-\infty}^x e^{-\frac{t^2}{2}} dt$$

where $\Delta f = (\beta + 1) f_m$

f_m = TV baseband
bandwidth

The actual spectral shape is difficult to determine for $\beta = 1.5$ since neither narrow-band or wideband approximations may be used. The spectral

This is a tabulated function:

$$P \left[\frac{46}{10} \right] = 0.9999978875$$

$$P \left[\frac{26}{10} \right] = 0.9953388119$$

and the total interfering power is then 0.0046590756 which is -23.3 db referenced to the total signal power. Since the total signal powers for the RBV and MSS signals are equal, the signal-to-interference ratio for the MSS signal is +23.3 db. Because of the conservative approximations made in this analysis, the actual signal-to-interference ratio should be significantly better than this and no significant interference should be experienced.

The spectrum of the MSS downlink signal is that of continuous phase NRZ PCM/FM as given by Bennett and Davey, "Data Transmission," p. 329, eq. 19-69

$$W_u(f) = \frac{2A^2 \sin^2 \left[\frac{(\omega - \omega_1) T}{2} \right] \sin^2 \left[\frac{(\omega - \omega_2) T}{2} \right]}{T \left[1 - 2 \cos (\omega - \omega) T \cos \beta T + \cos^2 \beta T \right]} \left[\frac{1}{\omega - \omega_1} - \frac{1}{\omega - \omega_2} \right]^2$$

$$+ \frac{2A^2 \sin^2 \left[\frac{(\omega + \omega_1) T}{2} \right] \sin^2 \left[\frac{(\omega + \omega_2) T}{2} \right]}{T \left[1 - 2 \cos (\omega + \omega) T \cos \beta T + \cos^2 \beta T \right]} \left[\frac{1}{\omega + \omega_1} - \frac{1}{\omega + \omega_2} \right]^2$$

The second term represents the power at negative frequencies and when real positive frequencies are considered the first term is doubled and the second term dropped. The first term was programmed on the time-share computer with $A = T = 1$. The program was first run to determine the modulated signal spectral shape (Figure 9-8). The program was next integrated over a region corresponding to the adjacent RBV data channel. The total power in the adjacent channel was found to be -64.2 db, referenced to the signal power in that channel.

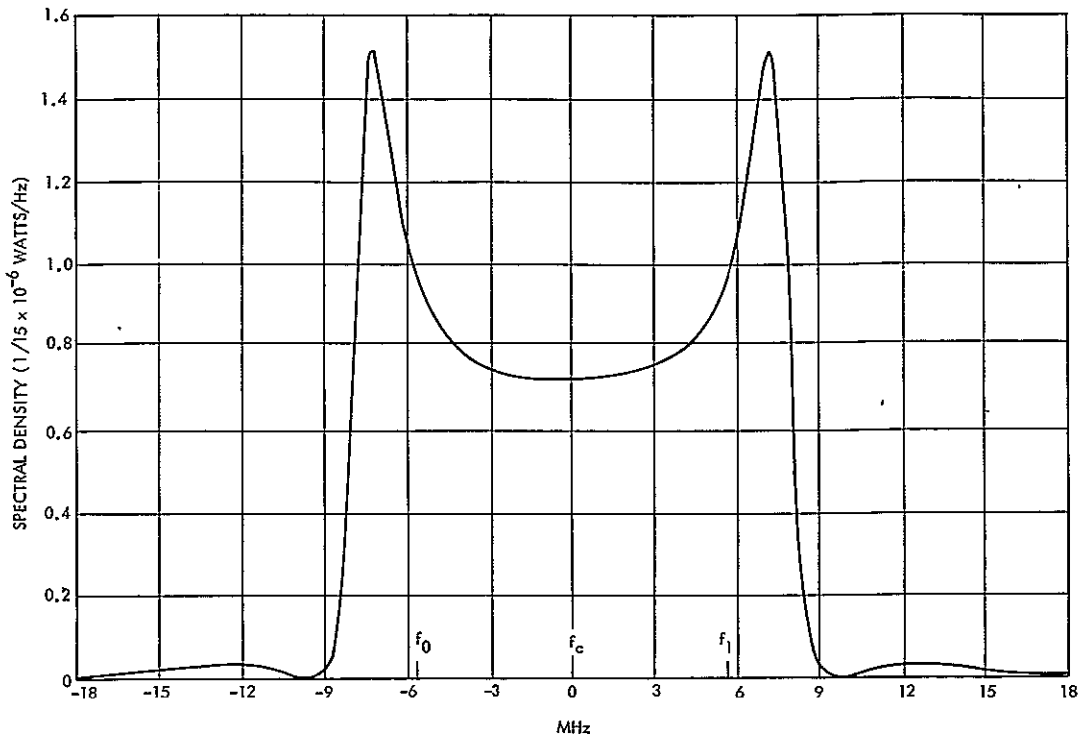


Figure 9-8

SIGNAL FREQUENCY SPECTRUM of MSS PCM/FM downlink data,
 $\beta = 0.75$

9.5 EFFECT OF RF LINK ON RBV SIGNAL-TO-NOISE-RATIO

The effects of the RF link signal-to-noise-ratio on the RBV sensors signal is shown in Figure 9-9. With two major noise sources, the total output signal-to-noise-ratio can be rewritten from the general case as

$$\frac{S_T}{N_T} = \frac{\frac{S_1}{N_1} \cdot \frac{S_2}{N_2}}{\frac{S_1}{N_1} + \frac{S_2}{N_2}}$$

If both of the noise sources are equal, the output signal-to-noise-ratio S_T/N_T is 3 db less than either S_1/N_1 or S_2/N_2 . If one of the noise sources is larger than the other S_T/N_T will approach the smaller of S_1/N_1 or S_2/N_2 .

In the ERTS application the major noise contributor for the RBV signal is the vidicon tube. Two of these sensors have an output signal-to-

noise ratio of 33 db, the third is 25 db. The other noise sources of importance are the thermal noise contribution of the RF link. When transmitting at an output level of 10 watts into the 30 foot MSFN antenna the RF link peak-to-peak signal to RMS noise is 38.7 db. Therefore the total S_T/N_T is 31.96 db the first two RBV's and 24.82 db for the third.

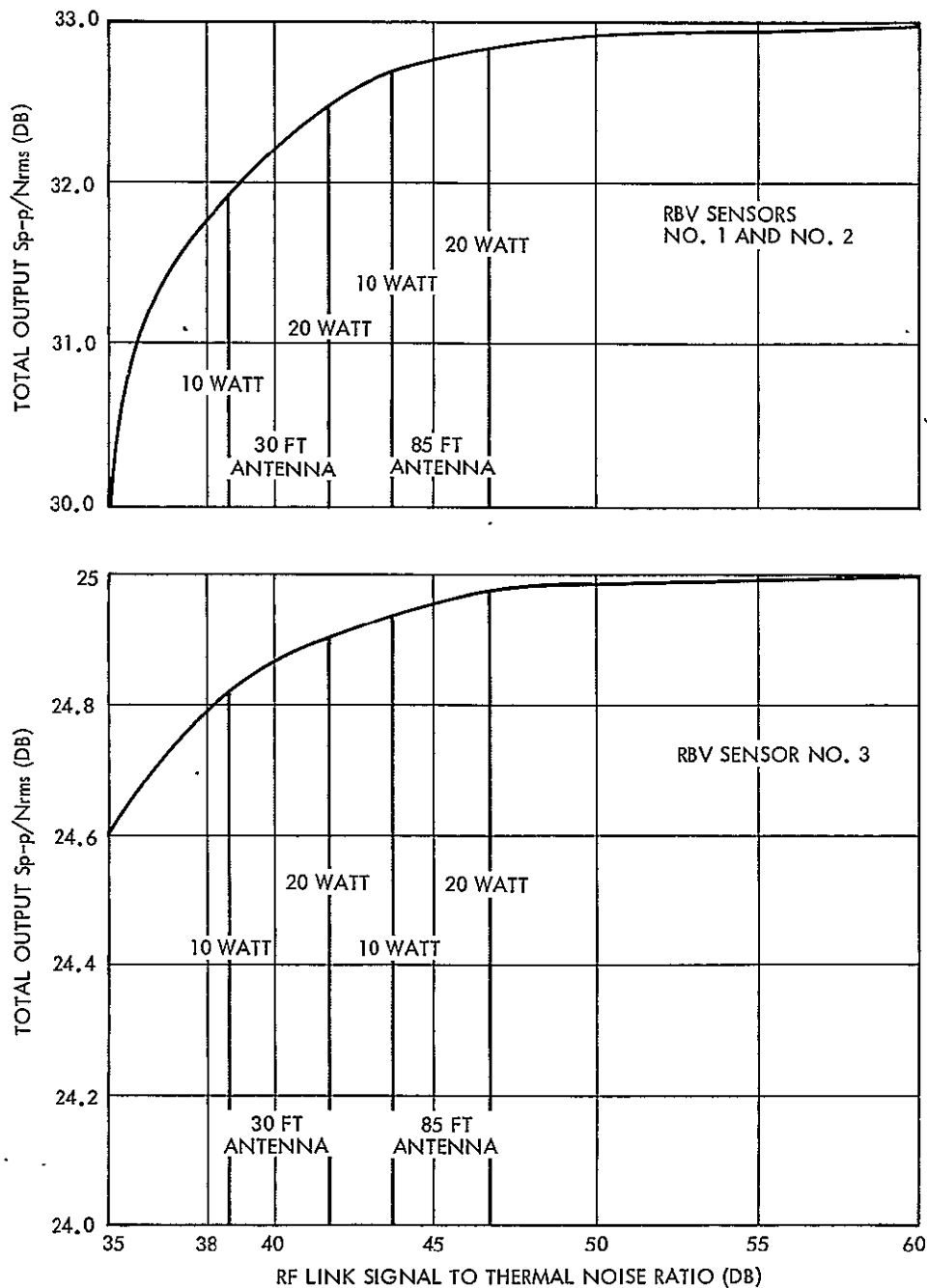


Figure 9-9
EFFECT OF LINK NOISE on system noise in the presence of RBV noise.

9.6 UNIFIED S-BAND DOWNLINK INTERMODULATION INTERFERENCE

The Unified S-band downlink uses a complex waveform to transmit several types of information from the spacecraft to the ground. Interference due to intermodulation must be considered. This section analyzes the interference and shows that the ERTS downlink will operate as designed.

Three major operating modes are considered. The first of these, the unstabilized spacecraft mode, is not analyzed since the downlink modulation consists of the 1 kbit/sec telemetry on the 1.25 MHz subcarrier oscillator only. The two stabilized spacecraft modes are:

Nonranging Mode:

- Ranging clock only (baseband)

- DCS data (1.024 MHz SCO)

- Telemetry 1 kbit/sec (1.25 MHz SCO)

- Telemetry playback 32 kbit/sec (300 kHz SCO)

- VTR PCM signals, 1 kbit/sec (1.65 and 225 kHz SCO's)

Ranging Mode:

- Ranging (baseband)

- DCS data (1.024 MHz SCO)

- Telemetry, 1 kbit/sec (1.25 MHz SCO)

9.6.1 Nonranging Mode

In the nonranging mode many intermodulation products are generated by the many subcarrier oscillators, due primarily to the nonlinear receiver phase detector characteristic. The presence of these intermodulation products when all subcarrier oscillators are on makes a separate ranging mode with a simplified baseband structure desirable. A list of intermodulation products generated by all possible combinations of Bessel functions of orders 0, ± 1 , and ± 2 is shown in Table 9-2 for the frequency range from the carrier to 165 kHz. The terms at zero frequency and 165 kHz are not intermodulation products, but represent the carrier and the first subcarrier oscillator signal, respectively.

Table 9-2. Intermodulation Products in the Nonranging Mode Falling at Baseband Frequencies Less Than 165 kHz

Frequency (kHz)	Level (db)	Frequency (kHz)	Level (db)
0.000	-4.14	87.000	-109.40
1.000	-36.42	88.000	-111.77
2.000	-90.87	89.000	-98.11
13.000	-81.60	89.000	-82.20
14.000	-61.81	90.000	-40.78
15.000	-77.08	91.000	-47.54
15.000	-61.17	92.000	-95.86
16.000	-77.72	93.000	-110.91
17.000	-97.51	94.000	-68.67
18.000	-105.81	95.000	-95.27
26.000	-65.63	96.000	-142.78
27.000	-73.20	103.000	-108.18
28.000	-154.07	104.000	-59.86
28.000	-138.16	105.000	-53.09
29.000	-83.71	106.000	-94.52
30.000	-48.41	108.000	-73.10
31.000	-83.71	109.000	-65.52
32.000	-138.16	117.000	-93.49
33.000	-74.74	120.000	-73.49
34.000	-61.04	121.000	-74.13
35.000	-93.76	122.000	-93.91
43.000	-133.67	130.000	-115.66
44.000	-85.35	131.000	-82.94
45.000	-78.59	132.000	-96.64
46.000	-104.10	133.000	-116.26
46.000	-120.01	134.000	-61.81
47.000	-117.76	135.000	-26.51
48.000	-77.69	136.000	-61.81
56.000	-87.42	137.000	-116.26
57.000	-95.00	137.000	-132.16
59.000	-72.62	138.000	-89.01
60.000	-31.19	139.000	-81.43
61.000	-37.96	148.000	-81.70
62.000	-86.28	149.000	-61.91
73.000	-80.06	150.000	-61.27
74.000	-31.74	150.000	-45.37
75.000	-24.97	151.000	-46.01
76.000	-66.40	152.000	-65.79
76.000	-82.31	163.000	-106.67
77.000	-95.97	164.000	-52.23
78.000	-131.30	165.000	-16.93

A list of intermodulation products occurring at higher frequencies is shown in Table 9-3. The only intermodulation products that are significant occur at 226 and 1249 kHz. Both of these products involve the DCS subcarrier oscillator ($1250 - 1024 = 226$; $1024 + 225 = 1249$) and will therefore be spread over a relatively wide spectral range. Intermodulation interference either to the ranging signal or to the data channels from the ranging signal cannot occur in this mode since only the clock components of the ranging signal are present and these do not fall near the data signals or major intermodulation products.

Table 9-3. Intermodulation Products in Nonranging Mode at Baseband Frequencies Greater Than 165 kHz

Frequency (kHz)	Level (db)	Frequency (kHz)	Level (db)
166.000	-53.10	725.000	-41.26
225.000	-16.70	751.000	-45.83
226.000	-19.98	784.000	-48.64
239.000	-47.34	785.000	-42.76
240.000	-44.06	799.000	-21.28
286.000	-53.10	859.000	-22.78
299.000	-45.83	860.000	-48.52
300.000	-10.94	889.000	-32.84
301.000	-45.83	890.000	-58.57
316.000	-63.15	916.000	-63.15
334.000	-48.64	934.000	-48.64
360.000	-44.06	949.000	-31.33
361.000	-47.34	950.000	-25.45
390.000	-34.01	964.000	-38.59
391.000	-37.29	1010.000	-58.57
451.000	-35.78	1024.000	-5.47
464.000	-63.15	1025.000	-31.20
465.000	-28.26	1084.000	-38.59
466.000	-63.15	1085.000	-32.71
499.000	-31.33	1099.000	-31.33
525.000	-26.75	1114.000	-48.64
526.000	-30.03	1115.000	-42.76
559.000	-32.84	1159.000	-32.84
560.000	-58.57	1160.000	-58.57
586.000	-63.15	1175.000	-41.26
616.000	-53.10	1189.000	-22.78
634.000	-38.59	1190.000	-48.52
664.000	-48.64	1249.000	-21.28
690.000	-44.06	1250.000	-15.40
691.000	-47.34		
724.000	-15.52		

9.6.2 Ranging Mode

The major intermodulation analysis effort consists of analyzing the ranging mode. The areas analyzed are: DCS and telemetry interference with ranging, ranging interference with telemetry, and ranging interference with DCS.

The effect of DCS and telemetry on ranging was analyzed by searching for intermodulation components close to the carrier. The components located are listed in Table 9-4. Considering the level of these components, DCS and telemetry interference with ranging is considered negligible.

To analyze the effect of the ranging code on the telemetry and DCS channels, the actual spectrum of the ranging code must be accurately known. The Mark I ranging code has been analyzed* and shown to consist

*Report #05952-H320-RO-)), "Preliminary Analysis of the LM and CSM Antenna Tracking Systems," 24 Oct 1967, prepared for NASA MSC under Contract NAS 9-4810, Appendix C.

Table 9-4. Intermodulation Products in the Ranging Mode at Baseband Frequencies Less Than 165 kHz

Frequency (kHz)	Level (db)
106.000	-210.02
120.000	-162.07

of 10 sets of harmonic line spectra, all having the sine x/x envelope function. These have been abstracted and listed in Table 9-5. The interference in each of the two channels is analyzed by counting the components which fall in the ground demodulator bandwidth, multiplying each component by the envelope function and summing the total power. Table 9-5 includes this analysis for a ranging power of one. The final signal-to-interference ratio is then found by comparing the relative power levels of the ranging signal to the signal being interfered with.

Table 9-5. Intermodulation Spectrum Between PRN and PCM/FM Telemetry

Code α	PRN Code Component	$P\alpha$ (db)	$f\alpha$ (Hz)	Interfering Harmonics	Sum of Harmonic Power
1	c1.	-3	495.833k	--	--
2	c1.X	-13.5	45k	X26-X29	-22.9 db
3	c1.A	-24	16k	X72-X84	-27.7 db
4	c1.B	-27	7.86k	X147-X172	-27.6 db
5	c1.C	-30.1	3.9k	X295-X346	-27.8 db
6	c1.X.A	-34.4	1.45k	X794-X931	-27.8 db
7	c1.X.B	-37.4	715	X1609-X1889	-27.7 db
8	c1.X.C	-40.5	355	X3240-X3803	-27.7 db
9	c1.A.B.C	-63	2	$X5.75 \times 10^5$ - $X6.75 \times 10^5$	-27.8 db
10	c1.X.A B.C	-73.4	0.18	$X6.38 \times 10^6$ - $X7.5 \times 10^6$	-27.8 db

NOTE: Total ranging power in telemetry band: -17.7 db referenced to total ranging power.

The total power in the telemetry band is found to be -17.7 db referenced to the total ranging power. Since the total ranging power is -20.0 db referenced to the carrier and the telemetry is -11.3 db, the signal-to-interference ratio is 26.4 db. This interference level is sufficiently low to avoid any appreciable degradation of telemetry by ranging interference. The above numbers assume a ranging modulation index of 0.1 radian. Because of the nonoptimum location of the telemetry subcarrier, this lower-than-normal ranging modulation index is desirable to keep interference at a minimum. Because of the relatively short maximum communication distance of the ERTS spacecraft, an acceptable ranging power budget is maintained.

The interference in the DCS band is lower since the DCS band is located at the null of the PRN ranging spectrum.

9.7 VHF TRANSMITTER DESIGN ALTERNATIVES

The design of the 137.86-MHz transmitter was set by two limit conditions

- 32 kbit/sec data must be transmitted using an omnidirectional antenna.
- Carrier power must be suitable for STADAN minitrack network.

The normal data rate is, of course, only 1 kbit/sec but the power output requirement is set by the higher, emergency-only data rate. One-half watt output was chosen to provide greater than 6-db margin over the minimum signal needed for a bit error rate of 1 in 10^6 .

The possible sources of supply of the 137.86-MHz transmitter were

- Modify the existing 136-MHz OGO 0.1-watt unit
- Procure an existing unit from some other source
- Design and build a new assembly based on circuit elements from other designs.

The first alternative was infeasible since the existing OGO unit was too low in power output and has no modulation capability. The second was discarded after a review of existing designs convinced us that a new design would be simpler, more efficient, and thus more reliable. In particular, the features of a new design which made it preferable were

- A biphasic modulator can be used. By switching between two signals of the same frequency but different phase, modulation can be accomplished at the output frequency. Any phase-shift may be used and the phase modulation stability can be much better than can be accomplished with a linear modulator.
- Crystal control at the output frequency. A 137.86-MHz seventh-overtone crystal may be used to provide the output frequency directly with no frequency multiplication. The simplicity of this approach will increase reliability, and efficiency should also be improved since multiplier stages are generally inefficient.
- High DC to RF conversion efficiency. The expected worst case power requirements are:

+23 volt input	1.5 watts
+28 volt input	1.80 watts
+33 volt input	2.20 watts

- Wide input voltage range. As indicated above, the unit will meet ERTS requirements with input voltages ranging from 23 to 33 volts, thus removing the requirement for a voltage converter.

9.8 COMMUNICATION LINK POWER BUDGETS

In calculating the performance of all links in the ERTS communication system, the standard measure of acceptable link performance for digital data has been a signal greater than that needed to produce a bit error rate of 1 in 10^6 bits. This criterion has been met for all links that carry digital data. For RBV data the detected SNR is 38.7 db for a MSFN ground station having a 30-foot paraboloid antenna.

In all calculations the required 6-db margin of the study specification is carried as a system loss. Hence the link is considered acceptable if a positive margin remains. The VHF command uplink specification (GSFC study specification, paragraph 7.6.1.3) calls for a margin of 20 db, whereas we compute the link as having 17.6 db (Table 9-6). The design of this link is unchanged from OGO, where it has proved totally satisfactory. In view of this experience we propose no change in design of the spacecraft equipment. As further discussed in Section 10, antenna design and placement have been arranged to provide good command link security in all spacecraft attitudes.

Table 9-6. Power Budget of the ERTS VHF Command Uplink

Parameter	Value
Transmitter power, dbm	+53.0
Transmitter antenna gain, db	+12.0
Space loss (0 deg elevation), db	-147.4
Polarization loss, db	-3.0
System margin, db	-6.0
Spacecraft antenna gain, db	-0.0
Spacecraft circuit loss (design value), db	-1.0
Receiver sensitivity (OGO receiver), dbm	-110.0
Margin, db	+17.6

The 1 kbit/sec VHF telemetry link makes use of a new transmitter (Section 9.7) having a half-watt power output and employing Manchester PSK modulation at an index of 1.25 radians. The link margin for 32 kbit/sec data on the 137.86-MHz carrier is identical to that shown on Table 9-7 except for noise power. For the 32 kbit/sec bandwidth the noise power becomes -121.5 db and the excess margin is thus 2.6 db.

Since Manchester-coded data is transmitted on the VHF beacon (Table 9-7), the spectrum in the immediate vicinity of the carrier will be relatively free of interference; a null occurs in the modulation spectrum at the carrier frequency. In Table 9-7 the value for spacecraft antenna gain is that provided by the OGO omnidirectional antenna (see Section 10). Table 9-8 shows the VHF carrier link budget.

Power budgets for unified S-band uplink carrier tracking, commanding, and telemetering are indicated in Tables 9-9, 9-10, and 9-11.

Table 9-11 lists the component parts of the total unified S-band downlink. The distribution of the total power between the carrier and various subcarriers is obtained by first choosing the relative power requirements and then through an iterative process employing tables of Bessel functions and their ratios, determining the proper modulation indices for each. Table 9-12 documents the results.

Table 9-7. Power Budget of the ERTS
VHF 1 kbit/sec Downlink

Parameter	Value
Sideband power (Note 1), dbm	+26.5
Spacecraft antenna gain (Note 2), db	0.0
Transmission line loss (design value), db	-2.0
Polarization loss (estimated), db	-1.0
Space loss (5 deg elevation) Note 3), db	-144.9
Receive antenna gain, db	+22.0
Antenna noise temperature, °K	1240
Receiver noise temperature, °K	360
System noise temperature, °K	1600
Noise power (KTB for 1 kbit/sec), db	-136.6
System margin, db	-6.0
Received power, db	-105.4
Received signal-to-noise ratio, db	31.2
Maximum bit error rate	10 ⁻⁶
Theoretical SNR in matched bandwidth, db	10.5
Degradation from theoretical (estimated), db	3.0
Required SNR, db	13.5
Margin, db	17.7

Notes:

- 1) 0.5-watt transmitter with 0.5-db modulation loss (±1.25 radian biphase)
- 2) OGO type omnidirectional antenna, See Section 10
- 3) 137.86 MHz, 1637 nautical miles

Table 9-8. Power Budget of the ERTS
VHF Beacon

Parameter	Value
Carrier power (Note 1), dbm	+17.0
Spacecraft antenna gain, db	-0.0
Transmission line loss (design value), db	-2.0
Polarization loss (estimated), db	-1.0
Space loss (0 deg elevation) (Note 2), db	-146.3
Receive antenna gain, db	+22.0
System margin, db	-6.0
Received carrier power, dbm	-116.3
Noise power in 100 Hz bandwidth (Note 3), dbm	-146.6
Received SNR, db	30.3
Required loop SNR, db	6.0
Margin, db	24.3

Notes:

- 1) 0.5-watt transmitter modulated ±1.25 radians
- 2) 137.86 MHz, 1914 nautical miles
- 3) From noise temperatures in VHF 1 kbit/sec downlink budget

Table 9-9. Unified S-Band Uplink Carrier Tracking Budget

Transmitter Power, dbm	+63 .
Transmitter antenna gain, db	+43
Space loss (0 deg elevation), db	-170.3
Polarization Loss	0.0
System margin	-6.0
Spacecraft antenna gain	0.0
Total received power, dbm	-70.3
Threshold carrier tracking, dbm	-125.0
Margin, db	54.7

Table 9-10. Power Budget of the ERTS Unified S-Band Command Link

Parameter	Value
Transmitter power, dbm	+63.0
Transmitter antenna gain, db	+43.0
Space loss, db	-170.3
Polarization loss, db	0.0
System margin, db	-6.0
Spacecraft antenna gain, db	0.0
Spacecraft circuit loss (design value), db	-5.0
Command carrier, modulation loss (Note 1), db	-3.1
Command subcarrier modulation loss (estimate), db	-2.0
Synchronization modulation loss (Note 2), db	-3.0
Received command data power, db	-83.4
Command noise power (KTB) (Note 3), db	-134.2
Theoretical data SNR for $10^{-6}P_e$, db	10.5
Degradation from theoretical (estimate), db	-6.0
Excess command margin, db	34.3

Notes:

- 1) 1.2-radian subcarrier deviation with 0.1-radian ranging deviation
- 2) 50 percent synchronization power
- 3) 1000°K antenna, 9 db NF receiver in 1-kHz noise bandwidth

Table 9-11. Power Budget for the ERTS Unified S-Band Downlink, Normal Mode

Parameter	Value
Transmitter power (Note 1), dbm	+29.0
Transmitter antenna gain (Note 2), db	+5.0
Transmitter circuit loss (Note 2), db	-1.5
Transmitter antenna pointing loss (estimate),	-0.1
Space loss (5 deg elevation) (Note 3), db	169.3
Receiving antenna gain (30 ft dish), db	+43.4
Receiving antenna pointing loss, db	0.0
Receiving circuit loss, db	0.5
Required system margin, db	-6.0
Total received power, dbm	-100.0
Receiver noise density, dbm	-177.5
Power to noise spectral density, db	77.5

Notes:

- 1) 800-milliwatt TETR transmitter
- 2) Shaped-beam antenna
- 3) 1640 nautical miles at 2287.5 MHz

Table 9-12. Link Margins for Unified S-Band Channels

	VTR 1	VTR 2	1 Kbit	32 Kbit	DCS	Ranging
Subcarrier oscillator frequency	165 kHz	225 kHz	1.25 MHz	300 kHz	1.024 MHz	
Noise bandwidth, db Hz	43.9	45.3	43.0	49.5	57.8	25.5*
SNR required, db	12.5	12.5	12.5	13.0	10.0	10.0
C/N required, db	56.4	57.8	55.1	62.5	67.8	35.5
Peak deviation, rad	0.32	0.38	0.29	0.63	1.04	0.1
Modulation loss, db	16.9	15.4	17.9	10.7	5.5	24.2
Carrier C/N required, db	73.3	73.2	73.0	73.2	73.3	59.7
Excess Margin	4.2	4.3	4.5	4.3	4.2	17.8

*350-Hz bandwidth (widest ranging receiver loop bandwidth; 40 Hz is threshold bandwidth)

The carrier suppression is 4.2 db. This results in a carrier SNR of 44.9 db. This carrier level is sufficient to permit the high doppler rate tracking. Under this signal level the receiver loop bandwidth will be 700 Hz with a noise bandwidth of 2000 Hz.*

The SNR requirements for the PCM subcarriers are based on both click noise and thermal noise at the discriminator output for 10^{-6} Pe. The DCS subcarrier SNR is based on discriminator threshold requirements and will provide an adequate output SNR of 22.3 db based on the FM improvement available with the relatively small DCS bandwidth and the high level of thermal noise already present in the DCS data.

Some additional margin could be gained for the unified S-band normal mode downlink by transmitting the DCS data in a 100-kHz band centered at 1.024 MHz, rather than on a subcarrier. This approach allows the use of the 150-kHz filter in the MSFN 1.024-MHz subcarrier demodulator and requires predetection recording. No interference to any other service is generated by intermodulation since the DCS signal is a hard-limited constant power signal. Approximately 4 db less power would be required for this subcarrier and, since the DCS subcarrier utilizes 44 percent of the downlink RF power, approximately 1.3 db additional margin could be obtained.

The selection of the modulation index for ranging is a compromise between ranging power budget and interference considerations. The ranging modulation index chosen for ERTS is 0.1 radian. Because of the short ranges involved, this modulation index results in a signal-to-noise ratio of 24.8 db in the ranging receiver's widest loop bandwidth and is more than adequate. By the use of this 0.1-radian modulation index, the signal-to-interference-ratio of the ranging signal on the 1.25 MHz (PCM) subcarrier oscillator is limited to 26.4 db.

During launch and should stabilization be lost the unified S-band omnidirectional antenna would be used. To offset the loss of gain only the 1 kbit/sec real time telemetry would be sent (Table 9-13).

*"Proceedings of the Apollo Unified S-Band Technical Conference," July 1965, p. 67, NASA Sp-87.

Table 9-13. Power Budget for the ERTS Unified S-Band Downlink, Unstabilized Spacecraft Mode

Parameter	Value
Transmitter power (Note 1), db	29.0
Transmitter antenna gain (Note 2), db	-5.0
Transmitter circuit loss (design value), db	-2.5
Space loss (5 deg elevation) (Note 3), db	-169.3
Receiving antenna gain, db	43.4
Receiving antenna pointing loss, db	0.0
Receiving circuit loss, db	-0.5
Required system margin, db	-6.0
Total received power, db	-110.9
Receiver noise density, db	-177.5
Power to noise spectral density, db	66.6
1 kbit/sec power to spectral density required (Note 4), db	55.1
Modulation loss (Note 5), db	1.8
Excess margin, db	9.7

Notes:

- 1) 800-milliwatt TETR transmitter
- 2) S-band omnidirectional antenna
- 3) 1640 nautical miles at 2287.5 MHz
- 4) See previous power budget
- 5) 1.66-radian peak carrier deviation

In the unstabilized spacecraft mode the unified S-band downlink carrier suppression by modulation is 7.5 db, which leads to a 26.1-db signal-to-noise ratio in the 2-kHz strong signal noise bandwidth of the ground receiver with the loop bandwidth switch in the 700-Hz threshold bandwidth position.

Communication of the wideband video data can be by three different antenna/receiver combinations; 30 ft MSFN, 40 ft STADAN, 85 ft STADAN. Power budgets for each are shown in Table 9-14.

With respect to Table 9-14, should one TWTA fail, the remaining TWTA will be operated in the 20-watt mode with both carriers. In this mode an additional 1.5-db degradation may be experienced, 1.0 db lost to intermodulation products and 0.5 db allowed for imbalance between the

Table 9-14. Power Budget for ERTS Wideband Telemetry Link

Parameter	30 ft Dish	40 ft Dish	85 ft Dish
Spacecraft transmitter power (Note 1), dbm	+40.0	+40.0	+40.0
Spacecraft antenna gain (design value), db	+5.0	+5.0	+5.0
Transmission line loss (design value), db	-1.0	-1.0	-1.0
Space loss (5 deg elevation) (Note 2), db	-169.2	-169.2	-169.2
Received antenna gain, db	+44.0	+45.5	+51.5
Antenna noise temperature, °K	125	125	125
Receiver temperature, °K	100	100	100
System temperature, °K	225	225	225
Noise power (20-MHz bandwidth), dbm	-104.6	-102.1	-102.1
System margin, db	-6.0	-6.0	-6.0
Received power, dbm	-87.2	-85.7	-79.7
Carrier-to-noise ratio, db	+17.4	+16.4	+22.4
FM improvement (modulation index is 1.5 for RBV data), db	+12.3	+12.3	+12.3
Signal peak-to rms factor, RBV data (estimate), db	+9.0	+9.0	+9.0
Detected signal-to-noise ratio (peak-to-peak signal to RMS noise) RBV data, db	+38.7	+37.7	+43.7
Theoretical carrier-to-noise ratio for 10 ⁻⁶	+13.2	+13.2	+13.2
Filter improvement for 16 Mbit/sec PCM/FM in 20-MHz bandwidth, db	+1.2	+1.2	+1.2
Bit synchronization degradation, db	-1.0	-1.0	-1.0
Excess margin, MSS data, db	+4.4	+3.4	+9.4

Notes:

- 1) 10/20 watt TWTA in 10-watt mode
- 2) 1640 nautical miles at 2265 MHz; 0.1 db less at 2230 MHz neglected

two carriers. The RBV output SNR is 32.2, 36.2 and 42.2 db for 30-, 40- and 85-foot stations, respectively. The MSS data margin is 2.9 db at the 30-foot stations, 1.9 db at 40-foot stations, and 7.9 at the 85-foot stations.

The FM improvement factor in Table 9-13 is based on

$$\frac{3}{2} \beta^2 \left(\frac{B_{if}}{B_s} \right)$$

where

β = modulation index

B_{if} = predetection bandwidth (20 MHz)

B_s = baseband signal bandwidth

The MSS data downlink optimization problem is virtually identical to the model studied by Shaft*. Shaft has shown that discriminator detection of PCM/FM may be optimized to approach a theoretically optimum PCM/FM detector within 1.0 db. Using continuous phase PCM/FM with $\beta = 0.75$, theoretical optimum discriminator detection requires a bit-energy-to-noise-density ratio of 13.2 db for a bit error rate of 1×10^{-6} according to the curves presented by Shaft.

*P. D. Shaft, "Error Rate of PCM/FM Using Discriminator Detection," IEEE Trans. on Space Electricity and Telemetry, pp. 131-136, December 1963.

CONTENTS

	Page
10. ANTIENNAS	10-1
10.1 VHF Antenna Pattern Test	10-1
10.1.1 Test Conditions	10-2
10.1.2 Test Results	10-3
10.1.3 Conclusions	10-21
10.2 Unified S-Band Omnidirectional Antenna Pattern Test	10-21

10. ANTENNAS

Radiation requirements for ERTS are substantially different than for OGO. The addition of unified S-band and wideband video communication equipment has led to five S-band antennas not previously required. Deletion of the 400-MHz telemetry channel and the substitution of one at 136 MHz instead are further differences. Radiation studies have been directed toward providing the required coverage as efficiently as appropriate both through the design and the placement of antennas.

Our proposal in June 1969 covered the design of a shaped-beam antenna for conveying the wideband video to earth. This antenna (described in Volume 3, Section 6) has a high gain toward the horizon at the expense of gain at the nadir. This is done to compensate for range losses. The result is that nowhere beneath the satellite is the field strength lower than at the horizon. At the horizon it is 5 db higher than an isotropic antenna would provide.

This same design is also employed for normal unified S-band communication. In the event of an unstabilized spacecraft, as for example during launch, omnidirectional coverage is required for both the unified S-band link and for the VHF link. To be certain the type of antenna selected and the planned position on the ERTS body provide adequate coverage for the communication links, without masking effects that impede signal quality, the antenna patterns for the VHF STADAN antenna and the unified S-band omnidirectional antenna have been measured on scale models. In both instances the measurements demonstrated adequate performance.

10.1 VHF ANTENNA PATTERN TEST

The objective of the VHF antenna pattern study was to determine if the location of the VHF STADAN antenna on ERTS provides operation satisfactory for the mission.

The VHF STADAN antenna on OGO is mounted at the end of a deployed boom, where its operation has been quite satisfactory. To avoid the need for deployment, it is desired to relocate the antenna on a fixed tripod support. Pattern measurements are designed to determine

if the tripod support allows antenna gain coverage of -15 dbi over 85 percent of the sphere surrounding the spacecraft. Since the most critical portion of the link is the downlink telemetry signal at 136 MHz, all data was obtained at 816 MHz, where wavelength matches that of 136 MHz at the scale used.

10.1.1 Test Conditions

A one-sixth scale model of the deployed OGO was employed to make the measurements. Figures 10-1 and 10-2 show two views of the model mounted on the TRW antenna pattern range. Figure 10-3 is a block diagram of the crossed dipole VHF antenna and a laboratory quadrature hybrid, Sage Model 751, showing the method for feeding the antenna.

The one-sixth scale model was illuminated at 816 MHz with linear polarization; for one-half of the test with E_{θ} polarization (shown as horizontal), and for the other half with E_{ϕ} polarization (shown as vertical).

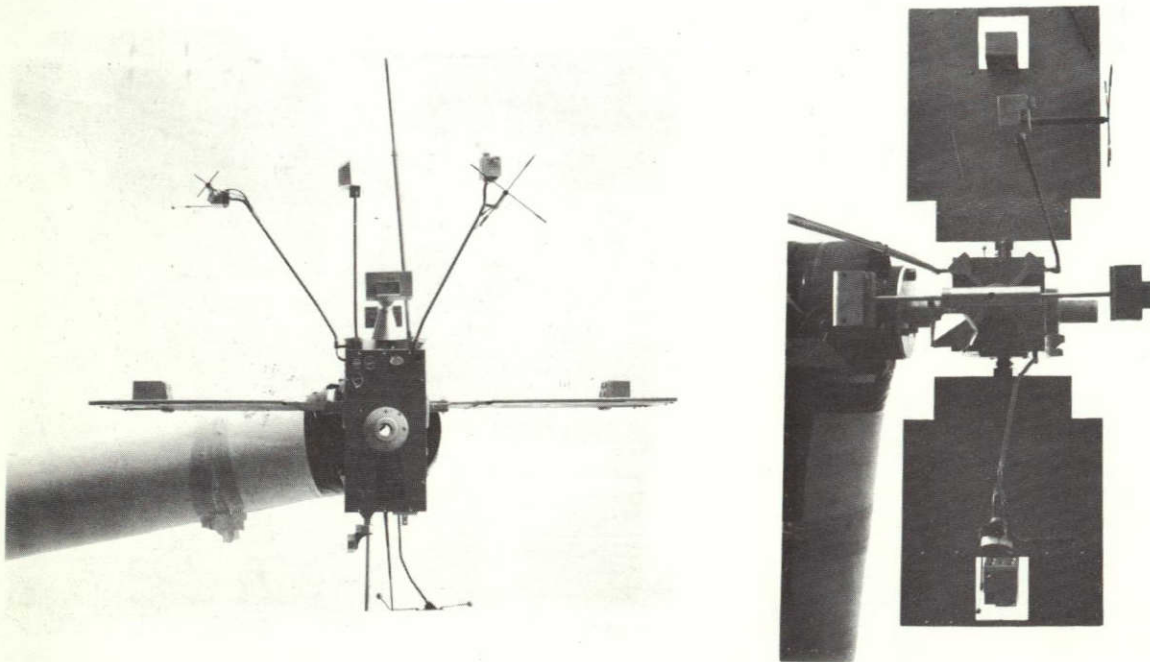


Figure 10-1
ANTENNA PATTERN test model of OGO
spacecraft, 1/6 scale

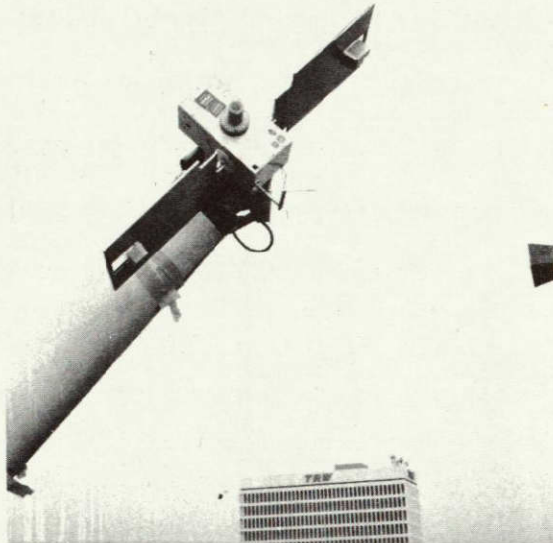


Figure 10-2
ERTS SPACECRAFT ANTENNA PATTERN
model, 1/6 scale

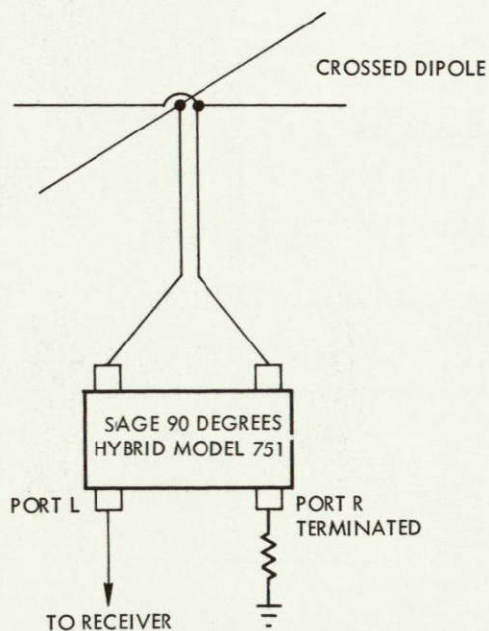
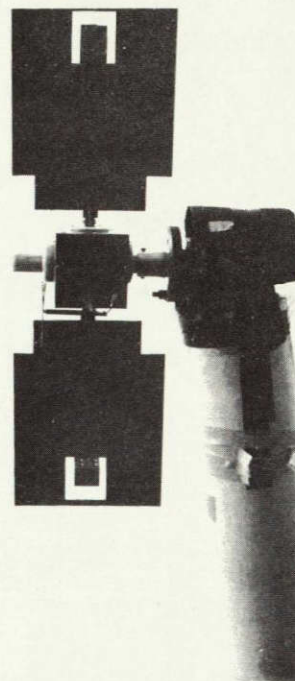


Figure 10-3
ANTENNA TEST MODEL block diagram

10.1.2 Test Results

Figures 10-4 through 10-11 show the resulting contour plots. Figures 10-4 and 10-5 are contours obtained on the OGO configuration with the antenna pattern recorder receiving data from Port L of the quadrature hybrid. In Figure 10-4 the illumination is vertical and in Figure 10-5 horizontal. Figure 10-6 is the contour plot of the OGO configuration with the contour plotter receiving from Port R of the quadrature hybrid with the illumination antenna vertical, and Figure 10-7 is the equivalent with horizontal polarization.

Figure 10-8 is the ERTS configuration, Port L, vertical

polarization; Figure 10-9 is the horizontal polarization equivalent. Figure 10-10 is the ERTS configuration, Port R, vertical polarization; and Figure 10-11 is the horizontal polarization data.

Integration of the patterns produced the following directivities:

- OGO configuration, Port L, directivity = 2.4 dbi (at peak)
- OGO configuration, Port, R, directivity = 4.32 dbi (at peak)
- ERTS configuration, Port L, directivity = 4.06 dbi (at peak)
- ERTS configuration, Port R, directivity = 2.25 dbi (at peak)

The actual losses in the VHF STADAN system on ERTS are conservatively estimated as approximately 2 db, accounted for by approximately 0.5 db in the transmitter passband of the dual diplexer coupler and 1.5 db in the coaxial cable, connectors, and antenna inefficiency. With this value as a baseline, the percent coverage factors for both the OGO and ERTS configurations were calculated (Figures 10-12 and 10-13):

<u>Configuration</u>	<u>Port</u>	<u>Polarization</u>	<u>Directivity (dbi)</u>	<u>Gain (dbi)</u>	<u>Coverage* (%)</u>
OGO	L	Horizontal-E θ	2.4	0.4	76
OGO	L	Vertical-E \emptyset	2.4	0.4	96
OGO	R	Horizontal-E θ	4.32	2.32	85
OGO	R	Vertical-E \emptyset	4.32	2.32	95
ERTS	L	Horizontal-E θ	4.06	2.06	90
ERTS	L	Vertical-E \emptyset	4.06	2.06	-
ERTS	R	Horizontal-E θ	2.25	0.25	92
ERTS	R	Vertical-E \emptyset	2.25	0.25	93

* at -15 dbi

PRECEDING PAGE BLANK NOT FILMED.

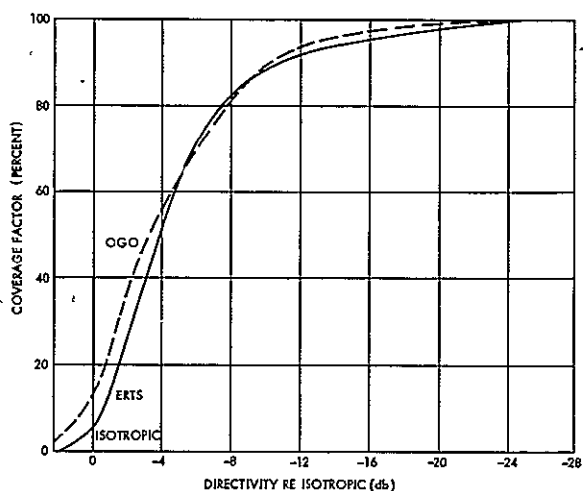


Figure 10-12
ANTENNA COVERAGE above stated loss
(ERTS and OGO installation, Port R,
vertical polarization)

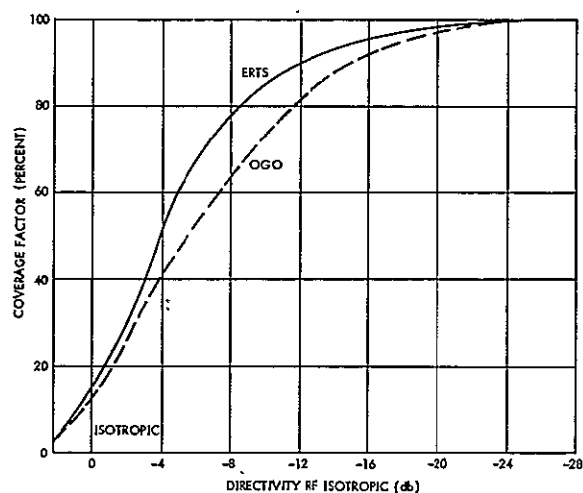


Figure 10-13
ANTENNA COVERAGE above stated loss
(ERTS and OGO installation, Port R,
horizontal polarization)

10.1.3 Conclusions

The peak antenna gains for both the OGO and ERTS VHF STADAN antenna installations are comparable. The percentage coverage factors are also comparable between the two installations. The pattern contour plots show that more deep holes in the antenna pattern coverage appear in the earth-facing side of the coverage for the ERTS configuration than in the OGO configuration. The percentage of signal lost, however, should not be greater than for OGO.

10.2 UNIFIED S-BAND OMNIDIRECTIONAL ANTENNA PATTERN TEST

The design objective for the unified S-band omnidirectional system is to provide a relatively good spherical coverage for the acquisition mode of spacecraft operation. In this mode the body may have any attitude with respect to a ground station as it rotates in pitch. Under these conditions the need is to communicate commands to the spacecraft and to receive 1 kbit/sec telemetry data.

The first approach to omnidirectional S-band coverage considered was to mount a cardioid pattern unit off one end of the spacecraft and a

fan beam unit at the other. This approach was thwarted by other spacecraft needs; the wideband tape recorder package mounted at the +Y end used all the available space.

The approach which was then investigated and which proved successful was to mount two log conical spiral antennas on the opposite Z panels. The radiation pattern for one of these antennas is shown on Figure 10-14 for the X-Z plane. Gain of this antenna is 5.5 db above a circularly polarized isotropic antenna. In the X-Y plane a near circular coverage is provided.

The pattern of Figure 10-14 was measured with a single log spiral antenna mounted in the center of a 30 x 66 inch ground plane and in the presence of mockups of the UHF crossed dipoles and a shaped-beam antenna. The UHF antenna was 24 inches from the log spiral unit under test and the shaped beam antenna 10, 20, and 30 inches. All three antennas were mounted in line. The log conical spiral antenna is that qualified for space flight in the TRW Model 169 program.

The conclusions of the test were:

- The effect of the UHF antenna on the log spiral is not significant
- The shaped-beam antenna produces a noticeable effect at 10 inches separation but negligible effect at 20 and 30 inch separations

With the pattern data of Figure 10-14 as a basis, the pattern with two such units mounted 30 inches apart on the Z panels of the spacecraft was estimated. The result is shown as Figure 10-15. The deep nulls shown will probably result in brief data dropout in a rolling spacecraft. The coverage appears to be more than adequate for command and telemetry requirements of the spacecraft since marginal signal strength is provided with -40 db gain for command signals and -17 db gain for 1 kbit/sec telemetry when in the acquisition mode of unified S-band subcarrier modulation levels.

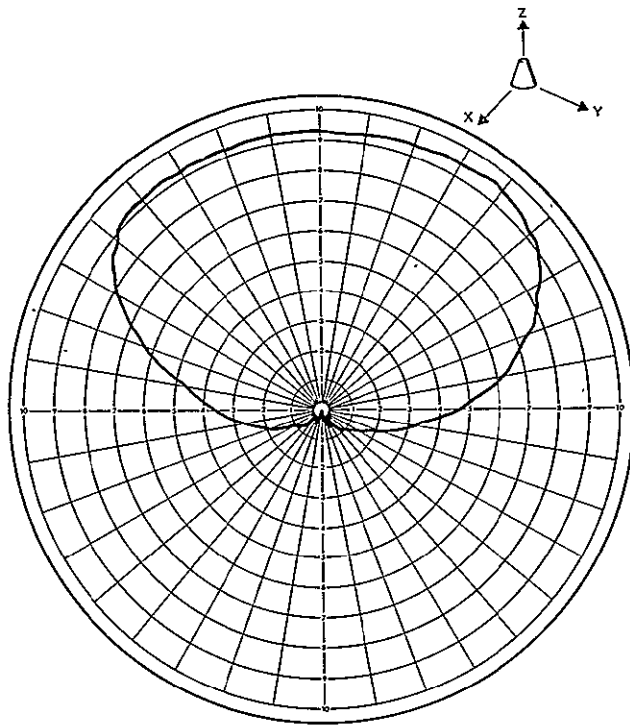


Figure 10-14
 RADIATION PATTERN of log conical spiral (Model 169) antenna (X-Z plane)

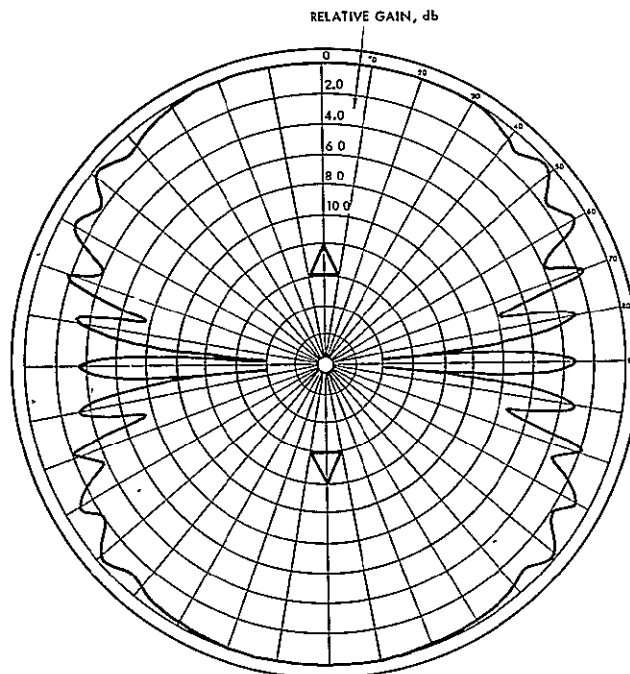


Figure 10-15
 RADIATION PATTERN of two widely spaced S-band conical spiral (Model 169) antennas

CONTENTS

	Page
11. ELECTRICAL POWER	11-1
11.1 Power System Sizing	11-1
11.2 Solar Array Design Factors	11-4
11.3 Alternate Array Designs	11-4
11.4 Depth of Battery Discharge	11-10
11.5 Negative Bus Peak Current Source	11-10

11. ELECTRICAL POWER

The electrical power subsystem requirements for ERTS have been studied in terms of their satisfaction by the OGO power subsystem. Included was the determination of a power profile showing the payload operational times. This profile also included all the original spacecraft subassemblies plus the recently identified unified S-band equipment. The entire subsystem was then reviewed in light of these requirements plus the body lighting conditions stemming from the ERTS orbit and orientation. In all respects except one with only minor adjustment, the OGO power subsystem design meets the ERTS mission requirements. The one exception is the need for supplying negative regulated power to the payload. Satisfaction of this need is accomplished through the addition of a 300-watt regulator-converter.

11.1 POWER SYSTEM SIZING

The average power required per orbit by the spacecraft and payload is essentially constant for the year. The budget presented in Table 11-1 is based on the following assumptions:

- 1) Normal mode 4 operation
- 2) Sensors on 20 minutes, 50 percent real time
- 3) Traveling wave tube warm-up 2 minutes
- 4) VHF and unified S-band transmitters ON always

The power required from the bus varies in time; a typical schedule of sensor operation is assumed to produce the profile of Figure 11-1. The components are a base load to which is added the following combinations of sensor and communication equipment loads:

Time History of Bus Current Based on 28 Volt Bus Voltage						
<u>Time*</u>	<u>0 to 10</u>	<u>10 to 20</u>	<u>20 to 30</u>	<u>30 to 80</u>	<u>80 to 90</u>	<u>90 to 103</u>
Base load, amperes	5.95	5.95	5.95	5.95	5.95	5.95

*Time equal zero corresponds to eclipse end; time equal sixty-nine corresponds to beginning of next eclipse.

<u>Time</u>	<u>0 to 10</u>	<u>10 to 20</u>	<u>20 to 30</u>	<u>30 to 80</u>	<u>80 to 90</u>	<u>90 to 103</u>
Data collection system	0.03	0.03	0.03	0.03	0.03	0.03
RBV, 155 watt	-	5.65	5.65	-	-	-
MSS, 60 watt	-	2.15	2.15	-	-	-
Wideband recorders, 2 record		-	6.0			
Wideband recorders, 2 playback		-	-	-	5.4	-
Wideband transmitter, 72 watt		2.8	-	-	2.8	-
-24 \pm 1/2 volt converter losses		1.5	1.9		1.0	
Total, amperes	5.98	18.18	21.68	5.98	15.18	5.98

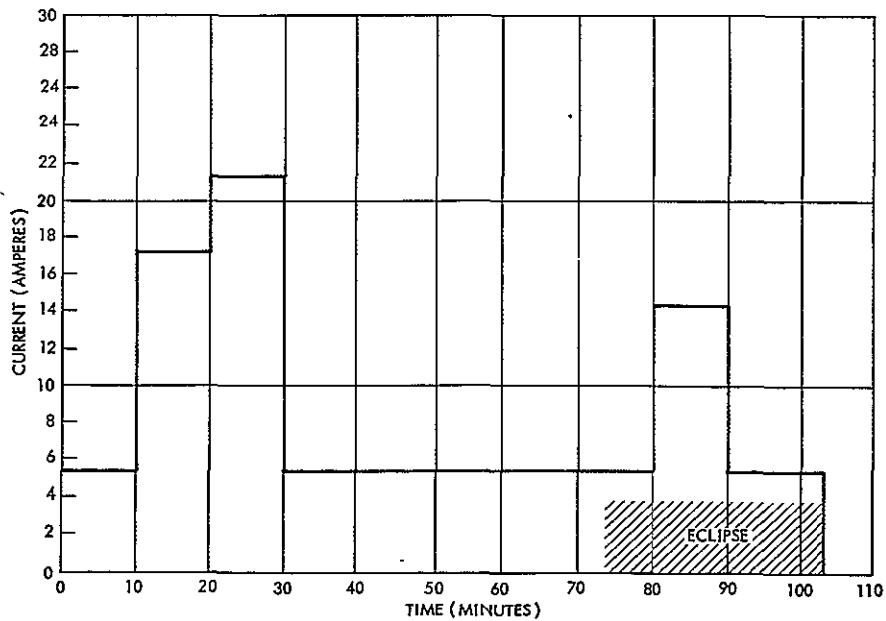


Figure 11-1
 PROFILE OF ELECTRICAL POWER at 28 volts in one orbit shows video playback in eclipse.

Table 11-1. Power Budget for ERTS

	Current (average) at 28 Volts
Continuous Loads	
Attitude control	2.78
Gyrocompass	0.26
Gyro heater	0.25
Reaction wheels, average	0.12
Communication bus minimum	1.13
Command receivers, decoders, command distribution unit, power control unit, low frequency timing assembly, special purpose telemetry, signal conditioner	
Other Steady Loads	
Equipment group (DDHA plus ADHA)	0.67
Narrowband tape recorder (10 percent play- back)	0.28
Stored command programmer, clock	0.7
Unified S-band system	0.34
137-MHz transmitter	<u>0.05</u>
Total Base Load	5.95 amperes
Variable Loads	
Data collection system, continuous	0.03
RBV 50 sec, 75 watt, 20 min, 155 watt	5.65
MSS 60 watt	2.15
Wideband recorder, each	
Record	3.0
Playback	2.7
Wideband transmitter, 10-watt mode	1.4 each
(Warm-up 2 min, 6 watts)	
Operate, driver 4 watts	
Operate, traveling wave tube 68 watts (2)	
-24-1/2 volts converter, losses, 20 min (15 percent of peak current)	1.9

11.2 SOLAR ARRAY DESIGN FACTORS

The total energy requirement which the solar array must support is the integral of the power profile plus a battery dissipation allowance:

	Energy Requirements (28 Volts)		
	<u>Watts</u>	<u>Time</u>	<u>Watt-Min</u>
Spacecraft plus DCS	164	103	16,900
Payload, real time	340	10	3,400
Payload, record	449	10	4,490
Payload, playback	251	10	2,510
Battery losses	14	103	<u>1,440</u>
		Total	28,740

Using these as the baseline the size of the power subsystem was established. The initial investigation was based on the solar module shown in Figure 11-2, 10 ohm-cm cells, and orientation such that the solar array shaft is parallel to the velocity vector. Figure 11-3 shows the theoretical solar array output with respect to position in orbit.

Shadowing of the array was determined with the aid of an ERTS model (see Figure 11-4). As can be deduced from this figure, the compartment holding the wideband tape recorder has a significant effect on shadow loss. The tests show a loss of 8 percent in total energy per revolution in the baseline configuration (that of Figure 11-4). The array will be wired to minimize the effects of shadowing on array output; a shadow on one module on the OGO disables a string of six other unshadowed modules, but this effect is eliminated for ERTS. This wiring plan (Figure 11-5) forms a series string of three adjacent modules such as A1, A2, and A3. In addition, array wiring is designed to minimize magnetic moment, as on OGO.

11.3 ALTERNATE ARRAY DESIGNS

Many possible solar array designs were investigated to maximize power. The key objectives of this study were

- Optimize voltage for the peak battery charge voltage requirement of 33 volts

11-5

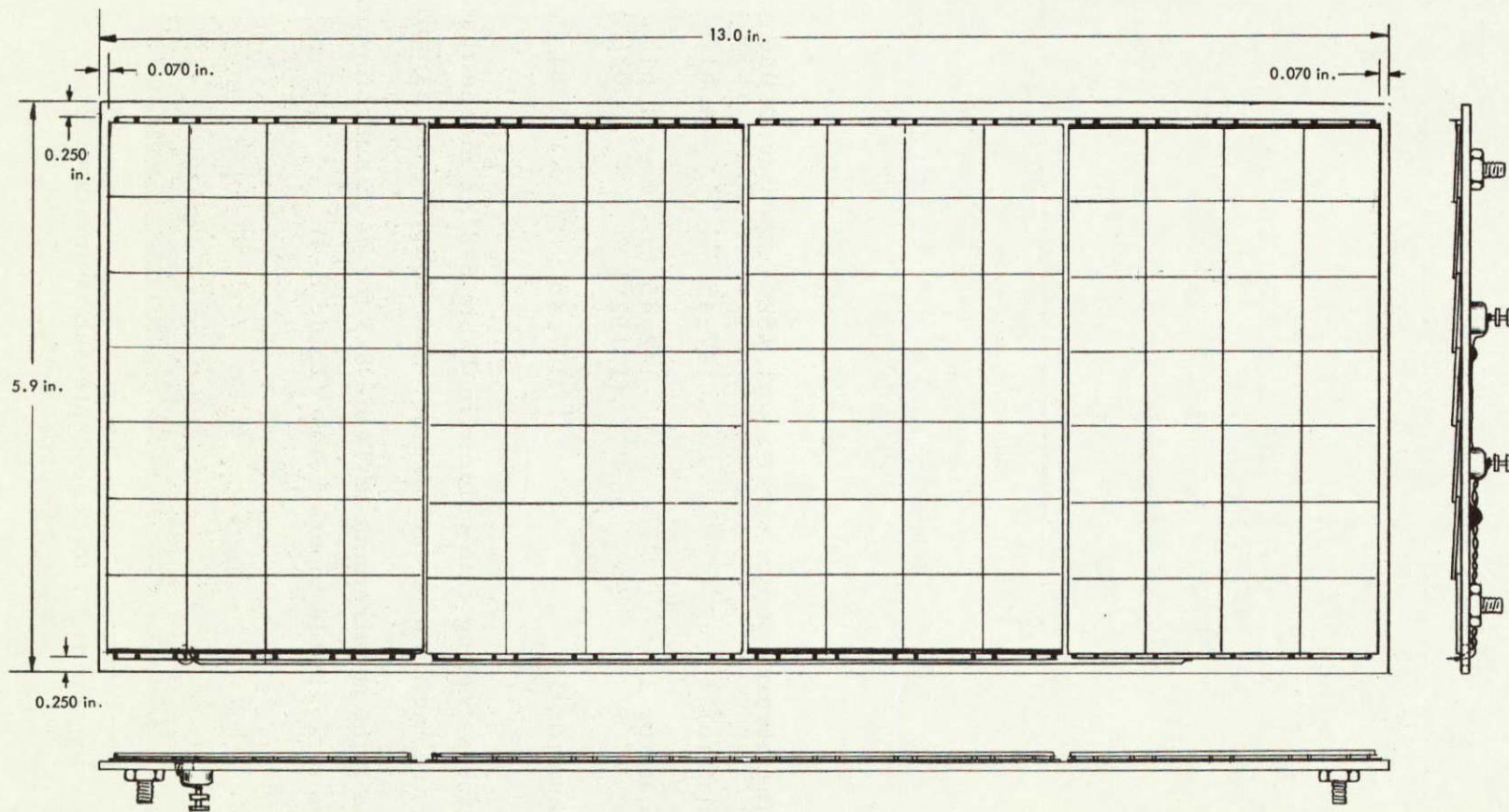


Figure 11-2
SOLAR SUB-PANEL LAYOUT

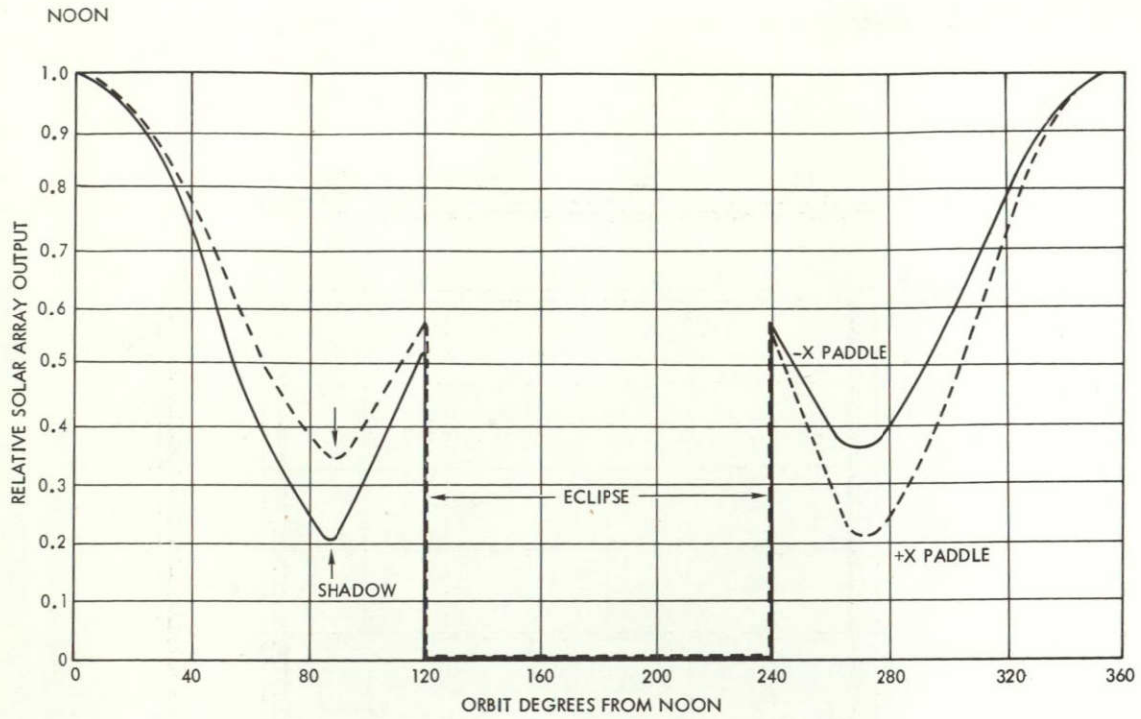


Figure 11-3
 ARRAY CURRENT, theoretical output with and without shading

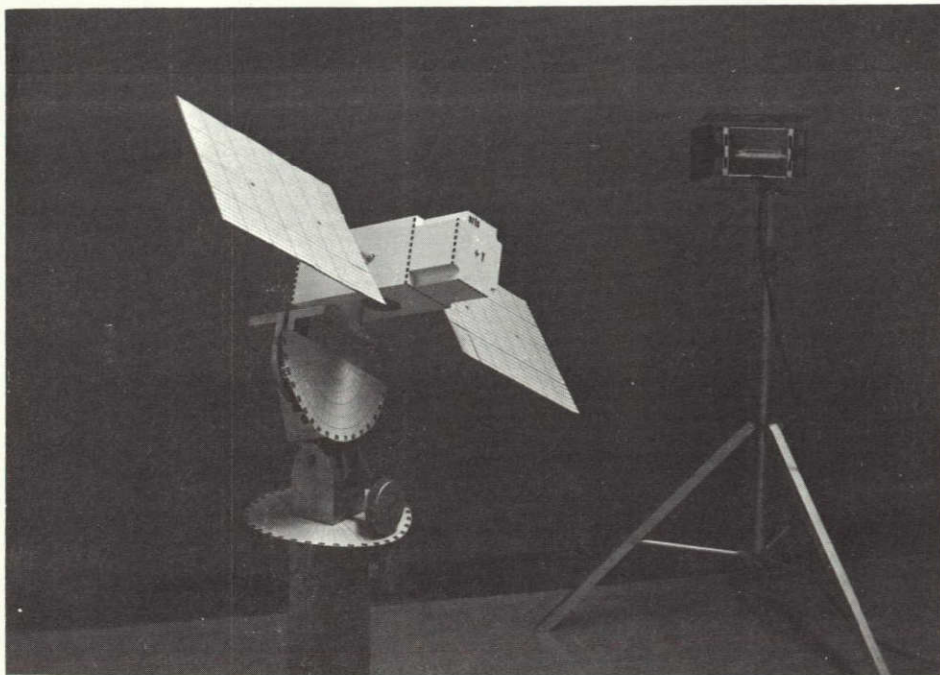


Figure 11-4
 ERTS SOLAR ARRAY shadow-orientation model

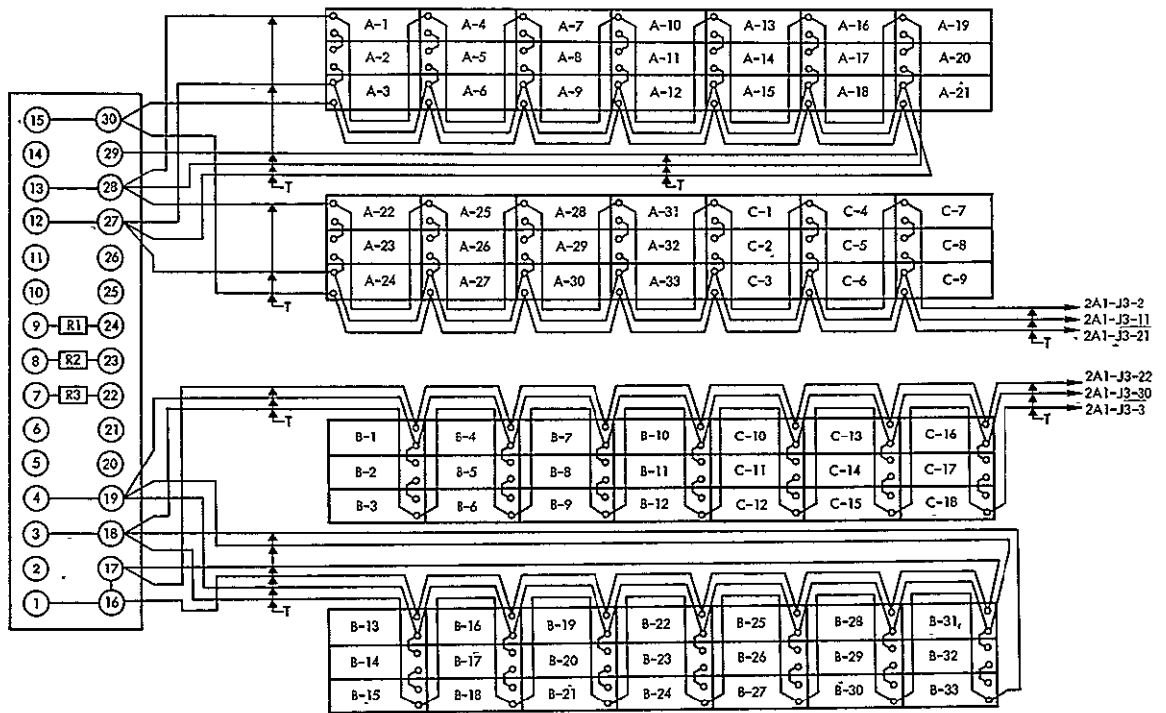


Figure 11-5

SOLAR ARRAY WIRING is designed to minimize effect of shadows on power.

- Provide as much power as possible at the end of three years
- Reduce cost of fabrication of array

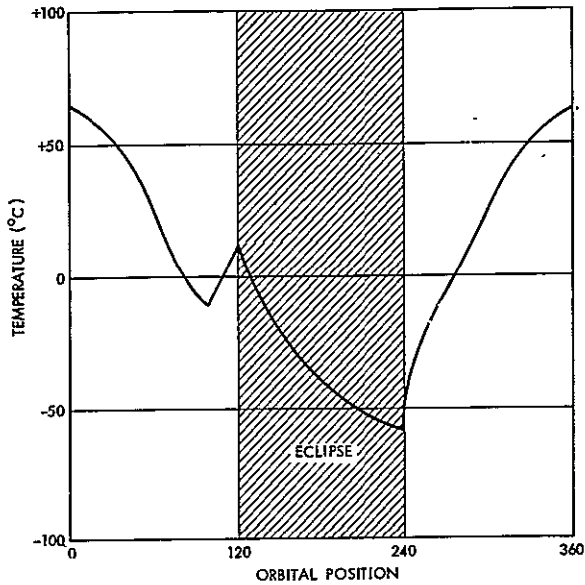
The temperature of the array is variable in the ERTS body orientation, as shown on Figure 11-6, as the result of variation in angle of arrival of sun energy.

Table 11-2 shows a range of possible solar paddle designs based on variation in number of cells in series and size of modules. A 13 x 17.9 inch module using 84 cells (OGO used 96) in series proved optimum (Figure 11-7). The large module permits packing more cells on a given array area, resulting in a 9.5 percent increase in array output.

Comparative data follows:

<u>Characteristic</u>	<u>Baseline</u>	<u>Alternate Larger Module</u>
Number of modules	168	56
Number of 2 x 2 cm cells	18,816	20,608

<u>Characteristic</u>	<u>Baseline</u>	<u>Alternate Larger Module</u>
Cells per module	112	368
Module size, inches	5.9 x 13	13 x 17.9
One sun, year end array output, watts	740	810



Despite the advantages, the increased cost of incorporating the larger module, calling for structural differences in array support points and requalification tests on an assembled paddle, led to the decision to retain the 5.9 x 13-inch module in the baseline design. The larger module remains a back-up choice for higher output if needed for payload growth.

Figure 11-6
ARRAY TEMPERATURE throughout one orbital revolution

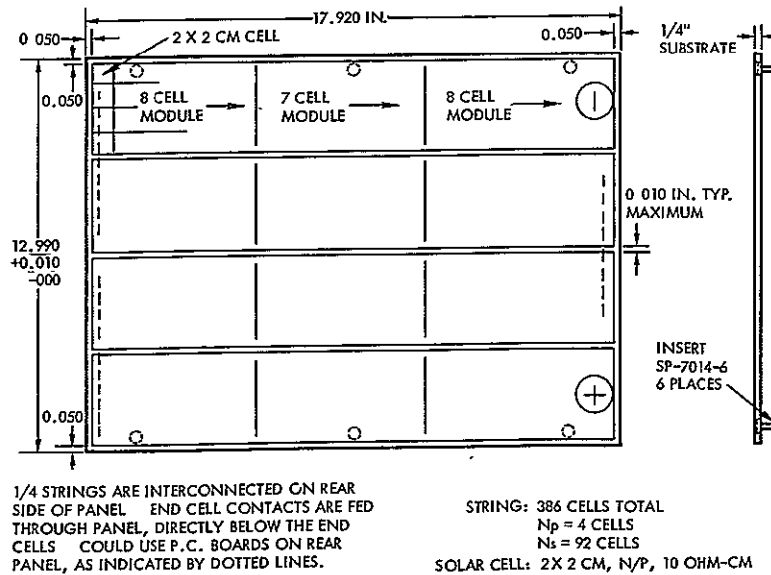



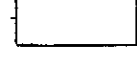



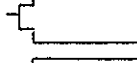



Figure 11-7
ALTERNATE ERTS SOLAR PANEL

Table 11-2. Tabulation of the various concepts considered for the ERTS solar array giving preliminary array worst case performance and optimum voltage at Year 2 for 2 and 10 ohm-cm cells, each 2 x 2 cm² size.

Concept Number	Number of Modules	Module Size (in.)	Number of Series Modules	Cells Per Modules	Total Number of Cells Per Array	Cell Packing Factor	Number of Series Cells	Array Configuration	Preliminary Array Performance at Year 1			
									10 ohm - cm		2 ohm - cm	
									Voltage at Maximum Power T = 61°C	Average* Array Power (watts)	Voltage at Maximum Power T = 61°C	Average* Array Power (watts)
1	144	5.9 x 13.0	3	112	16,128	0.850	84		30.1	425	32.5	429
	145**	5.9 x 13.0	5	112	16,240	0.850	80		28.7	427	31.0	431
2	155	5.9 x 13.0	5	112	17,360	0.850	80		28.7	441	31.0	445
	168**	5.9 x 13.0	3	112	18,816	0.850	84		30.1	515	32.5	520
3	48	13.0 x 17.9	1	368	17,664	0.920	92		33.0	465	35.6	470
4	52	13.0 x 17.9	1	368	19,136	0.920	92		33.0	487	35.6	492
6	96	8.9 x 13	2	167	16,032	0.840	88		31.6	422	34.1	426
7	104	8.9 x 13	2	167	17,368	0.840	88		31.6	442	34.1	446
5	48	13.0 x 17.9	1	345	16,560	0.862	69		24.8	436	26.7	440

* Average array power based on one complete orbit.

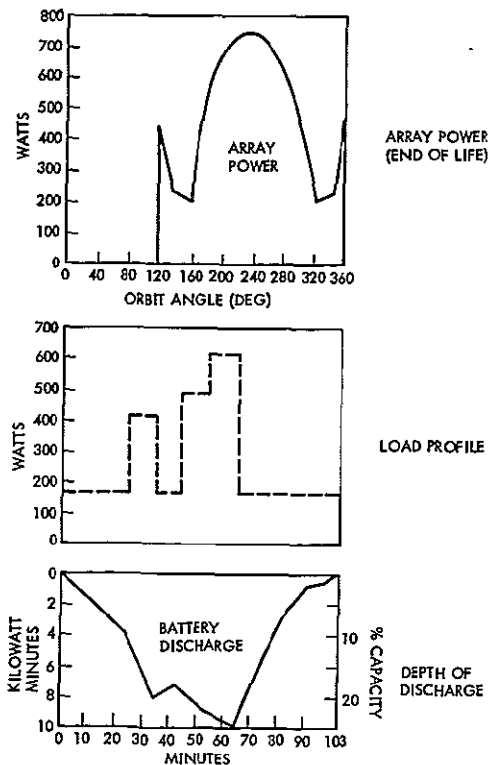
** Chosen baseline design.

11.4 DEPTH OF BATTERY DISCHARGE

Determination of depth of discharge requires a detailed analysis of the entire energy balance situation around the orbit with actual bus voltages and array voltage current curves. The study has assumed a set of worst case conditions:

- Full payload operation, 20 minutes (see Section 11.1)
- 10:00 AM node crossing
- 1 year in orbit
- 80 days after vernal equinox
- Baseline array (see Section 11.2)
- Realistic shadowing from model tests

The analysis, whose results are listed in Table 11-3, takes into account array output power obtained at the bus voltage as determined by the state of charge of the battery. Power load profile and depth of discharge are plotted on Figure 11-8. The conclusion reached is that battery depth of discharge will be about 24 percent after one year.



11.5 NEGATIVE BUS PEAK CURRENT SOURCE

The best method for supplying a 30-ampere current pulse to the shutter of the RBV camera was determined to be a 27-cell battery weighing 7.45 pounds. During this study the requirement changed to 18 amperes influencing the resultant solution in size only, calling for a battery of 1.1 ampere-hours instead of the 2.5 ampere-hours required for 30 amperes. The

Figure 11-8
POWER LOAD PROFILE and depth of discharge

Table 11-3. Power System Energy Balance (18,816 cells)
(100 percent battery charge at beginning of eclipse)

Event	Time Minutes	Solar Array ⁽¹⁾ Capability Watts	System Load Watts	Battery Average Rate		Battery Charge Watt ⁽²⁾	Discharge Watt Min.	Battery State of Charge ⁽³⁾ Watt Min.
				Charge Watt	Discharge Watt			
Eclipse, no payload	24	-	164	-	164	-	3940	-3940
Eclipse, payload on, playback	10	-	415		415		4150	-8090
Sunlight, payload off	5.7	304	164	140		798 x 0.81		-7444
Sunlight, payload off	5.7	211	164	47		268 x 0.81		-7227
Sunlight, payload on, real time	10	322	489		167		1670	-8897
Sunlight, payload on, record	10	546	613		67		670	-9567
Sunlight, payload off	3	720	164	556		1670 x 0.86		-8132
Sunlight, payload off	5.7	709	164	545		3103 x 0.84		-5522
Sunlight, payload off	8.6	611	164	447		3840 x 0.82		-2372
Sunlight, payload off	8.6	367	164	203		1745 x 0.81		- 957
Sunlight, payload off	5.7	216	164	52		296 x 0.81		- 717
Sunlight, payload off	<u>6.0</u>	336	164	172		1030 x 0.81		+ 118
	103.0							

(1) Assume use of 168 double OGO modules of 18,816 total cells and shadowing of video recorder.

(2) Assume approximately 86 to 81 percent watt-hour battery efficiency

(3) Referenced to full charge = 40,000 watt-minutes

object of this study was to supply a current pulse for 0.1 second of 30 amperes at -24, -12 + 0 volts. Open circuit voltage limit was set at 36 volts.

It is apparent that some energy storage device is required to supply the required pulse power. The energy per pulse is 24 volts x 18 amperes x 0.1 sec = 43.4 joules.

Capacitors and inductors are eliminated because of the size required. For a capacitor, $1/2 CE^2 = 43.4$ joules; if $E^2 \cong 1000$, then $C = 0.0864$ farad at 50 volts. For an inductor, $1/2 LI^2 = 43.4$ joules; if $I^2 = 100$, then $L = 0.0864$ henries at 10 ampere. This then leaves only a battery among the commonly available components for energy storage.

The discharge capacity required by the RBV shutters per cycle can be readily calculated from $\frac{ItT}{3600 p}$

where I = amplitude of pulse current, amperes

t = pulse duration, seconds

T = duration in seconds of payload operation per orbit

p = the pulse repetition time, seconds

or

$$\frac{(18)(0.1)(1200)}{(25)(3600)} = 0.025 \text{ ampere-hour}$$

Obviously the battery required to supply 0.024 ampere-hour of discharge capacity would be rather small. However, the discharge rate (18 ampere) now becomes the critical factor in the determination of the battery size. Internal impedance limits the discharge rate to approximately 20 times the nominal capacity. Then for an 18-ampere pulse amplitude a 0.9 ampere-hour cell would be adequate. A more detailed treatment of cell size selection appears below.

The battery power supply could be arranged in several configurations; those considered most feasible are shown in Figures 11-9 through 11-13. In all of these, except that of Figure 11-13, a separate battery is required.

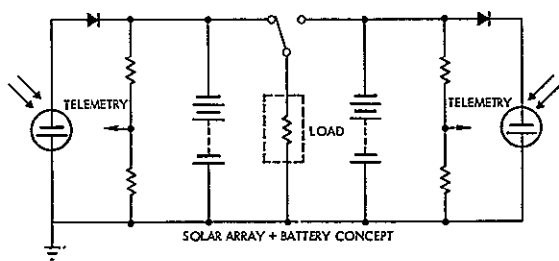


Figure 11-9
RBV SHUTTER power supply concept,
Configuration No. 1

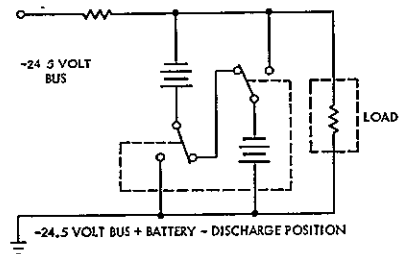


Figure 11-10
RBV SHUTTER power supply concept,
Configuration No. 2

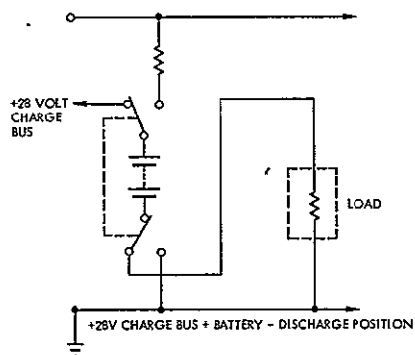


Figure 11-11
RBV SHUTTER power supply concept,
Configuration No. 3

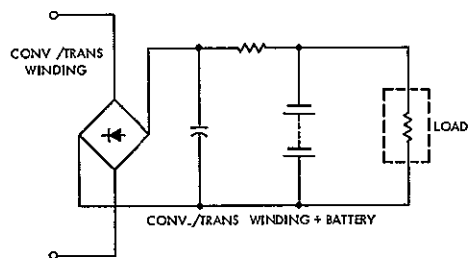


Figure 11-12
RBV SHUTTER power supply concept,
Configuration No. 4

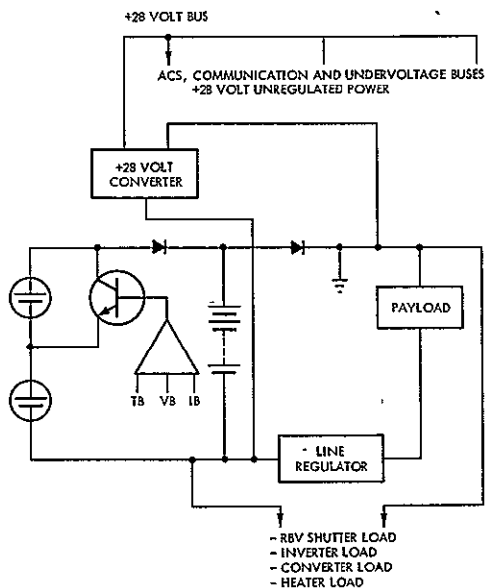


Figure 11-13
RBV SHUTTER power supply concept,
Configuration No. 5

Configuration No. 1 (Figure 11-9) calls for an added solar array module (approximately 112 2x2 cm cells) connected across the battery. The current limiting feature of the solar cell characteristic is well suited for limiting the charge current to a safe trickle charge value. Figure 11-9 shows the possibility of redundant supplies.

Configuration No. 2 (Figure 11-10) shows the required arrangement for charging from the -24.5 volt (payload) bus, requiring a resistor to limit the current to a trickle charge rate. In

addition, the battery would require switching such that two halves would be charged in parallel and discharged in series. To provide a minimum of 24 volts the battery would in effect require a minimum charge voltage of approximately:

$$V_c = \frac{1.45}{1.25} \times 24 = 27.8 \text{ volts}$$

which in effect is accomplished by the parallel charging arrangement.

Configuration No. 3 (Figure 11-11) utilizes the existing +28 volt (charge) bus with a trickle charge resistor. Upon discharge into the load of polarity of the battery must be reversed. The arrangement of Figure 11-11 accomplishes this.

Configuration No. 4 (Figure 11-12) utilizes an alternating current source that could either be in existence (attitude control system inverter or converter) or an added winding to one of the existing converters or inverters. This energy would then be rectified and supplied through a trickle charge resistor to the battery for charging.

Configuration No. 5 (Figure 11-13) would essentially reverse the existing charge bus placing the spacecraft ground at a positive potential with respect to the charge bus. Those loads that require a positive bus would be supplied by a converter within the power control unit. The RBV shutter power would then be taken from the existing pair of batteries (12 ampere-hours).

The order of merit seen in these alternate charging methods is as follows: 4, 1, 3, 2, 5. The switching approaches, 2 and 3, were discarded because of high current switching required. Reversing the spacecraft power bus, Configuration No. 5, could not be evaluated without a long study of existing wiring of the spacecraft but it is rejected because of the concomitant changes in the ground support equipment to reverse the bus. Alternates 1 and 4 are both quite feasible and straightforward, but the greater simplicity of Configuration 4 gives it preference.

Discussion with a cell vendor led to the selection of an HVO 1.1 cell type fitted with high pressure relief valve (50 psi) which could be

potted over to obtain sealed operation to meet the 18-ampere pulse requirement. Since the application is a pulse train load with trickle recharge, heat rejection and gas pressure generation should not be a problem in the battery design. The HVO 1.1 configuration has the following characteristics:

	<u>Cell</u>	<u>Battery</u>
Number of cells	-	28
Weight, lb	0.1	4.25
Height, in.	3	3-7/8
Width, in.	$1 \frac{21}{32}$	3-5/8
Length, in.	11/32	6-1/2

CONTENTS

	Page
12. ELECTRICAL INTEGRATION	12-1
12.1 Junction Box Requirements	12-1
12.2 Grounding and Bonding	12-1
12.3 Command Distribution Unit	12-2
12.4 Harnesses	12-7
12.5 Electromagnetic Interference	12-10
12.5.1 Multispectral Scanner	12-10
12.5.2 Return Beam Vidicon	12-11
12.5.3 RF System	12-12

12. ELECTRICAL INTEGRATION

12.1 JUNCTION BOX REQUIREMENTS

Study of the interconnection requirements for ERTS and the J boxes to meet these requirements optimally has demonstrated that the power distribution J-box, which provides subsystems with a power distribution point and an interface with the launch vehicle and external test equipment, should be reduced in size. The new design will provide a number of advantages, primarily ease of access to the spacecraft test points and availability of the in-flight jumper from the shroud access port. The junction box will be mounted on the +Y panel in the extended portion of the spacecraft (see Section 4) readily accessible for troubleshooting.

The payload electrical integration assembly has been simplified because of the reduced requirements on ERTS compared to OGO. The assembly for ERTS, as in OGO, will function as a gathering place for all subsystem signals routed to the payloads. The input gates receiving signals from the payload provide a means of conditioning the bilevel status telemetry from the payload. For the most part, interconnections of the type required could be provided by a single harness (thus eliminating the payload integration assembly, but a harness of this magnitude would become large and difficult to handle and would increase the time and cost of making changes to the payload or the spacecraft.

All other J boxes can remain the same as on OGO except that some electrical changes will be required in the central J box to handle the addition of the orbital switching assembly. The OGO 6 ordnance J box will be used in its original configuration except for simplifications since a number of ordnance functions have been deleted.

12.2 GROUNDING AND BONDING

Grounding for ERTS has been studied to determine what configurations will be required for a compatible observatory. A hybrid ground system will probably be required, but this is being reviewed further in the light of new equipment, including the payload equipment. To assure electromagnetic compatibility, it is planned that all new chassis assemblies will be fabricated to provide maximum shielding effectiveness within

the constraints of connector and shaft penetrations. When possible the assemblies will be constructed in the form of a seamless five-sided box with one cover plate. The mating edge between the cover plate and the box will be free of any insulating finish, and will either have a flange as a mating surface or a metal mesh gasket. In order to assure adequate pressure between the cover plate and the chassis, the screws or other fasteners holding the cover plate to the chassis will be no more than 4 inches apart, located at each corner as well as at intermediate points.

Electrical bonding will be established by a low impedance electrical path between conducting elements. All mating surfaces of the structure will be treated with a protective finish which is either electrically conductive or which can be penetrated under moderate pressure. Where surface pressure cannot be used, such as around movable joints or rotating shafts, flexible bonding straps will assure an adequately low impedance between members. A reasonable DC resistance between any two bonded members in ERTS, as measured by a bonding meter or milliohmeter, is 2 milliohms. All spacecraft assemblies will be bonded to the structure such that the DC impedance between the chassis and the structure is 2 milliohms or less.

12.3 COMMAND DISTRIBUTION UNIT

A method of command distribution for ERTS has been defined that performs all of the standard OGO functions and meets as well the following ERTS requirements:

- Matrix drive redundancy
- Monitoring of the status of new spacecraft commands
- Automatic timer shut off for all high-current payload equipment
- Negative polarity of -24.5 volt DC for payload power
- A minimum capacity of 358 commands
- Payload commands modified to meet the following Nimbus interface requirements:

Driver	Open Circuit Output (volts)		Source Impedance (ohms)	Maximum Load Capability (amp)
	Energized	Non-energized	Energized	
A	-24 ±1.0	0 ±0.5	2	1
B	0 ±0.5	-24.0 ±1.0	2	1

The matrix selected to meet these requirements is shown in Figure 12-1.

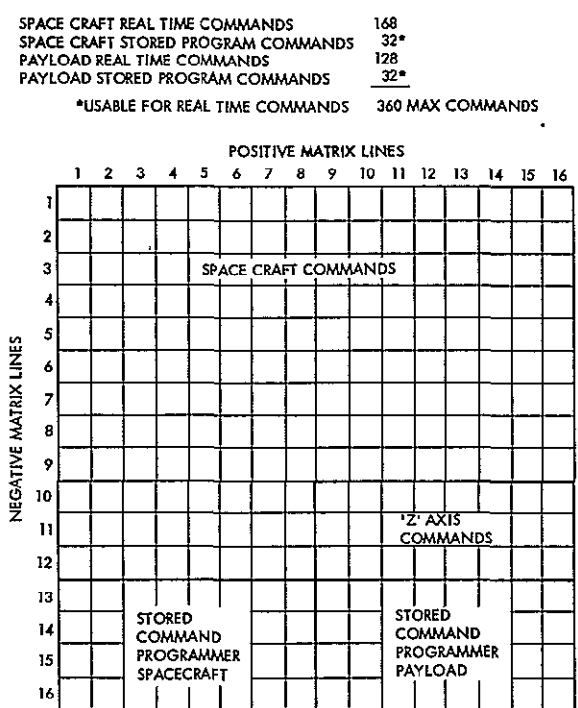


Figure 12-1
 COMMAND MATRIX assignments are arbitrary and may be varied by re-wiring the CDU.

In evaluating alternative approaches for ERTS, prime consideration was given to modifying the OGO 6 command distribution unit. The unit in OGO 6 had a command capability over and above that required for ERTS. A second factor was the OGO flight history; the units flown on OGO have a record of thousands of hours of successful operation. A third element in the design selection was cost. Modifying the OGO 6 unit for the ERTS configuration can be done in modules and these modular modifications avoid the requirement for a complete test qualification program.

Figure 12-2 shows redundant matrix drivers selected by

- Command to place the proper negative drivers in the matrix
- An enable pulse from the addressed decoder to power the selected group of drivers

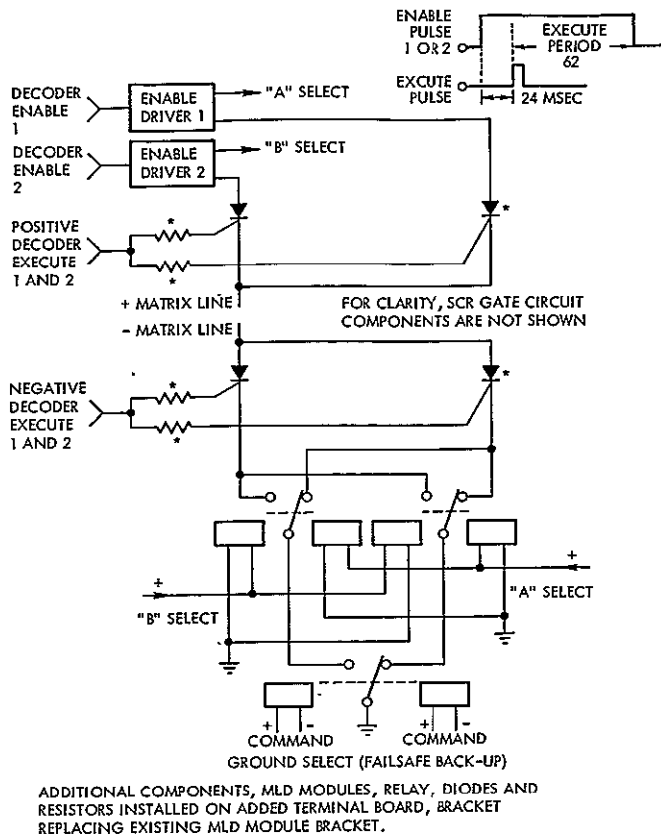


Figure 12-2
ADDED COMPONENTS for ERTS
redundant matrix

- All six items of the payload assemblies controlled by the timers had to be independent in their operation (six timers required).
- The timers must reset each time an "on" command is sent so that time will start from the last command sent; thus, a full time cycle must be provided from the last issued "on" command.

Six identical timers as shown in Figure 12-3 are provided, each one accepting a 0.05425 pulse/sec clock input from the low frequency timing assembly. Each timer divides the input clock by 79 yielding one output pulse for 79 input pulses for a total time delay of approximately 24 minutes. The normal override feature is provided by commands that uniquely turn off the selected timer to allow equipment control by its normal on-off function. A command resets all equipment timers to the operate mode.

The input drive signals to the line driver stored command receivers are cross-strapped so that both decoders can enter the appropriate line drivers.

Orbital operation safety was found to require automatic timer shut-off of all loads greater than 1 ampere. The high-current items of the payload require a total of six timers, one each for the RBV and MSS, two for the video tape recorders, and two for the wideband amplifiers. It has been found impractical to adapt the existing OGO 23-minute timer because of its size; the requirement for six such timers would severely limit the space allocation. The timers had to meet the following basic requirements:

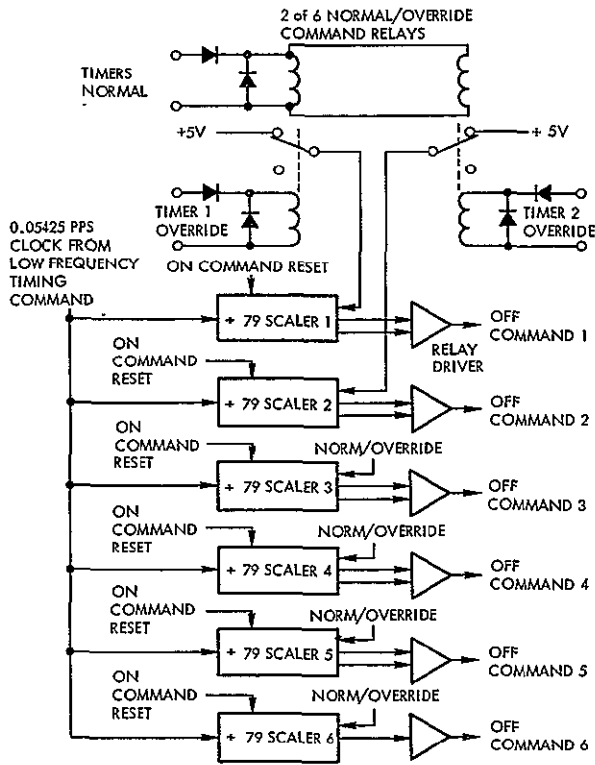


Figure 12-3
24-MINUTE TIMER

inhibit line. The clocking gates shown in Figure 12-5 inhibit the transfer of data into the shift register during readout. Transitions during the readout period are recognized by the primary storage relays and read into the registers following the readout cycle.

To facilitate operational use it was decided to install single-bit status reports for all new spacecraft command functions. Five 9-bit shift registers, loaded in parallel and read-out serially, provide status telemetry for 45 discrete status bits. Figure 12-4 shows one of the five registers and the shift clock selection circuitry. Primary storage relays remember the last commanded status through the readout cycle, permitting non-destructive readout. The primary storage relays are reset by the inverse command function where applicable or by the end of the word cycle as represented by the trailing edge of the fifth or last

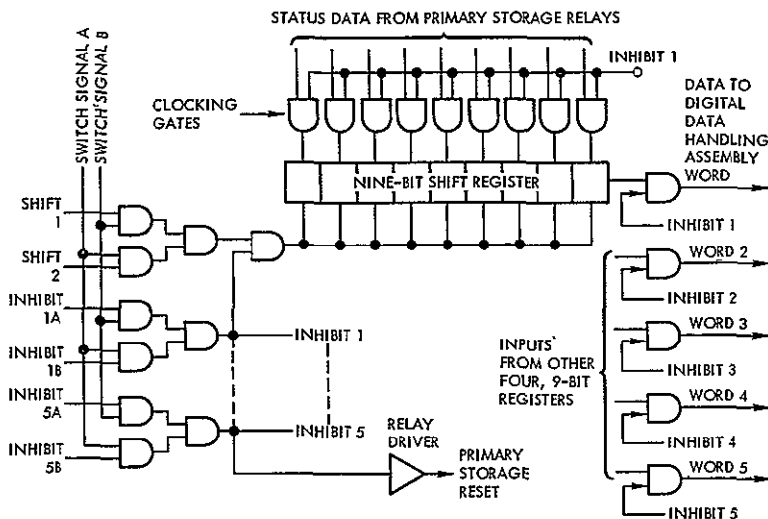


Figure 12-4
ONE OF FIVE 9-BIT
parallel/serial shift
registers to provide
command status
telemetry

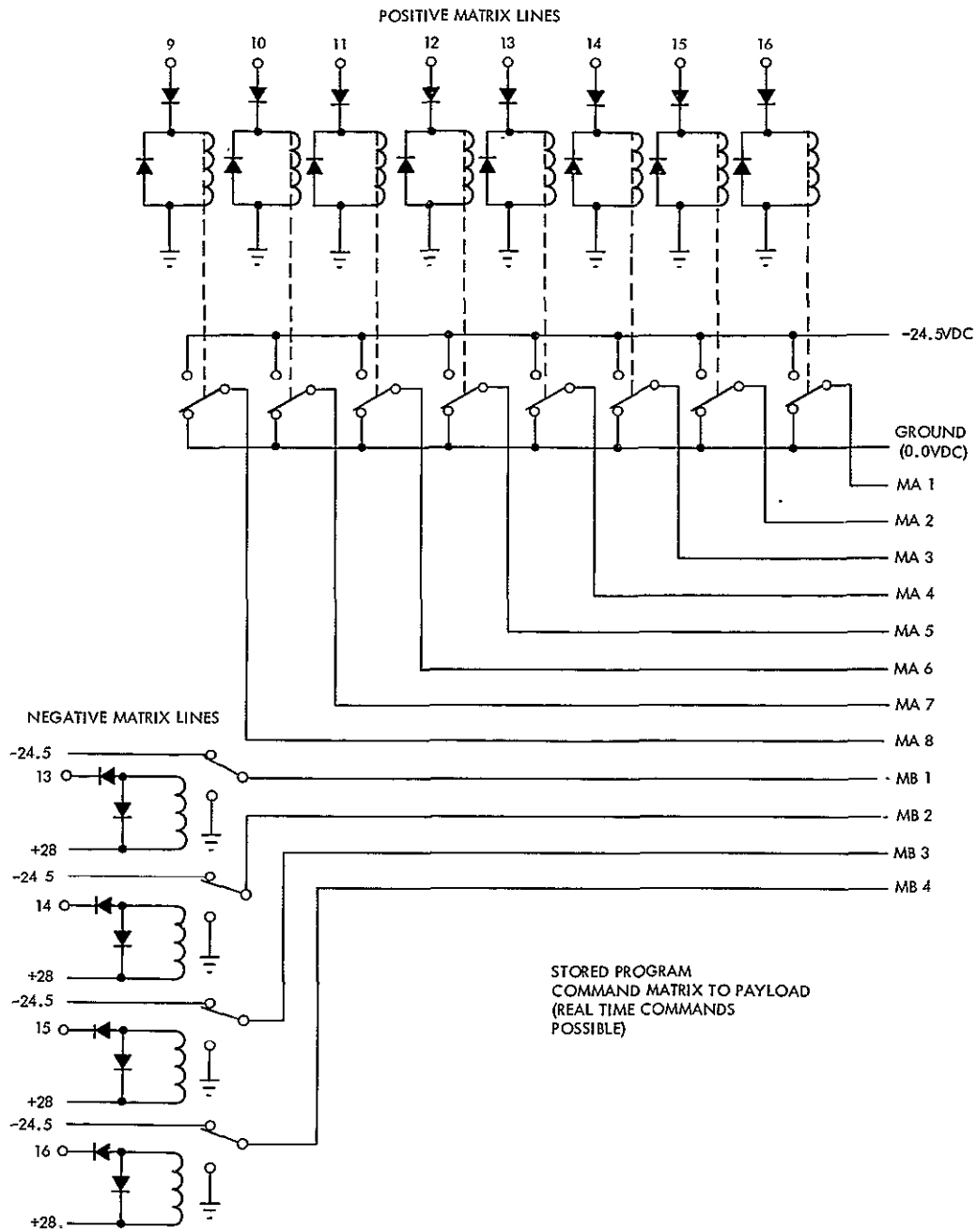


Figure 12-5
PAYLOAD INTERFACE for stored command matrix

Compatibility with the Nimbus command polarity interface requirements is shown in Figure 12-5. All payload commands from command storage or real time from the Z axis matrix are provided for by the

interface lines identified as MA or MB. The MA lines are switched from 0 volt DC (ground) to -24.5 volt DC for the 62-millisecond command interval. The MB lines are switched from -24.5 to 0 volt DC (ground) for the 62-millisecond command interval. One selected pair of lines are switched to the true state for each complete command issued, i. e., MA-1 and any one of four MB lines.

Study of total command requirements showed that 256 commands, suggested by the study specification, was not sufficient. A decision was made to provide increased capacity in the manner of OGO 6. Figure 12-6 shows how 24 commands are expanded to 128 commands. Each payload command requires the receipt of two commands from the ground station. The first sets the desired one of eight latching relays. The second drives an impulse relay that transfers one of 16 MA lines to -24 volt DC and pulses the ground transfer relays (K9 and K10) to complete the command. The selected relay K1 through K8 is set by the intended command while all others are reset by a system of ORing diodes that receive the selected command as a reset. Relays K11 through K26 are impulse relays that remain closed for the 62-millisecond command duration. Relays K9 and K10 are circuit redundant to ensure command completion in the event of a failure of K9 or K10.

12.4 HARNESSES

The harness design used on OGO was reviewed to verify that it was still appropriate. ERTS will utilize approximately 40 cable or harness assemblies for the interconnection of spacecraft subsystems and payload. Electrically ERTS interconnections will be similar to those on OGO, but mechanical configurations will be changed to accommodate the relocation of subsystem boxes. Cables for use with the payload equipment will be redesigned and significantly simpler than those on OGO. To minimize weight, the size of copper wire used in harnesses is as small as No. 30 average (0.01-inch diameter).

The basic considerations to be applied in planning the harnesses for ERTS include:

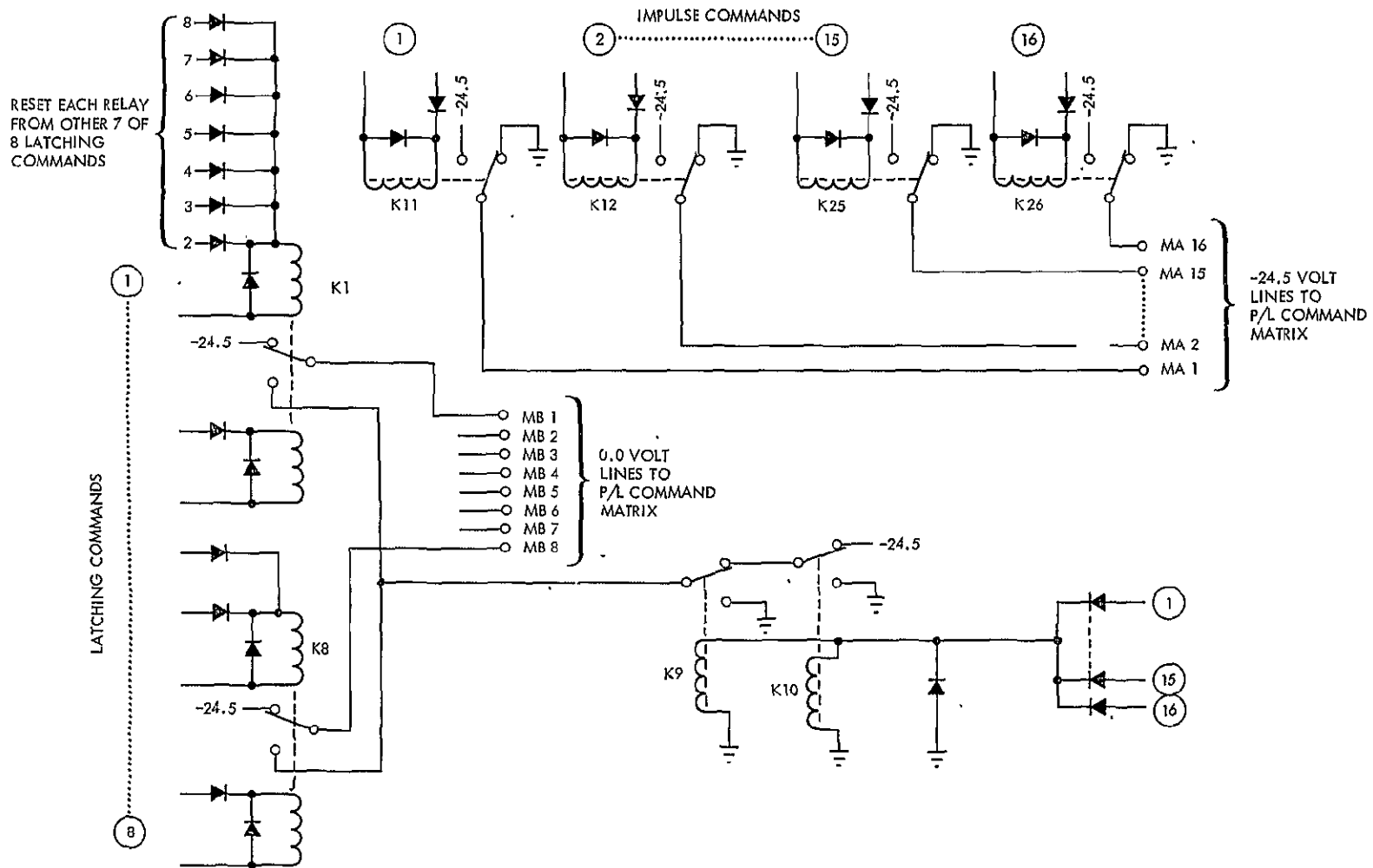


Figure 12-6
Z AXIS COMMAND MATRIX

- Cabling will be assigned according to five signal classifications: power lines, command lines, digital data lines, analog signal lines, and RF signal lines. The separation distance between classes will be at least 1 inch.
- Harnesses will be held in position close to the spacecraft structure.
- Wires between units will follow the most direct route.
- Twisted pair wiring will be used for all balanced or quasi-balanced circuits.
- All digital circuits and high impedance circuits will be shielded.
- All RF circuits will be coaxial cable.
- Shield continuity will be maintained over the entire length of a shield.
- Unshielded segments of shielded wires will be as short as possible.
- Shield terminations will be directly to the spacecraft structure or via the connector hardware. In no case will shields be connected to a common wire which is grounded at some remote point.
- In general, all shields will be grounded at each connector through which its circuit passes.

ERTS will be able to make use of the wrap-up designed, developed, and flown on all of the OGO's. Since the dual section wrap-up on OGO provides an excessive number of conductors for ERTS, the wrap-up assembly can be reduced to a single section and fewer conductors per cable element.

ERTS requirements are for 28 connections between the (+X) solar array and main body and 29 connections between the (-X) solar array and main body. A single section wrap-up assembly with eight wire elements, composed of three elements of 15 hook-up conductors each (total of 45 hook-up conductors) and five elements of 10 shielded conductors each (total of 50 shielded conductors) will provide a total of 95 conductors. Adequate wires are thus provided for parallel lines in the 12 high current circuits of the 45; 22 AWG hook-up conductors are reserved for this

purpose. The shielded conductors provide a high percentage of redundancy for the 33 signal and telemetry lines.

The single section wrap-up will mount in the (-X) position (see Volume 3, Section 2). The array harnesses will pass through the drive shaft entry holes on the (-X) side only, but branch in a "Y" joint to both (+X) and (-X) paddles.

The area originally occupied (in OGO 6) by the (+X) wrap-up will be vacant, and the entry holes in the drive shaft for the (+X) array harnesses eliminated. The shaft design is thus strengthened and simplified compared to OGO 6.

The wrap-up section for ERTS will have the following characteristics:

Weight	~2.7 lb
Torque	~30 in. lb at 60°F
Size	~5.25 in. diameter
Life expectancy	>50,000 cycles

Since the design is a scaled-down version of the OGO 6 design, which was qualified on that program, no additional qualification testing is required.

12.5 ELECTROMAGNETIC INTERFERENCE

The electrical and electromechanical equipment proposed for ERTS have been studied to search for possible RF interference. In particular the new ERTS equipment and the payload equipment, including the video tape recorders, multispectral scanner, and return beam vidicon, were reviewed to determine potential problems in mutual compatibility.

12.5.1 Multispectral Scanner

It is likely that some special electromagnetic compatibility considerations may be required to insure compatibility of the MSS on the spacecraft. In general, photo-sensing devices usually have nonlinear characteristics which means that modulated RF signals can be detected by the sensor in the form of interference.

Special high frequency shielding and possibly wave guide below cut-off apertures may be needed to prevent interference by the spacecraft 20-watt S-band transmitter. The 20-watt systems for ERTS will use special filters at the output of the TWT amplifiers to limit unwanted harmonic signals above S-band. High level RF fields usually cause compatibility problems with the input electronics of the sensors; therefore, a large amount of shielding may be required on the sensitive circuits of the MSS. It is recommended that shields associated with the MSS be circumferentially terminated. Conductive epoxy is a desirable circumferential shield termination method for signals above 10 MHz. From an electromagnetic compatibility standpoint it is desirable to locate the MSS detector systems as far as possible from the high-power high-frequency spacecraft transmissions systems. Also, it is recommended that special RF susceptibility tests be performed on the MSS detectors to insure they are not susceptible to RF modulated signals.

Another potential electromagnetic compatibility problem area with the MSS is in the drive mechanism for the scan mirror. The proposed scan system appears to require large current pulses to drive the mirror at a 15-Hz rate. The large current pulse could cause magnetic field coupling to sensitive circuits. These scan mirror circuits should be analyzed to determine if special shielding and filtering will be required to prevent electromagnetic compatibility problems. The low level output signals of the MSS will probably require shielding to prevent pick-up from spacecraft signals.

12.5.2 Return Beam Vidicon

Past experience with TV systems for space applications (such as Surveyor) indicates that the vidicon circuits are sensitive to magnetic fields. For this reason, special care should be exercised in the design of spacecraft cables carrying large currents in the vicinity of the RBV. Magnetic fields near the vidicon could distort picture information.

High-impedance vidicon circuits are also susceptible to high frequency fields such as those from spacecraft transmission systems, resulting not only from the high impedance circuits but from nonlinearities in the electronics of the vidicon.

The typical problem produced by RF susceptibility is a herringbone effect on the reproduced picture. For this reason, a special electromagnetic compatibility test should be performed on the RBV system to insure that it is not susceptible to modulate RF signals. The test signals should be at least 6 db above the spacecraft transmission signal levels. Modulation of RF signals will probably produce worst-case effects. If interferences are produced by high-frequency, high-power sources, it is recommended that a special waveguide below cut-off aperture be considered for the vidicon and its associated output amplifier.

12.5.3 RF System

The compatibility of the new S-band systems will be provided in the electromagnetic compatibility control for the ERTS program. The goals are to limit the signals produced by the RF system to desired signals only, by limiting the transmitter outputs and providing adequate shielding on subassemblies of the RF system and limiting bandwidths of signals used within the RF system. Filters at the wideband transmitter output are described in Section 6, Volume 3.

13. THERMAL

Flying OGO for an ERTS mission alters the basic thermal control concept. Thermal louvers, when on OGO, are never exposed to the sun, but they see it periodically on ERTS. Two spacecraft orientations have been seriously considered for ERTS use, one with the array axis perpendicular to the orbit plane and one with the axis in it (see Figure 13-1).

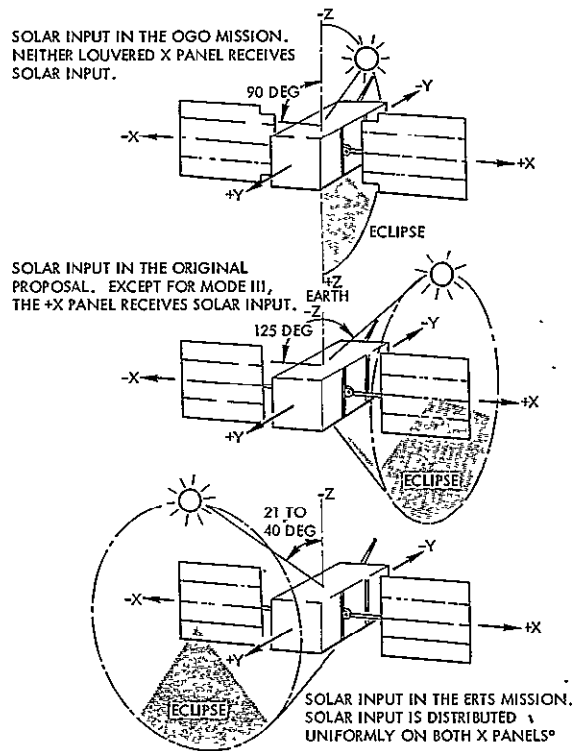


Figure 13-1

IMPACT OF ORIENTATION CHOICE. Selected orientation is thermally the best for the ERTS mission because external heat input is distributed uniformly on the observatory.

The latter has been selected as our baseline approach (see Section 1); however, documenting the analysis of each is appropriate here.

The principal difference between the orientation rejected and that adopted is that in the former only one set of thermal louvers continually sees the sun (except for eclipses); and in the latter both louvers see the sun inter-

mittantly in each orbit. Solar input to the panels containing louvers is shown below for OGO and for the two ERTS configurations considered. The fixtures include the earth's albedo and energy reflected from the solar arrays.

Solar Flux to the X Panels
(Btu/hr/ft²)

	-X Panel		+X Panel	
	Aft	Forward	Aft	Forward
OGO	0 to 13	0 to 13	0 to 13	0 to 13
Original ERTS	13	13	245	245
Final ERTS	116	30 to 72	116	30 to 72

Lower solar input to the X panels in the final ERTS configuration permits a change from the second surface mirrors required for the original configuration to aluminized teflon without affecting thermal control of the observatory even when the solar absorptance is fully degraded after a three-year exposure to the sun. The cost is reduced from approximately \$10,000 to \$100 by changing second surface mirrors to the aluminized teflon (see Table 13-1). The resulting thermal control subsystem keeps all ERTS equipment and the payload within the required temperature of $20 \pm 10^{\circ}\text{C}$.

Table 13-1. Second Surface Mirrors vs Aluminized Teflon. The cost is reduced by selecting aluminized teflon without affecting thermal control of the observatory.

	June 1969 Configuration Second Surface Mirrors	Present Configuration Aluminized Teflon
Solar absorptance*	0.10	0.25
Surface emittance	0.80	0.80
Absorbed solar input by the +X panel** (Btu/hr ft ²)		
Forward	24.5	18.0
Aft	24.5	29.0
Approximate cost per observatory	\$10,000	\$100

* Degraded after three years

** Maximum solar input multiplied by solar absorptance in the respective configurations.

Data is presented in Section 9 of Volume 3 which shows the mounting surface temperatures of all components to be within specified limits when in Mode 4. In addition, the thermal analysis computer program was run for the abnormal condition: all sensors turned off, spacecraft tracking sun in Mode 2. The Mode 2 condition is encountered only

during initial acquisition and any (unlikely) sun reacquisition sequences. The sun is normal to the spacecraft +Y panel under which are located the wideband tape recorders in this condition. Figure 13-2 shows the resultant steady-state temperatures.

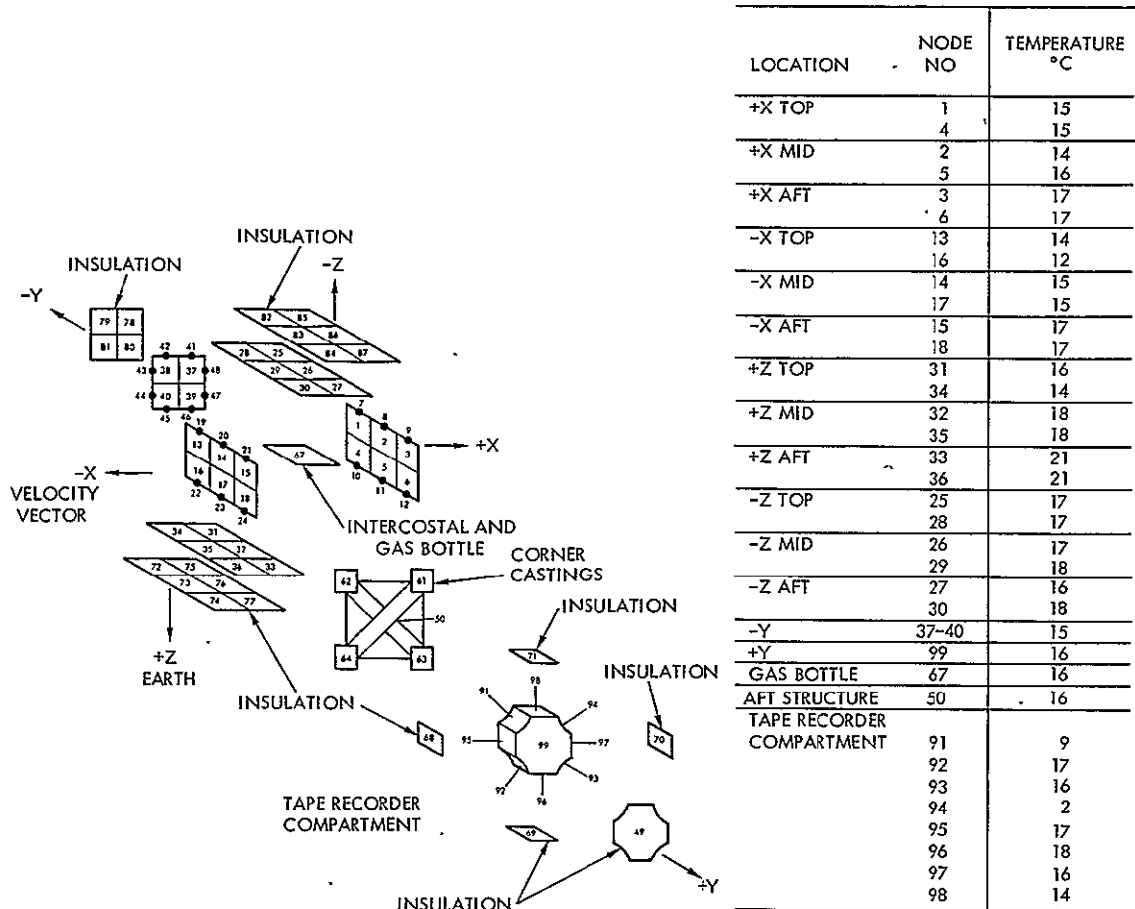


Figure 13-2
TEMPERATURE DISTRIBUTION IN ERTS during Mode 2 sun tracking with all sensors off.

14. SPACECRAFT HARDWARE

As required by Section 7.10 of the study specification, the list of assemblies has been continuously updated throughout the study, and the current list as of 15 January 1970 is given in Table 14-1. The extent of new design is described by subsystem in Volume 3. The concept changes which have resulted in changes to the equipment list are largely those of the revised study specification

- Downlink narrowband telemetry is placed in a new 137-MHz transmitter.
- A new unified S-band system for data, command, and tracking has been added.
- Wideband data switching has been made part of spacecraft design.
- A -24 volt battery is added to supply high current RBV shutter load.

In addition, and as a convenience, the clock has been packaged with the stored command programmer.

Table 14-1. Equipment List

Major Spacecraft Assembly Nomenclature	Anticipated Source	Use Existing Design with		Quantity for ERTS-A, -B and Spares			Units Available for ERTS			Flight History Program
		No Change	Minor Change	Required	Available	To Be Fabricated	Part Number	Serial Numbers	Program Accountability	
<u>Attitude Control</u>										
A-1 yaw gyro assembly *	TRW	x		3F	1F	2	201371-1	8	OGO 3900	OGO 1-6
A-2 gyro electronic assembly	TRW	x		3F	1F	2	202163-1	8	OGO 3900	OGO 1-6
A-3 horizon scanner electronic	TRW		New	3F, 1Q	0	4	-	-	At GSFC	
A-4 horizon scanner head A-C	TRW		New	3F, 1Q	2F ^x , 1Q ^x	4	-	-	At GSFC	
A-5 horizon scanner head B-D	TRW		New	3F, 1Q	2F ^x , 1Q ^x	4	-	-	At GSFC	
A-6 sun sensor (+X)	TRW		x	3F	1F	2	202384-1	3	OGO 3900	OGO 1-6
A-7 sun sensor (-X)	TRW		x	3F	1F	2	202744-1	3	OGO 3900	OGO 1-6
A-8 sensor electronic and logic assembly	TRW	x ^{xxx}		3F	1F	2	200932-2	4,2-1	OGO 3900	OGO 1-6
A-9 attitude control assembly	TRW		x	3F, 1Q	1F, 1P	2	200833-1	7,2-2	OGO 3900	OGO 1-6
A-10 drive electronics assembly	TRW	x ^{xxx}		3F	1F	2	200934-1	8,2-2	OGO 3900	OGO 1-6
A-11 rate gyro assembly	TRW	x		3F	1F	2	200935-1	4	OGO 3900	OGO 1-6
A-12 inverter assembly	Kinetics	x		3F	1F	2	C207540-2	8	OGO 3900	OGO 4-6
A-13 control switch assembly	TRW	x		3F	1F	2	228576-3	7	OGO 3900	OGO 3-6
A-14 orbital switch assembly	TRW		New	3F, 1Q	0	4	-	-	OGO 3900	
A-15 array drive mechanism	TRW	x		3F	2F	1	202540-2	4,11	OGO 3900	OGO 1-6
A-16 Z reaction wheel	Bendix		x	3F	2F	1	C218461-1	5,10	OGO 3900	OGO 1-6
A-17 Y reaction wheel	Bendix		x	3F, 1Q	0	4	-	-	-	Nimbus
A-18 X reaction wheel	Bendix		x	3F	0	3	-	-	-	Nimbus
A-19 array position transducer	Kearfott	x		3F	2F	1	-	-	OGO 3900	OGO 1-6
A-20 pneumatics tubing (set)	TRW		x	3F	0	3	-	-	OGO 3900	OGO 1-6
A-21 pneumatic tank	Airtec	x		3F, 1Q	1F	3	C111928-1	19	OGO 3900	OGO 1-6
A-22 nozzle booms	TRW		x	5F	0	5	-	-	OGO 3900	OGO 1-6
A-23 valves	Sterer	x		27F	6F	21	PT2-3002 243553-1	67,68 77,83 86,87	-	OGO 1-6
A-24 pressure switch	Hydra-Electric	x		27F	6F	21	PT2-3003	67,68 69,70 71,72	-	OGO 1-6
A-25 regulator	Sterer	x		3F	2F	1	PT2-3004	3,9	OGO 3900	OGO 1-6
A-26 high pressure transducer	Servonics	x		3F	1F	2	PT2-3000	-	OGO 3900	OGO 1-6
A-27 low pressure transducer	Servonics	x		3F	1F	2	PT2-3001	-	OGO 3900	OGO 1-6

Notes: F = Flight, Q = Qualification, T = Test, P = Prototype, S = Structural model

^x Mechanical and optical parts available from GFP A060

^{xxx} No change to existing units, detection of unnecessary function in new build
(i.e., OPEP control channel)

Table 14-1. Equipment List (Continued)

Major Spacecraft Assembly Nomenclature	Anticipated Source	Use Existing Design with		Quantity for ERTS-A, -B and Spares			Units Available for ERTS			Flight History Program
		No Change	Minor Change	Required	Available	To Be Fabricated	Part Number	Serial Numbers	Program Accountability	
<u>Power Supply</u>										
P-1 solar paddle (+X)	TRW		X	2F	0	2	100010-11	-	OGO 3900	OGO 1-6
P-2 solar paddle (-X)	TRW		X	2F	0	2	100010-12	-	OGO 3900	OGO 1-6
P-3 battery pack (No. 1 and 2)	TRW	X		6F, 4T	4T	6	232820-2	19, 20 25, 26	OGO 3900	OGO 1, 3-6
P-4 power control unit	TRW		X	3F	1F	2	232245-2	3	OGO 3900	OGO 4, 5, 6
P-5 charge control assembly	TRW	X		5F	2F	3	204553-1	6, 17	OGO 3900	OGO 1-6
P-6 charge control assembly	TRW	X		5F	2F	3	204553-2	5, 24	OGO 3900	OGO 1-6
P-7 converter No. 2	IT and T	X		6F	1F	5	C206566-1	7	OGO 3900	OGO 1-6
P-8 converter No. 5 (or 6)	IT and T	X		6F	2F	4	C206569-1	3 5	OGO 3900	OGO 1-6
P-9 converter No. 7 (or 8)	IT and T	X		6F	2F	4	C206805-1	4 4	OGO 3900	OGO 1-6
P-10 converter No. 9	IT and T	X		3F	1F	2	C206570-1	6	OGO 3900	OGO 1-6
P-11 payload bus converter	TRW		New	3F, 1Q	0	4	-	-	-	-
P-12 -24 volt battery	TRW		New	3F, 1Q	0	4	-	-	-	-
<u>Command and Data Handling</u>										
C-1 VHF receiver	TRW		X	6F	2F, 1P	4	217907-1	3, 14	OGO 3900	OGO 1-6
C-2 VHF dual duplexer assembly	Rantech		X	3F,	1F	2	218264-2	6	OGO 3900	OGO 3-6
C-3 VHF command decoder	TRW		X	6F,	2F	4	218303-1	9, 10	OGO 3900	OGO 1-6
C-4 VHF antenna	TRW		X	3F	2F	1	217530-1	9, 10	OGO 3900	OGO 3-6
C-5 special purpose telemetry unit	TRW		X	3F, 1Q,	1F, 1P	2	202650-2	6, 2-2	OGO 3900	OGO 1-6
C-6 VHF power monitor	Sanders		X	6F	1F	5	214252-2	4	OGO 3900	OGO 1, 3, 5
C-7 analog data handling assembly ADHA	TRW		X	6F	2F	4	201140-1	16, 18	OGO 3900	OGO 1-6
C-8 digital data handling assembly DDHA	TRW	X		6F	3F	3	218486-1	3, 7, 8	OGO 3900	OGO 1-6
C-9 low frequency tuning assembly, AFTA	TRW		X	6F	2F	4	218487-1	5, 6	OGO 3900	OGO 1-6
C-10 signal conditioner	TRW		X	3F	1F	2	201738-1	8	OGO 3900	OGO 1-6
C-11 tape recorder electronics	RCA		X	6F, 1Q	1P	6	207463-2	2-2	OGO 3900	OGO 1-6
C-12 tape recorder transport	RCA		X	6F, 1Q	1P	6	207464-5	2-2	OGO 3900	OGO 1-6
C-13 stored command programmer	TRW		New	6F, 1Q	0	7	-	-	-	-
C-14 wideband TLM transmitter driver	Frequency electronics		New	10F, 1Q	0	11	-	-	-	SGLS
C-15 video channel switching assembly	TRW		New	3F, 1Q	0	4	-	-	-	-

Table 14-1. Equipment List (Continued)

Major Spacecraft Assembly Nomenclature	Anticipated Source	Use Existing Design with		Quantity for ERTS-A, -B and Spares			Units Available for ERTS			Flight History Program
		No Change	Minor Change	Required	Available	To Be Fabricated	Part Number	Serial Numbers	Program Accountability	
C-16 TWTA	Watkins-Johnson		New	3F, 1Q	0	4	-	-	-	Mariner '69
C-17 USB and WBTLM shaped beam antenna	TRW		X	8F, 1Q	0	9	-	-	-	-
C-18 USB transponder	TRW		X	6F	0	7	-	-	-	TETR
C-19 dual baseband assembly	Dynatronic		X	3F, 1Q	0	4	-	-	-	Model 35
C-20 USB diplexer	SW		New	3F, 1Q	0	4	-	-	-	TETR
C-21 USB omni-antenna	TRW		New	6F	0	6	-	-	-	Model 35
C-22 VHF transmitter	TRW		New	6F, 1Q	0	7	-	-	-	-
C-23 wideband reject filter			New	6F, 1Q	0	7	-	-	-	-
<u>Electrical Integration</u>										
E-1 command distribution unit (3A2)	TRW		X	2F and spare modules	1F and spare modules	1 plus module	201529-3	8	OGO 3900	OGO 1-6
E-2 J box 3A5 (central)	TRW	X*		2F	0	2	222518-1		-	OGO 1-6
E-3 J box 3A7 (power distribution)	TRW		X	2F, 1Q	0	3			-	OGO 1-6
E-4 box 3A13 (ordnance)	TRW	X*		2F	0	2	214055-1		-	OGO 1-6
E-5 momentum control assembly	TRW	X		3F	0	3	247072-1		-	OGO 5,6
E-6 payload integration assembly	TRW		X	2F, 1Q	0	3	-		-	-
E-7 solar array wrap-up	TRW	X*		3F	0	3	232443		-	OGO 1-6
E-8 digital integration unit (4A46)	TRW	X		2F	0	2	231394-1		-	OGO 1-6
E-9 harnesses (set) subsystem	TRW		X	2F	0	2	List		-	OGO 1-6
E-10 harnesses payload	TRW		X	2F	0	2	List		-	-
<u>Structure /Thermal</u>										
S-1 spacecraft structure	TRW		X	2F, 1S	Piece-parts	3	107997-5		OGO 3900	OGO 1-6
S-2 solar array drive shaft	TRW	X		3F	1F	2	100669-2	Kit	OGO 3900	OGO 1-6
S-3 louver banks (+X, -X)	TRW		X	5F	1F	4	104017-10	Kit	OGO 3900	OGO 1-6
S-4 insulation (set)	TRW		X	3F	0	3	List		OGO 3900	OGO 1-6
S-5 horizon scanner bracket	TRW		X	2F	0	2	108393-50		OGO 3900	OGO 1-6
S-6 VHF antenna support	TRW		X	2F	0	2	-		OGO 3900	OGO 1-6
S-7 release system (set)	Hollex	X*		3F	1F	2	-	Kit	OGO 3900	OGO 1-6
S-8 interstage and separation	TRW		X	3F, 1S	Piece-parts	4	103990-2		OGO 3900	OGO 1-6
S-9 integration hardware (set)	TRW		X	3F	Piece-parts	3	-		OGO 3900	OGO 1-6
<u>Orbit Adjust System</u>										
V-1 thrusters No 1, 2, and 3	Spectromat		New	12F, 1Q	0	13	-	-	-	-

14-4

* Deletions only

CONTENTS

	Page
15 PERFORMANCE ASSURANCE	15-1
15.1 The Spacecraft Reliability Model	15-2
15.2 Review of Existing Assemblies, Extent of Compliance with ERTS Requirements	15-16
15.3 Configuration Management	15-16
15.4 Consolidated Parts, Materials, and Process List	15-20
15.5 Reliability Program Plan	15-20
15.6 Quality Program Plan	15-20
15.7 Test Monitoring and Control Plan	15-21
15.8 Program Plan for Soldered Electrical Connections	15-22
15.9 Review of TRW Failure Reporting Procedures	15-22

15. PERFORMANCE ASSURANCE

In accordance with Section 7.11 of the study specification the following tasks were completed.

- A system design specification for the ERTS observatory was prepared
- The ERTS reliability model was modified to reflect new equipment and more recent data
- A consolidated list of parts and materials was prepared
- A review of existing assemblies was conducted to determine extent of compliance with ERTS requirements
- A comparative review of TRW and NASA/GSFC failure reporting systems was made
- A comparative review was made of the TRW configurations management system with NASA/GSFC requirements

Documents were prepared and published governing TRW ERTS program plans for

- Configuration management
- Reliability
- Maintainability
- Quality
- Test monitoring and control
- Soldering
- Failure reporting
- Safety

The purpose of this activity was to assure a high and uniform standard of quality in the delivered spacecraft and associated equipment. This has been achieved as is evident in the documents presented as Volumes 6 through 12 separately bound to facilitate review.

The purpose of the system specification is to define at the interface to payload, booster and ground station user the minimum performance

guaranteed by the spacecraft contractor. This specification is submitted separately.

15.1 THE SPACECRAFT RELIABILITY MODEL

The purpose of developing a reliability model is to assure by a logical process that a high reliability will be achieved and to highlight weak links in the chain for further study. In the case of ERTS it was possible to build on the existing OGO reliability model by adding new in-line systems. Much of the design of the flight-proven OGO spacecraft has been incorporated into the ERTS design. For that equipment with demonstrated orbital reliability (MTBF) the demonstrated reliability was used as the building block to develop the ERTS reliability model. Using this technique the demonstrated reliability of six orbiting spacecraft forms the basic ERTS model with new and redesigned equipment added and OGO equipment not required for ERTS deleted.

Table 15-1 lists the OGO equipment to be used on ERTS that has minor changes to be incorporated and has demonstrated orbital experience. Table 15-2 lists the OGO equipment to be used on ERTS that is changed sufficiently to require reliability evaluation but which has demonstrated orbital experience. Table 15-3 lists the equipment which is of new design to ERTS or has not demonstrated orbital experience.

The reliability functional diagram for the ERTS spacecraft shown in Figure 15-1 describes the redundancy features of the design. Those items of design new to ERTS are shown with cross-hatching. This figure illustrates that the ERTS spacecraft is comprised mainly of equipment with demonstrated OGO orbital experience. Figures 15-2 and 15-3 illustrate the units with minor modifications, redundant OGO units and new units added and units deleted from the OGO design. Figures 15-4 through 15-8 show the individual subsystem reliability math models with new and modified units identified.

From September 5, 1964 to December 31, 1969 over 124,000 hours of successful operation have been logged on six OGO spacecraft. At 60 percent confidence, the probability of success for one year is at least 0.938 as shown in Figure 15-9. This is based on:

- 4-1/4 years of experience with OGO 1
- 3 years of experience with OGO 2
- 2-1/2 years of experience with OGO 3
- 1-1/2 years of experience with OGO 4
- 1-3/4 years of experience with OGO 5
- 1/2 year of experience with OGO 6

Table 15-1. OGO Units with No Change or Minor Change

Yaw gyro assembly	Battery pack
Gyro electronic assembly	Power control unit
Sun sensor (+X)	Charge control assembly
Sun sensor (-X)	Converter 2, 5, 7, and 9
Sensor electronic and logic assembly	VHF command receiver
Attitude control assembly	VHF diplexer
Drive electronics assembly	VHF antenna
Rate gyro assembly	VHF power monitor
Inverter assembly	Analog data handling assembly
Control switching assembly	Digital data handling assembly
Array drive mechanism	Low frequency timing assembly
Z reaction wheel	Signal conditioner
Y reaction wheel	Tape recorder
X reaction wheel	Command distribution unit
Array position transducer	Momentum control assembly
Pneumatics	Payload integration assembly
Solar paddle (+X)	Solar array wrap-up
Solar paddle (-X)	Digital integration unit

Reliability predictions for each equipment new to ERTS/OGO or modified from OGO equipment are presented in Table 15-4. The failure rates used are presented in Table 15-5.

The resulting ERTS observatory reliability prediction (excluding GFE) can be summarized as:

$$\begin{aligned}
 R_{\text{ERTS}} &= R_{\text{OGO orbital}} \times R_{\text{new boxes}} \times R_{\text{boxes modified}} \\
 &= 0.9375 \times 0.9097 \\
 &= 0.8525 \text{ for one year in orbit}
 \end{aligned}$$

Table 15-2. OGO Units with Modification Requiring Additional Reliability Analysis

Horizon scanner	Special purpose telemetry
VHF command decoders	Signal conditioner

Table 15-3. Units New to ERTS that Require Reliability Analysis

Orbital switching assembly	Dual baseband assembly
Payload bus converter	Unified S-band diplexer
-24 volt battery	Unified S-band omni antenna
Stored command programmer	VHF transmitter
Wideband telemetry transmitter driver	Wideband reject filter
Video channel switching assembly	Unified S-band and wideband telemetry shaped-beam antenna
Travelling wave tube assembly	Orbit adjust thruster
Unified S-band transponder	

Table 15-4. Reliability Predictions of New or Modified ERTS Equipment

	Part Count	Part Failure Rate (bits) [*]	Total Failure Rate (bits) [*]
<u>Horizon Scanner Electronics</u>			
Resistor, metal film	415	1.0	415.0
Resistor, wirewound	68	10.0	680.0
Capacitor, ceramic	60	4.0	240.0
Capacitor, solid tantalum	115	9.0	1035.0
Capacitor, mylar	5	20.0	100.0
Diode, general purpose (SI)	36	3.0	108.0
Diode, zener	74	37.0	2738.0
Transistor, low power (SI)	64	10.0	640.0
Transistor, high power (SI)	2	40.0	80.0
Transistor, field effect	4	60.0	240.0
Integrated circuit, analog amplifier	53	100.0	5300.0
Integrated circuit, MOS	3	100.0	300.0
Integrated circuit, TTL	5	25.0	125.0
Thermistor	8	35.0	280.0
50-pin connector	6	30.0	180.0
Connector pin	150	0.6	90.0
	918		12551.0
<u>Orbital Switching Assembly (Total Parts)</u>			
Resistor, carbon composition	77	2.0	154.0
Resistor, metal film	30	1.0	80.0
Capacitor, ceramic	30	4.0	120.0
Capacitor, solid tantalum	10	9.0	90.0
Diode, general purpose (SI)	35	3.0	105.0
Diode, zener	10	37.0	370.0
Diode, power rectifier (SI)	4	44.0	176.0
Transistor, low power (SI)	15	10.0	150.0
Integrated circuit, DTL	71	25.0	1775.0
Integrated circuit, analog amplifier	24	100.0	2400.0
Relay, latching	2	64.0	128.0
Integrated circuit, dual flip-flop	15	150.0	2250.0
	373		7798.0
<u>Orbital Switching Assembly (Critical Parts)</u>			
Resistor, carbon composition	20	2.0	40.0
Resistor, metal film	22	1.0	22.0
Capacitor, ceramic	5	4.0	20.0
Capacitor, solid tantalum	4	9.0	36.0
Diode, general purpose (SI)	12	3.0	36.0
Diode, zener	2	37.0	74.0
Diode, power rectifier (SI)	4	44.0	176.0
Transistor, low power (SI)	2	10.0	20.0
Integrated circuit, DTL	6	25.0	150.0
Integrated circuit, analog amplifier	4	100.0	400.0
Relay, latching	2	64.0	128.0
	83		1102.0
<u>Payload Bus Converter</u>			
Resistor, carbon composition	50	2.0	100.0
Capacitor, solid tantalum	3	9.0	27.0
Diode, general purpose (SI)	5	3.0	15.0
Transistor, low power (SI)	5	10.0	50.0
Transistor, high power (SI)	1	40.0	40.0
Transformer	4	14.0	56.0
Inductor	3	10.0	30.0
	71		318.0
$R_{\text{single payload bus converter}} = 0.9972$ $R_{\text{redundant (2 out of 3) payload bus converter}} = 0.9998$			

Notes

- 190 electronic parts are used in each of the four tracking channels
- 158 electronic parts are used in the electronics common to the four tracking channels.

$$R_{\text{common electronics}} = RCE = 0.9812$$

$$R_{\text{tracking channel including head}} = RTC = 0.9715$$

$$R_{\text{three out of four tracking heads}} = RT = 0.9954$$

$$R_{\text{horizon scanner}} = RCE \times RT = 0.9767$$

- The ERTS horizon scanner design is based on the existing advanced OGO unit. No flight experience is available on this unit.

*One bit = one failure per billion hours

Table 15-4. Reliability Predictions of New or Modified ERTS Equipment (Continued)

	Part Count	Part Failure Rate (bits) ^a	Total Failure Rate (bits) ^a
<u>Unified S-Band Baseband Assembly</u>			
Resistor, metal film	13	1.0	13.0
Capacitor, ceramic	6	4.0	24.0
Capacitor, glass	3	3.0	9.0
Capacitor, solid tantalum	6	9.0	54.0
Transistor, low power (SI)	4	10.0	40.0
Relay, latching	2	64.0	128.0
Connector, coaxial	8	10.0	80.0
Feedthrough filter	1	10.0	10.0
50-pin connector	1	30.0	30.0
	44		388.0
R _{base band} = 0.9966			
<u>Signal Conditioner Plus Signal Conditioner Auxiliary</u>			
Resistor, metal film	476	1.0	476.0
Capacitor, solid tantalum	32	9.0	288.0
Diode, general purpose (SI)	2	3.0	6.0
Transistor, low power (SI)	75	10.0	750.0
Connector pin	258	0.6	154.8
	585		1674.8
R _{signal conditioner} = 0.9854			
<u>Special Purpose Telemetry</u>			
Resistor, carbon composition	3	2.0	6.0
Resistor, metal film	18	1.0	18.0
Capacitor, solid tantalum	7	9.0	63.0
Diode, general purpose (SI)	17	3.0	51.0
Diode, zener	2	37.0	74.0
Transistor, low power (SI)	5	10.0	50.0
Integrated circuit, TTL	12	25.0	300.0
Relay, nonlatching	2	106.0	212.0
Sensor	1	3.0	3.0
	67		777.0
R _{special purpose telemetry} = 0.9932			
The special purpose telemetry design is modified from OGO.			
<u>Stored Command Programmer</u>			
• SCP/clock (command stored address determination, prior logic)			
Resistor, carbon composition	136	2.0	272.0
Capacitor, ceramic	45	4.0	180.0
Diode, zener	3	37.0	111.0
Transistor, low power (SI)	50	10.0	500.0
Integrated circuit, TTL	161	25.0	4025.0
MOS shift register	32	100.0	3200.0
	427		8288.0
• Discriminator/bit synchronizer			
Resistor, carbon composition	65	2.0	130.0
Capacitor, ceramic	22	4.0	88.0
Capacitor, glass	2	3.0	6.0
Capacitor, filter feedthrough	2	10.0	20.0
Capacitor, solid tantalum	21	9.0	189.0
Diode, general purpose (SI)	4	3.0	12.0
Transistor, low power (SI)	13	10.0	130.0
Integrated circuit, DTL	2	25.0	50.0
Inductor	6	10.0	60.0
50-pin connector	3	30.0	90.0
Filter, bandpass	2	40.0	80.0
Filter, band reject	1	40.0	40.0
	143		895.0
• Clock			
Resistor, carbon composition	12	2.0	24.0
Resistor, metal film	2	1.0	2.0
Capacitor, ceramic	7	4.0	28.0
Capacitor, mica	2	4.0	8.0
Diode, general purpose (SI)	1	3.0	3.0
Transistor, low power (SI)	3	10.0	30.0
Integrated circuit, DTL	7	25.0	175.0
Oscillator	1	150.0	150.0
Counter (MSI)	10	75.0	750.0
Time Delay	1	20.0	20.0
	46		1190.0

Table 15-4. Reliability Predictions of New or Modified ERTS Equipment (Continued)

	Part Count	Part Failure Rate (bits)	Total Failure Rate (bits)
• Stored Command Converter			
Resistor, carbon composition	139	2.0	278.0
Capacitor, ceramic	41	4.0	164.0
Diode, general purpose (SI)	47	3.0	141.0
Diode, zener	3	37.0	111.0
Transistor, high power (SI)	52	40.0	2080.0
Transformer	2	14.0	28.0
Fuse	2	100.0	200.0
RF choke	10	10.0	100.0
	296		3102.0
$R_{\text{single stored command programmer}} = R_A \times R_B \times R_C \times R_D$			
$= 0.8887$			
$R_{\text{redundant stored command programmer}} = 0.9876$			
Digital Command Decoder			
Resistor, carbon composition	12	2.0	24.0
Resistor, metal film	715	1.0	715.0
Capacitor, ceramic	305	4.0	1220.0
Capacitor, solid tantalum	14	9.0	126.0
Capacitor, mica	5	4.0	20.0
Capacitor, mylar	1	20.0	20.0
Diode, general purpose (SI)	696	3.0	2088.0
Diode, zener	4	37.0	148.0
Transistor, low power (SI)	175	10.0	1750.0
Transistor, high power (SI)	1	40.0	40.0
Transformer	50	14.0	700.0
Inductor	4	10.0	40.0
RF choke	1	10.0	10.0
50-pin connector	3	30.0	90.0
Sensor	1	3.0	3.0
	1987		6994.0
$R_{\text{single digital command decoder}} = 0.9412$			
$R_{\text{redundant digital command decoder}} = 0.9965$			
The digital command decoder is modified slightly from OGO			
VHF Transmitter			
Resistor, carbon composition	36	2.0	72.0
Capacitor, ceramic	20	4.0	80.0
Capacitor, glass	5	3.0	15.0
Capacitor, filter feedthrough	3	10.0	30.0
Capacitor, solid tantalum	1	9.0	9.0
Capacitor, variable	5	40.0	200.0
Diode, general purpose (SI)	3	3.0	9.0
Diode, zener	2	37.0	74.0
Transistor, low power (SI)	8	10.0	80.0
Transistor, high power (SI)	2	40.0	80.0
Transformer	5	14.0	70.0
Thermistor	1	35.0	35.0
Crystal, quartz	1	20.0	20.0
RF choke	7	10.0	70.0
50-pin connector	3	30.0	90.0
	103		937.0
$R_{\text{single VHF transmitter}} = 0.9918$			
$R_{\text{redundant VHF transmitter}} = 0.9994$			
VHF Receiver			
Resistor, carbon composition	460	2.0	920.0
Resistor, metal film	8	1.0	8.0
Resistor, wirewound	4	10.0	40.0
Capacitor, ceramic	32	4.0	128.0
Capacitor, glass	92	3.0	276.0
Capacitor, solid tantalum	44	9.0	396.0
Capacitor, variable	4	40.0	160.0
Diode, general purpose (SI)	32	3.0	96.0
Diode, zener	20	37.0	740.0
Transistor, low power (SI)	116	10.0	1160.0
Transistor, high power (SI)	4	40.0	160.0
Inductor	12	10.0	120.0
Thermistor	16	35.0	560.0
Crystal, quartz	8	20.0	160.0

	Part Count	Part Failure Rate (bits) ²	Total Failure Rate (bits) ²
Crystal filter	4	20.0	80.0
RF choke	4	10.0	40.0
50-pin connector	12	30.0	360.0
Filter, RFI	4	10.0	40.0
Connector pin	100	0.6	60.0
	876		5504.0

$$R_{\text{single VHF receiver}} = 0.9529$$

$$R_{\text{redundant VHF receiver}} = 0.9978$$

The VHF receiver is modified slightly from OGO.

Unified S-Band Transponder Receiver

Resistor, carbon composition	226	2.0	452.0
Resistor, metal film	174	1.0	174.0
Capacitor, ceramic	154	4.0	616.0
Capacitor, glass	105	3.0	315.0
Capacitor, solid tantalum	15	9.0	135.0
Capacitor, variable	14	40.0	560.0
Diode, general purpose (SI)	18	3.0	54.0
Diode, zener	8	37.0	296.0
Diode, varactor	4	40.0	160.0
Transistor, low power (SI)	44	10.0	440.0
Transistor, field effect	2	60.0	120.0
Inductor	33	10.0	330.0
Crystal, quartz	2	20.0	40.0
50-pin connector	32	30.0	960.0
DC amplifier (IC)	1	100.0	100.0
Filter, RFI	15	10.0	150.0
Sensistor	1	3.0	3.0
Filter, bandpass	1	40.0	40.0
Toroid	17	10.0	170.0
Diode, step recovery	1	100.0	100.0
Connector pin	114	0.6	68.4
	867		5283.4

$$R_{\text{single unified S-band receiver}} = 0.9548$$

$$R_{\text{redundant unified S-band receiver}} = 0.998$$

Unified S-band Transponder Transmitter

Resistor, carbon composition	68	2.0	136.0
Resistor, metal film	14	1.0	14.0
Resistor, wirewound	9	10.0	90.0
Capacitor, ceramic	36	4.0	144.0
Capacitor, glass	105	3.0	315.0
Capacitor, filter feedthrough	8	10.0	80.0
Capacitor, solid tantalum	10	9.0	90.0
Capacitor, variable	36	40.0	1440.0
Diode, general purpose (SI)	1	3.0	3.0
Diode, zener	7	37.0	259.0
Diode, varactor	8	40.0	320.0
Transistor, low power (SI)	11	10.0	110.0
Transistor, high power (SI)	1	40.0	40.0
Inductor	19	10.0	190.0
Thermistor	1	35.0	35.0
Crystal, quartz	1	20.0	20.0
50-pin connector	4	30.0	120.0
Filter, RFI	12	10.0	120.0
Sensistor	1	3.0	3.0
Diode, step recovery	4	100.0	400.0
	356		3929.0

$$R_{\text{single unified S-band transmitter}} = 0.9662$$

$$R_{\text{redundant unified S-band transmitter}} = 0.9989$$

Transmitter Driver

Resistor, carbon composition	33	2.0	66.0
Resistor, metal film	30	1.0	30.0
Capacitor, ceramic	36	4.0	144.0
Capacitor, glass	16	3.0	48.0
Capacitor, filter feedthrough	13	10.0	130.0
Capacitor, solid tantalum	19	9.0	171.0
Capacitor, foil tantalum	1	20.0	20.0
Diode, general purpose (SI)	7	3.0	21.0
Diode, varactor	1	40.0	40.0
Transistor, low power (SI)	12	10.0	120.0
Transistor, high power (SI)	1	40.0	40.0

Table 15-4. Reliability Predictions of New or Modified ERTS Equipment (Continued)

	Part Count	Part Failure Rate (bits)*	Total Failure Rate (bits)*
Integrated circuit, analog amplifier	5	100.0	500.0
Crystal, quartz	1	20.0	20.0
RF choke	12	10.0	120.0
50-pin connector	3	30.0	90.0
Diode, step recovery	1	100.0	100.0
	<u>191</u>		<u>1660.0</u>
R _{single transmitter driver} = 0.9856			
R _{redundant transmitter driver} = 0.9998			
<u>Video Switching Assembly</u>			
Connector, coaxial	1	10.0	10.0
50-pin connector	1	30.0	30.0
Coupler	4	50.0	200.0
Isolator	2	40.0	80.0
Transfer switch (RF)	1	20.0	20.0
	<u>9</u>		<u>340.0</u>
R _{video switching assembly} = 0.997			
<u>-24 Volt Battery</u>			
Resistor, wirewound	4	10.0	40.0
Diode, power rectifier (SI)	2	44.0	88.0
Transformer	1	14.0	14.0
	<u>7</u>		<u>142.0</u>
R _{-24 battery} = 0.9988			

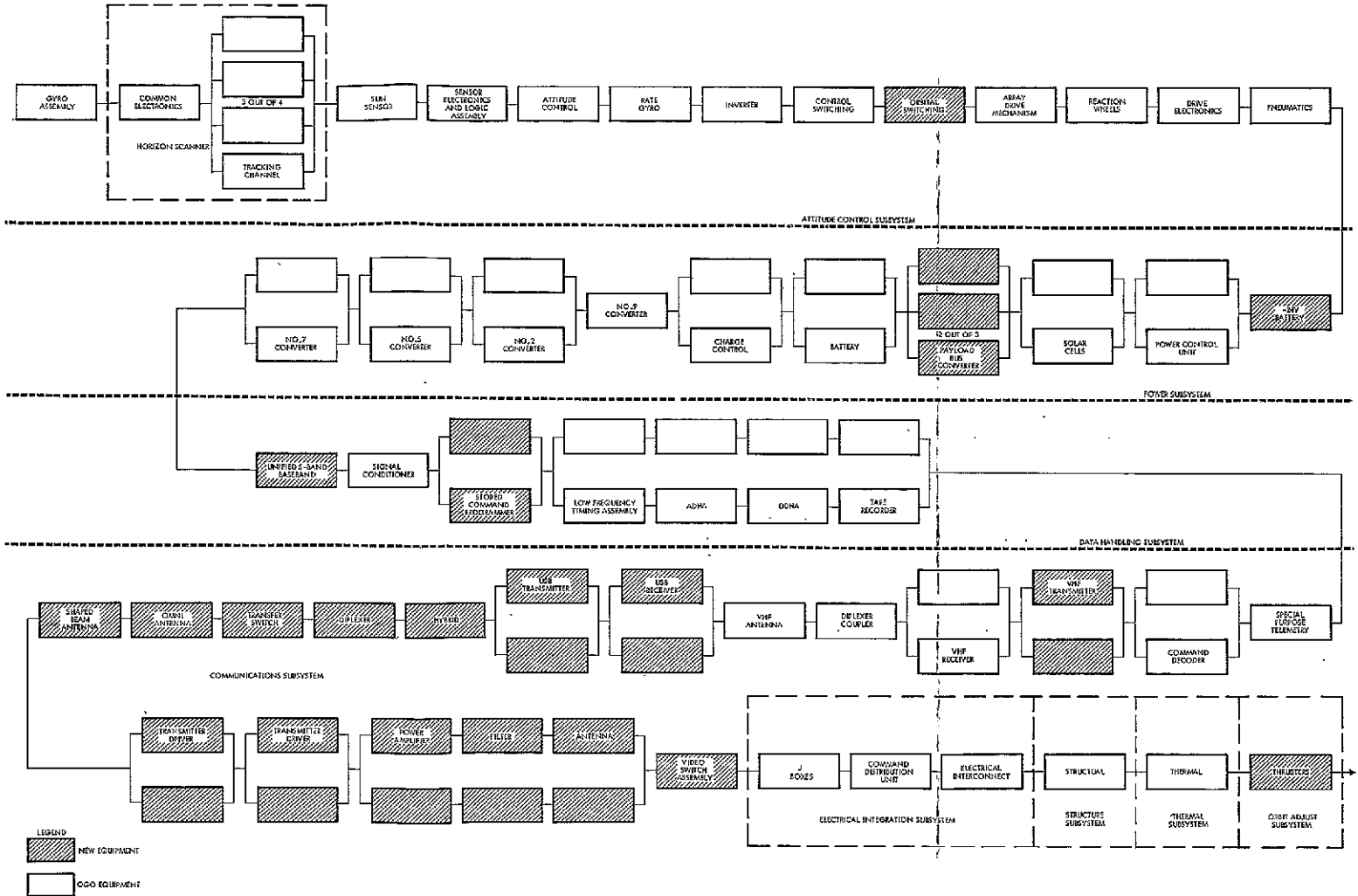
The predicted reliability is conservative because the reliability of modified OGO boxes are included without deleting the OGO-predicted reliability of those boxes. Also the predicted reliability of OGO boxes (wideband transmitters and tone decoder) not required for ERTS are not deleted. Additional reliability gain will also result from the use of redundant converters 2, 5, and 7, and the redundant low frequency timing assembly.

The subsystem reliability apportionment for the ERTS observatory (excluding GFE other than existing OGO equipment) is based on the OGO demonstrated orbital reliability, the OGO apportionment and the inclusion of the ERTS new and modified equipment. Using the overall predicted ERTS reliability the subsystem apportionments are defined:

- Altitude control 0.937
- Power 0.995
- Data handling 0.962
- Communications 0.971

Table 15-5. ERTS Failure Rates

Number	Bits	Description	Number	Bits	Description
1	2.00	Resistor, carbon composition	36	10.00	Connector, coaxial
2	1.00	Resistor, metal film	37	35.00	Thermistor
3	10.00	Resistor, wirewound	38	20.00	Crystal, quartz
4	50.00	Variable, wirewound resistor	39	0.01	Core, magnetic
5	50.00	Thin film resistor network	40	20.00	Crystal filter
6	4.00	Capacitor, ceramic	41	10.00	RF choke
7	3.00	Capacitor, glass	42	10.00	Feedthrough filter
8	30.00	Capacitor, polystyrene	43	100.00	Integrated circuit, voltage regulator
9	10.00	Capacitor, filter feedthrough	44	100.00	Power amplifier
10	9.00	Capacitor, solid tantalum	45	30.00	50-pin connector
11	20.00	Capacitor, foil tantalum	46	100.00	DC amplifier (integrated circuit)
12	40.00	Capacitor, variable	47	10.00	Filter, RFI
13	4.00	Capacitor, mica	48	3.00	Sensitor
14	20.00	Capacitor, mylar	49	40.00	Filter, bandpass
15	3.00	Diode, general purpose (SI)	50	10.00	Toroid
16	37.00	Diode, zener	51	40.00	Filter, band reject
17	136.00	Diode, 4-layer device	52	150.00	Oscillator
18	40.00	Diode, varactor	53	75.00	Counter (MSI)
19	100.00	Diode, tunnel	54	20.00	Time delay
20	44.00	Diode, power rectifier (SI)	55	50.00	Coupler
21	10.00	Transistor, low power (SI)	56	40.00	Isolator
22	40.00	Transistor, high power (SI)	57	100.00	MOS shift register
23	60.00	Transistor, field effect	58	50.00	Antenna
24	25.00	Integrated circuit, RTL	59	20.00	Transfer switch (RF)
25	25.00	Integrated circuit, DTL	60	100.00	Diode, step recovery
26	100.00	Integrated circuit, analog amplifier	61	80.00	Diplexer
27	100.00	Integrated circuit, MOS	62	130.00	Diplexer/coupler
28	150.00	Integrated circuit, hybrid	63	150.00	Integrated circuit, dual flip flop
29	25.00	Integrated circuit, TTL	95	50.00	Unified S-band shaped-beam antenna
30	14.00	Magnetic amplifier	96	50.00	Omni unified S-band antenna
31	14.00	Transformer	97	50.00	VHF antenna
32	10.00	Inductor	98	50.00	Wideband antenna
33	106.00	Relay, nonlatching	99	6716.00	TWTA
34	64.00	Relay, latching	100	0.60	Connector pin
35	100.00	Fuse			



FOLDOUT FRAME 1

Figure 15-1
ERTS RELIABILITY MODEL

FOLDOUT FRAME 2

- Electrical integration 0.983
- Structures 0.999
- Thermal 0.999
- Orbit adjust 0.999
- Antennas 0.999

ERTS observatory apportionment (other than existing OGO equipment) 0.853

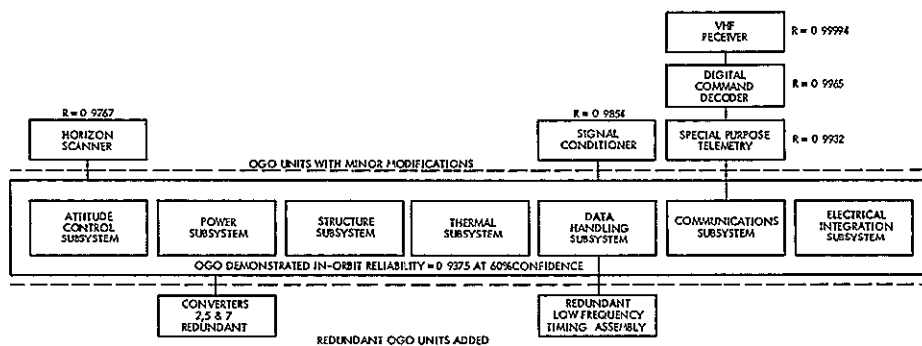


Figure 15-2

UNITS WITH MINOR MODIFICATIONS and redundant OGO units added

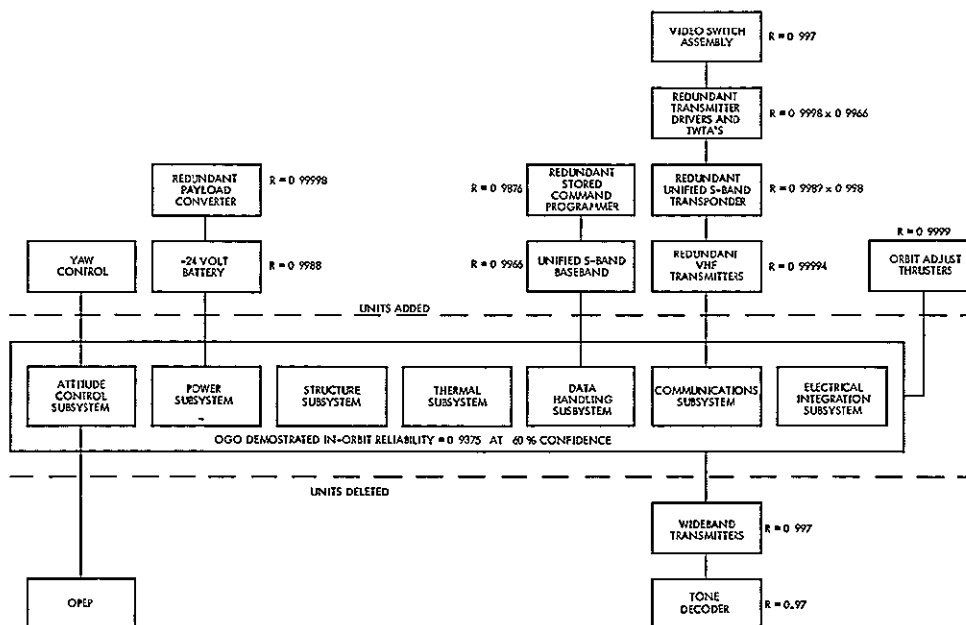


Figure 15-3

NEW UNITS ADDED AND UNITS DELETED

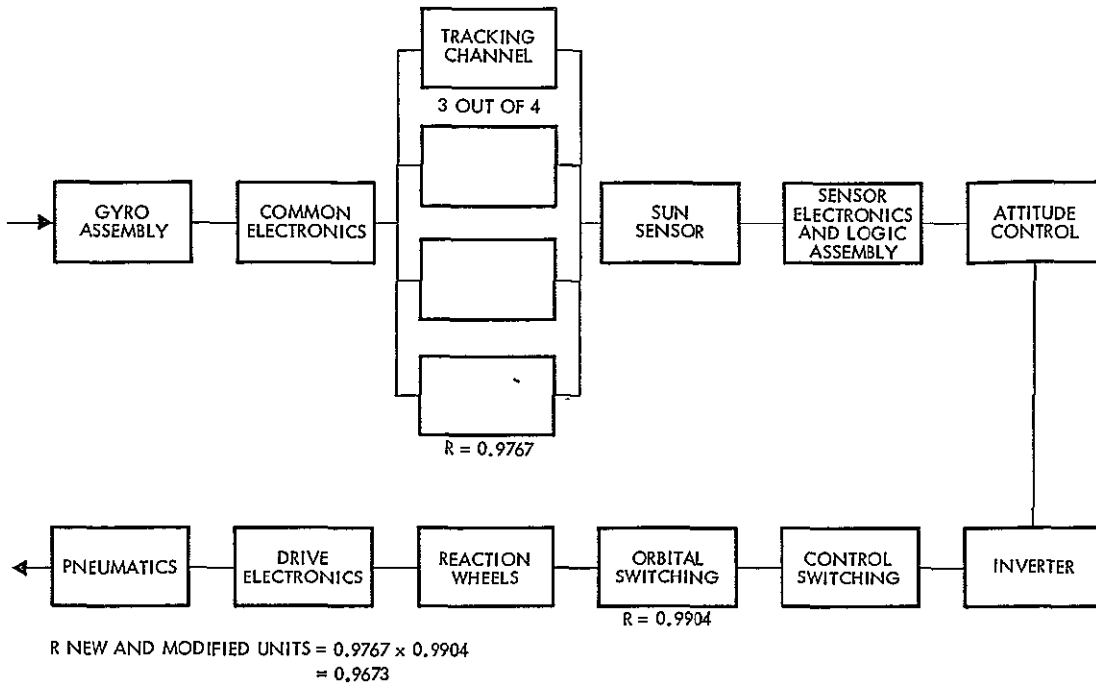


Figure 15-4
ATTITUDE CONTROL SUBSYSTEM RELIABILITY MODEL

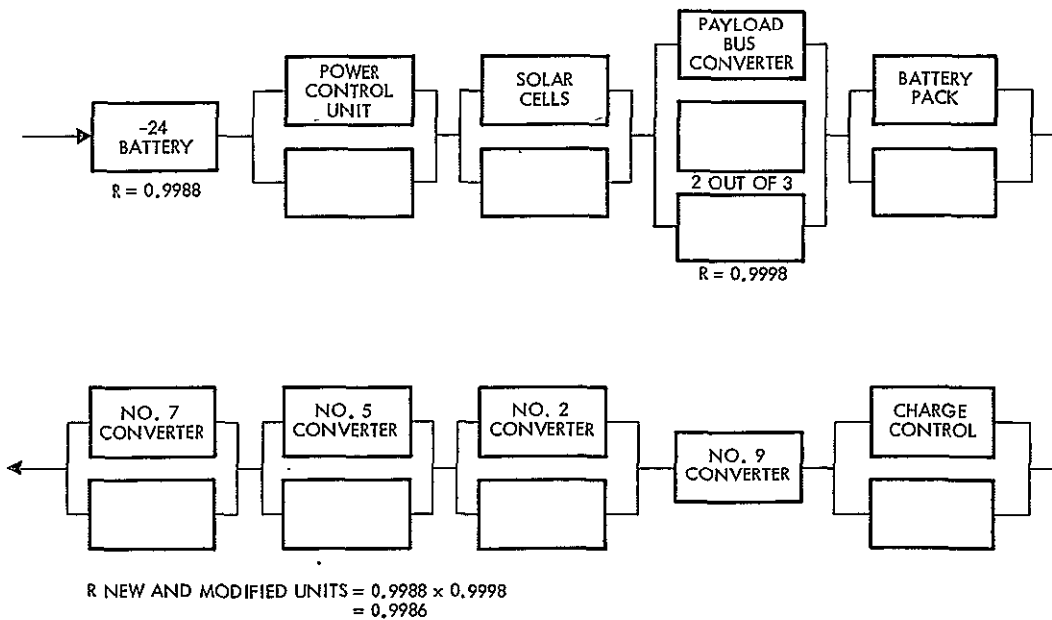


Figure 15-5
POWER SUBSYSTEM RELIABILITY MODEL

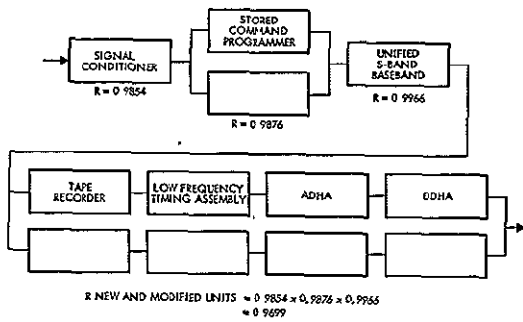


Figure 15-6
DATA HANDLING SUBSYSTEM
RELIABILITY MODEL

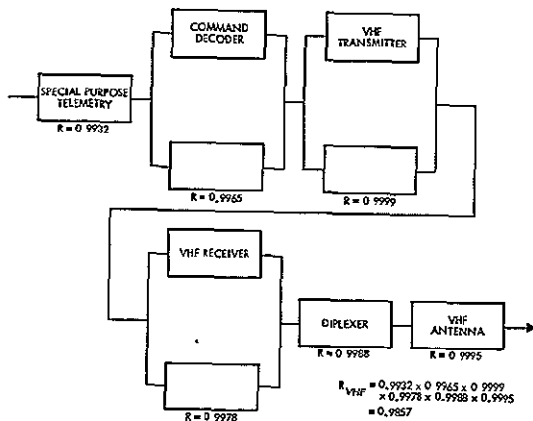


Figure 15-7a
VHF TRANSMITTERS AND RECEIVERS
RELIABILITY MODEL

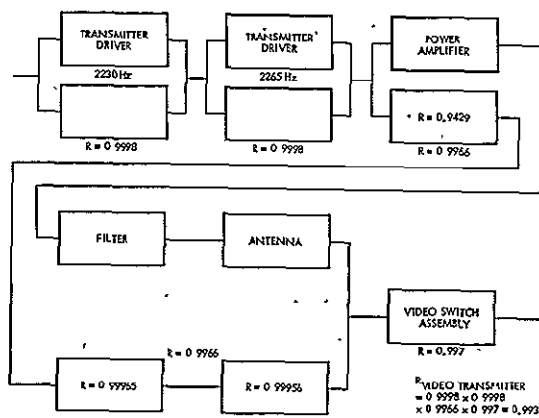


Figure 15-7c
VIDEO TRANSMITTER RELIABILITY MODEL

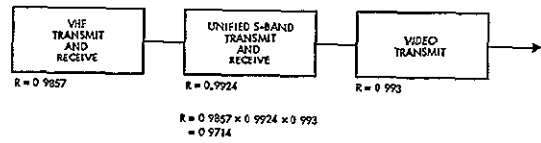


Figure 15-7
COMMUNICATIONS SUBSYSTEM
RELIABILITY MODEL

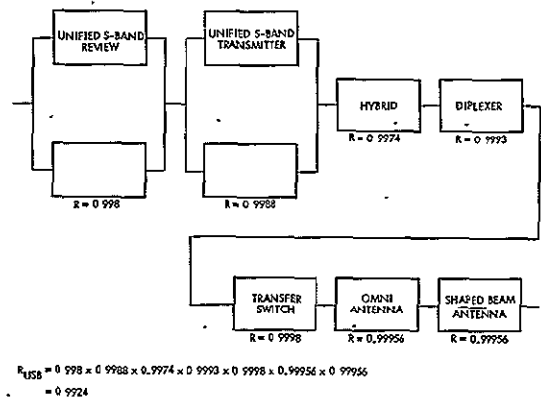


Figure 15-7b
UNIFIED S-BAND TRANSMITTERS AND
RECEIVERS RELIABILITY MODEL

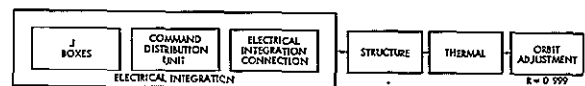


Figure 15-8
ELECTRICAL INTEGRATION, STRUCTURE,
THERMAL, AND ORBIT ADJUST SUB-
SYSTEMS RELIABILITY MODEL

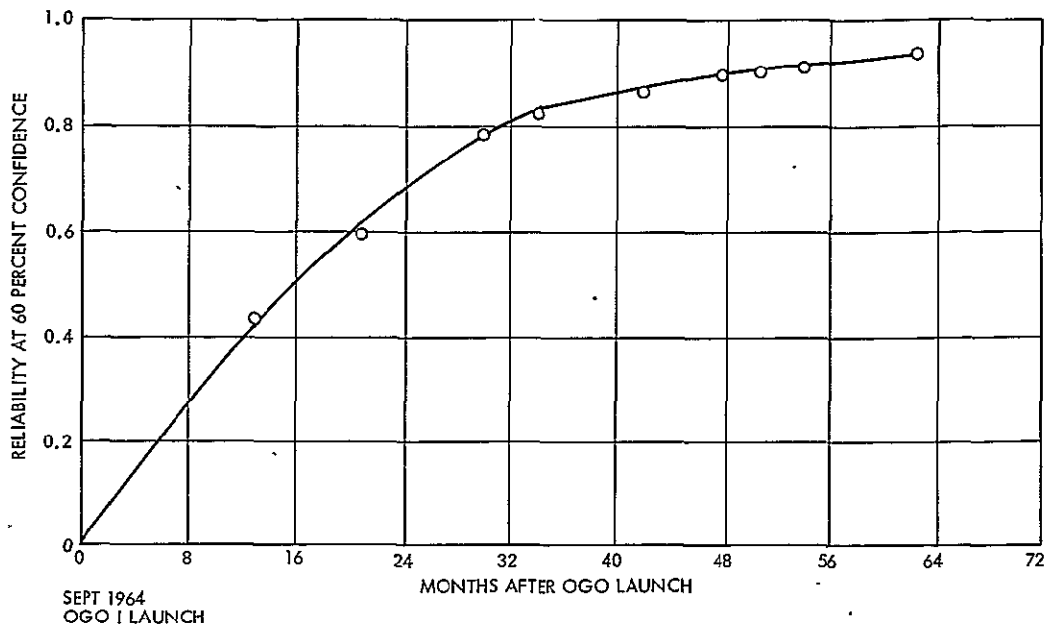


Figure 15-9
OGO DEMONSTRATED RELIABILITY

15.2 REVIEW OF EXISTING ASSEMBLIES, EXTENT OF COMPLIANCE WITH ERTS REQUIREMENTS

All existing assemblies (components) planned for use on ERTS-A and -B meet the requirements of NPC 250-1 and NHB 5300.4(1B). These assemblies were built to meet NASA/GSFC contract requirements in which NPC 250-1 and NPC 200-2 were imposed. The environmental test program imposed on the OGO contracts essentially meets the requirements of GSFC S-320-G-1 in that all existing assemblies proposed for ERTS have successfully completed environmental testing to TRW specifications D-13351 and D-13352. (See Section 4 for an analysis of vibration environment.) The existing assemblies planned for ERTS are identified in the hardware list of Section 14.

15.3 CONFIGURATION MANAGEMENT

The configuration management system was reviewed during the Phase B/C study to determine its compatibility with Goddard Management Instruction 8040.1. The study included a paragraph by paragraph comparison of the TRW system and GMI 8040.1 and resulted in the plan given

in Volume 9. The paragraph notation of GMI 8040.1 is used below to describe results of the comparison.

1. APPLICATION

The configuration management procedures of TRW have been developed in such a manner that they are capable of being applied to all TRW projects on a selective basis according to the project requirements. The ERTS configuration management plan establishes the procedures which will be observed by the responsible management levels and technical personnel of TRW involved in the development, test, and fabrication of the observatory as well as the ground data handling system.

2. DEFINITION

Configuration management is defined as:

- The identification of the technical description of a configured item contained within its engineering and related documentation
- The accounting for the engineering and manufacturing technical documentation to provide visibility into the configuration of hardware and software configured items at all times
- A system of configuration control that provides for a systematic and logical review of all changes to end items of hardware and software in accordance with their baseline requirements

3. PURPOSE

The ERTS configuration management system ensures that:

- The technical description of all end-items are documented by engineering drawings, specifications, procedures, and processes in a logical, timely, and effective manner
- The documentation of the technical description is accounted for and reported in a timely and effective manner
- All applicable engineering changes are reviewed in a systematic manner to determine their validity and impact. The system also ensures that all affected parties are cognizant of change impact.

4. APPLICABILITY

The procedures in the ERTS configuration management plan are applicable to the observatory segment and the ground data handling segment of the ERTS project. The procedures for configuration management of the data collection platform are contained within a separate DCS configuration management plan.

5. RESPONSIBILITIES

The overall responsibility for configuration management on each project is vested in the project manager. For the ERTS project, the authority for implementing and managing the procedures in the configuration management plan has been delegated to the configuration management manager through the manager for project performance assurance, who reports directly to the project manager. The configuration management manager also serves as chairman of the change evaluation and control board.

6. OBJECTIVES

The broad objectives of the ERTS configuration management system as defined in the project configuration management plan are:

- 1) Identify and provide formal documentation for end items to ensure that engineering drawings; specifications, and related documentation, including changes are identical to end items
- 2) Lend credence to the realistic development of schedules and cost data through the definition of hardware in terms of specifications and related design documentation and changes thereto
- 3) Ensure the coordination of design changes and ensure that the impact of proposed changes on performance requirements, schedules, cost, manpower and reliability, are documented and considered as part of the approval process
- 4) Provide a uniform means for reporting configuration management data

7. AUTHORITY

Approval of engineering changes within the ERTS project lies with the change evaluation and control board as defined within the ERTS configuration management plan. However, all Class I changes subsequent to the establishment of the Stage 2 baseline will require approval of the GSFC project manager.

8. NOT APPLICABLE

9. BASELINE CONCEPT

The Stage 1 and 2 baselines of GMI 8040.1 are compatible with TRW's development and production baselines. The attendant informal and formal change control requirements are documented in detail in the ERTS configuration management plan. The general requirements are:

- Informal change control results in a completely documented end item at all times up to the configuration freeze date. However, classification of changes are not required until the Stage 2 baseline.
- Formal change control beginning on each end item as they are included on the Stage 2 configured article list involves the complete evaluation of all configuration changes using the engineering change request, engineering change analysis, and engineering change directive as detailed in the configuration management plan.

10. CONFIGURATION CONTROL BOARD

The ERTS Change Evaluation and Control Board is instituted as the formal activity for reviewing and approving or disapproving all configuration changes on the ERTS project. In addition, two lower tier boards are used to detail the schedule and cost impacts of changes prior to review by the CECB.

- The Software Change Planning Board is composed of change accounting and planning personnel familiar with the detailed schedule and software development plan tasks and shall provide detailed visibility of software change impact to the CECB.
- The Change Planning Board provides the CECB with recommended effectivities and disposition of parts in addition to determining the change impact on manufacturing documentation.

Agendas and minutes of the CECB activity are provided by the CECB chairman.

11. CONFIGURED ARTICLE LISTS

Configured article lists of all end-item hardware and software will be maintained and kept current so that the configuration can be maintained current at all times. The descriptive portions of the list are compatible with GSFC 8040.1 and can be extracted and printed by the configuration data bank. The list for each end item will be attached to the DD-250 when the end item is accepted by the appropriate NASA designee.

15.4 CONSOLIDATED PARTS, MATERIALS AND PROCESSES LIST

A consolidated listing of all parts, materials and processes used in existing assemblies and in planned assemblies, where parts identification has been made, is supplied in Appendix C. In addition to referencing the part and material type designation, this list provides identification to the procurement specification and the planned or preferred sources of supply. The requirements delineated in the GSFC Preferred Parts List PPL-10 provide the minimum standard for the procurement or use of all ERTS parts.

15.5 RELIABILITY PROGRAM PLAN

The NASA/GSFC-approved OGO reliability program plan revised to meet ERTS requirements is presented in Volume 6. The reliability program plan covers all aspects of reliability for the Phase D contract and complies with the requirements of NPC 250-1 for spacecraft and ground data handling equipment. The plan was written in compliance with NPC 250-1 but was structured in accordance with the format of the draft copy of the new NASA "Reliability Program Provisions for Space Systems Contractors," NHB 5300.XXX (draft copy, May 1969) to incorporate the requirements for ground data handling, software, and sites.

The subcontractor reliability program plan requirements document identified as PAR 700-54 was completed during the study and is included in Volume 6.

15.6 QUALITY PROGRAM PLAN

The NASA/GSFC-approved OGO quality program plan has been modified to be compatible with NHB 5300.4(1B), Quality Program Provisions for Aeronautical and Space System Contractors (see Volume 7). Specific additional requirements have been stipulated as quality assurance responsibilities. The quality program plan establishes ERTS project quality requirements. The plan includes the observatory, associated GSE, and the ground data handling system. Detailed quality requirements are defined for TRW Systems and its subcontractors to effectively implement a quality system to ensure that all quality assurance requirements are met for acceptance and delivery of the contract end items.

TRW's OGO supplier and subcontractor quality assurance requirements plans have been revised to incorporate the ERTS requirement and are now reflected as PAR 700-52 and 700-53, product assurance requirements, in compliance with NPC 200-3 and NHB 5300.4(1B), respectively. The ERTS quality program plan includes discussion and establishes program requirements in the following areas:

- Introduction and general requirements
- Quality program management and planning
- Design and development controls
- Identification and data retrieval
- Procurement controls
- Fabrication controls
- Inspections and tests
- Nonconforming article and material control
- Metrology controls
- Inspection stamp controls
- Handling, storage, preservation, marking, labeling, packaging, packing, and shipping
- Sampling plans, statistical planning and analysis
- Government property control

In addition, the relationship between NHB 5300.4(1B), Quality Program Provisions, and existing TRW policies, instructions, and procedures included in the company Quality Assurance Manual, is presented to further describe the implementation of NASA/GSFC requirements.

15.7 TEST MONITORING AND CONTROL PLAN

The test monitoring and control plan developed during the study is presented in Volume 8. The plan assures proper test application, test conditions, completion and evaluation of requirements imposed from the initial procurement at the piece-part level through incoming inspection, manufacturing, component qualification and acceptance testing,

spacecraft and observatory testing, launch site testing, and other testing including end item testing by subcontractors. The contents of this plan are compatible with ERTS reliability and quality requirements and complement the ERTS test and launch support plans.

15.8 PROGRAM PLAN FOR SOLDERED ELECTRICAL CONNECTIONS

The TRW/ERTS program plan for soldered electrical connections complies with NHB 5300.4(3A), and ensures high reliability electrical connections for ERTS hardware (see Volume 10).

The plan includes the training and certification of personnel, facility and equipment requirements, and the preparation and application of the soldering process. TRW implements the requirements of NHB 5300.4(3A) as stipulated in the program plan for soldered electrical connections through the use of internal process specifications and fabrication inspection process procedures, as appropriate. For subcontracted assemblies, product assurance requirements (PAR700-53, 53) documents specify the NHB-5300.4(3A) requirements as applicable to hardware delivered to TRW for flight use. If TRW determines that a deviation to the NHB document or the program plan is necessary, a request for waiver to NASA/GSFC will be transmitted through the ERTS performance assurance office.

15.9 REVIEW OF TRW FAILURE REPORTING PROCEDURES

The TRW failure reporting procedure approved by GSFC for OGO meets the ERTS requirement for a system compatible with both government and contractor. The approved OGO procedure has been revised to provide more stringent controls such as combining the TRW failure report and discrepancy report and reporting of failure at lower levels of hardware. The recommended failure reporting system for the ERTS Phase D is presented in Volume 11. The system uses the TRW Test Information Retrieval System (TIRS) for in-house reporting and the GSFC 4-2 for reporting to NASA/GSFC.

The TIRS system has been operational on all new TRW projects since April 1969. It is a computerized system for recording, storing, and retrieving failure and discrepancy data from functional tests. The basic reporting form is the test discrepancy report, an eight-copy form

so arranged that the level of test being performed can be recorded. This permits recording lower assembly analysis during rework. Six levels of assembly can be recorded:

- Level 1: system
- Level 2: subsystem
- Level 3: assembly
- Level 4: subassembly
- Level 5: detail subassembly
- Level 6: part

The basic information from the test discrepancy report is fed directly into the computer through codes. The cause of failure, failure analysis and corrective action are provided by a free-form follow-up sheet that permits detailed analysis of up to 2200 characters. The follow-up sheet, the "Test Discrepancy Follow-up Sheet" (TDF), is completed by reliability engineers. Supplemental TDF's can be submitted to update in-process failures or to revise closed-out TDF's. Close-out of each TDR/TDF is made by the reliability engineer, signifying acceptance by the failure review board of the failure analysis and corrective action.

The TRW system failure reporting procedure was reviewed during the B/C study to determine compatibility with Goddard Management Instruction GMI 5310.1A. The study included a review on a paragraph-by-paragraph basis of the newly incorporated TIRS with GMI 5310.1A. The paragraph notation of GMI 5310.1A is used below for this comparison for Paragraph 2 through 7. Table 15-6 compares the TRW TDR/TDF with the GSFC 4-2.

The objectives of the failure reporting procedure are as follows:

- TIRS provides TRW and the ERTS project with a uniform and effective malfunction reporting system. Reporting to GSFC will be through the GSFC 4-2 form.
- TIRS provides a computerized depository of malfunction information that is quickly and selectively retrievable.

Table 15-6. Comparison of TRW TDR/TDF with GSFC 4-2

GSFC 4-2	Test Discrepancy Report and Follow-Up
1. Project	Unnumbered blank, in addition computer keyed to job number, line 02
2. Spacecraft	No corresponding space
3. Operation	
4. Units (hr/cycles)	Line 02, Block 39, cumulative operation, time/cumulative cycles
5. System or experiment	Line 03, Block 10
6. Date and time of failure	Line 01, failure data
7. Date of report	
8. Critical (yes/no)	Block 21, follow-up sheet
9. Component	Lines 03, subsystem or system level failures
10. Assembly	Lines 04 and 05
11. Subassembly (not listed)	Lines 06 and 07 (detail subassembly, lines 08 and 09)
12. Part (one space only)	Lines 10, 11, 12, and 13 for more than 1 part removed or reworked
13. Test failed	Line 01, code
14. Environment when failed	Line 01, code
15. Action to be taken	Line required per level of test Block 50 (line 6 or 8) Block 44 for line 04 (assembly) Blocks to be marked as well as space for instruction to be written
16. Reference log book number page, test procedure paragraph	No log book reference Test procedure and paragraph, line 02
17. Description	Lines for written description at level of test, i.e., assembly or subassembly, etc. Additional lines for changing or expanding description on follow-up sheet
18. Originator	Block 38, line 01
19. Cause	Freeform, follow-up sheet for cause to be written. If minor, line 14 has code space and comments block for cause and retest instructions
20. Corrective action	As above, comments block for minor action plus: retest instructions, follow-up form for additional information Codes line 14 Follow-up form codes, line 21 will change codes on 2 DR form
21. F/A performed, etc.	Would have to be written on follow-up sheet Blocks 15, 16, and 20 of lines 5, 7, and 9 have means to designate if failure was verified, type of defect (coded) and if primary or secondary
22. Rework, etc.	Space available for rework document, number, time, and written description plus quality assurance buy-off at each level, i.e., assembly subassembly lines 5, 7, and 9
23. Retest required	See retest instruction block
24. Retest results	Quality assurance buy-off blocks at every level
25. Unit may be used for flight	No space other than comments block, or continuation (free form) sheet. Follow-up sheet for written action by FRB or restrictions on units.

- TIRS is company-wide for all TRW Systems projects. Through biweekly summary and detailed reports each project is cognizant of problems on other projects.
- TIRS outputs provide TRW ERTS management and GSFC ERTS management with status and history reports of project malfunctions for design and flight readiness review.

The TRW Systems definitions are in agreement with those of attachments 1 and 2 to GMI 5310. 1A.

The scope of the TIRS system is as follows:

- All TRW Systems projects use the standard TIRS reporting system for reporting and documenting malfunctions or flight and prototype hardware.
- The TIRS reporting system begins with the first functional test at the detail subassembly level and continues through the mission until observatory power is turned off. The level of hardware as defined in the configured item parts list is the defining criteria.
- Malfunctions are reported on the Standard Test Discrepancy Report (Form 1075).
- Subcontractors may use the TRW Systems form or a subcontractor form approved by TRW. All TRW failures and subcontractor failures on the ERTS project will be reported to GSFC on the GSFC 4-2 form.
- All malfunctions (failures) are reviewed monthly by the Failure Review Board on each project. The failure description, cause of failure, and corrective action are reviewed by the board prior to formal close-out.
- All malfunctions (failures) are closed out by the Failure Review Board. The manager of performance assurance represents the project manager for close-out approval.
- The reporting of all discrepancies is through the normal quality control inspection procedure. Nonfunctional discrepancies (e. g., cosmetic types) are reported on discrepancy reports and functional discrepancies are reported on test discrepancy reports.

The responsibilities for malfunction reporting are as follows:

- The overall responsibility for malfunction reporting on each project is vested in the project manager. This responsibility is normally delegated to the performance assurance manager, who acts for the project manager.

- Each project malfunction reporting system is established, maintained, and coordinated in accordance with customer requirements and TRW Systems directives. A detailed plan is prepared for each project and controlled by the manager of performance assurance, who serves as chairman of the Failure Review Board.
- The unit engineer in conjunction with the reliability engineer and other specialists evaluates each malfunction or failure to determine the cause and recommended corrective action. These are described at the monthly meeting of the Failure Review Board and are documented on the TDR and on failure reports such as the GSFC 4-2 form that is submitted to GSFC.
- The manager of performance assurance or his designee represents the project manager at the Failure Review Board meetings. He reviews the failure reports and brings management inputs to the meetings.
- The TRW Systems Product Assurance Group has overall control of TIRS. Reports that are determined to cover discrepancies are handled through normal quality assurance procedures. TDR's that are determined to be failures are handled by reliability engineers. The determination is made by the responsible reliability engineer with concurrence through the project office and Failure Review Board.
- The central TDR receiving and distributing system including data storage and data retrieval is the responsibility of the TRW Product Assurance Group.
- Failure analysis and problem recurrence prevention are the responsibility of the division where the equipment was designed and built. TRW product assurance provides consulting and standards.

The Failure Review Board is instituted as a formal activity on each hardware project. The board has as a minimum the following members:

- Manager of performance assurance, chairman
- Reliability engineer, technical secretary
- Manufacturing
- Quality

The Failure Review Board provides the equivalent function performed by the GSFC Malfunction Report Review Team.

All TRW Systems failures are reported on the Test Discrepancy Report (TDR). The form combines the discrepancy and failure report for all functional failures beginning with the first functional test of a subassembly. A TDR is initiated no later than 8 hours after the discrepancy or failure. This is in agreement with GSFC requirements of 24 hours.

Reports to GSFC will be forwarded to arrive within 5 working days after discovery of the malfunction.

The originator and quality inspection personnel are charged with filling out the TDR with all known information. Quality inspectors must validate the information on each TDR when an inspection of test results is required. This is in agreement with GSFC requirements that the originator should fill out the form.

The TRW Systems TDR is an eight-copy form:

- Copy 2, a reliability flash copy, distributed immediately after initiation of the TDR
- Copy 3, a quality systems flash copy, distributed when initial disposition is made prior to rework, if any
- Copy 4, the final quality systems copy, distributed after all rework is completed and the TDR is closed
- Copy 5 is retained with the system or subsystem data package
- Copy 6 is forwarded to the Metrology Department when the TDR is the result of test equipment error
- Copy 7 is retained with the subassembly data package
- Copy 8 is retained with the detail subassembly data package

Copies 1, 4, 5, 7, and 8 are retained with the failed item until the failure is analyzed, cause of failure determined, and corrective action is taken. Copy 1 is distributed to reliability after rework is completed; Copy 4 is distributed to quality assurance after rework is completed.

The TRW Quality Assurance Group reviews each TDR for completeness and inputs to the computer. Rework of a failed item is verified by quality assurance. Each failure is reviewed by the Failure

Review Board. The Board meets on a monthly basis, or more often if required, and final recommendations are made to the project manager. The extent of the rework is reviewed by the Failure Review Board before final approval is made. Final close-out of each failure is through the Failure Review Board.

Copies of each TDR are released on a biweekly basis through computer printouts for distribution to interested projects and other personnel. Reliability and quality assurance personnel review the bi-weekly reports to assure completeness and accuracy and to perform statistical analyses.

15.10 SAFETY PLAN

The ERTS Safety Plan developed during the study for Phase D is presented in Volume 12. The plan provides overall direction for the protection of personnel and equipment. Briefings and system safety orientation of project personnel, examination of plans and operations for safety criteria, attendance at design reviews and documentation of safety hazards will be stressed throughout the ERTS project.

CONTENTS

	Page
16. INTEGRATION, TEST, AND LAUNCH	16-1
16.1 Observatory Qualification	16-1
16.2 Pneumatic Leak Test Study	16-3
16.3 Observatory Shock Test Study	16-5
16.4 Thermal Deformation Checks	16-6
16.5 ERTS Payload Study	16-8
16.5.1 Multispectral Scanner	16-8
16.5.2 Return Beam Vidicon	16-9
16.6 Functions Not Tested in All-Up Spacecraft Testing	16-10

16. INTEGRATION, TEST AND LAUNCH

Six areas have been studied during Phase B/C in the course of defining the procedures and policies best suited to the integration, test, and launch of ERTS:

- The policy for system qualification
- The pneumatic leak test
- The observatory shock test
- Measurement of thermal deformation
- Payload interfaces
- Nontestable functions

The results of these studies have been applied in preparing the sequence described in Volume 3 and the plans presented in Volume 12.

16.1 OBSERVATORY QUALIFICATION

Three alternative methods for qualifying the ERTS have been evaluated, making use of a prototype spacecraft, omitting prototype system tests, and making use of a spacecraft that is planned to serve both as prototype and flight. This third alternative is selected since it can provide all the test data required for qualification while adding little to the cost or schedule of the program.

The first alternative considers the full qualification program using a prototype spacecraft built exclusively for this purpose. This spacecraft contains operating prototype subsystems and is subjected to environmental tests to qualify the design for fabrication of the flight model spacecraft. The qualification test cycle would take approximately eight months and would start five months before integration of the ERTS-A begins.

The second alternative considers a flight spacecraft which is subjected only to flight acceptance test durations and test levels. This method adds no extra time to the schedule and assumes that the design has already been qualified by other methods both structurally and electrically.

The third alternative is a combination of the first two. This alternative considers a spacecraft, which is designated in advance to serve both as a prototype and flight model. This model is subjected to environmental tests which combine elements of flight acceptance and prototype testing. The combined elements in this case are environmental qualification test levels at acceptance test durations, component qualification program on new or major modified units, and subsystem compatibility testing on the bench using engineering models or prototype models of the unified S-band, VHF and wideband RF subsystems. The subsystem compatibility test are completed before the proto-flight is integrated.

The design analysis presented in Section 4 demonstrates that a prototype model spacecraft for ERTS is not necessary. The reasons for this conclusion lie in the similarity of the structure, weight, and environment of ERTS to those of OGO:

- Structure: The ERTS body is unchanged from OGO except for an improved panel construction.
- Weight: The total weight of ERTS is close to that of OGO, OGO 6 being slightly heavier.
- Weight distribution: The density of equipment in ERTS is about the same as OGO, the only substantial difference being the concentration at the OGO upper support points which is eliminated in ERTS.
- Environment: The booster-induced vibration and shock provided to ERTS by the Thor-Delta are quite similar to those provided to OGO by the Thor-Agena. The ERTS orbital environment is similar to the POGO environment.

The elimination of the prototype model saves five months of program time. Although the second alternative is the least costly of the three it introduces an uncomfortable amount of risk into the program, particularly with respect to observatory dynamics and electrical compatibility.

The third alternative calls for no extension of the schedule beyond that without a prototype, and costs the program only a subsystem electrical compatibility test, which increases integration and test costs by

six man-months. This model satisfies the requirements for a proto-flight spacecraft as defined in GSFC Environmental Test Specification S-320-G-1, Paragraph 4.11b. The proto-flight model concept is ideally suited to the ERTS program, for which a design-qualified structure exists along with other major subsystems.

16.2 PNEUMATIC LEAK TEST STUDY

The study to develop an accurate leak test method that produces results in a shorter time than the pressure decay and mass spectrometer methods has concluded that the radiotracer method should be adopted. The tracer concentration is so small that it does not require purging after the final on-stand test; the spacecraft can be launched with this tracer in the gas bottle.

The study evaluated two alternative approaches. The rejected alternative method consists of two parts. At high pressures a mass spectrometer is used to detect leaks, and at low pressures leak rates are measured by pressure decay.

The pressure decay method requires periodic measurement of pressure vessel temperature (accurate to approximately 0.05 percent) and gas pressure (accurate to approximately 0.07 percent). This data along with date, time, and barometric pressure is fed to a computer which calculates instantaneous standard volumes and a least square fit through these standard volumes. The slope of this line is the leak rate of the pneumatic low pressure system. In a 24-hour test this method is accurate to ± 2 scc/hr but is very sensitive to changes of temperature in the test environment. The high pressure, mass spectrometer, method requires the pneumatic system to be loaded to flight pressure in the pneumatic test cell with the spacecraft doors open. At flight pressure, the test cell doors are opened and a mass spectrometer "sniff" test is made on all joints and connections of the pneumatic system. This same procedure is followed after the pressure vessel is loaded to proof pressure ($1.5 \times$ flight pressure) and bled down to flight pressure.

The selected approach measures leak rates by utilizing a radiotracer leak detector. This method is currently being used on four other spacecraft programs at TRW. The spacecraft is placed in the pneumatic

test cell and pressurized to flight pressure with a trace of Kr⁸⁵ added to the normal flight gas. The spacecraft is enclosed in an airtight plastic bag. A radiation detector outside of the bagged spacecraft continuously samples the tracer gas concentration within the bagged volume. The radiation intensity of the gas is proportional to the tracer gas concentration and therefore the amount of gas that has leaked from the pneumatic system. The increase in radiation intensity with time is directly proportional to the leak rate. The system is calibrated by placing a standard known leak rate in the bagged volume and sampling the gas concentration change with the leak detector. The pneumatic vessel is loaded to proof pressure and bled down to flight pressure while the detector samples the tracer concentration. The accuracy of this method for the ERTS configuration is 0.8 scc/hr. Leak rates as low as 0.1 scc/hr have been measured on Intelsat III.

The recommended concentration of Kr⁸⁵ for the ERTS pneumatic volumes is 2×10^{-5} mci/cm³. This concentration gives the total system a radioactivity of 110.4 mci. This amount of radiation is so small that hazards are negligible, for personnel or equipment.

The radiotracer method does not require that the spacecraft doors be open during the test, a significant advantage over the mass spectrometer method, in that the possibility of affecting the integrity of the equipment is avoided. The radiotracer method can be used on-stand after final pressurization, allowing direct comparison of data with the in-plant leak tests.

The radiotracer method is more accurate as shown by the table below:

<u>Method</u>	<u>Accuracy</u>
Radiotracer	0.8 scc/hr
Mass spectrometer	1.0 scc/hr
Pressure decay	2.0 scc/hr

Test comparison is shown below:

<u>Method</u>	<u>Test Time</u>
Radiotracer	12 hr (high and low pressure)
Mass spectrometer	4 hr (high pressure only)
Pressure decay	24 to 96 hr (low pressure only)

These times are in addition to system pressurization which requires the same time in both cases. The pressure decay method is so dependent on environmental temperature stability that it could take as long as 96 hours to determine leak rate.

16.3 OBSERVATORY SHOCK TEST STUDY

The Phase B/C study has shown that the band release test will serve to satisfy the requirements for the simulated booster-induced shock test.

The first alternative is to conduct a simulated shock test as specified in our Phase B/C proposal for the prototype spacecraft. Since this type of test requires a special test setup, it will add one week to the environmental test cycle.

The second alternative is to follow the McDonnell-Douglas proposal (MDAC Delta Spacecraft Design Restraints, DAC-61687) which involves substituting the following sinusoidal vibration test for the qualification shock test:

<u>Frequency (HZ)</u>	<u>Acceleration (g's) (O-P)</u>
100 to 250	1.5 lateral 2.3 thrust
250 to 400	7.5
400 to 2000	15.0

The third alternative is to delete the shock test requirement based on the argument that ERTS is so nearly like OGO structurally that the actual launches of OGO should serve as design qualification with respect to shock.

The accepted approach calls for a separation band release test, using the structural model spacecraft, to determine the resulting shock

spectrum amplitudes and to apply this data instead of the simulated (vehicle-induced) shock test, providing that the band release levels are more severe. If they are not, the band release test can be modified to achieve the required levels by increasing band preloads or the quantity of ordnance charge. In the past, band separation tests have been more severe than the shock spectrum requirement specified by S-320-G-1.

Since a prototype model spacecraft is not proposed, the first alternative is not practical. The second alternative is not considered to be accurately representative of vehicle-induced or operational shocks. The third alternative is not responsive to the requirements of the environmental specifications S-320-G-1, which calls for a shock test during flight acceptance test.

The selected approach is ideally suited to the ERTS program. This method will not lengthen the test schedule because band release and array release tests are normally conducted after vibration anyway.

A separation band release clearance will be performed on the structural model anyway. The effect of the selected approach is that shock instrumentation needs to be included in this test. This method is suggested as an alternative shock test in the GSFC Environmental Specification S-320-G-1.

16.4 THERMAL DEFORMATION CHECKS

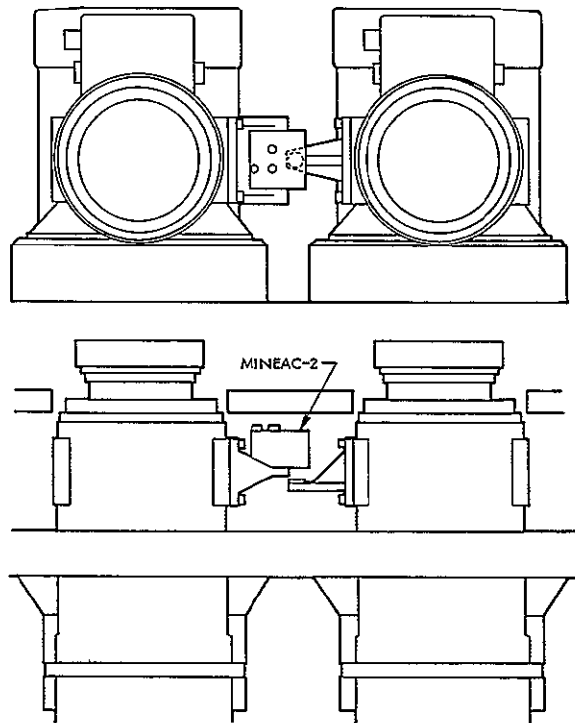
Sensor alignment checks during environmental testing using miniature electronic readout autocollimators have been studied for use in monitoring changes in alignment of sensors during environmental testing and flight. It is concluded that the potential accuracy of the measurements, the small size, and the low power consumption of these autocollimators make their use practical and desirable for thermal-vacuum tests and possible flight instrumentation.

The alignment of the RBV cameras and MSS with respect to the observatory horizon scanners and yaw gyro is critical and must be known within 5 arc second. It is desirable to know whether this alignment changes during thermal stresses on the observatory structure during thermal-vacuum testing, or during flight. Measurement of the relation of alignment of the components during thermal-vacuum testing by

reference to an external instrument, as during installation alignments, is complicated by lack of visibility of the component reference surfaces, and by the unknown thermal effects on any structure intervening between the reference surface and a measuring instrument.

To avoid these problems, it is possible to mount small autocollimators within the observatory to take advantage of the relatively stable and benign environment. The autocollimators occupy a volume of about 1.5 in.³ and weigh approximately 2 ounces. In operation a collimated beam is projected on a mirror on the surface to be measured, with the return image sensed by a photocell. A signal is generated which is proportional to the displacement between the projected beam and the return beam. The range of the units is 3.0 inches, and their accuracy is 1 arc second.

Several arrangements of autocollimators and other optical elements are possible, with the optimum selection depending on the lines of sight available within the observatory, which axes are critical in component alignment, and the accuracies required. One arrangement is shown in Figure 16-1.



To implement this approach, further study is required during Phase D to evaluate the autocollimators in environmental tests, and to determine accuracies with the appropriate optical arrangement. The instruments are currently being evaluated at TRW under company-funded research programs. The results of this program will directly affect the method used on ERTS.

Figure 16-1

AUTOCOLLIMATOR installed on RBV assembly will measure alignment shift in test

16.5 ERTS PAYLOAD STUDY

A study of the ERTS payload was undertaken to obtain information about payload interfaces in support of ERTS integration, test and launch operations.

16.5.1 Multispectral Scanner

Bench performance tests will be conducted on the MSS prior to delivery from Hughes and again after delivery at TRW. The bench test equipment will be supplied by Hughes and will consist of the following:

<u>Description</u>	<u>Function</u>
Scanner test set	Provides scanner power, readouts and commands
Scanner temperature controller	Maintains scanner at required temperature
Collimator, collimator controller, full field source power supply and cooler control	Provides source used in evaluation of the MSS system performance
Space background simulator (ERTS-B)	Calibration reference for Band 5
Tape recorder/reader system	----
Demultiplexer	----

Hughes will provide bench test handling fixtures, drill fixture, shipping containers, and an interface plan defining handling conditions and procedures. TRW will design and fabricate the spacecraft installation handling fixture, the design of which will be coordinated with Hughes and GSFC.

A detailed bench test plan will be generated by Hughes, along with a MSS subsystem test plan for inclusion in the observatory acceptance test plan.

Hughes also will provide personnel to support the installation of the MSS in the spacecraft integration and tests of the MSS.

16.5.2 Return Beam Vidicon

Bench performance tests will be conducted on the three-camera RBV system prior to delivery from RCA and again after delivery at TRW. The equipment, shown in Figure 16-2, will be supplied by RCA. RCA will provide bench test handling fixtures, shipping container and an interface plan defining handling conditions and procedures. TRW will design and fabricate an RBV base plate assembly and handling fixtures. This activity will be coordinated with RCA and GSFC.

A detailed bench test procedure will be generated by RCA.

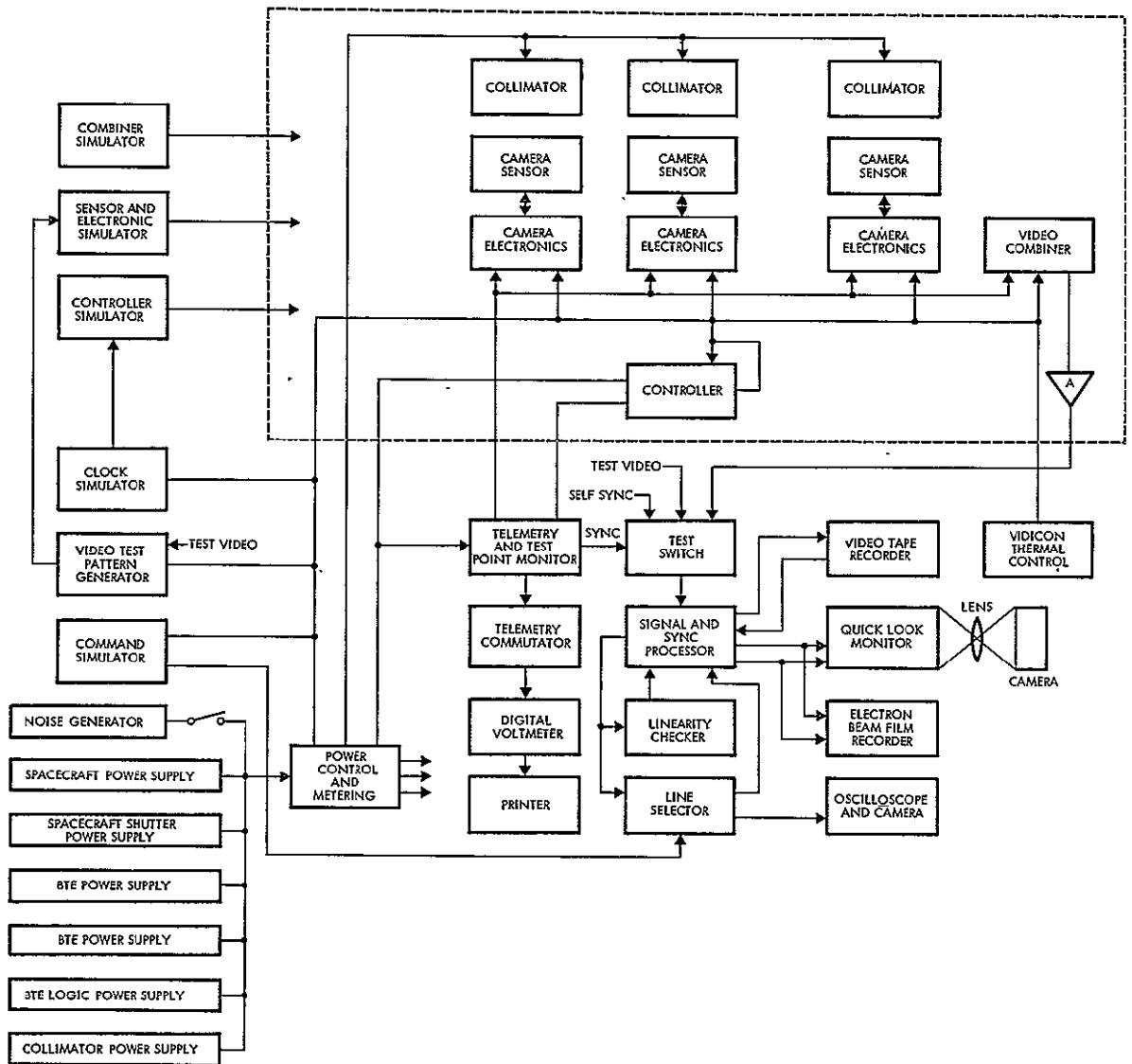


Figure 16-2
BENCH TEST EQUIPMENT block diagram (RBV)

RCA will provide personnel to support installation and all post-installation testing and will provide an RBV subsystem test plan for inclusion in the spacecraft acceptance test plan.

16.6 FUNCTIONS NOT TESTED IN ALL-UP SPACECRAFT TESTING

Study Specification Paragraph 7.12 asks identification of "all spacecraft functions that cannot for any reason be functionally demonstrated." For the purpose of this section, the "all-up" spacecraft is defined as fully assembled such as is evident in later stages of testing, all connections mated for flight, solar array installed, etc. Most of the instances where testing is not complete are directly due to some limitation of the environment and in each case the test not performed on the fully assembled spacecraft is performed at some earlier stage of assembly. This test plan has worked extremely well as evidenced by in-orbit success of OGO spacecraft. In six spacecraft, not a single instance of in-orbit difficulty has resulted from test oversight on the ground.

The areas where testing of the assembled spacecraft is not complete are:

- Full Deployment of Arrays. The arrays cannot be deployed fully because the hinge is not designed to support the weight of the array in a 1-g field. However, the release mechanism is tested subsequent to vibration and in thermal vacuum. The hinge deployment is tested at ambient and at cold conditions early in the test program.
- Horizon Tracker Sensitivity. The horizon tracker functions are fully tested on a partially assembled spacecraft with heated sources in the scanner field of view. This is not feasible with the arrays installed. Absolute sensitivity of the trackers is measured in the laboratory before assembly with the spacecraft. Control of the thermal environment is not precise enough to check sensitivity in the spacecraft area.
- Solar Array Rotation. Because the arrays have to be folded when installed on the spacecraft, rotation is not feasible during vibration, pre-ship system test, and on-stand testing. During the remaining integrated system tests, including thermal vacuum and solar simulation, shaft rotation is tested.
- Solar Array Illumination. Because of the folded configuration of the solar arrays when installed on

the spacecraft, they cannot be fully illuminated thereby preventing illumination tests in the all-up configuration. A solar array spacecraft compatibility test is performed during the integration cycle which proves that the spacecraft can operate from the power obtained from an illuminated array. At this time, the array is not mechanically attached but is connected electrically through the cables.

- Tape Recorder Bit Dropout. Tape recorder bit dropouts cannot be checked in the all-up configuration because of the necessity to have the door open and disconnect flight connectors to connect ground support equipment. This test is performed during the tape recorder bench tests. Tape recorder functional operation is tested by storage and playback of data right up to a few hours before launch.
- VHF Transmitter Radiated Power. Because of the folded configuration of the VHF antenna elements and the folded arrays in close proximity to the antennas, a true radiated power measurement cannot be made. Power measurements are made previously with the elements deployed when the arrays are not installed. In the all-up configuration, power measurements are made via telemetry power monitors. These have been a reliable measure of power output.
- VHF Receiver Sensitivity. A true receiver sensitivity check cannot be made on the VHF command receiver for the same reasons as stated above. During integration phase, hard-line sensitivity measurements are made. All during systems testing, RF link gross sensitivity measurements are made, but due to the noise environment, measurements below -110 db are suspect.
- Deployed Field of View (Horizon Tracker). A deployed field of view check cannot be made in the all-up configuration for two reasons; (1) the solar arrays cannot be deployed for reasons stated above, and (2) the horizon scanners have to be replaced with field of view test heads, thereby necessitating disconnecting flight connectors. During the integration cycle, field of view checks are made by simulating the deployed array envelope.
- Thermal Louver Operation. Proper thermal louver operation is tested during solar simulation. At this time, the observatory is not in the all-up configuration (arrays are simulated) but is as close as practical to the all-up configuration.

The conclusion of this study is that testing is adequately complete-
no new functions added for ERTS are not functionally tested. All of the
above cited conditions are identical to the OGO situation. None con-
stitute a threat to success in orbit.

CONTENTS

	Page
17. GROUND SUPPORT EQUIPMENT	17-1
17.1 Thermal-Vacuum Fixture	17-1
17.2 Observatory Handling Fixture	17-2
17.3 Center of Gravity Fixture	17-3
17.4 Alignment Table Adapter	17-4
17.5 Sensor Installation Equipment	17-4
17.6 ERTS RF Station	17-5
17.7 Test Control Center	17-6
17.8 Peripheral EGSE	17-6
17.9 Launch Site Signal Monitoring	17-7

17. GROUND SUPPORT EQUIPMENT

A study of GSE requirements for ERTS was performed to determine which items of OGO GSE, both mechanical and electrical, could be used on ERTS without modification, which items require modification, and which requirements necessitate new equipment. The items of equipment and the operations studied included the following.

17.1 THERMAL-VACUUM FIXTURE

The requirement for a "coning" sun exposure during solar simulation will be met by designing a new fixture for the TRW 22 x 46 foot chamber.

The direction of sun impingement during solar simulation is the major difference between the requirement placed on the ERTS fixture compared to that for OGO. Relative to the ERTS axes the sun rotates about the Y axis at the +Y end, whereas OGO required illumination only on either Z side and -Y end.

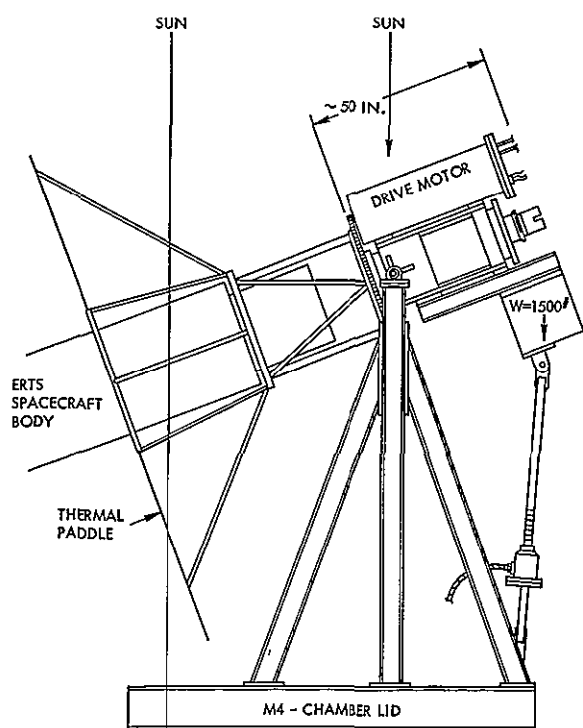
To permit the ERTS simulation, two methods seemed sufficiently promising to warrant study. The first involved installing the observatory in the TRW cylindrical chamber used for OGO 5 and 6. The fixture would be designed to position the observatory with the Y axis at specified angles off the line to the sun simulator in the top of the chamber. The fixture would then rotate the observatory about its Y axis to provide the proper sun aspect. The advantage of this method is a realistic simulation of the solar effect, with a minimization of analytical assumptions. The disadvantages were the design and fabrication of a fixture that would partially invert the observatory and rotate it about two axes, and the increased cost of operation of this chamber over the spherical chamber.

The second method consisted of an extensive modification of the fixture used for OGO 1 and 3. In this method the observatory is suspended from the top of the spherical chamber and xenon lamps are installed in the bottom to illuminate the +Y end. The intensity of the solar simulator in the side of the chamber is adjusted to that of the component

of one sun that would be normal to the observatory sides as the observatory is rotated about its Y axis. Rotation continues in one direction until eclipse, then the observatory is rotated back to the starting point while the sun simulators are off, during eclipse. Primarily because of the requirement for a clear sun view on the +Y end, and the necessity for continuous rotation, the OGO fixture must be modified to include a new support structure and rotation drive, but the basic suspension method and test setup procedures would be the same as for OGO.

The advantages of the second method are a fixture simple to design and fabricate, and no requirement for unusual handling of the observatory. The disadvantage is an analytical assumption about the solar simulation, in that the sides of the observatory are subjected to a normal component of one sun, rather than one sun impinging at an angle to the surface.

It was concluded that the sun simulation in the cylindrical chamber is superior technically, and that the more sophisticated test setup in the cylindrical chamber is justified at an additional cost of approximately \$20,000 for the fixture and \$24,000 per test in chamber operating costs. Figure 17-1 illustrates this chosen approach.



17.2 OBSERVATORY HANDLING FIXTURE

The OGO universal handling fixture (Figure 17-2) will be utilized in observatory integration and test, rather than the horizontal and vertical dollies (Figure 17-3) because of safer erection capability and convenience of roll ring design.

Two sets of handling fixtures were built for OGO, the horizontal

Figure 17-1
FIXTURE FOR THERMAL VACUUM test rotates spacecraft as in orbit.

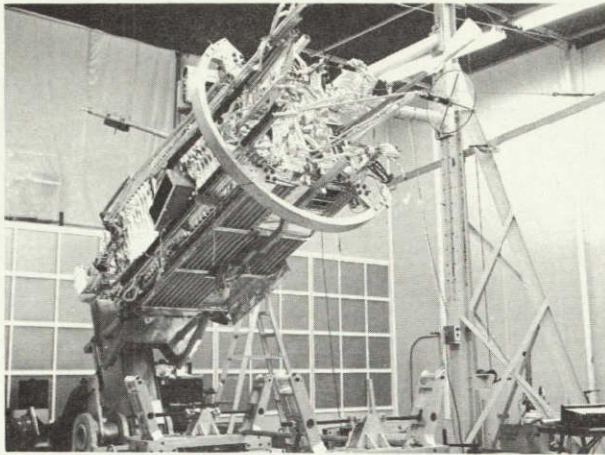


Figure 17-2
OGO UNIVERSAL HANDLING FIXTURE
will be unchanged for ERTS.

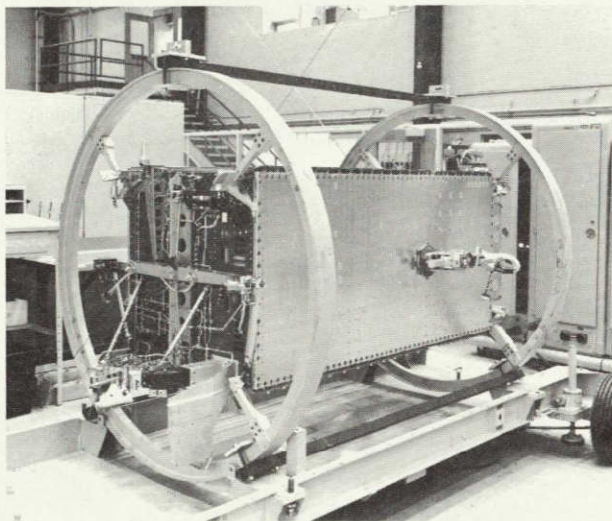


Figure 17-3
HORIZONTAL DOLLY will be retained
for back-up test use.

and vertical dollies at the start of the program and the universal handling fixture after OGO 3. The handling dollies are lighter and more maneuverable, but erection and lowering require the installation of a strongback spanning the length of the observatory, and the handling of that large an item near the observatory involves some risk of damage.

The universal handling fixture is less maneuverable but more stable, and erects and lowers the observatory smoothly in a cantilevered mode. Also the roll-rings used with the universal handling fixture divide in quarters, providing ease of access, which will be required during installation of the multispectral scanner as well as in other instances.

17.3 CENTER OF GRAVITY FIXTURE

The OGO center of gravity fixture (Figure 17-4) will be used on ERTS, rather than taking advantage of a possibly quicker method using spin balance techniques, because a new adapter and new procedures make the change not cost effective.

During 1963, TRW developed equipment and procedures for fast, accurate determination of the center of gravity using a technique of spinning the test article slowly and measuring the inbalance (see Figure 17-5). This technique was studied for use on ERTS, but it is

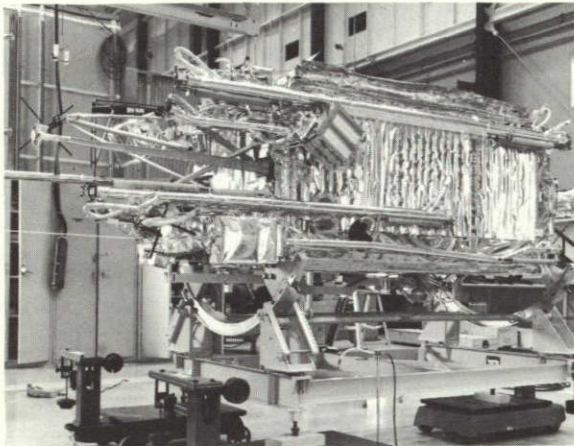


Figure 17-4

CENTER OF GRAVITY FIXTURE will be used for weight and center of gravity determination.

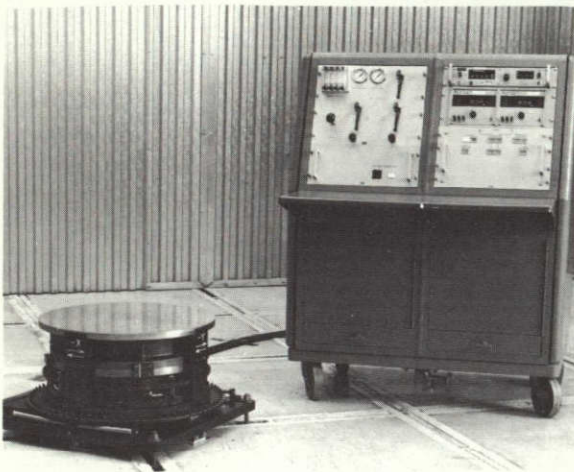


Figure 17-5

CENTER OF GRAVITY test equipment used for small spacecraft will not be used for ERTS.

aid the installation of the sensor assemblies, which weigh over 100 pounds, rather than a floor-supported lifting device, because of simplicity of design and operation. Consideration was given to a rolling or articulated device supported from the floor which would be used to position the sensors while mounting bolts were installed. This technique would have the advantage of positive control of the sensor at all times, but would have the disadvantages of complex design and construction, difficulty in positioning the fixture near the observatory, and complex operation.

concluded that the three-scale method employed on OGO yields sufficiently accurate data, and reduction in test time with the spinning technique would not exceed one day. Since fixtures and procedures for the three-scale method exist, no expenditures for spinning are justified.

17.4 ALIGNMENT TABLE ADAPTER

A new adapter, as shown in Figure 17-6, is required to mount the observatory on a rotary table during alignments. Observatory alignments will be performed in cylindrical coordinates on TRW's alignment facility. This requires the placing of the observatory on a rotary indexing table in the vertical position. A simple structure will be provided to mate with the rotary table and the interface castings.

17.5 SENSOR INSTALLATION EQUIPMENT

Slings will be provided to

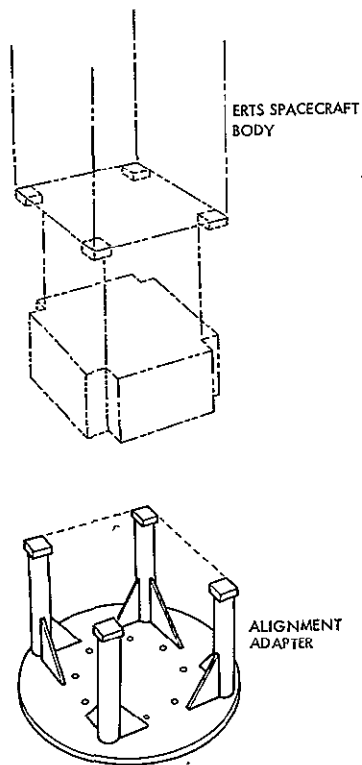


Figure 17-6
PROPOSED ALIGNMENT FIXTURE

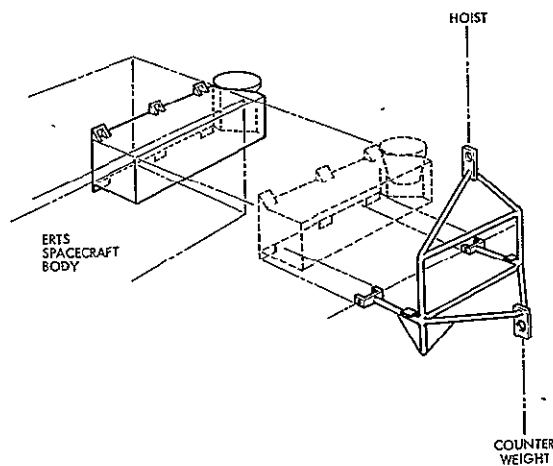


Figure 17-7
HOIST SLING

The design selected is a sling, to be used with the overhead hoist, which is counterbalanced to allow the sensor package to extend horizontally from the hoist cable. This design is simple, easily fabricated and easily used (see Figure 17-7). It does not provide positive control of the sensor position at all times, and its use is subject to hoist availability. These disadvantages are overcome, however, by ordinary spacecraft technician care in handling and planning.

17.6 ERTS RF STATION

When the complement of ERTS radio frequency test equipment was defined, a study was undertaken to see if the OGO test van could be used for the RF station as before. With the addition of the S-band systems to the spacecraft, RF acquisition and data reduction in the system test becomes more complicated. Moreover, line lengths are critical between the receiving electrical GSE and the payload test equipment. It is desirable that distance between the RF receivers and the payload test equipment be kept to a minimum

and that the same cables should be used during all parts of the test program, including tests at the launch site.

Lastly the bulk of test equipment is more than can be housed in the OGO test van. To mount some of the test equipment remotely from the van or the spacecraft conflicts with the goal of keeping all the equipment with short cable runs in a single group. Placing all of the equipment in a group near the spacecraft is the most logical from the standpoints of line length, and accessibility to the payload test equipment.

The conclusion of this study was that all RF test equipment should be located in a functional group in the test area adjacent to the observatory.

17.7 TEST CONTROL CENTER

Test equipment from the CGO test control center that remains applicable to ERTS is most conveniently combined in a new three-bay console. This approach is preferable to adapting the OGO five-bay console to ERTS because of the inefficient use of space thereby entailed in the test area.

Changes required in the control center because the inclusion of the unified S-band command systems and the long command word make the existing configuration for command generation obsolete. Moreover, the status panels in the control center are no longer all applicable. One possible approach is to change the nomenclature on the status lights as required and make minor wiring changes for the new configuration. Alternately, the changes could be accomplished by replacing the command generator and command decoder by blank panels. The third and selected alternative is to lay out a new, smaller console and utilize the equipment needed from the old control center console.

Since the first two alternatives still lead to a needlessly large five-bay console, the third alternative is clearly advantageous for the tests. Since the cost of the new console is not large, a three-bay console has been adopted for two test stations, one for the test talker and the other for the test conductor.

17.8 PERIPHERAL EGSE

Differences between ERTS and OGO in attitude control and ordnance require changes in the test and monitoring equipment used in ground checkout. The deletion of OGO's boom group deployment switches

requires that changes be made in the ordnance monitor panel and additions to the RF subsystems call for changes in the spacecraft control and monitor panel. The best approach appears to be to fabricate two new face panels to be installed on the existing chassis in Rack B of the peripheral electrical ground support equipment. A small amount of re-wiring is required in the attitude control test set so that the rate generator will control the yaw gyro. To rearrange the indicator and switches requires disassembly of the front panel and chassis and unsoldering of the components. It is a simple task, however, once this work is done, to fabricate new face panels with cutouts only for the indicators required. The new face panels could then be reassembled with the switch and indicators needed. All the unused functions are deleted, and that possibility of confusion avoided.

An alternate approach is to leave the panels as they are and change the nomenclature to reflect the new spacecraft functions. This approach would leave all of the switches and indicators on the face of the panels, some of which would have no function, increasing the chance of confusion or error in monitoring or switching. As a consequence it was abandoned.

17.9 LAUNCH SITE SIGNAL MONITORING

At the launch site the spacecraft S-band antennas point in a direction away from RF center at Building 840. Alternate methods for receiving usable S-band data at Building 840 were studied.

One approach would use a plane reflector, approximately 10 by 10 feet mounted on the RF antenna tower adjacent to the launch pad. Exact antenna angles and elevations would be determined during the S-band range checkout during launch site activation. The power budget as follows appears to have adequate margin:

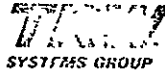
	<u>S-Band</u>	<u>USB</u>
Receive antenna gain (8 ft dish on 450 ft tower), db	+ 32	+ 32
Observatory transmitter power, db	+ 40	+ 27
Observatory antenna gain, db	+ 6	+ 6
Propagation loss (10 mi range), db	-124	-124

	<u>S-Band</u>	<u>USB</u>
Antenna/reflector loss, db	- 10	- 10
Net transmission level, dbm	- 56	- 69
Receive sensitivity (0 db S/N IF), dbm	- 91	- 98
S/N margin, db	+ 35	+ 29

An alternative approach studied is to mount a receiving horn with semi-rigid coax cables connecting to a transmitting antenna in the gantry greenhouse. The receiving horn would be placed in the antenna field and the transmit horn pointed toward Building 840 at South Vandenberg. An alternative is to have a hat or collector over each antenna with a semi-rigid coaxial cable running to dishes on the side of the greenhouse that faces Building 840.

Both of these alternatives require coaxial cabling and horns or dishes to be mounted on the greenhouse. With the gantry pulled back from the pad, the greenhouse system would be of no use. The second method of mounting hats around the antennas could lead to an accident in which an antenna element is bent or broken. Moreover, the test set up would be destroyed when the shroud was installed. Utilizing a reflector away from the greenhouse avoids any need for equipment to be mounted on the gantry and problems when the gantry is moved or when the shroud is installed. It was therefore adopted.

APPENDIX A
PAYLOAD INTERFACE SPECIFICATION



ONE SPACE PARK • REDONDO BEACH, CALIFORNIA

CODE IDENT 11982

TITLE

PAYLOAD INTERFACE
SPECIFICATION
ERTS SPACECRAFT/OBSERVATORY

DATE 1/30/70 NO. D-13504

SUPERSEDING: _____

PRELIMINARY

PREPARED BY: W. Kesler

APPROVAL SIGNATURES:

_____	DATE	<u>RE Russell</u>	DATE
<u>RE Franzen</u>	2/4/70	<u>P. W. Massey</u>	2/4/70
<u>J. H. Gail</u>	2/4/70	<u>T. E. Brown</u>	2-4-70

1.0 SCOPE

This specification establishes interface design requirements for the payload on Earth Resources Technology Satellites A and B.

2.0 APPLICABLE DOCUMENTS

The following documents of the exact issue shown, form a part of this specification to the extent specified herein. In the case of TRW Systems documents, the latest issue shall apply. In the case of conflict between documents referenced here and the detail content of Section 3, the detailed requirements of Section 3 shall be considered the superseding requirement.

SPECIFICATIONSNASA

S-733-P-4 20 September 1968	GSFC specification for Two-Inch Return Beam Vidicon Camera System
--------------------------------	--

S-731-P-100 24 June 1969	GSFC Specification, Multispectral Scanner System
-----------------------------	---

TRW Systems

D-13500	ERTS Spacecraft System
D-13353	Environmental Design Qualification Test - ERTS/Spacecraft
D-13354	Environmental Acceptance Test - ERTS/ Spacecraft

Hughes Aircraft Company

TBD

Interface Specification, Multispectral
Scanner, Flight Equipment Subsystem

DRAWINGS

TRW Systems

C-121199

Interface Control Drawing, ERTS Payload

OTHER DOCUMENTS

Manuals

NASA

Revision 2
December 1967

Nimbus Handbook for Experimenters
(Nimbus D)

3.0 REQUIREMENTS

3.1 Payload Mechanical Interface. The total volume occupied by the payload shall be less than 13 cubic feet. The face of the spacecraft oriented toward the earth (+Z) shall have adequate area for mounting payload sensors. The sensors shall be contained within the spacecraft body structure and shall be mounted on the interior surface of the plates, which form the face, as defined in TRW Systems Specification No. D-13500.

3.1.1 Mounting Adapter Bracket. Payload items designed to the Nimbus Sensory Ring Modular Concept, as defined by Nimbus Handbook for Experimenters, shall be attached to the spacecraft by means of a TRW designed mounting adapter bracket. The bracket, shown in Figure 1, shall be designed to provide mechanical interface between the ERTS spacecraft and the items defined by the Nimbus Sensory Ring Modular Concept.

The mounting adapter bracket shall provide the capability of preloading the payload modules to 144 ± 72 pounds.

The physical location and mechanical mounting interface provided within the spacecraft for all payload items shall be as defined by TRW Systems Drawing No. C-121199.

3.1.2 Payload Weight. As a design goal, the maximum total payload weight including payload harnesses shall be 450 pounds.

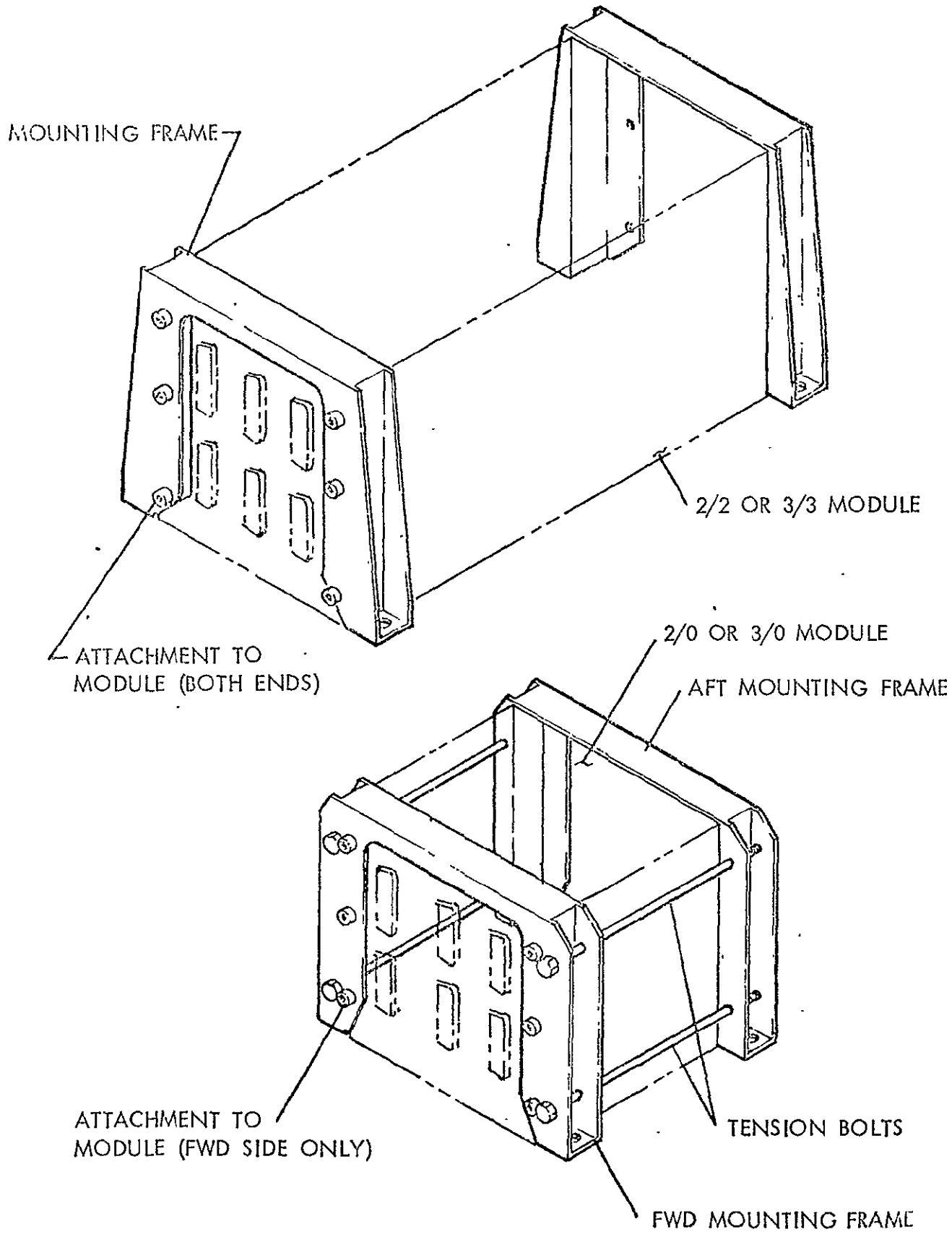


Fig. 1 A-6

3.1.2.1 The allocated weight of the ERTS-A and B payload is defined by Table I.

TABLE I

<u>Payload Item</u>	<u>ERTS - A</u>	<u>ERTS - B</u>
RBV Camera (3)	93.6	93.6
RBV Electronics (3)	36.0	36.0
FBV Camera Controller	7.0	7.0
RBV Video Combiner	9.0	9.0
RBV Baseplate	15.0	15.0
MSS Scanner	105.0	120.0
MSS Multiplexer	9.8	9.8
Video Tape Recorder/ Reproducer and Electronics (2)	136.0	136.0
DCS Receivers (2)	5.0	5.0
DCS Antenna	0.8	0.8
Payload Harnesses	<u>18.0</u>	<u>18.0</u>
TOTAL	435.20	450.20

3.1.3 Accessibility. Payload design shall be such that all electrical connectors, alignment adjustment points, alignment indices, and test points are accessible when the spacecraft \pm Z doors are open. Test connectors and calibration and/or simulation openings in payload assemblies shall be located so they are accessible when the spacecraft/observatory is in the folded configuration.

3.1.4 Alignment. Payload sensors which must be aligned, or whose alignment relative to the spacecraft axes must be defined, shall incorporate alignment surfaces or indices provided by the Payload Contractor.

For items requiring alignment with respect to all three axes, two mutually perpendicular alignment surfaces shall be provided. For alignment with respect to two axes, one surface shall be sufficient. These surfaces shall be visible when the item is installed in the spacecraft. Detailed requirements shall be coordinated with each Payload Contractor. Sensor/spacecraft/observatory alignment shall be provided to 0.1 degree or better, when required.

3.1.5 Field of View. The spacecraft shall provide an unobstructed Earth looking field of view as defined in NASA Specification No. S-731-P-100 and NASA Specification No. S-733-P-4 for the Multi Spectral Scanner and Return Beam Vidicon cameras respectively.

3.1.6 Shape of Openings. Openings required by payload sensors may have any shape which does not compromise the structural integrity or the gas sealing capability of any portion of the spacecraft. The Payload Contractor shall provide a protective cover for sensor openings. The cover shall be red and have provisions to allow for ease of installation and removal. Labeling shall include payload assembly identification and the words "non-flight" or "remove before flight".

3.1.7 Gas Seals. As a design goal, gas seals shall be provided around payload sensor openings to minimize the possibility of contamination to optics or other exposed surfaces of sensors, if required.

3.1.8 Mounting Base Flatness. Mounting surface interfaces for both payload and spacecraft shall be flat within ± 0.005 inches.

3.1.9 Uncompensated Momentum. To maintain Multi-Spectral Scanner relative picture error to 100 feet or less per 25 second period, allowable payload steady state uncompensated momentum shall not be greater than:

Roll Axis (Y-Y):	0.0002 Ft-Lb-Seconds
Pitch Axis (X-X):	0.0004 Ft-Lb-Seconds
Yaw Axis (Z-Z):	0.0005 Ft-Lb-Seconds

3.2.1 Payload Power.

3.2.1.1 Average Power. Spacecraft provided power allocated to the payload shall be at least 75 watts per orbital period.

3.2.1.2 Maximum Power. The maximum regulated bus power provided by the spacecraft to the payload shall be 400 watts, and provide capability to accept transients to 600 watts. On the unregulated negative bus, the spacecraft shall provide up to 5 watts of power, together with a transient load of up to 18 amperes, for 0.1 second.

3.2.1.3 Payload Input Power. The spacecraft system bus voltage shall be $28 \begin{smallmatrix} +5.5 \\ -4.5 \end{smallmatrix}$ vdc. Power inputs to the payload may be supplied from the positive spacecraft/observatory unregulated and unfiltered power source.

Primary payload power shall be supplied from a regulated negative power converter assembly consisting of 2 converters with the following characteristics for each:

Output Voltage:	Minus 24.5 \pm 0.5 vdc
Output Current:	0 to 12.5 amperes
Output Impedance:	Less than or equal to 0.07 Ohms over Frequency Range of DC to 1 kHz Less than or equal to 0.30 Ohms over Frequency Range of 1 kHz to 50 kHz

A battery shall be supplied to provide minus 24 to minus 35 vdc source power for the RBV camera shutter assembly.

3.2.2 Payload Harnesses. The spacecraft shall provide the required electrical harnesses between payload assembly interfaces and spacecraft subsystems. The spacecraft shall provide inter-payload assembly harnesses, as required.

3.2.3 Commands. A total of 160 commands shall be provided by the spacecraft for use by the payload. Thirty-two of these commands shall be available for use with the stored command programmer or used in real time. A payload command relay shall be energized by the simultaneous occurrence of a negative going voltage pulse on an "A" matrix line and a positive going pulse on a "B" matrix line.

The command lines to the payload shall be energized for 50 to 65 milliseconds upon activation of the command. The open-circuit energized output voltage of the "A" command lines shall be minus 24.0 \pm 1.0 vdc with a source impedance of 2 ohms, or less. The

energized open circuit output voltage of the "B" command lines shall be zero \pm 0.5 volts with a source impedance of 2 ohms, or less. These polarities are reversed for non-energized lines.

3.2.4 Timing Signals. Timing signals with the following characteristics at the source shall be supplied to the payload:

- (a) Frequencies available: 1.6 MHz, 50 kHz, and 1 Hz.
- (b) Accuracy of frequencies: One part in 10^6 for one year.
- (c) Waveform: Coherent square wave.
- (d) True Amplitude: 5.25 ± 0.75 volts at no-load and 1.3 ± 0.3 , minus 0.2 volts for a 600 ohm load.
- (e) False Amplitude: $0.2 \begin{matrix} +0.10 \\ -0.15 \end{matrix}$ vdc at no-load and 600 ohm loads.
- (f) Fault Protection: Maximum permissible DC fault voltage applied to a timing signal output line shall be between ± 30 volts.

3.2.5 Coded Clock. The spacecraft coded clock signal shall be provided to both video tape recorders simultaneously as three words within the narrowband PCM telemetry format. These three words shall consist of 25 bit binary coded time. Clock update shall be synchronous with PCM telemetry data and shall occur once every 1.152 seconds.

3.2.5.1 Input Signal Characteristics. The telemetry signals shall consist of two-level rectangular waveform, the levels being designed "true" and "false". Transmission of "true" followed by "false" represents a one bit in the PCM format and "false" followed by "true" represents a zero.

3.2.5.2 Symmetry and Jitter. The duration of a "true" and a "false" level during a bit shall be 50 ± 5 percent of a bit period. Jitter (bit time variation) shall be less than five percent of nominal bit width.

3.2.5.3 Level Amplitudes. "True" level shall be 1.5 vdc into a 600 ohm load. "False" level shall be zero to plus 0.3 vdc no-load and with 600 ohm load.

3.2.5.4 Rise and Fall Times. Rise and fall times (10 percent to 90 percent of actual peak amplitude) shall be 1.0 microsecond maximum, respectively.

3.2.5.5 Fault Voltage. The maximum permissible DC fault voltage applied to a coded clock output shall be between ± 30 vdc.

3.2.6 Telemetry Interfaces.

3.2.6.1 Narrowband Telemetry System. The narrowband telemetry system shall include two identical equipment groups, designated Equipment Group One and Equipment Group Two. Each equipment group shall consist of an analog data handling assembly and a digital data handling assembly. Under normal conditions, Equipment Group One shall be assigned to the handling of real time telemetry data and Equipment Group Two to the handling of recorded data, however, their functions may be interchanged by ground command.

The bit rates of the narrowband telemetry shall be:

<u>Real Time</u>	<u>Data Storage</u>
1 or 32 kbps	1 kbps

The two equipment groups shall be synchronized with respect to main commutator word sampling. Subcommutator word sampling shall be synchronous only with respect to the complete subcommutator frame cycle (i. e., at initial turn-on of an equipment group, the particular subcommutator word which is first sampled is random.)

3.2.6.2 Bi-Level Telemetry Inputs. Bi-level (discrete) input gating shall be provided for multiplexing of single-bit digital data (such as relay on-off levels) by the telemetry equipment groups. Control signals shall not be provided to sources which use bi-level gating. Sources which use bi-level gating shall have a telemetry output as follows:

$$\text{Minus } 10 \text{ V} \leq V_{\text{ON}} \leq \text{Minus } 5 \text{ V}$$

$$\text{Minus } 1.0 \text{ V} \leq V_{\text{OFF}} \leq \text{Zero}$$

The source impedance in the ON condition will be one megohm or less; in the OFF condition, 50,000 ohms or less. Under fault conditions, bi-level inputs shall not exceed minus 25 or plus 0.8 vdc.

3.2.6.3 Negative Analog Telemetry Inputs.

3.2.6.3.1 Output Voltage. The analog output signal shall be negative only and shall lie in the zero to minus 6.375 vdc range.

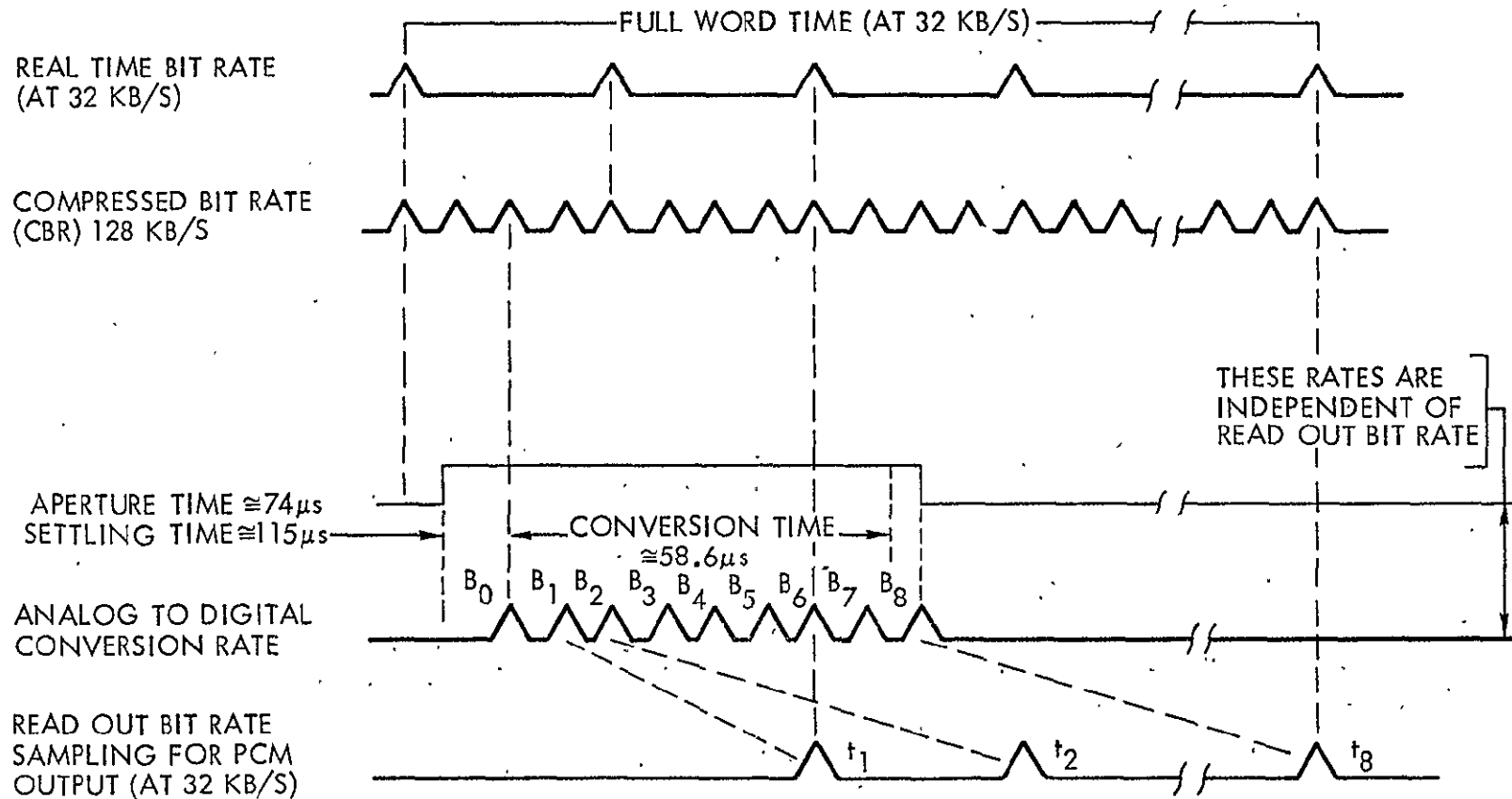
3.2.6.3.2 Output Impedance. When a separate output line to each equipment group is used for each analog data output, the output impedance shall be less than 8000 ohms resistive and less than 50 picofarads capacitive for one percent accuracy. Under certain conditions (e.g. high output capacitance) higher output resistances may be used.

3.2.6.3.3 Signal Output Lines. A single output line to both equipment groups or isolated output lines to each equipment group may be used, however, crosstalk may occur for the single line approach depending upon analog data output impedance.

3.2.6.3.4 Sample Duration. The analog data shall be sampled for a conversion time not to exceed 73 microseconds. (Refer to Figure 1 for the timing diagram for sampling of analog outputs.)

3.2.6.3.5 Signal Sample Current. The analog payload output shall be able to supply a current of at least 10 microamperes at the time of comparison without suffering degradation in calibration or performance when connected to one equipment group. A current of at least 20 microamperes shall be similarly accommodated when an analog output is connected to both equipment groups.

The analog payload output shall also be able to supply a worst case current surge of six milliamperes (12 milliamperes when connected to both equipment groups) commencing at the start of the aperture time (see Figure 2) without degradation. A transient current of this magnitude may be required prior to actual analog signal conversion (during settling time).



THIS EXAMPLE ILLUSTRATES LOGIC TIMING FOR THE MAX REAL TIME BIT RATE OF 32KB/S

Figure 2

3.2.6.3.6 Wire Type. Analog data output signals shall be transmitted from the payload to the analog data handling assembly on miniature coaxial cable. The analog signal return shall be through circuit ground.

3.2.6.3.7 Fault Voltage. Maximum permissible D.C. fault voltage applied to an analog data output line shall be between 33.5 vdc and minus 33.5 vdc.

3.2.6.4 Positive Analog Telemetry Inputs. Positive analog telemetry inputs and spacecraft telemetry equipment interfaces, for negative analog telemetry inputs, shall be as defined in Paragraph 3.2.6.3 except for the following:

3.2.6.4.1 Output Voltage. The analog output signal shall be positive only and shall lie in the zero to plus 5.120 vdc range.

3.2.6.4.2 Output Impedance. When a separate analog data output line to each equipment group is used for each analog data output, the output impedance shall be less than 1000 ohms resistive and less than 100 picofarads capacitive for eight bit quantization accuracy.

3.2.6.5 Video S-Band Telemetry Interface.

3.2.6.5.1 Multi Spectral Scanner. The Multi Spectral Scanner shall provide a twisted-pair data input, a twisted-pair clock input and a twisted-pair word rate input to the channel switching assembly at a nominal data rate of approximately 15 Megabits. The logic levels shall be:

One 3.0 to 5.0 Milliamps into 50 Ohms

Zero 0.0 to 0.1 Milliamps into 50 Ohms

One wire of the twisted pair shall provide the levels above while the other provides the logical complement. The data format shall be NRZ. The clock signal shall be a square wave at the bit rate frequency, and the word rate signal shall be a square wave at 1/6 the bit rate frequency.

The wideband telemetry assembly shall provide an output modulation index of 0.65 ± 10 percent with the data input.

3.2.6.5.2 Return Beam Vidicon. The Return Beam Vidicon shall provide to the channel switching assembly a four MHz bandwidth analog input signal with a voltage swing from 0.0 ± 0.05 vdc to minus 1.65 ± 0.1 vdc with a 50 ohms impedance.

The wideband telemetry assembly shall provide modulation index of 1.5 ± 20 percent for this signal.

3.2.6.5.3 Video Tape Recorder. The Video Tape Recorders shall provide recorded versions of the Multi Spectral Scanner and the Return Beam Vidicon video signals. Impedance and voltage characteristics shall be TBD. The output modulation characteristics shall simulate the real-time signal modulations as closely as possible.

3.2.6.6 Unified S-Band Telemetry Interface.

3.2.6.6.1 Data Collection System. The Data Collection System shall provide to the baseband assembly a signal with the following characteristics

Voltage: 1.0 V rms \pm 10 percent
Bandwidth: 15 Hz to 135 kHz
Impedance: 600 Ohms

The Data Collection System will be modulated on the 1.024 MHz subcarrier.

3.2.6.6.2 Video Tape Recorder Auxiliary Channels. The Video Tape Recorder Number One and Video Tape Recorder Number Two shall provide one kHz narrowband telemetry housekeeping data to the Unified S-Band base-band assembly for modulation on subcarrier frequencies of 165 kHz and 225 kHz respectively. Signal characteristics shall be (TBD).

3.3 Environmental Conditions. The payload shall be designed to withstand the environmental conditions specified in TRW Systems Specification Nos. D-13353 and D-13354.

3.4 Thermal Interfaces.

3.4.1 Interface Requirements. The thermal interface between the spacecraft/observatory subsystems and the payload shall be as follows:

- (a) Maximum heat dissipation (power density) for each payload assembly mounted on panels under an active louver control shall be less than 0.22 watts per square inch of the payload mounting surface.
- (b) Maximum heat dissipation for each payload assembly mounted on panels covered with insulation or mounted to the interior structure of the spacecraft, shall be less than 0.08 watts per square inch of the payload mounting surface.

- (c) For each payload sensor with a view port at 20°C average temperature during normal operation, the heat energy flow out through the opening shall be greater than the energy flow in.
- (d) The mean energy input to an opening facing the earth (+Z panel) per one orbit shall be considered to be:

Solar Energy: 74 BTU/Hr-Ft²

Earth Emission: 52 BTU/Hr-Ft²

3.4.2 Operating Temperatures. Payload assemblies (components) contained within the main body of the spacecraft/observatory will be mounted on flat panels, except for the Multi Spectral Scanner and the items defined in paragraph 3.1.1 which are mounted to the bracket shown in Figure 1. The mounting panel temperatures at the periphery of the payload modules and the mean radiation environment temperatures shall be controlled to 20±10°C. The environment shall be regarded as having an infrared emittance of 0.80.

3.4.3 Design Qualification Temperatures. Payload assemblies (components) within the spacecraft/observatory shall be designed to be capable of operating in a temperature environment of zero to plus 40°C.

3.4.4 Surface Coatings. The external surface of payload assemblies (components) that contact spacecraft radiating panels shall be electrically conducting. Examples of non-corrosive surface coatings which meet this requirement include:

Aluminum: Alodine 600

Magnesium: Dow 23

Remaining surfaces shall be treated or coated to be thermally black and have an emittance of not less than 0.72 at a temperature of 18°C.

4.0 Not Applicable

5.0 Not Applicable

6.0 Notes

NIMBUS Sensory Ring Modules (concept)

- 1 Camera Controller
- 3 Camera Electronics
- 1 Video Combiner

APPENDIX B
DESIGN ANALYSIS REPORT

PREPARED D. G. Cross 1/20/70 REPORT NO. _____
CHECKED _____
MODEL ERTS B/C Study

PAGE _____

DESIGN ANALYSIS REPORT
APPENDIX

STRUCTURAL AND DYNAMIC ANALYSIS

The ERTS structure has been reviewed for its ability to withstand launch and orbital environments successfully. An on-line structural analysis program has been used to obtain member loads in the primary interstage and box structure, and to obtain modal frequencies of the structure. Modal analysis was completed for the basic OGO interstage and for a modified interstage design with diagonals added between adjacent bipod pairs to reduce interstage warping under lateral loads. The critical design limit load condition for the primary structure is the burnout condition of 10.1 G axial compression together with a 2.0 G +X/+Z lateral load. The bipod legs and separation system will require some redesign.

Side panels for the box are proposed as .600 in. thick honeycomb to support on-board equipment. Strength and stiffness are adequate to support the equipment masses during dynamic loading, and to prevent modal coupling with the primary structure (Modal frequency above 100 Hz).

Thermal distortions have been estimated for the MSS Scanner, RBV Camera, Horizon Scanners, and Yaw Gyro. Relative displacements between any two sensitive instruments are well within the requirement of 0.10 degrees-of-arc for all orbital thermal conditions.

Secondary structures for MSS Scanner and RBV Camera mounting have been sized and compared. Channel longerons have been selected for the MSS Scanner, and a secondary honeycomb panel for the RBV Cameras in order to provide sufficient stiffness to maintain local modal frequencies above 25 Hz.

The solar paddle structural frame has been modeled on the AS 147 Computer Program to determine modal frequencies, mode shapes, and dynamic responses to sinusoidal qualification vibration. Results are satisfactory in terms of expected frequencies and accelerations relative to the OGO paddle.

**STRUCTURAL ANALYSIS -
PRIMARY BOX & INTERSTAGE**

STATIC ANALYSIS - RUN 1.1

MEMBER DESC.	CRIT. COND.	P LIM.	P ULT	P ALL	M.S.
1. BIPOD LEG	4: BURNOUT	3790	5680	5050*	*
2. BOX LOWER EDGE	" "	300	450	540	+ .20
3. BOX LOW. DIAG.	" "	332	497	3520	Hi
4. BOX CORNER VERT.	5: X/2 "	1770	2658	15600	Hi

BURNOUT:
- 10.1g AX.
± 2.0g LAT.
LIMIT
@ 1500 LB

* Bipod leg is critical in flange crippling. Ultimate capability is really somewhat higher in post-buckling strength. However, thicknesses will be increased for the ERTS bipod leg to prevent flange crippling.

DYNAMIC ANALYSIS - RUN 1.2 & 1.3

MODE & DESCR.	FREQUENCY, Hz	
	RUN 1.2 OGO INTERST.	RUN 1.3 BIPOD DIAGS.
1. First Lateral	15.9	16.1
2. First Torsion	31.8	38.4
3. Second Lateral	34.9	52.0 †
4. First Axial	54.7	56.3
5. First Box Shear	57.3	77.7

† Second lateral mode of the spacecraft can be significantly increased by including diagonal bracing between adjacent bipod braces, thereby reducing the amount of diagonal warping of the interstage truss.

LOADING CASE NO. 1 CLASS 1

JOINT	F1		F2		F3	
14	.0000E	0	-.1333E	4	.0000E	0
15	.0000E	0	-.1333E	4	.0000E	0
16	.0000E	0	.1333E	4	.0000E	0
17	.0000E	0	.1333E	4	.0000E	0

STATIC ANALYSIS

F4 F5 F6

UNIT +Z MOMENT
M = 80000 IN-LB

LOADING CASE NO. 2 CLASS 1

JOINT	F1		F2		F3	
9	.5000E	3	.0000E	0	.0000E	0
10	.5000E	3	.0000E	0	.0000E	0
11	.5000E	3	.0000E	0	.0000E	0
12	.5000E	3	.0000E	0	.0000E	0

F4 F5 F6

UNIT +X SHEAR
V = 2000 LB

LOADING CASE NO. 3 CLASS 1

JOINT	F1		F2		F3	
14	.0000E	0	.1250E	4	.0000E	0
15	.0000E	0	.1250E	4	.0000E	0
16	.0000E	0	.1250E	4	.0000E	0
17	.0000E	0	.1250E	4	.0000E	0

F4 F5 F6

UNIT -Y COMPR.
P = 5000 LB

LOADING CASE NO. 4 CLASS 1 CRITICAL

JOINT	F1		F2		F3	
14	.7500E	3	.3800E	4	.0000E	0
15	.7500E	3	.3800E	4	.0000E	0
16	.7500E	3	.3800E	4	.0000E	0
17	.7500E	3	.3800E	4	.0000E	0

F4 F5 F6

ERTS BURNOUT
10.1 g -Y AX
2.0 g +X LAT

LOADING CASE NO. 5 CLASS 1 CRITICAL

JOINT	F1		F2		F3	
14	.5310E	3	.3800E	4	.5310E	3
15	.5310E	3	.3800E	4	.5310E	3
16	.5310E	3	.3800E	4	.5310E	3
17	.5310E	3	.3800E	4	.5310E	3

F4 F5 F6

ERTS BURNOUT
10.1 g +Y AX
2.0 g +X/+Z LAT

LOADING CASE NO. 6 CLASS 1

JOINT	F1		F2		F3	
14	.7500E	3	-.9370E	3	.0000E	0
15	.7500E	3	-.9370E	3	.0000E	0
16	.7500E	3	-.9370E	3	.0000E	0
17	.7500E	3	-.9370E	3	.0000E	0

F4 F5 F6

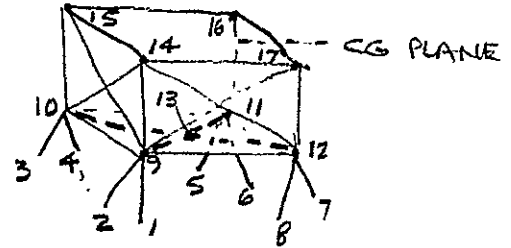
ERTS LIFTOFF
-2.5 g -Y AX
2.0 g +X LAT

BEGINNING INVERSION OF STIFFNESS MATRIX
U COMPUTED
U INVERSE COMPUTED
INVERSION COMPLETE

JOINT DEFLECTIONS

JOINT	X1	X2	X3	X4	X5	X6
1	.0000E 0	.0000E 0	.0000E 0			
2	.0000E 0	.0000E 0	.0000E 0			
3	.0000E 0	.0000E 0	.0000E 0			
4	.0000E 0	.0000E 0	.0000E 0			
5	.0000E 0	.0000E 0	.0000E 0			
6	.0000E 0	.0000E 0	.0000E 0			
7	.0000E 0	.0000E 0	.0000E 0			
8	.0000E 0	.0000E 0	.0000E 0			
9	.1460E-1	.1492E-1	.2600E-2			
10	.1460E-1	.1492E-1	-.2600E-2			
11	.1550E-1	.2359E-1	.3505E-2			
12	.1550E-1	.2359E-1	-.3505E-2			
13	.1810E-1	.0000E 0	-.9038E-11			
14	.3773E-1	.2459E-1	-.3222E-2			
15	.3773E-1	.2459E-1	.3222E-2			
16	.4666E-1	.4789E-1	.5714E-2			
17	.4666E-1	.4789E-1	-.5714E-2			

RUN 1.1
STATIC



MEMBER LOADS

MEM	JT.	F1	F2	F3	F4	F5	F6
1	1	.1774E 4	.0000E 0	.0000E 0			
	9	-.1774E 4	.0000E 0	.0000E 0			
2	2	.7168E 3	.0000E 0	.0000E 0			
	9	-.7168E 3	.0000E 0	.0000E 0			
3	3	.7168E 3	.0000E 0	.0000E 0			
	10	-.7168E 3	.0000E 0	.0000E 0			
4	4	.1774E 4	.0000E 0	.0000E 0			
	10	-.1774E 4	.0000E 0	.0000E 0			
5	5	.2733E 4	.0000E 0	.0000E 0			
	11	-.2733E 4	.0000E 0	.0000E 0			
6	6	.3790E 4	.0000E 0	.0000E 0			
	11	-.3790E 4	.0000E 0	.0000E 0			
7	7	.3790E 4	.0000E 0	.0000E 0			
	12	-.3790E 4	.0000E 0	.0000E 0			
8	8	.2733E 4	.0000E 0	.0000E 0			
	12	-.2733E 4	.0000E 0	.0000E 0			
9	9	.2219E 3	.0000E 0	.0000E 0			
	10	-.2219E 3	.0000E 0	.0000E 0			
10	10	.3860E 2	.0000E 0	.0000E 0			
	11	-.3860E 2	.0000E 0	.0000E 0			
11	11	.2991E 3	.0000E 0	.0000E 0			
	12	-.2991E 3	.0000E 0	.0000E 0			
12	12	.3860E 2	.0000E 0	.0000E 0			
	9	-.3860E 2	.0000E 0	.0000E 0			
13	9	.3317E 3	.0000E 0	.0000E 0			
	13	-.3317E 3	.0000E 0	.0000E 0			
14	13	.3317E 3	.0000E 0	.0000E 0			
	11	-.3317E 3	.0000E 0	.0000E 0			
15	10	.3317E 3	.0000E 0	.0000E 0			
	13	-.3317E 3	.0000E 0	.0000E 0			

BIPOD LEG
MAX LIMIT

Box LOWER EDGE
MAX LIMIT

Box LOWER DIAG.
MAX LIMIT
(Same as Case 5)

16	13	-.3317E	3	.0000E	0	.0000E	0
	12	.3317E	3	.0000E	0	.0000E	0
17	9	.6258E	3	.0000E	0	.0000E	0
	14	-.6258E	3	.0000E	0	.0000E	0
18	10	.6258E	3	.0000E	0	.0000E	0
	15	-.6258E	3	.0000E	0	.0000E	0
19	11	.1573E	4	.0000E	0	.0000E	0
	16	-.1573E	4	.0000E	0	.0000E	0
20	12	.1573E	4	.0000E	0	.0000E	0
	17	-.1573E	4	.0000E	0	.0000E	0
21	9	.6673E	3	.0000E	0	.0000E	0
	17	-.6673E	3	.0000E	0	.0000E	0
22	12	.2934E	4	.0000E	0	.0000E	0
	14	-.2934E	4	.0000E	0	.0000E	0
23	10	.1299E	4	.0000E	0	.0000E	0
	14	-.1299E	4	.0000E	0	.0000E	0
24	9	.1299E	4	.0000E	0	.0000E	0
	15	-.1299E	4	.0000E	0	.0000E	0
25	11	<u>.2934E</u>	<u>4</u>	.0000E	0	.0000E	0
	15	-.2934E	4	.0000E	0	.0000E	0
26	10	.6673E	3	.0000E	0	.0000E	0
	16	-.6673E	3	.0000E	0	.0000E	0
27	12	.2303E	4	.0000E	0	.0000E	0
	16	-.2303E	4	.0000E	0	.0000E	0
28	11	.2303E	4	.0000E	0	.0000E	0
	17	-.2303E	4	.0000E	0	.0000E	0
29	14	-.8593E	3	.0000E	0	.0000E	0
	15	.8593E	3	.0000E	0	.0000E	0
30	15	-.1191E	4	.0000E	0	.0000E	0
	16	.1191E	4	.0000E	0	.0000E	0
31	16	<u>-.1524E</u>	<u>4</u>	.0000E	0	.0000E	0
	17	.1524E	4	.0000E	0	.0000E	0
32	17	-.1191E	4	.0000E	0	.0000E	0
	14	.1191E	4	.0000E	0	.0000E	0

Box SIDE PANEL DIAG.
 (Almost max limit, -25 lb)

Box UPPER EDGE (Midplane)
 Max LIMIT

JOINT EQUILIBRIUM CHECK

JOINT	F1	F2	F3	F4	F5	F6
1	-.2077E	3	-.1496E	4	.9306E	3
2	.3761E	3	-.6044E	3	-.8394E	2
3	.3761E	3	-.6044E	3	.8394E	2
4	-.2077E	3	-.1496E	4	-.9306E	3
5	.3201E	3	-.2304E	4	-.1434E	4
6	-.1988E	4	-.3196E	4	.4438E	3
7	-.1988E	4	-.3196E	4	-.4438E	3
8	.3201E	3	-.2304E	4	.1434E	4
9	.7991E-	6	.1863E-	7	.6370E-	6
10	.4210E-	6	.6277E-	6	.5178E-	6
11	.8196E-	6	.1051E-	5	.4098E-	6
12	.3949E-	6	.9090E-	6	-.2086E-	6
13	-.1461E-	5	.0000E	0	-.1045E-	5
14	.7500E	3	.3800E	4	-.7302E-	6
15	.7500E	3	.3800E	4	-.8568E-	7
16	.7500E	3	.3800E	4	-.5960E-	7
17	.7500E	3	.3800E	4	-.2012E-	6

JOINT DEFLECTIONS

JOINT	X1	X2	X3	X4	X5	X6
1	.0000E 0	.0000E 0	.0000E 0			
2	.0000E 0	.0000E 0	.0000E 0			
3	.0000E 0	.0000E 0	.0000E 0			
4	.0000E 0	.0000E 0	.0000E 0			
5	.0000E 0	.0000E 0	.0000E 0			
6	.0000E 0	.0000E 0	.0000E 0			
7	.0000E 0	.0000E 0	.0000E 0			
8	.0000E 0	.0000E 0	.0000E 0			
9	.1237E- 1	.1311E- 1	.1237E- 1			
10	.8043E- 2	.1925E- 1	.8947E- 2			
11	.1327E- 1	.2539E- 1	.1327E- 1			
12	.8947E- 2	.1925E- 1	.8043E- 2			
13	.1282E- 1	.0000E 0	.1282E- 1			
14	.2629E- 1	.1974E- 1	.2629E- 1			
15	.2452E- 1	.3624E- 1	.3346E- 1			
16	.3522E- 1	.5274E- 1	.3522E- 1			
17	.3346E- 1	.3624E- 1	.2452E- 1			

MEMBER LOADS

MEM	JT.	F1	F2	F3	F4	F5	F6
1	1	.8259E 3	.0000E 0	.0000E 0			
	9	-.8259E 3	.0000E 0	.0000E 0			
2	2	.8259E 3	.0000E 0	.0000E 0			
	9	-.8259E 3	.0000E 0	.0000E 0			
3	3	.1505E 4	.0000E 0	.0000E 0			
	10	-.1505E 4	.0000E 0	.0000E 0			
4	4	.3002E 4	.0000E 0	.0000E 0			
	10	-.3002E 4	.0000E 0	.0000E 0			
5	5	<u>1.3681E 4</u>	<u>.0000E 0</u>	<u>.0000E 0</u>			
	11	-.3681E 4	.0000E 0	.0000E 0			
6	6	.3681E 4	.0000E 0	.0000E 0			
	11	-.3681E 4	.0000E 0	.0000E 0			
7	7	.3002E 4	.0000E 0	.0000E 0			
	12	-.3002E 4	.0000E 0	.0000E 0			
8	8	.1505E 4	.0000E 0	.0000E 0			
	12	-.1505E 4	.0000E 0	.0000E 0			
9	9	.1458E 3	.0000E 0	.0000E 0			
	10	-.1458E 3	.0000E 0	.0000E 0			
10	10	-.2230E 3	.0000E 0	.0000E 0			
	11	.2230E 3	.0000E 0	.0000E 0			
11	11	-.2230E 3	.0000E 0	.0000E 0			
	12	.2230E 3	.0000E 0	.0000E 0			
12	12	.1458E 3	.0000E 0	.0000E 0			
	9	-.1458E 3	.0000E 0	.0000E 0			
13	9	<u>-.3317E 3</u>	<u>.0000E 0</u>	<u>.0000E 0</u>			
	13	.3317E 3	.0000E 0	.0000E 0			
14	13	-.3317E 3	.0000E 0	.0000E 0			
	11	.3317E 3	.0000E 0	.0000E 0			
15	10	-.3317E 3	.0000E 0	.0000E 0			

BIPOD LEG
 (Almost Max Limit, -110 lb)

Box Lower Dmg.
 MAX LIMIT
 (Same as Case 4)

	13	.3317E	3	.0000E	0	.0000E	0
16	13	-.3317E	3	.0000E	0	.0000E	0
	12	.3317E	3	.0000E	0	.0000E	0
17	9	.4288E	3	.0000E	0	.0000E	0
	14	.4288E	3	.0000E	0	.0000E	0
18	10	.1099E	4	.0000E	0	.0000E	0
	15	-.1099E	4	.0000E	0	.0000E	0
19	11	<u>.1770E</u>	<u>4</u>	<u>.0000E</u>	<u>0</u>	<u>.0000E</u>	<u>0</u>
	16	-.1770E	4	.0000E	0	.0000E	0
20	12	.1099E	4	.0000E	0	.0000E	0
	17	-.1099E	4	.0000E	0	.0000E	0
21	9	.6428E	3	.0000E	0	.0000E	0
	17	-.6428E	3	.0000E	0	.0000E	0
22	12	.2248E	4	.0000E	0	.0000E	0
	14	-.2248E	4	.0000E	0	.0000E	0
23	10	.2248E	4	.0000E	0	.0000E	0
	14	-.2248E	4	.0000E	0	.0000E	0
24	9	.6428E	3	.0000E	0	.0000E	0
	15	-.6428E	3	.0000E	0	.0000E	0
25	11	<u>.2959E</u>	<u>4</u>	<u>.0000E</u>	<u>0</u>	<u>.0000E</u>	<u>0</u>
	15	-.2959E	4	.0000E	0	.0000E	0
26	10	.1354E	4	.0000E	0	.0000E	0
	16	-.1354E	4	.0000E	0	.0000E	0
27	12	.1354E	4	.0000E	0	.0000E	0
	16	-.1354E	4	.0000E	0	.0000E	0
28	11	.2959E	4	.0000E	0	.0000E	0
	17	-.2959E	4	.0000E	0	.0000E	0
29	14	-.9563E	3	.0000E	0	.0000E	0
	15	.9563E	3	.0000E	0	.0000E	0
30	15	-.1427E	4	.0000E	0	.0000E	0
	16	.1427E	4	.0000E	0	.0000E	0
31	16	-.1427E	4	.0000E	0	.0000E	0
	17	.1427E	4	.0000E	0	.0000E	0
32	17	-.9563E	3	.0000E	0	.0000E	0
	14	.9563E	3	.0000E	0	.0000E	0

EX VERTICAL
MAX LIMIT

EX SIDE PANEL DIRG.
MAX LIMIT

JOINT EQUILIBRIUM CHECK

JOINT	F1	F2	F3	F4	F5	F6
1	-.9672E	2	-.6964E	3	.4333E	3
2	.4333E	3	-.6964E	3	-.9672E	2
3	.7896E	3	-.1269E	4	.1763E	3
4	-.3515E	3	-.2531E	4	-.1575E	4
5	.4311E	3	-.3104E	4	-.1931E	4
6	-.1931E	4	-.3104E	4	.4311E	3
7	-.1575E	4	-.2531E	4	-.3515E	3
8	.1763E	3	-.1269E	4	.7896E	3
9	.7600E-	6	.8941E-	7	.7283E-	6
10	.4023E-	6	.9462E-	6	.6258E-	6
11	.1125E-	5	.1431E-	5	.7078E-	6
12	.4992E-	6	.7451E-	6	-.2496E-	6
13	-.1744E-	5	.0000E	0	-.1346E-	5
14	.5310E	3	.3800E	4	.5310E	3
15	.5310E	3	.3800E	4	.5310E	3
16	.5310E	3	.3800E	4	.5310E	3
17	.5310E	3	.3800E	4	.5310E	3

STRUCTURAL ANALYSIS PROGRAM

STRUCTURE TYPE = 1
 NUMBER OF JOINTS = 21
 NUMBER OF MEMBERS = 50
 NUMBER OF JOINTS CONSTRAINED = 9
 NUMBER OF MATRIX ELEMENTS ALTERED = 0
 YOUNG'S MODULUS OF ELASTICITY = .100000E 8
 SHEAR MODULUS = .400000E 7

JOINT COORDINATES

JOINT	X (IN)	Y (IN)	Z (IN)
1	-12.5000	.0000	-26.2000
2	-26.2000	.0000	-12.5000
3	-26.2000	.0000	12.5000
4	-12.5000	.0000	26.2000
5	12.5000	.0000	26.2000
6	26.2000	.0000	12.5000
7	26.2000	.0000	-12.5000
8	12.5000	.0000	-26.2000
9	-15.0000	-18.0000	-15.0000
10	-15.0000	-18.0000	15.0000
11	15.0000	-18.0000	15.0000
12	15.0000	-18.0000	-15.0000
13	.0000	-18.0000	.0000
14	-15.0000	-52.0000	-15.0000
15	-15.0000	-52.0000	15.0000
16	15.0000	-52.0000	15.0000
17	15.0000	-52.0000	-15.0000
18	-15.0000	-88.0000	-15.0000
19	-15.0000	-88.0000	15.0000
20	15.0000	-88.0000	15.0000
21	15.0000	-88.0000	-15.0000

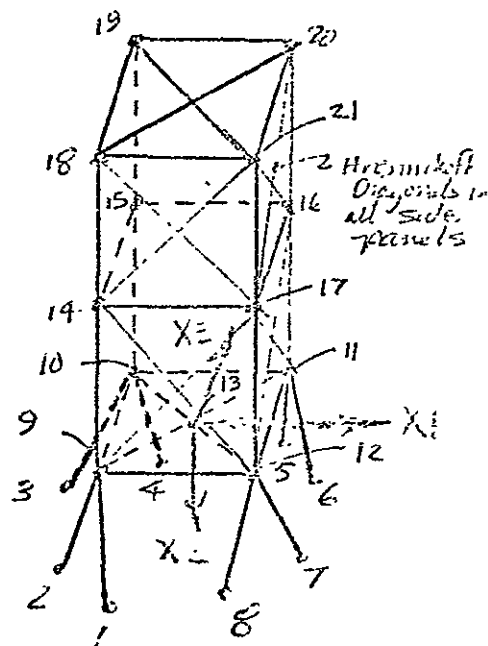
JOINT CONSTRAINTS

JOINT	X1	X2	X3	X4	X5	X6
1	1	1	1			
2	1	1	1			
3	1	1	1			
4	1	1	1			
5	1	1	1			
6	1	1	1			
7	1	1	1			
8	1	1	1			
13	-1	1	-1			

ERTS COMPUTER
 RUN 1.2-

Dynamic Model Anal.
 Improved Model

Full Box: 3 levels
 for mass' dist.
 12/17/67



BEAM PROPERTIES

MEMBER	JOINT	JOINT	AREA	I-YY	I-ZZ	J	REF.	JT.
1	1	9	.2930	.000000	.000000	.000000		0.
2	2	9	.2930	.000000	.000000	.000000		0.
3	3	10	.2930	.000000	.000000	.000000		0.
4	4	10	.2930	.000000	.000000	.000000		0.
5	5	11	.2930	.000000	.000000	.000000		0.
6	6	11	.2930	.000000	.000000	.000000		0.
7	7	12	.2930	.000000	.000000	.000000		0.
8	8	12	.2930	.000000	.000000	.000000		0.
9	9	10	.1280	.000000	.000000	.000000		0.
10	10	11	.1280	.000000	.000000	.000000		0.
11	11	12	.1280	.000000	.000000	.000000		0.
12	12	9	.1280	.000000	.000000	.000000		0.
13	9	13	1.1000	.000000	.000000	.000000		0.
14	13	11	1.1000	.000000	.000000	.000000		0.
15	10	13	1.1000	.000000	.000000	.000000		0.
16	13	12	1.1000	.000000	.000000	.000000		0.
17	9	14	.2200	.000000	.000000	.000000		0.
18	10	15	.2200	.000000	.000000	.000000		0.
19	11	16	.2200	.000000	.000000	.000000		0.
20	12	17	.2200	.000000	.000000	.000000		0.
21	9	17	.8610	.000000	.000000	.000000		0.
22	12	14	.8610	.000000	.000000	.000000		0.
23	10	14	.8610	.000000	.000000	.000000		0.
24	9	15	.8610	.000000	.000000	.000000		0.
25	11	15	.8610	.000000	.000000	.000000		0.
26	10	16	.8610	.000000	.000000	.000000		0.
27	12	16	.8610	.000000	.000000	.000000		0.
28	11	17	.8610	.000000	.000000	.000000		0.
29	14	15	.4000	.000000	.000000	.000000		0.
30	15	16	.4000	.000000	.000000	.000000		0.
31	16	17	.4000	.000000	.000000	.000000		0.
32	17	14	.4000	.000000	.000000	.000000		0.
33	14	18	.2200	.000000	.000000	.000000		0.
34	15	19	.2200	.000000	.000000	.000000		0.
35	16	20	.2200	.000000	.000000	.000000		0.
36	17	21	.2200	.000000	.000000	.000000		0.
37	18	19	.1280	.000000	.000000	.000000		0.
38	19	20	.1280	.000000	.000000	.000000		0.
39	20	21	.1280	.000000	.000000	.000000		0.
40	21	18	.1280	.000000	.000000	.000000		0.
41	14	21	.8610	.000000	.000000	.000000		0.
42	17	18	.8610	.000000	.000000	.000000		0.
43	15	18	.8610	.000000	.000000	.000000		0.
44	14	19	.8610	.000000	.000000	.000000		0.
45	16	19	.8610	.000000	.000000	.000000		0.
46	15	20	.8610	.000000	.000000	.000000		0.
47	17	20	.8610	.000000	.000000	.000000		0.
48	16	21	.8610	.000000	.000000	.000000		0.
49	18	20	.8610	.000000	.000000	.000000		0.
50	21	19	.8610	.000000	.000000	.000000		0.

WEIGHT PROPERTIES G = 1.00

JOINT	X1	X2	X3	X4	X5	X6
1	.0000E 0	.0000E 0	.0000E 0			
2	.0000E 0	.0000E 0	.0000E 0			
3	.0000E 0	.0000E 0	.0000E 0			
4	.0000E 0	.0000E 0	.0000E 0			
5	.0000E 0	.0000E 0	.0000E 0			
6	.0000E 0	.0000E 0	.0000E 0			
7	.0000E 0	.0000E 0	.0000E 0			
8	.0000E 0	.0000E 0	.0000E 0			
9	.3240E 0	.3240E 0	.3240E 0			
10	.3240E 0	.3240E 0	.3240E 0			
11	.3240E 0	.3240E 0	.3240E 0			
12	.3240E 0	.3240E 0	.3240E 0			
13	.0000E 0	.0000E 0	.0000E 0			
14	.3240E 0	.3240E 0	.3240E 0			
15	.3240E 0	.3240E 0	.3240E 0			
16	.3240E 0	.3240E 0	.3240E 0			
17	.3240E 0	.3240E 0	.3240E 0			
18	.3240E 0	.3240E 0	.3240E 0			
19	.3240E 0	.3240E 0	.3240E 0			
20	.3240E 0	.3240E 0	.3240E 0			
21	.3240E 0	.3240E 0	.3240E 0			

BEGINNING MODAL ANALYSIS

DO YOU WISH TO HAVE THE MODAL OUTPUT SAVED ON FILE /MODES/(1=YES/0=NO) 1

HOW MANY NATURAL FREQUENCIES ARE DESIRED? 12

NATURAL FREQUENCIES

MODE	FREQ(CPS)	FREQ(RAD/SEC)	
1	.15893662E 2	.99862825E 2] 1st LATERAL → 16, no change
2	.15893662E 2	.99862825E 2	
3	.31819559E 2	.19992818E 3] 1st TORSION → 33, up 21%
4	.34850806E 2	.21897407E 3	
5	.34850807E 2	.21897408E 3] 2nd LATERAL → 52, up 47%
6	.54714620E 2	.34378209E 3	
7	.57311119E 2	.36009638E 3] 1st AXIAL → 56
8	.73238943E 2	.46017385E 3	
9	.73238943E 2	.46017385E 3] 1st BOX SHEAR → 57 } no change
10	.92066691E 2	.57847208E 3	
11	.94319094E 2	.59262434E 3	
12	.94319094E 2	.59262435E 3	

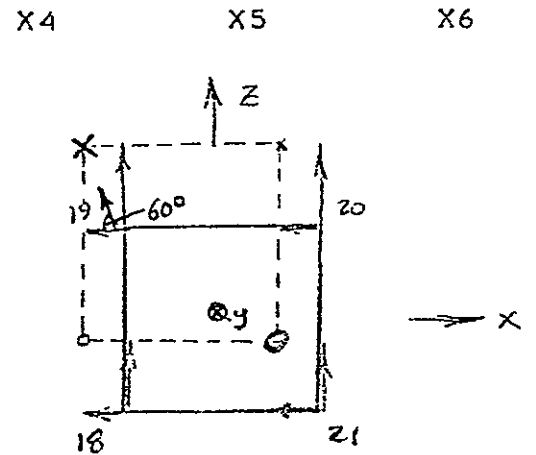
Run 1.3 (INTERSTAGE DIMENSIONALS ADDED)

HOW MANY MODE SHAPES ARE DESIRED? 12

MODE 1
 FREQUENCY (CPS) = $\frac{15.8937}{1.0000}$
 GENERALIZED MASS = 1.0000

JOINT	X1	X2	X3	X4	X5	X6
1	.0000E 0	.0000E 0	.0000E 0	.0000E 0	.0000E 0	.0000E 0
2	.0000E 0	.0000E 0	.0000E 0	.0000E 0	.0000E 0	.0000E 0
3	.0000E 0	.0000E 0	.0000E 0	.0000E 0	.0000E 0	.0000E 0
4	.0000E 0	.0000E 0	.0000E 0	.0000E 0	.0000E 0	.0000E 0
5	.0000E 0	.0000E 0	.0000E 0	.0000E 0	.0000E 0	.0000E 0
6	.0000E 0	.0000E 0	.0000E 0	.0000E 0	.0000E 0	.0000E 0
7	.0000E 0	.0000E 0	.0000E 0	.0000E 0	.0000E 0	.0000E 0
8	.0000E 0	.0000E 0	.0000E 0	.0000E 0	.0000E 0	.0000E 0
9	.8701E- 2	-.3228E- 1	.2986E- 3	.8701E- 2	-.3228E- 1	.2986E- 3
10	-.1522E- 1	.9937E- 1	.1249E- 1	-.1522E- 1	.9937E- 1	.1249E- 1
11	.8701E- 2	.3228E- 1	.2986E- 3	.8701E- 2	.3228E- 1	.2986E- 3
12	-.1522E- 1	-.9937E- 1	.1249E- 1	-.1522E- 1	-.9937E- 1	.1249E- 1
130000E 00000E 0
14	-.1220E 0	-.6941E- 1	.2688E 0	-.1220E 0	-.6941E- 1	.2688E 0
15	-.1625E 0	.2137E 0	.2895E 0	-.1625E 0	.2137E 0	.2895E 0
16	-.1220E 0	.6941E- 1	.2688E 0	-.1220E 0	.6941E- 1	.2688E 0
17	-.1625E 0	-.2137E 0	.2895E 0	-.1625E 0	-.2137E 0	.2895E 0
18	-.3415E 0	-.8696E- 1	.6859E 0	-.3415E 0	-.8696E- 1	.6859E 0
19	-.3632E 0	.2677E 0	.6970E 0	-.3632E 0	.2677E 0	.6970E 0
20	-.3415E 0	.8696E- 1	.6859E 0	-.3415E 0	.8696E- 1	.6859E 0
21	-.3632E 0	-.2677E 0	.6970E 0	-.3632E 0	-.2677E 0	.6970E 0

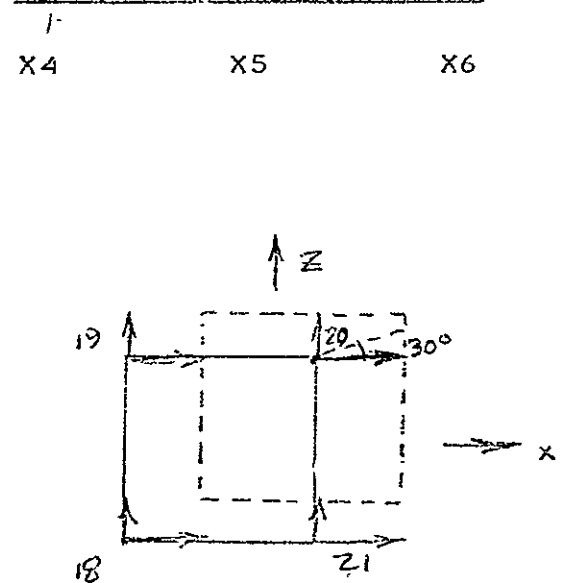
1ST LATERAL +Z/-X



MODE 2
 FREQUENCY (CPS) = $\frac{15.8937}{1.0000}$
 GENERALIZED MASS = 1.0000

JOINT	X1	X2	X3	X4	X5	X6
1	.0000E 0	.0000E 0	.0000E 0	.0000E 0	.0000E 0	.0000E 0
2	.0000E 0	.0000E 0	.0000E 0	.0000E 0	.0000E 0	.0000E 0
3	.0000E 0	.0000E 0	.0000E 0	.0000E 0	.0000E 0	.0000E 0
4	.0000E 0	.0000E 0	.0000E 0	.0000E 0	.0000E 0	.0000E 0
5	.0000E 0	.0000E 0	.0000E 0	.0000E 0	.0000E 0	.0000E 0
6	.0000E 0	.0000E 0	.0000E 0	.0000E 0	.0000E 0	.0000E 0
7	.0000E 0	.0000E 0	.0000E 0	.0000E 0	.0000E 0	.0000E 0
8	.0000E 0	.0000E 0	.0000E 0	.0000E 0	.0000E 0	.0000E 0
9	.1263E- 1	-.9988E- 1	.1522E- 1	.1263E- 1	-.9988E- 1	.1522E- 1
10	.5137E- 4	-.3066E- 1	-.8497E- 2	.5137E- 4	-.3066E- 1	-.8497E- 2
11	.1263E- 1	.9988E- 1	.1522E- 1	.1263E- 1	.9988E- 1	.1522E- 1
12	.5137E- 4	.3066E- 1	-.8497E- 2	.5137E- 4	.3066E- 1	-.8497E- 2
130000E 00000E 0
14	.2875E 0	-.2148E 0	.1669E 0	.2875E 0	-.2148E 0	.1669E 0
15	.2661E 0	-.6593E- 1	.1267E 0	.2661E 0	-.6593E- 1	.1267E 0
16	.2875E 0	.2148E 0	.1669E 0	.2875E 0	.2148E 0	.1669E 0
17	.2661E 0	.6593E- 1	.1267E 0	.2661E 0	.6593E- 1	.1267E 0
18	.6913E 0	-.2691E 0	.3743E 0	.6913E 0	-.2691E 0	.3743E 0
19	.6799E 0	-.8260E- 1	.3528E 0	.6799E 0	-.8260E- 1	.3528E 0
20	.6913E 0	.2691E 0	.3743E 0	.6913E 0	.2691E 0	.3743E 0
21	.6799E 0	.8260E- 1	.3528E 0	.6799E 0	.8260E- 1	.3528E 0

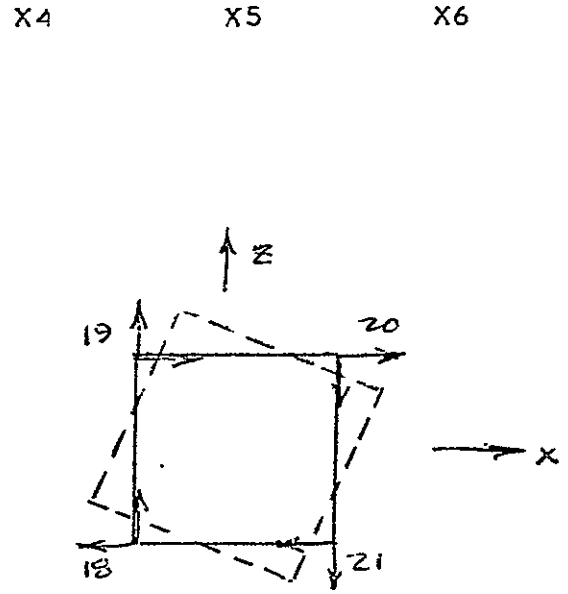
1ST LATERAL +X/+Z



MODE 3
 FREQUENCY (CPS) = 31.8196
 GENERALIZED MASS = 1.0000

JOINT	X1	X2	X3	X4	X5	X6
1	.0000E 0	.0000E 0	.0000E 0			
2	.0000E 0	.0000E 0	.0000E 0			
3	.0000E 0	.0000E 0	.0000E 0			
4	.0000E 0	.0000E 0	.0000E 0			
5	.0000E 0	.0000E 0	.0000E 0			
6	.0000E 0	.0000E 0	.0000E 0			
7	.0000E 0	.0000E 0	.0000E 0			
8	.0000E 0	.0000E 0	.0000E 0			
9	-.2397E 0	.9636E-9	.2397E 0			
10	.2397E 0	.1803E-9	.2397E 0			
11	.2397E 0	-.9121E-9	-.2397E 0			
12	-.2397E 0	.2150E-10	-.2397E 0			
130000E 0			
14	-.3654E 0	.9044E-9	.3654E 0			
15	.3654E 0	.1237E-9	.3654E 0			
16	.3654E 0	-.7032E-9	-.3654E 0			
17	-.3654E 0	.9597E-10	-.3654E 0			
18	-.4413E 0	.1307E-8	.4413E 0			
19	.4413E 0	.9438E-10	.4413E 0			
20	.4413E 0	-.9974E-9	-.4413E 0			
21	-.4413E 0	.8325E-10	-.4413E 0			

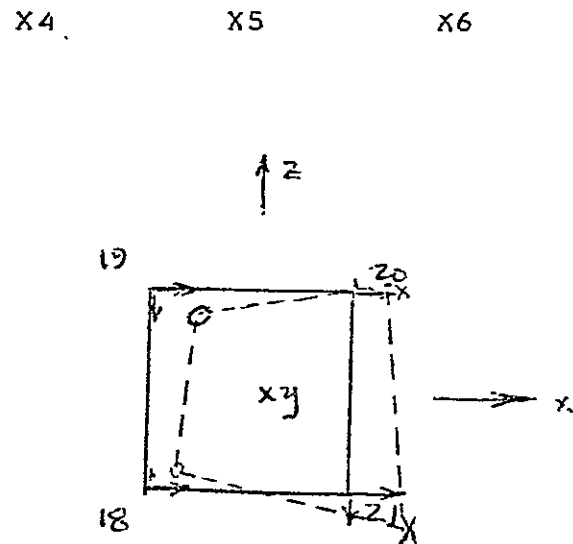
1st TORSION



MODE 4
 FREQUENCY (CPS) = 34.8508
 GENERALIZED MASS = 1.0000

JOINT	X1	X2	X3	X4	X5	X6
1	.0000E 0	.0000E 0	.0000E 0			
2	.0000E 0	.0000E 0	.0000E 0			
3	.0000E 0	.0000E 0	.0000E 0			
4	.0000E 0	.0000E 0	.0000E 0			
5	.0000E 0	.0000E 0	.0000E 0			
6	.0000E 0	.0000E 0	.0000E 0			
7	.0000E 0	.0000E 0	.0000E 0			
8	.0000E 0	.0000E 0	.0000E 0			
9	-.6549E 0	-.1518E 0	.2231E-1			
10	-.7280E 0	-.2513E 0	.3187E 0			
11	-.6549E 0	.1518E 0	.2231E-1			
12	-.7280E 0	.2513E 0	.3187E 0			
130000E 0			
14	-.3617E 0	-.1087E 0	.1116E 0			
15	-.3499E 0	-.1799E 0	.6388E-1			
16	-.3617E 0	.1087E 0	.1116E 0			
17	-.3499E 0	.1799E 0	.6388E-1			
18	.5093E-1	-.1419E 0	.1528E-2			
19	.5833E-1	-.2347E 0	-.2847E-1			
20	.5093E-1	.1419E 0	.1528E-2			
21	.5833E-1	.2347E 0	-.2847E-1			

2nd LATERAL + x/-z

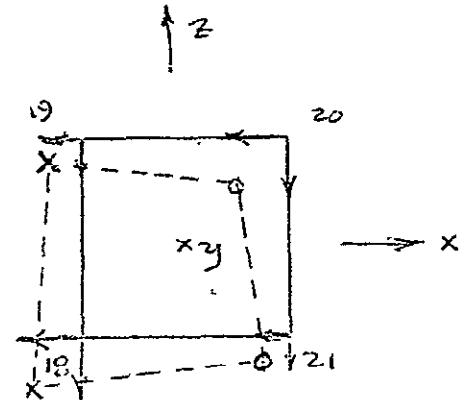


MODE 5
 FREQUENCY (CPS) = 34.8508
 GENERALIZED MASS = 1.0000

JOINT	X1	X2	X3	X4	X5	X6
1	.0000E 0	.0000E 0	.0000E 0	.0000E 0	.0000E 0	.0000E 0
2	.0000E 0	.0000E 0	.0000E 0	.0000E 0	.0000E 0	.0000E 0
3	.0000E 0	.0000E 0	.0000E 0	.0000E 0	.0000E 0	.0000E 0
4	.0000E 0	.0000E 0	.0000E 0	.0000E 0	.0000E 0	.0000E 0
5	.0000E 0	.0000E 0	.0000E 0	.0000E 0	.0000E 0	.0000E 0
6	.0000E 0	.0000E 0	.0000E 0	.0000E 0	.0000E 0	.0000E 0
7	.0000E 0	.0000E 0	.0000E 0	.0000E 0	.0000E 0	.0000E 0
8	.0000E 0	.0000E 0	.0000E 0	.0000E 0	.0000E 0	.0000E 0
9	.6705E 0	.2892E 0	.5344E 0	.5344E 0	.2892E 0	.6705E 0
10	.4949E 0	.5050E-1	.2846E 0	.2846E 0	.5050E-1	.4949E 0
11	.6705E 0	-.2892E 0	.5344E 0	.5344E 0	-.2892E 0	.6705E 0
12	.4949E 0	-.5050E-1	.2846E 0	.2846E 0	-.5050E-1	.4949E 0
130000E 00000E 0
14	.2857E 0	.2071E 0	.1906E 0	.1906E 0	.2071E 0	.2857E 0
15	.3139E 0	.3616E-1	.2308E 0	.2308E 0	.3616E-1	.3139E 0
16	.2857E 0	-.2071E 0	.1906E 0	.1906E 0	-.2071E 0	.2857E 0
17	.3139E 0	-.3616E-1	.2308E 0	.2308E 0	-.3616E-1	.3139E 0
18	-.5492E-1	.2702E 0	-.4499E-1	-.4499E-1	.2702E 0	-.5492E-1
19	-.3716E-1	.4718E-1	-.1971E-1	-.1971E-1	.4718E-1	-.3716E-1
20	-.5492E-1	-.2702E 0	-.4499E-1	-.4499E-1	-.2702E 0	-.5492E-1
21	-.3716E-1	-.4718E-1	-.1971E-1	-.1971E-1	-.4718E-1	-.3716E-1

Znd LATERAL - X/-Z

X4 X5 X6

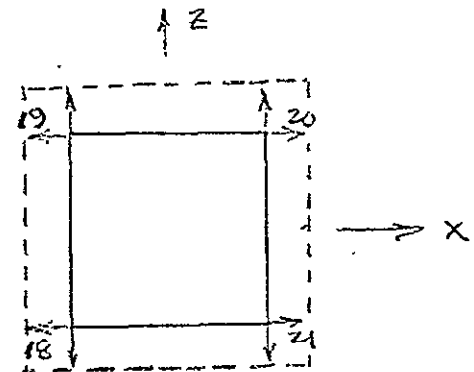


MODE 6
 FREQUENCY (CPS) = 54.7146
 GENERALIZED MASS = 1.0000

JOINT	X1	X2	X3	X4	X5	X6
1	.0000E 0	.0000E 0	.0000E 0	.0000E 0	.0000E 0	.0000E 0
2	.0000E 0	.0000E 0	.0000E 0	.0000E 0	.0000E 0	.0000E 0
3	.0000E 0	.0000E 0	.0000E 0	.0000E 0	.0000E 0	.0000E 0
4	.0000E 0	.0000E 0	.0000E 0	.0000E 0	.0000E 0	.0000E 0
5	.0000E 0	.0000E 0	.0000E 0	.0000E 0	.0000E 0	.0000E 0
6	.0000E 0	.0000E 0	.0000E 0	.0000E 0	.0000E 0	.0000E 0
7	.0000E 0	.0000E 0	.0000E 0	.0000E 0	.0000E 0	.0000E 0
8	.0000E 0	.0000E 0	.0000E 0	.0000E 0	.0000E 0	.0000E 0
9	-.4363E-5	.2815E 0	-.4363E-5	-.4363E-5	.2815E 0	-.4363E-5
10	-.4363E-5	.2815E 0	.4363E-5	.4363E-5	.2815E 0	-.4363E-5
11	.4363E-5	.2815E 0	.4363E-5	.4363E-5	.2815E 0	.4363E-5
12	.4363E-5	.2815E 0	-.4363E-5	-.4363E-5	.2815E 0	-.4363E-5
130000E 00000E 0
14	-.8651E-1	.4987E 0	-.8651E-1	-.8651E-1	.4987E 0	-.8651E-1
15	-.8651E-1	.4987E 0	.8651E-1	.8651E-1	.4987E 0	-.8651E-1
16	.8651E-1	.4987E 0	.8651E-1	.8651E-1	.4987E 0	.8651E-1
17	.8651E-1	.4987E 0	-.8651E-1	-.8651E-1	.4987E 0	-.8651E-1
18	-.1430E-1	.6544E 0	-.1430E-1	-.1430E-1	.6544E 0	-.1430E-1
19	-.1430E-1	.6544E 0	.1430E-1	.1430E-1	.6544E 0	-.1430E-1
20	.1430E-1	.6544E 0	.1430E-1	.1430E-1	.6544E 0	.1430E-1
21	.1430E-1	.6544E 0	-.1430E-1	-.1430E-1	.6544E 0	-.1430E-1

1st AXIAL, +y

X4 X5 X6

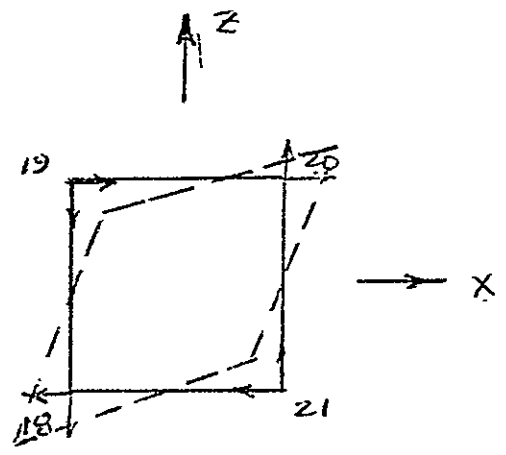


MØDE 7
 FREQUENCY (CPS) = 57.3111
 GENERALIZED MASS = 1.0000

1ST Box SHEAR

JØINT	X1	X2	X3
1	.0000E 0	.0000E 0	.0000E 0
2	.0000E 0	.0000E 0	.0000E 0
3	.0000E 0	.0000E 0	.0000E 0
4	.0000E 0	.0000E 0	.0000E 0
5	.0000E 0	.0000E 0	.0000E 0
6	.0000E 0	.0000E 0	.0000E 0
7	.0000E 0	.0000E 0	.0000E 0
8	.0000E 0	.0000E 0	.0000E 0
9	-.1438E- 1	.1858E 0	-.1438E- 1
10	.1438E- 1	-.1858E 0	-.1438E- 1
11	.1438E- 1	.1858E 0	.1438E- 1
12	-.1438E- 1	-.1858E 0	.1438E- 1
130000E 0
14	-.5165E 0	.8798E- 1	-.5165E 0
15	.5165E 0	-.8798E- 1	-.5165E 0
16	.5165E 0	.8798E- 1	.5165E 0
17	-.5165E 0	-.8798E- 1	.5165E 0
18	-.1581E- 1	-.4415E 0	-.1581E- 1
19	.1581E- 1	.4415E 0	-.1581E- 1
20	.1581E- 1	-.4415E 0	.1581E- 1
21	-.1581E- 1	.4415E 0	.1581E- 1

X4 X5 X6



MØDE 8
 FREQUENCY (CPS) = 73.2389
 GENERALIZED MASS = 1.0000

JØINT	X1	X2	X3
1	.0000E 0	.0000E 0	.0000E 0
2	.0000E 0	.0000E 0	.0000E 0
3	.0000E 0	.0000E 0	.0000E 0
4	.0000E 0	.0000E 0	.0000E 0
5	.0000E 0	.0000E 0	.0000E 0
6	.0000E 0	.0000E 0	.0000E 0
7	.0000E 0	.0000E 0	.0000E 0
8	.0000E 0	.0000E 0	.0000E 0
9	.1643E- 1	-.3162E- 1	-.7004E- 1
10	-.3390E 0	-.4039E 0	.3458E 0
11	.1643E- 1	.3162E- 1	-.7004E- 1
12	-.3390E 0	.4039E 0	.3458E 0
130000E 0
14	.3586E 0	-.4254E- 2	-.3122E 0
15	.3227E 0	-.5434E- 1	-.2702E 0
16	.3586E 0	.4254E- 2	-.3122E 0
17	.3227E 0	.5434E- 1	-.2702E 0
18	.2055E 0	.4625E- 1	-.2630E 0
19	-.3491E 0	.5908E 0	.3857E 0
20	.2055E 0	-.4625E- 1	-.2630E 0
21	-.3491E 0	-.5908E 0	.3857E 0

X4 X5 X6

STRUCTURAL ANALYSIS PROGRAM

ADDING DIAGONALS
TO INTERSTAGE

BEGINNING MODAL ANALYSIS

DO YOU WISH TO HAVE THE MODAL OUTPUT SAVED ON FILE /MODES/?(1=YES/0=NO) 0
HOW MANY NATURAL FREQUENCIES ARE DESIRED? 12

NATURAL FREQUENCIES

MODE	FREQ(CPS)		FREQ(RAD/SEC)
1	.16059863E	2 1-LAT	.10090709E 3
2	.16059863E	2	.10090709E 3
3	.38417666E	2 TOR	.24138532E 3
4	.52003670E	2 2-LMT	.32674870E 3
5	.52003670E	2	.32674870E 3
6	.56292361E	2 1-AXI	.35369533E 3
7	.57882185E	2 1-SHR	.36368449E 3
8	.77736453E	2	.48843254E 3
9	.77736454E	2	.48843254E 3
10	.98664469E	2	.61992714E 3
11	.98664469E	2	.61992714E 3
12	.10314233E	3	.64806240E 3

ESTS COMPUTER
RUN 1:3 -

Full Box Model -
Interstage Diagonals
Added, otherwise, 1.2
12/18/65

HOW MANY MODE SHAPES ARE DESIRED? 7

MODE 1
 FREQUENCY (CPS) = $\frac{16.0599}{1.0000}$
 GENERALIZED MASS = $\frac{16.0599}{1.0000}$

1st LATERAL +X/+Z

JØINT	X1	X2	X3	X4	X5	X6
1	.0000E 0	.0000E 0	.0000E 0			
2	.0000E 0	.0000E 0	.0000E 0			
3	.0000E 0	.0000E 0	.0000E 0			
4	.0000E 0	.0000E 0	.0000E 0			
5	.0000E 0	.0000E 0	.0000E 0			
6	.0000E 0	.0000E 0	.0000E 0			
7	.0000E 0	.0000E 0	.0000E 0			
8	.0000E 0	.0000E 0	.0000E 0			
9	.4293E- 1	-.8597E- 1	.4082E- 1			
10	.1330E- 1	-.1400E- 1	-.3390E- 3			
11	.4293E- 1	.8597E- 1	.4082E- 1			
12	.1330E- 1	.1400E- 1	-.3390E- 3			
130000E 0			
14	.2746E 0	-.2150E 0	.2063E 0			
15	.2489E 0	-.3500E- 1	.1706E 0			
16	.2746E 0	.2150E 0	.2063E 0			
17	.2489E 0	.3500E- 1	.1706E 0			
18	.6359E 0	-.2713E 0	.4628E 0			
19	.6212E 0	-.4417E- 1	.4423E 0			
20	.6359E 0	.2713E 0	.4628E 0			
21	.6212E 0	.4417E- 1	.4423E 0			

MODE 2
 FREQUENCY (CPS) = $\frac{16.0599}{1.0000}$
 GENERALIZED MASS = $\frac{16.0599}{1.0000}$

1st LATERAL +Z/-X

JØINT	X1	X2	X3	X4	X5	X6
1	.0000E 0	.0000E 0	.0000E 0			
2	.0000E 0	.0000E 0	.0000E 0			
3	.0000E 0	.0000E 0	.0000E 0			
4	.0000E 0	.0000E 0	.0000E 0			
5	.0000E 0	.0000E 0	.0000E 0			
6	.0000E 0	.0000E 0	.0000E 0			
7	.0000E 0	.0000E 0	.0000E 0			
8	.0000E 0	.0000E 0	.0000E 0			
9	.2617E- 2	-.1854E- 1	.1544E- 1			
10	-.4005E- 1	.8511E- 1	.4285E- 1			
11	.2617E- 2	.1854E- 1	.1544E- 1			
12	-.4005E- 1	-.8511E- 1	.4285E- 1			
130000E 0			
14	-.1557E 0	-.4636E- 1	.2595E 0			
15	-.1928E 0	.2128E 0	.2833E 0			
16	-.1557E 0	.4636E- 1	.2595E 0			
17	-.1928E 0	-.2128E 0	.2833E 0			
18	-.4079E 0	-.5850E- 1	.6448E 0			
19	-.4291E 0	.2685E 0	.6585E 0			
20	-.4079E 0	.5850E- 1	.6448E 0			
21	-.4291E 0	-.2685E 0	.6585E 0			

MODE 3
 FREQUENCY (CPS) = 38.4177
 GENERALIZED MASS = 1.0000

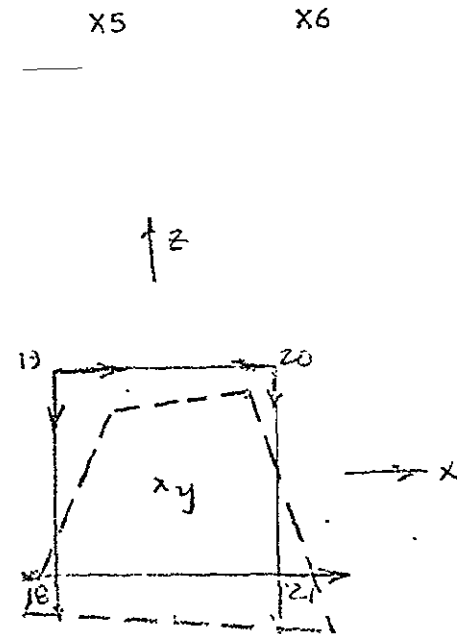
1st TORSION

JOINT	X1	X2	X3	X4	X5	X6
1	.0000E 0	.0000E 0	.0000E 0			
2	.0000E 0	.0000E 0	.0000E 0			
3	.0000E 0	.0000E 0	.0000E 0			
4	.0000E 0	.0000E 0	.0000E 0			
5	.0000E 0	.0000E 0	.0000E 0			
6	.0000E 0	.0000E 0	.0000E 0			
7	.0000E 0	.0000E 0	.0000E 0			
8	.0000E 0	.0000E 0	.0000E 0			
9	-.1684E 0	-.2394E-9	.1684E 0			
10	.1684E 0	-.3671E-10	.1684E 0			
11	.1684E 0	-.1143E-9	-.1684E 0			
12	-.1684E 0	-.1847E-9	-.1684E 0			
130000E 0			
14	-.3585E 0	-.3310E-9	.3585E 0			
15	.3585E 0	-.2491E-9	.3585E 0			
16	.3585E 0	-.1283E-9	-.3585E 0			
17	-.3585E 0	-.3044E-9	-.3585E 0			
18	-.4785E 0	-.3471E-9	.4785E 0			
19	.4785E 0	-.1683E-9	.4785E 0			
20	.4785E 0	-.3555E-9	-.4785E 0			
21	-.4785E 0	-.3885E-9	-.4785E 0			

MODE 4
 FREQUENCY (CPS) = 52.0037
 GENERALIZED MASS = 1.0000

2nd LATERAL +x, -z

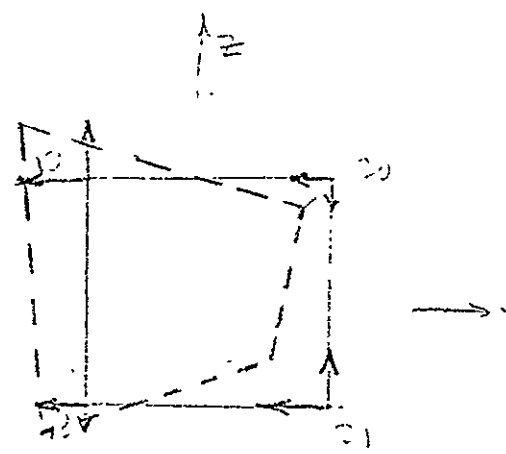
JOINT	X1	X2	X3	X4	X5	X6
1	.0000E 0	.0000E 0	.0000E 0			
2	.0000E 0	.0000E 0	.0000E 0			
3	.0000E 0	.0000E 0	.0000E 0			
4	.0000E 0	.0000E 0	.0000E 0			
5	.0000E 0	.0000E 0	.0000E 0			
6	.0000E 0	.0000E 0	.0000E 0			
7	.0000E 0	.0000E 0	.0000E 0			
8	.0000E 0	.0000E 0	.0000E 0			
9	.1530E-1	.9979E-1	.5641E 0			
10	-.3093E 0	-.1640E 0	.6431E 0			
11	.1530E-1	-.9979E-1	.5641E 0			
12	-.3093E 0	.1640E 0	.6431E 0			
130000E 0			
14	-.1642E 0	.9960E-1	.4599E 0			
15	-.5325E-1	-.1637E 0	.4329E 0			
16	-.1642E 0	-.9960E-1	.4599E 0			
17	-.5325E-1	.1637E 0	.4329E 0			
18	-.5321E-1	.2180E 0	-.8707E-1			
19	.1050E 0	-.3584E 0	-.1256E 0			
20	-.5321E-1	-.2180E 0	-.8707E-1			
21	.1050E 0	.3584E 0	-.1256E 0			



MODE 5
 FREQUENCY (CPS) = 52.0037
 GENERALIZED MASS = 1.0000

2nd LATERAL, -X/+Z

JOINT	X1	X2	X3	X4	X5	X6
1	.0000E 0	.0000E 0	.0000E 0			
2	.0000E 0	.0000E 0	.0000E 0			
3	.0000E 0	.0000E 0	.0000E 0			
4	.0000E 0	.0000E 0	.0000E 0			
5	.0000E 0	.0000E 0	.0000E 0			
6	.0000E 0	.0000E 0	.0000E 0			
7	.0000E 0	.0000E 0	.0000E 0			
8	.0000E 0	.0000E 0	.0000E 0			
9	.5550E 0	.9507E-1	-.3043E-2			
10	.6433E 0	.1668E 0	-.3252E 0			
11	.5550E 0	-.9507E-1	-.3043E-2			
12	.6433E 0	-.1668E 0	-.3252E 0			
130000E 0			
14	.4582E 0	.9489E-1	-.1764E 0			
15	.4280E 0	.1665E 0	-.6634E-1			
16	.4582E 0	-.9489E-1	-.1764E 0			
17	.4280E 0	-.1665E 0	-.6634E-1			
18	-.8404E-1	.2077E 0	-.4961E-1			
19	-.1271E 0	.3645E 0	.1074E 0			
20	-.8404E-1	-.2077E 0	-.4961E-1			
21	-.1271E 0	-.3645E 0	.1074E 0			



MODE 6
 FREQUENCY (CPS) = 56.2924
 GENERALIZED MASS = 1.0000

1st Axial

JOINT	X1	X2	X3	X4	X5	X6
1	.0000E 0	.0000E 0	.0000E 0			
2	.0000E 0	.0000E 0	.0000E 0			
3	.0000E 0	.0000E 0	.0000E 0			
4	.0000E 0	.0000E 0	.0000E 0			
5	.0000E 0	.0000E 0	.0000E 0			
6	.0000E 0	.0000E 0	.0000E 0			
7	.0000E 0	.0000E 0	.0000E 0			
8	.0000E 0	.0000E 0	.0000E 0			
9	-.7700E-2	.2596E 0	-.7700E-2			
10	-.7700E-2	.2596E 0	.7700E-2			
11	.7700E-2	.2596E 0	.7700E-2			
12	.7700E-2	.2596E 0	-.7700E-2			
130000E 0			
14	-.9256E-1	.4964E 0	-.9256E-1			
15	-.9256E-1	.4964E 0	.9256E-1			
16	.9256E-1	.4964E 0	.9256E-1			
17	.9256E-1	.4964E 0	-.9256E-1			
18	-.1543E-1	.6634E 0	-.1543E-1			
19	-.1543E-1	.6634E 0	.1543E-1			
20	.1543E-1	.6634E 0	.1543E-1			
21	.1543E-1	.6634E 0	-.1543E-1			

MODE 7
 FREQUENCY (CPS) = 57.8322
 GENERALIZED MASS = 1.0000

1st Box SHEAR

JOINT	X1	X2	X3	X4	X5	X6
1	.0000E 0	.0000E 0	.0000E 0			
2	.0000E 0	.0000E 0	.0000E 0			
3	.0000E 0	.0000E 0	.0000E 0			
4	.0000E 0	.0000E 0	.0000E 0			
5	.0000E 0	.0000E 0	.0000E 0			
6	.0000E 0	.0000E 0	.0000E 0			
7	.0000E 0	.0000E 0	.0000E 0			
8	.0000E 0	.0000E 0	.0000E 0			
9	.2004E- 1	-.1728E 0	.2004E- 1			
10	-.2004E- 1	.1728E 0	.2004E- 1			
11	-.2004E- 1	-.1728E 0	-.2004E- 1			
12	.2004E- 1	.1728E 0	-.2004E- 1			
130000E 0			
14	.5167E 0	-.9093E- 1	.5167E 0			
15	-.5167E 0	.9093E- 1	.5167E 0			
16	-.5167E 0	-.9093E- 1	-.5167E 0			
17	.5167E 0	.9093E- 1	-.5167E 0			
18	.1571E- 1	.4453E 0	.1571E- 1			
19	-.1571E- 1	-.4453E 0	.1571E- 1			
20	-.1571E- 1	.4453E 0	-.1571E- 1			
21	.1571E- 1	-.4453E 0	-.1571E- 1			

PARTICIPATION FACTOR

MODE	X1	X2	X3	X4	X5	X6
1	.1190E 1	.4563E- 9	.8569E 0			
2	-.7925E 0	.8095E- 9	.1234E 1			
3	.1315E- 8	-.9226E- 9	.1804E- 8			
4	-.2978E 0	.1267E- 8	.1223E 1			
5	.1214E 1	.3037E- 8	-.3326E 0			
6	-.1746E- 8	.1840E 1	-.7114E- 9			
7	.1412E- 9	.2799E- 8	-.3950E- 9			

PREPARED D. G. CROSS

CHECKED _____

MODEL ERTS B/C STUDY

B/C STUDY

INTERSTAGE & BOX - TRUSS AXIAL LOADS

INTERSTAGE-AXIAL LOAD CAPABILITY

1. BIPOD LEGS

$L = 21.4 \text{ in}$

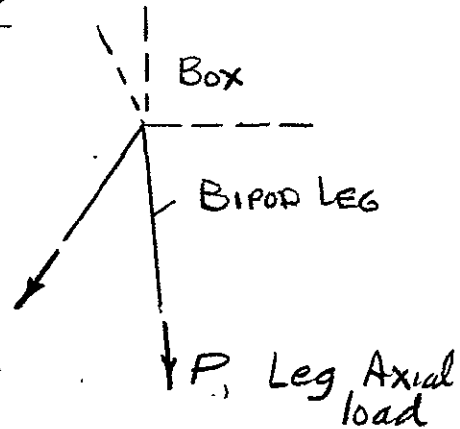
$E = .10 \times 10^6 \text{ psi}$

$A = .293 \text{ in}^2$

$I_{mn} = .122 \text{ in}^2$

$I_p = .218 \text{ in}^2$

Nom. dim's
(.060 t)



CASE 1 DESIGN ULTIMATE LOAD, BURNOUT

- 3890 lb. Compression + 625 in-lb Bending

- o Column Instability, M.S. = +.89
- o Maximum Stress, M.S. = +2.4
- o Flange Crippling, M.S. = +.30 ← CRIT.

CASE 2 DESIGN ULTIMATE LOAD, LIFTOFF

+ 2430 lb Tension + 1940 in-lb Bending

- o Foot Bending Stress, M.S. = +.17 (Cons.)
- o Separation Flange, M.S. = +.90
- o Flange Webs, M.S. = +.25 ← CRIT

Resultant Allowable Axial Load, Ultimate
in Bipod Leg (no change in geometry)

- 5050 lb compression
- OR + 3040 lb tension

INTERSTAGE BIPOD

060/ERTS

Head Area
REF. PG

19°

17.875 ± 0.05

.060 (TYP)

1.150

A

A

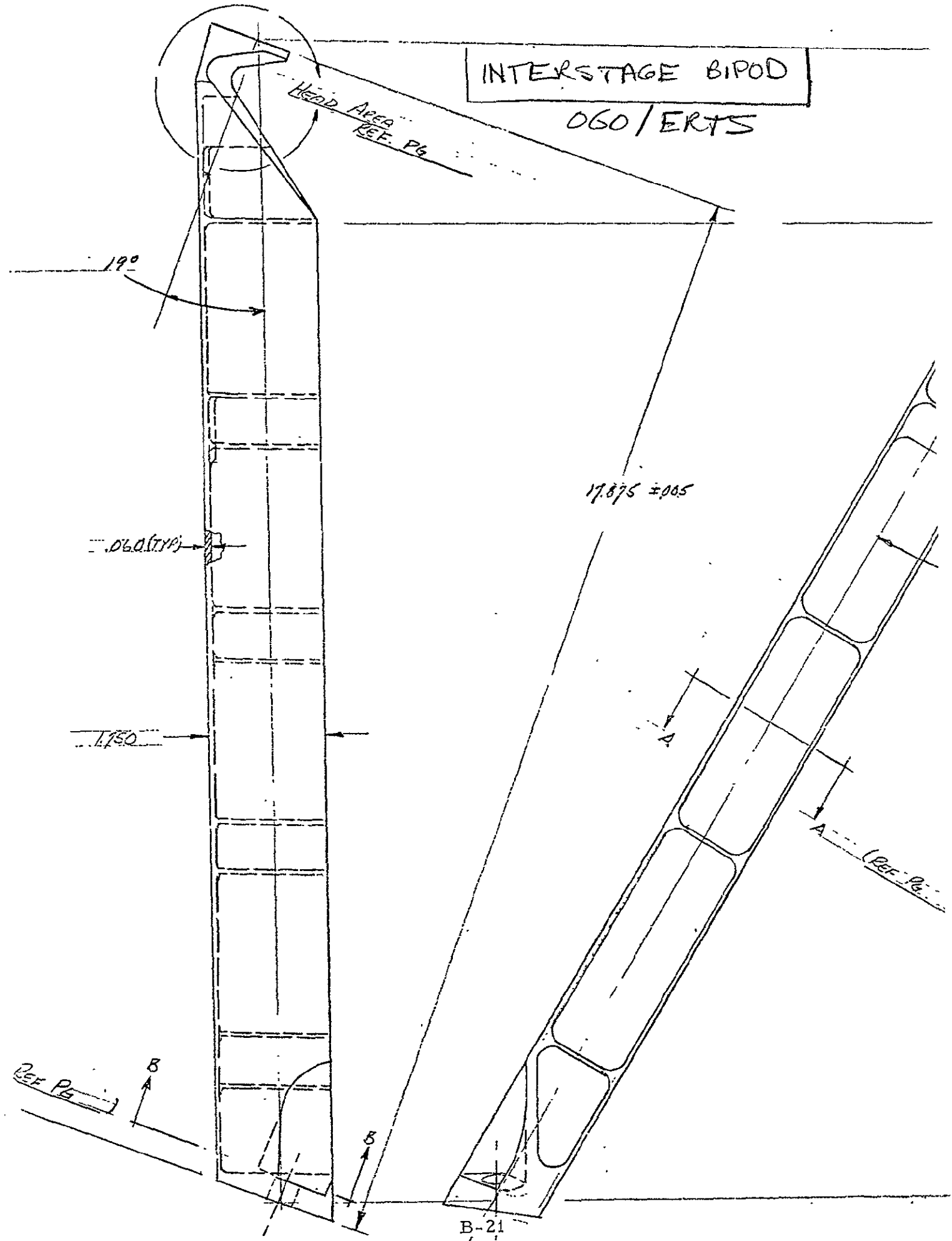
(Ref. Pg.)

Ref. Pg.

B

B

B-21



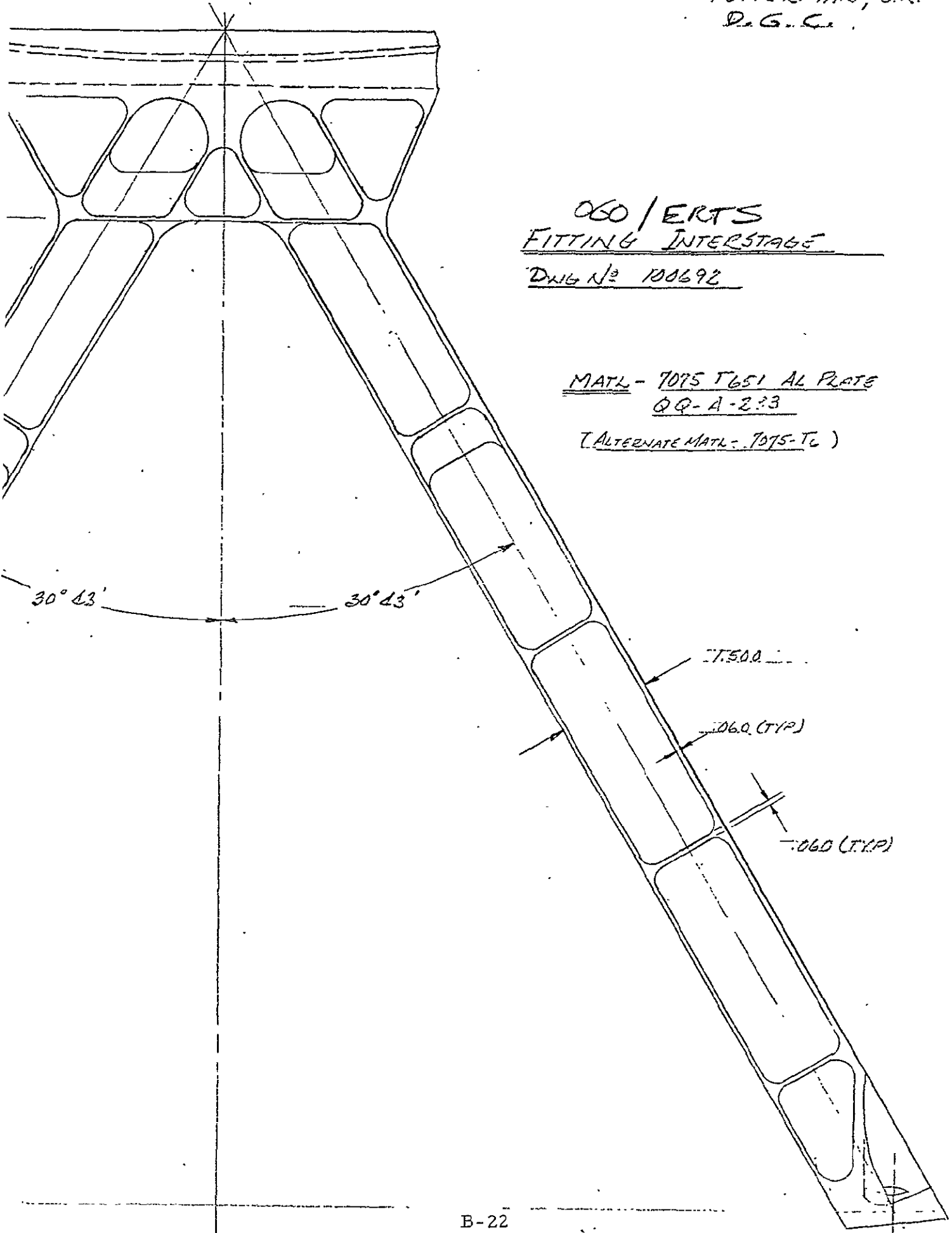
FUTTERMAN, S.R.
D.G.C.

OGO / ERTS
FITTING INTERSTAGE

DWG No 100692

MATL - 7075 T651 AL PLATE
QQ-A-233

(ALTERNATE MATL - 7075-T6)



PREPARED FUTTERMAN, S.R.
 CHECKED D. G. C. 1/16/70
 MODEL 060 / ERTS

REPORT NO. _____ PAGE _____

FITTING, INTERSTAGE



REF. DWG. NO. 100692 (CONT'D)

COLUMN STABILITY CHECK

CRITICAL CONDITION - BUENOUT, 12.9 g DOWN + 3.0 g LATERAL

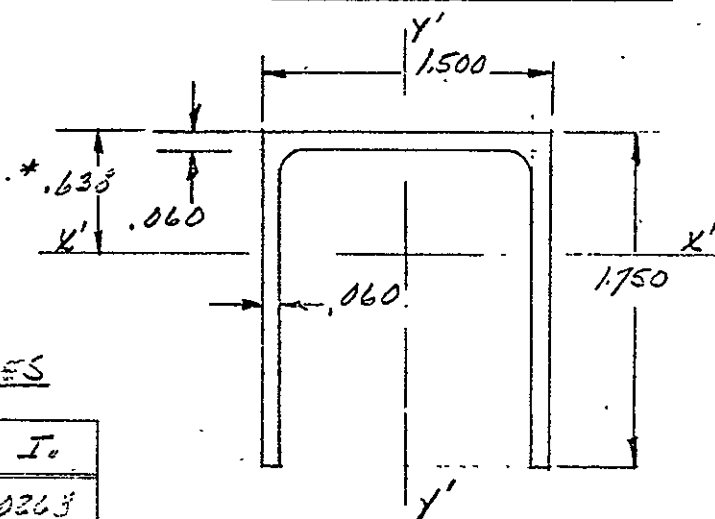
P_c = 3890 # @ θ = 45°

SPRING LOAD = 335 #

DAC
ULT (F=1.5 incl.)

REF. PG.

REF. PG.



BASIC SECTION PROPERTIES

EL	AREA	Y	AY	AY ²	I _c
1	.1050	.875	.0920	.0805	.0263
2	.1050	.875	.0920	.0805	.0263
3	.0823	.020	.0025	.0001	—
Σ	.2923	—	.1865	.1611	.0536

SECTION A-A

REF PG

$$* \bar{Y} = \frac{.1865}{.2923} = .633$$

$$I_{x'x'} = .0536 + .1611 - .1865 \times .633 = .096 \text{ IN}^4$$

$$I_{y'y'} = \frac{1.750 \times 1.500^3 - 1.690 \times 1.330^3}{12} = .122 \text{ IN}^4$$

$$I_p = .096 + .122 = .218 \text{ IN}^4$$

$$\text{AREA} = .2923 \text{ IN}^2$$

L' ASSUMED 22 IN

$$P_{x'} = .573 \text{ IN.}$$

$$P_{y'} = .647 \text{ IN.}$$

PREPARED FUTTERMAN, S.R.

REPORT NO.

PAGE

CHECKED D.G.C. 1/16/70FITTING, INTERSTAGEMODEL '060' / ERAS

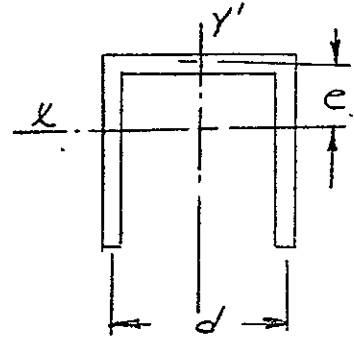
STL

REF DING N^o 100692 (CONT'D)COLUMN STABILITY CHECK (CONT'D)RADIUS OF GYRATION BASED ON TORSIONAL STABILITY.

$$P_B = \sqrt{\frac{\Gamma}{I_P} + \frac{G_c}{\pi^2 E_c} \times \frac{L^2 K}{I_P}}$$

REFERENCE (BLEICH)

$$K = \sum \frac{bt^3}{3}$$



$$\Gamma = \frac{d^2}{4} \left[I_x + e^2 A \left(1 - \frac{d^2 A}{4 I_y} \right) \right]$$

(CHANNEL)

FOR SECTION A-A REF PGS

$$K = \frac{.06^3}{3} (1.750 + 1.750 + 1.380) = .0000319$$

$$\Gamma = \frac{(1.44)^2}{4} \left[.096 + .608^2 \times .2928 \left(1 - \frac{1.44^2 \times .2928}{4 \times .122} \right) \right]$$

$$\Gamma = .519 (.096 - .370 \times .2928 \times .242) = .0363$$

$$P_B = \left[\frac{.0363}{.218} + \frac{.039 (22)^2 .0000319}{.218} \right]^{\frac{1}{2}}$$

$$P_B = \underline{.410 \text{ IN}}$$

*REF MIL HSB 5

PREPARED FUTTERMAN, S.R.

REPORT NO.

PAGE

CHECKED D.G.C. 1/16/70FITTING INTERSTAGEMODEL '060' / EKTS

STL

REF. DNG N° 100692 (CONT'D)COLUMN STABILITY CHECK (CONT'D)EFFECTIVE RADIUS OF GYRATION FOR COMBINED TORSION AND FLEXURAL STABILITY

$$P_E^4 - \left[\frac{P_x^2 + P_0^2}{1 - \frac{A Y_0^2}{I_P}} \right] P_E^2 + \left[\frac{P_x^2 \times P_0^2}{1 - \frac{A Y_0^2}{I_P}} \right] = 0$$

$$Y_0 = e - \left(\frac{d^2 A}{4 I_Y} \right)$$

REF BLEICH

FOR SECTION A-A

$$Y_0 = .600 - \left(\frac{1.44^2 \times .2937}{4 \times .125} \right) = -.657 \text{ in}$$

$$P_E^4 - \left[\frac{(.573)^2 + (.410)^2}{1 - .570} \right] P_E^2 + \left[\frac{(.573)^2 \times (.410)^2}{1 - .570} \right] = 0$$

$$P_E^4 - 1.152 P_E^2 + .1283 = 0$$

$$P_E^2 = \frac{1.152 \pm \sqrt{1.152^2 - 4 \times .1283}}{2} = \frac{1.152 \pm .906}{2}$$

$$P_E^2 = .123$$

(MIN.)

$$P_E = .351$$

(MIN.)

$$L' = 22" \quad \frac{L'}{P_E} = 62.6$$

$$F_c = \frac{\pi^2 E}{(L'/P)^2} = \frac{\pi^2 \times 10^7}{(62.6)^2} = 25200 \text{ #/IN}^2$$

$$f_c = \frac{3890}{.2928} = 13300 \text{ #/IN}^2$$

$$\text{GENERAL COLUMN CHECK } M/S: \frac{25200}{13300} - 1 = \underline{.89}$$

PREPARED FUTTERMAN, S.R.

REPORT NO.

PAGE

CHECKED D.G.C. 1/16/70

FITTING - INTERSTAGE

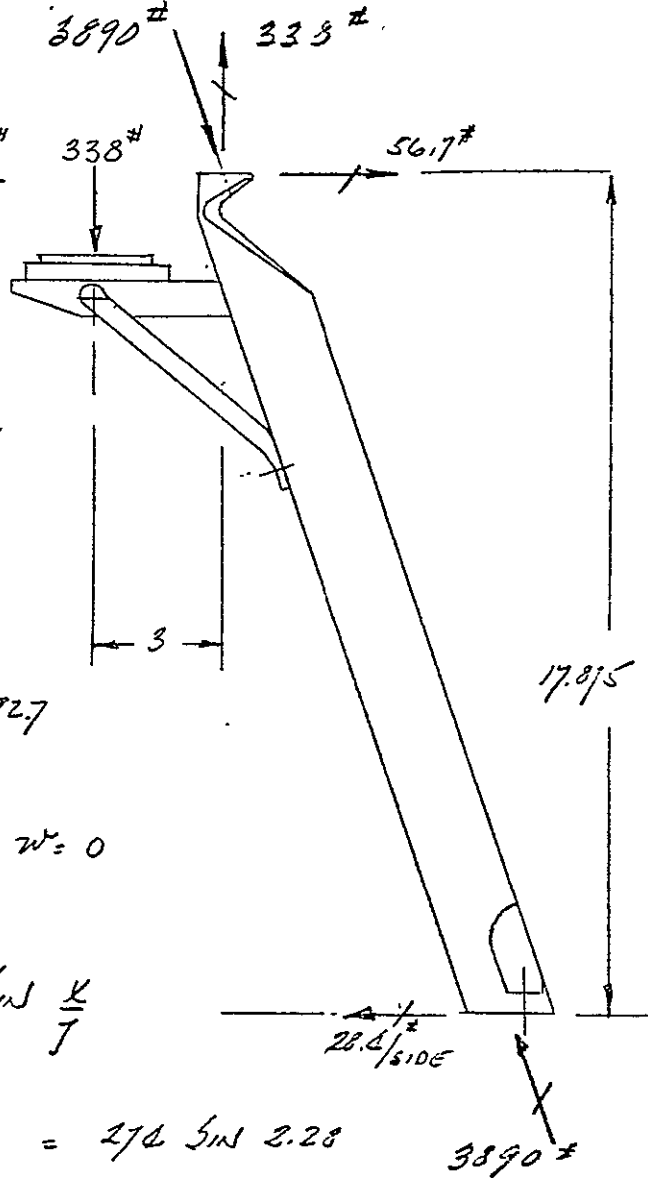
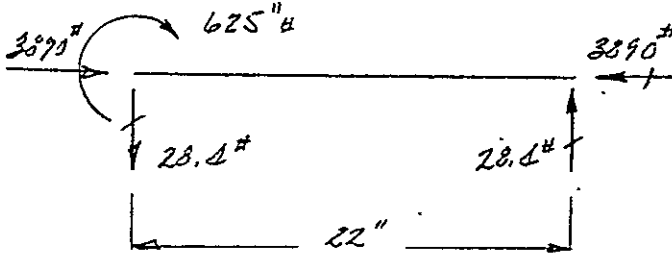
MODEL '060' / ERTS



REF DWG 110692 (CONT'D)

COLUMN STABILITY CHECK (CONT'D)

BEAM COLUMN CHECK



ASSUMED LOADING CONFIG.
(CRIT. LEG OF BRGD)

BEAM COL EQU. REF 'BEUMI'

$$M = C_1 \sin \frac{x}{j} + C_2 \cos \frac{x}{j} + w j^2$$

$$j^2 = \frac{EI^*}{P} = \frac{10^7 (0.36)}{3890} = 92.7$$

$$j = 9.65$$

$$C_1 = \frac{M_2}{4j} \quad C_2 = 0 \quad w = 0$$

$$M = \frac{M_2}{4j} \sin \frac{x}{j} = \frac{625}{22/9.65} \sin \frac{x}{j}$$

$$M_{MAX} @ x=22 = \frac{625 \times 9.65}{22} \sin \frac{22}{9.65} = 274 \sin 2.28$$

$$= 274 (0.7589) = 208 \text{ inch-pounds}$$

$$f_b = \frac{208 \times 0.638}{.096} = 3850 \text{ psi}$$

* IEFFECTIVE ASSUMED FROM $P_e = .351$ REF PG.

$$I^* = .2923 \times .351^2 = .036 \text{ in}^4$$

PREPARED FUTTERMAN, S.R.
 CHECKED D.G.C. 1/16/70
 MODEL '060' IERTS

REPORT NO.

PAGE

FITTING - INTERSTAGE

REF DWG N^o 100692 (CONT'D)BEAM COLUMN CHECK (CONT'D)

$$f_b = 3850 \text{ #/in}^2$$

$$f_c = 13300 \text{ #/in}^2$$

$$f_N = 13300 + 3850 = 17150 \text{ #/in}^2$$

$$F_{CC} = \bar{\sigma}_c = K_c \eta_c E \left(\frac{t}{b}\right)^2 \quad \text{WHERE } \bar{\sigma} > .75 \sigma_{cy}$$

$$K_c = 3.62$$

REF NACA REPT TN---

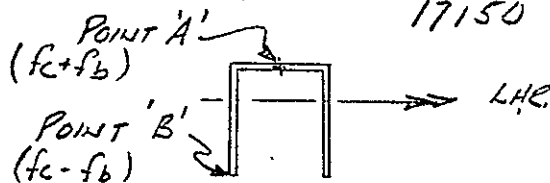
$$\eta_c = \frac{(1 - \nu_e^2)}{(1 - \nu_p^2)} \times \frac{E_s}{E} \left[\frac{1}{2} + \frac{1}{2} \sqrt{\frac{1}{4} + \frac{3}{2} \left(\frac{E_c}{E_s}\right)} \right]$$

$$F_{CC} = 58000 \text{ #/in}^2$$

$$b/t = 25 \text{ (4 SIDES S.S.)}$$

BEAM COLUMN CHECK

$$M/S = \frac{58000}{17150} - 1 = \underline{2.37}$$

NOTE:

THE AREA (POINT 'A') UNDER MAXIMUM STRESS HAS NO FREE EDGES AND THEREFORE HAS THE BETTER ALLOWABLE. THE FREE EDGE (POINT 'B') HAS STRESSES LESS THAN THE 13300 #/IN² STRAIGHT COLUMN STRESS BUT IS CRITICAL DUE TO ITS LOWER ALLOWABLE STRESS. THIS CHECK, FOR LOCAL INSTABILITY IS MADE ON THE FOLLOWING PAGE.

PREPARED FUTTERMAN, S.R.

REPORT NO.

PAGE

CHECKED D.G.C. 1/16/70

FITTING - INTERSTAGE

MODEL 060 / ERTS



REF DWG NO 100692 (CONT'D)

LOCAL INSTABILITY CHECK

POST BUCKLING STRENGTH

FRANGES

$F_{cc} = 20000 \text{ #/IN}^2$ REF NACA TN -
 $b/t = 29.5 \text{ I.E.F.}$
 $(b/t = 35)$ $P_{cc} = 20000 (2 \times .06 \times 1.72) = 4130 \#$
 $P_{cc} = 30000 \times .05 \times 1.72 = 2550$

HEEL

$F_{cc} = 58000 \text{ #/IN}^2$ REF NACA TN -
 $b/t = 25 \text{ N.E.F.}$ $P_{cc} = 58000 (.06 \times 1.47) = 5100$
 $(b/t = 30)$ $P_{cc} = 58000 \times .05 \times 1.47 = 4280$

TOTAL ALLOWABLE LOAD = 9230 #
6115 min

DESIGN NET COMP LOAD = 3890 #

$M/S = \frac{9250}{3890} = 1.40$
1.54 min

BUCKLING STRENGTH (BASED ON UNIFORM STRESS FIELD)

$f_c = 13300 \text{ #/IN}^2$

$\sigma_{cr} = \frac{K \pi^2 E}{12(1-\nu^2)} \left(\frac{t}{b}\right)^2$ (FRANGE CRITICAL)

$K = 1.50$

REF NACA TN 3751

$a/b = \frac{1}{1.75} = 2.29$

$\sigma_{cr} = \frac{1.50 \times \pi^2 (10.5) \times 10^6}{12(1-.3^2)} \left(\frac{.06}{1.72}\right)^2 = 17250 \text{ #/IN}^2$

$M/S = \frac{17250}{13300} = 1.30$
(1.11 min)

PREPARED FUTTERMAN, S.R.
 CHECKED D.G.C. 1/16/70
 MODEL '060' / E.R.T.S.

REPORT NO. _____ PAGE _____

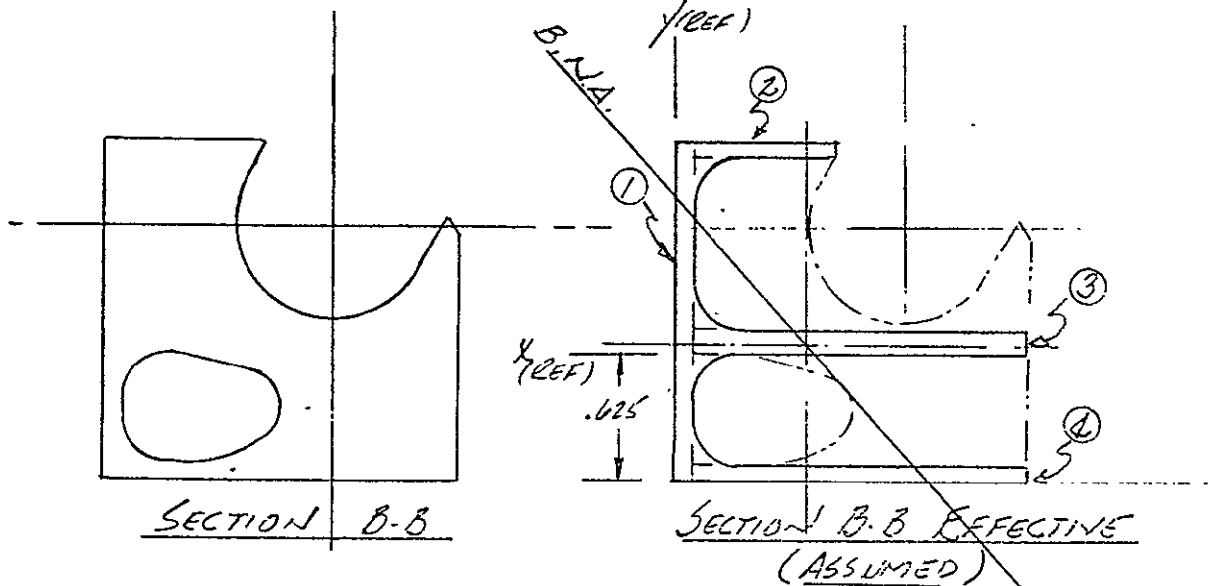
FITTING - INTERSTAGE



REF. DWG. N° 100692 (CONT'D)

SECTION B-B

REF P6



SECTION PROPERTIES

- ① $1.75 \times .06 = .1050 \text{ IN}^2$
- ② $.71 \times .06 = .0426 \text{ IN}^2$
- ③ $1.68 \times .15 = .2520 \text{ IN}^2$
- ④ $1.63 \times .06 = .1008 \text{ IN}^2$

SEG	AREA	X	AX	AX ²	Y	AY	AY ²	I _{OX}	I _{OY}	A _{XY}
1	.1050	.030	.00315	.00009	.250	.02625	.00656	.02630	-	.00077
2	.0426	.415	.01763	.00736	1.075	.04665	.05103	-	.00179	.01926
3	.2520	.900	.22680	.20412	.075	.01890	.00142	.00472	.05920	.17010
4	.1008	.900	.09072	.08163	-.590	-.05993	.03569	-	.02370	-.05398
Σ	.5002	-	.33831		-	.02132	.07473	.03152	.05469	.13627

$\bar{X} = \frac{.33835}{5002} = .6773$ $\bar{Y} = \frac{.02132}{5002} = .00427$

$I_x = .03152 + .09475 - .5002 (.00427)^2 = .12627 \text{ IN}^4$

$I_y = .13627 + .03469 - .5002 (.6773)^2 = .14851 \text{ IN}^4$

$I_{xy} = .13627 - .5002 (.00427)(.6773) = .11109 \text{ IN}^4$

PREPARED FUTTERMAN, S. R.
 CHECKED D.G.C. 1/16/70
 MODEL '060' / ER93

REPORT NO.

PAGE

FITTING - INTERSTAGE

REF DWG N° 100692 (CONT'D)

SECTION B-B (CONT'D)SECTION PROPERTIES (CONT'D)

$$\tan 2\alpha = \frac{2 I_{xy}}{I_x - I_y} = \frac{2 \times .11109}{.14851 - .12427} = 9.18$$

$$2\alpha = 83.8^\circ$$

$$\alpha = 41.9^\circ$$

$$I_y' = I_y \cos^2 \alpha + I_x \sin^2 \alpha - 2 I_{xy} \cos \alpha \sin \alpha$$

$$I_y' = .14851 (.7643)^2 + .12427 (.6679)^2 - 2 (.11109) (.14851) (.6679)$$

$$I_y' = .0275 \text{ in}^4$$

BENDING + AXIAL LOAD STRESS CHECK

CRITICAL CONDITION - LIFT OFF, 3.75 g UP + 3 g LATERAL
@ $\theta = 45^\circ$ REF PG

$$P = 2430 \#$$

$$f_b = \frac{Mc}{I} \quad M = 2430 \times .80 = .1940 \text{ in} \cdot \#$$

$$f_b = \frac{1940 \times .875}{.0275} = 61800 \#/\text{in}^2$$

$$f_t = \frac{1940}{.5002} = 3880 \#/\text{in}^2$$

$$F_{TU} = 77000 \#/\text{in}^2$$

REF MIL H32-5

SECTION B-B, BEND + TEN.

MS

$$\frac{77000}{61800 + 3880}$$

=

$$\frac{.17}{}$$

(CONSERVATIVE)

PREPARED FUTTERMAN, S.R. 3/26/63

REPORT NO.

PAGE

CHECKED D.G.C. 1/16/70

FITTING - INTERSTAGE

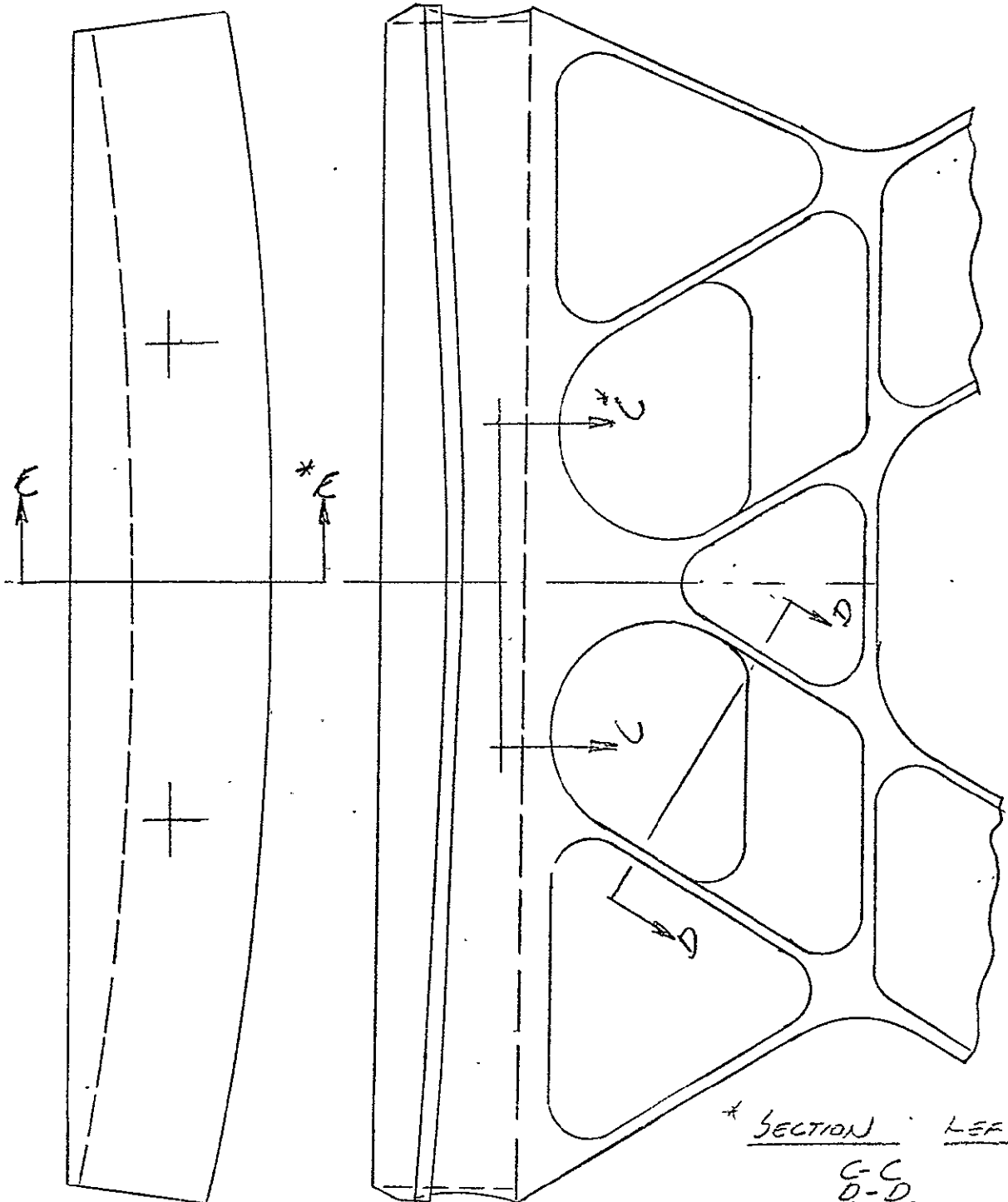
MODEL '060' / EXTS



REF DWG. No 100692 (CONT'D)

HEAD AREA CHECK

REF PG.



PREPARED FUTTERMAN, S.R. 3/26/63 REPORT NO.

PAGE

CHECKED D.G.C. 1/16/70

FITTING - INTERSTAGE



MODEL '060' / ERTS

REF. DWG. N° 100692 (CONT'D)

HEAD AREA, CHECK (CONT'D)

CRITICAL CONDITION - LIFT OFF, (2.5g FWD + 2.0g LATERAL @ 45°)

REF Pg.

MAXIMUM CORNER LOAD DUE TO SPACECRAFT INERTIA.

$$P_{ci} = 2.5(1.035)250 + 2.0(1.035)990 = 2696 \# \text{ vertical}$$

REF Pg

CORNER LOAD DUE TO 102375 SPRING

$$P_{cs} = 225 \#$$

REF Pg

DESIGN LOAD

$$P_c = 1.5(2696 + 225) = 4350 \#$$

$$P_v = P_c \cos 30^\circ + S \sin 30^\circ = P_c \cos 18^\circ$$

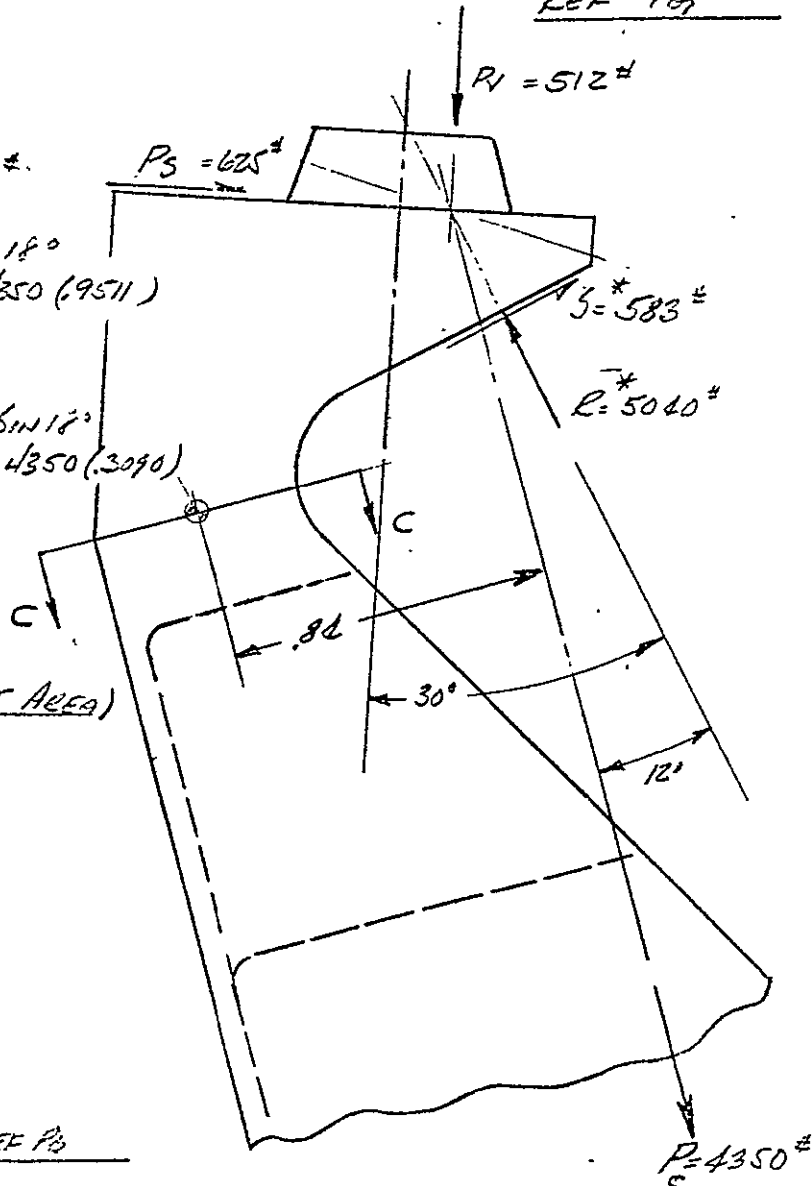
$$P_v = 5040(.933) + 583(1.500) = 4350(.9511)$$

$$P_v = 512 \#$$

$$P_s = P_c \sin 30^\circ - S \cos 30^\circ - P_c \sin 18^\circ$$

$$P_s = 5040(.500) - 583(.866) - 4350(.3090)$$

$$P_s = 625 \#$$



SECTION C-C (THROAT AREA)

$$M = 4350 (.84)$$

$$M = 3650 \# \text{ in}$$

$$P_T = 4350 \# \text{ (TENSION)}$$

* LOADS FROM 100699 REF Pg

PREPARED FUTTERMAN, S.R.

REPORT NO.

PAGE

CHECKED D. G. C. 1/16/70

FITTING - INTERSTAGE

MODEL '060' / EKTS -



REF DWS N² 100692 (CONT'D)

SECTION C-C (CONT'D)

$M = 3650 \#$ $P_T = 4350 \#$

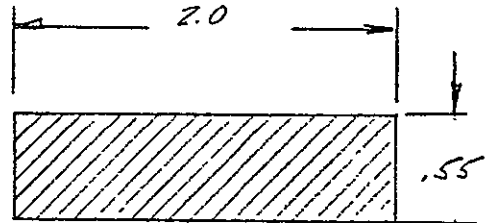
$f_b = \frac{6M}{bt^2} = \frac{6(3650)}{2(.55)^2}$

$f_b = 36100 \#/\text{IN}^2$

$f_t = \frac{4350}{.55 \times 2.0} = 4300 \#/\text{IN}^2$

$F_{T0} = 77050 \#/\text{IN}^2$

REF AXIS



SECTION C-C
(ASSUMED EFFECTIVE)

$M/S = \frac{77050}{36100 + 4300} - 1 = \underline{\underline{.90}}$

PREPARED FUTTERMAN, S.R. 3/27/65 REPORT NO.

PAGE

CHECKED D.G.C. 1/16/70

FITTING - INTERSTAGE

MODEL '060'



REF. DWG. NO. 100692 (CONT'D)

HEAD AREA CHECK (CONT'D)

SECTION D-D

$$M = \frac{3650}{\cos 30^\circ} = 2100 \#$$

$$P_t = \frac{4350}{2.5 \sin 30^\circ} = 4350 \#$$

$$f_b = \frac{M C}{I} = \frac{2100 \times .772}{.039}$$

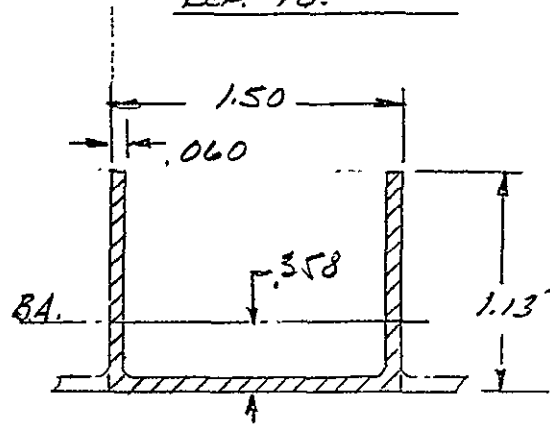
$$f_b = 41,600 \#/in^2$$

$$f_t = \frac{P_t}{A} = \frac{4350}{.218}$$

$$f_t = 20,000 \#/in^2$$

$$F_{TD} = 77000 \#/in^2$$

REF. PG.



SECTION D-D

(ASSUMED EFFECTIVE)

$$I = .039 in^4, A = .218 in^2$$

REF ANGLE

$$M/S = \frac{77000}{61600} - 1 = \underline{\underline{.25}}$$

PREPARED FUTTERMAN, SR 3/27/63

REPORT NO.

PAGE

CHECKED D.G.C. 7/15/70

FITTING - INTERSTAGE



MODEL '080' LEPTS

REF. DWG. NO 100672 (CONT'D)

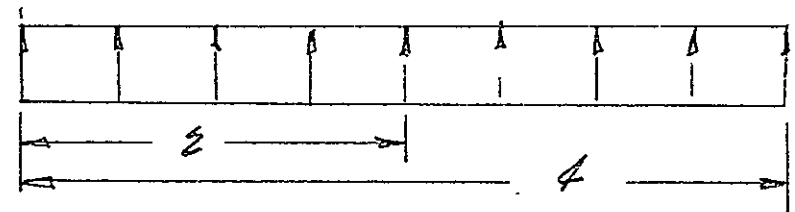
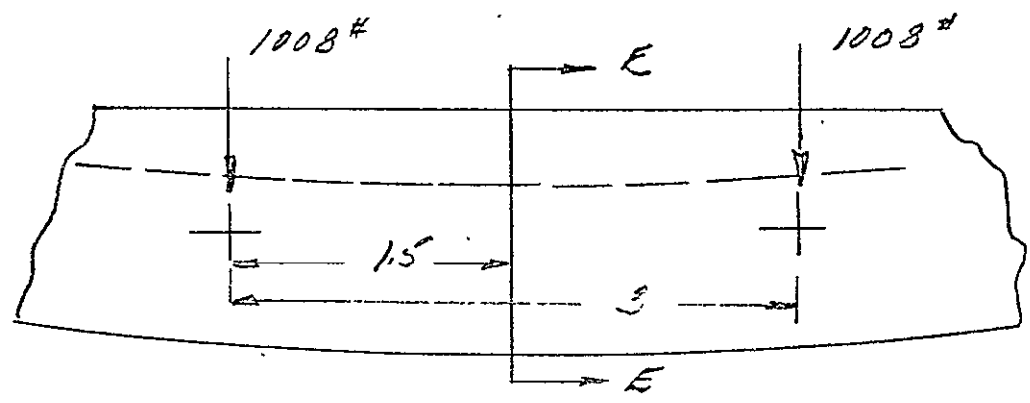
HEAD AREA CHECK (CONT'D)

SECTION E-E

REF PG

DESIGN LOAD $w = 1009/2 = 504 \#/IN$

REF PG



$w = 504 \#/IN$
(FROM 100699)

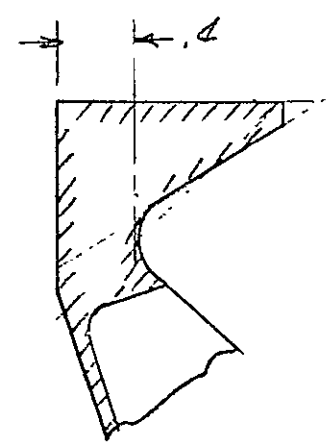
$$M/E = 1008(1.5 - 1.0) = 504 \#$$

$$f_b = \frac{M C}{I} = \frac{504 \times .8}{.058}$$

$$f_b = 6950 \#/IN^2$$

$$F_{TU} = 77000 \#/IN^2 \quad \text{REF ANCS}$$

$$M/S = \frac{77000}{6950} - 1 = \underline{\text{HIGH}}$$



SECTION E-E
 $I = .058 IN^4$

BOX MEMBERS - AXIAL LOAD CAPABILITY

(REF. ERTS COMPUTER RUN 1-1-INTERSTAGE AND BOX AS 3-D TRUSS)

2. Box Lower Edge Member, Dwg. 103746-3

$A = .064 \text{ in}^2$, Angle

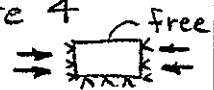
$b = 1.0 \text{ in}$, $t = .032 \text{ in}$.

$l = 1.5 \text{ in}$. between panel attachments

$E = 10 \times 10^6 \text{ psi}$
 $F_{cy} = 39000 \text{ psi}$ } 2024-T3 Sheet

$F_{cr} = K \frac{E}{1-\nu^2} \left(\frac{t}{b}\right)^2$; $K = .74$ @ $a/b = 1.5$
Roark Table XVI Case 4

$= \frac{.74 (10^7)}{.91} \left(\frac{3.2 \times 10^{-2}}{1.0}\right)^2 = 8400 \text{ psi}$



$P_{cr} = .064 \text{ in}^2 (8400 \text{ psi}) = \underline{540 \text{ lb}}$ Crippling Allowable
Panel supports prevent overall buckling failures

3. Box Lower Diagonal, Dwg. 100316-28

$A = 1.10 \text{ in}^2$, I-beam

$I \approx 4(.232 \text{ in}^2)(.44 \text{ in})^2 = .180 \text{ in}^4$

$L = 21.2 \text{ in}$, Euler column length

$b = 4.25 \text{ in}$, $t = .040 \text{ in}$ web

$E = 10 \times 10^6 \text{ psi}$
 $F_{cy} = 39000 \text{ psi}$ } 2024-T351 Extr. Caps
Webs

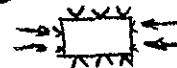
$P_y = (39000 \text{ psi})(1.10 \text{ in}^2) = 42700 \text{ lb (N.C.)}$

3. DIAGONALS (CON'D)

$$F_{cr} = K \frac{E}{1-\nu^2} \left(\frac{t}{b}\right)^2 ; K = 3.29 @ a/b > 3$$

Roark Table XVI Case 1

$$= \frac{3.29 (10^7) (4.0 \times 10^{-2})^2}{(.91) (4.25)^2}$$



$$= 3200 \text{ psi}$$

$$P_{cr} = (1.10 \text{ in}^2)(3200 \text{ psi}) = \underline{3520 \text{ lb LIM}}$$

Euler Buckling:

$$P_{cr} = \frac{\pi^2 (10^7) (.180)}{(2.12 \times 10^1)^2} = \underline{26600 \text{ lb ULT}}$$

4. BOX-CORNER VERTICALS, DWG. 100285

(103712, Box Assy)

$$A = .220 \text{ in}^2, \text{ Angle @ Base}$$

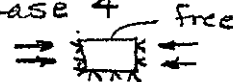
$$b = 1.0 \text{ in}, t = .110 \text{ in}$$

$$l = 1.40 \text{ in, between panel attachment}$$

$$\left. \begin{aligned} E &= 10 \times 10^6 \text{ psi} \\ F_{cy} &= 71000 \text{ psi} \end{aligned} \right\} \begin{aligned} &7075-T6S1 \\ &\text{Extrusion} \end{aligned}$$

$$F_{cr} = K \frac{E}{1-\nu^2} \left(\frac{t}{b}\right)^2 ; K = .784 @ a/b = 1.4$$

Roark Table XVI Case 4



$$= \frac{.785 (10^7) (1.10 \times 10^{-1})^2}{.91 (1.0)^2} = 104,000 \text{ psi}$$

N.C.

$$P_{cr} = (71000 \text{ psi})(.220 \text{ in}^2) = 15600 \text{ lb (N.C.)}$$

5 & 6. SIDE PANELS (Configuration Same as 060-Z Panel)

HONEYCOMB FACESHEET COMPRESSION

$h = .600$ in panel depth (facesheet N.A. to N.A.)

$t_f = .025$ in facesheet thickness, 2024-T3

$s = .125$ in core cell size

$t_c = .0007$ in core foil thickness

$\rho_c = 3.1$ psf core density

$\left. \begin{array}{l} (F_{cy} = 39000 \text{ psi}) \\ E'_c = 49000 \text{ psi} \\ G'_c = 24000 \text{ psi} \end{array} \right\}$

(5052 Alum.)
Avg "L" & "W" dir
min. values

Intracell Buckling Strength

$$F_{cw} = .75 E \left(\frac{t_f}{s} \right)^{3/2}$$

$$= .75 (10^7) \left(\frac{.025}{.125} \right)^{3/2} = 670,000 \text{ psi } \underline{\underline{N.C.}}$$

Facesheet Wrinkling Strength

$$F_{cw} = .43 \sqrt[3]{E E'_c G'_c}$$

$$= .43 \left[(10)(.049)(.024) \times 10^{18} \right]^{1/3} = 98,000 \text{ psi } \underline{\underline{N.C.}}$$

6. SIDE PANELS (CON'D)

Panel Bending

10g's vibration lateral response
in qual sine test

$$\begin{aligned}
 a &= 60 \text{ in} & \alpha &= b/a = 0.50 & I_o &= .0045 \text{ in}^4/\text{in} \\
 b &= 30 \text{ in} & & & Z_o &= .0150 \text{ in}^3/\text{in} \\
 Q &= 200 \text{ lb (10g's)} = 2000 \text{ lb} & & & F_{ur} &= 39000 \text{ psi} \\
 & \text{normal load, ultimate} & & & (h = .60 \text{ in}) \\
 & & & & z &= .025 \text{ in}
 \end{aligned}$$

$$\begin{aligned}
 M &= Q \left(\frac{.125 \alpha}{1 + 1.61 \alpha^3} \right) \\
 &= \frac{200(.125)(.50)}{1 + 1.61(.50)^3} \\
 &= 10.4 \text{ in-lb/in}
 \end{aligned}$$

Roark Table X
Case 36

Simply-Supported Rect. Panel
Under uniform normal pressure

$$f_b = 10.4 / .0150 = 6900 \text{ psi (Not critical)}$$

Panel Lateral Frequency

$$\begin{aligned}
 f_n &\approx 3.52 \sqrt{\frac{EI_o(1 + 2.21 \alpha^3)}{W (.01185 b^2 \alpha)}} \\
 &= 3.52 \left[\frac{(10^7)(.45 \times 10^{-2})(1.276)}{(.2 \times 10^3)(5.33)} \right]^{1/2}
 \end{aligned}$$

Based on max.
deflection of plate
; frequency of a
uniform loaded beam

$$= 258 \text{ Hz, High. No anticipated problems with intercostal coupling}$$

PREPARED D. G. CROSS 1/13/70
 CHECKED _____
 MODEL ERTS B/C STUDY

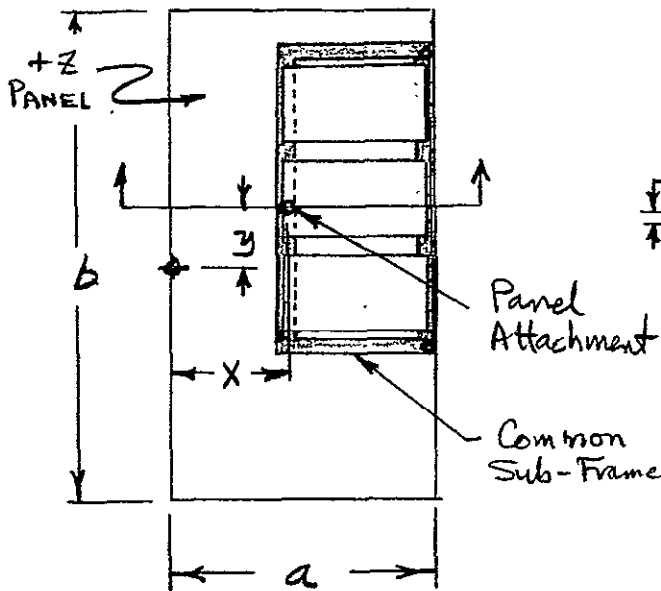
REPORT NO.

PAGE

**STRUCTURAL ANALYSIS -
THERMAL DISTORTION**

THERMAL DISTORTION OF SENSOR MOUNTS

FIRST CONCEPT FOR RBV CAMERA SUPPORT -
DIRECT ATTACHMENT TO PANEL



$h = .625$
 $x = 15.0, a = 30.0$
 $y = 16.0, b = 67.0$
 $\Delta T = 2.0^\circ F$
 $\alpha = 12.9 \times 10^{-6}$
 $\text{in/in-}^\circ F$

$\theta = w/x$

$w = \frac{\alpha \Delta T (1+\nu) 4a^2}{\pi^3 h} f\left(\gamma \equiv \frac{x}{a}, \beta \equiv \frac{y}{a}, \alpha \equiv \frac{b}{2a}\right)$

where $f(\gamma, \beta, \alpha) = \sum_{m=1,3,5,\dots}^{\infty} \frac{\sin m\pi\gamma}{m^3} \left(1 - \frac{\cosh m\pi\beta}{\cosh m\pi\alpha}\right)$

Ref. Timoshenko, "Theory of Plates and Shells", 2nd Ed., pg 164

PREPARED D G. Cross . . . 1/13/70

REPORT NO.

PAGE

CHECKED _____

STRUCTURAL ANALYSIS—
THERMAL DISTORTION

MODEL ERTS B/C STUDY

Calculations of θ

$$\eta = \frac{15.0}{30.0} = .500$$

$$\beta = \frac{16.0}{30.0} = .533$$

$$\alpha = \frac{67.0}{2(30.0)} = 1.118$$

$$f(\eta, \beta, \alpha) = \boxed{m=1} : \sin \frac{\pi}{2} \left(1 - \frac{\cosh 1.68}{\cosh 3.71} \right) = +.864$$

$$\boxed{m=3} : \frac{\sin \frac{3\pi}{2}}{27} \left(1 - \frac{\cosh 5.04}{\cosh 11.13} \right) = -.037$$

$$f(\eta, \beta, \alpha) = \underline{+.827}$$

$$w = \frac{(12.9 \times 10^{-6})(2.0^{\circ}\text{F})(1.3)(4)(.30 \times 10^2)^2(.827)}{\pi^3 (.625)}$$

$$= .515 \times 10^{-2} \text{ in}$$

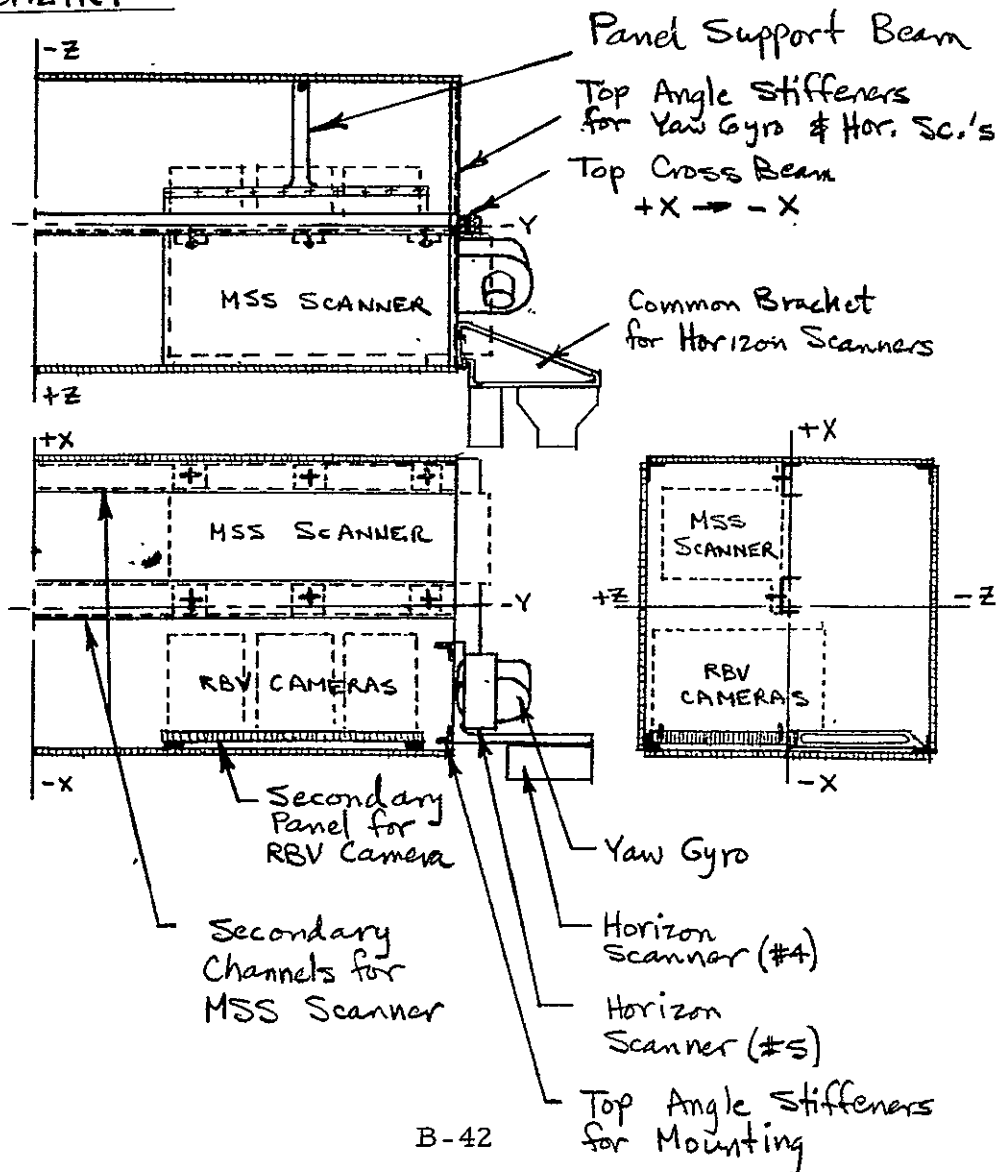
$$\theta = \left(\frac{.00515}{15.0} \right) \left(\frac{180^{\circ}}{\pi \text{ rad}} \right) = .0197 \text{ degrees of arc} \\ (\sim 1.18 \text{ minutes})$$

**STRUCTURAL ANALYSIS -
THERMAL DISTORTION**

THERMAL DISTORTION OF SENSOR MOUNTS

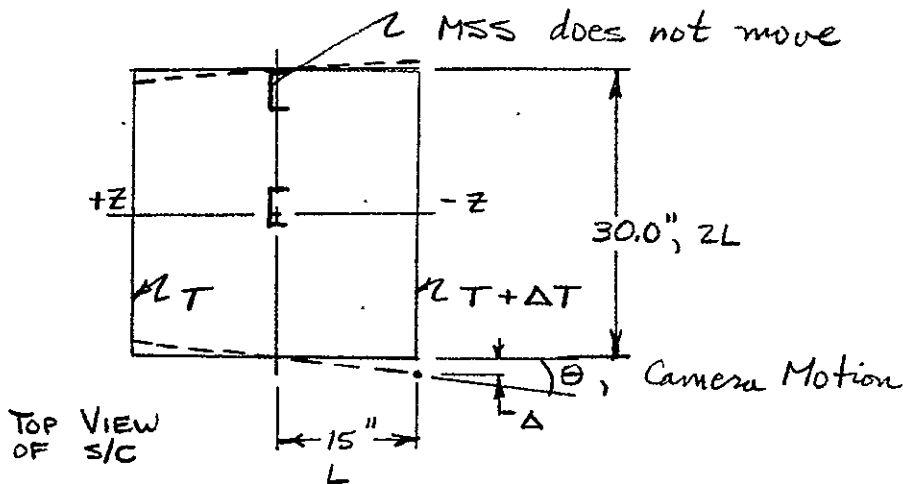
REQUIREMENT : The maximum angular distortion of any one of the four sensors relative to any other (RBV Camera assembly, MSS Sensor, Horizon Scanner and Yaw Gyro) is to be maintained to less than 0.10 degrees-of-arc during all orbital conditions.

GEOMETRY



**STRUCTURAL ANALYSIS -
THERMAL DISTORTION**

CASE 1 : Differential Temperatures
between Opposite Panels +z vs -z :



$$\theta = \Delta / L ; \Delta = L \alpha \Delta T$$

$$\therefore \theta = \alpha (\Delta T)$$

$$\Delta T = 10^\circ \text{F}$$

$$\alpha = 12.9 \times 10^{-6} \text{ in/in-}^\circ\text{F}$$

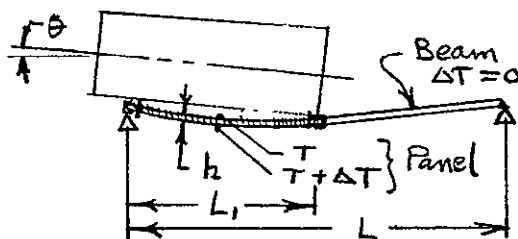
for 2024-T4 Alum.

$$\theta = (12.9 \times 10^{-6} \text{ in/in-}^\circ\text{F})(10^\circ \text{F})(57.3^\circ/\text{rad})$$

$$= \underline{.739 \times 10^{-2}} \text{ degrees-of-arc (vs } \pm 10 \text{ deg. all.)}$$

NON-CRITICAL

CASE 2: Temperature Gradient through Secondary
Panel for RBV Camera Mount



$$\alpha = 12.9 \times 10^{-6} \text{ in/in-}^\circ\text{F}$$

$$\Delta T = 0.5^\circ \text{F}$$

$$h = 0.5 \text{ in}$$

$$L_1 = 15 \text{ in}, L = 30 \text{ in}$$

$$\theta = \frac{L_1(L-L_1)(\alpha \Delta T)}{2h(L)} = \frac{15(15)(6.45 \times 10^{-6})}{2(0.5)(30)} [57.3^\circ/\text{rad}] = \underline{.277 \times 10^{-2}} \text{ degrees-of-arc}$$

B-43

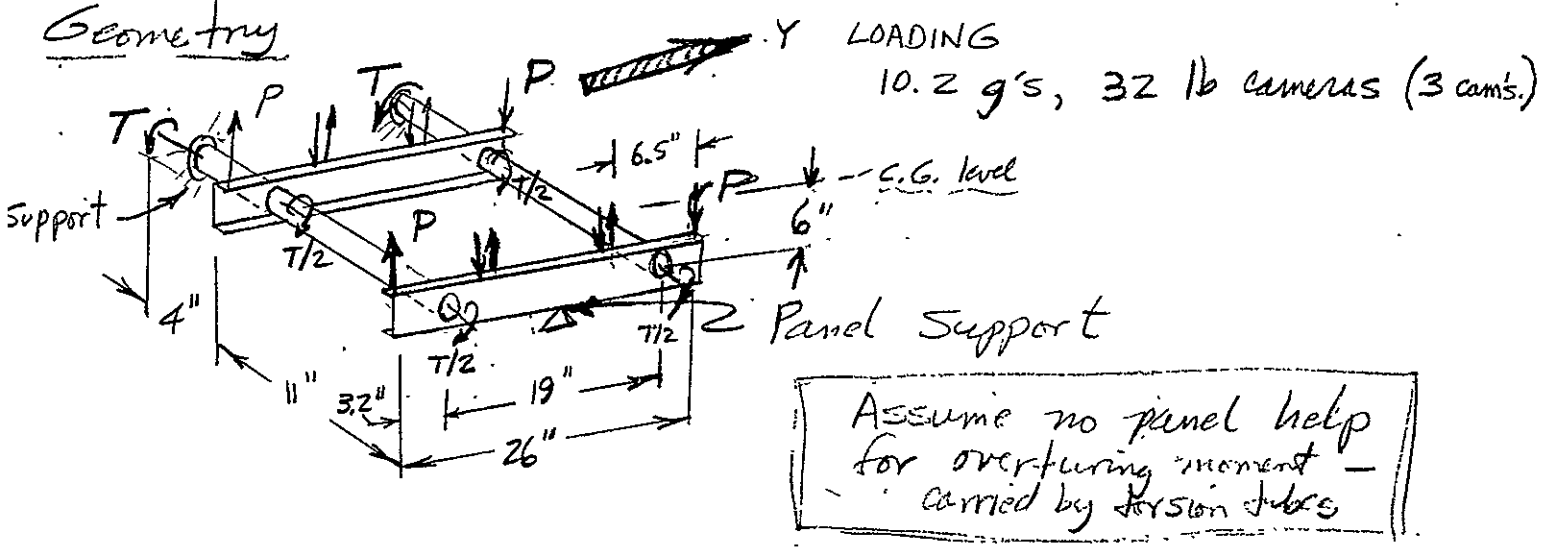
NON-CRITICAL

Mounting Frame for Camera

- Initial Structural Sizing, Y LOADS

12/4/69

Geometry



$$P = (32 \text{ lb})(10.2 \text{ g's})\left(\frac{1}{2}\right)\left(\frac{6 \text{ in}}{6.5 \text{ in}}\right) = \begin{matrix} 151 \text{ lb limit} \\ 226 \text{ lb ult} \end{matrix}$$

$$T = \frac{1}{2}(3)(32 \text{ lb})(10.2 \text{ g})(6 \text{ in}) = 2940 \text{ in-lb limit}$$

Torque in each tube at support

- $F_{tu} = 50000$
- $F_{su} = 30000$
- $F_{ty} = 38000 \text{ psi}$
- $F_{sy} = 22800 \text{ psi}$

Tube Check 1.5" x .040 Alum.

2024-T42

$$T_{DES} = (1.5 F_{tu})(2940) = \underline{4320 \text{ in-lb ult}}$$

$$f_s = 2T / \pi D^2 t = \frac{2(4320)}{\pi (1.5)^2 (.040)} = 30400 \text{ psi ult}$$

$$\therefore \boxed{T_{ult} = 4260 \text{ in-lb ult}} \quad \text{vs } 30000 \text{ psi } F_{su}$$

$$F_{scrapping} = E \left(\frac{1}{\lambda \beta} \right)^2 \left[1.8 + \sqrt{1.2 + .201 (\beta \sqrt{\lambda})^3} \right]$$

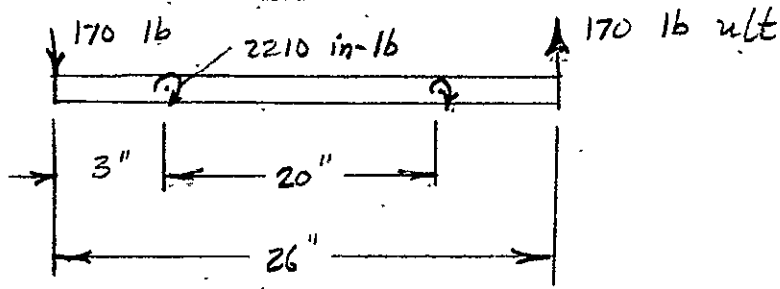
$\lambda = R/t = .75/.040 = 18.7$
 $\beta = l/R = 9/.75 = 5.3$
 $\beta \sqrt{\lambda} = 22.9$

$$= \frac{10^7}{[(1.87)(1.53) \times 10^2]^2} \left[1.8 + \sqrt{1.2 + .201 (22.9)^3} \right] = 51900 \text{ psi}$$

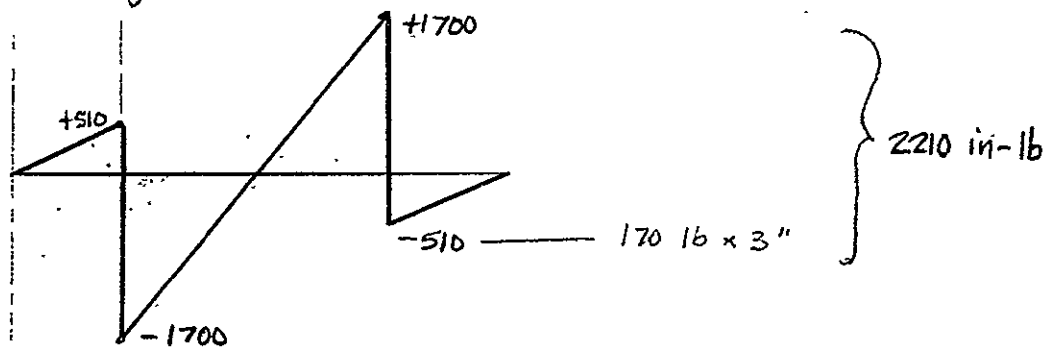
50.94 Crapping
Non Cr/2

12/4/69

Beam Check 2" web, 1" flange, .125 wall [



Moment Diagram (F1, F2)

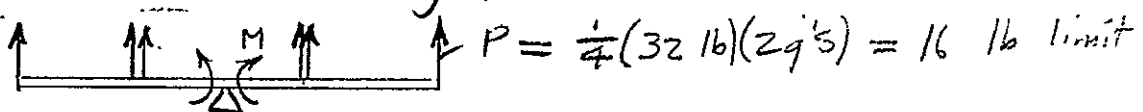


$$M_{DES} = 1700 \text{ in-lb ult}$$

$$I = \frac{1}{2}(2")^2(1")(.125) + \frac{1}{12}(2")^3(.125) = .333 \text{ in}^4$$

$$c = 1" \quad f_b = \frac{1700(1")}{.333} = 5100 \text{ psi Non Critical}$$

2nd Condition : 2g's limit lateral



$$M = [(16 \text{ lb})(13 \text{ in}) + 2(16 \text{ lb})(2.5 \text{ in})](1.5 \text{ F.S.}) = 470 \text{ in-lb ult}$$

Non Critical

15/4/59

Frequency Estimate (Jones Method)
in Y direction

$$K_{\theta} = \left(\frac{6J}{L} \right) (2 + \frac{1}{2}) \quad J = \frac{\pi}{4} D^3 t$$

(1.5 panel thick) $= \frac{\pi}{4} (1.5)^3 (0.040) = .106 \text{ in}^4$

$$= \frac{(.4 \times 10^7) (.106) (3)}{7.65} \quad L = 4'' + \frac{1}{3}(11'')$$

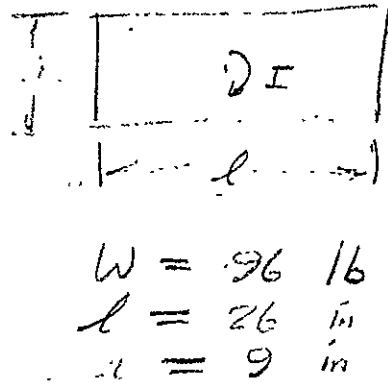
$$= 7.65''$$

$K = 1.667 \times 10^5 \text{ in-lb/rad ftal}$

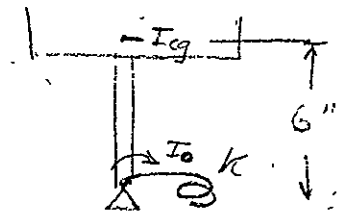
$$I_y = \frac{1}{12} \frac{W}{j} (l'' + a'')$$

$$= \frac{22}{12(256)} ((26)''^2 + 9'')^{741}$$

$$= 15.5 \text{ lb-in-sec}^2$$



$$I_{\text{panel}} = 15.5 + 22 \text{ lb} \left(\frac{26''}{2} \right)^2$$



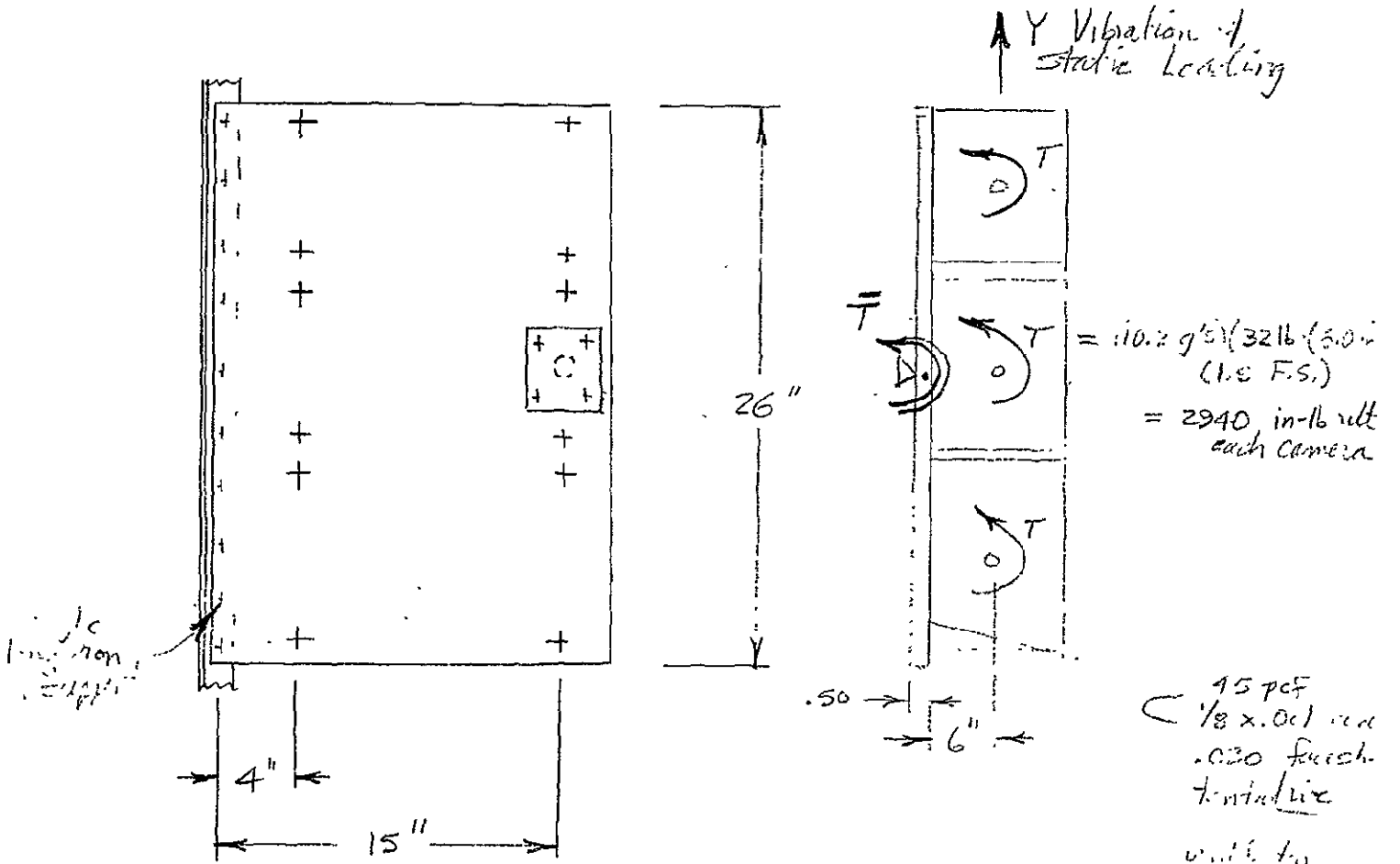
$I_0 = 24.5 \text{ lb-in-sec}^2$

$$\omega = \frac{1}{2\pi} \sqrt{k/I} = \sqrt{\frac{16.67 \times 10^4}{24.5}} / 2\pi = 13.1 \text{ Hz}$$

Low relative to 25 Hz requirement

Alternate Structure for Secondary Camera Mount - Hangar

12/8/69



45 pcf
1/8 x .001 in
.020 finish
tinted
with tin

Weight = (10)(26) [$\frac{4.5}{1728} (.5) + 2(.020)(.1)(1.5)$]
 W = 2.85 lb

Panel Torsional Loading
 $t = .020, G = 4 \times 10^6 \text{ psi}, G_c = 38 \times 10^6 \text{ psi}$
 $h = .50, b = .26, l = 7'' \text{ effective}$
 $T = 8820 \text{ in-lb total, 1st.}$

$$J = 2tb(zh+t)^2(1-\alpha)$$

where $\alpha = \frac{2(\coth \gamma_c b - 1)}{\gamma_c b \sinh \gamma_c b}$; $\gamma_c = \sqrt{\frac{4tG_c}{Gt(2h+t)}}$

$$\gamma_c = \sqrt{\frac{4(.50)(.01)}{(.02)(1.02)^2}} = .980; \gamma_c b = 25.4; \alpha = .0788$$

$$\therefore J = 2(.020)(26)(1.02)^2(.9212) = \boxed{.998 \text{ in}^4}$$

27 cfs
B-47
Equiv. to 2-2.0" x .160 wall tubes 1.5" x .040

VS .732 total
for two tubes...

Honeycomb structure:

9/8/67

$$\epsilon_s = \frac{\bar{T} A_1}{2tb(2h+t)(1-\alpha)} \quad ; \quad \epsilon_c = \frac{\bar{T} \gamma_c A_2}{4b h(1-\alpha)}$$

here $\Lambda_1 = 1 - \frac{1}{\cosh \frac{1}{2} \gamma_c b}$ \rightarrow $\Lambda_2 = \tanh \frac{1}{2} \gamma_c b \rightarrow \underline{1}$ as large $\gamma_c b$

$$\therefore \epsilon_s = \frac{88000}{2(.030)(.9217)} = 1030 \text{ psi with face sheets tens.}$$

$$\epsilon_c = \frac{88000(.980)}{4(26)(.26)(.910)} = 100 \text{ psi with core shear}$$

NonCritical

Thermally-Sized Honeycomb

12/22/69

$$\bar{h} = .50 \text{ in}, \quad t_c = .030, \quad \rho_c = 8.1 \text{ pcf} \quad ; \quad s = .125 \text{ in} / t_c = .002 \text{ in}$$

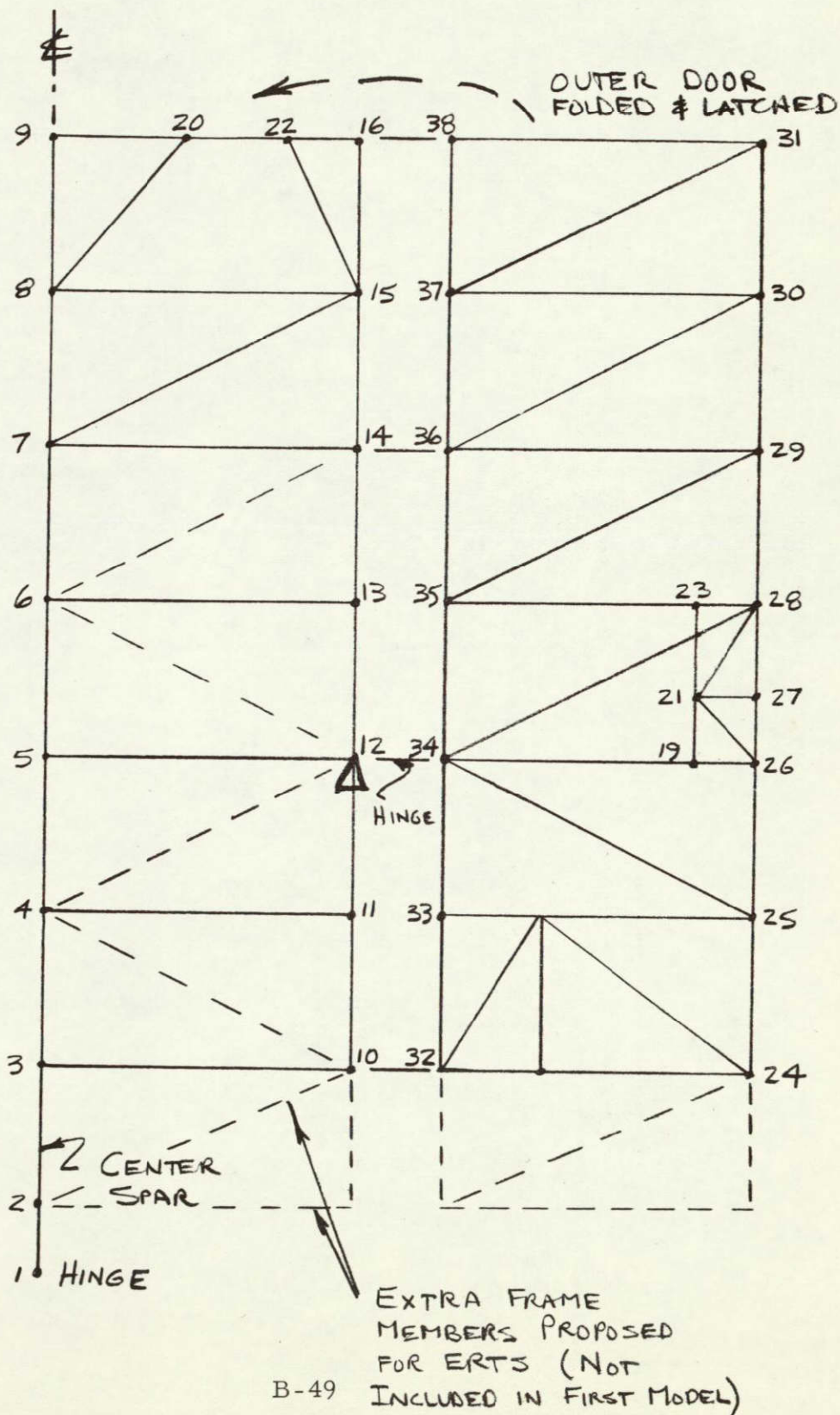
$$h = .44 \text{ in}, \quad 2h+t = .910, \quad G_c = 81200 \text{ psi}$$

$$\gamma_c = \sqrt{\frac{4hG_c}{Gt(2h+t)}} = \sqrt{\frac{4(.44)(.0203)}{.030(.910)^2}} = 1.20 \text{ in}^{-1}$$

$$\alpha \approx 2 / \gamma_c b = \frac{2}{1.20(26)} = .0640$$

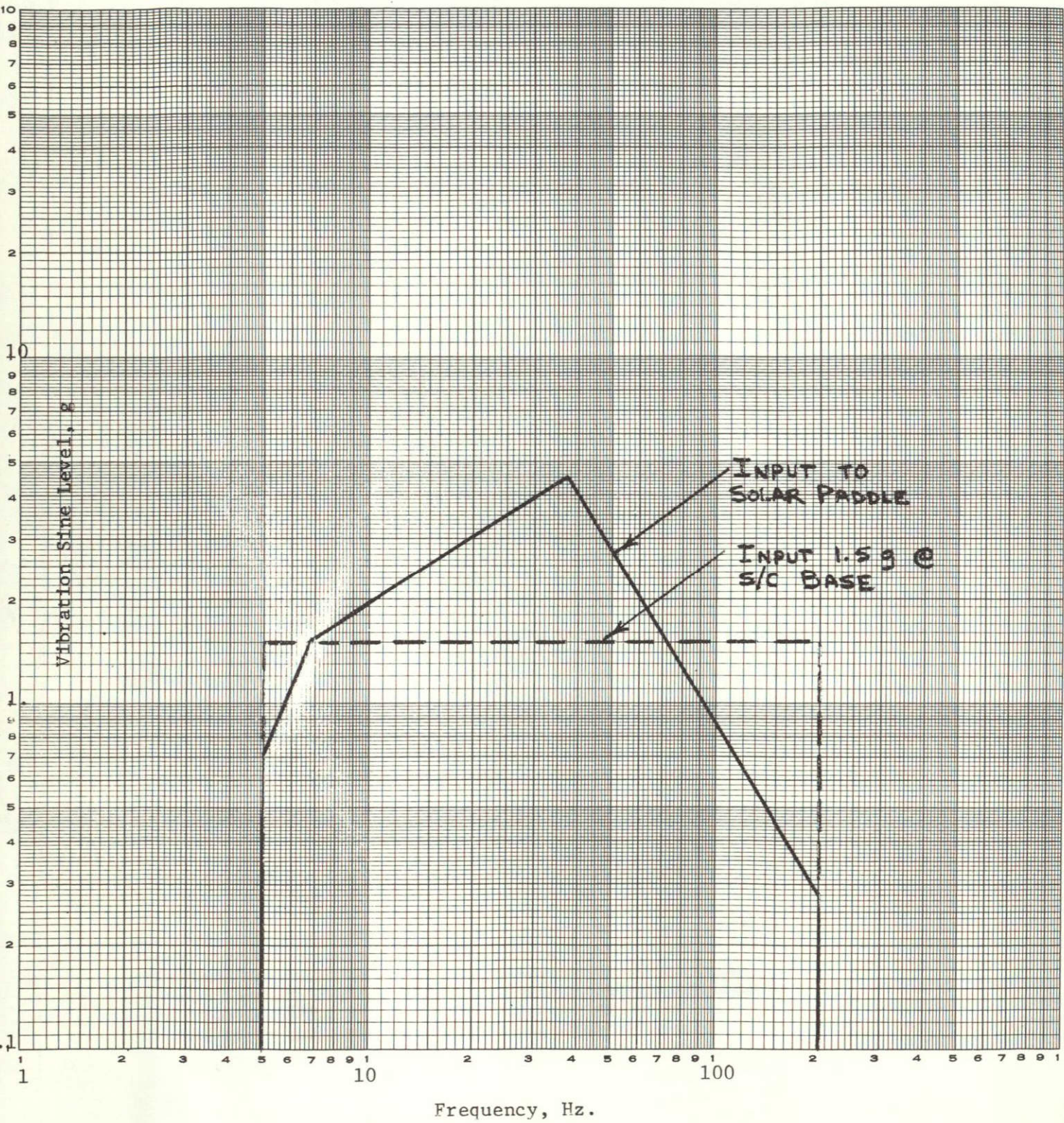
$$J = 2(.030)(26)(.910)^2(.9360) = \boxed{1.210 \text{ in}^4} \rightarrow \underline{\underline{30 \text{ Hz}}}$$

STRUCTURAL ANALYSIS
SOLAR ARRAY



B-49

QUALIFICATION VIBRATION SINE INPUT TO SOLAR ARRAY FROM 5-200 Hz.



DYNAMIC ANALYSIS -
SOLAR ARRAY

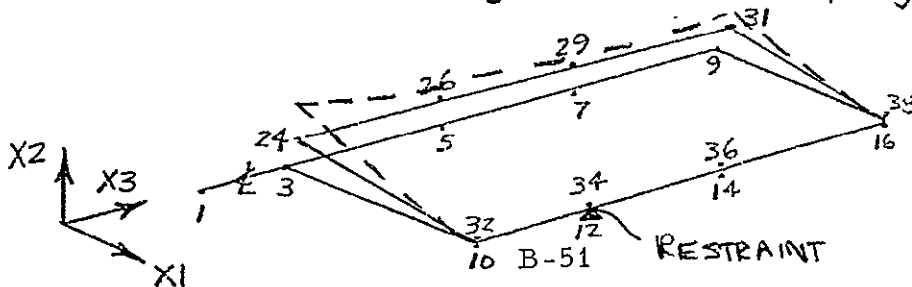
DYNAMIC SINUSOIDAL RESPONSE (g's)
 AXIS INPUT : S/C - X ; PANEL - X2, OUT-OF-PLANE
 MODE : 1 ; FREQUENCY 8 Hz

responses with * are
higher at 7 Hz

JT.	X1	X2	X3	JT.	X1	X2	X3
1				20		6.30	
2				21		1.04	0.28
3		*1.09		22		*6.63	
4		*1.50		23	0.31	*0.90	0.36
5		*2.13		24	4.27	18.45	0.43
6		*2.96		25	2.08	9.54	0.44
7		*3.93		26	0.26	2.53	0.45
8		*4.98		27	0.12		0.46
9		*6.08		28	0.39	0.96	0.46
10		2.78		29	0.70	1.76	0.47
11		1.35		30	1.53	6.29	0.48
12		-		31	2.79	12.12	0.48
13		*2.21		32		2.78	
14		*3.82		33		1.83	
15		*5.38		34		1.03	
16		*6.84		35		*2.19	
17	0.82	6.38	0.16	36		*3.82	
18	0.37	3.70	0.16	37		*5.40	
19	0.21	2.22	0.36	38		*6.85	

Note : Only those responses above .1g are listed

MODE SHAPE : Symmetrical Flapping of Outer Doors



**DYNAMIC ANALYSIS -
SOLAR ARRAY**

DYNAMIC SINUSOIDAL RESPONSE (g's)

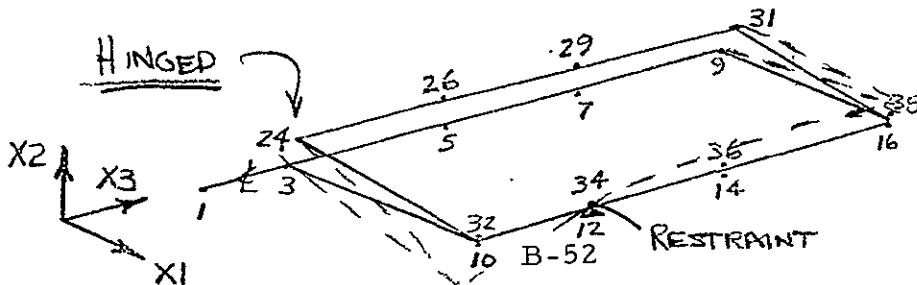
AXIS INPUT : S/C - Z ; PANEL-X1 ; IN-PLANE

MODE : 2 ; FREQUENCY 21 Hz

JT.	X1	X2	X3	JT	X1	X2	X3
1	3.98	-	-	20	3.18	2.83	0.62
2	-	-	-	21	3.25	0.53	1.59
3	5.39	-	-	22	3.24	5.60	1.63
4	4.72	-	-	23	3.57	0.82	1.59
5	-	-	-	24	4.28	3.77	1.55
6	3.58	-	-	25	3.71	1.93	1.58
7	5.20	-	-	26	3.16	0.48	1.67
8	4.98	-	-	27	3.17	-	1.70
9	3.18	-	-	28	3.37	0.55	1.75
10	5.49	18.07	1.95	29	4.11	0.94	1.80
11	4.72	8.71	1.95	30	4.96	0.85	1.82
12	3.21	-	1.94	31	4.48	1.41	1.83
13	3.58	4.14	1.94	32	5.30	18.07	1.93
14	5.19	3.70	1.93	33	3.81	8.90	1.93
15	4.86	1.44	1.91	34	3.21	-	1.92
16	3.24	7.39	1.91	35	3.96	4.33	1.93
17	4.57	11.61	1.76	36	5.10	3.70	1.93
18	3.64	2.73	1.76	37	5.02	1.38	1.94
19	3.21	0.40	1.59	38	3.32	7.39	1.95

Note : Only those responses above .1g are listed

MODE SHAPE : Anti-symmetrical Torsion



DYNAMIC SINUSOIDAL RESPONSE (g's)

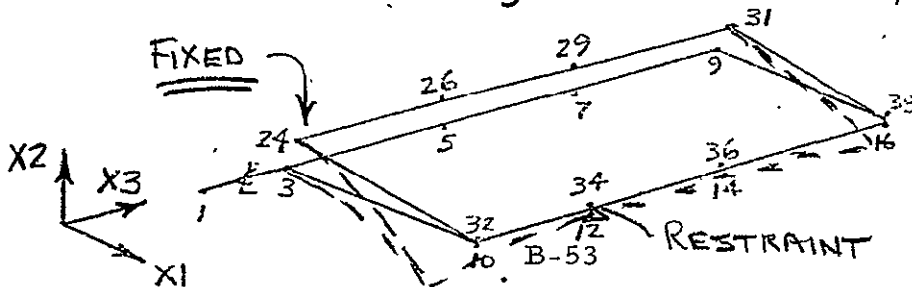
AXIS INPUT : S/C-X ; PANEL-X2, OUT-OF PLANE
MODE : 3 ; FREQUENCY 25 + Hz

Responses with * are
critical at 26 Hz

JT.	X1	X2	X3	JT	X1	X2	X3
1				20		9.76	
2				21	0.35	3.16	2.49
3		2.68		22		0.76	0.63
4		4.16		23	1.07	4.35	2.49
5		5.92		24	5.29	1.72	3.17
6		*6.55		25	2.45	1.80	3.07
7		*9.14		26	0.56	1.67	2.85
8		*11.98		27	0.36		2.76
9		14.98		28	1.42	5.12	2.63
10	0.16	*20.82	0.29	29	2.50	*8.76	2.46
11		12.48	0.37	30	2.04	*4.11	2.35
12	0.28	—	0.44	31	1.49	5.46	2.29
13		3.85	0.53	32	0.33	*20.82	0.54
14		4.75	0.63	33	0.46	12.98	0.57
15		2.60	0.60	34	0.19	2.25	0.59
16	0.10	3.74	0.62	35	0.36	4.13	0.64
17		18.23	1.25	36	0.28	*4.75	0.63
18	1.34	8.67	1.25	37	0.54	2.96	0.68
19	0.47	2.13	2.49	38	0.56	3.74	0.67

Note : Only those responses above .1 g are listed

MODE SHAPE : Symmetrical Flapping of Assy.



APPENDIX C
PARTS "A" AND "B" PARTS,
MATERIALS AND
PROCESSES LISTS

. ERTS PROJECT PARTS, MATERIALS AND PROCESSES LISTS
COMPATIBLE WITH GSFC PPL-10

SCOPE

This list of parts, materials and processes is submitted in compliance with Item 7.11.4 on Page 35 of the GSFC Design Study Specification for ERTS-A and -B. Use of OGO residual inventories from NAS-5-3900 contract as well as ERTS procurement of the following categories of items contained herein meets the requirements of the GSFC Preferred Parts List, PPL-10:

- o JANTX parts
- o ERMIL parts
- o Parts contained in the current TRW Preferred Parts List
- o Other TRW PT Specification or MIL parts which are procured and screened to meet the requirements of PPL-10.

The listings include, in tabular presentation, the procurement specification, the preferred/planned sources of supply and other information.

CONTENT

Section I lists the parts employed on OGO equipment which are considered suitable for ERTS application. The list also includes interchangeable alternate replacements to upgrade new procurement to current high reliability types. Where no listing appears in the ERTS part number column the FOOGO part number is valid for current procurement.

Section II identifies parts for use in new or modified ERTS designs. Many of the parts listed in Section II are also listed in Section I, since Section I provides a cross reference for the confirmation or conversion of FOOGO parts to current high reliability types.

Section III provides a listing of those materials and processes employed in the OGO programs which are current types valid for ERTS use. Also included are those additional materials and processes currently identifiable for ERTS.

Procurement of mechanical parts such as fasteners and electronic parts assembly "hardware" shall be in accordance with the TRW Systems Mechanical Preferred Parts Manual (MPPM).

SUMMARY

This listing of parts, materials and processes identifies approximately 95% of the total requirements. The list will be finalized upon completion of design identification early in the developmental program.

Parts identification has not been completed for components in the following ERTS assemblies:

- o Stored Command Programmer Converter
- o Payload Converter

APPROVED SOURCES

The following is provided for code identification for the listings in Sections I, II and III. "QPL" indicates listings in the Qualified Products List (DOD). In Section III, "QAPSD" indicates multiple listings in the TRW Quality Assurance Preferred Suppliers Directory. These are lists of TRW approved suppliers, who have demonstrated the capability of meeting requirements of the applicable specifications listed. "ASL" indicates multiple listing in the TRW Approved Suppliers List. Numbers prefixed with "CC" indicate Commodity Code number assigned by Quality Assurance (TRW) for the QAPSD (see above). Where no QPL or QAPSD is listed and a source name is entered, a mandatory source is not intended. Materials and Processes conforming to D.O.D. specifications are normally widely available and may be obtained in a competitive manner.

MANUFACTURER	ABBREVIATION	FEDERAL SUPPLY CODE IDENTIFICA- TION (FSCI)
Aerovox Corporation	AERO	96095
Allen & Bradley Company	A-B	01121
Amelco (See Teledyne)	Amelc	16170
American Machine and Foundry Co., Potter and Brumfield Division	P&B	77342
Amphenol Corp., Amphenol RF Division	Amph	74868
Angstrohm Precision Inc.	ANGS	17745
Babcock Electronics Corp., Relays Division	Bbck	09026
Cannon (See ITT Cannon)	Can	71468
Cinch Mfg. Co. and Howard B. Jones Div.	Cinch	71785
Coast Coil Co.	Coast	05245
Continental Device Corp.	CDC	07910

MANUFACTURER	ABBREVIATION	FEDERAL SUPPLY CODE IDENTIFICA- TION (FSCI)
Corning Glass Works, Electronics Components Div.	Corning	16299
Crystalonics (See Teledyne)	Cryst	12498
Dale Electronics Inc.	Dale	91637
Deutsch Co., Electronic Components Division	Deut	11139
Deutsch Filters Relay Division	DFilt	99699
Dickson Electronics Corp.	Dick	12954
Double A Products Co.	Db1A	24785
Electro-Film	ElFlm	
Electro-Midland	ElMid	
Erie Technological Products of Canada Ltd.	Erie	12294
Essex Wire Corp., Wire and Cable Div.	Essex	04217
Fairchild Camera and Instrument Corp., Semiconductor Div.	FSC	07263
Fenwal Electronics Inc.	Fenw	15801
General Electric Co., Semi-Conductor Products Dept.	GE	09214
General RF Fittings Inc.	GRFF	95077
General Time Corp.	GenTm	24733

MANUFACTURER	ABBREVIATION	FEDERAL SUPPLY CODE IDENTIFICA- TION (FSCI)
Hadley Mfg. Co. Inc.	Hadley	90218
Haveg Industries Inc.	Haveg	-
Heliotec General Corp., Electro Group	Helio	
Hewlett-Packard Co.	HPA	28480
Hoffman Industries	HFMN	28951
Hudson Wire Co.	HUDSN	84667
Indiana General Corp., Electro Mechanical Div.	IndGn	16636
International Wire and Cable Co.	InWir	15661
IRC Division of TRW Inc.	IRC	07716
ITT Cannon Electric Inc.	Can	71468
JFD Electronics Co.	JFD	73899
Johanson Mfg. Co.	Joh	91293
Kelvin Electric Co.	Kelv	07088
McCoy Electronics Co.	McCoy	00136
Mepco Division of Sessions Clock Co.	Mepco	80031
Microdot Inc.	Micro	98278

MANUFACTURER	ABBREVIATION	FEDERAL SUPPLY CODE IDENTIFICA- TION (FSCI)
Motorola Semiconductor Products Inc.	MOT	04713
National Semiconductor Corp.	NAT	12040
Omni Spectra Inc.	OMNI	
Parko Electronics Co. Inc.	PRK	13979
Phelps-Dodge Copper Products Corp., Habirshaw Cable & Wire Div.	PhlpD	94142
Potter Co., The West Coast Division	POT	19781
Potter & Brumfield (See American Machine and Foundry Co.)	P&B	77342
Precision Tube Co. Inc.	PT	82413
Pyle & National Co.	Pyle	49367
Radio Corp. of America, Electronic Components and Devices	RCA	86684
Raychem Corp.	Raych	06090
Raytheon Co., Components Div., Semiconductor Operation	Ray	07933
Reeves Hoffman	RevH	82567
Sangamo Electric Co.	Sang	53021
Shallcross Mfg. Co.	Shalc	54294
Signetics Corp.	SIG	18324

C-6

MANUFACTURER	ABBREVIATION	FEDERAL SUPPLY CODE IDENTIFICA- TION (FSCI)
Siliconix Inc.	SIL	17856
Solitron Devices Inc., Transistor Div.	SOL	21845
Sprague Electric Co.	Sprg	56289
Teledyne Inc. Crystalonics Division	Cryst	12498
Teledyne Systems Co., Communications Div. (Amelco)	Amelc	16170
Texas Instruments Inc., Semiconductor & Components Div.	TI	01295
Times Wire and Cable Division of International Silver Co.	Times	07145
Triad Transformer Corp.	Triad	81095
TRW Capacitor Division	TRWC	84411
TRW Semiconductors Inc.	TRWS	01281
TRW Systems Group, TRW Inc.	TRWSY	11982
Ultronix Inc.	Ultr	05347
Union Carbide Corp., Electronics Division	UC	05397
Uniform Tubes	UT	93306
United Control Corp.	Unct	97896

C-8

MANUFACTURER	ABBREVIATION	FEDERAL SUPPLY CODE IDENTIFICA- TION (FSCI)
United Transformer Co., Division of TRW Inc.	UTC	80223
Unitrode Corp.	Uni	12969
U. S. Capacitor Corp.	USCC	16546
Valor Inst Inc.	Valor	00262
Vanguard Electronics Co.	Van	03550
Victory Engineering Corp.	Vetry	83186
Vitramon Inc.	Vit	95275
Westinghouse Electric Corp, Semiconductor Dept.	WH	05277

SECTION I

APPROVED FOOGO PARTS AND ALTERNATE REPLACEMENTS

PART TYPE	PAGE
Capacitors	1 - 3
Connectors	4
Crystals	5
Filters, Fuses, Heater Elements	6
Inductors (Including "Chokes" and "Coils")	7
Microwave (RF) Devices	8
Relays	9
Resistors and Thermistors	10 - 12
Semiconductors	
Diodes	13 - 17
Transistors	18 - 23
Integrated Circuits	24
Solar Cells, Switches, Timers	25
Transformers	26
Wire and Cable	27 - 28

C-9

FOOGO PART NUMBER	ERTS PART NUMBER	SPECIFICATION	APPROVED SOURCES	REMARKS
CK05CW	M39014/01-xxxx	MIL-C-39014/1	Aerovox, Potter, Erie	CKR05BX xxxxP # 11
CK06CW	M39014/02-xxxx	MIL-C-39014/2	Aerovox, Potter, Erie	CKR06BX xxxxP # 11
CK12CW	M39014/05-xxxx	MIL-C-39014/5	Aerovox, Potter, Erie	CKR12BX xxxxP # 11
CK13CW	M39014/06-xxxx	MIL-C-39014/6	Aerovox, Potter, Erie	CKR13BX xxxxP # 11
CK16AX	M39014/06-xxxx	MIL-C-39014/6	Aerovox, Potter, Erie	CKR13BX xxxxP # 11
CKR19BX	M39014/06-xxxx	MIL-C-39014/6	Aerovox, Potter, Erie	Use CKR13 series # if possible
C-10 CL25Bxxxxxx3	PT4-1061	PT4-1061	Sprague	
CPV08 series	PT4-1079	PT4-1079	Sprague	
CS13	M39003/01-xxxx	MIL-C-39003/1	Sprague, UC	CSR13 xxxxKP
CTMxxxVAK	PT4-1078/1-xxxS	PT4-1078	Sprague, TRW Cap.	
CTMxxxVBK	PT4-1079-xxxK	PT4-1079	Sprague	
CTMxxxVDK	PT4-1079-xxxK	PT4-1079	Sprague	
CYFM10C	PT4-1055/1, CYFR10Gxxxx	PT4-1055	Corning	
CY10C	PT4-1055/1, CYFR10Gxxxx	PT4-1055	Corning	
CY12C	PT4-1081/1	PT4-1081	Vitramon	PT4-1055/1*, CYFR10G*

#For flight equipment "P" or "R" failure rate required ("L" or "M" not acceptable.

*Review possible use of PT4-1055 with specialist.

CAPACITORS

FOOGO PART NUMBER	ERTS PART NUMBER	SPECIFICATION	APPROVED SOURCES	REMARKS
CY15C	PT4-1055/2, CYFR10Gxxxx	PT4-1055	Corning	
CY20C	PT4-1055/3, CYFR20Gxxxx	PT4-1055	Corning	
CY30C	PT4-1055/4, CYFR30Gxxxx	PT4-1055	Corning	
PT4-1000	PT4-1077/5-01	PT4-1077	JFD	Variable, slot head
PT4-1004	PT4-1080	PT4-1080	Sangamo	
PT4-1006			Johanson	PT4-1077/3-01 variable: 250V, slot head
PT4-1010B	M39014/05	MIL-C-39014/5	Aerovox, Potter, Erie	
PT4-1010C	M39014/05	MIL-C-39014/5	Aerovox, Potter, Erie	
PT4-1010D	M39014/05	MIL-C-39014/5	Aerovox, Potter, Erie	
PT4-1010E	M39014/06	MIL-C-39014/6	Aerovox, Potter, Erie	
PT4-1010F	M39014/06	MIL-C-39014/6	Aerovox, Potter, Erie	
PT4-1010G	PT4-1062	PT4-1062	Aerovox, Potter, Erie	
PT4-1011G 104M	PT4-1062-001	PT4-1062	Aerovox, Potter, Erie	
PT4-1011J 504F	PT4-1062-005	PT4-1062	Aerovox, Potter, Erie	
PT4-1011K 105M	PT4-1062-007	PT4-1062	Aerovox, Potter, Erie	
PT4-1011L 2052	PT4-1062-009	PT4-1062	Aerovox, Potter, Erie	
PT4-1012	M39003/01-xxxx	MIL-C-39003/1	Sprague, UC	

FCCGO PART NUMBER	ERTS PART NUMBER	SPECIFICATION	APPROVED SOURCES	REMARKS
PT4-1013-38			UC	PT4-1059*
PT4-1017-5			Sprague, TRWC Aero, Pot, Erie	PT4-1079* PT4-1062*
PT4-1037H	PT4-1066-2	PT4-1066	Gen. Electric	
PT4-1047BG-xxxxK	M39014/05-xxxx	MIL-C-39014/5	Aero, Pot, Erie	
PT4-1048	PT4-1062	PT4-1062	Aero, Pot, Erie	ceramic
PT4-1055/1	PT4-1055/1	PT4-1055	Corning	glass
PT4-1055/2	PT4-1055/2		Corning	glass
C-12 PT4-1055/3	PT4-1055/3		Corning	glass
PT4-1055/4	PT4-1055/4	PT4-1055	Corning	glass
PT4-1059	PT4-1059	PT4-1059	Un. Carb.	solid ta
PT4-1066	PT4-1066	PT4-1066	GE	ta foil
PT4-1078/1	PT4-1078/1	PT4-1078	Sprague, TRWC	nylon
4BN 1055()G			U.S. Cap JFD	PT4-1067* PT4-1089*

VARIABLE CAPACITORS

PT4-1077/3	PT4-1077/3	PT4-1077/3	Johanson
VC16G			JFD
VC25G			JFD

*Evaluate electrical and dimensional parameters and review with Specialist.

CONNECTORS

FOOGO PART NUMBER	ERTS PART NUMBER	SPECIFICATION	APPROVED SOURCES	REMARKS
PT2-5 Series	PT2-94-X	PT2-88	Cannon	
PT2-7-2	PT2-7-2	PT2-7	Cinch	
PT2-7-55	PT2-7-55	PT2-7	Cinch	
PT2-14-2	PT2-14-2	PT2-14	GRFF	TNE
PT2-17-3	PT2-17-3	PT2-17	GRFF	TM
PT2-18-4			Deutsch	PT2-88*
PT2-43			Bendix	NAS1599*
PT2-48			Bendix	NAS1599*
PT2-50				
PT2-62	PT2-94-X	PT2-88	Cannon	
PT2-84/1	PT2-84/1	PT2-84	Omni	OSM218

*Evaluate for substitution

CRYSTALS

FOOGO PART NUMBER	ERTS PART NUMBER	SPECIFICATION	APPROVED SOURCES	REMARKS
PT4-12000	PT4-12006-X	PT4-12006	MCCOY, REVH	
PT4-12003-1	PT4-12009-X	PT4-12009		
PT4-12003-2	PT4-12009-X	PT4-12009		
PT4-12003-3	PT4-12009-X	PT4-12009		
PT4-12003-4	PT4-12009-X	PT4-12009		
PT4-12003-5	PT4-12008-X	PT4-12008		
PT4-12014-X	PT4-12014-X	PT4-12014		
PT4-13002-X	PT4-1200X-X	PT4-120XX	MCCOY, REVH	

FILTERS

FOOGO PART NUMBER	ERTS PART NUMBER	SPECIFICATION	APPROVED SOURCES	REMARKS
PT4-1016	PT4-1039-1		Erie	
PT4-1039-1	PT4-1039-1		Erie	
PT4-1063/1				Feed thru
C-15 PT4-13016-6	PT4-13016-6			Feed thru
1270-024			Erie	Low Pass, hif

FUSE

PT3-1006	PT3-1006		Electro-Midland	
----------	----------	--	-----------------	--

HEATER ELEMENT/STRIP

PT4-13009-7	PT4-13048/1		Electro-film	
-------------	-------------	--	--------------	--

FOOGO PART NUMBER	ERTS PART NUMBER	SPECIFICATION	APPROVED SOURCES	REMARKS
PT6-1-3	PT6-18/x-x	MIL-T-27	Vanguard	
PT6-3-3				
PT6-3-4				
PT6-3-6				
PT6-3-7				
PT6-3-8				
PT6-3-9				
PT6-3-10				
PT6-3-11				
PT6-3-12				
PT6-14-x				
PT6-18/4				
PT6-18/6	PT6-18/6-x	MIL-T-27	Vanguard	

MICROWAVE (INCLUDING RF) DEVICES

FOOGO PART NUMBER	ERTS PART NUMBER	SPECIFICATION	APPROVED SOURCES	REMARKS
PT4-13027/11	PT4-13027/11	PT4-13027	*	Isolator
PT4-13034/20	PT4-13034/20	PT4-13034	*	Coupler

C-17

*Sources to be reviewed before procurement action.

RELAYS

FOOGO PART NUMBER	ERTS PART NUMBER	SPECIFICATION	APPROVED SOURCES	REMARKS
PT2-1000				(a)
1001	PT2-1060	PT2-1060	Babcock	
1002	PT2-1031-x	PT2-1031	P&B, Bbck, DFilt	(a) M5757/21
1004	(b)			/12
1005-1	PT2-1034-x	PT2-1034	P&B, Bbck, DFilt	(a)
1005-2	PT2-1034-x	PT2-1034		(a)
1008	PT2-1034-x	PT2-1034		(z) /10
1011	PT2-1035-x	PT2-1035		(a) /21
1012	PT2-1034-x	PT2-1034		(a) /13-084
1013	PT2-1034-x	PT2-1034		(z) /10-015
1015	PT2-1035-x	PT2-1035	P&B, Bbck, DFilt	(a) /12
1029-1	(b)			(a)
1034	PT2-1034-x	PT2-1034	P&B, Bbck, DFilt	(a)
1035	PT2-1035-x	PT2-1035		(a)
1037	PT2-1034-x	PT2-1034		
1039	PT2-1034-x	PT2-1034	P&B, Bbck, DFilt	/13-014
1047-1				(a) /23
1048-1	PT2-1034-x	PT2-1034	P&B, Bbck, DFilt	/13
PT2-1049-1	(b)			M5757/12
421-26				(a) M5757/39

(a) See Parts Specialist for specification.

(b) See Parts Specialist - one general purpose replacement to be developed for these sensitive relays (sensitive relays

RESISTORS

FOCGO PART NUMBER	ERTS PART NUMBER	SPECIFICATION	APPROVED SOURCES	REMARKS
PT4-7BxxxxF	RNR60	MIL-R-55182	Mepco, IRC	
PT4-7CxxxxF	RNR60	MIL-R-55182	Mepco, IRC	
PT4-7ExxxxF	RNR60	MIL-R-55182	Mepco, IRC	
PT4-13VxxxxJ	RWR89SRxxxxFR	MIL-R-39007	Dale	
PT4-15-xxxxJ	RCR07GxxxxJS	MIL-R-39008	Allen-Bradley	
PT4-18E	RBR56L	MIL-R-39005	Kelvin, Ultronix Shallcross	
PT4-18-P	RBR56L	MIL-R-39005	Kelvin, Ultronix Shallcross	
RBR56LxxxxxTP	RBR56LxxxxxTP	MIL-R-39005	Kelvin, Ultronix Shallcross	
RC05	RCR05	MIL-R-39008	Allen-Bradley	
RC07	RCR07	MIL-R-39008	Allen-Bradley	
RC12G	RCR07	MIL-R-39008	Allen-Bradley	
RC20	RCR20	MIL-R-39008	Allen-Bradley	
RC32	RCR32	MIL-R-39008	Allen-Bradley	
RC42	RC42	MIL-R-11	Allen-Bradley	

FCCGO PART NUMBER	ERTS PART NUMBER		SPECIFICATION	APPROVED SOURCES	REMARKS
RE60	RER60		MIL-R-39009	Dale	
RE65	RER65		MIL-R-39009	Dale	
RE70	RER70		MIL-R-39009	Dale	
RN55 or RNC55	RNR55H	RNC55H	MIL-R-55182	Angstrohm Mepco, IRC	
RN60 or RNC60	RNR60H	RNC60H	MIL-R-55182	Mepco, IRC	
RN65 or RNC65	RNR65H	RNC65H	MIL-R-55182	Mepco, IRC	
C-20 RN70	RNR70C	RNN70C	MIL-R-55182	Mepco	
RW57	RWR74		MIL-R-39007	Dale	
RW59	(a)		MIL-R-39007	Dale	RWR80, RWR89
RW69	(a)		MIL-R-39007	Dale	RWR80, RWR89
RWP18	RWR80		MIL-R-39007	Dale	

(a) Select appropriate values from RWR80 or RWR89

		RESISTORS/THERMISTORS		
FOOGO PART NUMBER	ERTS PART NUMBER	SPECIFICATION	APPROVED SOURCES	REMARKS
PT4-1-1	PT4-81/21	PT4-81 ↓	} Fenwal Electronics Victory Engineering	
PT4-1-2	PT4-81/21			
PT4-1-3	PT4-81/21			
PT4-2-821G	PT4-81/13-26		TI :	
PT4-6	PT4-81/2-01		} Fenwal Electronics Victory Engineering	PT4-81/2-02(a)
PT4-6-1	PT4-81/x			PT4-81/3-01 non-mag.
PT4-14	PT4-81/x	PT4-81	(a)	

C-21

(a) See specialist for detail specification.

SEMICONDUCTORS, DIODES

FOOGO PART NUMBER	ERTS PART NUMBER	SPECIFICATION	APPROVED SOURCES	REMARKS
HFA0242.	PT4-2297-011	PT4-2297	H-P	
HFA0153	PT4-2284-011	PT4-2284	H-P	
HFA2350	PT4-2298-021	PT4-2298	H-P	
HFA2351	PT4-2298-011	PT4-2298	H-P	
PT4-2001	1N647 JAN-TX	MIL-S-19500/240	GE, TI, TRWS	Alt. 1N649 JAN-TX PT4-2279-021
-2003	1N3600 JAN-TX	MIL-S-19500/213	CDC, GE, FSC	PT4-2311-011*, 1N459
-2004	PT4-2302-021	PT4-2302	MOT, TRWS	1N4371A
-2005	1N3064 JAN-TX	MIL-S-19500/144	CDC, GE, FSC	PT4-2311-011*
-2006	1N3154 JAN-TX , PT4-2327-011	PT4-2327 MIL-S-19500/158	MOT, TRWS	PT4-2311-011*
-2007	1N3064 JAN-TX	MIL-S-19500/144	CDC, GE, FSC	PT4-2311-011*
2009	PT4-2311-011 ,	PT4-2311 MIL-S-19500/231	CDC, GE, FSC	Alt. 1N3600 JAN-TX*
-2010	1N3064 JAN-TX	MIL-S-19500/144	CDC, GE, FSC	PT4-2311-011*
-2012	1N914 JAN-TX	MIL-S-19500/116	CDC, GE, FSC	PT4-2311-011*
-2033	PT4-2278-131	PT4-2278	TRWS, CRYST	PCLXX (15PF)
-2036	PT4-2279-091	PT4-2279	GE, TI, TRWS	PCLXX (47PF)
-2037			FSC	(a) FA4320E
-2038	1N3155 JAN-TX	MIL-S-19500/158	MOT, TRWS	
PT4-2044	1N748 JAN-TX , PT4-2270-031	PT4-2270 MIL-S-19500/127	CDC, MOT, TRWS	

C-22

* Approximate replacement, design approval required to substitute.

(a) Review and see specialist for current specification

SEMICONDUCTORS, DIODES

FOOGO PART NUMBER	ERTS PART NUMBER	SPECIFICATION	APPROVED SOURCES	REMARKS
PT4-2049	IN914 JAN-TX	MIL-S-19500/116	CDC, FSC, GE	PT4-2311-011*, IN916
2051	IN825	PT4-2272-021 MIL-S-19500/159 PT4-2272	CDC, MOT, TRWS	
2052				SCR3A101, IN3888 IN1878 JAN-TX*, PT4-2326*
2053	IN969B	PT4-2271-061 MIL-S-19500/117 PT4-2271	CDC, MOT, TRWS	
2057				1N1202A JAN-TX*, 1N250B
2065	IN649	PT4-2279-031 MIL-S-19500/240 PT4-2279	GE, TI, TRWS	
2071	IN3064	MIL-S-19500/144 PT4-3064	CDC, FSC, GE	PT4-2311-011*
2087-2	IN757A	PT4-2283-321 MIL-S-19500/127 PT4-2283	CDC, MOT, TRWS	
2231	IN4944	MIL-S-19500/359	UNITRODE	SF4
2239	IN827 JAN-TX	PT4-2272-031 MIL-S-19500/159 PT4-2272	CDC, MOT, TRWS	
2267	PT4-2267-xx1	PT4-2267	H-P	HPA2301
2269	PT4-2269-xx1	PT4-2269	FSC, CDC, GE	
PT4-2270-051	IN750 JAN-TX	MIL-S-19500/127	MOT, CDC, TRWS	

C-23

* Approximate replacement, design approval required to substitute (or see Specialist for alternate part).

SEMICONDUCTORS, DIODES

FOOGO PART NUMBER	ERTS PART NUMBER	SPECIFICATION	APPROVED SOURCES	REMARKS
PT4-2270-091	IN754 JAN-TX	MIL-S-19500/127	MOT, CDC, TRWS	
2273-031	PT4-2273-031	PT4-2273	MOT, CDC, TRWS	IN4573A
2276	PT2350	PT4-2350	TRWS	
2278	PT4-2278	PT4-2278	TRWS, CRYST	PC1xx
2279	IN649 JAN-TX	MIL-S-19500/240	TI, TRWS, GE	
2286	PT4-2286-011	PT4-2286	Varian	VAB806ED*
2288	PT4-2288	PT4-2288	UNI, MOT, SOL	1N3613
2294-021	PT4-2294-021	PT4-2294		FCT1122
2311	PT4-2311	PT4-2311	FSC, CDC, GE	FDH600
PT4-2321	PT4-2321	PT4-2321	TRWS	PS1701x
TFR610	PT4-2330			UTRH51
1N250B JAN	1N1202A JAN-TX			PT4-2057
1N485B JAN	1N485B JAN-TX			PT4-2311-011*, 1N3064 JAN-TX*
1N647 JAN	1N647 JAN-TX	PT4-2279-021 MIL-S-19500/240 PT4-2279	TI, TRW, GE	1N649 JAN-TX and PT4-2279-031
1N746A JAN	1N746A JAN-TX	PT4-2270-011 MIL-S-19500/127 PT4-2270	MOT, CDC, TRWS	

C-24

* Approximate replacement, design approval required to substitute (or see Specialist for alternate part).

SEMICONDUCTORS, DIODES

FOOGO PART NUMBER	ERTS PART NUMBER		SPECIFICATION	APPROVED SOURCES	REMARKS
1N747A JAN	1N747A JAN-TX	PT4-2270-021	PT4-2270, MIL-S-19500/127	MOT, CDC, TRWS	
1N748A JAN	1N748A JAN-TX	PT4-2270-031			
1N750A JAN	1N750A JAN-TX	PT4-2270-051			
1N751A JAN	1N751A JAN-TX	PT4-2270-061			
1N753A JAN	1N753A JAN-TX	PT4-2270-081			
1N754A JAN	1N754A JAN-TX	PT4-2270-091			
1N755 JAN	1N755A JAN-TX	PT4-2270-101			
1N756 JAN	1N756A JAN-TX	PT4-2270-111			
1N757 JAN	1N757A JAN-TX	PT4-2270-121			
1N758A JAN	1N758A JAN-TX	PT4-2270-131			
1N759 JAN	1N759A JAN-TX	PT4-2270-141	PT4-2270, MIL-S-19500/127		
1N821 JAN	1N821 JAN-TX	PT4-2272-071	MIL-S-19500/159 PT4-2272	MOT, CDC, TRWS	
1N830 JAN	1N830 JAN #		MIL-S-19500/229 (Navy)		
1N965B JAN	1N965B JAN-TX	PT4-2271-021	MIL-S-19500/117 PT4-2271	MOT, CDC, TRWS	
1N968B JAN	1N968B JAN-TX	PT4-2271-051	MIL-S-19500/117 PT4-2271	MOT, CDC, TRWS	

C-25

Screening to the JAN-TX level will be required. See Specialist

SEMICONDUCTORS, DIODES

FOOGO PART NUMBER	ERTS PART NUMBER	SPECIFICATION	APPROVED SOURCES	REMARKS
1N1186 JAN	PT4-2301-011	PT4-2301	GE, MOT, WestH	
1N1204 JAN	1N1204A JAN-TX	MIL-S-19500/260	MOT, GE	
1N2984B JAN	1N2984E JAN-TX	MIL-S-19500/124	MOT, TRWS	PT4-2174*
1N3027 JAN	1N3027B JAN-TX	MIL-S-19500/115	MOT, TRWS	PT4-2138*
1N3062 JAN			FSC, CDC, GE	PT4-2311*
1N3064 JAN	1N3064 JAN-TX , PT4-2269-011	MIL-S-19500/144 PT4-2269	FSC, CDC, GE	PT4-2311*
1N3070 JAN	1N3070 JAN-TX	MIL-S-19500/169	CDC, FSC, TI	
1N4781 JAN	PT4-2266-011	PT4-2266	MOT, CDC	
1N5153 JAN				*
5082-0240			H-P	Step Recovery*

*Approximate replacement - see Specialist.

SEMICONDUCTORS, TRANSISTORS

FOOGO PART NUMBER	ERTS PART NUMBER	SPECIFICATION	APPROVED SOURCES	REMARKS
K5001	PT4-7188	PT4-7188		
PT4-7000				2N221 JAN-TX*, 2N707A
PT4-7001	2N720A JAN-TX , PT4-7232	MIL-S-19500/182 PT4-7232	MOT, FSC, TI, AMEL	2N910 JAN-TX* PT4-7178*
PT4-7002	2N2906 JAN-TX	MIL-S-19500/291	MOT, FSC, TI, AMEL	2N 859
PT4-7003	2N2906 JAN-TX	MIL-S-19500/291	MOT, FSC, TI, AMEL	2N 859
PT4-7004				*2N 18A
PT4-7005				*2N 703
PT4-7006	2N2219A JAN-TX	MIL-S-19500/251	MOT, FSC, TI	
PT4-7007	2N2369A JAN-TX , PT4-7158	MIL-S-19500/317 PT4-7158	FSC, MOT, TI	
PT4-7008	2N3251A JAN-TX	MIL-S-19500/323		PT4-7200*
PT4-7009	2N930 JAN-TX	MIL-S-19500/253	MOT, FSC, TI, GE	
PT4-7010				2N 834 *
PT4-7013	2N2906A JAN-TX	MIL-S-19500/291	MOT, TI	

* Approximate replacement, design approval required to substitute - see Specialist.

Screening to the JAN-TX level is required.

SEMICONDUCTORS, TRANSISTORS

Part No.	Part Description	Specification	Manufacturer	Notes
FTL-7014	2N3251A JAN-TX	MIL-S-19500/323	MOT, FSC, TI	PT4-7200*
FTL-7016				2N1742, 2N3127 JAN# 2N3283 JAN# *
FTL-7021	2N2880 JAN-TX ; PT4-7176-011	MIL-S-19500/315 PT4-7176	FSC, MOT, TI	2N1890 JAN-TX*
PT4-7024				
PT4-7034	2N910 JAN # ; PT4-7232-011	MIL-S-19500/274 PT4-7232	AMEL, FSC, MOT, TI	
PT4-7046	2N2880 JAN-TX , PT4-7176-011	MIL-S-19500/315 PT4-7176	FSC, MOT, SOL, TI	2N1721, 2N2880
PT4-7047			WESTINGHOUSE	SW006, 2N2124, 2N2126 PT4-7231 *
PT4-7049	2N2060 JAN-TX	MIL-S-19500/270	FSC, MOT, TI	PT4-7157*, 2N2920 JAN-TX*
C-28 PT4-7059	2N2946A JAN-TX, PT4-7156-011	MIL-S-19500/382 PT4-7156	TI	
PT4-7062	2N1711 JAN-TX	MIL-S-19500/225	MOT, FSC, TI	
PT4-7063				2N 834*
PT4-7071	2N2060 JAN-TX	MIL-S-19500/270	FSC, MOT, TI	PT4-7157*, 2N2920 JAN-TX*
PT4-7072	2N2060 JAN-TX	MIL-S-19500/270	FSC, MOT, TI	2N2920 JAN TX, PT4-7157*
PT4-7074			FSC, MOT, TI	2N2906A JAN-TX*
PT4-7076				2N885*
PT4-7080	2N2880 JAN-TX , PT4-7176-011	MIL-S-19500/315 PT4-7176	FSC, MOT, SOL, TI	

* Approximate replacement, design approval required to substitute - see Specialist.

Screening to the JAN-TX level is required.

SEMICONDUCTORS, TRANSISTORS

FOOGO PART NUMBER	ERTS PART NUMBER	SPECIFICATION	APPROVED SOURCES	REMARKS
PT4-7081	2N708 JAN-TX	MIL-S-19500/312		2N914 JAN-TX*
PT4-7093				2N930 JAN-TX 2N2484 JAN-TX PT4-7162-011
PT4-7101	2N2222A JAN-TX , PT4-7163-011	MIL-S-19500/255 PT4-7163	FSC, MOT, TK	
PT4-7102	2N2907A JAN-TX , PT4-7164-011	MIL-S-19500/291 PT4-7164	MOT, TI	
PT4-7103	PT4-7165-011	PT4-7165	FSC, MOT, TI, SSP	2N2851
PT4-7113				2N2907A JAN-TX* or PT4-7164*, 2N2415
PT4-7150	PT4-7231 -011	PT4-7231	SOL, TI	2N4002
PT4-7156	2N2946 JAN-TX , PT4-7156-011	MIL-S-19500/382 PT4-7156	TI	
PT4-7164	2N2222A JAN-TX , PT4-7163-011	MIL-S-19500/255 PT4-7163	FSC, MOT, TI	
PT4-7164	2N2907A JAN-TX , PT4-7164-011	MIL-S-19500/291 PT4-7164	FSC, MOT, TI	2N918
PT4-7170	2N918 JAN-TX , PT4-7170-011	MIL-S-19500/301 PT4-7170	MOT, TI	2N-7170-041
PT4-7173				2N2369A

*Approximate replacement - review and see Specialist.

SEMICONDUCTORS, TRANSISTORS

FOOGO PART NUMBER	ERTS PART NUMBER	SPECIFICATION	APPROVED SOURCES	REMARKS
PT4-7177	PT4-7229-011	PT4-7229	MOT, TI	2N4853
PT4-7178	PT4-7178-011 , PT4-7178	PT4-7178	MOT, TI	2N3501
PT4-7209				2N4138*
PT4-7225	PT4-7225	PT4-7225	FSC	2N3503 2N3599
PT4-7231	PT4-7231-xx1	PT4-7231	SOL, TI	2N4002, 2N3599
PT4-7248	PT4-7248-011	PT4-7248	FSC, TI	2N5005
PT4-7253			MOT	2N4416*
2N328A JAN	2N2904 JAN-TX	MIL-S-19500/290	MOT	2N358A JAN* 2N2904 JAN-TX* 2N2222A JAN-TX*
2N358A JAN			MOT	
2N490/B USAF	PT4-7229-011	PT4-7229	MOT, TI	2N4853
2N599 JAN				2N2907A JAN-TX* or PT4-7164*
2N720A JAN	2N720A JAN-TX , PT4-7232-011	MIL-S-19500/182 PT4-7232	AMEL, FSC, MOT, TI	PT4-7178* 2N910 JAN-TX*

C-30

* Review and see specialist.

SEMICONDUCTORS, TRANSISTORS

FOOGO PART NUMBER	ERTS PART NUMBER	SPECIFICATION	APPROVED SOURCES	REMARKS
2N869 JAN	2N2906A JAN-TX	MIL-S-19500/291	MOT, TI	
2N918 JAN	2N918 JAN-TX	MIL-S-19500/301	FSC, MOT	PT4-7170-XX1 DCX
2N999 JAN	PT4-7235-011	PT4-7235	FSC, GE, MOT	
2N1041 USN				PT4-7248-021* OR 2N5005, OR TPA0400DMA
2N1049A USN				2N1049A JAN # *
2N1118 USA	2N2906A JAN-TX	MIL-S-19500/291	MOT, TI	
2N1131 USA				#
2N1132 JAN	2N2904A JAN-TX	MIL-S-19500/290	MOT, TI	2N2906A JAN-TX*
2N1197 JAN				PT4-2070*
2N1305 JAN				2N2907A JAN-TX* OR PT4-7164*
2N1306 JAN				PT4-7163* OR 2N2222 JAN-TX
2N1480 USA	2N3501 JAN-TX, PT4-7178	MIL-S-19500/366 PT4-7178	MOT, TI	
2N1484 USA				#

* Approximate replacement - review and see Specialist

Screening to the JAN-TX level is required.

SEMICONDUCTORS, TRANSISTORS

FOOGO PART NUMBER	ERTS PART NUMBER	SPECIFICATION	APPROVED SOURCES	REMARKS
2N1908 JAN				2N4399* PT4-7247*
2N2605 JAN	PT4-7154-011	PT4-7154	MOT, TI	2N2605 JAN #
2N2851 JAN	PT4-7165-011	PT4-7165	FSC, SSP, TRWS	2N2851
2N2920 JAN	2N2920 JAN-TX, PT4-7157-011	MIL-S-19500/355 PT4-7157	FSC, MOT, TI	-
2N2927 JAN				#
2N2946 JAN	2N2946A JAN-TX, PT4-7156-011	MIL-S-19500/382	TI	
C-32 2N2975 JAN	2N2920 JAN-TX PT4-7157-011	MIL-S-19500/355 PT4-7157	FSC, MOT, TI	
2N3599 JAN	PT4-7231-XX1		SOL, TI	
2N3733 JAN				RCA*
2N3866 JAN				RCA*
2N4428 JAN				#
2N4429 JAN	PT4-7214-011	PT4-7214	TRWS	
2N4430 JAN	PT4-7204-011	PT4-7204	TRWS	
2N4936 JAN				#
2N5522 JAN	PT4-7207	PT4-7207	AMEL, UC	2N3954

*Approximate replacement - review and see Specialist

Screening to the JAN-TX level is required.

SEMICONDUCTORS, INTEGRATED CIRCUITS

FOOGO PART NUMBER	ERTS PART NUMBER	SPECIFICATION	APPROVED SOURCES	REMARKS
uA702A	PT4-5007	PT4-5007	FSC	Eval. Pkg.
7A723	PT4-5027	PT4-5027	FSC	-
MC1595L	PT4-5030-011	PT4-5030	FSC	-
MC1596G	PT4-5031-011	PT4-5031	FSC	
PT4-4054	PT4-4054-011	PT4-4054	FSC, MOT, TI	DTUL945
PT4-4055	PT4-4055-011	PT4-4055	FSC, MOT, TI	DTUL946
PT4-4067	PT4-4067-011	PT4-4067	FSC, MOT, TI	SH2001F
C-33 PT4-4128			SIL	DG126L, DG129L* FET, SW.
PT4-5006	PT4-5016-011	PT4-5016	NAT, SIL, UC	LM101A
PT4-5007	PT4-5007-011	PT4-5007	FSC	uA702A
PT4-5014	PT4-5014-011	PT4-5014	FSC, MOT, NAT, TI	uA710
PT4-5016	PT4-5016-011	PT4-5016	NAT, SIL, UC	LM101A
PT4-5022	PT4-5022	PT4-5022	NAT, SIL	LM102
SNT 54L 51T			NAT, TI	* TTL
SNT 54L 04T			NAT, TI	* PT4-4132
SNT 54L 00T			NAT, TI	* PT4-4132

* Review with component specialist

FOOGO PART NUMBER	ERTS PART NUMBER	SPECIFICATION	SOLAR CELLS APPROVED SOURCES	REMARKS
PT2-2054	PT7-29	PT7-29	HFMN, HELIO	
SWITCHES				
PT2-2004-15	PT2-2014-28	PT2-2014	UNCT	
PT2-2008	PT2-2015-X	PT2-2015	METALS & CONTROLS (TI)	
TIMERS				
PT2-1020	PT2-1020	PT2-1020	GENTM	TIMER OSCILLATOR
PT2-1021	PT2-1021	PT2-1021	GENTM	TIMER
PT2-1022	PT2-1022	PT2-1022	GENTM	TIMER
516002-1			PRK	RELAY, TIME DELAY PT2-1018*, PT2-1019* PLUS SCREENING

C-34

* EVALUATE FOR REPLACEMENT

TRANSFORMERS

FOOGO PART NUMBER	ERTS PART NUMBER	SPECIFICATION	APPROVED SOURCES	REMARKS
DIT 21	PT6-1065/X-X	MIL-T-27	UTC	
PT6-1000-1	PT6-1065/X-X		COAST	3150
PT6-1000-2	PT6-1065/X-X		COAST	3152
PT6-1003-1	PT6-1065/XX-X		HADLEY	14259-1
PT6-1003-2	PT6-1065/XX-X		HADLEY	14259-2
PT6-1006	PT6-1065/XX-X		VALOR	PT6-1092-2
PT6-1007	PT6-1065/XX-X		HADLEY	14222
C-35 PT6-1008	PT6-1065/XX-X		HADLEY	14231
PT6-1010	PT6-1065/XX-X		HADLEY	14202
PT6-1011	PT6-1065/XX-X		HADLEY	14203
PT6-1012	PT6-1065/XX-X		HADLEY	14204
PT6-1013	PT6-1065/XX-X		HADLEY, COAST	14205, 2166
PT6-1018	PT6-1065/XX-X		TRIAD	46139
PT6-2011	PT6-1065/XX-X		INDGN	CF-401-Q3 FERRITE COLIFORM
TF4RX13YY-D1-T37	PT6-1065/XX-X	MIL-T-27		

WIRE & CABLE

FOOGO PART NUMBER	ERTS PART NUMBER	SPECIFICATION	APPROVED SOURCES	REMARKS
PT3-1-2-XX-X	PT3-38-1-XX-X	PT3-38	RAYCH	#
PT3-1-12-XX-X				*PT3-53N-XX-X
PT3-2	PT3-59-XX-X	PT3-59	RAYCH	MIN COAX
PT3-3	PT3-55 (SOLDERING ONLY)			PT3-55 FOR SOLDERING SEE SPECIALIST FOR WELDING
PT3-8-29	PT3-55-1-XX-X	PT3-55	RAYCH	
PT3-10-2	PT3-33-XX-X	PT3-33	RAYCH	SHIELDED CABLE
PT3-12-2	PT3-59-XX-X	PT3-59	RAYCH	MIN COAX
PT3-13-1-XX-X	PT3-53A-XX-X	PT3-53	RAYCH	
PT3-13-3-XX-X	PT3-53B-XX-X	PT3-53	RAYCH	
PT3-13-4-XX-X	PT3-53B-XX-X	PT3-53	RAYCH	
PT3-15-1			RAYCH	PT3-59*
PT3-19-1				*FLEX RIBBON
PT3-19-2				*FLEX RIBBON
PT3-29	PT3-29-XX-X	PT3-29		COAX, SEMI-RIGID

* Evaluate, review with specialist

If AWG 26 or smaller size, use "-2" (not "-1"). If AWG 24 or larger size, either "-1" or "-4" are satisfactory.

		WIRE & CABLE		
FOOGO PART NUMBER	ERTS PART NUMBER	SPECIFICATION	APPROVED SOURCES	REMARKS
PT3-33	PT3-33-XX-X	PT3-33	RAYCH	
PT3-38-2	PT3-38-1-XX-X	PT3-38	RAYCH	#
PT3-57	PT3-59-XX-X	PT3-59	RAYCH	MIN COAX E-7
PT3-59	PT3-59-XX-X	PT3-59	RAYCH	MIN COAX E3, E-9
QQ-W-343	QQ-W-343	QQ-W-343	HUDSN, PHLPD, INWIR	FEDERAL SPEC.

C-37

If AWG 26 or smaller size, use "-2" (not "-1"). If AWG 24 or larger size, either "-1" or "-4" are satisfactory.

ERTS PARTS LIST - SECTION II

(PARTS FOR NEW DESIGN)

PART TYPE	PAGE NO.
CAPACITORS	
Fixed, Solid Tantalum	1 - 4
Fixed, Ceramic	5 - 7
Variable, Tubular	7
Fixed, Glass Dielectric	8 - 13
COILS	14 - 17
CONNECTORS	
Circular, Subminiature and Miniature	18
Rectangular, Subminiature	18
Coaxial, Subminiature	18 - 20
Contacts, Pins and Sockets and Accessories	20
CRYSTALS	21
FILTERS	22
INDUCTORS	23
RELAYS	24
RESISTORS	
Fixed, Carbon Composition	25
Fixed, Wire-Wound, Power	26 - 27
Fixed, Film	26 - 27
Fixed, Wire-Wound, Accurate	28
SEMICONDUCTORS	
Diodes	29 - 34
Transistors	35 - 37
Integrated Circuits	38
SWITCHES	39
TRANSFORMERS	40
WIRE AND CABLE	41 - 43

C-38

CAPACITORS

PART NUMBER	DESCRIPTION	SPECIFICATION	APPROVED SOURCES	REMARKS
M39003/01-2482	FIXED, SOLID TA, POL, 6 VDC, 6.8 UF PORM 10%	MIL-C-39003/1	UC, SPRAGUE	CSR13B685KP
M39003/01-2484	47 UF			B476KP
-2487	150 UF			B157KP
-2491	330 UF 6 VDC			B337KP
-2494	4.7 UF 10 VDC			C475KP
-2497	33 UF			C336KP
-2501	100 UF			C107KP
-2505	220 UF 10 VDC			C227KP
-2508	3.3 UF 15 VDC			D335KP
-2511	22 UF			D226KP
-2514	68 UF			D686KP
-2517	150 UF 15 VDC			D157KP
-2520	1.5 UF 20 VDC			E155KP
-2523	2.2 UF			E225KP
-2526	10 UF			E106KP
-2529	15 UF			E156KP
-2532	33 UF			E336KP
M39003/01-2535	47 UF 20 VDC	MIL-C-39003/1	UC, SPRAGUE	CSR13 E476KP

PART NUMBER	DESCRIPTION	SPECIFICATION	APPROVED SOURCES	REMARKS
M39003/01-2538	FIXED, SOLID TA, POL, 20 VDC, 68 UF FORM 10%	MIL-C-39003/1	UC, SPRAGUE	CSR13E686KP
	-2541 100 UF 20 VDC			E107KP
	-2544 6.8 UF 35 VDC			F685KP
	-2546 22 UF			F226KP
	-2549 33 UF			F336KP
	-2552 47 UF 35 VDC			F476KP
	-2554 .0047 UF 50 VDC			G472KP
	-2557 .0068 UF			G682KP
	-2560 .01 UF			G103KP
	-2563 .015 UF			G153KP
	-2566 .022 UF			G223KP
	-2569 .033 UF			G333KP
	-2572 .047 UF			G473KP
	-2575 .068 UF			G683KP
	-2578 .10 UF			G104KP
	-2581 .15 UF			G154KP
	-2584 .22 UF			G224KP
M39003/01-2587	.33 UF 50 VDC	MIL-C-39003/1	UC, SPRAGUE	CSR13G334KP

C-40

CAPACITORS

PART NUMBER	DESCRIPTION	SPECIFICATION	APPROVED SOURCES	REMARKS	
M39003/01-2590	FIXED, SOLID TA, POL, 50 VDC, .47 UF FORM 10%	MIL-C-39003/1	UC, SPRAGUE	CSR13G474KP	
-2593	.68 UF			G684KP	
-2596	1.0 UF			G105KP	
-2599	1.5 UF			G155KP	
-2602	2.2 UF			G225KP	
-2605	3.3 UF			G335KP	
-2608	4.7 UF			G475KP	
-2611	6.8 UF			G685KP	
-2614	10 UF			G106KP	
-2617	15 UF			G156KP	
-2620	22 UF	50 VDC		G226KP	
-2622	.10 UF	75 VDC		H104KP	
-2625	.15 UF			H154KP	
-2628	.22 UF			H224KP	
-2631	.33 UF			H334KP	
-2634	.47 UF			H474KP	
-2637	.68 UF			H684KP	
M39003/01-2640	1.0 UF	75 VDC	MIL-C-39003/1	UC, SPRAGUE	CSR13H105KP

C-41

CAPACITORS

PART NUMBER	DESCRIPTION	SPECIFICATION	APPROVED SOURCES	REMARKS
M39003/01-2643	FIXED, SOLID TA, POL, 75 VDC, 1.5 UF FORM 10%	MIL-C-39003/1	UC, SPRAGUE	CSR13H155KP
-2646	2.2 UF			H225KP
-2649	3.3 UF			H335KP
-2652	4.7 UF			H475KP
-2655	6.8 UF			H685KP
-2658	10 UF			H106KP
-2661	15 UF	75 VDC		H156KP
-2687	.10 UF	100 VDC		J104KP
-2690	.15 UF			J154KP
-2693	.22 UF			J224KP
-2696	.33 UF			J334KP
-2699	.47 UF			J474KP
-2702	.68 UF			J684KP
-2705	1.0 UF			J105KP
-2708	1.5 UF			J155KP
M39003/01-2711	2.2 UF	MIL-C-39003/1	UC, SPRAGUE	CSR13J225KP

C-42

CAPACITORS

PART NUMBER	DESCRIPTION	SPECIFICATION	APPROVED SOURCES	REMARKS
M39014/01-0241	FIXED, CERAMIC, GEN PUR, 200 VDC, 10 PF FORM 10%	MIL-C-39014/1	AEROVOX, POTTER	CKR05BX100KP
-0244	15 PF			150KP
-0247	22 PF			220KP
-0250	33 PF			330KP
-0253	47 PF			470KP
-0258	68 PF			680KP
-0259	100 PF			101KP
-0263	150 PF			151KP
-0265	220 PF			221KP
-0268	330 PF			331KP
-0271	470 PF			471KP
-0274	680 PF			681KP
M39014/01-0277	1000 PF	MIL-C-39014/1		CKR05BX102KP
M39014/02-0242	1500 PF	MIL-C-39014/2		CKR06BX152KP
-0246	2200 PF			222KP
-0249	3300 PF			332KP
-0252	4700 PF			472KP
M39014/02-0255	6800 PF	MIL-C-39014/2	AEROVOX, POTTER	CKR06BX682KP

C-43

CAPACITORS

PART NUMBER	DESCRIPTION	SPECIFICATION	APPROVED SOURCES	REMARKS
M39014/02-0257	FIXED, CERAMIC, GEN PUR, 200 VDC, 10000 PF PORM 10%	MIL-C-39014/2	AEROVOX, POTTER	CKR06BX103KP
-0260	15000 PF 100 VDC			153KP
-0262	22000 PF			223KP
-0263	33000 PF			333KP
-0265	47000 PF			473KP
-0267	68000 PF			683KP
C-44 M39014/02-0270	100000 PF	MIL-C-39014/2		CKR06BX104KP
M39014/05-0251	10 PF	MIL-C-39014/5		CKR12BX100KP
-0253	22 PF			220KP
-0255	33 PF			330KP
-0257	47 PF			470KP
-0260	68 PF			680KP
-0264	100 PF			101KP
-0266	150 PF			151KP
-0269	220 PF			221KP
-0271	330 PF			331KP
-0274	470 PF			471KP
M39014/05-0277	680 PF 100 VDC	MIL-C-39014/5	AEROVOX, POTTER	CKR12BX681KP

CAPACITORS

PART NUMBER	DESCRIPTION	SPECIFICATION	APPROVED SOURCES	REMARKS
M39014/05-0282	FIXED, CERAMIC, GEN PUR, 100 VDC, 1000 PF FORM 10%	MIL-C-39014/5	AEROVOX, POTTER	CKR12BX102KP
-0285	1500 PF			152KP
-0288	2200 PF			222KP
-0290	3300 PF			332KP
-0292	4700 PF			472KP
-0294	6800 PF			682KP
C M39014/05-0296	10000 PF	MIL-C-39014/5	AEROVOX, POTTER	CKR12BX103KP
C-45 M39014/06-0121	15000 PF	MIL-C-39014/6	AEROVOX	CKR13BX153KP
-0123	22000 PF			223KP
-0125	33000 PF			333KP
-0127	47000 PF			473KP
-0129	68000 PF			683KP
M39014/06-0133	100000 PF 100 VDC	MIL-C-39014/6	AEROVOX	CKR13BX104KP
PTL-1077/5-01	VARIABLE, GLASS DIELECTRIC, TUBULAR, 1000 VDC, 1 TO 16 PF, 750 Q AT 20 MHZ	PT4-1077/5	JFD	
PTL-1077/6-01	1 TO 36 PF, 550 Q AT 20 MHZ	PT4-1077/6	JFD	

CAPACITORS

PART NUMBER	DESCRIPTION	SPECIFICATION	APPROVED SOURCES	REMARKS
PT4-1055/1-OR5C	FIXED, GLASS DIELECTRIC, 500 VDC, .5 PF FORM .25 PF	PT4-1055/1	CORNING	CYFRLOGXXXX (S)
PT4-1055/1-1ROC	1.0 PF			
PT4-1055/1-1R5C	1.5 PF			
PT4-1055/1-2R2C	2.2 PF			
PT4-1055/1-2R7C	2.7 PF			
PT4-1055/1-3ROC	3.0 PF			
C-46 PT4-1055/1-3R3C	3.3 PF			
PT4-1055/1-3R6C	3.6 PF			
PT4-1055/1-3R9C	3.9 PF			
PT4-1055/1-4R3C	4.3 PF			
PT4-1055/1-4R7C	4.7 PF			
PT4-1055/1-5R1C	5.1 PF			
PT4-1055/1-5R6C	5.6 PF			
PT4-1055/1-6R2C	6.2 PF			
PT4-1055/1-6R8C	6.8 PF			
PT4-1055/1-7R5C	7.5 PF			
PT4-1055/1-8R2C	8.2 PF			
PT4-1055/1-9R1C	9.1 PF	PT4-1055/1	CORNING	CYFRLOGXXXX (S)

(S) ACCEPTABLE SUBSTITUTE

CAPACITORS

PART NUMBER	DESCRIPTION	SPECIFICATION	APPROVED SOURCES	REMARKS
PT4-1055/1-100C	FIXED, GLASS DIELECTRIC, 500 VDC, 10 PF PORM .25 PF	PT4-1055/1	CORNING	CYFRLOGXXX (S)
PT4-1055/1-110C	11 PF			
PT4-1055/1-120C	12 PF			
PT4-1055/1-130G	13 PF PORM 2%			
PT4-1055/1-150G	15 PF			
PT4-1055/1-160G	16 PF			
C-47 PT4-1055/1-180G	18 PF			
PT4-1055/1-200G	20 PF			
PT4-1055/1-220G	22 PF			
PT4-1055/1-240G	24 PF			
PT4-1055/1-270F	27 PF PORM 1%			
PT4-1055/1-300F	30 PF			
PT4-1055/1-330F	33 PF			
PT4-1055/1-360F	36 PF			
PT4-1055/1-390F	39 PF			
PT4-1055/1-430F	43 PF			
PT4-1055/1-470F	47 PF			
PT4-1055/1-510F	51 PF 500 VDC	PT4-1055/1	CORNING	CYFRLOGXXX (S)

(*) ACCEPTABLE SUBSTITUTE

CAPACITORS

PART NUMBER	DESCRIPTION	SPECIFICATION	APPROVED SOURCES	REMARKS
PT4-1055/1-560F	FIXED, GLASS DIELECTRIC, 500 VDC, 56 PF FORM 1%	PT4-1055/1	CORNING	CYFRLOGXXXX (S)
PT4-1055/1-620F	63 PF			
PT4-1055/1-680F	68 PF			
PT4-1055/1-750F	75 PF			
PT4-1055/1-820F	82 PF			
PT4-1055/1-910F	91 PF			
C-48 PT4-1055/1-101F	100 PF			
PT4-1055/1-111F	110 PF			
PT4-1055/1-121F	120 PF			
PT4-1055/1-131F	130 PF			
PT4-1055/1-151F	150 PF 500 VDC			
PT4-1055/1-161F	160 PF 300 VDC			
PT4-1055/1-181F	180 PF			
PT4-1055/1-201F	200 PF			
PT4-1055/1-221F	220 PF			
PT4-1055/1-241F	240 PF 300 VDC	PT4-1055/1		
PT4-1055/2-271F	FIXED, GLASS DIELECTRIC, 500 VDC, 270 PF FORM 1%	PT4-1055/2		
PT4-1055/2-301F	300 PF 500 VDC	PT4-1055/2	CORNING	CYFRLOGXXXX (S)

(S) ACCEPTABLE SUBSTITUTE

CAPACITORS

PART NUMBER	DESCRIPTION	SPECIFICATION	APPROVED SOURCES	REMARKS
PT4-1055/2-331F	FIXED, GLASS DIELECTRIC, 500 VDC, 330 PF FORM 1%	PT4-1055/2	CORNING	CYFR10GXXXX (S)
PT4-1055/2-361F	360 PF			
PT4-1055/2-391F	390 PF			
PT4-1055/2-431F	430 PF			
PT4-1055/2-471F	470 PF			
PT4-1055/2-511F	510 PF	500 VDC		
PT4-1055/2-561F	560 PF	300 VDC		
PT4-1055/2-621F	620 PF			
PT4-1055/2-681F	680 PF			
PT4-1055/2-751F	750 PF			
PT4-1055/2-821F	820 PF			
PT4-1055/2-911F	910 PF			
PT4-1055/2-102F	1000 PF			
PT4-1055/2-112F	1100 PF			
PT4-1055/2-122F	1200 PF	300 VDC	PT4-1055/2	CYFR10GXXXX
PT4-1055/3-132F	FIXED, GLASS DIELECTRIC, 500 VDC, 1300 PF FORM 1%	PT4-1055/3		CYFR20GXXXX
PT4-1055/3-152F	1500 PF			
PT4-1055/3-162F	1600 PF	500 VDC	PT4-1055/3	CYFR20GXXXX (S)

C-49

(C) ACCEPTABLE SUBSTITUTE

CAPACITORS

PART NUMBER	DESCRIPTION	SPECIFICATION	APPROVED SOURCES	REMARKS
PT4-1055/3-182F	FIXED, GLASS DIELECTRIC, 500 VDC, 1800 PF FORM 1%	PT4-1055/3	CORNING	CYFR20GXXXX (S)
PT4-1055/3-202F	2000 PF			
PT4-1055/3-222F	2200 PF			
PT4-1055/3-242F	2400 PF			
PT4-1055/3-272F	2700 PF			
PT4-1055/3-302F	3000 PF			
C-50 PT4-1055/3-332F	3300 PF	500 VDC		
PT4-1055/3-362F	3600 PF	300 VDC		
PT4-1055/3-392F	3900 PF			
PT4-1055/3-432F	4300 PF			
PT4-1055/3-472F	4700 PF			
PT4-1055/3-512F	5100 PF	300 VDC	PT4-1055/3	CYFR20GXXXX
PT4-1055/4-562F	FIXED, GLASS DIELECTRIC, 500 VDC, 5600 PF FORM 1%	PT4-1055/4		CYFR30GXXXX
PT4-1055/4-622F	6200 PF	500 VDC		
PT4-1055/4-682F	6800 PF	300 VDC		
PT4-1055/4-752F	7500 PF			
PT4-1055/4-822F	8200 PF			
PT4-1055/4-912F	9100 PF	300 VDC	PT4-1055/4	CYFR30GXXXX (S)

(S) ACCEPTABLE SUBSTITUTE

CAPACITORS

PART NUMBER	DESCRIPTION	SPECIFICATION	APPROVED SOURCES	REMARKS
PT4-1055/4-103F	FIXED, GLASS DIELECTRIC, 300 VDC, 10000 PORM 1%	PT4-1055/4	CORNING	CYFR30GXXXX (S)

C-51

(S) ACCEPTABLE SUBSTITUTE

COILS

PART NUMBER	DESCRIPTION	SPECIFICATION	APPROVED SOURCES	REMARKS
PT6-18/1-3	R.F., FIXED, .15 UH PORM 10%, 38 Q, 0.1 OHM, 1100 MA DC	PT6-18/1	VANGUARD	
PT6-18/1-5	.22 UH, 33 Q, 0.14 OHM, 935 MA DC			
PT6-18/1-7	.33 UH, 30 Q, 0.21 OHM, 780 MA DC			
PT6-18/1-9	.47 UH, 30 Q, 0.35 OHM, 590 MA DC			
PT6-18/1-11	.68 UH, 28 Q, 0.65 OHM, 450 MA DC			
PT6-18/1-13	1.0 UH, 25 Q, 1.10 OHMS, 350 MA DC			
PT6-18/1-15	1.5 UH, 28 Q, 0.22 OHM, 745 MA DC			
PT6-18/1-17	2.2 UH, 30 Q, 0.40 OHM, 550 MA DC			
PT6-18/1-19	3.3 UH, 45 Q, 0.85 OHM, 380 MA DC			
PT6-18/1-21	4.7 UH, 45 Q, 1.2 OHMS, 320 MA DC			
PT6-18/1-23	6.8 UH, 50 Q, 2.0 OHMS, 245 MA DC			
PT6-18/1-25	10 UH, 55 Q, 3.7 OHMS, 180 MA DC			
PT6-18/1-27	15 UH, 45 Q, 2.8 OHMS, 205 MA DC			
PT6-18/1-29	22 UH, 50 Q, 3.3 OHMS, 190 MA DC			
PT6-18/1-31	33 UH, 45 Q, 3.8 OHMS, 187 MA DC			
PT6-18/1-33	47 UH, 45 Q, 4.5 OHMS, 165 MA DC			
PT6-18/1-35	68 UH, 50 Q, 6.7 OHMS, 135 MA DC			
PT6-18/1-37	100 UH, 50 Q, 8.2 OHMS, 125 MA DC	PT6-18/1	VANGUARD	

25-5

COILS

PART NUMBER	DESCRIPTION	SPECIFICATION	APPROVED SOURCES	REMARKS
PT6-18/1-39	R.F., FIXED, 150 UH PORM 10%, 28 Q, 16 OHMS, 85 MA DC	PT6-18/1	VANGUARD	
PT6-18/1-41	220 UH, 26 Q, 21 OHMS, 73 MA DC			
PT6-18/1-43	330 UH, 26 Q, 37 OHMS, 62 MA DC			
PT6-18/1-45	470 UH, 27 Q, 56 OHMS, 50 MA DC			
PT6-18/1-47	680 UH, 28 Q, 70 OHMS, 42 MA DC			
PT6-18/1-49	1000 UH, 28 Q, 102 OHMS, 38 MA DC	PT6-18/1		
PT6-18/4-3	R.F., FIXED, 0.15 UH PORM 10%, 85 Q, 0.03 OHM, 3000 MA DC	PT6-18/4		
PT6-18/4-5	.22 UH, 75 Q, 0.03 OHMS, 3000 MA DC			
PT6-18/4-7	.33 UH, 70 Q, 0.05 OHM, 2500 MA DC			
PT6-18/4-9	.47 UH, 60 Q, 0.08 OHM, 2000 MA DC			
PT6-18/4-11	.68 UH, 55 Q, 0.12 OHM, 1500 MA DC			
PT6-18/4-13	1.0 UH, 50 Q, 0.24 OHM, 1100 MA DC			
PT6-18/4-15	1.5 UH, 45 Q, 0.43 OHM, 850 MA DC			
PT6-18/4-17	2.2 UH, 45 Q, 0.80 OHM, 610 MA DC			
PT6-18/4-19	3.3 UH, 55 Q, 0.15 OHM, 1400 MA DC			
PT6-18/4-21	4.7 UH, 70 Q, 0.30 OHM, 1000 MA DC			
PT6-18/4-23	6.8 UH, 65 Q, 0.55 OHM, 800 MA DC			
PT6-18/4-25	10 UH, 60 Q, 0.73 OHM, 650 MA DC	PT6-18/4	VANGUARD	

COILS

PART NUMBER	DESCRIPTION	SPECIFICATION	APPROVED SOURCES	REMARKS
PT6-18/4-27	R.F., FIXED, 15 UH PORM 10%, 80 Q, 1.4 OHMS, 500 MA DC	PT6-18/4	VANGUARD	
PT6-18/4-29	22 UH, 75 Q, 1.8 OHMS, 430 MA DC			
PT6-18/4-31	33 UH, 85 Q, 3.5 OHMS, 300 MA DC			
PT6-18/4-33	47 UH, 80 Q, 4.0 OHMS, 275 MA DC			
PT6-18/4-35	68 UH, 75 Q, 4.7 OHMS, 250 MA DC			
PT6-18/4-37	100 UH, 75 Q, 6.0 OHMS, 220 MA DC	PT6-18/4		
PT6-18/6-1	R.F., TOROIDAL, 1.0 UH PORM 5%, 70 Q, 0.35 OHM, 750 MA DC	PT6-18/6		
PT6-18/6-3	1.5 UH, 60 Q, 0.50 OHM, 630 MA DC			
PT6-18/6-5	2.2 UH, 60 Q, 0.90 OHM, 470 MA DC			
PT6-18/6-7	3.3 UH, 60 Q, 1.3 OHMS, 390 MA DC			
PT6-18/6-9	4.7 UH, 60 Q, 1.8 OHMS, 330 MA DC			
PT6-18/6-11	6.8 UH, 60 Q, 2.2 OHMS, 300 MA DC			
PT6-18/6-13	10 UH, 60 Q, 2.6 OHMS, 280 MA DC			
PT6-18/6-16	15 UH, 75 Q, 1.5 OHMS, 450 MA DC			
PT6-18/6-18	22 UH, 80 Q, 2.3 OHMS, 380 MA DC			
PT6-18/6-20	33 UH, 80 Q, 3.3 OHMS, 320 MA DC			
PT6-18/6-22	47 UH, 80 Q, 4.7 OHMS, 260 MA DC			
PT6-18/6-24	68 UH, 80 Q, 6.8 OHMS, 220 MA DC	PT6-18/6	VANGUARD	

C-54

COILS

PART NUMBER	DESCRIPTION	SPECIFICATION	APPROVED SOURCES	REMARKS
PT6-18/6-26	R.F., TOROIDAL, 100 UH PORM 5%, 80 Q, 9.7 OHMS, 180 MA DC	PT6-18/6	VANGUARD	
PT6-18/6-27	.10 UH, 55 Q, 0.04 OHM, 2200 MA DC			
PT6-18/6-29	.15 UH, 60 Q, 0.06 OHM, 1800 MA DC			
PT6-18/6-31	.22 UH, 65 Q, 0.08 OHM, 1500 MA DC			
PT6-18/6-33	.33 UH, 65 Q, 0.11 OHM, 1300 MA DC			
PT6-18/6-35	.47 UH, 65 Q, 0.17 OHM, 1100 MA DC			
PT6-18/6-37	.68 UH, 70 Q, 0.27 OHM, 900 MA DC	PT6-18/6	VANGUARD	

C-55

CONNECTORS

PART NUMBER	DESCRIPTION	SPECIFICATION	APPROVED SOURCES	REMARKS
NAS1662-12	ELECTRICAL, CIRCULAR, MINIATURE, ENVIR RESISTING, PIN CONTACT, SIZE 12	NAS1662	DEUTSCH	
NAS1662-16	PIN CONTACT, SIZE 16	NAS1662		
NAS1662-20	PIN CONTACT, SIZE 20	NAS1661		
NAS1663-12	ELECTRICAL, CIRCULAR, MINIATURE, ENVIR RESISTING, SOCKET CONTACT, SIZE 12	NAS1663		
NAS1663-16	SOCKET CONTACT, SIZE 16	NAS1663		
NAS1663-20	SOCKET CONTACT, SIZE 20	NAS1663	DEUTSCH	
NAS1668-12	ELECTRICAL, CIRCULAR, MINIATURE, ENVIR RESISTING, GROMMET SEALING PLUG, SIZE 12	NAS1668	DEUTSCH, CANNON	
NAS1668-16	GROMMET SEALING PLUG, SIZE 16	NAS1668		
NAS1668-20	GROMMET SEALING PLUG, SIZE 20	NAS1668	DEUTSCH, CANNON	
PT2-16-11	ELECTRICAL, RECTANGULAR, SUBMIN, SCREW LOCK ASSY, FEMALE	PT2-16	CAN, CINCH, DOUBLE A	
PT2-16-12	MALE			
PT2-16-13	MALE			
PT2-16-14	MALE			
PT2-16-15	MALE	PT2-16	CAN, CINCH, DOUBLE A	
PT2-82-2	ELECTRICAL, COAXIAL, SUBMIN, STRAIGHT PLUG	PT2-82	AMPHENOL	

C-56

CONNECTORS

PART NUMBER	DESCRIPTION	SPECIFICATION	APPROVED SOURCES	REMARKS
PT2-82-9	ELECTRICAL, COAXIAL, SUBMIN, RIGHT ANGLE PLUG	PT2-82	AMPHENOL	
PT2-82-10	BULKHEAD JACK			
PT2-82-11	BULKHEAD RECEPTACLE			
PT2-82-12	FEED-THROUGH ADAPTER	PT2-82	AMPHENOL	
PT2-88/2-BAPNR3	ELECTRICAL, CIRCULAR, SUBMIN, ENVIR RESISTING, BAYONET COUPLING, PIN, WALL MOUNT RCPT	PT2-88	DEUTSCH	
C-57 PT2-88/2-BASNR3	SOCKET, WALL MOUNT RECPT			
PT2-88/2-PAPNR3	PIN, PLUG			
PT2-88/2-PASNR3	SOCKET, PLUG	PT2-88	DEUTSCH	
PT2-90/2-1	ELECTRICAL, CIRCULAR, SUBMIN, ENVIR RESISTING, BAYONET COUPLING, PIN	PT2-90		
PT2-90/2-2	SOCKET			
PT2-90/2-3	PIN			
PT2-90/2-4	SOCKET	PT2-90	DEUTSCH	
PT2-94-1	ELECTRICAL, RECTANGULAR, SUBMIN, GEN PUR, 9 PINS	PT2-94	CANNON	
PT2-94-2	15 PINS			
PT2-94-3	25 PINS			
PT2-94-4	37 PINS	PT2-94	CANNON	

CONNECTORS

PART NUMBER	DESCRIPTION	SPECIFICATION	APPROVED SOURCES	REMARKS
PT2-94-5	ELECTRICAL, RECTANGULAR, SUBMIN, GEN PUR, 50 PINS	PT2-94	CANNON	
PT2-94-6	9 SOCKETS			
PT2-94-7	15 SOCKETS			
PT2-94-8	25 SOCKETS			
PT2-94-9	37 SOCKETS			
PT2-94-10	50 SOCKETS	PT2-94		
C-58 PT2-95-1	ELECTRICAL, RECTANGULAR, SUBMIN, PIN TYPE REMOVABLE CONTACT	PT2-95		
PT2-95-2	SOCKET TYPE REMOVABLE CONTACT			
PT2-95-3	PIN TYPE REMOVABLE CONTACT			
PT2-95-4	SOCKET TYPE REMOVABLE CONTACT	PT2-95	CANNON	

CRYSTALS, QUARTZ

PART NUMBER	DESCRIPTION	SPECIFICATION	APPROVED SOURCES	REMARKS
PT4-12005-	4K Hz-20K Hz, HC-13 PKG	PT4-12005	MC COY, REEVES-HOFFMAN	
PT4-12006-	1M Hz-3M Hz, TO-8 PKG	PT4-12006		
PT4-12007-	10M Hz-20M Hz, TO-5 PKG	PT4-12007		
PT4-12008-	20M Hz-50M Hz, TO-5 PKG	PT4-12008		
PT4-12009-	50M Hz-125M Hz, TO-5 PKG	PT4-12009		
PT4-12011-	3M Hz-10M Hz, TO-8 PKG	PT4-12011		
C-59 PT4-12012-	100K Hz-300K Hz, HC-13 PKG	PT4-12012		
PT4-12012-	300K Hz-600K Hz, HC-6 PKG	PT4-12012		
PT4-12013-	800K Hz-1M Hz, E7-1 PKG	PT4-12013		
PT4-12014-	125M Hz-200M Hz, TO-5	PT4-12014	MC COY, REEVES-HOFFMAN	

FILTERS

PART NUMBER	DESCRIPTION	SPECIFICATION	APPROVED SOURCES	REMARKS
PT4-1039-1	CAPACITOR, FEED-THRU, CERAMIC DIELECTRIC, 5 A, 200 VDC	PT4-1039	ERIE	
PT4-13016-6	RFI, SUPPRESSION, BROADBAND, CERAMIC DIELECTRIC, 10 A, 50 VDC	PT4-13016	ERIE, USCC	

INDUCTORS

PART NUMBER	DESCRIPTION	SPECIFICATION	APPROVED SOURCES	REMARKS
PT6-2066/67-1	FILTER, ENCAPSULATED, .06 OHM	100 WVDC MAX, PT6-2066/67	TRW SYSTEMS	
PT6-2066/67-2	.12 OHM			
PT6-2066/67-3	.30 OHM			
PT6-2066/67-4	.62 OHM			
PT6-2066/67-5	1.1 OHMS			
PT6-2066/67-6	1.8 OHMS			
C-61 PT6-2066/67-7	4.0 OHMS			
PT6-2066/67-8	8.4 OHMS	100 WVDC PT6-2066/67	TRW SYSTEMS	

NOT REPRODUCIBLE

RELAYS

PART NUMBER	DESCRIPTION	SPECIFICATION	APPROVED SOURCES	REMARKS
PT2-1034-8	GEN PUR, HALF CRYSTAL CAN, 26 V, 870 OHM PORM 15%	PT4-1034 ..	DFILT, P&B	
PT2-1034-15	2PDT	PT4-1034		
PT2-1035PBLPX26	MAGNETIC LATCH, HALF CRYSTAL CAN, 2PDT, LOW CURRENT TO 2A, 26 V, 810 OHM MIN, PLAIN CAN	PT4-1035 :		
PT2-1035PB3SX26	SIDE MOUNT			
PT2-1035PB7SX26	FLANGE MOUNT	PT4-1035	DFILT, P&B	

RESISTORS

PART NUMBER	DESCRIPTION	SPECIFICATION	APPROVED SOURCES	REMARKS
RC42GF100J TO RC42GF226J	COMPOSITION, 2 W, 10 OHMS TO 22 MEGO PORM 5%	MIL-R-11/7	ALLEN-BRADLEY	
RCR05GF100JS TO RCR05GF226JS	1/8 W, 2.7 OHMS TO 22 MEGO PORM 5%	MIL-R-39008/4		
RCR07G2R7JS TO RCR07G226JS	1/4 W, 2.7 OHMS TO 22 MEGO PORM 5%	MIL-R-39008/1		
RCR20G2R7JS TO RCR20G226JS	1/2 W, 2.7 OHMS TO 22 MEGO PORM 5%	MIL-R-39008/2		
C-63 RCR32G2R7JS TO RCR32G226JS	1 W, 2.7 OHMS TO 22 MEGO PORM 5%	MIL-R-39008/3	ALLEN-BRADLEY	
RCR07G2R7JS				

IDENTIFIES THE NOMINAL RESISTANCE IN OHMS, USING TWO SIGNIFICANT FIGURES FROM THE FOLLOWING TABLE. THE THIRD FIGURE INDICATES THE NUMBER OF ZEROS TO FOLLOW; E.G., 163 = 16 K. IF THE VALUE IS LESS THAN 10 OHMS, BOTH FIGURES ARE SIGNIFICANT AND "R" LOCATES THE DECIMAL POINT; E.G., 2R7 = 2.7 OHMS.

10	15	22	33	47	68
11	16	24	36	51	75
12	18	27	39	56	82
13	20	30	43	62	91

PART NUMBER	DESCRIPTION	SPECIFICATION	APPROVED SOURCES	REMARKS
RER65FR100P TO RER65F5621P	WIREWOUND, POWER, CHASSIS MOUNT, 10 W, 0.1 TO 5620 OHMS PORM 1%	MIL-R-39009/1	DALE	
RER70FR100P TO RER70F1212P	15 W, 0.1 TO 12100 OHMS	MIL-R-39009/1	DALE	
RER75FR100P TO RER75F3922P	30 W, 0.1 TO 39200 OHMS	MIL-R-39009/1	DALE	

RNC50H49R9FR TO RNC50H1003FR	FILM, 1/20 W, 49.9 OHMS TO 100 K PORM 1%	MIL-R-55182/7	MEPCO, ANGSTROHM
RNC55H49R9FR TO RNC55H1003FR	1/10 W 49.9 OHMS TO 100 K		MEPCO, ANGSTROHM, IRC
RNC60H49R9FR TO RNC60H4993FR	1/8 W 49.9 OHMS TO 499 K		MEPCO, IRC
RNC65H49R9FR TO RNC65H1004FR	1/4 W 49.9 OHMS TO 1 MEGO	MIL-R-55182/7	MEPCO, IRC

RNC50H49R9FR

IDENTIFIES THE NOMINAL RESISTANCE IN OHMS, USING THREE SIGNIFICANT FIGURES FROM THE FOLLOWING TABLE. THE FOURTH FIGURE INDICATES THE NUMBER OF ZEROS TO FOLLOW; E.G., 1693 = 169 K. IF THE VALUE IS LESS THAN 100 OHMS, ALL THREE FIGURES ARE SIGNIFICANT AND "R" LOCATES THE DECIMAL POINT; E.G., 49R9 = 49.9 OHMS.

100	121	147	178	215	261	316	383	464	562	681	825
102	124	150	182	221	267	324	392	475	576	698	845
105	127	154	187	226	274	332	402	487	590	715	866
107	130	158	191	232	280	340	412	499	604	732	887
110	133	162	196	237	287	348	422	511	619	750	909
113	137	165	200	243	294	357	432	523	634	768	931
115	140	169	205	249	301	365	442	536	649	787	953
118	143	174	210	255	309	374	453	549	665	806	976

RESISTORS

PART NUMBER	DESCRIPTION	SPECIFICATION	APPROVED SOURCES	REMARKS
RNN70C24R9FR TO RNN70C1004FR	FILM, 1/2 W, 24.9 OHMS TO 1 MEGO PORM 1%	MIL-R-55182/6	MEPCO	
RWR80SR100FR TO RWR80S2671FR	WIREWOUND, POWER, 2 W, 0.1 TO 2670 OHMS PORM 1%	MIL-R-39007/8	DALE	
RWR81SR500FR TO RWR81S1001FR	1 W, 0.5 TO 1000 OHMS	MIL-R-39007/9		
RWR84SR100FR TO RWR84S1242FR	7 W, 0.1 TO 12.4 K OHMS	MIL-R-39007/10		
C-65 RWR89SR100FR TO RWR89S4121FR	3 W, 0.1 TO 4.12 K OHMS	MIL-R-39007/11	DALE	

RWR80SR100FR

IDENTIFIES THE NOMINAL RESISTANCE IN OHMS, USING THREE SIGNIFICANT FIGURES FROM THE FOLLOWING TABLE. THE FOURTH FIGURE INDICATES THE NUMBER OF ZEROS TO FOLLOW; E.G., 1693 = 169 K. IF THE VALUE IS LESS THAN 100 OHMS, ALL THREE FIGURES ARE SIGNIFICANT AND "R" LOCATES THE DECIMAL POINT; E.G., 49R9 = 49.9 OHMS.

100	121	147	178	215	261	316	383	464	562	681	825
102	124	150	182	221	267	324	392	475	576	698	845
105	127	154	187	226	274	332	402	487	590	715	866
107	130	158	191	232	280	340	412	499	604	732	887
110	133	162	196	237	287	348	422	511	619	750	909
113	137	165	200	243	294	357	432	523	634	768	931
115	140	169	205	249	301	365	442	536	649	787	953
118	143	174	210	255	309	374	453	549	665	806	976

RESISTORS

PART NUMBER	DESCRIPTION	SPECIFICATION	APPROVED SOURCES	REMARKS:
RER56LL0R00TP TO RER56L22602TP	WIREWOUND, ACCURATE, 1/8 W, 10 OHMS TO 220 K PORM .01%	MIL-R-39005/5	KELVIN, ULTRONIX	
RER56LL0R00BP TO RER56L22002BP	10 OHMS TO 220 K PORM .1%	MIL-R-39005/5	KELVIN, ULTRONIX	
RER56LR1000FP TO RER56L22002FP	0.1 OHM TO 220 K PORM 1%	MIL-R-39005/5	KELVIN, ULTRONIX	

RER56LR1000FP

C-66

DASH NUMBER IDENTIFIES NOMINAL RESISTANCE IN OHMS USING FOUR SIGNIFICANT FIGURES. THE FIRST THREE ARE CHOSEN FROM THE FOLLOWING TABLE. ADD ZERO FOR THE FOURTH SIGNIFICANT DIGIT. THE FIFTH DIGIT INDICATES THE NUMBER OF ZEROS TO FOLLOW; E.G., 11802 = 118 K. IF THE VALUE IS LESS THAN 1000 OHMS, ALL FOUR FIGURES ARE SIGNIFICANT AND "R" LOCATES THE DECIMAL POINT; E.G., 845R0 = 845 OHMS.

100	121	147	178	215	261	316	383	464	562	681	825
102	124	150	182	221	267	324	392	475	576	698	845
105	127	154	187	226	274	332	402	487	590	715	866
107	130	158	191	232	280	340	412	499	604	732	887
110	133	162	196	237	287	348	422	511	619	750	909
113	137	165	200	243	294	357	432	523	634	768	931
115	140	169	205	249	301	365	442	536	649	787	953
118	143	174	210	255	309	374	453	549	665	806	976

DIODES

PART NUMBER	DESCRIPTION	SPECIFICATION	APPROVED SOURCES	REMARKS
JAN-TX1N3893	SILICON, SWITCH, 9 A, 200 NS	MIL-S-19500/304	GE, MOT, SOL	1N3893
JAN-TX1N746A	SILICON, VOLTAGE REFERENCE, 200 MW, 3.3 V PORM 7%	MIL-S-19500/127	MOT, CDC, TRWS	1N746A
JAN-TX1N747A	3.6 V			1N747A
JAN-TX1N748A	3.9 V			1N748A
JAN-TX1N749A	4.3 V			1N749A
JAN-TX1N750A	4.7 V			1N750A
JAN-TX1N751A	5.1 V			1N751A
JAN-TX1N752A	5.6 V			1N752A
JAN-TX1N753A	6.2 V			1N753A
JAN-TX1N754A	6.8 V			1N754A
JAN-TX1N755A	7.5 V			1N755A
JAN-TX1N756A	8.2 V			1N756A
JAN-TX1N757A	9.1 V			1N757A
JAN-TX1N758A	10 V			1N758A
JAN-TX1N759A	12 V 200 MW	MIL-S-19500/127		1N759A
JAN-TX1N827	SILICON, TEMP. COMP, VOLTAGE REF, 6.2 V, 11 MV, TEMP STABILITY	MIL-S-19500/159	MOT, CDC, TRWS	1N827

C-67

DIODES

PART NUMBER	DESCRIPTION	SPECIFICATION	APPROVED SOURCES	REMARKS
JAN-TX1N938B	SILICON, TEMP COMP, VOLTAGE REF, 9.0 V, 16 MV, TEMP STABILITY	MIL-S-19500/156	MOT, CDC, TRWS, DICK	1N938B
JAN-TX1N964B	SILICON, VOLTAGE REFERENCE, 220 MW, 13 V FORM 7%	MIL-S-19500/117		1N964B
JAN-TX1N965B	15 V			1N965B
JAN-TX1N966B	16 V			1N966B
JAN-TX1N967B	18 V		MOT, CDC, TRWS, DICK	1N967B
JAN-TX1N968B	20 V		MOT, CDC, TRWS	1N968B
JAN-TX1N969B	22 V			1N969B
JAN-TX1N970B	24 V			1N970B
JAN-TX1N971B	27 V			1N971B
JAN-TX1N972B	30 V 220 MW	MIL-S-19500/117	MOT, CDC, TRWS	1N972B
PT4-2266-031	SILICON, TEMP COMP, VOLTAGE REF, 8.5 V, 66 MV	PT4-2266	MOT, CDC	1N483A
PT4-2273-031	SILICON, TEMP COMP, VOLTAGE REF, 6.4 V, 10 MV	PT4-2273	MOT, CDC, TRWS	1N4573A
PT4-2274-021	SILICON, TEMP COMP, VOLTAGE REF, 6.7 V, 21 MV	PT4-2274	CDC	FCT-1122
PT4-2278-011	SILICON, VOLTAGE-VARIABLE CAP, 5.5-7.5 PF, 5.1:1 RANGE	PT4-2278	TRWS, CRYST	PC 139

C-68

DIODES

PART NUMBER	DESCRIPTION	SPECIFICATION	APPROVED SOURCES	REMARKS
PT4-2278-021	SILICON, VOLTAGE-VARIABLE CAP, 8.5-11.5 PF, 5.2:1 RANGE	PT4-2278	TRWS, CRYST	PC 135
PT4-2278-031	13-17PF, 5.3:1 RANGE			PC 124
PT4-2278-041	19-25PF, 5.4:1 RANGE			PC 136
PT4-2278-051	28-38PF, 5.4:1 RANGE			PC 128
PT4-2278-061	40-54PF, 5.4:1 RANGE	PT4-2278	TRWS, CRYST	PC 137
PT4-2288-011	SILICON, RECTIFIER, 935MA, 450 V	PT4-2288	UNITRODE, MOT, SOL	1N3613
PT4-2344-011	SILICON, SWITCHING RECTIFIER: FORWARD CURRENT 1.0A AT 1.0V, 75 NS REVERSE RECOVERY TIME TO 5MA	PT4-2344	UNITRODE	UTX225
PT4-2340-011	SILICON, IMPEDENCE 25 MEGOHM, TC +25 TO 150°C, MIN -.05, MAX +.65 PEAK POINT CURRENT .22MA	PT4-2340	MOTOROLA	1N5283
PT4-2340-021	IMPEDENCE 19 MEGOHM, TC MIN -.06 MAX +.57, PEAK POINT CURRENT .24MA			1N5284
PT4-2340-031	IMPEDENCE 14 MEGOHM, TC MIN -.10 MAX +.50, PEAK POINT CURRENT .27MA			1N5285
PT4-2340-041	IMPEDENCE 9 MEGOHM, TC MIN -.12 MAX +.45, PEAK POINT CURRENT .30MA			1N5286
PT4-2340-051	IMPEDENCE 6.60 MEGOHM, TC MIN -.14 MAX +.40, PEAK POINT CURRENT .33MA	PT4-2340	MOTOROLA	1N5287

C-69

DIODES

PART NUMBER	DESCRIPTION	SPECIFICATION	APPROVED SOURCES	REMARKS
PT4-2340-061	SILICON, IMPEDENCE 4.10 MEGOHM, TC +25 TO 150°C, MIN -.18, MAX +.30 PEAK POINT CURRENT .39MA	PT4-2340	MOTOROLA	1N5288
PT4-2340-071	IMPEDENCE 3.30 MEGOHM, TC MIN -.20 MAX +.25, PEAK POINT CURRENT .43MA			1N5289
PT4-2340-081	IMPEDENCE 2.70 MEGOHM, TC MIN -.22 MAX +.22, PEAK POINT CURRENT .47MA			1N5290
PT4-2340-091	IMPEDENCE 1.90 MEGOHM, TC MIN -.25 MAX +.14, PEAK POINT CURRENT .56MA			1N5291
C-70 PT4-2340-101	IMPEDENCE 1.55 MEGOHM, TC MIN -.27 MAX +.10, PEAK POINT CURRENT .62MA			1N5292
PT4-2340-111	IMPEDENCE 1.35 MEGOHM, TC MIN -.28 MAX +.07, PEAK POINT CURRENT .68MA			1N5293
PT4-2340-121	IMPEDENCE 1.15 MEGOHM, TC MIN -.30 MAX +.03, PEAK POINT CURRENT .75MA			1N5294
PT4-2340-131	IMPEDENCE 1 MEGOHM, TC MIN -.31 MAX 0.00, PEAK POINT CURRENT .82MA			1N5295
PT4-2340-141	IMPEDENCE .880 MEGOHM, TC MIN -.32 MAX -.02, PEAK POINT CURRENT .91MA			1N5296
PT4-2340-151	IMPEDENCE .800 MEGOHM, TC MIN -.34 MAX -.04, PEAK POINT CURRENT 1.00MA			1N5297
PT4-2340-161	IMPEDENCE .700 MEGOHM, TC MIN -.35 MAX -.05, PEAK POINT CURRENT 1.10MA	PT4-2340	MOTOROLA	1N5298

DIODES

PART NUMBER	DESCRIPTION	SPECIFICATION	APPROVED SOURCES	REMARKS
PT4-2340-171	SILICON, IMPEDENCE .640 MEGOHM, TC +25 TO 150°C, MIN -.36, MAX -.09 PEAK POINT CURRENT 1.20MA	PT4-2340	MOTOROLA	1N5299
PT4-2340-181	IMPEDENCE .580 MEGOHM, TC MIN -.37 MAX -.10, PEAK POINT CURRENT 1.30MA			1N5300
PT4-2340-191	IMPEDENCE, .540 MEGOHM, TC MIN -.38 MAX -.12, PEAK POINT CURRENT 1.40MA			1N5301
PT4-2340-201	IMPEDENCE, .510 MEGOHM, TC MIN -.39 MAX -.13, PEAK POINT CURRENT 1.50MA			1N5302
PT4-2340-211	IMPEDENCE, .475 MEGOHM, TC MIN -.40 MAX -.14, PEAK POINT CURRENT 1.60MA			1N5303
PT4-2340-221	IMPEDENCE, .420 MEGOHM, TC MIN -.40 MAX -.16, PEAK POINT CURRENT 1.80MA			1N5304
PT4-2340-231	IMPEDENCE, .395 MEGOHM, TC MIN -.41 MAX -.18, PEAK POINT CURRENT 2.00MA			1N5305
PT4-2340-241	IMPEDENCE, .370 MEGOHM, TC MIN -.42 MAX -.19, PEAK POINT CURRENT 2.20MA			1N5306
PT4-2340-251	IMPEDENCE, .345 MEGOHM, TC MIN -.42 MAX -.20, PEAK POINT CURRENT 2.40MA			1N5307
PT4-2340-261	IMPEDENCE, .320 MEGOHM, TC MIN -.43 MAX -.22, PEAK POINT CURRENT 2.70MA			1N5308
PT4-2340-271	IMPEDENCE, .300 MEGOHM, TC MIN -.43 MAX -.22, PEAK POINT CURRENT 3.00MA	PT4-2340	MOTOROLA	1N5309

DIODES

PART NUMBER	DESCRIPTION	SPECIFICATION	APPROVED SOURCES	REMARKS
PT4-2340-281	SILICON, IMPEDENCE .280 MEGOHM, TC +25 TO 150°C, MIN -.44, MAX -.24 PEAK POINT CURRENT 3.30MA	PT4-2340	MOTOROLA	1N5310
PT4-2340-291	IMPEDENCE, .265 MEGOHM, TC MIN -.44 MAX -.25, PEAK POINT CURRENT 3.60MA			1N5311
PT4-2340-301	IMPEDENCE, .255 MEGOHM, TC MIN -.45 MAX -.26, PEAK POINT CURRENT 3.90MA			1N5312
PT4-2340-311	IMPEDENCE, .245 MEGOHM, TC MIN -.45 MAX -.27, PEAK POINT CURRENT 4.30MA			1N5313
C-72 PT4-2340-321	IMPEDENCE, .235 MEGOHM, TC MIN -.45 MAX -.28, PEAK POINT CURRENT 4.70MA	PT4-2340	MOTOROLA	1N5314

TRANSISTORS

PART NUMBER	DESCRIPTION	SPECIFICATION	APPROVED SOURCES	REMARKS
JAN-TX2N918	NPN, SILICON, LOW POWER, TO-18	MIL-S-19500/301	MOT, FSC	
JAN-TX2N2222	NPN, SILICON, SWITCHING, TO-18	MIL-S-19500/255	MOT, FSC	
JAN-TX2N2369A	NPN, SILICON, SWITCHING, TO-18	MIL-S-19500/317	FSC, MOT, TI	
JAN-TX2N2857	NPN, SILICON, TO-18	MIL-S-19500/343	FSC, MOT, TI	
JAN-TX2N2907A	PNP, SILICON, SWITCHING, TO-18	MIL-S-19500/291	MOT, TI	
JAN-TX2N2920	UNITIZED, DUAL, NPN, SILICON	MIL-S-19500/355	MOT, TI	
JAN-TX2N3375	NPN, SILICON, HIGH-POWER, TO-60	MIL-S-19500/341	MOT, TI	
PT4-7156-011	CHOPPER, SILICON, PNP, TO-46	PT4-7156	MOT, TI	2N2946
PT4-7159-011	MULTIPLE, SILICON, COMPLEMENTARY PAIR	PT4-7159	MOT, FSC, TI	MD6002
PT4-7160-011	NPN, HIGH SPEED, MEDIUM CURRENT, TO-5	PT4-7160	MOT, FSC, TI	2N3253
PT4-7161-011	PNP, HIGH SPEED, MEDIUM CURRENT, TO-5	PT4-7161	MOT, FSC, TI	2N3467
PT4-7162-011	NPN, LOW NOISE, SILICON, TO-18	PT4-7162	MOT, FSC, TI	2N2484
PT4-7172-011	NPN, GEN PUR, HIGH V, AMPL, TO-18	PT4-7172	FSC, MOT, RAY	2N915
PT4-7173-011	NPN, SILICON, TO-18	PT4-7173	FSC, MOT, RAY	2N2369A
PT4-7174-011	NPN, SILICON, MDM PWR, VHF AMPL, TO-18	PT4-7174	FSC, MOT	2N3137
PT4-7175-011	NPN, SILICON, HIGH PWR, VHF AMPL, TO-60	PT4-7175	MOT, RCA, NAT	2N3632

C-73

TRANSISTORS

PART NUMBER	DESCRIPTION	SPECIFICATION	APPROVED SOURCES	REMARKS
PT4-7176-011	NPN, SILICON, INTERMEDIATE PWR, TO-59	PT4-7176	FSC, SOL, TI, MOT	2N2880
PT4-7178-011	NPN, SILICON, GEN PURPOSE, HIGH VOLTAGE, TO-5	PT4-7178	MOT, TI	2N3501
PT4-7187-011	NPN, SILICON, UHF AMPL & OSC, TO-46	PT4-7187	FSC	MT1060
PT4-7187-021	NPN, SILICON, UHF AMPL & OSC, TO-46	PT4-7187	FSC	MT1060A
PT4-7206-011	PNP, SILICON, MATCHED PAIR, TO-5	PT4-7206	FSC, TI	2N4025
PT4-7206-021	TO-5 (6 LEAD)	PT4-7206	FSC, TI	2N4022
PT4-7206-031	TO-5 (6 LEAD)	PT4-7206	FSC, TI	2N4023
PT4-7213-011	NPN, SILICON, HIGH SPEED SWITCH- ING FLATPACK	PT4-7213	FSC, MOT, TI	MD2369AF
PT4-7215-011	NPN, SILICON, LOW POWER, UHF AMPL, TO-5 (SOLID HEADER)	PT4-7215	TRWS	2N4428
PT4-7216-011	NPN, SILICON, FLATPACK	PT4-7216	MOT, TI, FSC	MD2219F
PT4-7217-011	PNP, SILICON, FLATPACK	PT4-7217	MOT, TI	MD2905A
PT4-7229-011	P-N PLANAR UNIJUNCTION, TO-18	PT4-7229	MOT, TI	2N4853
PT4-7231-011	NPN, SILICON, HIGH POWER, TO-63	PT4-7231	SOL, TI	2N4002
PT4-7247-011	PNP, HIGH POWER, TO-3	PT4-7247	SOL, TI	2N4399
PT4-7248-011	PNP, POWER, TO-59	PT4-7248	SOL, TI	TPAO4000MA
PT4-7248-021	TO-59	PT4-7248	SOL, TI	2N5005

C-74

TRANSISTORS

PART NUMBER	DESCRIPTION	SPECIFICATION	APPROVED SOURCES	REMARKS
PT4-7253-011	FET, JUNCTION, N-CHANNEL, UHF, TO-18 (4 LEAD)	PT4-7253	MOT	2N4416

INTEGRATED CIRCUITS

PART NUMBER	DESCRIPTION	SPECIFICATION	APPROVED SOURCES	REMARKS
PT4-4047-011	DUAL, 4-INPUT, EXPANDABLE NAND GATE	PT4-4047	SIGNETICS, SPRAGUE	SE416J
PT4-4048-011	DUAL, RST FLIP-FLOP	PT4-4048	SIGNETICS	SE424J
PT4-4049-011	DUAL, 4-INPUT BUFFER/DRIVER	PT4-4049	SIGNETICS	SE455J
PT4-4050-011	QUAD, 2-INPUT NAND GATE	PT4-4050	SIGNETICS	SE480J
PT4-4051-011	DUAL, 4-INPUT, NAND/NOR GATE	PT4-4051	FSC, TI, MOT	DTUL930
PT4-4052-011	DUAL, 4-INPUT BUFFER	PT4-4052	.	DTUL932
PT4-4053-011	DUAL, 4-INPUT EXTENDER	PT4-4053	.	DTUL933
PT4-4054-011	CLOCKED FLIP-FLOP, RS OR JK	PT4-4054	.	DTUL945
PT4-4055-011	QUAD, 2-INPUT NAND/NOR GATE	PT4-4055	FSC, TI, MOT	DTUL946
PT4-4056-011	2-INPUT, MONOSTABLE MULTIVIBRATOR	PT4-4056	FSC, MOT	DTUL951
PT4-4057-011	TRIPLE, 3-INPUT NAND/NOR GATE	PT4-4057	FSC, TI, MOT	DTUL962
PT4-4087-011	LOW POWER, CLOCKED FLIP-FLOP	PT4-4087	AMELCO	LPDTUL9040
PT4-4088-011	LOW POWER, DUAL 3-INPUT GATE	PT4-4088	AMELCO, FSC	LPDTUL9041
PT4-4089-011	LOW POWER, DUAL 3-INPUT GATE WITH EXTENDER INPUT	PT4-4089	AMELCO, FSC	LPDTUL9042
PT4-4090-011	LOW POWER, QUAD 2-INPUT GATE	PT4-4090	AMELCO, FSC	LPDTUL9046
PT4-5007-011	WIDEBAND, DC AMPLIFIER	PT4-5007	FSC	UA702A

C-76

SWITCHES

PART NUMBER	DESCRIPTION	SPECIFICATION	APPROVED SOURCES	REMARKS
PT2-2014-13	THERMOSTATIC, SPST, SNAP ACTG, HERMETIC SEALED, OPEN 52°F, CLOSE 42°F	PT2-2014	UNITED CONTROL	
PT2-2014-14	OPEN 86°F, CLOSE 95°F			
PT2-2014-15	OPEN 115°F, CLOSE 125°F			
PT2-2014-17	OPEN 60°F, CLOSE 51°F			
PT2-2014-18	OPEN 85°F, CLOSE 90°F			
PT2-2014-21	OPEN 75°F, CLOSE 80°F			
PT2-2014-22	OPEN 70°F, CLOSE 80°F			
PT2-2014-23	OPEN 105°F, CLOSE 110°F			
PT2-2014-24	OPEN 100°F, CLOSE 105°F			
PT2-2014-32	OPEN 65°F, CLOSE 70°F			
PT2-2014-33	OPEN 60°F, CLOSE 65°F			
PT2-2014-34	OPEN 55°F, CLOSE 60°F			
PT2-2014-35	OPEN 86°F, CLOSE 95°F	PT2-2014	UNITED CONTROL	

C-77

TRANSFORMERS

PART NUMBER	DESCRIPTION	SPECIFICATION	APPROVED SOURCES	REMARKS
PT6-1065/16-1	POWER, ENCAPSULATED, 50 WVDC MAX	PT6-1065	TRW SYSTEMS	
PT6-1065/17-1				
PT6-1065/18-3				
PT6-1065/54-2				
PT6-1065/60-1				
PT6-1065/61-1				
PT6-1065/80-1				
PT6-1065/81-1				
PT6-1065/82-1				
PT6-1065/83-1	POWER, ENCAPSULATED, 200 WVDC MAX	PT6-1065	TRW SYSTEMS	

C-78

WIRE AND CABLE

PART NUMBER	DESCRIPTION	SPECIFICATION	APPROVED SOURCES	REMARKS
MIL-W-583	WIRE, MAGNET, ELECTRICAL	MIL-W-583	HUDSN, PHLPD, ESSEX	
MS21985-16-9	HOOK-UP, EXTRUDED TEFLON INS, 16 AWG, 600-VOLT, WHITE	MS21985	QPL	
MS21985-18-9	18 AWG			
MS21985-20-9	20 AWG			
MS21985-22-9	22 AWG			
MS21985-24-9	24 AWG			
C-79 MS21985-26-9	26 AWG			
MS21985-28-9	HOOK-UP, EXTRUDED TEFLON INS, 28 AWG, 600-VOLT, WHITE	MS21985	QPL	
PT3-33B18-9	FLAT BRAID SHIELD, 18 AWG	PT3-33	RAYC	
PT3-33B20-9	20 AWG			
PT3-33B22-9	22 AWG			
PT3-33B24-9	24 AWG			
PT3-33F26-9	26 AWG			
PT3-33F28-09	28 AWG			
PT3-33F30-09	FLAT BRAID SHIELD, 30 AWG	PT3-33		
PT3-38-1-18-9	HOOK-UP, IRRADIATED, POLYALKENE INSULATION, 18 AWG	PT3-38		
PT3-38-1-20-9	HOOK-UP, IRRADIATED, POLYALKENE INSULATION, 20 AWG	PT3-38	RAYC	

WIRE AND CABLE

PART NUMBER	DESCRIPTION	SPECIFICATION	APPROVED SOURCES	REMARKS
PT3-38-1-22-9	HOOK-UP, IRRADIATED, POLYALKENE INSULATION, 22 AWG	PT3-38	RAYC	
PT3-38-1-24-9	24 AWG			
PT3-38-2-26-9	26 AWG			
PT3-38-2-28-9	28 AWG			
PT3-38-2-30-9	HOOK-UP, IRRADIATED, POLYALKENE INSULATION, 30 AWG	PT3-38	RAYC	
QQ-W-343	ELECTRICAL, COPPER INSULATED	QQ-W-343 (FEDERAL SPEC)	HUDSN, PHLPD, INWIR	

WIRE AND CABLE

PART NUMBER	DESCRIPTION	SPECIFICATION	APPROVED SOURCES	REMARKS
PT3-29-3	COAXIAL, SEMI-RIGID, RF, 50 OHMS, COPPER TUBE, UNPLATED	PT3-29	PT, UT	
PT3-29-4	COPPER TUBE, UNPLATED			
PT3-29-5	COPPER TUBE, UNPLATED			
PT3-29-6	ALUMINUM TUBE, UNPLATED			
PT3-29-11	COPPER PLATED, ALUMINUM	PT3-29	PT, UT	
PT3-49-75-1	COAXIAL, TEFLON DIELECTRIC, 75 OHMS, DOUBLE BRAID	PT3-49	TIMES, HAVEG, MICRO	
C-81 RG-142B/U	COAXIAL, DOUBLE BRAID	MIL-C-17/70	QPL	
RG-187A/U	COAXIAL, SINGLE BRAID	MIL-C-17/68	QPL	
RG-188A/U	COAXIAL, TEFLON JACKET, FLEXIBLE, SINGLE BRAID	MIL-C-17/69	QPL	

SECTION III - MATERIALS AND PROCESSES

	MATERIAL OR PROCESS TYPE DESIGNATION	PROCUREMENT SPECIFICATION	SUBSTITUTE OR SUPERSEDING SPECIFICATION	PLANNED SOURCE OF SUPPLY <u>1/</u>	CODE NO. <u>2/</u>
1	Dry Unbonded MoS ₂ Films	PR1-1		TRW Systems Group	11982
2	Cleaning Fluid System Comp.	PR2-2		Cemarc Division, Cemarc Corp., Inglewood, Calif.	001354
3	Cleaning Aluminum	PR2-3		Anadite Inc. South Gate, Calif.	005267
4	Abrasive Cleaning	PR2-4		TRW Systems Group	11982
5	Solvent Cleaning	PR2-8		TRW Systems Group	11982
6	Surface Prep. for Bonding	PR2-12		Golden State Casting Port Hueneme, Calif.	005371
7	Surface Prep. Adhesives, Coatings	PR2-22		TRW Systems Group	11982
8	Fusion Welding	PR3-1		Cromer Mfg. & Eng. Los Angeles, Calif.	0020480
9	Resistance Welding	PR3-2		TRW Systems Group	11982
10	Brazing, Salt Bath	PR3-3		QAPSD	008827
11	Tinning & Soldering Electronic Comp.	PR3-5		TRW Systems Group	11982
12	Installation of Conv. Rivets	PR3-9		TRW Systems Group	11982
13	Resistance Welding Stranded Wire	PR3-17		TRW Systems Group	11982
14	Soldering, Electrical and Electronic	PR3-21		TRW Systems Group	11982
15	Potting with Silicone	PR4-1		TRW Systems Group	11982
16	Bonding with Epoxys	PR4-2		TRW Systems Group	11982
17	Thermal Interface Mat.	PR4-5		TRW Systems Group	11982
18	Potting Connectors	PR4-7		TRW Systems Group	11982
19	Bonding with Conductive Epoxy	PR4-11	PR4-12	*	
20	Cond. Epoxy for R. F. Shield	PR4-12		TRW Systems Group	11982

* See Listed Substitute or Superseding Specification for Planned Source of Supply.

	MATERIAL OR PROCESS TYPE DESIGNATION	PROCUREMENT SPECIFICATION	SUBSTITUTE OR SUPERSEDING SPECIFICATION	PLANNED SOURCE OF SUPPLY <u>1/</u>	CODE NO. <u>2/</u>
21	Cover Glass Bonding, EPD X-74	PR4-14		TRW Systems Group	11982
22	Cover Glass Bonding	PR4-15		TRW Systems Group	11982
23	Vac. Impreg. Transformer	PR4-16		TRW Systems Group	11982
24	Structural Adhesive	PR4-18		TRW Systems Group	11982
25	Applications of Sealing Compound	PR4-20		TRW Systems Group	11982
26	Bonding with Film Adhesive	PR4-21		TRW Systems Group	11982
27	Embedding Elect. Parts, Assys, with Epoxy Resin	PR4-24		TRW Systems Group	11982
28	Silicone Bonding	PR4-27		TRW Systems Group	11982
29	Adhesive Bonding of Electronics	PR4-34		TRW Systems Group	11982
30	Clear Protective Coating	PR5-1	PR5-11	*	
31	Epoxy Protective Finish	PR5-2		TRW Systems Group	11982
32	Conformal Coating, Electronic Assemblies	PR5-5	PR5-14	*	
33	Grease Plating	PR5-6		TRW Systems Group	11982
34	Coating of High Frequency Coils	PR5-8		TRW Systems Group	11982
35	Repairable Coatings for Cordwood Modules	PR5-11		TRW Systems Group	11982
36	Coating Thermoplastic	PR5-12		TRW Systems Group	11982
37	Conf. Coat. Elect. Circuit Board Assys	PR5-14		TRW Systems Group	11982
38	Application Thermal Control Coating	PR5-17		TRW Systems Group	11982
39	Conformal Coating, Electronic Circuit Board Assemblies (Polyurethane)	PR5-22		TRW Systems Group	11982
40	Gold Plating	PR6-3		Anchor Plating So. El Monte, Calif.	CC5336

* See listed Substitute or Superseding Specification for Planned Source of Supply.

	MATERIAL OR PROCESS TYPE DESIGNATION	PROCUREMENT SPECIFICATION	SUBSTITUTE OR SUPERSEDING SPECIFICATION	PLANNED SOURCE OF SUPPLY <u>1/</u>	CODE NO. <u>2/</u>
41	Solder Coat. Electrodeposited	PR6-5		TRW Systems Group	11982
42	Hard Anodizing	PR6-6	PR6-23 and MIL-A-8625	*	
43	Electroplating Aluminum	PR6-7		Anchor Plating So. El Monte, Cal.	CC5336
44	Vac-Deposited Aluminum	PR6-11		Vac. Metallizing Co. Van Nuys, Calif.	CC238
45	Supplementary Treatment of Hard Anodizing	PR6-23		TRW Systems Group	11982
46	Installation of Hardware etc.	PR7-1		TRW Systems Group	11982
47	Fab. of Wire and Cable	PR7-2		TRW Systems Group	11982
48	Grounding of Shielded Wire	PR7-3		TRW Systems Group	11982
49	Assembly of RF Connectors	PR7-4		TRW Systems Group	11982
50	Printed Wiring Boards	PR7-5		See ASL	
51	RF Hardware and Part Installation	PR7-11		TRW Systems Group	11982
52	Electronic Assembly on Printed Wiring	PR7-18		TRW Systems Group	11982
53	Instal. Threaded Fasteners	PR9-18		TRW Systems Group	11982
54	Instal. Temp. Tabs, Probes	PR9-40		TRW Systems Group	11982
55	Instal. of Min. Threaded Inserts	PR9-109		TRW Systems Group	11982
56	Key Locked Inserts	PR9-110		TRW Systems Group	11982
57	Rack and Panel Connectors	PR9-113		TRW Systems Group	11982
58	Tightening Threaded Fasteners	PR9-131		TRW Systems Group	11982
59	Fab. of Alum. Honeycomb	PR10-7		See ASL	
60	Low Pressure Epoxy Laminate	PR10-14		TRW Systems Group	11982

C-84

* See listed Substitute or Superseding Specification for Planned Source of Supply.

	MATERIAL OR PROCESS TYPE DESIGNATION	PROCUREMENT SPECIFICATION	SUBSTITUTE OR SUPERSEDING SPECIFICATION	PLANNED SOURCE OF SUPPLY <u>1/</u>	CODE NO. <u>2/</u>
81	Gold Plating	P6-2	PR6-3	*	
82	Anodizing and Coloring Alum.	P6-4	MIL-A-8625	*	
83	Electroplating Alum. Alloy	P6-5	PR6-7	*	
84	Black Oxide Finish	P6-9	MIL-C-13924	*	
85	Hard Anodizing	P6-10	PR6-6	*	
86	Fab. and Instal. Elect. Harnesses	P7-3	PR7-2	*	
87	Aluminum Foil	MT2-2		Aluminum Co. of America	09192
88	H. S. Reflector Sheet	MT2-4		<u>3/</u>	
89	Sintered Bronze, MoS ₂	MT2-5		Booker-Cooper, Inc. North Hollywood, Cal.	
90	Cu-Ni Alloy Wire and Ribbon	MT2-7	MT11-1, Type II Class A180	*	
91	Silicone Rubber, RTV	MT3-2	MIL-S-23586	*	
92	Cu-Clad Epoxy-Glass Laminate	MT3-4		Mica Corporation Culver City, Cal.	06216
93	Primer for RTV Silicone Compounds	MT3-25		General Electric Waterford, N. Y.	01139
94	Tape, Lacing and Tying	MT3-38		See ASL	
95	Thermal Control Paint, U.V. Stable	MT6-7		Dow Corning Corp. Eng. Prod. Div. Elizabethtown, Ken.	
96	Coating, Epoxy Resin Base	MT6-9		Finch Paint and Chemical Co.	98502
97	Heat Shrinkable Tube	MT13-4		See ASL	
98	Aluminized Plastic Film	MT3-14		See ASL	
99	Lead Wire & Ribbons	MT11-1		See ASL	

* See listed Substitute or Superseding Specification for Planned Source of Supply.

	MATERIAL OR PROCESS TYPE DESIGNATION	PROCUREMENT SPECIFICATION	SUBSTITUTE OR SUPERSEDING SPECIFICATION	PLANNED SOURCE OF SUPPLY <u>1/</u>	CODE NO. <u>2/</u>
100	Sleeving	MIL-3-2		See ASL	
101	Insul. Tubing, Heat Shrinkable	MIL-3-4		See ASL	
102	Ceramic Insulating Materials	MIL-I-10		QPL	
103	Laminated Plastic Rod & Tube	MIL-P-79		Synthane Corp.	78397
104	Aluminum Foil	MIL-A-148		Crawford Foil Co. Hawthorne, Calif.	
105	Packaging Bearing Parts	MIL-B-197		TRW Systems Group	11982
106	Black Finish for Copper	MIL-F-495		Enthone Inc.	02258
107	Magnet Wire	MIL-W-583		MIL Spec. Supply Inc Van Nuys, Calif.	
108	Synthetic Resin Insulation	MIL-I-631		QPL	
109	Lacing Twine	MIL-T-713		Gudebrod Bros. Silk Company	82110
110	Propellant Powder, M ₁ O	JAN-T-715		Hercules Powder Co.	28284
111	Laminated Glass Cloth Sheets	MIL-P-997		QPL	
112	Glass Fabric	MIL-Y-1140		Ferro Corp., Fiber Glass Division	22645
113	Laminated Paper-Base Sheets	MIL-P-3115	L-P-513	*	
114	Pretreatment of Mag. Alloy	MIL-M-3171		Anadite Inc. South Gate, Calif.	CC5267
115	Packaging Materials Corr. Inhibitor	MIL-P-3420		QPL	
116	Bare Copper Wire	MIL-W-3861	QQ-W-343	*	
117	Grease	MIL-I-4343		QPL	
118	Surface Treatment	MIL-S-5002		Anadite Inc. South Gate, Calif.	CC5267
119	CRES, Plate, Sheet and Strip	MIL-S-5059		Ducommun Metals and Supply Co.	18702
120	Epoxy Adhesive	MIL-A-5090		Shell Chem. Co.	22893

	MATERIAL AND PROCESS TYPE DESIGNATION	PROCUREMENT SPECIFICATION	SUBSTITUTE OR SUPERSEDING SPECIFICATION	PLANNED SOURCE OF SUPPLY 1/	CODE NO. 2/
121	CRES Flex Cable	MIL-C-5424		Ducommun Metals and Supply Co.	18702
122	Heat Resistant Acrylic Sheet	MIL-P-5425		QPL	
123	Chemical Conversion Films	MIL-C-5541		QPL or QAPSD	CC7201
124	4140 Alloy Steel Bars A.Q.	MIL-S-5626		Ducommun	18702
125	Testing of Cable	MIL-C-5688		TRW Systems Group	11982
126	Silicone Rubber, Low, High Temp. Res..	MIL-R-5847	ZZ-R-765	*	
127	Classification of Castings	MIL-C-6021		TRW Systems Group	11982
128	Lubricating Oil	MIL-L-6085		Texaco, Inc.	99748
129	Heat Treatment of Al. Alloy	MIL-H-6088		QAPSD	CC2601
130	Nitriding Steels	MIL-S-6090		Ducommun	CC2611
131	Steel, Corr. and Heat Resistant	MIL-S-6721		Ducommun	18702
132	4130 Alloy Steel Bars, A.Q.	MIL-S-6758		Ducommun	18702
133	Spot & Seam Resistance Weld	MIL-W-6858		QAPSD	CC8870
134	Penetrant Inspection	MIL-I-6866		QAPSD	CC3755
135	Heat Treatment of Steel	MIL-H-6875		QAPSD	CC2610
136	Hydraulic Tube, 6061 Al.	MIL-T-7081		Tubesales Los Angeles, Cal.	
137	Heat Treatment of Be-Cu	MIL-H-7199		QAPSD	CC2603
138	Aluminum Core Material	MIL-C-7438		Aluminum Co. of America	09192
139	Electrical Insulation Sleeving	MIL-I-7444		MIL Spec Supply, Inc. Van Nuys, Calif.;	
140	18-8-CRES Bar & Wire, A.Q.	MIL-S-7720		Ducommun	18702

* See listed Substitute or Superseding Specification for Planned Source of Supply.

	MATERIAL OR PROCESS TYPE DESIGNATION	PROCUREMENT SPECIFICATION	SUBSTITUTE OR SUPERSEDING SPECIFICATION	PLANNED SOURCE OF SUPPLY 1/	CODE NO. 2/
141	Brazing	MIL-B-7883		QAPSD	008826
142	1020 & 1025 Steel, A. Quality	MIL-S-7952		Ducommun	18702
143	Interchangeability Parts	MIL-I-8500		TRW Systems Group	11982
144	Zinc Chromate Primer	MIL-P-8585		QPL	
145	Welding of Alum. Alloys	MIL-W-8604		TRW Systems Group	11982
146	Welding of CRES & HR Alloys	MIL-W-8611		TRW Systems Group	11982
147	Epoxy Resin Adhesive	MIL-A-8623		QPL	
148	Anodic Coating	MIL-A-8625		QAPSD	007202
149	Hydraulic Tube CRES	MIL-T-8808		Tubesales Los Angeles, Calif.	
150	Solid Film Lubricant	MIL-L-8937		QPL or QAPSD	007236
151	Pure Beryllium Sheet	MIL-B-8964		Brush Beryllium Co.	05451
152	Titanium Sheet, Strip, Plate	MIL-T-9046		ARMCO Steel Corp., Advanced Mat'ls. Div.	78019
153	Titanium Bars, Forgings	MIL-T-9047		Fansteel/	06992
154	Glass Cloth for Laminate	MIL-C-9084		Ram Chemicals Inc.	22401
155	Epoxy Resin, L. P. Laminating	MIL-R-9300		QPL	
156	Tin Plating	MIL-T-10727		QAPSD	007278
157	Alum. Backed Adhesive Tape	MIL-T-11291	L-T-0080	*	
158	Silver Sheet and Strip	MIL-S-13282		Handy and Harmon	25166
159	Black Oxide Finish	MIL-C-13924		Enthone Inc.	02258
160	Copper Clad Laminate	MIL-P-13949		QPL	
161	Finish for Ground Signal Eq.	MIL-F-14072		TRW Systems Group	11982


* See listed Substitute or Superseding Specification for Planned Source of Supply.

	MATERIAL OR PROCESS TYPE DESIGNATION	PROCUREMENT SPECIFICATION	SUBSTITUTE OR SUPERSEDING SPECIFICATION	PLANNED SOURCE OF SUPPLY 1/	CODE NO. 2/
162	Copper Plating	MIL-C-14550		TRW Systems Group	11982
163	Insulation Tape	MIL-I-15126		Minnesota Mining and Mfg. Co.	76381
164	Brazing Alloy, Silver	MIL-B-15395		Handy and Harmon	25166
165	Nylon Rods and Bars	MIL-P-17091	L-P-410	*	
166	Insulation Sleeving, Glass Fiber, Sil. Rubber Treatment	MIL-T-18057		Insulectro Corp. Los Angeles, Calif.	
167	Epoxy - Glass Laminate	MIL-P-18177		QPL	
168	Argon, Technical	MIL-A-18455		The Matheson Co., Inc. Los Angeles, Calif.	
169	Silver Sheet, Strip, Wire, Rod	MIL-S-19424	MIL-S-13282	*	
170	Diallyl Phthalate Molding Resin	MIL-P-19833		QPL	
171	Alum. Alloy Brazing Alloys	MIL-B-20148		Ducommun Metals and Supply Co.	18702
172	Polyamid Molding Plastic	MIL-M-20693		Cadillac Plastic and Chemical Co.	95696
173	Sealing Compounds	MIL-S-22473		Cadillac Plastic and Chemical Co.	95696
174	Sealing Compound Silicone	MIL-S-23586		QPI	
175	Glass - Epoxy L.P. Lam. Resin	MIL-P-25421		Coast Pro Seal and Mfg. Co.	83527
176	H. T. Fluid Resistant Rubber	MIL-R-25897		Chomerics Inc.	18565
177	Electroless Nickel	MIL-C-26074		QAPSD	CC7272
178	Anodizing Magnesium	MIL-M-45202		Anadite Inc. South Gate, Cal.	CC5267
179	Gold Plating	MIL-G-45204		TRW Systems Group	11982
180	Polyethylene Terephthalate Plastic	MIL-P-55010		Cadillac Plastics	

* See listed Substitute or Superseding Specification for Planned Source of Supply.

C-90

	MATERIAL OR PROCESS TYPE DESIGNATION	PROCUREMENT SPECIFICATION	SUBSTITUTE OR SUPERSEDING SPECIFICATION	PLANNED SOURCE OF SUPPLY 1/	CODE NO. 2/
181	Printed Wiring	MIL-P-55110		TRW Systems Group	11982
182	Finishing of Metal & Wood	MIL-STD-171		TRW Systems Group	11982
183	Lock Wire	MS 20995		Aircraft Supply Glendale, Calif.	
184	Insert, Std. dims - Helical Coil	MS 33537		Helicoil Corp.	91767
185	Insert, Screw Thds. - dims for Assembly and Hole	MS 33646		TRW Systems Group	11982
186	Safety Wiring Practices	MS 33540		TRW Systems Group	11982
187	Polyester Sheet & Strip	L-P-377		Cadillac Plastic and Chemical Co.	95696
188	Plastic Film, Polyethylene	L-P-378		Cadillac Plastic and Chemical Co.	95696
189	Nylon Rods and Bars	L-P-410		Cadillac Plastic and Chemical Co.	95696
190	Laminated Paper Base Sheets	L-P-513		Synthane Corp.	78397
191	Tape	L-T-80		Minnesota Mining and Mfg. Co.	76381
192	Pressure Sensitive Tape	L-T-100		Minnesota Mining and Mfg. Co.	76381
193	Silver Alloy Brazing Flux	O-F-499		Handy and Harmon	25166
194	Polyester Thread	V-T-285		Cadillac Plastic and Chemical Co.	95696
195	Pasted-Mica, Insulation	HH-I-538		Carborundum Co. Refractories and Elect. Division	07521
196	Rubber, Silicone, Low, High, and Tear Res.	ZZ-R-765		A.B. Boyd Co. Los Angeles, Cal.	

	MATERIAL OR PROCESS TYPE DESIGNATION	PROCUREMENT SPECIFICATION	SUBSTITUTE OR SUPERSEDING SPECIFICATION	PLANNED SOURCE OF SUPPLY <u>1/</u>	CODE NO. <u>1/</u>
197	2024 Aluminum Bar, Shapes	QQ-A-200/3		Aluminum Co. of Amer./ Reynolds Alum. Supply Co. of Calif.	09192 04355
198	6061 Aluminum Bar, Shapes	QQ-A-200/8			
199	6063 Aluminum Bar, Shapes	QQ-A-200/9			
200	7075 Aluminum Bar, Shapes	QQ-A-200/11			
201	1100 Aluminum Bar, Rod	QQ-A-225/1			
202	2011 Aluminum Bar, Rod	QQ-A-225/3			
203	2017 Aluminum Bar, Rod	QQ-A-225/5			
204	2024 Aluminum Bar, Rod	QQ-A-225/6			
205	5052 Aluminum Bar, Rod	QQ-A-225/7			
206	6061 Aluminum Bar, Rod	QQ-A-225/8			
207	7075 Aluminum Bar, Rod	QQ-A-225/9			
208	1100 Plate and Sheet	QQ-A-250/1			
209	2014 Plate and Sheet	QQ-A-250/3			
210	2024 Plate and Sheet	QQ-A-250/4			
211	2024 Clad Plate and Sheet	QQ-A-250/5			
212	5052 Plate and Sheet	QQ-A-250/8			
213	6061 Plate and Sheet	QQ-A-250/11			
214	7075 Plate and Sheet	QQ-A-250/12		Aluminum Co. of Amer./ Reynolds Alum. Supply Co. of Calif.	09192 04355

	MATERIAL OR PROCESS TYPE DESIGNATION	PROCUREMENT SPECIFICATION	SUBSTITUTE OR SUPERSEDING SPECIFICATION	PLANNED SOURCE OF SUPPLY <u>1/</u>	CODE NO. <u>2/</u>
215	2024 Alum. Extrusions	QQ-A-267	Superseded by QQ-A-200/3	*	
216	2024 Alum. Bar, Rod	QQ-A-268	Superseded by QQ-A-225/6	*	
217	7075 Alum. Extrusions	QQ-A-277	Superseded by QQ-A-200/11	*	
218	7075 Alum. Bar, Rod, Wire	QQ-A-282	Superseded by QQ-A-225/9	*	
219	5052 Alum. Bar, Rod	QQ-A-315	Superseded by QQ-A-225/7	*	
220	5052 Alum. Plate & Sheet	QQ-A-318	QQ-A-250/8	*	
221	6061 Alum. Alloy Plate & Sheet	QQ-A-325	QQ-A-225/8	*	
222	6061 Alum. Plate & Sheet	QQ-A-327	QQ-A-250/11	*	
223	2017 Alum. Bar & Rod	QQ-A-351	QQ-A-225/5	*	
224	2024 Alum. Plate & Sheet	QQ-A-355	QQ-A-250/4	*	
225	3003 Alum.	QQ-A-359			
226	2024 Clad Alum. Plate & Sheet	QQ-A-362	QQ-A-250/5	*	
227	2011 Alum. Bar, Rod	QQ-A-365	QQ-A-225/3	*	
228	Alum. Alloy Forging	QQ-A-367	QQ-A-225/1	*	
229	1100 Alum. Alloy Bar, Rod	QQ-A-411	QQ-A-225/1	*	
230	1100 Alum. Alloy Plate & Sheet	QQ-A-561	QQ-A-250/1	*	
231	Permanent Mold Castings	QQ-A-596		Reynolds Alum. Supply Co. of California	04355
232	Alum. Alloy Sand Casting	QQ-A-601		Reynolds Alum. Supply Co. of California	04355

C-92

* See listed Substitute or Superseding Specification for Planned Source of Supply.

	MATERIAL OR PROCESS TYPE DESIGNATION	PROCUREMENT SPECIFICATION	SUBSTITUTE OR SUPERSEDING SPECIFICATION	PLANNED SOURCE OF SUPPLY 1/	CODE NO. 2/
233	Brass, Flat Products	QQ-B-613		Ducommon Metals and Supply Co.	18702
234	Brass Rod & Flat Products	QQ-B-626		Ducommon Metals and Supply Co.	18702
235	Naval Brass	QQ-B-637		Ducommon Metals and Supply Co.	18702
236	Phosphor Bronze	QQ-B-750		Ducommon Metals and Supply Co.	18702
237	Be-Cu Bar, Rod & Wire	QQ-C-530		Brush Beryllium Co.	05451
238	Be-Cu Strip	QQ-C-533		Brush Beryllium Co.	05451
239	Flat Copper Products	QQ-C-576		Ducommon Metals and Supply Co.	18702
240	Copper-Silicon Alloy	QQ-C-591		Ducommon Metals and Supply Co.	18702
241	Mag. Bars, Rods, & Shapes	QQ-M-31		Dow Chemical Co. Gov. Affairs Dept.	96717
242	Mag. Alloy Plate & Sheet	QQ-M-44		Dow Chemical Co. Gov. Affairs Dept.	96717
243	Cadmium Plating	QQ-P-416		QAPSD	CC7257
244	Alum. Welding Rods	QQ-R-566		Ducommon Metals and Supply Co.	18702
245	Silver Plating	QQ-S-365		QAPSD	CC7276
246	Silver Solder	QQ-S-561		Handy and Harmon	25166
247	Solder	QQ-S-571		QPL	
248	CRES Bars & Shapes	QQ-S-763		Ducommon Metals and Supply Co.	18702
249	Copper Alloy Wire	QQ-W-321		MIL Spec Supply Inc Van Nuys, Calif.	

	MATERIAL OR PROCESS TYPE DESIGNATION	PROCUREMENT SPECIFICATION	SUBSTITUTE OR SUPERSEDING SPECIFICATION	PLANNED SOURCE OF SUPPLY 1/	CODE NO. 2/
250	Uninsulated Copper Wire	QQ-W-343		MIL Spec Supply Inc Van Nuys, Calif.	
251	Ni-Cr-Fe Alloy Wire	QQ-W-390		MIL Spec Supply Inc Van Nuys, Calif.	
252	Steel Wire	QQ-W-412		Ducommun Metals and Supply Co.	18702
253	CRES Wire	QQ-W-423		Ducommun Metals and Supply Co.	18702
254	High Carbon Steel Wire	QQ-W-428		Ducommun Metals and Supply Co.	18702
255	Gloss Enamel	TT-E-489		Sherwin-Williams Co	15210
256	Semi-Gloss Enamel	TT-E-529		Sherwin-Williams Co	15210
257	3003 Alum. Alloy Tube	WW-T-700/2D		Tubesales Los Angeles, Calif.	
258	2024 Alum. Alloy Tube	WW-T-700/3D		Tubesales Los Angeles, Calif.	
259	5052 Alum. Alloy Tube	WW-T-700/4D		Tubesales Los Angeles, Calif.	
260	6061 Alum. Alloy Tube	WW-T-700/6D		Tubesales Los Angeles, Calif.	
261	2024 Alum. Alloy Tube	WW-T-785	Superseded by WW-T-700/3	*	
262	5052 Alum. Alloy Tube	WW-T-787	Superseded by WW-T-700/4	*	
263	3003 Alum. Alloy Tube	WW-T-788	Superseded by WW-T-700/2	*	
264	6061/62 Alum. Alloy Tube	WW-T-789	Superseded by WW-T-700/6	*	
265	Copper Tube	WW-T-799		Ducommun Metals and Supply Co.	18702

* See listed Substitute or Superseding Specification for Planned Source of Supply.

	MATERIAL OR PROCESS TYPE DESIGNATION	PROCUREMENT SPECIFICATION	SUBSTITUTE OR SUPERSEDING SPECIFICATION	PLANNED SOURCE OF SUPPLY <u>1/</u>	CODE NO. <u>2/</u>
266	Silicone Rubber	ZZ-R-765		Chomerics Inc.	18565
267	Metal Test Methods	FED-STD-151		QAPSD	007050
268	Colors	FED-STD-595		TRW Systems Group	11982
269	GMC 800 Chem. Polish	None		Greater Mountain Chem. Co.	09402
270	NRC-2 Alum-Mylar	None		National Research Corp.	42831
271	11110 Gasket	None		Technical Wire Products Inc.	07700
272	M 1709 Epoxy	None		Bee Chemical Co. Gardena, Calif.	
273	HT-A-327 Lubricant	None		Houghton and Co.	73277
274	KK-949A Lubricant			Bray Oil Co.	98308
275	KK-949B Lubricant	0258914		Bray Oil Co.	98308
276	CL Hardner	None		Shell Chem. Co.	22893
277	A4094 Primer, Silicone	0258913		Dow Corning Corp. Midland, Mich.	71984
278	Stycast 1090 Epoxy Resin	0258738		Emerson & Cuming Canton, Mass.	04552
279	RTV 11 Rubber, Silicone	None		General Electric Silicone Prod. Dept.	01139
280	Thermolite 12 Catalyst	0258737		M & T Chemical Co.	12941
281	Silastic 731	0258741		Dow Corning Corp.	71984
282	Epon 828 Resin	0258907		Shell Chem. Co. Pittsburg, Calif.	22893